

# Copper Phenoxyl Complexes

Inaugural-Dissertation

zur

Erlangung des Doktorgrades

der Mathematisch-Naturwissenschaftlichen Fakultät

der Universität zu Köln

vorgelegt von

Katharina Butsch

aus Bonn

Köln, 2010

Gutachter:

Prof. Dr. Axel Klein

Prof. Dr. Uwe Ruschewitz

Prof. Dr. Wolfgang Kaim

Prüfungsvorsitz:

Prof. Dr. Günter Schwarz

Tag der mündlichen Prüfung:

20.10.2010

## Danksagung:

Ein besonderer Dank geht an Herrn Prof. Dr. A. Klein für das interessante Promotionsthema, zahlreiche fachliche Diskussionen und die vielen Freiheiten, die mir bei der Durchführung der praktischen Arbeiten gewährt wurden.

Für die finanzielle Unterstützung bedanke ich mich bei der Studienstiftung des Deutschen Volkes.

Ich danke allen, die mit zahlreichen Messungen und gutem Rat zur vorliegenden Arbeit beigetragen haben: Frau I. Müller, Herrn Dr. I. Pantenburg und Herrn Dr. J. Neudörfl von der XRD Abteilung; Frau N. Tosun und Frau S. Kremer für die EA-Messungen; Herrn P. Kliesen für IR-/Raman- und NIR-Absorptions-Messungen, Herrn Dr. M. Valldor für die magnetischen Messungen sowie Frau D. Naumann von der NMR-Abteilung.

Ein großes Dankeschön auch an Herrn T. Günther und Herrn Prof. Dr. A. Berkessel für die Bereitstellung der salen-type Liganden und Herrn A. Kaiser für die Bereitstellung des [(dppe)NiCl<sub>2</sub>].

Ich bedanke mich bei Frau S. Mihm für die Einarbeitung in die Programme X-Red und X-Shape und bei den Herren A. Uthe und A. Schüren für die Einarbeitung in die ESR-Spektroskopie und Hilfe bei den 4 K Messungen.

Ein großer Dank gilt auch dem Arbeitskreis Klein für die permanente Unterstützung, die zahlreichen Diskussionen und Tassen Kaffee und das tolle Arbeitsklima: Herrn S. Elmas, Frau C. Hamacher, Herrn A. Kaiser, Herrn R. Lepski, Frau A. Lüning, Frau Y. von Mering, Herrn R. Pohl, Herrn B. Rausch, Herrn A. Schüren, Frau K. Stirnat und Herrn A. Uthe. Ein besonderer Dank gilt Frau S. Nitsche, ohne die es zwei Jahre lang sehr langweilig im Labor gewesen wäre!

Ich bedanke mich auch bei allen, die diese Arbeit Korrektur gelesen haben, besonders aber bei Herrn C. Biewer und bei Frau L. Butsch.

Ein weiterer Dank geht an die „lila Truppe“ und Frau Prof. Dr. BDL für viele gute Tips und den Tritt in den Hintern.

Danke an alle, denen ich in den letzten 2.5 Jahren auf die Nerven gegangen bin und die das mit stoischer Ruhe ertragen haben: meiner Familie und meinen Freunden!

## Abstract:

The work described in the following was inspired by radical copper enzymes such as Galactose Oxidase (GO). GO catalyses the two-electron oxidation of terminal alcohols to the corresponding aldehydes using air oxygen. Transfer of two electrons is possible, since GO contains two magnetically coupled one-electron redox centres: a tyrosylate ligand from the apo-protein, which exists either in the tyrosylate or the tyrosyl radical form and is bound to a copper ion possessing two stable oxidation states (+I and +II). The catalytic activity of GO can be assigned to the Cu–OTyr (Tyr = Tyrosine, or more general Cu–Oaryl) motive, which is also found in all complexes synthesised and characterised in this thesis.

The ligands specifically designed for this study, contain substituted, non-substituted or aromatically enlarged phenoxy moieties and belong to various compound classes: O,N,O pincer ligands, O,O',N donor ligands, salen type ligands, phenol-substituted triazole ligands, phenalene ligands, benzoquinone ligands and acridine ligands. All of them were used to synthesise Cu<sup>II</sup> complexes, selected ligands (e.g. O,O',N, donor ligands) were additionally coordinated to Ni<sup>II</sup>, Zn<sup>II</sup>, Fe<sup>II</sup>, Fe<sup>III</sup> and Co<sup>II</sup>.

All compounds were fully characterised using NMR or EPR spectroscopy, UV/vis/NIR-absorption spectroscopy, emission spectroscopy, cyclic voltammetry, spectroelectrochemistry, elemental analysis and XRD. These studies focus on (a) the electrochemical properties of the two one-electron redox couples Cu<sup>II</sup>/Cu<sup>I</sup> and [PhO<sup>•+</sup>]/[PhO], (b) the influence of ligand- and complex structure on both redox pairs and (c) the catalytic activity of the complexes resulting from their electrochemical properties. The latter was investigated by test reactions using benzyl alcohol as substrate and an *in situ* generated catalyst.

Furthermore, detailed investigations on reactions yielding the active radical species Cu<sup>II</sup>–[OPh<sup>•+</sup>] under catalysis conditions were performed using a phenol-substituted triazole ligand system. Two methods were compared, one starting from a Cu<sup>I</sup> precursor, which is oxidised by air oxygen to yield the copper radical complex and the second starting from Cu<sup>II</sup> complexes which undergo a disproportionation reaction forming the active radical species and a Cu<sup>I</sup> byproduct.

## Kurzzusammenfassung:

Die im Folgenden beschriebenen Arbeiten wurden inspiriert von Radikal-Kupfer Enzymen wie der Galactose Oxidase (GO). GO katalysiert die Zwei-Elektronen-Oxidation von terminalen Alkoholen zu den korrespondierenden Aldehyden unter Verwendung von Luftsauerstoff. Die Elektronenübertragung wird durch magnetische Kopplung zweier Ein-Elektronen-Redoxzentren ermöglicht: ein Tyrosylat-Ligand aus dem Apo-Protein, der entweder als Tyrosylat oder als Tyrosyl-Radikal vorliegt, koordiniert dazu an das Kupferion, das in zwei stabilen Oxidationsstufen (+I und +II) vorliegen kann. Die katalytische Aktivität von GO kann auf das Strukturmotiv Cu–OTyr (oder vereinfacht Cu–OPh) reduziert werden. Alle Verbindungen, die im Rahmen dieser Arbeit synthetisiert und charakterisiert wurden weisen ein solches Strukturmotiv auf.

Durch gezieltes Ligandendesign wurden Systeme erhalten, die substituierte, unsubstituierte, oder aromatisch erweiterte Phenoleinheiten enthalten. Die verwendeten Liganden gehören zu den Klassen der O,N,O-Pincer-Liganden, O,O',N-Donor-Liganden, salen-typ-Liganden, Phenol-substituierten Triazol-Liganden, Phenalenon-Liganden, Benzochinon-Liganden und Acridin-Liganden. Die Liganden wurden vorrangig zur Synthese von Cu<sup>II</sup> Komplexen verwendet, mit ausgesuchten Liganden wurden zusätzlich auch Ni<sup>II</sup>, Zn<sup>II</sup>, Fe<sup>II</sup>, Fe<sup>III</sup> und Co<sup>II</sup> Komplexe hergestellt (v.a. mit den O,O',N-Donor-Liganden).

Alle Verbindungen wurden vollständig charakterisiert unter Verwendung von NMR- oder ESR-Spektroskopie, UV/vis/NIR-Absorptionspektroskopie, Emissionsspektroskopie, Cyclovoltammetrie, Spektroelektrochemie, Elementaranalyse und Röntgenbeugung am Einkristall. Im Mittelpunkt der Untersuchungen standen dabei (a) die elektrochemischen Eigenschaften der beiden Ein-Elektronen-Redoxzentren Cu<sup>II</sup>/Cu<sup>I</sup> und [PhO<sup>•+</sup>]/[PhO] bzw. (b) der Einfluss struktureller Veränderungen der Liganden und Komplexe auf die Eigenschaften der beiden Redoxpaare und schließlich (c) der Einfluss der elektrochemischen Eigenschaften auf das katalytische Potential der Komplexe. Letzteres wurde in Testreaktionen untersucht, bei denen Benzylalkohol als Substrat verwendet und der Katalysator *in situ* generiert wurde.

An einem ausgewählten Komplexsystem (mit Phenol-substituiertem Triazol-Ligand) wurden ferner detaillierte Untersuchungen zur Generierung der aktiven Species Cu<sup>II</sup>–[OPh<sup>•+</sup>] vorgenommen. Hier wurden zwei Methoden verglichen, die Verwendung von Cu<sup>I</sup> Prekursoren, die mittels Luftsauerstoff zur Cu<sup>II</sup>-Radikal-Spezies oxidiert werden, und die Disproportionierung von Cu<sup>II</sup> Komplexen in die radikalische Komplex-Spezies und ein Cu<sup>I</sup> Nebenprodukt.

# Content:

<b>1.0</b>	<b>Introduction</b>	1
1.1	Metal functions in biological systems	1
1.2	Copper containing enzymes	5
1.3	The enzyme Galactose Oxidase	10
1.4	Model systems for Galactose Oxidase	16
1.5	Phenoxy radicals and their stabilisation	19
1.6	Motivation of this thesis	22
<b>2.0</b>	<b>O,N,O-pincer complexes</b>	25
<b>2.1</b>	<b>Derivatives of Pyridine-2,6-dicarboxylic acid (pydicH<sub>2</sub>) as O,N,O-pincer ligands and their Cu<sup>II</sup> complexes</b>	25
2.1.1	Introduction	25
2.1.2	Syntheses of pydicH <sub>2</sub> ester ligands and their copper complexes	26
2.1.3	EPR spectroscopy	32
2.1.4	Electrochemical measurements	33
2.1.5	Absorption spectroscopy and spectroelectrochemical measurements	35
2.1.6	Conclusions on the suitability of pydicH <sub>2</sub> ester complexes as GO model systems	37
<b>2.2</b>	<b>Bis-phenoxido-pincer ligands and their copper complexes</b>	37
2.2.1	Introduction	37
2.2.2	Synthesis and characterisation of the ligands	39
2.2.3	Synthesis of the complexes	41
2.2.4	NMR spectroscopy	43
2.2.5	EPR spectroscopy	44
2.2.6	Electrochemical measurements	47
2.2.7	Absorption spectroscopy and spectroelectrochemical measurement	49
2.2.8	Luminescence properties	55
2.2.9	Conclusions on the suitability of bis-phenoxido pincer complexes as GO model systems	57
<b>3.0</b>	<b>Radicals delocalised in aromatic systems</b>	58
<b>3.1</b>	<b>Introduction</b>	58
<b>3.2</b>	<b>9-Hydroxyphenalenone (opoH) ligand and complexes</b>	58
3.2.1	Introduction	58
3.2.2	Synthesis and structure analysis of the opo complexes	61

3.2.3	Electrochemical properties	65
3.2.4	Absorption spectroscopy and spectroelectrochemistry	67
<b>3.3</b>	<b>Benzo-[h]-quinoline-10-ol (bqOH) complexes</b>	<b>69</b>
3.3.1	Introduction	69
3.3.2	Synthesis of bqOH complexes	70
3.3.3	EPR spectroscopy	71
3.3.4	Electrochemical properties	71
3.3.5	UV/vis absorption spectroscopy	72
<b>3.4</b>	<b>Acridine complexes</b>	<b>74</b>
3.4.1	Introduction	74
3.4.2	Synthesis and structure of ligands and complexes	75
3.4.3	EPR spectroscopy	76
3.4.4	Electrochemical properties	77
3.4.5	UV/vis absorption spectroscopy and spectroelectrochemistry	78
<b>3.5</b>	<b>Radicals in aromatic ligands – conclusions</b>	<b>81</b>
<b>4.0</b>	<b>Copper complexes with salen type ligands (N<sub>2</sub>O<sub>2</sub> donor set)</b>	<b>83</b>
4.1	Introduction	83
4.2	Synthesis and structure of the copper complexes	85
4.3	EPR spectroscopy	87
4.4	Electrochemical properties	88
4.5	Absorption spectroscopy and spectroelectrochemistry	90
4.6	Conclusion on the suitability of the salen type complexes as GO model systems	92
<b>5.0</b>	<b>An O,N chelating triazol ligand (triazH) and its copper complex [Cu(triaz)<sub>2</sub>]</b>	<b>93</b>
5.1	Introduction	93
5.2	Synthesis and Structure of [Cu(triaz) <sub>2</sub> ]	94
5.3	EPR spectroscopy	96
5.4	Cyclic voltammetry	97
5.5	Absorption spectroscopy and spectroelectrochemistry	98
5.6	Summary on the suitability of [Cu(triaz) <sub>2</sub> ] as a GO model system	99
<b>6.0</b>	<b>Highly flexible O,O',N Ligands and their Co, Fe, Ni, Cu and Zn complexes</b>	<b>100</b>
6.1	Introduction	100
6.2	Ligand preparation	102

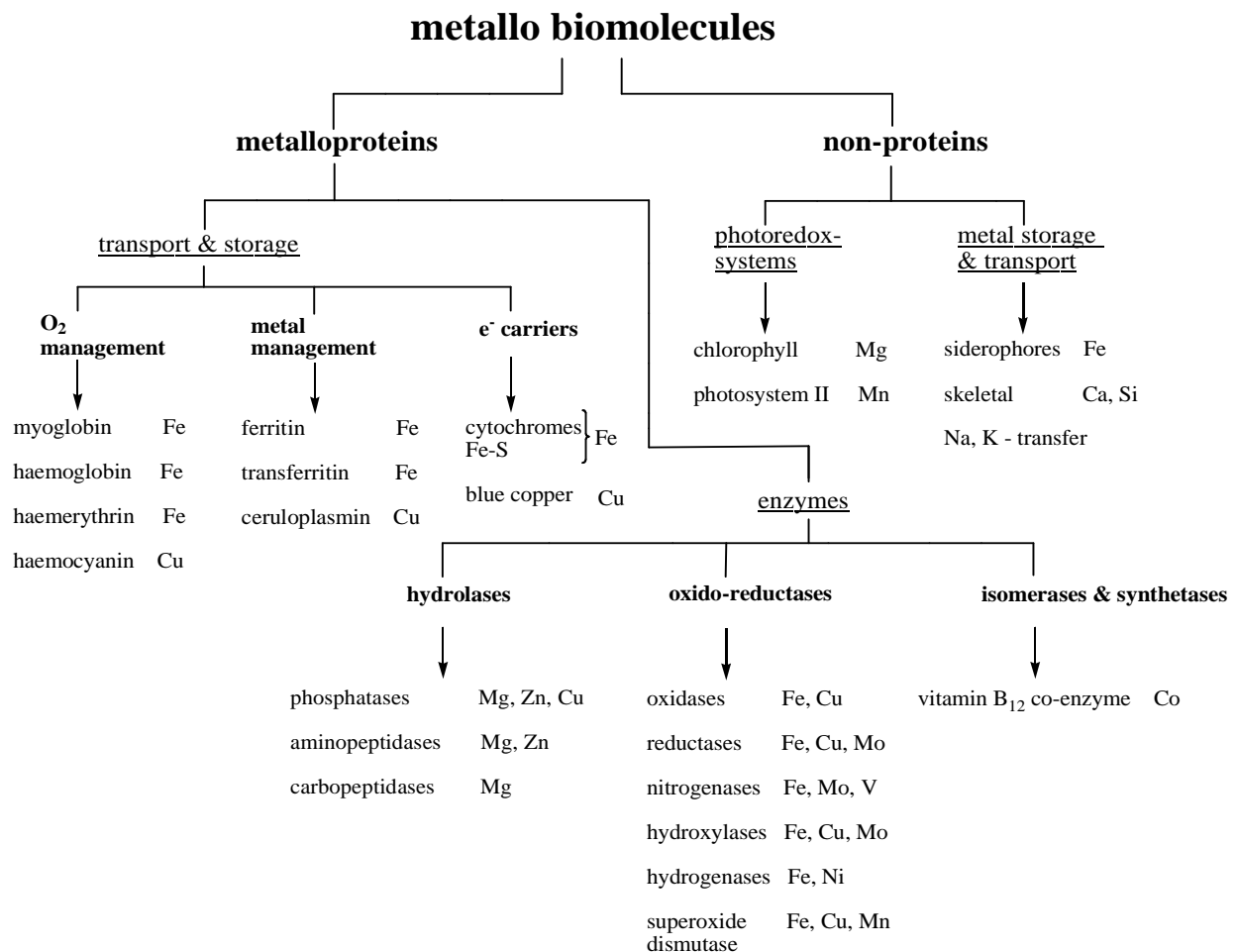
6.3	Complex synthesis	103
6.4	NMR spectroscopy	104
6.5	Crystal and molecular structures from XRD	106
6.6	EPR spectroscopy of Co <sup>II</sup> , Cu <sup>II</sup> and Fe <sup>III</sup> compounds	111
6.7	Magnetic measurements	114
6.8	UV/vis/NIR absorption spectroscopy	115
6.9	Electrochemical investigations	120
6.10	Conclusion on the suitability of O,O',N donor complexes as GO models	123
<b>7.0</b>	<b>Catalytic test reactions</b>	<b>124</b>
7.1	Introduction	124
7.2	Phenoxyl radical generation by a copper disproportionation reaction	126
7.3	Phenoxyl radical stability	127
7.4	Variation of the copper source	129
7.5	Influences of the base	130
7.6	Catalytic oxidation using the phenoxy radical complex [Cu(triaz) <sub>2</sub> (L) <sub>n</sub> ] <sup>•k+</sup>	135
7.7	Catalytic activity of copper complexes from Chapters 2, 3 and 4	137
<b>8.0</b>	<b>Summary</b>	<b>140</b>
<b>9.0</b>	<b>Experimental</b>	<b>144</b>
9.1	Instrumentation	144
9.2	Synthesis	145
9.3	Disproportionation Experiments	161
<b>10.0</b>	<b>Literature</b>	<b>164</b>
<b>11.0</b>	<b>Appendix</b>	<b>176</b>



# 1.0 Introduction

## 1.1 Metal functions in biological systems

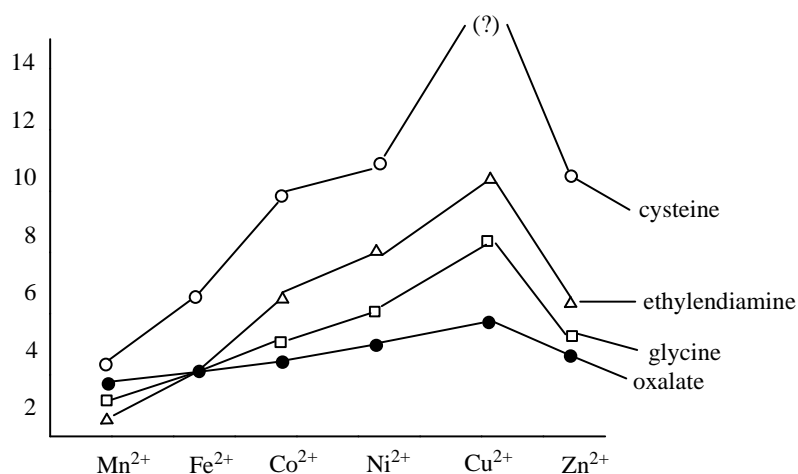
Approximately one third of all enzymes and proteins require metal ions for their biological function.<sup>[1]</sup> Redox inactive metal ions such as  $Mg^{2+}$ ,  $Ca^{2+}$  and  $Zn^{2+}$  are mainly important for enzyme structure and/or configuration. Since function and structure are inseparable in biological systems these metals are crucial. Redox active metals as manganese, iron, cobalt and copper are important for electron transfer (uptake, release and storage), dioxygen binding or oxygenation / oxidation catalysis (substrate binding and activation).<sup>[1]</sup> Scheme 1 shows an overview over metal containing biomolecules with selected examples.



Scheme 1: Classification of metal dependent biomolecules in living organisms<sup>[2]</sup>

In a simple bioinorganic approach, the inner core of a metalloprotein (Scheme 1) can be described as a metal complex and the physical properties and reactivity is then discussed in terms of “established” parameters for the description of transition metal complexes: oxidation state of the metal, coordination number, coordination polyhedron and the specific role ligands can play ( $\sigma$ -donator,  $\pi$ -acceptor etc.). The inner core is also referred as coenzyme and together with the apoenzyme it forms the holoenzyme, which is the main working metalloprotein.<sup>[3]</sup>

Ligands for the coordination of metals in biological systems can be proteins (part of the apoenzyme), with amido-, amino-, amidato-, carbonyl- or carboxylate-functions located at the N or C termini of the peptide backbone; with amino-, amido-, imidazolyl-, imidazolate-, guanidine-, carbamate-, carboxylate-, carbonyl-, phenol-, phenolate-, hydroxyl-, hydroxylate-, thioether-, thiol-, thiolate- or disulfide functions located in the amino acid-side chains, or exogenic ligands. The latter group contains specifically designed multidentate (multifunctional) ligands as chlorins, corrins, porphyrins, pterins or ubiquitous small ions or molecules as  $I^-$ ,  $Cl^-$ ,  $CN^-$ ,  $H_2O$ ,  $PO_4^{3-}$ ,  $O_2$ ,  $N_2$ ,  $NO$ ,  $\alpha$ -ketoglutarate, etc.<sup>[1]</sup> Some metal / ligand combinations are superior to others, as can be predicted by the HSAB (hard and soft acids and bases) principle. This concept distinguishes between hard and soft *Lewis* acids and *Lewis* bases, while “hard” means small, highly charged and not polarisable ions or molecules, the term “soft” describes big and well polarisable ions and molecules with low charge.<sup>[4]</sup> Thermodynamically the combinations of soft acids and bases as well as hard acids with hard bases are stable. In the context of coordination chemistry the HSAB principle ascribes the preference of ligands with soft donor functions to soft metal ions and hard metal ions to ligands with hard donor functions. E.g. in metalloenzymes tyrosinate strongly favours  $Fe^{III}$ , histidine coordinates to  $Zn^{II}$ ,  $Cu^{II}$ ,  $Cu^I$  and  $Fe^{II}$ , methionine often coordinates to  $Fe^{II}$ ,  $Fe^{III}$ ,  $Cu^I$  and  $Cu^{II}$ , while glutamate and aspartate prefer  $Fe^{III}$ ,  $Mn^{III}$ ,  $Fe^{II}$ ,  $Zn^{II}$ ,  $Mg^{II}$  or  $Ca^{II}$  and finally cysteinate bonds relatively unselective to  $Zn^{II}$ ,  $Cu^{II}$ ,  $Cu^I$ ,  $Fe^{III}$ ,  $Fe^{II}$ ,  $Mo^{IV-VI}$  and  $Ni^{I-III}$ .<sup>[3]</sup> Scheme 2 presents binding constants of divalent metal ions with biological relevance to typical ligands providing different donor sets: oxalate (O,O); glycine (N,O); ethylenediamine (N,N) and cysteine (N,S). Remarkably, all these ligands form the strongest bonds to  $Cu^{2+}$  ions. The differences in binding strength increase with increasing softness of the ligands (soft ligands are expected to fit best to  $Cu^{2+}$  ions). As a result copper complexes are the most stable divalent complexes found in bio-systems.

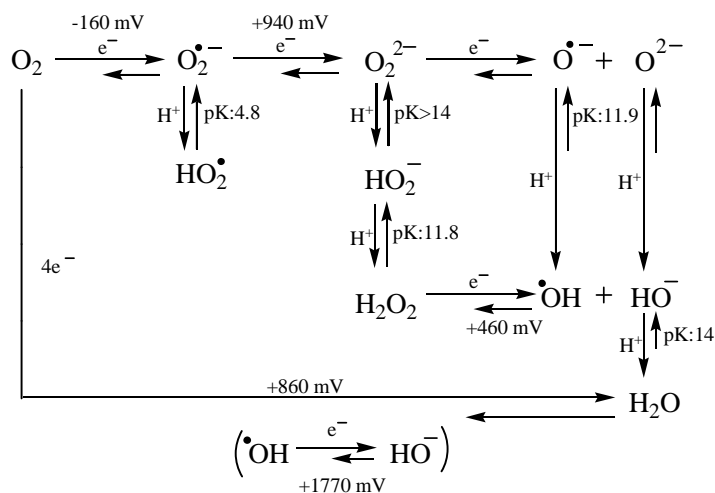


Scheme 2: Binding constants ( $\log K$ ) for some (biological) ligands with the divalent ions  $\text{Mn}^{2+}$ ,  $\text{Fe}^{2+}$ ,  $\text{Co}^{2+}$ ,  $\text{Ni}^{2+}$ ,  $\text{Cu}^{2+}$  and  $\text{Zn}^{2+}$ [5]

The role ligands play in metalloproteins is, of course, not limited to binding. Additionally, ligands can provide cooperative and allosteric interactions, they organise reactive sites in multicentre enzymes and realise electron transfer via superexchange pathways, they provide a hydrophobic environment with surface recognition sites, binding pockets for substrate binding and activation, they possess specific charge and hydrogen bonding sites and therefore assist in catalysis, they stabilise reactive (exogenous) ligands and finally induce a rack<sup>[6]</sup> or entatic<sup>[7-9]</sup> state around the metal ion.<sup>[1]</sup> The latter aspect is highly important for bioinorganic coordination chemistry. Entatic catalysis enables enzymes to activate small, symmetric molecules with high binding energy e.g. during  $\text{N}_2$ -fixation, during reductive  $\text{CH}_4$  synthesis from  $\text{CO}_2$  and  $\text{H}_2$  and in  $^3\text{O}_2$  metabolism at very moderate conditions ( $\sim 298\text{ K}$ ,  $1\text{ atm}$ ,  $\text{pH}\sim 7$ ). Especially the oxygen metabolism plays an important role for living systems. One aspect in this respect is the utilisation of energy included in dioxygen, another aspect is detoxification by removing superoxide and peroxides, which are strongly oxidising agents. Scheme 3 illustrates the step by step reduction of  $^3\text{O}_2$  molecules. In the course of the oxygen metabolism the involved metal ions need to coordinate reliably to various different intermediate oxygen species.

Dioxygen binding to low valent metal ions such as  $\text{Fe}^{2+}$  and  $\text{Cu}^+$  leads to activation of the kinetically inert  $\text{O}_2$  molecule.  $\text{Cu}^+$  is a  $\pi$ -donor and therefore the  $\text{Cu}$ -dioxygen binding is stabilised.<sup>[5]</sup> Furthermore, oxygen activating metals need a redox potential similar to the redox potential of dioxygen. The redox potential of oxygen in water is  $-0.33\text{ V}$  vs. NHE at  $\text{pH } 7$ ;<sup>[3]</sup> for

the sake of comparability the values are transferred to  $\text{FeCp}_2/\text{FeCp}_2^+$  (Ferrocen/Ferrocenium) where the potential lies at about  $E(\text{O}_2/\text{O}_2^{\bullet-}) = -0.07 \text{ V}^{[11,12]}$  which is realised very well by copper compounds. Therefore, copper containing enzymes are ideal suited for oxygen dependent reactions and  $^3\text{O}_2$  metabolism.<sup>[13–31]</sup>



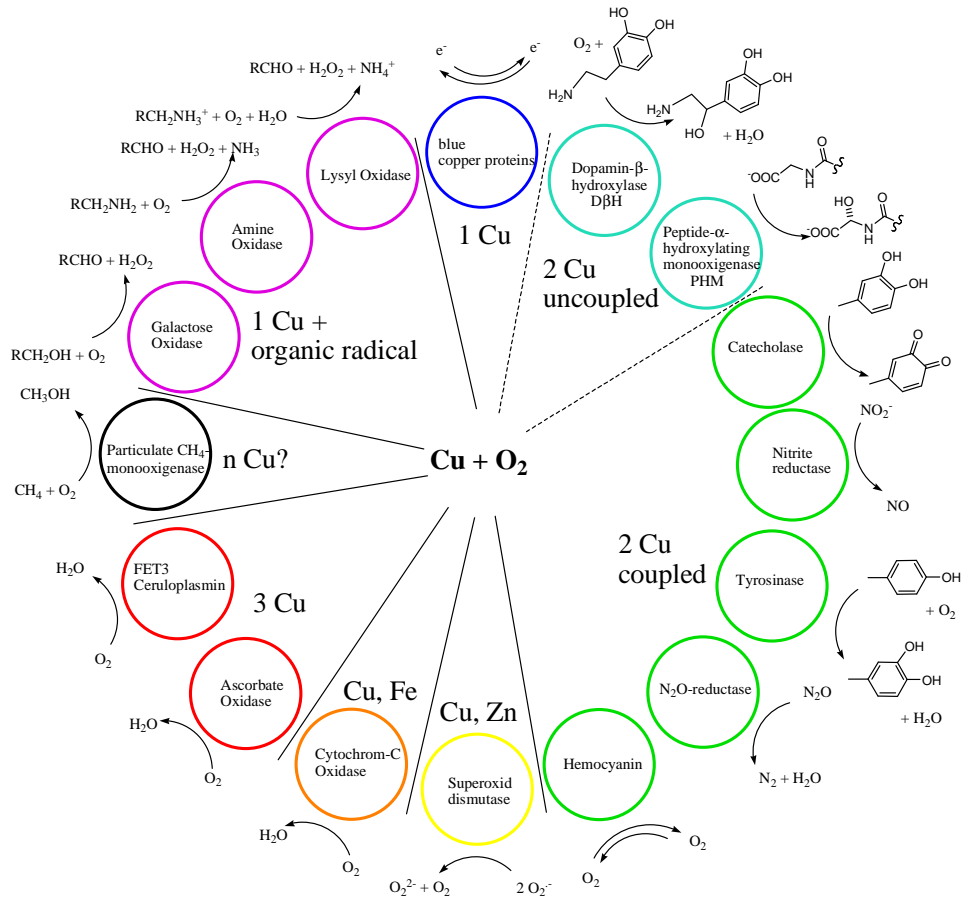
Scheme 3: Summary of reactions important for the dioxygen reduction, electrochemical potentials are given vs. NHE<sup>[10]</sup>

Although iron and copper containing proteins both catalyse oxidation and oxygenation reactions due to similarities in their redox behaviour, there are important differences between the two metals:<sup>[3]</sup>

- (1) The  $\text{Cu}^{\text{I}}/\text{Cu}^{\text{II}}$  redox potentials generally lie higher than those of  $\text{Fe}^{\text{II/III}}$ ; implying that the oxidised copper species are more stable than the oxidised iron species. Copper proteins, e.g. caeruloplasmin, catalyse the iron  $\text{Fe}^{\text{II/III}}$  oxidation and therefore helps in regulation of the iron metabolism.
- (2) In water (neutral pH or sea water) the oxidised copper species ( $\text{Cu}^{\text{II}}$ ) is well soluble, while materials containing  $\text{Cu}^{\text{I}}$  are nearly insoluble.<sup>[32]</sup> In case of iron, the solubility of the reduced species ( $\text{Fe}^{\text{II}}$ ) is higher.
- (3) During evolution copper became relevant lately (compared to iron);<sup>[5,33,34]</sup> thus iron is mainly found in intracellular media, while copper is abundant in extracellular media. (The displacement of iron and manganese in oxidising enzymes by copper presumably is due to the high binding strength of copper ions to biological ligands (Scheme 2), which minimises the danger of losing the metal ion during the catalytic reaction.)<sup>[5]</sup>

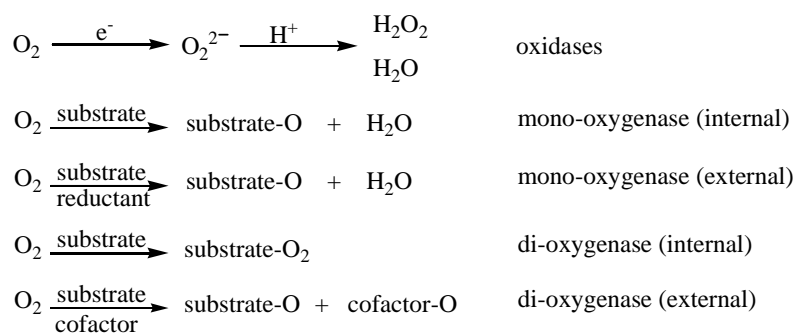
### 1.2 Copper containing enzymes

Copper enzymes are involved in oxygen transport, activation as well as degradation of toxic side products deriving from the use of oxygen, superoxide and peroxides (Scheme 4).



Scheme 4: Most important copper containing enzymes and their reactions [36,37,38]

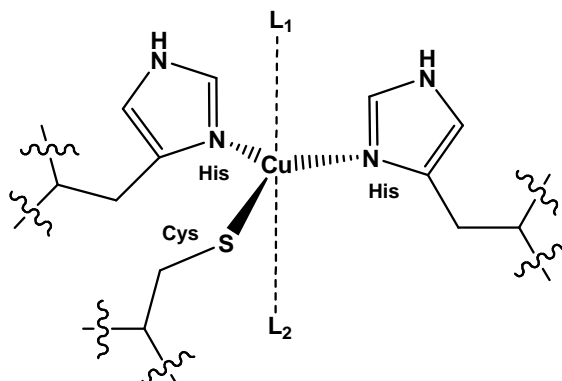
Most copper enzymes belong to the classes of oxidases and oxygenases (Scheme 5). Oxidases reduce dioxygen to superoxide, peroxide or water, while oxygenases mediate the incorporation of dioxygen into organic substrates, either both oxygen atoms in one organic substrate (intramolecular dioxygenases) or into a substrate and an organic cofactor (intermolecular dioxygenases). Alternatively, one oxygen atom is transferred to the substrate while the second atom is reduced to water (monooxygenases). If an additional reductant is necessary, the monooxygenases are called external, if the substrate itself is the reductant they are called internal. [35]



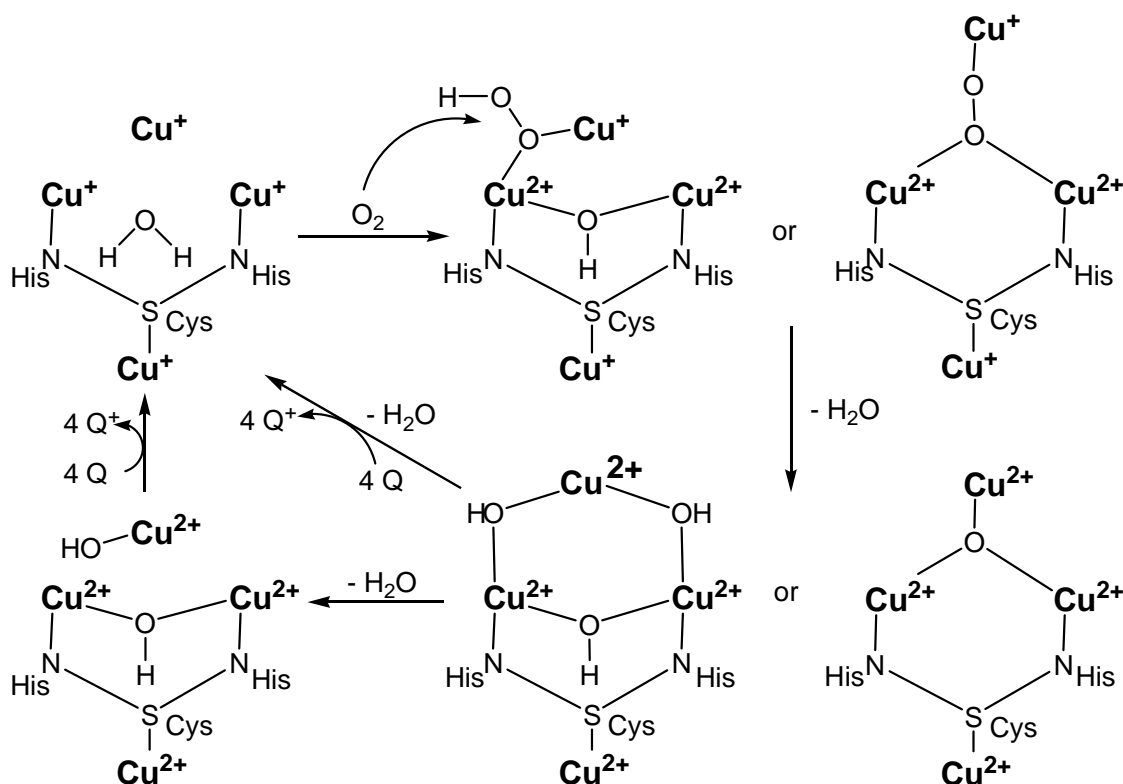
Scheme 5: Classification of oxidases and oxygenases

Internal oxygenation reactions require transfer (storage and controlled release) of more than one electron. Since only a single electron is supplied per copper atom, a higher number of electrons has to be achieved by combination of several redox centres (Scheme 4).

Single electron transfer is the only reaction which can be catalysed by simple mononuclear copper enzymes. Examples of mononuclear enzymes (class I + II) are blue copper proteins (class I) such as azurin<sup>[39]</sup> or plastocyanin<sup>[40]</sup>. Their name is derived from their intense blue colour, which is a result of ligand to metal charge transfer (LMCT) from the cysteinyl ligand (a thiolate, Scheme 6) to  $\text{Cu}^{\text{II}}$ .<sup>[41]</sup> The cysteinyl ligand, as a typical non-innocent ligand<sup>[42]</sup>, transfers electron density to the metal site. This causes extraordinary magnetic properties of the  $\text{Cu}^{2+}$  ion with small hyperfine splitting constants ( $A_{\parallel\text{Cu}}$ ) in the EPR spectra.<sup>[43]</sup> Furthermore, the geometry of the copper atom is highly distorted tetrahedral, with angle deviations up to  $22^\circ$  from the ideal  $109^\circ$ .<sup>[44]</sup> This geometry results in a destabilisation of the  $\text{Cu}^{\text{II}}$  state, which favours a square pyramidal geometry. From the electrochemical point of view this all leads to highly interesting enzyme properties, since the reduction potential of  $\text{Cu}^{\text{II}}$  in blue copper proteins lies between 0.28 V vs.  $\text{FeCp}_2/\text{FeCp}_2^+$  (rusticyanin) and  $-0.22$  V vs.  $\text{FeCp}_2/\text{FeCp}_2^+$  (stellacyanin).<sup>[3]</sup>

Scheme 6: Essential components of the copper site in “blue” copper proteins<sup>[36]</sup>

For the transfer of more than one electron, copper sites are coupled to one or more additional electron transfer sites. Such redox centres can be magnetically coupled via covalent metal–metal bonds (not present in biological systems) or by bridging ligands, e.g. dioxygen itself (class III). If several non-coupled copper ions are found, such as in dopamine- $\beta$ -hydroxylase (D $\beta$ H) and peptide- $\alpha$ -hydroxylating monooxygenase (PHM) (Scheme 4), they may be considered as “one copper atom species”.<sup>[37]</sup> The uncoupled metal sites are not bridged by organic molecules and the distance between two metal ions is larger than 7 Å, as verified by crystal structure analysis.<sup>[45,46]</sup> Nevertheless, the separated metal ions in D $\beta$ H and PHM cooperate during the catalytic cycle. One copper ion, coordinating to a methionine residue (Cu<sub>M</sub>), binds to the substrate while a hydrogen atom is eliminated from the substrate; the intermediate complex species is then reduced to a hydroperoxide species<sup>[47]</sup> by a single electron transfer from the second copper ion, which only bonds to histidine residues (Cu<sub>H</sub>). It was postulated that either substrate molecules close the gap between the two ions<sup>[46]</sup> or that a superoxide channelling occurs instead of an electron transfer.<sup>[48]</sup>

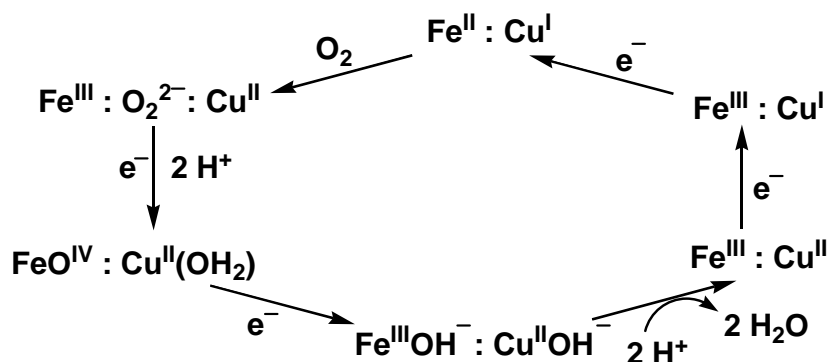


Scheme 7: General mechanism of a four electron reduction found in multi-centre copper oxidases, Q = substrate<sup>[38]</sup>

The highest number of coupled copper sites can be found in so called “blue oxidases” in which a three atom cluster (class II + class III) connected to a fourth single copper ion (class I) exists. Such copper cluster can be found in laccase,<sup>[49]</sup> ceruloplasmin<sup>[50]</sup> and ascorbat-oxidase<sup>[51]</sup>. In general, they all use the four electron reduction of O<sub>2</sub> to 2 H<sub>2</sub>O for substrate specific oxidation.<sup>[36]</sup> The separated copper ion (d > 13 Å) is responsible for a simple electron transfer from the substrate to the copper cluster, while the three copper ions in the cluster (separated by 3.4 Å to 5.1 Å) mediate the O<sub>2</sub> reduction.<sup>[52]</sup> Scheme 7 visualises different states of oxidation and the coordination of the copper ions during this reaction.

Enzymes such as the “particular methane-monooxygenase” (pMMO), phenoxazinone-synthase (PHS) or dihydrogeodin/sulochrin-oxidase (DHGO/SO) have not been fully characterised yet, but they are supposed to belong to the three-copper-atom cluster enzymes.<sup>[38]</sup>

Alternatively to coupling of several copper sites with each other, a copper ion can be coupled with other metal ion (a rare combination). This is found e.g. in cytochrom-*c*-oxidase, in which an iron ion is coupled to the copper ion. Cytochrom-*c*-oxidase is located in the mitochondria membrane and catalyses, as part of the respiratory chain, the final (four electron) reduction of O<sub>2</sub> to two H<sub>2</sub>O.<sup>[53-55]</sup> The very complex enzyme contains thirteen subunits and three copper ions, two iron ions, one zinc ion and one magnesium ion.<sup>[56]</sup> One of the crucial sites of the cytochrom-*c*-oxidase main unit is the copper-iron centre. It consists of a cytochrom heme iron part (in its high spin state) and a copper part with three histidine ligands (Cu<sub>B</sub>). In the oxidised state, Fe<sup>III</sup> (S =  $\frac{5}{2}$ ) and Cu<sup>II</sup> (S =  $\frac{1}{2}$ ) ions are anti-ferromagnetically coupled (total spin S = 2), in the reduced state a diamagnetic Cu<sup>+</sup> ion exists in combination with a Fe<sup>II</sup> high spin species (S = 0). Due to the even number of unpaired spins, the enzyme is predestined for a dioxygen binding.<sup>[3]</sup>



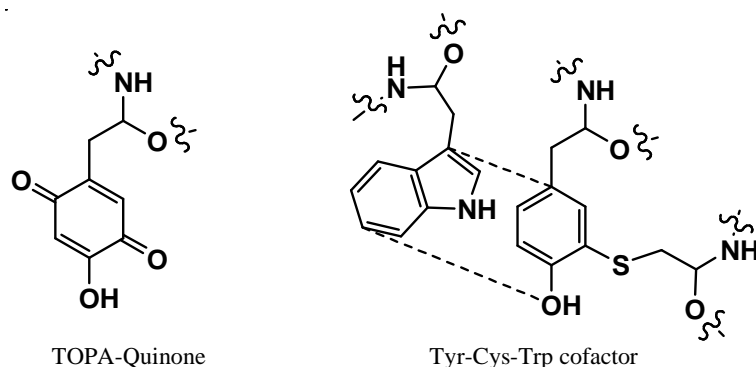
Scheme 8: Assumed catalytic cycle for the reaction of cytochrom-*c*-oxidase<sup>[2]</sup>



Both metal ions are separated by 4-5 Å<sup>[57,58]</sup> and it is likely that the dioxygen molecule binds to both metal ions. During the catalytic cycle (Scheme 8) a hydroperoxo-copper<sup>II</sup> species<sup>[52]</sup> is formed (not shown) and transformed to an oxoferryl<sup>IV</sup> species<sup>[59]</sup> upon protonation.

Another copper containing bimetallic active site is abundant in the copper-zinc dependent superoxide-dismutase (Zn,Cu-SOD)<sup>[60,61]</sup> catalysing the dismutation (that is disproportionation) of the superoxide anion  $O_2^{\bullet-}$  ( $2 O_2^{\bullet-} \rightleftharpoons O_2^{2-} + O_2$ ).<sup>[61]</sup> This reaction is part of the cell detoxification. Besides the copper-zinc SOD, iron and manganese containing SODs are known as well.<sup>[60,61,62]</sup> Due to the fact that the superoxide radical anion is highly reactive (and therefore toxic), an enzymatic activation of the substrate is not necessary, instead the challenge lies in stabilising the enzyme towards aggressive species<sup>[63,64]</sup> and to guarantee a fast substrate transport to the active site. The latter is realised by a channel in the protein scaffold containing hydrogen bridges.<sup>[36]</sup> The active centre contains the non-redox active Zn<sup>II</sup> and a copper ion bridged by histidine side chains, which are necessary for the substrate orientation.<sup>[60,65]</sup> The copper ion mediates two redox reactions via a covalent substrate bond, an oxidation is performed ( $O_2^{\bullet-}$  to  $O_2$ ) if the copper ion is in its Cu<sup>II</sup> state, or a reduction ( $O_2^{\bullet-}$  to  $H_2O_2$ ) if the ion is in its Cu<sup>I</sup> state.<sup>[36,66]</sup>

Another possible combination is a copper site coupled to an organic radical.<sup>[67]</sup> Scheme 4 lists three important examples belonging to the class of radical copper enzymes, Scheme 9 depicts the organic “cofactors”: amine oxidase<sup>[68]</sup> in which the copper ion is coupled to a so called TOPAquinone (TOPA = trioxyphenylalanine = 2,4,5-trihydroxyphenylalanine) radical, lysyl oxidase<sup>[69]</sup> which contains a quinine derived ligand radical and Galactose Oxidase<sup>[14]</sup> in which a tyrosyl radical is part of the reactive centre (Scheme 9).



Scheme 9: Internal cofactors of amine oxidase and lysyl oxidase (left) and galactose oxidase (right) carrying a radical during the catalytic reaction

From the viewpoint of inorganic or coordination chemistry, the combination of a redox active metal ion with a non-innocent organic ligand in its radical state is highly interesting. In the following the properties of the enzyme Galactose Oxidase, the best understood copper radical enzyme with regard to biology (enzyme structure and mechanism) and bioinorganic chemistry (applicable model systems), are described in detail.

### 1.3 The enzyme Galactose Oxidase

Galactose Oxidase (GO, EC 1.1.3.9) is an extracellular monomeric enzyme (68 kDa) which was isolated first in 1959 from the fungus *Polyporus circinatus* (later re-determined as *Cladobotrium (Dactylium) dendroides*).<sup>[70]</sup> Due to the fact that this fungus is (parasitically) associated with plants, it was suggested that GO secretion occurs in order to decompose galactose containing (hemi)cellulose.<sup>[70b]</sup> GO catalyses the oxidation of terminal alcohols to aldehydes with H<sub>2</sub>O<sub>2</sub> as a side product.<sup>[3,71]</sup> The main biological function and with it the enzyme's substrate could not be determined yet, because GO is highly nonspecific. E.g. GO converts *D*-galactose, *D*-raffinose, dihydroxyacetone,<sup>[72]</sup> benzyl alcohol and several of its *meta*- and *para*-substituted derivatives to the corresponding aldehydes.<sup>[73]</sup> Substrate diversity is untypical for enzyme catalysis. Normally enzymes are highly specialised and consequently committed to a single substrate. As a possible explanation it was suggested that the function of GO is rather the production of hydrogen peroxide than the oxidation of substrates.<sup>[74]</sup> However, GO exhibits high stereoselectivity (>95%) for abstraction of the *pro-S* hydrogen of oxidisable substrates, the substrate's C $\alpha$  apparently serves as a stereo selectivity determinant.<sup>[75]</sup>

The catalytic cycle consists of two different reactions: the substrate oxidation (Equation 1) and the oxygen reduction (Equation 2), the latter reorganises the ground state of the enzyme.<sup>[76-78]</sup> These catalytic reactions require a two electron transfer and therefore the mononuclear copper site in GO needs to be supported by a second redox centre. In the case of GO this is a tyrosyl radical cation [Tyr]<sup>•+</sup> (Scheme 4). The two electrons released from the substrate are transferred to the metal (Cu<sup>II</sup>/Cu<sup>I</sup> redox couple) as well as to the organic tyrosyl radical.



The three dimensional structure of GO is known since 1991 when Ito *et al.* crystallised the protein with H<sub>2</sub>O in the assumed position of the substrate. The protein structure consists of three big  $\beta$ -structure domains and one  $\alpha$  helix, which leads to high protein stability, so that GO remains active even in 6 M urea. The copper ion is located on the surface of the second largest domain, an antiparallel  $\beta$  sheet.<sup>[72]</sup> The oxidised form contains a Cu<sup>2+</sup> ion, which is coordinated in a square pyramidal fashion. The amino acids Tyr 272 (O–Cu = 1.94 Å), His 496 (N–Cu = 2.11 Å) and His 581 (N–Cu = 2.15 Å) form the pyramid's base, while in the axial position a weakly bound (2.69 Å) tyrosinate residue (Tyr 495) is located. An exogenic ligand is incorporated into the coordination sphere and occupies the substrate binding site *in vivo*. This exogenous ligand is a water molecule at pH = 7 (O–Cu = 2.8 Å), while in acetate buffer solution (pH = 4.5) an acetato ligand (O–Cu = 2.3 Å) is coordinating to the copper ion. The coordination polyhedron is nearly perfect square pyramidal when bearing an acetato ligand, while the square base of the pyramid is distorted when the aqua complex is formed (Figure 1).<sup>[15]</sup> This distortion is part of the entatic state of GO<sup>[7,8]</sup> and the highest activity of GO is observed around pH = 7.

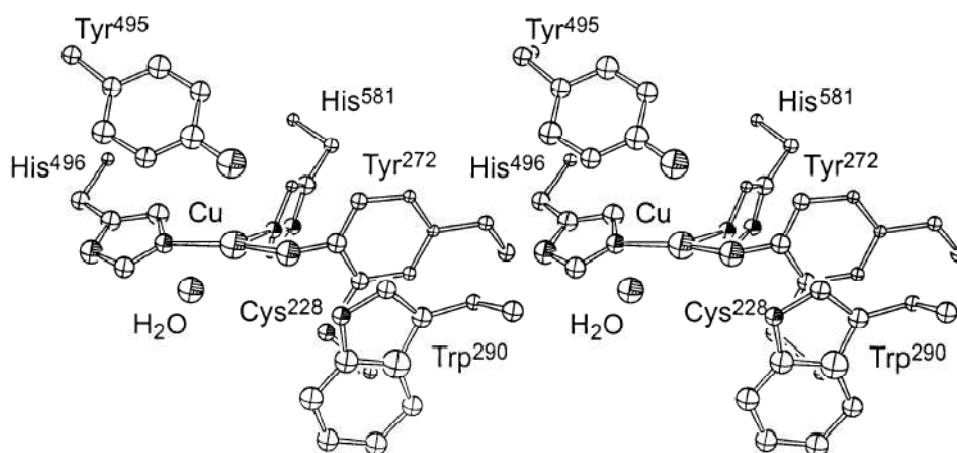
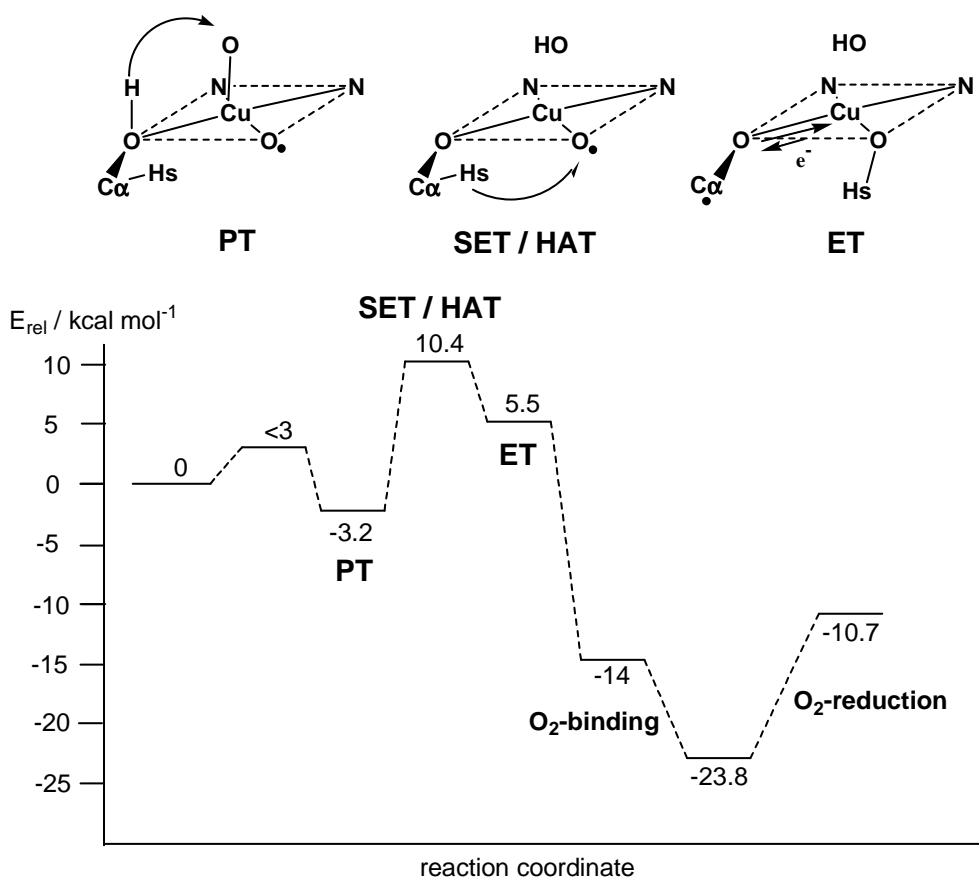


Figure 1: Stereo view of the active centre of Galactose Oxidase (GO) from ref. [72]

The tyrosyl radical cation [Tyr]<sup>•+</sup> is located in the first coordination sphere and delocalised (via a thioether bond) into the second coordination sphere, thus it is called a secondary „built-in“ cofactor. The two tyrosyl ligands which are part of the copper coordination sphere are not chemically equivalent and the radical is exclusively located at the equatorial Tyr 272.

A probable mechanism (Scheme 10) can be drawn based on numerous spectroscopic, catalytic and theoretical studies.<sup>[79]</sup>



Scheme 10: Enzyme structure<sup>[73]</sup> and energetic profile during the catalytic reaction<sup>[79]</sup>

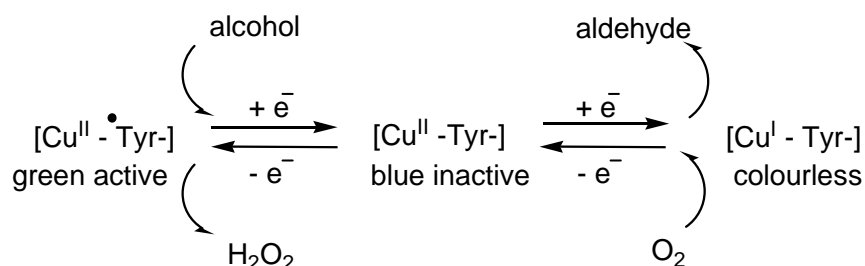
Scheme 10 shows that the overall catalytic cycle is exothermic by  $11 \text{ kcal mol}^{-1}$ . The first reaction step is a proton transfer (PT) between the substrate and Tyr 495 (that serves as an internal base<sup>[80,81]</sup>), which proceeds isothermally and very fast.<sup>[82]</sup> The Tyr 495 dissociates from the copper ion and forms a hydrogen bond with the substrate-oxygen. This reaction step is exothermic by  $3.2 \text{ kcal mol}^{-1}$ .<sup>[79]</sup> The decrease of the coordination number from five to four might facilitate the reduction of  $\text{Cu}^{\text{II}}$  to  $\text{Cu}^{\text{I}}$  and stabilise the reduced copper state.<sup>[72,83]</sup>

The second step, a hydrogen atom transfer (HAT) to Tyr 272, occurs simultaneously with an electron transfer to the equatorial tyrosine.<sup>[79]</sup> Due to the fact that the active site of GO is EPR silent<sup>[72]</sup> the formation of the GO radical state cannot be observed by EPR measurements (EPR measurements might help to distinguish between an axial or an equatorial tyrosyl radical). The hydrogen atom transfer is closely linked or even concerted (in an  $\text{E}_{\text{R}2}$  mechanism) to a single electron transfer (SET). In case of a step by step reaction, the intermediate is a substrate derived ketyl radical, which has a remarkable potential difference to the enzyme site. This might be the

driving force for the complete oxidation process leading to the aldehyde product and a  $\text{Cu}^{\text{I}}$  site. Isotopic exchange reactions indicate that the hydrogen atom transfer is the rate-limiting step.<sup>[75]</sup> Finally a very exothermic electron transfer between substrate and copper ion occurs and the aldehyde molecule is released from the enzyme.<sup>[79]</sup>

After dissociation of Tyr 495 and product,  $\text{Cu}^{\text{I}}$  is coordinated by three ligands with trigonal planar symmetry (a T-shaped form is discussed alternatively).<sup>[47,72,79,82]</sup> Later on, this species takes part in the regeneration reaction. The re-oxidation of the copper atom might be supported by the coordination polyhedron: the square-pyramidal geometry is generally favoured for the  $\text{Cu}^{\text{II}}$  state.<sup>[82]</sup> The radical is more stable in the axial position if both tyrosine residues are deprotonated.<sup>[84-86]</sup>

Over the whole catalytic reaction three different states of the GO enzyme can be defined by their different spectroscopic properties. Scheme 11 and Table 1 summarise the spectroscopic properties of the different GO states.



Scheme 11: Mechanistic scheme of the catalytic reaction and the regeneration reaction of GO<sup>[72]</sup>

Table 1: Analytical properties of the three redox states of natural GO

Properties	$\text{Cu(II)Tyr}^{\bullet}$	$\text{Cu(II)Tyr}$	$\text{Cu(I)Tyr}$
Colour	green	blue	colourless
absorption bands	445 nm ( $6436 \text{ Lmol}^{-1}\text{cm}^{-1}$ ) <sup>[a]</sup> ; 810 nm ( $4133 \text{ Lmol}^{-1}\text{cm}^{-1}$ ) <sup>[b]</sup>	314 nm, 365 nm, 422 nm, 510 nm, 625 nm, 785 nm	-
Activity	active	inactive	inactive <sup>[c]</sup>
oxidation potential <sup>[d]</sup>	-	+ 0.01 V <sup>[11,87,88]</sup>	- 0.24 V <sup>[11,88]</sup>
EPR	silent ( $S = 0$ ) <sup>[81][e]</sup>	$g_{\parallel} = 2.299$ ; $g_{\perp} = 2.073$ <sup>[70]</sup>	silent ( $S = 0$ )

[a] Assigned to LMCT, ( $\pi-\pi^*$  transition) with the radical Tyr 272<sup>[89]</sup>

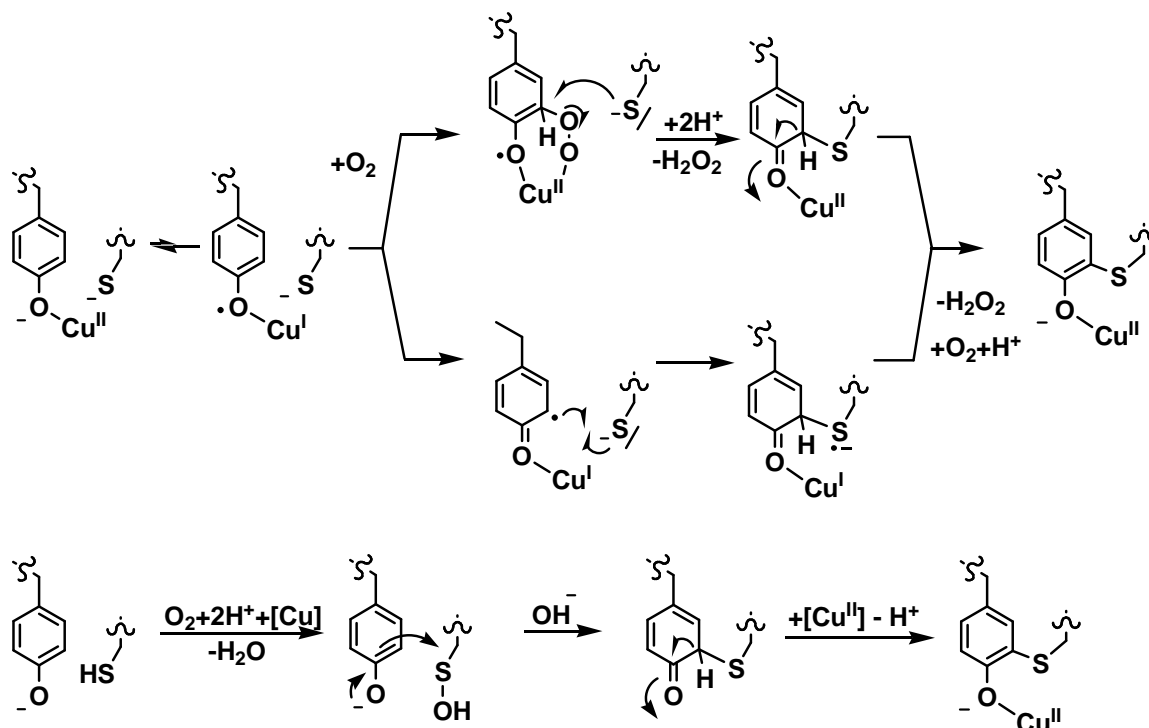
[b] Assigned to LMCT due to charge resonance (IL) between Tyr 495 and Tyr 272<sup>[81]</sup>

[c] Before regeneration; therefore sometimes described as active in  $\text{H}_2\text{O}_2$  synthesis

[d] Potentials vs.  $\text{FeCp}_2/\text{FeCp}_2^+$

[e]  $[\text{Tyr}]^{\bullet+}$  in apo-GO:  $g_{\parallel} = 2.0073$ ,  $g_{\perp} = 2.0017$ <sup>[81]</sup>

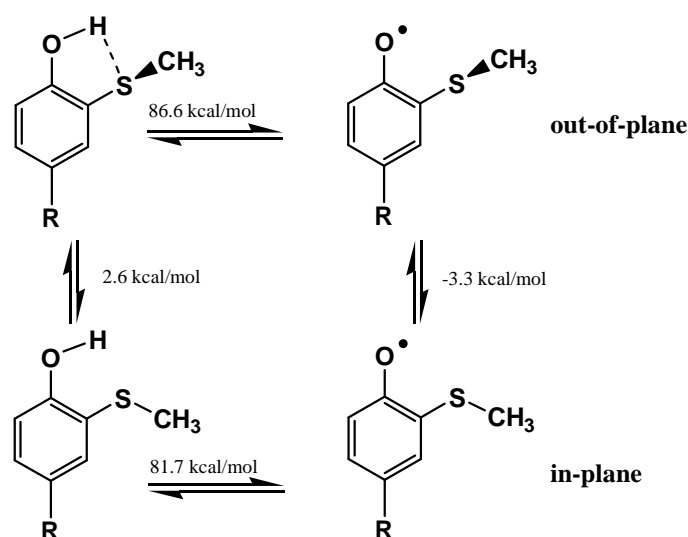
The radical which appears at Tyr 272 during the catalytic reaction is linked to the Trp 290 by a sulfur bridge formed by the Cys 228. This cystein residue binds covalently to the *ortho*-C-atom of Tyr 272.<sup>[15]</sup> The sulfur bridge is formed via a posttranslational self processing (splitting of the 17 amino acid-prosequence located at the N-terminus and formation of the sulfur bridge). The active enzyme configuration is automatically produced upon addition of Cu<sup>II</sup> (Scheme 12).<sup>[90]</sup>



Scheme 12: Possible formation reactions for the thioether bond in GO<sup>[91,92]</sup>

A number of studies have been performed to examine the thioether bond's influence on the radical stability<sup>[89,93–100]</sup> but this still remains a controversial point. A first hypothesis (1997/1998) claimed that the sulfur bridge enlarges the aromatic system of Tyr 272 and therefore supports the generation and stabilisation of the free radical. Model systems showed that the thioether substituted tyrosyl radical is stabilised by approximately 540 mV in relation to an unsubstituted tyrosyl radical,<sup>[101,102]</sup> while EPR measurements show high electron density on the sulfur atom but not in the  $\pi$ -system of the ligand.<sup>[89]</sup> These findings were in line with studies on model compounds bearing an enlarged  $\pi$ -system which does not have any influence on the radical stabilisation.<sup>[103–105]</sup> The sulfur bridge also induces a conjugative effect which stabilises the negative charge of the tyrosinate ligand and leads to a lower  $pK_a$  value.<sup>[89]</sup> Because of these and

other reasons, a mutation of Trp 290 destabilises the enzyme (1993/1994).<sup>[106-108]</sup> Other experimental trails on model compounds<sup>[109]</sup> and simulation of the catalytic activity<sup>[79]</sup> (2000) did not confirm any influence of the thioether bond. So it has been assumed that the stabilising effect of the thioether bond primarily is shielding of the free radical from the solvent.<sup>[71]</sup> Furthermore, it has been suggested that the true reason for the occurrence of  $\pi$ - $\pi$  interactions mediated by the sulfur bridge is to maintain the cofactor orientations and to guarantee a diamagnetic ground state of the enzyme.<sup>[110]</sup> Investigations of Dooley *et al.* (2007) have shown that the sulfur bridge influences the radical stability as well as the kinetic parameters and the binding affinity of some substrates e.g. *D*-galactose.<sup>[111]</sup> Recent investigations of Pedulli *et al.* (2008) showed that there are two different configurations of the thioether bond, an “in-plane” and an “out-of-plane” configuration (Scheme 13).



Scheme 13: Different thioether configurations calculated for *ortho*-(Methylthio)tyrosine, R = CH<sub>2</sub>CH(NH<sub>2</sub>)COOH<sup>[112]</sup>

Both configurations can be transformed into each other by rotation of the –SR group. The “out-of-plane” configuration promotes the oxidation reaction by supporting the proton transfer from the substrate to the Tyr 272, while the coplanar state destabilises the phenolic OH-bond. Pedulli *et al.* even assign the 10000 times lowered catalytic efficiency of model compounds to this conformation depending proton transfer properties of the wild type enzyme and propose that the switching of the –SR bond might not be reproducible in model systems.<sup>[112]</sup>

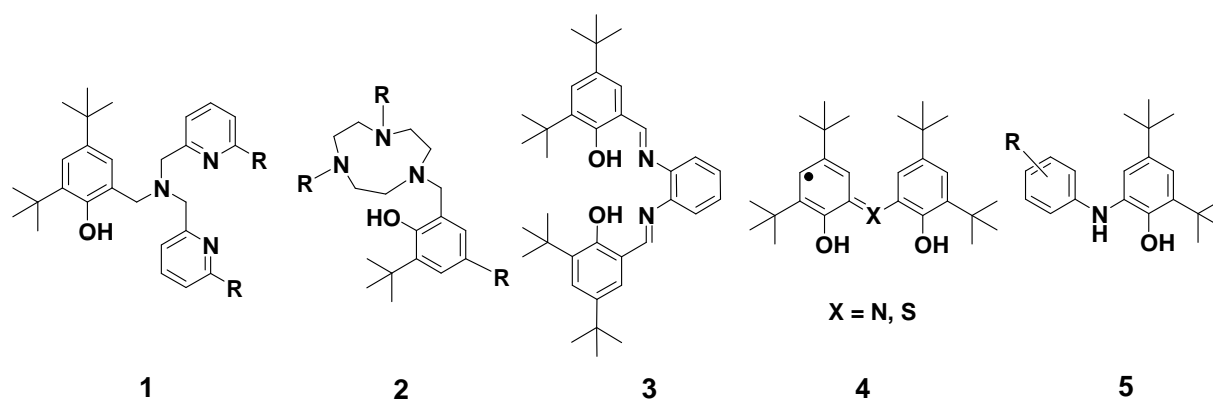
## 1.4 Model systems for Galactose Oxidase

Generally, models for metalloenzymes can be subdivided into two groups: the structural models, which shall depict the enzyme structure as exactly as possible, and the functional models, which possess the same catalytic properties as the enzyme. Since the 1990s great efforts have been made to synthesise model systems for GO. The well disclosed but extraordinary structure of GO and the urge to understand its catalytic mechanism *in vivo* has been the motivation for the synthesis and investigation of a number of structural models.<sup>[113-116]</sup> The intention to find the catalytically relevant structure elements of native GO and the motivation to improve the model compounds applicability in organic synthesis (in line with the criteria of “green chemistry“) resulted in a larger number of functional models. Functional GO models are highly interesting regarding the catalysed reaction: the selective oxidation of alcohols to aldehydes at the same time preventing the formation of carboxylic acids as side products.

In synthetic organic chemistry various strategies have been developed to achieve selective alcohol oxidation. Oxidising agents like sodium dichromate in sulphuric acid are used in stoichiometric amounts (*Jones Reaction*).<sup>[117a]</sup> But as a downside, the reactions performed in aqueous medium lead to the formation of the corresponding acids via formation of the hydrates as reaction intermediates. A variation of the *Jones Reagent* is pyridine chlorochromate (PCC, called *Corey's Reagent*)<sup>[117b]</sup> which is used in CH<sub>2</sub>Cl<sub>2</sub> solution. A different reaction strategy is to perform a *Swern Oxidation* with DMSO (S<sup>IV</sup>) and oxalylchloride<sup>[118]</sup>. Oxidising agents that can be used in substoichiometric amounts are ruthenium compounds e.g. the *Ley-Griffith Reagent* (tetrapropylammonium perruthenate (TRAP) and N-methylmorpholine N-oxide (NMO)<sup>[119]</sup>. Within this reaction the Ru<sup>IV</sup> species is oxidised to Ru<sup>VI</sup> as the active species) or the *Dess-Martin periodinane* (the active species contains I<sup>V</sup>).<sup>[120]</sup> None of these reactions can be called “green”. Green (or sustainable) chemistry means a minimal use of energy and minimal production or use of hazardous compounds, which shall be realised by achieving maximal efficiency of reactions with few or no side products.<sup>[121]</sup> A GO comparable reaction strategy is an oxidation using air oxygen and catalytic amounts of Pd(OAc)<sub>2</sub> / DMSO<sup>[122]</sup> but this is a quite expensive method. So a copper catalysed (copper enzyme mimicking) oxidation strategy using air oxygen as the oxidising agent is still sought for. Furthermore, selective alcohol oxidation is not only important to laboratory chemists, but also concerns industrial chemistry, which is proven by the high number of patents in this field.<sup>[123]</sup>



Plenty of studies on functional GO model systems including diverse ligand types are provided in literature. In the following the five main groups of ligands are described (Scheme 14) which differ essentially in number and nature of the donor atoms and the resulting coordination geometry.



Scheme 14: Ligands used for GO model systems: 1) tripodal N-donor-ligands<sup>[124–131]</sup>, 2) 1,4,7-triacetylononan (TACN) based ligands<sup>[100,132–136]</sup>, 3) salen type ligands<sup>[84,137–140]</sup> 4) thio- / iminosemiquinone ligands<sup>[141–143]</sup> 5) *o*-iminobenzosemiquinone ligands<sup>[144–149]</sup>

As expected, the use of tripodal and TACN-based ligands leads to  $\eta^5$  (distorted) square pyramidal coordination, while the salen type ligands are  $\eta^4$  coordinated and form square planar or tetrahedral copper complexes. The semiquinone ligands, which coordinate  $\eta^3$  or  $\eta^2$  respectively, are not able to predetermine the coordination polyhedra and the coordination sphere depends on the coligands.

Due to the fact that copper complexes containing hard donor sites (like oxygen atoms) are often binuclear (e.g. bridging by anionic oxido functions like deprotonated acid or alcohol groups), synthetic strategies (ligand design) have to be developed to protect the metal ions from dimerisation.<sup>[71,142,147]</sup> Ligand types like tripodal ligands or (semi)quinone-ligands are usually not as bulky as salen type ligands or TACN-based ligands, so that the former undergo dimerisation more often than the latter.<sup>[71]</sup>

Several GO model systems were successfully applied in catalytic oxidation reactions. Table 2 summarises some important catalysts and the reaction conditions.

Table 2: Different GO model systems and their efficiency in catalytic test reactions

catalyst <sup>[a]</sup>	substrate	external base	solvent/ atmosphere	T (K) / t (h)	yield / TON	Ref.
tripodal ligand (1) *	benzyl alcohol	NaOH	MeCN / O <sub>2</sub>	298 / 24	272 cycles	131b
salen type ligand <sup>[b]</sup> (3)	benzyl alcohol	-	CH <sub>2</sub> Cl <sub>2</sub> / air	293 / 1	20-75%	137
tosylamine ligand <sup>[c]</sup>	benzyl alcohol	KOH	MeCN / O <sub>2</sub>	293 / 3	14%	114
TEMPO- ligand <sup>[d]</sup>	alcohols	KO <sup>tert</sup> Bu or NaOH	2 MeCN:1 H <sub>2</sub> O / air	298 / 1-24	0-100 %	143,150,151
imino- semiquinonate * (4)	benzyl alcohol, ethanol	NEt <sub>3</sub>	THF / air	293 / 20	55 %	141
semiquinonate * (4)	alcohols	NEt <sub>3</sub>	CH <sub>2</sub> Cl <sub>2</sub> / Ar	294 / 45	> 95%	139
N <sub>2</sub> O <sub>2</sub> <sup>[152][b]</sup>	benzyl alcohol	<sup>n</sup> Bu <sub>4</sub> NOMe	CH <sub>2</sub> Cl <sub>2</sub> / air	298 / –	70%	138

[a] Catalysts can be isolated before application (\*) or can be formed *in situ*; for identifying the different ligand types (Scheme 14)

[b] The complex was previously isolated as radical species

[c] 2-(2-tosylaminoethylimino)methyl-4,6-di<sup>tert</sup>butylphenol fixed on Merrifield resin

[d] TEMPO = 2,2,6,6-tetramethylpiperidinyl-1-oxy

From these examples some general conclusions concerning the requirements of a GO model system can be drawn: the great diversity of applied ligands implicates that neither the exact coordination geometry nor the donor set is limiting the pool of catalysts. Furthermore, all catalysts need an external base for substrate deprotonation (the salen type copper complex of Stack *et al.*<sup>[137]</sup> precisely is not a catalyst, since it is applied in stoichiometric amounts), finally it can be concluded that all reported catalysts are far less effective than the natural enzyme (especially regarding lifetime and TON).

Nevertheless the catalytic systems are not equivalent: ligands which possess a N<sub>2</sub>O<sub>2</sub> donor set recently turned out to be favourable because of their superior properties for the phenoxyl radical generation. Two main strategies can be found for the radical generation. A widely used method is to start the catalytic cycle using a Cu<sup>I</sup> compound and generating the active species by exposure of the Cu<sup>I</sup> compound to O<sub>2</sub>. Another way is to take advantage of a disproportionation reaction described as a coligand effect that follows Equation 3:<sup>[130,153]</sup>

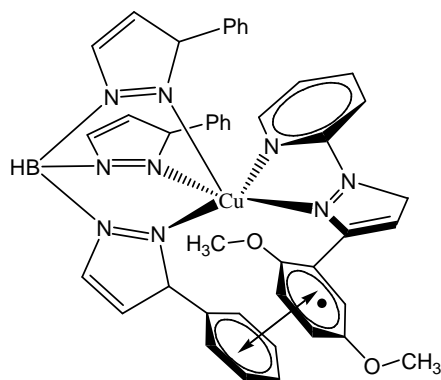


This effect was previously observed for the tripodal ligand *N*-(2-pyridylmethyl)-*N*-(2''-hydroxy-3',5'-di<sup>tert</sup>butylbenzyl)-*N*-(2''-hydroxy-3''-methylthio-5''-methylbenzyl)amine which was dissolved in MeCN and reacted with  $\text{Cu}(\text{ClO}_4)_2$ <sup>[153]</sup> or  $\text{Cu}(\text{OTf})_2$  in the presence of  $\text{NEt}_3$ <sup>[130]</sup>. In case the ligand system has a  $\text{N}_2\text{O}_2$  donor set the disproportionation reaction equilibrium was found to be on the phenoxyl radical (right). If a ligand with a  $\text{N}_3\text{O}$  donor set is used, only a very small amount of the copper phenoxyl radical species can be detected.<sup>[71,130]</sup> An explanation for this difference in phenolate ligand reactivity towards copper could not be given yet. If a radical generating disproportionation reaction is impossible (since there are no phenolate moieties) the formation of  $\text{Cu}^{\text{III}}$  complex species is observed.<sup>[154]</sup>

When the phenoxyl radical is finally generated, it needs to be stabilised by the ligand scaffold of a model complex. Since bioinorganic chemistry is highly focussed on that aspect of ligand design, the radical stabilisation will be discussed detailed in the following chapter.

## 1.5 Phenoxyl radicals and their stabilisation

Tyrosyl radicals can be found in different stable (i.e. detectable) cofactors of metalloenzymes:<sup>[67]</sup> in ribonucleotide reductase R2,<sup>[155]</sup> in photo system II,<sup>[156]</sup> in prostaglandin synthase<sup>[157]</sup> and cytochrome *c* peroxidase.<sup>[158]</sup> In other metalloenzymes the radical bearing tyrosyl residue is covalently modified as, for example, in amine oxidase<sup>[68]</sup> which includes a TOPA-quinone (TOPA = trioxyphenylalanine = 2,4,5-trihydroxyphenylalanine) involved in catalysis and finally GO (Chapter 1.3).



Scheme 15: Copper complex containing a  $\pi$ - $\pi$  stabilised phenoxyl radical<sup>[103,159,160]</sup>

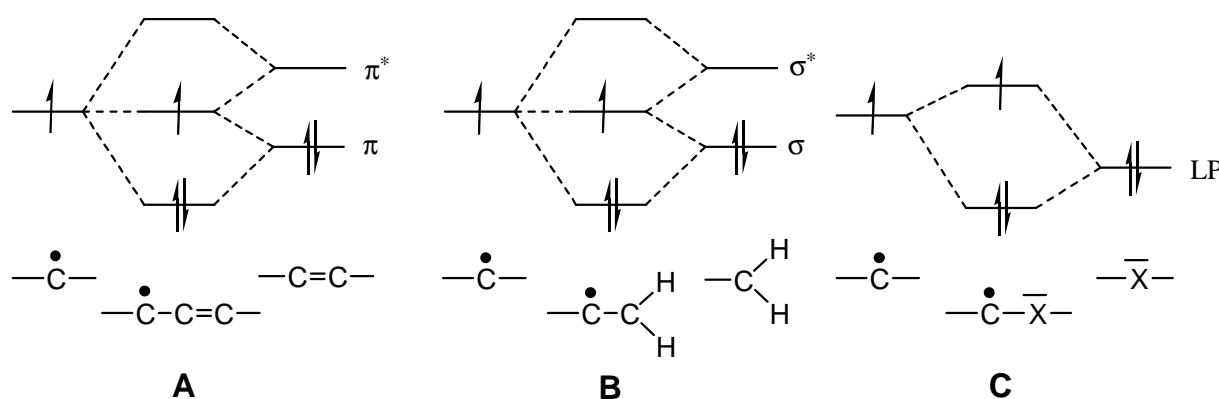
The tyrosylate/tyrosyl analogue found in nearly all GO model complexes is the phenolate/phenoxyl redox couple. The problem of stabilising the phenoxyl part of the redox couple was in the focus of a number of studies on GO modelling. Some approaches were made for mimicking the  $\pi$ - $\pi$  interactions found in GO (Scheme 15).<sup>[103–105,159,160]</sup> In this model compounds the  $\pi$ - $\pi$  interactions did not seem to influence the chemical reactivity of the phenolate / phenoxyl oxidation potential. Another approach was to mimic the covalent thioether modification:<sup>[112,161–164]</sup> While a model complex published in 1998 by Wieghardt *et al.* shows catalytic activity in oxidation catalysis<sup>[163]</sup> a detailed study on thioether derivatives of this and other established functional GO model compounds revealed no catalytic activity of the thioether complexes.<sup>[162,164]</sup>

The vast majority of functional GO model complexes possess *ortho* (C3) and *para* (C5) substituted phenoxyl moieties, in most cases *tert*butyl groups (1.4). Such (bulky) groups are known to stabilise aromatic radicals thermodynamically and kinetically.<sup>[165,166]</sup> Some less frequent alternatives for stabilising substituents are –Me, –*iso*Pr, –NO<sub>2</sub>, –OMe, –SMe, –SPh, –S*iso*Pr, and –F.<sup>[71]</sup> Nevertheless, in some studies on tripodal ligands with mixed substituents (*tert*butyl- combined with a methylthioether-group<sup>[167,168]</sup> or *tert*butyl with nitro- and methoxy-groups<sup>[169]</sup>) the compounds reveal reactivities similar to the 2,4-di-*tert*butyl-substituted derivatives.<sup>[137]</sup>

Only a few investigations have been carried out so far focussing on the influence of substituent variation: One comparative study, carried out on tripodal ligands, revealed that oxidation potentials and chemical stability of the copper phenoxyl complexes strongly correlate to the Hammett-parameter of the substituent located in *para* position to the hydroxyl function in the phenol ring (the higher the electron-donating capacity of the substituent the more stable the resulting phenoxyl radical).<sup>[115]</sup> Another important study was performed by Stack *et al.* who compared different salen type ligands bearing –SPh or –S*iso*Pr groups as well as partly unprotected (either C3 or C5 bear protons) or fully unprotected (C3 and C5 bear protons) phenolate ligands.<sup>[84]</sup> The resulting copper complexes show high phenoxyl oxidation potentials (0.8 V - 1.0 V), EPR active copper phenoxyl species and low catalytic capacity (turn over number between 0 and 9). Importantly, these findings do not imply that non-stabilised phenoxyl radicals are useless as GO mimicking oxidation catalysts. As an example, a well working non stabilised copper phenoxyl complex was presented in 2006 by McGrady *et al.*<sup>[170]</sup> These results reflect the dilemma between radical stabilisation and reactivity - a well stabilised radical contains less

energy and is therefore less reactive as a simple non-stabilised one. On the other hand a non-stabilised radical possesses a very short life time and is therefore difficult to detect. In the following some important aspects on radical stabilisation are summarised:

- The most common and most effective way is to use a  $\pi$ -system for resonance stabilisation by delocalisation of the unpaired spin (Scheme 16, **A**). The stabilisation occurs by a three centre three electron interaction, for which the allyl radical is the simplest example. Further substitution of the  $\pi$ -system by heteroatom-groups has a destabilising effect on the radical.<sup>[171]</sup>
- The radical stabilisation by alkyl substitution (Scheme 16, **B**) is based on a similar mechanism, overlapping orbitals are composed by combination of two C–H bonds. Interestingly, an increasing size of the attached alkyl group does not necessarily lead to enhanced stabilisation.<sup>[171]</sup>
- A radical stabilising effect can also be achieved by a two centre three electron interaction of a radical with an adjacent lone pair (Scheme 16, **C**). In this case the interaction becomes more effective if the lone pair orbitals are high lying.<sup>[171]</sup>



Scheme 16: Orbital interaction diagrams for the different radical stabilisation methods<sup>[171]</sup>

- Substitution in  $\beta$ -position of the radical is mainly inductive and electronegative substituents uniformly destabilise the radical.<sup>[171]</sup>
- Furthermore the stabilisation of a radical is a cumulative effect if several substituents were present, sometimes also described as a “saturation effect”,<sup>[172]</sup> which is valid for simple alkyl radicals as well as for resonance stabilised radicals.<sup>[173]</sup>

- A special case are the so called “captodative” stabilised radicals, which contain one electron donating and one electron withdrawing substituent.<sup>[172,174–177]</sup> The most prominent examples for this type of radicals are derived from amino acid and peptides such as the glycine-2-yl radical.<sup>[174,178,179]</sup>

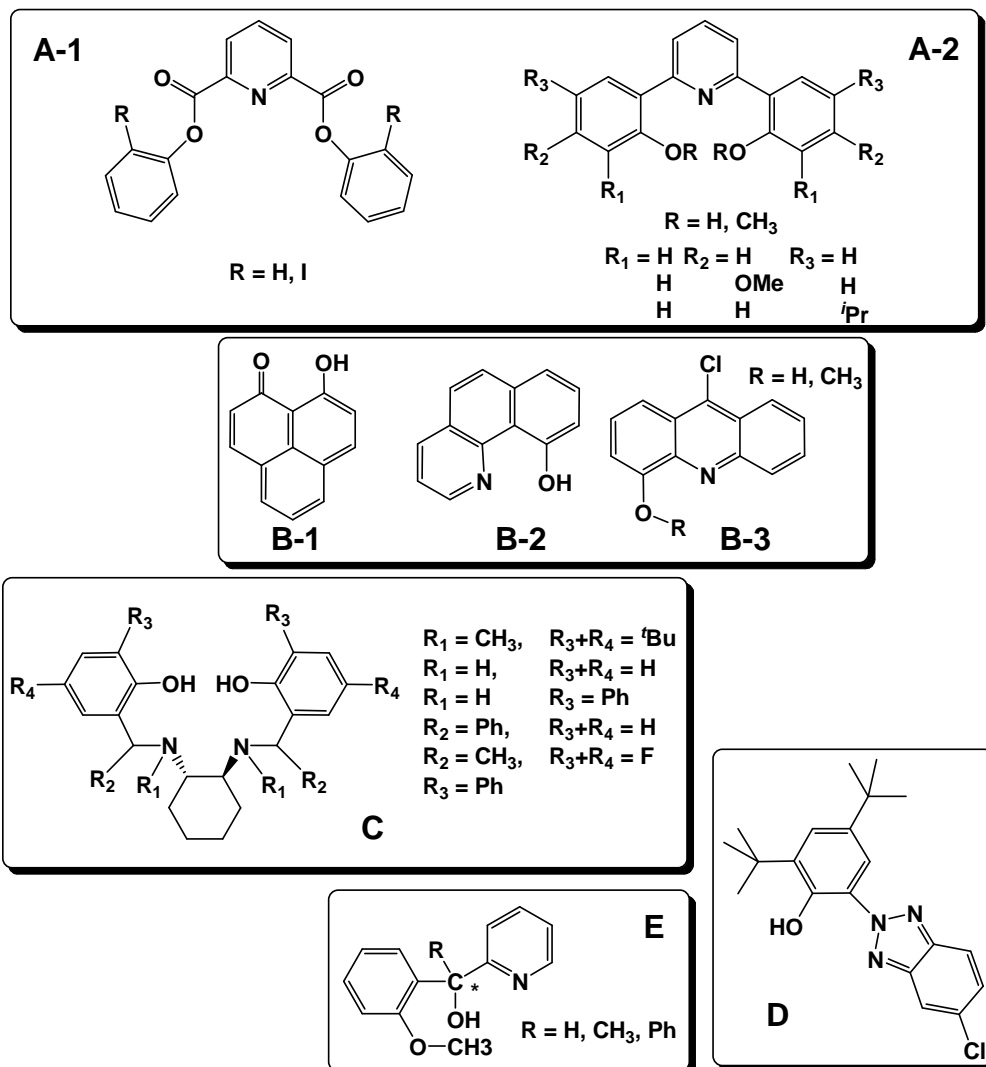
All these aspects of radical stabilisation have to be considered as requirements of a catalytic oxidation. A “dogmatic” attitude towards designed GO mimicking model systems is that the radical species need to provide the following skills: *The phenoxyl radical has to be generated from a deprotonated phenol moiety, which should contain stabilising groups in ortho and para position to the hydroxy function, most favourable are <sup>tert</sup>butyl groups. Furthermore the ligand has to contain strongly binding donor functions which stabilise the copper–ligand bond during the reaction and provide a distorted coordination geometry around the copper ion to destabilise the Cu<sup>II</sup> state. At last the phenolate / phenoxyl part of the ligand has to be positioned within a Cu–O–C bond angle of about 130° and a dihedral angle of about 90° to guarantee the coupling of the unpaired copper centred electron with the single electron from the phenoxyl part.*

## 1.6 Motivation of this thesis

The general aim of this thesis is the fundamental investigation of the structural requirements enabling phenoxyl copper complexes to perform a GO type of electrochemistry and thus catalysis. The challenge is rather to understand the origin of oxidative properties than to synthesise new “second generation” catalysts by optimisation of known copper complex systems. To this end copper complexes of various phenoxy ligands have been synthesised, analysed and thoroughly characterised, focussing on the complex structures, their electrochemical properties and their catalytic behaviour in alcohol oxidation reactions. Since the crucial species in the assumed catalytic oxidation reactions are phenoxyl radicals, special emphasis was put on the detection of such radicals and to analyse the impact of structural motives (variation of the phenoxyl ligands and the coligands) on their stability. Spectroelectrochemistry (thin-layer electrolysis coupled to detection of spectroscopic changes<sup>[180]</sup>), which allows to generate and study copper phenoxyl species *in situ*, is extremely well suited for this purpose. From the various spectroscopic methods which can be used for spectroelectrochemistry UV/vis/NIR absorption

spectroscopy is ideal to analyse phenoxyl radicals.

Concerning the design of the (new) ligands we have been presuming the following lines:

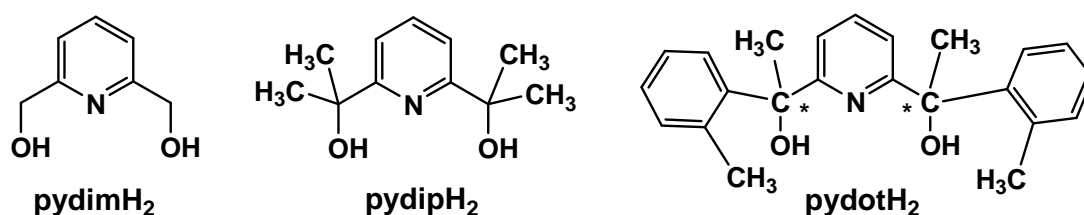


Scheme 17: Overview over the ligands designed for copper phenoxyl complexes; ligands **A** cf. Chapter 2; **B** cf. Chapter 3; **C** cf. Chapter 4; **D** cf. Chapter 5 and **E** cf. Chapter 6.

- Variation of the donor set from two (N,O and O,O; **B-1, B-2, B-3, D**) to three (O,N,O and O,O',N; **A-1, A-2, E**) and four (N<sub>2</sub>O<sub>2</sub>; **C**) donor atoms
- Varying stabilisation of the phenoxyl units: assorted from non-stabilised phenols (all H atoms; **A-1, A-2, C, E**) to partly stabilised phenols (*ortho*-I; *meta*-OMe; *para*-*iso*Pr; **A-1, A-2, ortho**-Ph **C**) and fully stabilised phenols (substituents *ortho* and *para*: F, Ph; *tert*Bu; **C, D**) and aromatically stabilised (phenol: **C, A-1, A-2**; phenalene: **B-1**; benzo-quinoline: **B-2** acridine: **B-3**)

- Contribution of the N-donor to the redox chemistry using aromatic (e.g. pyridine, acridine; **A-1**, **A-2**, **B-2**, **B-3**, **E**), heterocyclic (e.g. triazol; **D**), imine (**C**), *tert*-amine(**C**), *sec*-amine(**C**) functions
- Influence of (de)protonation abilities of the ligands: possessing proton transfer skills (phenol-ligands; **A-2**, **B-1**, **B-2**, **B-3**, **C**, **D**, **E**) and lacking proton transfer skills (phenol-esters (**A-1**) or phenol-ethers (**A-2**, **B-3**, **C**))

The starting point of the investigation is the class of tridentate ligands of the so called pincer type (**A**). Following the more general definition, pincer ligands possess a central (heterocyclic) arene system and additional donor groups in *ortho* position providing a tridentate and “pincer” like coordination.<sup>[181]</sup> Copper complexes of pincer type ligands (Scheme 18) have been synthesised recently and showed effective binding of copper to the central pyridine N atom and variable structural motives including square pyramidal and octahedral distorted coordination geometries.<sup>[182-184]</sup> Related oxido-pincer complexes of early transition metals have been used in oxygenation catalysis.<sup>[180,185]</sup>



Scheme 18: Overview on the developed and analysed oxido-pincer ligands<sup>[182-184]</sup>

Transformation of the donor set, such as rearrangement (O,O',N; **E** instead of O,N,O; **A**), addition of a fourth donor function (N<sub>2</sub>O<sub>2</sub> ligands; **C**) or diminishing the number of donor atoms in combination with altering the arene type (O,N-triazole; **D**) is the motivation for most of the new ligands. Furthermore, ligands with extended aromatic scaffolds (phenalene **B-1**, phenanthren **B-2** and anthracen **B-3**) will be used. They have been chosen with regard to their different anellation state.

From all ligands homo- and heteroleptic copper complexes were prepared and characterised. Selected ligands were further coordinated to other 3d transition metal ions such as Fe<sup>2+</sup>, Fe<sup>3+</sup>, Co<sup>2+</sup>, Ni<sup>2+</sup> and Zn<sup>2+</sup>. These complexes were synthesised and analysed with the objective of a better understanding of the copper analogues.

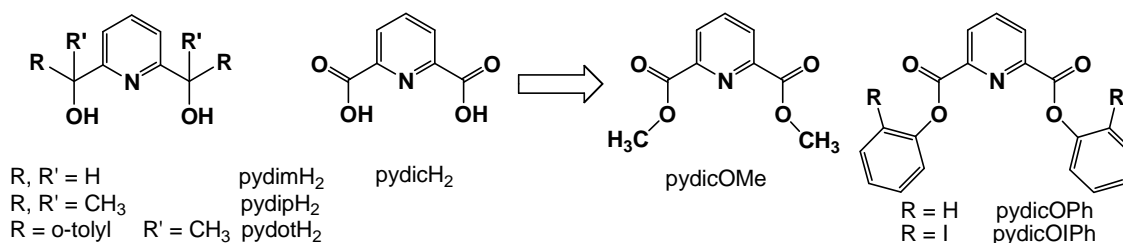


## 2.0 O,N,O-pincer complexes

### 2.1 Derivatives of Pyridine-2,6-dicarboxylic acid (pydicH<sub>2</sub>) as O,N,O-pincer ligands and their Cu<sup>II</sup> complexes

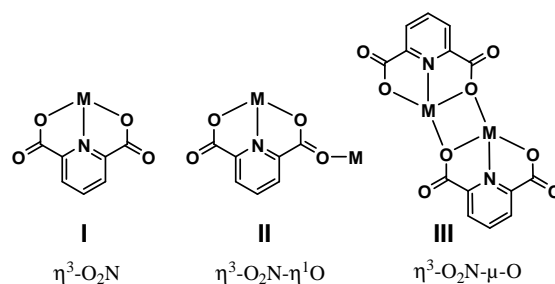
#### 2.1.1 Introduction

Pyridine-2,6-dicarboxylic esters are interesting oxido pincer ligands with an O,N,O donor set. They are structurally related to the O,N,O pincer ligands based on pyridine-2,6-dimethanol as well as to 2,6-dicarboxylic acid (pydicH<sub>2</sub>) as shown in Scheme 19.<sup>[183,184]</sup>



Scheme 19: General structure of the pyridine-2,6-dicarboxylic ester ligands used in this study

Deprotonated pydic<sup>2-</sup> normally coordinates in a tridentate mode, using the N donor atom and the two O<sup>-</sup> donor functions (Scheme 20, I). Complexes are known for hard metal ions like lanthanides<sup>[186-189]</sup>, early transition metals such as V<sup>3+</sup><sup>[190]</sup> and V<sup>5+</sup><sup>[191,192]</sup> but also for (medium) soft metal ions such as Fe<sup>2+</sup><sup>[193]</sup>, Fe<sup>3+</sup><sup>[194]</sup>, Ru<sup>2+</sup><sup>[195-197]</sup>, Co<sup>2+</sup><sup>[198]</sup>, Ni<sup>2+</sup><sup>[198,199]</sup>, Cu<sup>2+</sup><sup>[198,200]</sup>, Zn<sup>2+</sup><sup>[198]</sup>, Pd<sup>2+</sup><sup>[201]</sup> and Pt<sup>2+</sup><sup>[201-203]</sup>. In Mn<sup>2+</sup> containing polymeric networks a tetradentate coordination with one bridging carboxylate function (Scheme 20, II) has been observed,<sup>[204]</sup> a similar structure motive has been found for Ce<sup>4+</sup>.<sup>[198]</sup> Structures with a  $\mu$ -oxido bridge between two metal centres (Scheme 20, III) are known as well.<sup>[205]</sup>



Scheme 20: Binding modes of pydic<sup>2-</sup>

Various pydic complexes have been utilised in catalysis. Especially ruthenium complexes, bearing terpyridine coligands are used in catalytic oxidation processes such as alkene epoxidation,<sup>[206-211]</sup> or selective alcohol oxidation<sup>[212,213]</sup> (the latter performed with benzyl alcohol). In contrast to Galactose Oxidase (GO), which performs alcohol oxidation via a phenoxyl radical species (Chapter 1), the ruthenium pydic catalysts are used in combination with H<sub>2</sub>O<sub>2</sub> as external oxidising agent, applied in stoichiometric amounts or excess. Thus, this catalyst just mediates the H<sub>2</sub>O<sub>2</sub> depending alcohol oxidation and the reaction is clearly GO unlike.

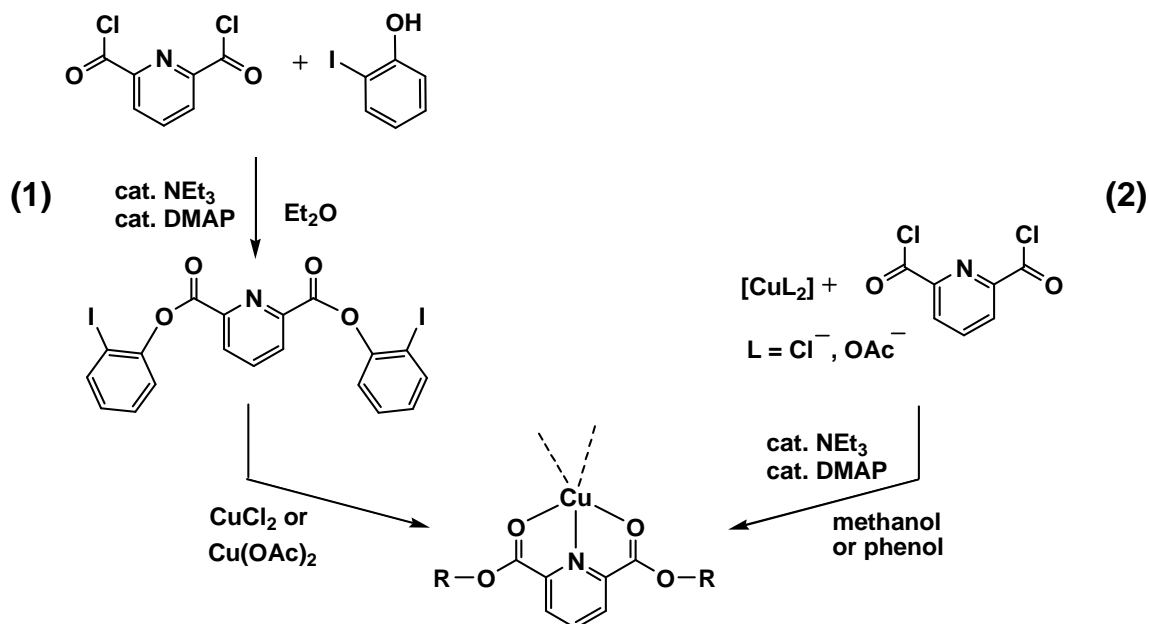
Alkyl- or arylester derivatives of pydicH<sub>2</sub> have been used as ligands as well (Scheme 19) e.g. dimethyl ester (pydicOMe)<sup>[214]</sup>, diethyl ester (pydicOEt)<sup>[215,216-218]</sup>, the di<sup>iso</sup>propyl ester (pydicO<sup>i</sup>Pr)<sup>[215]</sup>, the di<sup>n</sup>butyl ester (pydicO<sup>n</sup>Bu)<sup>[218]</sup> and the diphenyl ester (pydicOPh)<sup>[219]</sup> and several asymmetric esters<sup>[216,217,220,221]</sup>. In contrast to the pydic<sup>2-</sup> ligand which contains four equivalent, negatively charged oxygen atoms for coordination, the pydic carboxylic esters provide two sets of different oxygen atoms. They allow the formation of three different isomers O<sub>carbonyl</sub>-M-O<sub>carbonyl</sub> (**CC** isomer), O<sub>carbonyl</sub>-M-O<sub>alkoxy</sub> (**CA** isomer) and O<sub>alkoxy</sub>-M-O<sub>alkoxy</sub> (**AA** isomer). The three isomers have already been observed in metal complexes.<sup>[CC: 215, CA: 215, AA: 222,223]</sup> The **AA** isomers are strongly disfavoured, due to steric and electronic effects. The carbonyl oxygen donor offers  $\pi$  orbitals for metal ion coordination and forms stronger bonds than the alkoxy or aryloxy oxygen donor. The two known **AA** isomeric complexes are organometallic species, a Rh<sup>1+</sup> complex and a Fe<sup>2+</sup> complex.<sup>[222,223]</sup> With regard to copper, there are only a few examples for the formation of **CA** isomers<sup>[215,224]</sup> beside the normally formed **CC** isomers.

In this thesis some copper complexes containing the pydic carboxylic ester ligands pydicOMe, pydicOPh and pydicOIPh should be synthesised. These complexes are expected to exist in the **CC** isomeric forms, hence generation of phenoxyl radicals in the ligand should not lead to spin coupling between radical site and copper ion. Thus pydic aryloxyester complexes are suitable to investigate physical and catalytic properties of systems containing two independent redox centres.

### 2.1.2 Synthesis of pydicH<sub>2</sub> ester ligands and their copper complexes

Two different reaction strategies were used to synthesise copper complexes (Scheme 21). The first route is known in the literature<sup>[215]</sup> and consists of two subsequent steps, a ligand

synthesis and isolation followed by a complex formation reaction (1). The second route is a one-pot synthesis using pyridine-2,6-dicarboxylic acid dichloride (pydicCl<sub>2</sub>) a copper source and the corresponding alcohol (methanol or phenol) to form the ligand in the presence of the coordinating metal ion (2). This route has been worked out in the frame of this thesis.



Scheme 21: Two reaction strategies to synthesise copper complexes of pydic ester ligands

The ligand synthesis (1) was performed using *ortho*-iodo phenol and pydicCl<sub>2</sub> in a DMAP (dimethyl 4-aminopyridine) catalysed ester condensation using catalytic amounts of NEt<sub>3</sub>.

The resulting pydicOIPh ligand (obtained in 82% yield and characterised by <sup>13</sup>C and <sup>1</sup>H NMR and elemental analysis) was crystallised from acetone by slow evaporation to give single crystals suitable for XRD. The structure was resolved in the orthorhombic space group *Pbca*. The molecular structure depicted in Figure 2 shows the ligand providing a binding pocket for the formation of CC isomeric complexes. The planes of both phenol rings are tilted away from the pyridine ring (61° and 64°) one iodo substituent is located above the pyridine ring plane, while the other resides beneath this plane. The two carbonyl functions are slightly tilted from the pyridine plane, each pointing in the same direction as the iodo substituent of the corresponding phenol ring. The ligand's conformation might result from packing effects in the crystal leading to the formation of  $\pi$ - $\pi^*$  stacked dimers (Figure 2). Additionally, the iodo substituents of the molecules forming a dimer are pointing towards each other with an I...I distance of 4.350(1) Å, while relevant H bridges are missing in the crystal structure.

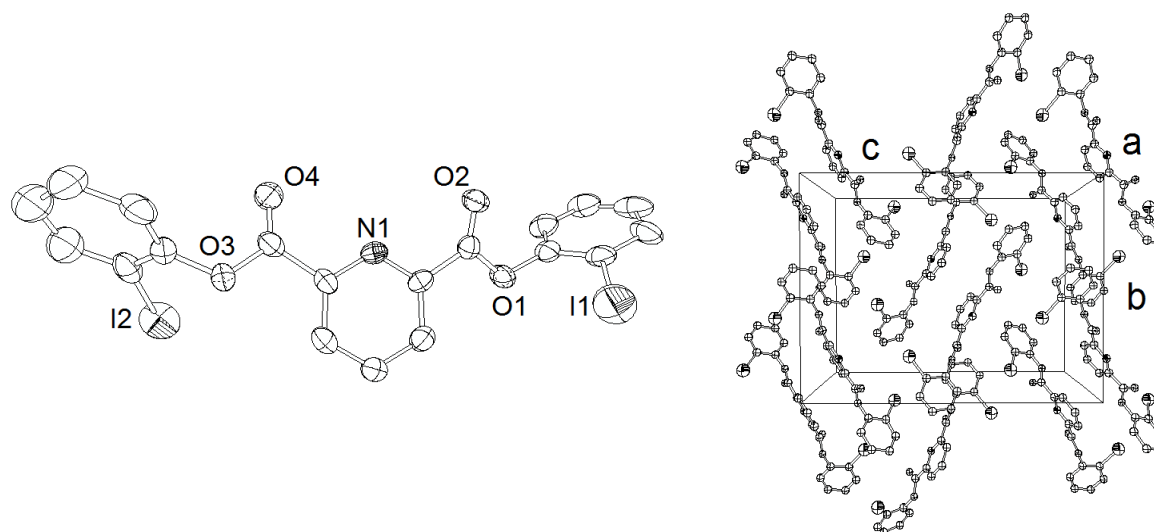


Figure 2: ORTEP representation (50% probability level) of the molecular structure of pydicOIPh (bis(2-iodophenyl) pyridine-2,6-dicarboxylate) (left); packing along the *a* axis of pydicOIPh in the crystal (right); H atoms were omitted for clarity

Complex formation using pydicOIPh was performed in methanol at 298 K using anhydrous  $\text{CuCl}_2$ . The obtained product was a brown powder (67% yield), which was analysed to be  $[(\text{pydicOIPh})\text{CuCl}_2]$ . The complex was characterised by elemental analysis, EPR spectroscopy, absorption spectroscopy, electrochemical and spectroelectrochemical measurements.

The alternative reaction strategy is a concerted *in situ* formation of ligand and complex (Scheme 21, synthesis **2**). Starting materials of the ligand (DMAP,  $\text{NEt}_3$ ,  $\text{pydicCl}_2$  and the corresponding alcohol) were mixed with  $\text{Cu}(\text{OAc})_2$  or  $\text{CuCl}_2$  respectively and reacted for 16 h at 298 K. First experiments were performed using all starting materials as purchased (and therefore containing small amounts of water). Both reactions, starting from  $\text{Cu}(\text{OAc})_2$  and from  $\text{CuCl}_2$ , lead to the formation of blue-green crystals, hence both compounds were clearly analysed by XRD as well as by elemental analysis. The product of the reaction using  $\text{Cu}(\text{OAc})_2$  was found to be  $[(\text{pydic})\text{Cu}(\text{OH}_2)_2]_n$ , while the reaction using  $\text{CuCl}_2$  yielded  $[\text{Cu}(\text{OH}_2)_6][(\text{Cu}(\text{pydic})\mu\text{-Cl})_2]$ . Both compounds result from the hydrolysis of  $\text{pydicCl}_2$  to  $\text{pydic}^{2-}$  in the presence of water while no ester was formed. The reaction yields were rather low (12 and 24%).

Figure 3 shows the polymeric chain and the mononuclear unit of the complex  $[(\text{pydic})\text{Cu}(\text{OH}_2)_2]_n$ ; the crystal structure (monoclinic  $P2_1/c$ ) has been reported before<sup>[225]</sup> thus will not be described here.

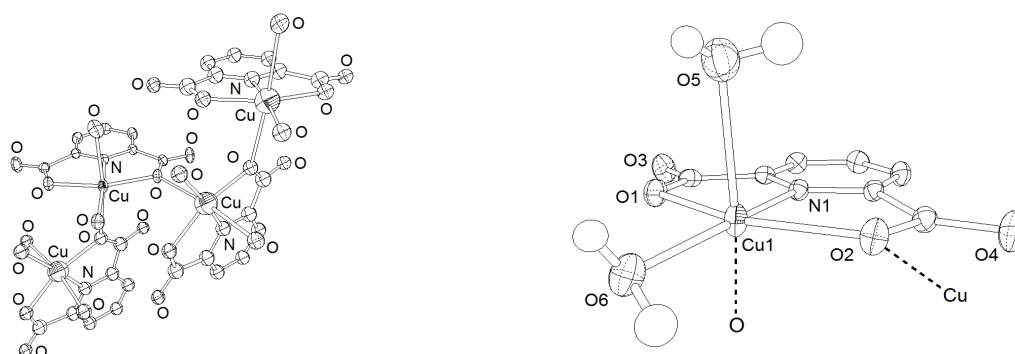


Figure 3: ORTEP-representation (50% probability level) of the crystal structure of  $[(\text{pydic})\text{Cu}(\text{OH}_2)_2]_n$  (left) and representation of a monomeric unit inside the polymeric chain (right), H atoms are omitted for clarity<sup>[225]</sup>

When using  $\text{CuCl}_2$  and  $\text{pydicCl}_2$  in a 1:1 stoichiometry, a complex salt of the general formula  $[\text{Cu}(\text{OH}_2)_6][(\text{Cu}(\text{pydic})\mu\text{-Cl})_2]$  was formed and crystallised from methanol solution. XRD revealed a crystal structure, which was solved and refined in the triclinic space group  $P\bar{1}$ . The structure as shown in Figure 4 (data in Table 3) will be briefly discussed. The complex cation  $[\text{Cu}(\text{OH}_2)_6]^{2+}$  is a Jahn-Teller elongated octahedron ( $\text{Cu2-O5} = 1.986(1) \text{ \AA}$ ;  $\text{Cu2-O6} = 1.964(1) \text{ \AA}$  and  $\text{Cu2-O11} = 2.561(1) \text{ \AA}$ ), in line with previous reports on related compounds.<sup>[226]</sup> The H atoms of  $[\text{Cu}(\text{OH}_2)_6]^{2+}$  were not found during the crystal structure refinement. Nevertheless, due to the observed counter ion  $[\text{Cu}(\text{OH}_2)_6]^{2+}$ , the deprotonation of  $\text{pydicH}_2$  in the complex is obvious.

The complex anion, a binuclear  $\mu$ -chlorido bridged complex, shows a distorted square pyramidal geometry around each copper atom. With a short equatorial bond  $\text{Cu-Cl}_{\text{eq}} = 2.212(1) \text{ \AA}$  and a long axial bond  $\text{Cu-Cl}_{\text{ax}} = 2.695(1) \text{ \AA}$ , while the  $\text{Cu-N}$  bond is rather short ( $1.927(4) \text{ \AA}$ ). Both  $\text{pydic}^{2-}$  ligands are completely coplanar which is obvious from the symmetry in the binuclear complex cation. (For further angles and distances see Appendix.)

The formation of the compound  $[\text{Cu}(\text{OH}_2)_6][(\text{Cu}(\text{pydic})\mu\text{-Cl})_2]$  was unexpected, due to the different stoichiometries of starting materials (ligand to copper ratio 1:1 and copper to chloride ratio 1:2) and product (ligand to copper ratio 2:3 and copper to chloride ratio 3:2). The formation of the  $\mu\text{-Cl}$ -bridged dimer might be due to the chosen reaction conditions (polar, aqueous methanol solution) favouring the formation of the  $[\text{Cu}(\text{OH}_2)_6]^{2+}$  counter ion, or charged species in general, while the chloride ligands might be released as  $\text{HCl}$ , which is removed from the reaction mixture either by acid base chemistry (reaction medium was basic) or by evaporation of gaseous  $\text{HCl}$ .

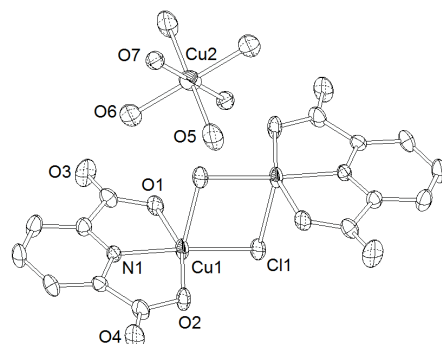


Figure 4: ORTEP representation (50% probability level) of molecular structure of  $[\text{Cu}(\text{OH}_2)_6][(\text{Cu}(\text{pydic})\mu\text{-Cl})_2]$ , H atoms were omitted for clarity

In a second attempt, the one-pot synthesis was performed using freshly distilled starting materials and anhydrous  $\text{CuCl}_2$ . The reaction using methanol as solvent was performed at 298 K and yielded a green-yellow crystalline powder after 16 h reaction time, which was isolated by evaporation of the solvent. The reaction using phenol as solvent had to be performed at 339 K to melt the phenol. The excess phenol was removed from the reaction mixture by stirring at 358 K for 96 h. During this time the phenol solidified in the upper part of the round bottom flask and left behind a brownish oil. The oil was transferred to another flask and cooled to room temperature on which it solidified as microcrystalline green-brown powder.

The compound obtained from the reaction with methanol was analysed by elemental analysis, recrystallised from methanol yielding single crystals suitable for XRD and showed to be  $(\text{HNEt}_3)[(\text{pydicOMe})\text{CuCl}_3]$ . The compound isolated from the reaction with phenol revealed  $(\text{HNEt}_3)[(\text{pydicOPh})\text{CuCl}_3]$ . This proves that under water free conditions *in situ* formation of a pydic alkyloxy or aryloxy ligand and coordination to a copper ion (one-pot) is possible. Yields of both reactions are moderate (32% and 54%) and similar to the overall yield of reaction strategy 1 (Scheme 21) which was 55% for  $[(\text{pydicOIPh})\text{CuCl}_2]$ .

Crystal structure solution and refinement of  $(\text{HNEt}_3)[(\text{pydicOMe})\text{CuCl}_3]$  were carried out in the triclinic space group  $P\bar{1}$ , the molecular structure is depicted in Figure 5, Table 3 summarises the refinement parameters. In the crystal structure of  $(\text{HNEt}_3)[(\text{pydicOMe})\text{CuCl}_3]$  the copper ion is coordinated in distorted octahedral shape, exclusively carbonyl oxygen atoms of the O,N,O-ester ligand bind to the copper ion (CC isomer). The axial Cu–Cl bonds are 2.305(1) Å and 2.306(1) Å long (with  $\text{Cl1-Cu-Cl3} = 172.87(2)^\circ$ ), while the equatorial Cu–Cl2 bond is shorter (2.255(1) Å). The two Cu–O bonds  $\text{Cu-O2} = 2.552(1)$  Å and  $\text{Cu-O4} = 2.504(1)$  Å are non-equivalent and rather long, the Cu–N bond lies within the typical range (2.065(1) Å).<sup>[183]</sup> Two

hydrogen bridges are formed between the triethyl ammonium ion and two chlorido ligands of the complex anion ( $H22 \cdots Cl1 = 2.702(1) \text{ \AA}$  and  $H22 \cdots Cl2 = 2.474(1) \text{ \AA}$   $Cl1 \cdots H22 \cdots Cl2 = 78.64(1)^\circ$ ).

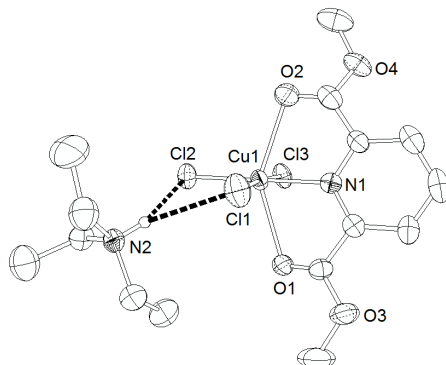


Figure 5: ORTEP representation (50% probability level) of the molecular structure of  $(HNEt_3)[(pydicOMe)CuCl_3]$ , H atoms are omitted for clarity.

Table 3. Crystal structure and refinement data of copper complexes and the ligand pydicOIPh

	$[Cu(OH_2)_6][Cu(pydic)\mu-Cl)_2]$	$(HNEt_3)[(pydicOMe)_2CuCl_3]$	pydicOIPh
formula	$C_{14}H_{18}Cl_2Cu_3N_2O_{14}$	$C_{15}H_{25}N_2O_4Cl_3Cu$	$C_{19}H_{11}I_2NO_4$
f. w. /g mol <sup>-1</sup>	671.73	467.26	571.09
crystale shape	needle	plate	block
colour	turquoise	green-brown	colourless
crystal system	triclinic	triclinic	orthorhombic
space group	$P\bar{1}$ (No. 2)	$P\bar{1}$ (No. 2)	$Pbca$ (No. 61)
a / $\text{\AA}$	8.185(3)	7.706(5)	13.520(5)
b / $\text{\AA}$	9.500(3)	10.274(5)	14.455(5)
c / $\text{\AA}$	9.682(2)	13.666(5)	19.496(5)
$\alpha$ / $^\circ$	69.01(3)	93.846(5)	90
$\beta$ / $^\circ$	66.97(3)	92.271(5)	90
$\gamma$ / $^\circ$	89.04(4)	107.216(5)	90
volume / $\text{\AA}^3$ , Z	640.2(3), 1	1029(9), 2	3810(2), 8
F(000)	329	482	2160
density / g cm <sup>-3</sup>	1.742	1.508	1.991
abs. coeff / mm <sup>-1</sup>	2.737	1.471	3.325
refl. coll.	7673	12430	34795
data / restr. / param.	2846 / 0 / 160	4602 / 0 / 235	4654 / 0 / 235
h, k, l,	-10 < h < 10 -12 < k < 12 -12 < l < 12	-9 < h < 10 -13 < k < 13 -18 < l < 18	-17 < h < 17 -19 < k < 19 -25 < l < 25
goof on F <sup>2</sup>	0.902	0.675	0.856
R <sub>int</sub>	0.0594	0.1262	0.0939
final R indices	R1 = 0.0533	R1 = 0.0397	R1 = 0.0338
[I > 2 $\sigma$ (I)]	wR2 = 0.1322	wR2 = 0.0544	wR2 = 0.0431
R indices (all data)	R1 = 0.0937 wR2 = 0.1499	R1 = 0.1468 wR2 = 0.0720	R1 = 0.1284 wR2 = 0.0514
largest diff.	1.710 and -1.147	0.361 and -0.313	0.577 and -0.568
p. a. h. /e $\text{\AA}^{-3}$			

All copper complexes were further characterised by EPR spectroscopy, cyclic voltammetry, absorption spectroscopy and with spectroelectrochemical methods.

### 2.1.3 EPR spectroscopy

EPR spectroscopy is a very specific and perfectly suited method to investigate Cu<sup>II</sup> complexes in the solid state and in solution. This is due to the high abundance of the two copper nuclei <sup>63</sup>Cu (69.17%) and <sup>65</sup>Cu (30.83%), both having a nuclear spin of  $I = 3/2$ .<sup>[227]</sup> The coupling of the spin of the unpaired electron in the Cu<sup>II</sup> d<sup>9</sup> system to the nuclear spin of Cu<sup>II</sup> and other atoms is an excellent measure for the electron density distribution between the metal and the ligand(s).<sup>[227,228]</sup> The shape (symmetry) of the anisotropic spectra (crystalline, amorphous, glassy frozen solution, protein samples) gives additional information on the local geometry around the copper ion (coordination polyhedron). Therefore the complexes [(pydic)Cu(OH<sub>2</sub>)<sub>2</sub>]<sub>n</sub>, [Cu(OH<sub>2</sub>)<sub>6</sub>][(Cu(pydic)μ-Cl)<sub>2</sub>], [(pydicOIPh)CuCl<sub>2</sub>], (HNEt<sub>3</sub>)[(pydicOMe)CuCl<sub>3</sub>] and (HNEt<sub>3</sub>)[(pydicOPh)CuCl<sub>3</sub>] were analysed by EPR spectroscopy in the solid state (HNEt<sub>3</sub>)[(pydicOMe)CuCl<sub>3</sub>] and (HNEt<sub>3</sub>)[(pydicOPh)CuCl<sub>3</sub>] were additionally measured in acetone solution. Table 4 summarises the EPR data and selected spectra are shown in Figure 6.

Table 4: X-band EPR data of the phenoxido-pincer copper complexes<sup>[a]</sup>

compound	$g_{av}$	$g_{//}$	$g_{\perp}$	$\Delta g$	state
[(pydic)Cu(OH <sub>2</sub> ) <sub>2</sub> ] <sub>n</sub>	2.151	2.217	2.118	0.099	solid
[Cu(OH <sub>2</sub> ) <sub>6</sub> ][(Cu(pydic)μ-Cl) <sub>2</sub> ]	2.150	2.291	2.080	0.211	solid
[(pydicOIPh)CuCl <sub>2</sub> ]	2.150	2.260	2.095	0.165	solid
[(pydicOIPh)CuCl <sub>2</sub> ]	2.114	2.177	2.082	0.095	acetone
(HNEt <sub>3</sub> )[(pydicOMe)CuCl <sub>3</sub> ]	2.102	2.189	2.059	0.130	solid
(HNEt <sub>3</sub> )[(pydicOMe)CuCl <sub>3</sub> ]	2.124	2.188	2.092	0.096	acetone
(HNEt <sub>3</sub> )[(pydicOPh)CuCl <sub>3</sub> ]	2.159	2.260	2.109	0.151	solid
(HNEt <sub>3</sub> )[(pydicOPh)CuCl <sub>3</sub> ]	2.150	2.229	2.111	0.118	acetone

[a] Samples measured at 298 K;  $g_{av}$  = averaged  $g$  value =  $(g_{//} + 2 g_{\perp})/3$ ;  $\Delta g = g_{//} - g_{\perp}$

All spectra recorded from solid and dissolved samples exhibit axial symmetry with  $g_{//} > g_{\perp}$  which is typical for octahedral elongated or square pyramidal Cu<sup>II</sup> complexes.<sup>[215,228-231]</sup> Although the  $g$  anisotropy ( $\Delta g$ ) varies strongly (from 0.096 to 0.211) the averaged  $g$  values are quite similar.



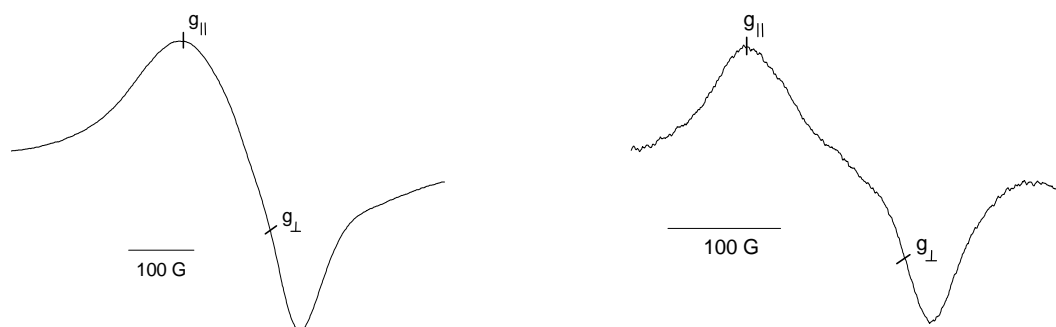


Figure 6: X-band EPR spectra of  $(\text{HNEt}_3)[(\text{pydicOPh})\text{CuCl}_3]$  (left) and  $(\text{HNEt}_3)[(\text{pydicOMe})\text{CuCl}_3]$  (right) measured at 298 K in acetone solution

From XRD the geometries of the complexes  $(\text{HNEt}_3)[(\text{pydicOMe})\text{CuCl}_3]$  and  $[(\text{pydic})\text{Cu}(\text{OH}_2)_2]_n$  are known to be distorted octahedral or square pyramidal, while  $[\text{Cu}(\text{OH}_2)_6][(\text{Cu}(\text{pydic})\mu\text{-Cl})_2]$  contains two different copper ions, one with octahedral elongated surrounding and two ions with square pyramidal geometry. The EPR spectra of the two copper species containing compound cannot be resolved. For  $[\text{Cu}(\text{OH}_2)_6]^{2+}$  the EPR parameters have been reported to  $g_{||} = 2.309$  and  $g_{\perp} = 2.065$ .<sup>[226]</sup> Since the EPR data of all complexes are quite similar, it is verified that the geometries of  $(\text{HNEt}_3)[(\text{pydicOPh})\text{CuCl}_3]$  and  $[(\text{pydicOIPh})\text{CuCl}_2]$ , which have not been crystallised so far, are also distorted octahedral or square pyramidal. Furthermore, the spectra recorded on dissolved samples are also quite similar to those of solid samples. Therefore the geometry of the complexes seems to be conserved upon dissolving in acetone.

### 2.1.4 Electrochemical measurements

The electrochemical properties of the new complexes were studied by cyclic voltammetry. Measurements were carried out at room temperature in  $\text{MeCN}/^n\text{Bu}_4\text{NPF}_6$  solution. A representative plot is shown in Figure 7, Table 5 summarises the observed potentials.

The redox properties of the isolated ligand pydicOIPh were analysed and compared to the corresponding copper complex to distinguish between ligand centred and copper centred reduction.  $[(\text{pydicOIPh})\text{CuCl}_2]$  shows one reversible, metal centred reduction at 0.11 V ( $\text{Cu}^{\text{II}}/\text{Cu}^{\text{I}}$ ) and two irreversible processes, a ligand centred reduction and a ligand centred oxidation. The ligand centred processes of free and coordinated ligand occur at almost the same potentials

supporting the assignment of [(pydicOIPh)CuCl<sub>2</sub>] to be a **CC** isomer. In a **CC** isomer both phenol moieties are not affected by the copper coordination, while in **AC** or **AA** isomers the bond between the copper ion and the phenol oxygen atom should influence the phenoxy oxidation potential.

Table 5: Electrochemical data of pydicOIPh and the oxido-pincer Cu<sup>II</sup> complexes<sup>[a]</sup>

compounds	$E_{pa}$ ox/ligand	$E_{1/2}$ Cu <sup>I</sup> /Cu <sup>II</sup>	$E_{pc}$ red/ligand
pydicOIPh	0.72	-	-1.42
[(pydicOIPh)CuCl <sub>2</sub> ]	0.72	0.11	-1.33
(HNEt <sub>3</sub> )[(pydicOMe)CuCl <sub>3</sub> ]	0.84	0.14	-1.33
(HNEt <sub>3</sub> )[(pydicOPh)CuCl <sub>3</sub> ]	1.13	0.10	-1.45
K <sub>2</sub> [CuCl <sub>4</sub> ]	1.12	0.08	-1.07, -1.48

[a] From cyclic voltammetry in MeCN/<sup>n</sup>Bu<sub>4</sub>NPF<sub>6</sub> solutions; potentials in V vs. FeCp<sub>2</sub>/FeCp<sub>2</sub><sup>+</sup>

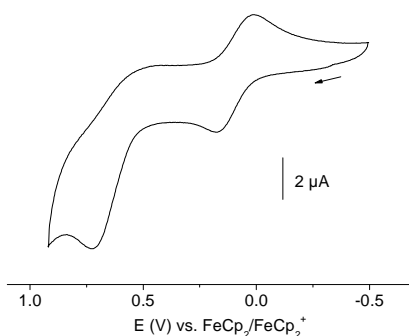
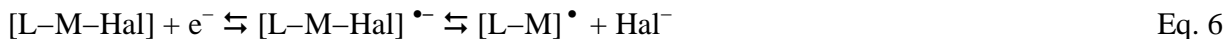


Figure 7: Cyclic voltammogramm of [(pydicOIPh)CuCl<sub>2</sub>] measured in MeCN/<sup>n</sup>Bu<sub>4</sub>NPF<sub>6</sub> at 298 K with 100 mV/s scan rate

The complexes (HNEt<sub>3</sub>)[(pydicOMe)CuCl<sub>3</sub>] and (HNEt<sub>3</sub>)[(pydicOPh)CuCl<sub>3</sub>] are investigated in comparison to the dissolved K<sub>2</sub>[CuCl<sub>4</sub>]. The complexes show similar redox properties, with a copper centred reversible reduction process occurring at about 0.1 V. Further reduction occurs irreversibly and might be associated to a Cl<sup>-</sup> cleavage, since very similar behaviour is found for [CuCl<sub>4</sub>]<sup>2-</sup> (Eq. 6).



Irreversible oxidations were observed for (HNEt<sub>3</sub>)[(pydicOMe)CuCl<sub>3</sub>], (HNEt<sub>3</sub>)[(pydicOPh)CuCl<sub>3</sub>] and K<sub>2</sub>[CuCl<sub>4</sub>]. Neither (HNEt<sub>3</sub>)[(pydicOMe)CuCl<sub>3</sub>] nor, of course, [CuCl<sub>4</sub>]<sup>2-</sup> possess a [OPh]<sup>•+</sup>/[OPh] redox couple, but show oxidation in a similar range as (HNEt<sub>3</sub>)[(pydicOPh)CuCl<sub>3</sub>]. So the oxidised species needs to be further analysed to allow an

unequivocal assignment. This was done by spectroelectrochemical characterisation presented below.

### 2.1.5 Absorption spectroscopy and spectroelectrochemical measurements

Absorption measurements (1000 – 200 nm) were performed in MeCN solution. The data are summarised in Table 6. Extinction coefficients  $\epsilon$  help to distinguish between absorption bands of ligand centred  $\pi$ - $\pi^*$  transitions (sharp absorption bands with large values for  $\epsilon$ ) charge transfer (broad absorption bands with lower values for  $\epsilon$ ) and d-d transitions (very broad absorption bands and small values for  $\epsilon$ ).

The complexes all show an absorption band at 462 nm which is assigned to be a LMCT between copper ion and chlorido ligands. The UV absorption bands, which are ligand centred  $\pi$ - $\pi^*$  transitions, vary significantly with the different substituents at the ester function.

While the complexes [(pydicOIPh)CuCl<sub>2</sub>], (HNEt<sub>3</sub>)[(pydicOMe)CuCl<sub>3</sub>] and (HNEt<sub>3</sub>)[(pydicOPh)CuCl<sub>3</sub>] show d-d absorption bands in the range of 800 to 900 nm, K<sub>2</sub>[CuCl<sub>4</sub>] shows a d-d band at 1074 nm indicating the differences in the ligand field strength, chlorido ligands are weak ligands to Cu<sup>II</sup>.

Table 6: Absorption maxima for the copper complexes<sup>[a]</sup>

compound	$\lambda$ / nm ( $\epsilon$ / Lmol <sup>-1</sup> cm <sup>-1</sup> )
[(pydicOIPh)CuCl <sub>2</sub> ]	289 (2747), 462 (425), 847 (72)
K <sub>2</sub> [CuCl <sub>4</sub> ] <sup>[b]</sup>	312, 346sh, 462, 1074
(HNEt <sub>3</sub> )[(pydicOMe)CuCl <sub>3</sub> ]	261 (4826), 462 (357), 823 (64)
(HNEt <sub>3</sub> )[(pydicOPh)CuCl <sub>3</sub> ]	261 (4134), 307 (2255), 462 (714), 900 (55)

[a] Measured in MeCN

[b] Due to a KCl impurity in the K<sub>2</sub>[CuCl<sub>4</sub>] salt the extinction coefficients  $\epsilon$  are not determined

Spectroelectrochemistry is a helpful method to analyse the spectroscopic properties of (potentially labile) oxidised or reduced species and means that electrochemistry (thin layer electrolysis performed at suitable potentials) is coupled to a second spectroscopic detection method. In general this method might be NMR, EPR, IR, Raman, absorption spectroscopy or else. The type of method should be chosen with regard to the system which is analysed: e.g. EPR can be used for compounds becoming paramagnetic upon electrochemical processes, IR

spectroscopy can be used for compounds showing indicative vibrations (e.g. complexes containing CO or NO ligands). For copper complexes absorption spectroscopy is a very helpful detection method. For the metal centred redox processes a decent change of the d-d transition and/or metal involved charge transfer is expected, while ligand centred processes lead to a change of  $\pi$ - $\pi^*$  transition. Furthermore, electrochemically induced processes such as (de)protonation reactions, halogenide cleavage or dimerisation should lead to typical changes of the absorption spectra and thus can be identified by this method. Generation of phenoxyl radicals also leads to indicative absorption bands at the same time allowing conclusion on the radical stability (by the absorption energy of the CT absorption band) and validating interactions between radical and copper ion or between two radicals of one complex.

Oxidative spectroelectrochemical measurements (at +1.5 V) in MeCN// $\text{Bu}_4\text{NPF}_6$  using  $(\text{HNEt}_3)[(\text{pydicOPh})\text{CuCl}_3]$  and  $[(\text{pydicOIPh})\text{CuCl}_2]$  were carried out to determine whether electrochemical oxidation generates phenoxyl radicals (Figure 8).

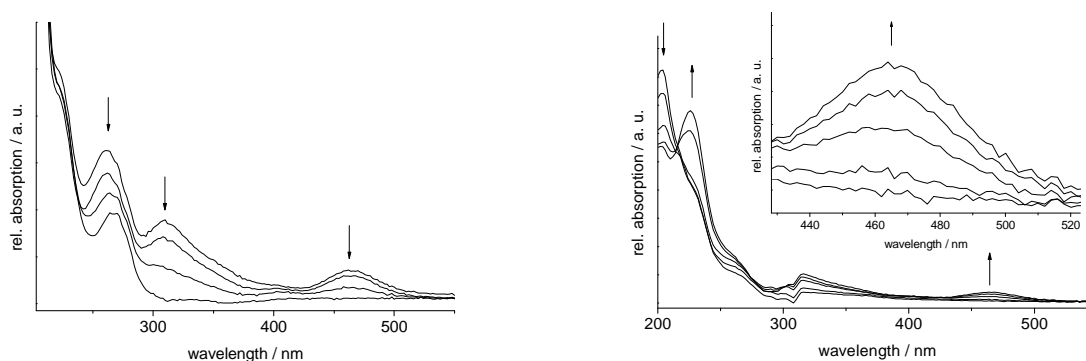


Figure 8: Absorption spectra recorded upon oxidative spectroelectrochemistry (+1.5 V) of  $(\text{HNEt}_3)[(\text{pydicOPh})\text{CuCl}_3]$  (left) and  $[(\text{pydicOIPh})\text{CuCl}_2]$  (right) in MeCN// $\text{Bu}_4\text{NPF}_6$  solution

During the electrochemical oxidation of  $(\text{HNEt}_3)[(\text{pydicOPh})\text{CuCl}_3]$  a decreasing intensity for the ligand centred absorption band at 261 nm (assigned to  $\pi$ - $\pi^*$  transition) is observed, while the absorption bands at 306 nm and 462 nm vanish. This is not typical for the formation of phenoxyl radicals but presumably indicates the decomposition of  $(\text{HNEt}_3)[(\text{pydicOPh})\text{CuCl}_3]$  upon oxidation.

Oxidation of  $[(\text{pydicOIPh})\text{CuCl}_2]$  leads to a new absorption band rising at 466 nm, while the absorption maximum at 203 nm ( $\pi$ - $\pi^*$  transition) is shifted to 226 nm. The band at 466 nm is assigned to be a charge transfer between  $\text{Cu}^{\text{II}}$  and a partly stabilised (*ortho*-I) phenoxyl radical generated upon oxidation.

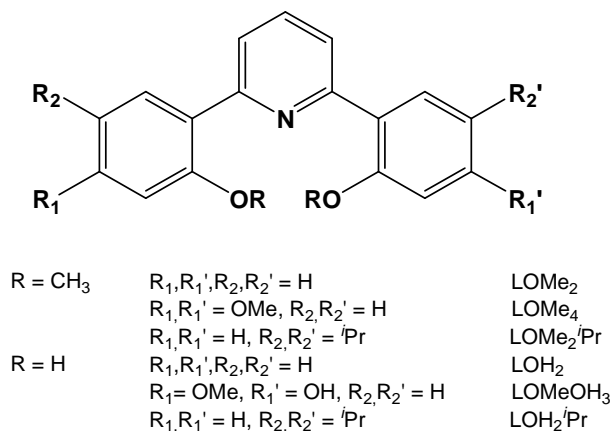
### 2.1.6 Conclusions on the suitability of pydicH<sub>2</sub> ester complexes as GO model systems

The complexes [(pydicOIPh)CuCl<sub>2</sub>] and (HNEt<sub>3</sub>)[(pydicOPh)CuCl<sub>3</sub>] both contain phenol moieties, which generally might allow the formation phenoxyl radicals. Electrochemical investigations showed that the potentials of the Cu<sup>II</sup>/Cu<sup>I</sup> redox couple lie in the typical range, while the ligand centred oxidation occurs at rather high potentials. The latter is not desirable for GO mimicking activity. Furthermore, spectroelectrochemistry showed that oxidation of (HNEt<sub>3</sub>)[(pydicOPh)CuCl<sub>3</sub>] does not lead to a phenoxyl radical species, while oxidation of [(pydicOIPh)CuCl<sub>2</sub>] leads to a phenoxyl radical. Therefore (HNEt<sub>3</sub>)[(pydicOPh)CuCl<sub>3</sub>] is surely not suitable as GO model complex, while the suitability of [(pydicOIPh)CuCl<sub>2</sub>] should be examined in a catalytic test reaction (Chapter 7). Modification of the O,N,O pincer ligands might improve their suitability, ligands which lack competitive donor functions (such as the carbonyl oxygen) guarantee a coordination of the phenoxy part of the ligand. A promising alternative would thus be the use of bis-phenoxido pincer ligands, which is described in the following.

## 2.2 Bis-phenoxido-pincer ligands and their copper complexes

### 2.2.1 Introduction

The class of bis-phenoxido pincer ligands (Scheme 22) is derived from the pydic-ester ligand type (Chapter 2.1). In contrast to the latter the bis-phenoxido pincer ligands solely possess three donor atoms (O<sub>phenol</sub>-N<sub>pyridine</sub>-O<sub>phenol</sub>), so a copper-phenoxido coordination is guaranteed.



Scheme 22: General structure of bis-phenoxido pincer ligands with various substituents

The synthesis of 2,6-bis-(2-hydroxyphenyl)pyridine ligand ( $\text{LOH}_2$ ) from 2,6-bis-(2-hydroxyphenyl)pyridine ( $\text{LOMe}_2$ ) has already been reported.<sup>[232]</sup> Also a similar ligand system, the asymmetric 2-(2-hydroxy-5-methylphenyl)-6-(2-hydroxyphenyl)pyridine ( $\text{LOH}_2\text{Me}$ ), which was synthesised via a *Kröhnke* pyridine synthesis is known.<sup>[233]</sup> Further substituted derivatives of  $\text{LOH}_2$  such as 2-(2-methoxynaphtyl)-6-(2-methoxyphenyl)pyridine, 2,6-bis-(2-methoxynaphtyl)pyridine and the hydroxy-derivatives<sup>[234]</sup> as well as fluorinated derivatives are known.<sup>[235]</sup> Complexes of the latter have not been described yet, but  $\text{LOH}_2$  and  $\text{LOH}_2\text{Me}$  were used to synthesise copper complexes (Figure 9).<sup>[233,236]</sup>

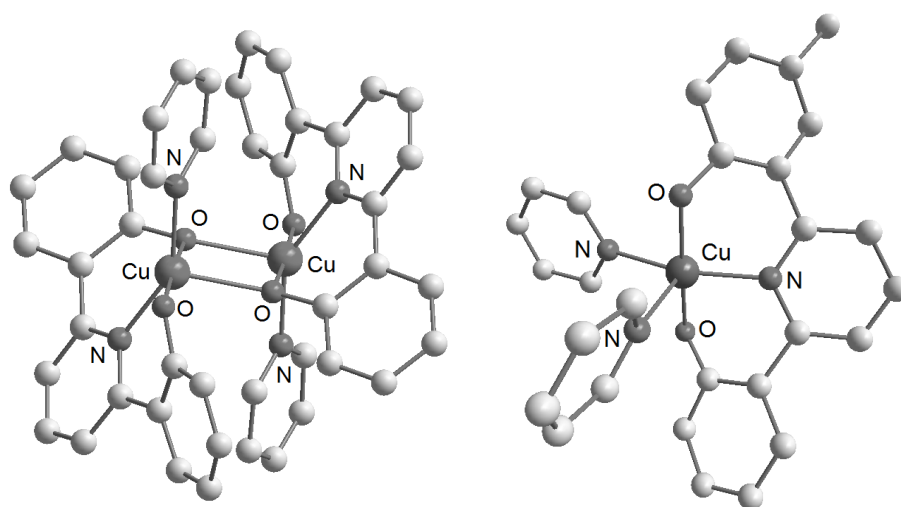


Figure 9: Molecular structure of  $[\text{Cu}(\text{LO}_2)(\text{py})]_2$ <sup>[236]</sup> (left), and  $[\text{Cu}(\text{LO}_2\text{Me})(\text{py})_2]$ <sup>[233]</sup> (right); H atoms omitted for clarity

$\text{Cu}^{\text{II}}$  complexes including the deprotonated  $\text{LOH}_2$  and  $\text{LOH}_2\text{Me}$  are normally isolated as multinuclear species, while mononuclear complexes are obtained upon treating multinuclear species with excess pyridine. This does not work in any case as the formation of  $[(\text{LO}_2)\text{Cu}(\text{py})]_2$  shows (Figure 9).<sup>[236]</sup>

Interestingly, the phenoxido-pincer ligands show a strongly distorted geometry upon coordination to large transition metal ions. This is due to the small binding pocket provided by these ligands. In the complex  $[(\text{LO}_2)\text{Be}(\text{OH}_2)]$ <sup>[237]</sup>, where the small  $\text{Be}^{2+}$  ion is located above the O,N,O plane, the planar ligand offers a binding pocket with  $\text{O1}\cdots\text{N1}$  and  $\text{O2}\cdots\text{N1} = 2.62 \text{ \AA}$  and  $\text{O1}\cdots\text{O2} = 2.59 \text{ \AA}$ . This means that in a planar ligand geometry the O donor atoms lie markedly closer than the approximate length of an O–Cu–O binding motive (approximately  $3.66 \text{ \AA}$  as inferred from the sum of covalence radii). As a result, both phenoxido moieties are twisted upon coordination to copper.

The aim of the present study was to synthesise mononuclear copper complexes with the known phenoxido-pincer ligands (LOH<sub>2</sub> and LOMe<sub>2</sub>) and with some new derivatives (LOMe<sub>4</sub>, LOH<sub>3</sub>OMe, LOMe<sub>2</sub><sup>*i*</sup>Pr and LOH<sub>2</sub><sup>*i*</sup>Pr). The electrochemical and optical properties were investigated with regard to the compound's ability to form phenoxyl radicals of the resulting complexes.

### 2.2.2 Synthesis and characterisation of the ligands

While the ligands 2,6-Bis(2-methoxyphenyl)pyridine (LOMe<sub>2</sub>) and 2,6-Bis(2-hydroxyphenyl)pyridine (LOH<sub>2</sub>) have been described before,<sup>[232,236,238]</sup> the derivatives (LOMe<sub>4</sub>, LOH<sub>3</sub>OMe, LOMe<sub>2</sub><sup>*i*</sup>Pr and LOH<sub>2</sub><sup>*i*</sup>Pr) are new compounds. LOMe<sub>4</sub> was synthesised via a *Kumada* coupling reaction and was isolated as its MgBr<sub>2</sub> complex. This is inferred from NMR spectroscopy and elemental analysis. The free LOMe<sub>4</sub> ligand was obtained by extraction of the organic complex solution with an aqueous solution of cryptand. Cheaper methods like acidifying the dissolved magnesium complex, filtration over silica or treatment with crown ether remained unsuccessful. LOH<sub>3</sub>OMe was obtained from LOMe<sub>4</sub> by demethoxylation using an excess of pyridinium hydrochloride. The reason for incomplete demethoxylation in the presence of a huge excess pyridinium hydrochloride is still unclear. The remaining methoxy group was found to be in *meta* position at the phenol core (non-coordinating) using appropriate NMR correlation experiments (H,H-COSY, HMBC, HSQC and NOESY).

The ligand LOMe<sub>2</sub><sup>*i*</sup>Pr was synthesised via a *Suzuki* coupling reaction in good yield (84%) and high purity. Demethoxylation using an excess of pyridinium hydrochloride yielded the ligand LOH<sub>2</sub><sup>*i*</sup>Pr (67%) in high purity. All ligands were fully characterised by NMR and elemental analysis. Additionally LOMe<sub>2</sub> and LOMe<sub>4</sub> could be obtained as single crystals from acetone. X-ray diffraction resulted the structure of LOMe<sub>2</sub> (solved in the monoclinic space group *Cc*) and LOMe<sub>4</sub> (solved in the chiral orthorhombic space group *P2<sub>1</sub>2<sub>1</sub>2<sub>1</sub>*<sup>[239]</sup>). Figure 10 shows the two molecular structures (for details of the crystal measurement and refinement see appendix). The crystal structure of LOMe<sub>2</sub> has already been reported in the monoclinic space group *Ia*.<sup>[232]</sup> Although *Ia* is a non-standard but equivalent setting of *Cc*, the molecular parameters in both structures are not identical (Figure 10). The  $\pi$ -overlap between the three ring planes is expected to be crucial for the spectroscopic and electrochemical properties of the free ligands and their

metal complexes (Table 7).

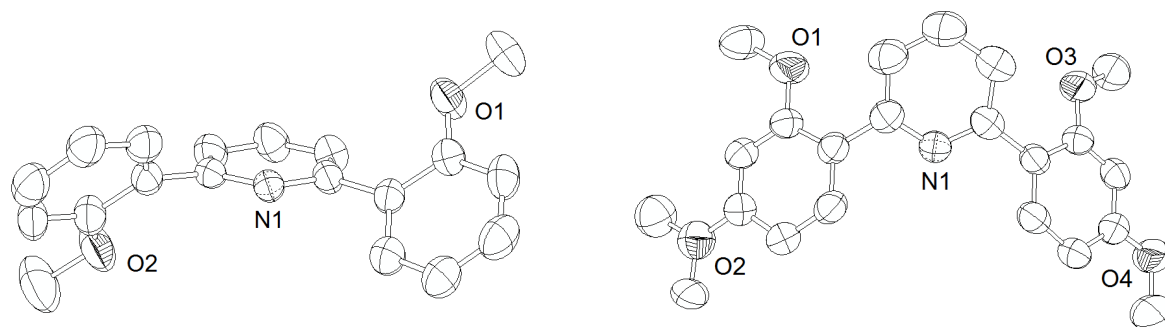


Figure 10: Molecular structure of LOMe<sub>2</sub> (left) and LOMe<sub>4</sub> (right), thermal ellipsoids represent 50% probability; H atoms were omitted for clarity

Table 7: Selected data of the molecular structures of LOMe<sub>2</sub> and LOMe<sub>4</sub>

dihedral angles	LOH <sub>2</sub>	LOMe <sub>2</sub>	LOMe <sub>4</sub>
planeO1-planeN	~26 <sup>[a]</sup>	44.40(6)	35.39(9)
planeO2-planeN	~30 <sup>[a]</sup>	51.75(8)	40.31(9)
planeO1-planeO2	~51 <sup>[a]</sup>	78.92(8)	38.06(9)

[a] Averaged values from three independent molecules from ref [232]

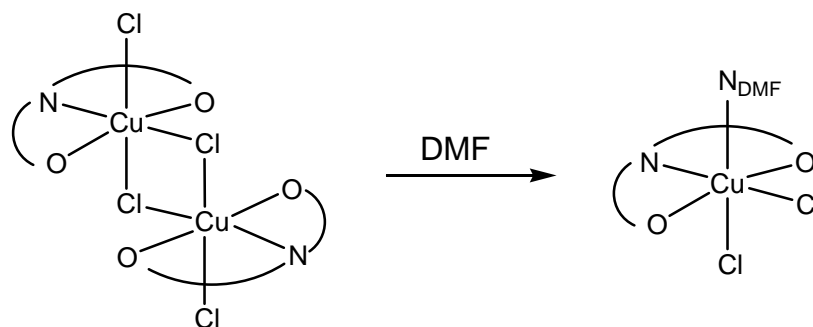
In the ligand LOMe<sub>2</sub> both phenol rings are markedly tilted from the central pyridine ring. As a result the two methoxy groups point into different directions one group lying above the pyridine ring plane and the other one below. Thus the  $\pi$ -overlap between the different ring planes in LOMe<sub>2</sub> is negligible. In LOMe<sub>4</sub> both tilt angles are smaller and both methoxy groups point in the opposite direction of the binding pocket. One of the methyl groups in 4-position is disordered (1:3). The tilt angles of the LOH<sub>2</sub> ligand are the smallest found in this series and the two hydroxy groups point into the same direction. In summary all three ligands exhibit molecular structures which result from steric interactions and do not represent the geometry presumed for their tridentate coordination mode. In order to coordinate in a bis-chelate manner they have to undergo conformational changes by rotation of the phenyl substituents. The corresponding rotation energies are probably rather small, while on the other hand, the systems might gain energy from more efficient  $\pi$ -delocalisation in the all-planar conformation. However, from a study on LOH<sub>2</sub>Me and its copper complex [Cu(LO<sub>2</sub>Me)(py)<sub>2</sub>]<sup>[233]</sup> it is evident that one of the phenol substituents is in a coplanar arrangement to the central pyridine core (supported by a O–H $\cdots$ N hydrogen bond), while in the corresponding Cu<sup>II</sup> complex all three rings are tilted toward each other, due to the small cavity provided by the O,N,O donor atoms (the mentioned protons fit into



the cavity). Thus an all-planar configuration cannot be expected for the Cu<sup>II</sup> or Ni<sup>II</sup> complexes. The geometry of LOMe<sub>2</sub><sup>*i*</sup>Pr and LOH<sub>2</sub><sup>*i*</sup>Pr is hardly predictable since the <sup>*iso*</sup>propyl group in *para* position is not expected to exhibit a strong sterical effect. In principle, both ligands can be twisted similar to LOH<sub>2</sub>, LOMe<sub>2</sub> or LOMe<sub>4</sub>.

### 2.2.3 Synthesis of the complexes

The synthesis of copper complexes containing phenoxido pincer ligands is mainly determined by the initial goal to generate mononuclear compounds. For LOH<sub>2</sub> and its derivatives the formation of oligonuclear copper complexes with copper atoms bridged by negatively charged oxido ligand functions (phenolates) was reported.<sup>[233,236]</sup> The already known strategy to form mononuclear complexes by adding suitable ligands like pyridine to multinuclear complexes<sup>[233]</sup> turned out to be insufficiently controllable: due to the unknown nuclearity of the starting materials (stoichiometry) the reaction yielded by-products as [Cu(py)<sub>2</sub>Cl<sub>2</sub>], which could be crystallised from the reaction mixture. Therefore more reliable strategies for the synthesis of mononuclear complexes had to be applied. The ligands were used in their protonated or methoxylated state, which prohibits the formation of oligonuclear species through oxido ligand bridging. Nevertheless the complex forming reactions with CuCl<sub>2</sub> in methanol yielded brown compounds, indicating the formation of binuclear complexes (or compounds with even higher nuclearity). Multinuclear compounds have been described to exhibit a brownish colour, while mononuclear derivatives are green.<sup>[233]</sup> Most likely the obtained compounds are binuclear chlorido bridged complexes: [(LOMe<sub>2</sub>)CuCl<sub>2</sub>]<sub>2</sub>, [(LOH<sub>2</sub>)CuCl<sub>2</sub>]<sub>2</sub>, [(LOMe<sub>4</sub>)CuCl<sub>2</sub>]<sub>2</sub>, [(LOMe<sub>2</sub><sup>*i*</sup>Pr)CuCl<sub>2</sub>]<sub>2</sub> and [(LOH<sub>2</sub><sup>*i*</sup>Pr)CuCl<sub>2</sub>]<sub>2</sub>. This assumption could be verified by EPR spectroscopy (see below). The copper atoms in these dimeric products are assumed to be octahedrally coordinated, bridged by two of the chlorido ligands (Scheme 23). The solids can be dissolved in DMF resulting reliably in octahedrally configured mononuclear species [(O,N,O)CuCl<sub>2</sub>(DMF)] (Scheme 23) as indicated by their absorption spectra and EPR spectroscopy (see below). In other donating solvents such as MeCN, DMF or DMSO the cleavage of the chlorido bridge can also be observed (see below).



Scheme 23: Proposed structure for the binuclear complexes  $[(\text{O},\text{N},\text{O})\text{CuCl}_2]_2$  and monomers obtained in DMF solution

But the mononuclear species obtained in MeCN solution rapidly disproportionate (Eq. 7). This is in line with recent reports on related chlorido bridged copper complexes<sup>[229]</sup> and with the previously reported pentacoordinated complexes  $[(\text{RR}'\text{pydimH}_2)\text{CuCl}_2]$  ( $\text{RR}'\text{pydimH}_2 =$  oxido pincer ligands based on 2,6-bis(hydroxymethyl) pyridine).<sup>[183]</sup>



An alternative synthesis is to perform ligand exchange reactions in MeCN starting from  $[\text{Cu}(\text{MeCN})_4](\text{TFA})_2$  (TFA = trifluoroacetic acid) as precursor. In the case of  $\text{LOMe}_2$  no reaction took place, while for  $\text{LOMe}_4$  the complex  $[(\text{LOMe}_4)\text{Cu}(\text{TFA})_2]$  was obtained as a light green solid. Additionally the complexes  $[(\text{LOH}_3\text{OMe})\text{Cu}(\text{TFA})_2]$  and  $[(\text{LOMe}_2^i\text{Pr})\text{Cu}(\text{TFA})_2]$  were obtained, while the reaction of  $\text{LOH}_2^i\text{Pr}$  and  $[\text{Cu}(\text{MeCN})_4](\text{TFA})_2$  (in 1:1 stoichiometry) yielded  $[(\text{LOH}^i\text{Pr})_2\text{Cu}]$  in some way. The pincer ligand in  $[(\text{LOH}_2)\text{CuCl}_2]_2$  is completely protonated, but can easily be deprotonated in methanol solution by adding an excess of  $\text{KO}^{tert}\text{Bu}$  or  $\text{NEt}_3$ . The deprotonated species  $[(\text{LOH})\text{CuCl}]$  precipitates immediately and can be isolated by filtration.

In addition to  $\text{Cu}^{\text{II}}$  complexes, which were the main focus of this study, some  $\text{Ni}^{\text{II}}$  derivatives were synthesised for comparison of the coordination geometry (detectable by UV/vis/NIR-, NMR- or EPR spectroscopy) and electrochemistry (higher potentials for the metal centred redox processes). The nickel compounds were synthesised using ligand exchange reactions starting from  $[(\text{PPh}_3)_2\text{NiBr}_2]$ . The obtained dimeric compounds  $[(\text{LOMe}_2)\text{NiBr}_2]_2$ ,  $[(\text{LOH}_2)\text{NiBr}_2]_2$ ,  $[(\text{LOMe}_4)\text{NiBr}_2]_2$ ,  $[(\text{LOMe}_2^i\text{Pr})\text{NiBr}_2]_2$  and  $[(\text{LOH}_2^i\text{Pr})\text{NiBr}_2]_2$  were rapidly formed in methanol. Obtained yields are low when using  $\text{LOH}_2$ ,  $\text{LOMe}_2$  and  $\text{LOMe}_4$  (45-79%). This is due to the formation of triphenylphosphane oxide (detectable by NMR spectroscopy) which had to be removed by repeated washing using non-polar solvents. Somehow this side reaction was

observed in negligible amounts for LOMe<sub>2</sub><sup>i</sup>Pr and LOH<sub>2</sub><sup>i</sup>Pr and as a result the yields of [(LOMe<sub>2</sub><sup>i</sup>Pr)NiBr<sub>2</sub>]<sub>2</sub> and [(LOH<sub>2</sub><sup>i</sup>Pr)NiBr<sub>2</sub>]<sub>2</sub> were good (74% and 93%).

### 2.2.4 NMR spectroscopy

Due to their paramagnetism, no NMR spectra could be obtained for the Cu<sup>II</sup> complexes. Ni<sup>II</sup> compounds are not necessarily diamagnetic, if their geometry is square planar or distorted octahedral they are suitable for NMR analyses, while tetrahedral complexes are paramagnetic and NMR spectroscopy is strongly hampered. Due to the small binding pocket of the bis-phenoxido pincer ligands the nickel complexes need to be strongly distorted. For some binuclear complexes [(O,N,O)NiBr<sub>2</sub>]<sub>2</sub>, <sup>1</sup>H NMR spectra were obtained and can be compared to spectra of the free ligands. <sup>13</sup>C NMR spectra were recorded for the free ligands while low solubility of the nickel complexes did not allow such measurements.

Table 8: Selected <sup>1</sup>H NMR data for the free ligands and their Mg<sup>II</sup> and Ni<sup>II</sup> complexes<sup>[a]</sup>

compound	Py4	Py3,5	Ph6	Ph4	Ph5	Ph3	OMe/OH
LOMe <sub>2</sub>	7.84	7.84	7.97	7.39	7.15	7.07	3.92
[(LOMe <sub>2</sub> )NiBr <sub>2</sub> ] <sub>2</sub>	8.52	8.30	8.04	7.59	7.35	7.22	4.10
LOH <sub>2</sub>	8.00	7.72	7.69	7.35	7.05	7.00	9.88
[(LOH <sub>2</sub> )NiBr <sub>2</sub> ] <sub>2</sub>	8.00	8.00	7.86	7.32	7.00	7.00	11.67
LOMe <sub>4</sub>	7.69	7.78	8.01	-	6.68	6.68	3.91/3.87
[(LOMe <sub>4</sub> )MgBr <sub>2</sub> ]	8.63	8.29	6.87	-	6.93	8.01	4.19/3.98
[(LOMe <sub>4</sub> )NiBr <sub>2</sub> ] <sub>2</sub>	8.94	8.55	7.00	-	7.04	8.18	4.40/4.05
LOMe <sub>2</sub> <sup>i</sup> Pr	7.73	7.73	7.73	7.25	-	6.98	3.86
[(LOMe <sub>2</sub> <sup>i</sup> Pr)NiBr <sub>2</sub> ] <sub>2</sub> <sup>[b]</sup>	-	-	-	-	-	-	-
LOH <sub>2</sub> <sup>i</sup> Pr	8.03	8.03	7.75	7.21	-	6.98	-
[(LOH <sub>2</sub> <sup>i</sup> Pr)NiBr <sub>2</sub> ] <sub>2</sub>	8.54	8.25	7.89	7.25	-	6.91	-

[a] Chemical shifts  $\delta$  in ppm, measured in [D<sub>6</sub>]-acetone

[b] The Ni<sup>II</sup> coordination the compound is paramagnetic and NMR correlation experiments could not be performed, <sup>1</sup>H signals are  $\delta$  = 14.65; 9.44; 8.15; 7.93; 7.41; 3.88; 3.56; 1.57 ppm.

From Table 8 it is evident that the <sup>1</sup>H signals of the ligands show remarkable low field shifts upon coordination. Especially the shift differences of the pyridine ring protons indicate the metal

ion coordination, while the shift differences of phenol ring protons are not so huge. The observed shift differences of the methoxy and hydroxy proton signals indicate that both oxido donors are coordinated in any case. The spectra were found to be unchanged after days, proving the stability of the formed complexes in acetone solution.

$[(\text{LOH}_2)\text{NiBr}_2]_2$  shows proton signals for two OH protons, revealing that the complex formation is not inducing a deprotonation of the coordinated OH groups. However the  $\delta$  value has shifted from 9.88 to 11.67 ppm indicating that the protons are far more acidic. For the ligand  $\text{LOH}_2^i\text{Pr}$  and its nickel complex no hydroxy proton was found in the NMR spectra, in line with the expected increased acidity of this proton (already without metal ion coordination). At least, for the nickel complex of  $\text{LOMe}_2^i\text{Pr}$  no interpretable NMR spectrum was recorded: all  $^1\text{H}$  signals are strongly broadened and correlation experiments to assign the signals could not be performed. This is clearly due to paramagnetism, which could either be caused by a strong distortion of this complex, or by paramagnetic “impurities” such as a mononuclear penta-coordinated complex species.

### 2.2.5 EPR spectroscopy

EPR spectra of all copper compounds were measured in solid state and in DMF solutions at 298 K and at 110 K (DMF was glassy frozen under this conditions), data are listed in Table 9. The free ligands and most nickel complexes were found to be diamagnetic, but also the paramagnetic nickel complex  $[(\text{LOMe}_2^i\text{Pr})\text{NiBr}_2]_2$  did not show an EPR signal under the conditions described above. All observed  $g$  values lie in the range expected for  $\text{Cu}^{\text{II}}$  complexes, while a close look reveals decent differences in the signal symmetry and subtle variations in  $g$  values and  $g$  anisotropy ( $\Delta g$ ). The signal form of  $\text{Cu}^{\text{II}}$  is a direct hint to the complex geometry.<sup>[228]</sup>

The binuclear complexes  $[(\text{O,N,O})\text{CuCl}_2]_2$  from the preparation in methanol exhibit ill-resolved axial spectra (no hyperfine splitting) and no indication of a half-field signal (Figure 11). Such spectra are typical for chloride bridged binuclear species with octahedral configuration (OD),<sup>[215,229]</sup> or square pyramidal geometry (SP)<sup>[230,231]</sup> indicating a marginal influence of the sixth ligand.<sup>[240]</sup>

Table 9: X-band EPR data of the phenoxido-pincer copper complexes<sup>[a]</sup>

Compound	$g_{av}$	$g_{  }$	$g_{\perp}$	$A_{  Cu}$	$\Delta g$	symmetry <sup>[b]</sup>	solvent / T [K]
$[(LOH_2)CuCl_2]_2$	2.178	2.327	2.104	-	0.223	OD	solid / 298
$[(LOMe_2)CuCl_2]_2$	2.170	2.230	2.140	-	0.090	OD	solid / 298
$[(LOMe_4)CuCl_2]_2$	2.158	2.333	2.070	-	0.263	OD	solid / 298
$[(LOMe_2^iPr)CuCl_2]_2$	2.140	2.254	2.083	-	0.171	OD	solid / 298
$[(LOH_2^iPr)CuCl_2]_2$	2.124	2.220	2.076	-	0.145	OD	solid / 298
$[(LOH)CuCl_2]$	2.181	2.346	2.099	-	0.351	OD	solid / 110
$[(LOH_2)CuCl_2(DMF)]$	2.164	2.331	2.081	139 G	0.250	OE or SP	DMF / 110
$[(LOMe_2)CuCl_2(DMF)]$	2.166	2.336	2.081	129 G	0.255	OE or SP	DMF / 110
$[(LOMe_4)CuCl_2(DMF)]$	2.163	2.296	2.097	123 G	0.199	OE or SP	DMF / 110
$[(LOH)CuCl(DMF)_2]$	2.156	2.313	2.078	170 G	0.235	OE or SP	DMF / 110
$[(LOMe_4)Cu(TFA)_2]$	2.146	2.326	2.056	165 G	0.270	OE or SP	solid / 110
$[(LOH_3OMe)Cu(TFA)_2]$	2.121	2.229	2.067	-	0.162	OE or SP	solid / 110
$[(LOMe_2^iPr)Cu(TFA)_2]$	2.152	2.315	2.070	-	0.245	OE or SP	solid / 298

Compound	$g_{av}$	$g_1$	$g_2$	$g_3$	$\Delta g$	symmetry <sup>[b]</sup>	solvent / T [K]
$[(LOH^iPr)_2Cu]$	2.176	2.323	2.153	2.053	0.270	OM	solid / 298
$[(LOH^iPr)_2Cu]$	2.097	2.110	2.097	2.084	0.026	OM	DMF / 298

[a]  $g_{av}$  = averaged  $g$  value =  $(g_{||} + 2 g_{\perp})/3$ ;  $\Delta g = g_{||} - g_{\perp}$

[b] Symmetry assignment based on EPR spectroscopy (see text), OD = octahedral dimeric, OE = octahedral elongated, SP = square pyramidal; OM = octahedral monomeric

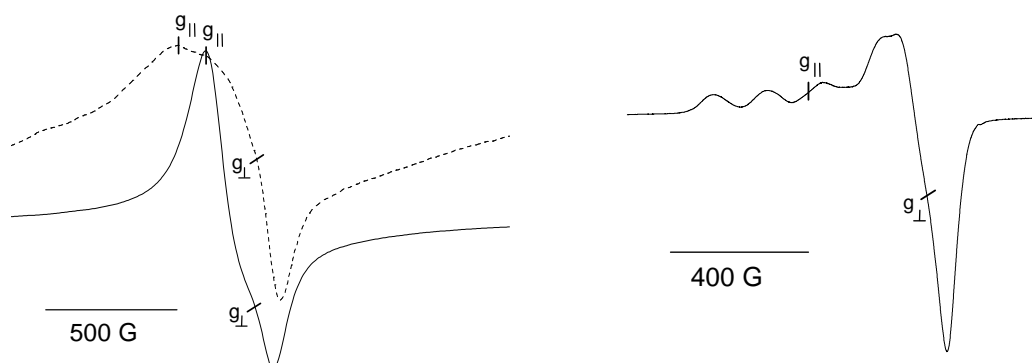


Figure 11: X-band EPR spectra of  $[(LOMe_2)CuCl_2]_2$  (left, solid line),  $[(LOH_2)CuCl_2]_2$  (left, dashed line) and  $[(LOMe_4)Cu(TFA)_2]$  measured in solid state at 298 K

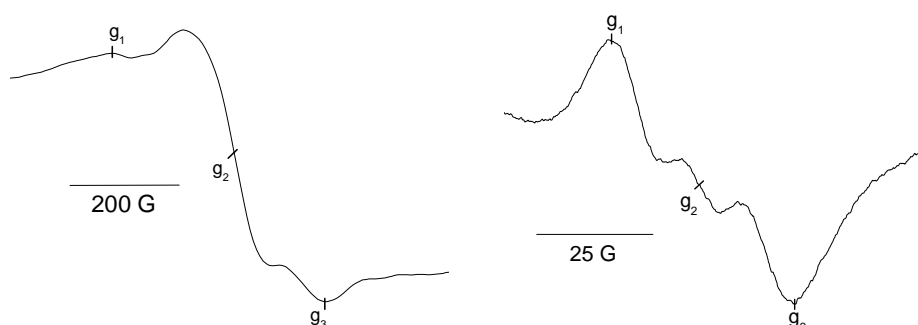
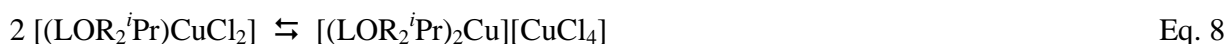


Figure 12: X-band EPR spectra of  $[(LOH^iPr)_2Cu]$  in the solid state (left) and dissolved in DMF (right), spectra measured at 298 K

The species observed in (glassy frozen) DMF solutions all exhibit axial spectra with coupling constants ( $A_{\parallel\text{Cu}}$ ) about 140 G for the  $g_{\parallel}$  component, which are typical for square-based pyramidal (SP), tetragonally elongated octahedral (OE) but also trigonal bipyramidally (TBP) configured  $\text{Cu}^{\text{II}}$  complexes.<sup>[226,241-244]</sup> However, the three cases can be winnowed by their  $g$  value range. TBP compounds usually have  $g_{\parallel}$  values around 2.0 and  $g_{\perp}$  around 2.2, while for the other two configurations  $g_{\parallel} > g_{\perp}$  with  $g_{\perp} > 2.04$  can be expected.<sup>[228]</sup> Following this classification the complexes [(O,N,O)CuCl<sub>2</sub>(DMF)] are mononuclear octahedral or square pyramidal complexes (Scheme 23). The  $g$  anisotropy ( $\Delta g$ ) is quite similar for all complexes.

The complex [(LOH)CuCl]<sub>2</sub> exhibits a spectrum which is very similar to those of the  $\mu$ -Cl bridged complexes. Thus the presence of a dimer in the solid state can be concluded. This implies that the deprotonated oxido function bridges two copper ions. In DMF solution this complex is mononuclear as inferred from the EPR spectrum. However, it cannot be determined if this species contains one or two DMF ligands, since their presence in axial position will not have significant influence (assuming a square planar arrangement of the O,N,O and the Cl coligand).

For the solid complex [(LOMe<sub>4</sub>)Cu(TFA)<sub>2</sub>] an axial spectrum (Figure 11) was found, which is very similar to those of the mononuclear complexes containing chlorido ligands, hence they are assumed to have similar geometries, while a hyperfine structure as found for [(LOMe<sub>4</sub>)Cu(TFA)<sub>2</sub>] was not observed for [(LOMe<sub>2</sub><sup>*i*</sup>Pr)Cu(TFA)<sub>2</sub>] and [(LOH<sub>3</sub>OMe)Cu(TFA)<sub>2</sub>]. The complex [(LOH<sup>*i*</sup>Pr)<sub>2</sub>Cu] is the only compound that exhibits rhombic spectra (Figure 12); in DMF solution the signal is highly symmetric ( $g_{\text{av}} = g_2$ ), thus it might be considered to be isotropic. The complex is clearly octahedrally configured and due to the shape of the O,N,O binding pocket, the geometry is assumed to be strongly distorted. The complexes [(LOH<sub>2</sub><sup>*i*</sup>Pr)CuCl<sub>2</sub>]<sub>2</sub> and [(LOMe<sub>2</sub><sup>*i*</sup>Pr)CuCl<sub>2</sub>]<sub>2</sub> measured in DMF contain more than one copper species. The spectra show strong half field signals and in case of [(LOH<sub>2</sub><sup>*i*</sup>Pr)CuCl<sub>2</sub>]<sub>2</sub> the signal seems to contain that observed for [(LOH<sup>*i*</sup>Pr)<sub>2</sub>Cu]. This points to a coordinative disproportionation of the complex following Eq. 8.



Similar reactions were previously observed for pyridine dimethanol pincer complexes and in case of  $\text{Cu}^{\text{II}}$  species it was found that these reactions mainly take place if the complexes are well soluble.<sup>[184]</sup> This explains, why disproportionation is exclusively observed for this two bis-phenoxido pincer complexes. The <sup>*iso*</sup>propyl residues obviously lead to an increase in ligand and complex

solubility.

## 2.2.6 Electrochemical measurements

Cyclic voltammetry performed on the copper dichlorido complexes was carried out using DMF as solvent and  ${}^n\text{Bu}_4\text{NPF}_6$  as electrolyte. Representative plots are shown in Figure 13 and data are summarised in Table 10. Solely the compound  $[(\text{LOMe}_4)\text{Cu}(\text{MeCN})](\text{TFA})_2$  was measured in MeCN to ensure comparability to most of the literature work on related GO model compounds. The nickel complexes were included in this study for comparison, but they had to be measured in THF solution since they are not stable in MeCN or DMF. The assignment of redox processes is based on the assumption that  $\text{Ni}^{\text{II}}$  and  $\text{Cu}^{\text{II}}$  might exhibit similar ligand centred oxidation or reductions, while the metal based electrochemistry differs largely ( $\text{Cu}^{\text{II}}$  might be easily reduced ( $\text{Cu}^{\text{II}}/\text{Cu}^{\text{I}}$  couple), whereas for  $\text{Ni}^{\text{II}}$  oxidation ( $\text{Ni}^{\text{II}}/\text{Ni}^{\text{III}}$ ) should be observed at comparable low potentials).

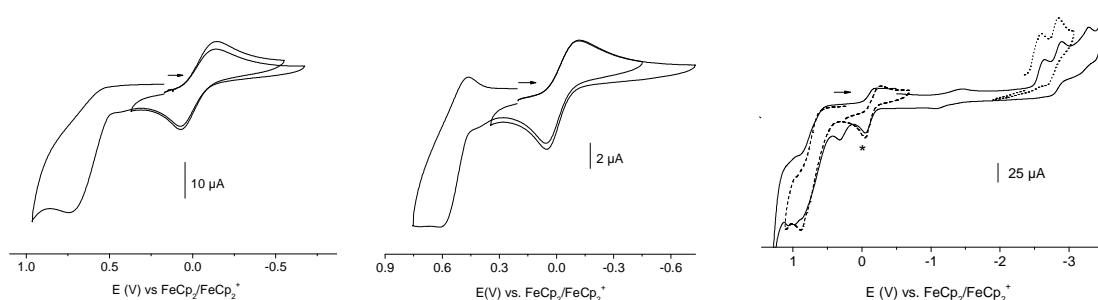


Figure 13: Cyclic voltammograms of  $[(\text{LOMe}_4)\text{CuCl}_2(\text{DMF})]$  (left),  $[(\text{LOMe}_2^i\text{Pr})\text{CuCl}_2(\text{DMF})]$  (middle) and  $[(\text{LOH}_2)\text{CuCl}_2(\text{DMF})]$  (right) measured in  $\text{DMF}/{}^n\text{Bu}_4\text{NPF}_6$  at 298 K with 100 mV/s scan rate; \* marks an oxidation wave corresponding to the deprotonated species

The copper complexes show reversible reductions at potentials around 0 V, while the corresponding  $\text{Ni}^{\text{II}}$  complexes are irreversibly oxidised at around +0.4 V. The (irreversible) ligand centred oxidation is strongly depending on the substitution pattern at the phenolate cores. For unsubstituted ligands the potentials of the  $[\text{OPh}]^{\bullet+}/[\text{OPh}]$  redox couple are quite similar, lying around 0.7 - 1.0 V (Table 10). The complex  $[(\text{LOH})\text{CuCl}(\text{DMF})_2]$  which contains the deprotonated  $\text{LOH}^-$  ligand, shows a far lower ligand oxidation potential. The  $[\text{OPh}]^{\bullet+}/[\text{OPh}]$

redox couple of  $\text{LOH}_2^i\text{Pr}$  and its copper complexes show irreversible oxidation at potentials around 0.3 - 0.7 V, in contrast  $\text{LOMe}_2^i\text{Pr}$  and its complexes exhibit reversible ligand centred oxidation at markedly lower oxidation potential ( $E_{1/2} = 0.54$  V and 0.36 V).

Table 10: Electrochemical data of free oxido-pincer ligands and their  $\text{Cu}^{\text{II}}$  and  $\text{Ni}^{\text{II}}$  complexes<sup>[a]</sup>

Ligands	$E_{pa}$ ox/ligand	$E_{1/2}$ $\text{Cu}^{\text{I}}/\text{Cu}^{\text{II}}$	solvent
$\text{LOH}_2$	0.93	-	DMF
$\text{LOMe}_2$	0.80	-	DMF
$\text{LOMe}_4$	0.98	-	DMF
$\text{LOH}_3\text{OMe}$	0.76	-	DMF
$\text{LOMe}_2^i\text{Pr}$	0.54	-	DMF
$\text{LOH}_2^i\text{Pr}$	0.63	-	DMF
Cu chlorido complexes	$E_{pa}$ ox/ligand	$E_{1/2}$ $\text{Cu}^{\text{I}}/\text{Cu}^{\text{II}}$	solvent
$\text{LOH}_2$	1.01	-0.11	DMF
$\text{LOH}^-$	0.28	-0.03	DMF
$\text{LOMe}_2$	0.90	-0.04	DMF
$\text{LOMe}_4$	0.72	-0.01	DMF
$\text{LOMe}_2^i\text{Pr}$	0.54 <sup>[b]</sup>	-0.01	DMF
$\text{LOH}_2^i\text{Pr}$	0.78	-0.03	DMF
Cu TFA complexes	$E_{pa}$ ox/ligand	$E_{1/2}$ $\text{Cu}^{\text{I}}/\text{Cu}^{\text{II}}$	solvent
$\text{LOMe}_4$	1.54	0.21	MeCN
$\text{LOH}_3\text{OMe}$	0.35	[245]	MeCN
$\text{LOMe}_2^i\text{Pr}$	0.36 <sup>[b]</sup>	-0.09	DMF
$[(\text{LOH}^i\text{Pr})_2\text{Cu}]$	0.35	-0.09	DMF
Ni complexes <sup>[c]</sup>	$E_{pa}$ ox/ligand	$E_{pa}$ $\text{Ni}^{\text{II}}/\text{Ni}^{\text{III}}$	solvent
$\text{LOH}_2$	0.82	0.41	THF
$\text{LOMe}_2$	> 1.04	0.56	THF
$\text{LOMe}_4$	0.96	0.52	THF
$\text{LOMe}_2^i\text{Pr}$	0.78	0.53	THF
$\text{LOH}_2^i\text{Pr}$	0.94	0.60	THF

[a] From cyclic voltammetry in solvent/<sup>n</sup>Bu<sub>4</sub>NPF<sub>6</sub> solutions; potentials in V vs. FeCp<sub>2</sub>/FeCp<sub>2</sub><sup>+</sup>

[b] Redox waves are reversible, potentials are  $E_{1/2}$  values

[c] Assumed to be dimeric in THF solution

Irreversible reduction waves were observed on cathodic scans, which were assigned to ligand centred processes. The complex  $[(\text{LOH}_2)\text{CuCl}_2(\text{DMF})]$  shows waves corresponding to the deprotonated complex  $[(\text{LOH})\text{CuCl}(\text{DMF})_2]$  at its reversed scan after reduction, which points to a deprotonation of the complex upon reduction. This is very uncommon, since deprotonation normally occurs after oxidation to remove the resulting positive charge, while reduction normally



is balanced by protonation.

### 2.2.7 Absorption spectroscopy and spectroelectrochemical measurement

The complexes [(O,N,O)CuCl<sub>2</sub>(DMF)] show typical weak ligand field (d-d) transitions around 1000 nm ( $\epsilon < 100 \text{ Lmol}^{-1}\text{cm}^{-1}$ ) indicative for a Jahn-Teller distorted square pyramidal or octahedral complex<sup>[246]</sup> (Figure 14 and Table 11). The energy of the ligand field absorptions for the Cu-OMe containing compounds lies at somewhat lower energy (9116 cm<sup>-1</sup>; 9681 cm<sup>-1</sup>; 10277 cm<sup>-1</sup>) compared to the Cu-OH containing derivatives (10764 cm<sup>-1</sup>; 10917 cm<sup>-1</sup>). This reflects the weaker ligand field imposed by the methoxy donor functions compared to hydroxy donor functions. The ligands exhibit strong absorption bands in the UV range of the spectrum. The two absorption bands discernible at around 270 and 310 nm are assigned to ligand centred  $\pi-\pi^*$  transitions and do not shift markedly upon coordination (Table 11).

An obstacle for analysing the dissolved copper complexes is complex disproportionation, which depends on the solvent's polarity and is supported by MeCN (Eq. 8).<sup>[183]</sup> Detection and quantification of this side reaction is carried out by examination of [CuCl<sub>4</sub>]<sup>2-</sup> which exhibits typical absorption bands (in MeCN a charge transfer absorption band is observed at 462 nm<sup>[247]</sup>). Time dependent measurements of [(LOH<sub>2</sub>)CuCl<sub>2</sub>]<sub>2</sub> dissolved in MeCN show an absorption band at 462 nm, which, starting from an intensity of 0.90 a. u., in one hour increases to an intensity of 2.09 a. u.; the formation of [CuCl<sub>4</sub>]<sup>2-</sup> in MeCN is faster (logK = 3.7) than in water (logK = 0.01)<sup>[247]</sup>. In DMF solution an absorption band at 438 nm is present for all complexes thus it is expected to be originated by [CuCl<sub>4</sub>]<sup>2-</sup> in DMF solution. In the case of [(LOH)CuCl<sub>2</sub>] it's starting intensity is 0.17 a. u., 0.19 a. u. after one hour and after 16 h the band has an intensity of 0.40 a. u. indicating a slow formation of [CuCl<sub>4</sub>]<sup>2-</sup>.

For [(LOMe<sub>2</sub>)CuCl<sub>2</sub>]<sub>2</sub> the disproportionation product is also detectable, but in contrast to [(LOH<sub>2</sub>)CuCl<sub>2</sub>]<sub>2</sub> the corresponding absorption band decreases during an hour from 2.08 a. u. to 0.80 a. u. in MeCN solution and from 0.85 a. u. to 0.75 a. u. in DMF. Therefore DMF seems to be the best solvent for absorption spectroscopy. The well soluble complexes [(LOMe<sub>2</sub><sup>*i*</sup>Pr)CuCl<sub>2</sub>(DMF)] and [(LOH<sub>2</sub><sup>*i*</sup>Pr)CuCl<sub>2</sub>(DMF)] exhibit strong absorption in the range of 438 nm in DMF solution, which is assigned to [CuCl<sub>4</sub>]<sup>2-</sup>. This indicates coordinative

disproportionation of the complexes and is in line with findings of EPR spectroscopy. Table 11 gives an overview of the essential absorption bands of the copper and nickel compounds.

Table 11: Absorption maxima for free ligands and Cu<sup>II</sup> and Ni<sup>II</sup> complexes<sup>[a]</sup>

compound	$\lambda_1$ / nm ( $\epsilon$ / Lmol <sup>-1</sup> cm <sup>-1</sup> )	$\lambda_2$ / nm ( $\epsilon$ / Lmol <sup>-1</sup> cm <sup>-1</sup> )	$\lambda_3$ / nm ( $\epsilon$ / Lmol <sup>-1</sup> cm <sup>-1</sup> )
LOMe <sub>2</sub>	316 (10000)	-	-
LOH <sub>2</sub>	318 (10300)	-	-
LOMe <sub>4</sub>	316 (10010)	371 (3610)	-
LOMe <sub>2</sub> <sup>i</sup> Pr	306 (2696)	-	-
LOH <sub>2</sub> <sup>i</sup> Pr	322 (1797)	-	-
[(LOMe <sub>2</sub> )CuCl <sub>2</sub> (DMF)]	304 (-)	375 (740)	1097 (86)
[(LOMe <sub>4</sub> )CuCl <sub>2</sub> (DMF)]	312 (14860)	369 (2320)	1033 (100)
[(LOMe <sub>2</sub> <sup>i</sup> Pr)CuCl <sub>2</sub> (DMF)]	316 (7832)	433 (630)	966 (127)
[(LOH <sub>2</sub> )CuCl <sub>2</sub> (DMF)]	316 (-)	-	929 (66)
[(LOH <sub>2</sub> <sup>i</sup> Pr)CuCl <sub>2</sub> (DMF)]	327 (10836)	436 (550), 480 (364)	916 (67)
[(LOMe <sub>2</sub> )NiBr <sub>2</sub> ] <sub>2</sub>	328 (5351)	612sh (123), 643 (131)	714 (88)
[(LOH <sub>2</sub> )NiBr <sub>2</sub> ] <sub>2</sub>	350 (10892)	617sh (160), 648 (185)	720 (92)
[(LOMe <sub>4</sub> )NiBr <sub>2</sub> ] <sub>2</sub>	378 (12056)	627 (55)	673sh (49)
[(LOMe <sub>2</sub> <sup>i</sup> Pr)NiBr <sub>2</sub> ] <sub>2</sub>	362 (6107)	637 (245)	673sh (229)
[(LOH <sub>2</sub> <sup>i</sup> Pr)NiBr <sub>2</sub> ] <sub>2</sub>	336 (10003)	612sh (119), 640 (134)	676 (123)

[a] Free ligands and copper complexes measured in DMF and nickel complexes measured in THF

Depending on the solvent's donor strength the resulting mononuclear complexes showed different absorption spectra (Figure 14). The shift of the d-d absorption band proves that solvent molecules are incorporated as ligands and the energy of the absorption bands in Table 12 reflect the expected ligand strength of NEt<sub>3</sub> > MeCN > DMF in the assumed species [(LOH<sub>2</sub>)CuCl<sub>2</sub>(solv)].

Table 12: Long-wavelength absorption of [(LOH<sub>2</sub>)CuCl<sub>2</sub>]<sub>2</sub> in various solvents

solvent	$\lambda$ / nm	$\epsilon$ / Lmol <sup>-1</sup> cm <sup>-1</sup>
NEt <sub>3</sub>	810	204
MeCN	909	44
DMF	941	67

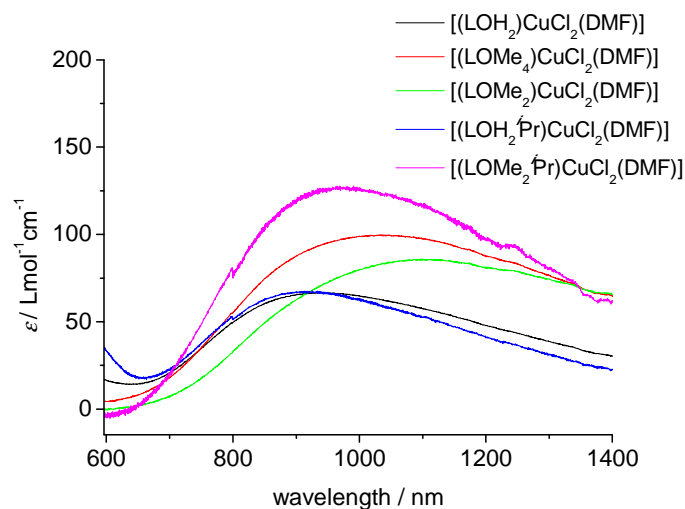


Figure 14: NIR-absorption spectra of [(O,N,O)CuCl<sub>2</sub>(DMF)] complexes

Absorption properties of the nickel complexes were studied in THF solution. As shown in Figure 15, the absorption maxima assigned to charge transfer and d-d transition in the range of 400 to 700 nm are very similar and in line with octahedral complex geometry. However, the intensity of the absorption bands varies strongly.

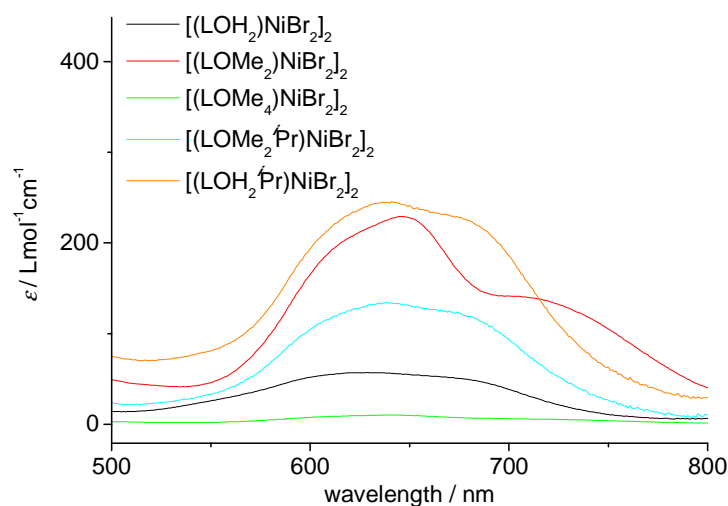


Figure 15: Vis-absorption of the [(O,N,O)NiBr<sub>2</sub>]<sub>2</sub> complexes measured in THF solution

The LOH<sub>2</sub> ligand had already been analysed regarding its acid/base properties. This has been done using absorption spectroscopy of the different (de)protonated species combined with

calculations.<sup>[233]</sup> From this study it is already known that an absorption band at 318 nm belongs to the fully protonated LOH<sub>2</sub> ligand (the absorption is assigned to  $\pi-\pi^*$  transition). An absorption maximum at 349 nm indicates the singly deprotonated Ligand LOH<sup>-</sup>, while an absorption band at 408 nm denotes the completely deprotonated LO<sup>2-</sup> ligand. The absorption spectrum of the complex [(LOH<sub>2</sub>)CuCl<sub>2</sub>(DMF)] thus confirms that the ligand remains protonated upon coordination.

The first spectroelectrochemical experiments (using an optical transparent thin-layer electrode "OTTLE" cell) were devoted to the question if the ligands tolerate the change in oxidation state of the copper atom from Cu<sup>II</sup> to Cu<sup>I</sup>. From these experiments it is obvious that the ligand centred absorption bands slightly decrease in intensity (10 to 30%). While the complex [(LOH)CuCl(DMF)<sub>2</sub>] (containing a singly deprotonated ligand) exhibits a shift of the corresponding long-wavelength absorption to lower energy (from 343 nm to 358 nm), the other complexes do not show a significant shift of the long-wavelength absorption bands (Table 13 and Figure 16).

Table 13: Data of absorption-titration experiments and spectroelectrochemical measurements<sup>[a]</sup>

titration	$\lambda$ / nm	equivalents			
with CuCl <sub>2</sub>	278, 318, 436 <sup>[a]</sup>	0-5			
with CuCl <sub>2</sub> ("Bu <sub>3</sub> N as base)	278, 360	0-3			
spectroelectrochemistry	oxidation	parent (Cu <sup>II</sup> )	Cu <sup>II</sup> →Cu <sup>I</sup>	reduction	
[(LOH <sup>i</sup> Pr) <sub>2</sub> Cu]	254, 325	254, 284, 362	254, 363	-	
[(LOH)CuCl(DMF) <sub>2</sub> ]	278, 322, 410sh	278, 343	277, 358	278, 351sh, 408	
[(LOH <sub>2</sub> )CuCl <sub>2</sub> (DMF)]	278, 316, 439	278, 316, 436 <sup>[b]</sup>	278, 318	278, 310, 425 <sup>[c]</sup>	
[(LOH <sub>2</sub> <sup>i</sup> Pr)CuCl <sub>2</sub> (DMF)]	286, 376, 447sh	253, 322	253, 327	-	
[(LOMe <sub>2</sub> )CuCl <sub>2</sub> (DMF)]	258, 324, 342sh	258, 304	258, 306	-	
[(LOMe <sub>4</sub> )CuCl <sub>2</sub> (DMF)]	264, 321, 371	264, 312	264, 314	-	
[(LOMe <sub>2</sub> <sup>i</sup> Pr)CuCl <sub>2</sub> (DMF)]	253, 296, 347	253, 309, 436 <sup>[b]</sup>	253, 310	-	
[(LOMe <sub>2</sub> <sup>i</sup> Pr)Cu(TFA) <sub>2</sub> ]	253, 343	253, 309	253, 308	-	

[a] Measured in DMF, all absorption bands in nm

[b] Assigned to [CuCl<sub>4</sub>]<sup>2-</sup>

[c] Further reduction leads to absorption bands at 278 nm, 350sh nm, 408 nm and 353 nm

It can be concluded that coordination is retained upon reduction to Cu<sup>I</sup> and the ligand easily follows the subsequent change of the coordination geometry, the latter might be simplified by a strong distorted complex geometry.

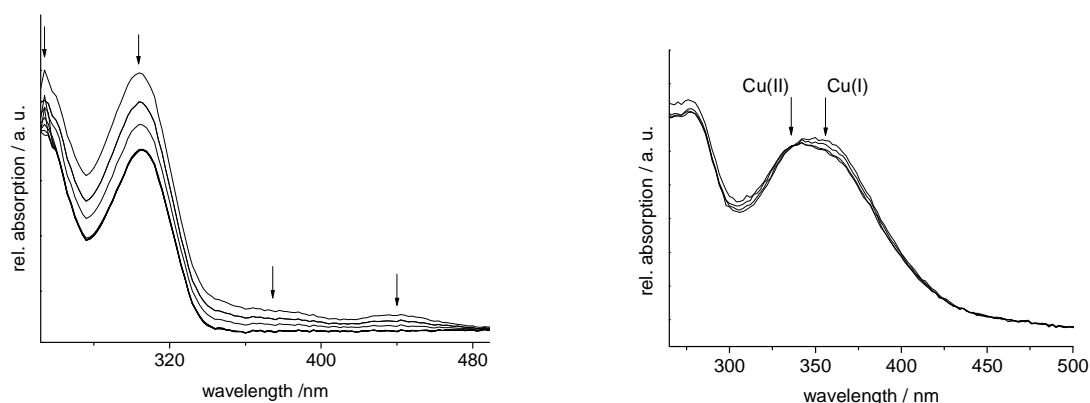


Figure 16: Absorption spectra of  $[(\text{LOMe}_2)\text{CuCl}_2(\text{DMF})]$  (left) and  $[(\text{LOH})\text{CuCl}(\text{DMF})_2]$  (right) measured upon electrochemical reduction ( $\text{Cu}^{\text{II}}$  to  $\text{Cu}^{\text{I}}$ ) in  $\text{DMF}/\text{Bu}_4\text{NPF}_6$  at 298 K

The ligand centred oxidation of the complexes occurs irreversibly as shown by cyclic voltammetry. Nevertheless the spectroscopic response upon oxidation was studied. For all complexes a long-wavelength absorption band lying in the range of 325 - 440 nm increases, the precise absorption wavelength depends on the ligand substitution (Figure 17). The new absorption band can be assigned to the phenoxyl radical species.<sup>[248]</sup> Interestingly, these absorption bands are shifted bathochromic with regard to the long-wavelength absorption bands of the parent species. Only  $[(\text{LOH})\text{CuCl}(\text{DMF})_2]$  and  $[(\text{LOH}^i\text{Pr})_2\text{Cu}]$ , which contain partly deprotonated ligands, show a phenoxyl radical charge transfer, which is shifted hypsochromic. Absorption bands in the range of 400 to 600 nm cannot be observed for the radical complexes. Comparison of the oxidation behaviour of  $[(\text{LOMe}_2^i\text{Pr})\text{CuCl}_2(\text{DMF})]$  and  $[(\text{LOMe}_2^i\text{Pr})\text{Cu}(\text{TFA})_2]$  proves that phenoxyl radical generation during electrochemical oxidation (indicated by the accessory absorption band) is not influenced by the coligand of the complexes.

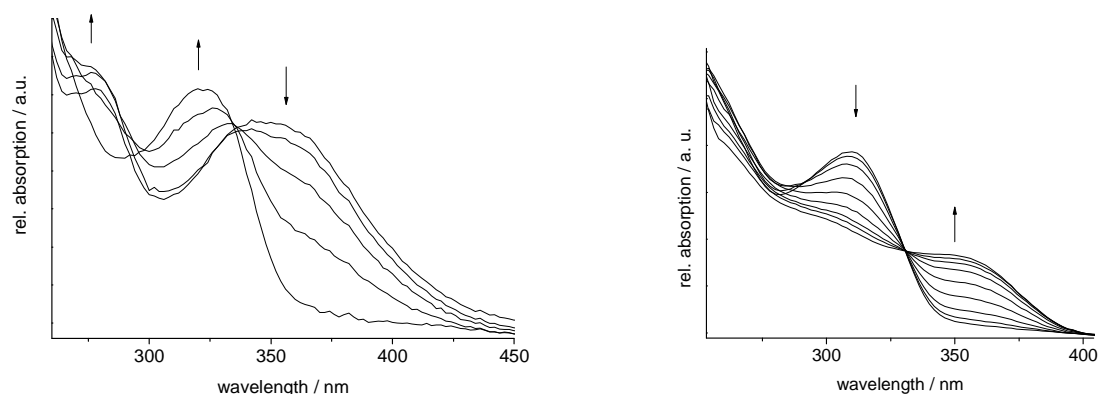


Figure 17: Absorption spectra recorded upon electrochemical oxidation (+1.0 V) of  $[(\text{LOH})\text{CuCl}(\text{DMF})_2]$  (left) and  $[(\text{LOMe}_2^i\text{Pr})\text{CuCl}_2(\text{DMF})]$  (right) in  $\text{DMF}/\text{Bu}_4\text{NPF}_6$  solution

Additionally some titration experiments were carried out to investigate the acid base properties of the metal complexes (Figure 18, left).<sup>[249-251]</sup> 0.3 mL  $n\text{Bu}_3\text{N}$  (1.3 mmol) were added to 3 mL of a  $\text{LOH}_2$  solution (0.6 mmol). Since no spectral changes were observed it can be concluded that the free ligand is not deprotonated under these conditions. To this mixture small portions (10  $\mu\text{L}$ ) of  $\text{CuCl}_2$  in DMF were added. The corresponding absorption spectra showed a decreasing absorption at 318 nm (corresponding to the ligand  $\text{LOH}_2$ ), while a new absorption band at 360 nm appeared (Figure 18, left). From the spectral fingerprint the proceeding reaction can be assigned to be the deprotonation of the coordinated ligand (formation of  $\text{LOH}^-$ ). Further addition of base did not change the recorded spectra, thus a fully deprotonated complex species, containing  $\text{LO}^{2-}$  is not accessible using  $n\text{Bu}_3\text{N}$  ( $pK_a = 10.9$ ). Titration of the ligand  $\text{LOH}_2$  under the same conditions without base leads to the formation of  $[(\text{LOH}_2)\text{CuCl}_2(\text{DMF})]$ , as indicated by comparison of the resulting spectrum with that of the isolated complex (Table 13).

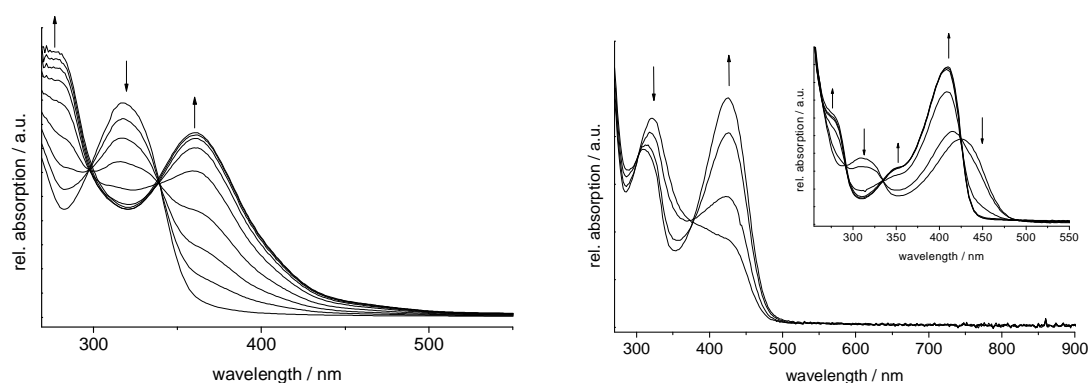


Figure 18: Absorption spectra recorded upon titration of a  $\text{LOH}_2/\text{NBu}_3$  solution with  $\text{CuCl}_2$  in DMF (left); spectroelectrochemical reduction ( $-2.7$  V) of  $[(\text{LOH}_2)\text{CuCl}_2(\text{DMF})]$  (right), inset shows reduction at  $-2.9$  V presumably leading to  $[(\text{LO})\text{CuCl}]^{2-}$  in  $\text{DMF}/n\text{Bu}_4\text{NPF}_6$  solution

Since a deprotonation upon reduction is a very uncommon process (nevertheless this has to be inferred by the CV experiments) optical spectroelectrochemistry of the reduction processes of  $[(\text{LOH}_2)\text{CuCl}_2(\text{DMF})]$  and  $[(\text{LOH})\text{CuCl}(\text{DMF})_2]$  was performed. Under reducing conditions ( $-2.7$  V) the absorption band of the complex  $[(\text{LOH}_2)\text{CuCl}_2(\text{DMF})]$  at 318 nm vanishes while a new absorption band appears at 425 nm (Figure 18, right). Further reduction ( $-3.0$  V) finally led to a strong absorption band at 408 nm, which is unequivocally indicative for the doubly deprotonated ligand. The origin of the absorption maximum at 425 nm remains unclear. When studying the complex containing the deprotonated ligand  $[(\text{LOH})\text{CuCl}(\text{DMF})_2]$  only the absorption band at 408 nm evolved immediately under reductive electrolysis. A coupling of

deprotonation and reduction of [(LOH<sub>2</sub>)CuCl<sub>2</sub>(DMF)] is further supported by the reductive spectroelectrochemistry of the complexes with methoxylated ligands (e.g. [(LOMe<sub>2</sub>)CuCl<sub>2</sub>(DMF)] and [(LOMe<sub>4</sub>)CuCl<sub>2</sub>(DMF)]). A general overview of titration experiments and spectroelectrochemical measurements is presented in Table 13.

To quantify the acidity of the complex [(LOH<sub>2</sub>)CuCl<sub>2</sub>(DMF)] and with it the basicity of the deprotonated system, pH titration experiments were carried out. These experiments were performed in methanol since the complex system is not stable in water or the alternative medium DMSO/H<sub>2</sub>O. However, *pK<sub>a</sub>* values obtained in methanol should be handled carefully since the pH scale is solvent depending and does not alter linearly.<sup>[252]</sup> The pH titration in methanol gave a *pK<sub>a</sub>*(1) value of 3.70 for the first deprotonation step (Eq. 9). In comparison to the *pK<sub>a</sub>* value obtained for the free ligand (10.5)<sup>[233]</sup> the acidity of the ligand has increased by a factor of about 10<sup>7</sup> by coordination to Cu<sup>II</sup>. A second deprotonation could not be induced using KOH as a base reflecting that the pH scale in water and methanol are not well comparable. Furthermore this shows that the fully deprotonated complex species can be considered to be a very strong base. The corresponding *pK<sub>a</sub>*(2) value of the free ligand has been determined to about 14.<sup>[238]</sup>



### 2.2.8 Luminescence properties

The ligands geometry (e.g. coplanarity of the aromatic rings) is assumed to be largely influenced by the coordinating metal as well as by substitution of the phenol core. These influence was established by emission spectroscopy in DMF solution. The ligand LOMe<sub>4</sub> and its complexes indeed show blue luminescence upon irradiation into the long-wavelength absorption band ( $\pi$ - $\pi^*$  transition), while unfortunately for LOH<sub>2</sub> or LOMe<sub>2</sub> ligands and their complexes no emission could be observed at 298 K in DMF solution. Comparable emission has been reported for the Zn<sup>II</sup> complex [(LO)<sub>4</sub>(py)<sub>4</sub>Zn<sub>4</sub>] in the solid state.<sup>[236]</sup> The corresponding emission for the ligands LOH<sub>2</sub> and LOMe<sub>2</sub> and their complexes is assumed to be quenched in DMF solution (radiation less decay). The emission maxima (around 470 nm) and the Stokes shifts (around

5400  $\text{cm}^{-1}$ ) are more or less the same for all compounds, while the intensities of the emissions and the quantum yields vary markedly (Table 14 and Figure 19). The emissions can be assigned to evolve from a  $^3\pi-\pi^*$  excited state. The quantum yield for the magnesium compound is higher than for the nickel and copper derivative, probably reflecting that the ion fits better into the narrow binding pocket of the ligand (see discussion on the molecular structures) thus providing a rigid system (better  $\phi$  than the free ligand).

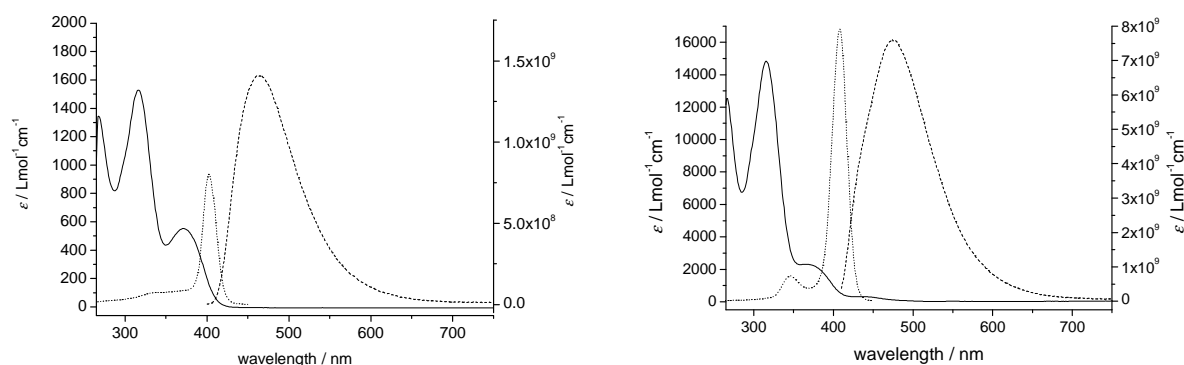


Figure 19: left: Absorption (solid line), excitation ( $\lambda_{\text{em}} = 464$  nm, dotted line) and emission spectra ( $\lambda_{\text{exc}} = 390$  nm, dashed line) of  $[(\text{LOMe}_4)\text{MgBr}_2]$  in DMF solution at 298 K; right: Absorption (solid line), excitation ( $\lambda_{\text{em}} = 475$  nm, dotted line) and emission spectra ( $\lambda_{\text{exc}} = 390$  nm, dashed line) of  $[(\text{LOMe}_4)\text{CuCl}_2(\text{DMF})]$  in DMF solution at 298 K

Table 14: Absorption, excitation and emission data of  $\text{LOMe}_4$  and its metal complexes

compound	abs. $\lambda_{\text{max}}$ <sup>[a]</sup>	exc. $\lambda_{\text{max}}$ <sup>[a][b]</sup>	em. $\lambda_{\text{max}}$ <sup>[c]</sup>	Stokes shift / $\text{cm}^{-1}$	$\phi$ <sup>[d]</sup>
$\text{LOMe}_4$	270 (21260); 298sh (16150); 307sh (17110); 313 (18160); 367 (1110)	361; 392	466	5137	$0.21 \cdot 10^{-3}$
$[(\text{LOMe}_4)\text{MgBr}_2]$	316 (1530); 371 (550)	344sh; 402	464	5449	$3.52 \cdot 10^{-3}$
$[(\text{LOMe}_4)\text{NiBr}_2(\text{DMF})]$	318 (6600); 372 (3860)	307sh; 380sh 395	467	5469	$0.12 \cdot 10^{-3}$
$[(\text{LOMe}_4)\text{CuCl}_2(\text{DMF})]$	316 (14820); 371sh (2290); 439sh (330)	346; 408	475	5901	$0.53 \cdot 10^{-3}$

[a] Absorption, excitation and emission maxima in nm, extinction coefficients  $\epsilon$  in  $\text{Lmol}^{-1}\text{cm}^{-1}$  as measured in DMF solution

[b] Excitation spectra obtained for the maximum emission wavelength

[c] Maximum emission recorded with excitation at  $\lambda_{\text{exc}} = 390$  nm

[d] Quantum yield



### 2.2.9 Conclusions on the suitability of bis-phenoxido pincer complexes as GO model systems

The O,N,O-phenoxido-pincer systems possess a flexible ligand scaffold and various residues can be introduced to the phenol cores. The substituents influence different parameters of the free ligands and complexes. An important aspect is the solubility, which can be increased by using substituents such as *iso*-propyl groups. Increasing solubility, although desired for homogeneous catalysts, in this case leads to a side reaction, the so called coordinative disproportionation. The primarily formed complex systems are binuclear but can be transferred reliably into mononuclear complexes by dissolving in DMF.

Furthermore, the different substituents influence the electrochemical properties of the complexes. The potentials of the  $[\text{OPh}]^{\bullet+}/[\text{OPh}]$  redox couples and the reversibility of the corresponding oxidation processes vary markedly. The ligand centred oxidation of unsubstituted or *meta*-substituted complexes processes mainly irreversibly, even at high scan rates. This largely limits comparison of different measurements but indicates that the formed radicals are highly reactive. Ligands and complexes containing *para-iso*-propyl residues at the phenoxido moieties show reversible oxidation processes. Although the potentials of the  $[\text{OPh}]^{\bullet+}/[\text{OPh}]$  redox couple in corresponding complexes are far higher than the  $[\text{OTyr}]^{\bullet+}/[\text{OTyr}]$  redox couple found in GO (0.01 V), the bis-phenoxido-pincer complexes settle quite well among other known GO model systems. For salen type complexes a potential range for the ligand oxidation of 0.83 V<sup>[148]</sup> to 0.08 V<sup>[137,253]</sup> is observed, potentials for TACN-containing complexes lie between 0.44 V<sup>[132]</sup> and -0.10 V,<sup>[136]</sup> while tripodal complexes show potentials with  $E_{1/2} > 0.80$  V and -0.16 V.<sup>[115]</sup>

The potentials for the reversible copper reduction of all phenoxido-pincer complexes are quite similar but higher than the  $\text{Cu}^{\text{II}}/\text{Cu}^{\text{I}}$  potential found in wild type GO (-0.24 V). This shows that the  $\text{Cu}^{\text{I}}$  state is more favoured for the phenoxido-pincer complexes.

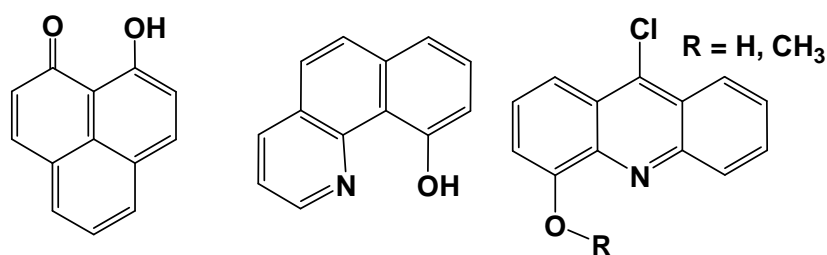
The ligands  $\text{LOH}_2$ ,  $\text{LOH}_3\text{OMe}$  and  $\text{LOH}_2^i\text{Pr}$  as well as their complexes exhibit acid base properties, which seem to be coupled to reductive electrochemistry. Hence copper complexes of bis-phenoxido pincer ligands might be able to act as internal bases in alcohol oxidation. The physical properties of some phenoxido pincer complexes are promising although the corresponding phenoxyl radical species are not (fully) stabilised. Quantification of the catalytic abilities has to be made under reaction conditions in catalytic test reactions (Chapter 7).

## 3.0 Radicals delocalised in aromatic systems

### 3.1 Introduction

As outlined in Chapter 2, substituents in varying positions of the phenoxy ligand influence the stability of the formed radicals. Electron donating substituents generally stabilise phenoxy radicals, while withdrawing substituents are destabilising if they are not located in *ipso*-position, the position of highest electron density.<sup>[171]</sup> Alternatively, radicals can be delocalised in extended aromatic systems. This also leads to high stability of the generated radicals.<sup>[254–256]</sup> Aromatic delocalisation seems to reduce the radical reactivity by “diluting” the amount of spin density per atom.<sup>[166]</sup> Some aromatic systems which have been successfully applied for phenoxy radical stabilisation are the phenalene system,<sup>[257,258]</sup> phenoxazine systems and derivatives,<sup>[259]</sup> flavenoides,<sup>[260]</sup> fluorenyl systems<sup>[261]</sup> or quinoide systems<sup>[42,262]</sup>.

In this thesis, three aromatic scaffolds (each consisting of three anellated six-membered rings) were chosen to investigate the influence of aromatic radical stabilisation on Galactose Oxidase (GO) like phenoxy radicals (Scheme 24): 9-hydroxyphenalene, a phenalene derivative (cf. 3.2), benzo-[h]-quinoline-10-ol a hetero-phenanthrene (cf. 3.3) and 4-alkoxy-9-chloro acridine, a hetero aromatic anthracen analogue, (cf. 3.4).



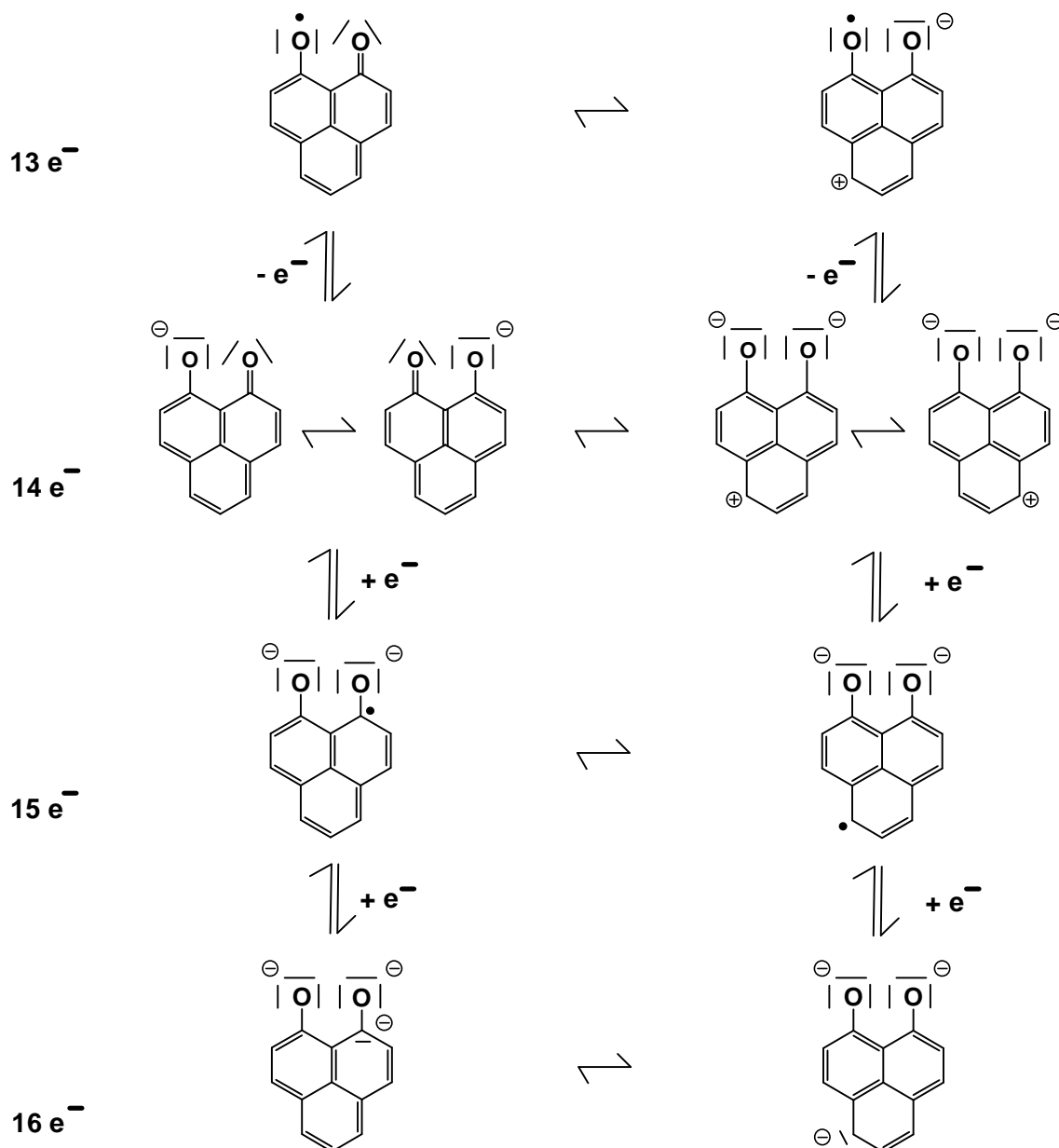
Scheme 24: Aromatic phenoxy type ligands used in this study 9-hydroxyphenalene (left), benzo-[h]-quinoline-10-ol (middle) and 4-alkoxy-9-chloro acridine (right)

### 3.2 9-Hydroxyphenalene (opoH) ligand and complexes

#### 3.2.1 Introduction

9-Hydroxyphenalene (opoH) (Scheme 24, left) was first synthesised by Koelsch *et al.*<sup>[263]</sup> It is a very interesting system for studying proton tautomerism<sup>[264]</sup> and tunnelling

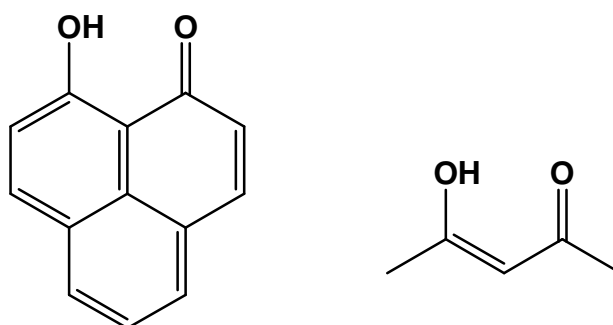
effects<sup>[265]</sup>. Complexes of the deprotonated  $\text{opo}^-$  ligand can be easily reduced (Scheme 25) and have been investigated towards their conducting abilities.<sup>[266–269]</sup>



Scheme 25: Resonance structure of  $\text{opo}^-$  and its reduced and oxidised species

From the coordination chemical point of view,  $\text{opoH}$  can be considered as an acetylacetonate ( $\text{acacH}$ ) analogue (Scheme 26).  $\text{Acac}$  is a frequently used ligand in transition metal chemistry and homoleptic, mononuclear complexes of all transition metals (despite of  $\text{Ag}$  and  $\text{Hg}$ ) as well as for most lanthanides and main group metals have been synthesised and analysed by XRD.  $\text{Opo}$  complexes are expected to be very similar to the corresponding  $\text{acac}$  complexes, however, only a few have been reported so far. Most known  $\text{opo}$  complexes contain main group metals like  $\text{B}^{\text{III}}$ ,<sup>[266,267,270]</sup>  $\text{Si}^{\text{IV}}$ ,<sup>[271]</sup>  $\text{Ge}^{\text{IV}}$ <sup>[271]</sup> or  $\text{Be}^{\text{II}}$ <sup>[270]</sup>. Additionally, there

are a few opo complexes of the f-elements  $\text{Eu}^{\text{III}}$ ,<sup>[272]</sup>  $\text{Er}^{\text{III}}$ ,<sup>[273]</sup>  $\text{Nd}^{\text{III}}$ <sup>[273]</sup> and  $\text{Yb}^{\text{III}}$ <sup>[273]</sup>, while complexes with d-block metals are known for  $\text{Mn}$ ,<sup>[274]</sup>  $\text{Co}$ ,<sup>[274]</sup>  $\text{Ni}$ ,<sup>[274]</sup>  $\text{Fe}$ ,<sup>[274]</sup>  $\text{Cu}$ ,<sup>[274]</sup>  $\text{Zn}$ ,<sup>[274]</sup>  $\text{Rh}$ ,<sup>[275]</sup>  $\text{Pd}$ <sup>[275]</sup> and  $\text{Pt}$ <sup>[275]</sup>. The transition metal complexes have been investigated in view of their photophysical properties but not with regard to their electrochemical properties, complexes of Rh, Pd and Pt have been synthesised and analysed with regard to their cytotoxicity, which has been found to be similar to that of *Cisplatin*, although the originating mechanism is different (phenalenone compounds are intercalating systems).<sup>[275]</sup>



Scheme 26: 9-Hydroxyphenalenone (opoH) (left), a derivative of acetylacetonone (acacH) (right)

Haddon *et al.* synthesised a boron complex containing opo ligands following Eq. 10.



The electrochemical properties of the resulting boron complex and other complexes containing main group metals have been characterised using cyclic voltammetry and spectroelectrochemical EPR spectroscopy.<sup>[270,276]</sup>

Reduction of such complexes led to ligand centred radicals. If more than one opo ligand was present, the reductive radical generation occurred step by step and each ligand has been found to stabilise one unpaired electron (Table 15). Oxidation processes of opo complexes have not been reported.

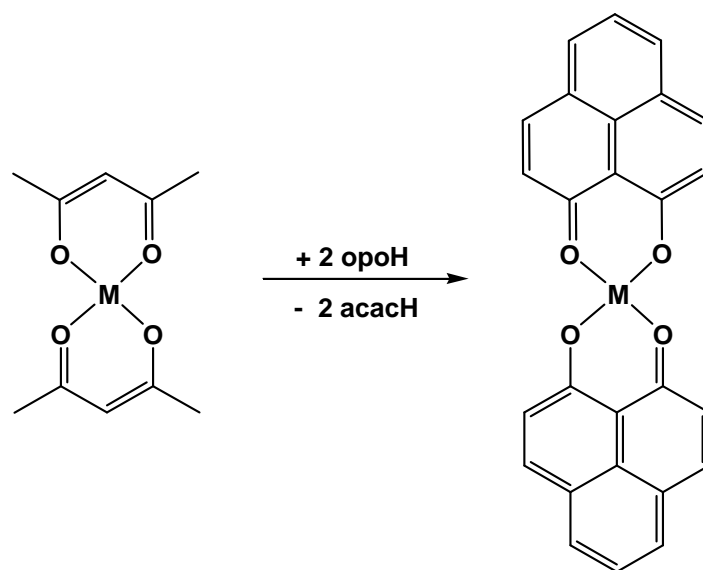
Table 15: Electrochemical potentials of main group metal complexes<sup>[a]</sup>

compound	$E_{1/2}1$	$E_{1/2}2$	$E_{1/2}3$	Lit.
$[(\text{opo})_2\text{Be}]$	-0.73	-1.03	-	270
$[(\text{opo})_2\text{B}]^+$	-0.70	-0.99	-	270
$[(\text{opo})_3\text{Ge}]^+$	-0.94	-1.06	-1.44	271
$[(\text{opo})_3\text{Si}]^+$	-0.95	-1.19	-1.51	271

[a] All potentials in V vs.  $\text{FeCp}_2/\text{FeCp}_2^+$

### 3.2.2 Synthesis and structure analysis of the opo complexes

Complex synthesis was performed by ligand exchange reactions using the corresponding acac complexes as precursors (Scheme 27). The acac complexes were synthesised as published in *Gmelins Handbuch der anorganischen Chemie*.<sup>[277]</sup> The driving force of the exchange reactions probably is the far lower solubility of the opo complexes which is due to  $\pi$ -stacking effects of opo in the solid state. Complex synthesis using  $\text{Cu}^{\text{II}}$ ,  $\text{Fe}^{\text{III}}$ ,  $\text{Ni}^{\text{II}}$  and  $\text{Zn}^{\text{II}}$  compounds were attempted.



Scheme 27: Synthesis of opo complexes

$[\text{Cu}(\text{opo})_2]$ ,  $[\text{Zn}(\text{opo})_2]$ , and  $[\text{Fe}(\text{opo})_3]$  could be obtained as intensely coloured solids in high yields (78-98%). They were characterised by elemental analysis, NMR spectroscopy (or EPR spectroscopy respectively), cyclic voltammetry, UV/vis absorption spectroscopy and spectroelectrochemical methods. Single crystals of the complex  $[\text{Fe}(\text{opo})_3]$ , which is soluble in THF, were obtained by slow evaporation and submitted to a XRD study. Unfortunately, the obtained crystals were of low quality and lacking reflexes in the range of high  $2\theta$  angles. Nevertheless, the crystal structure could be solved and refined in the triclinic space group  $P\bar{1}$ . The refinement parameters - R values and GooF - are not good enough to allow a discussion of the crystal structure (for full data see Appendix). The quality of the molecular structure of  $[\text{Fe}(\text{opo})_3]$ , which is expressed by thermal ellipsoids and standard deviations, is good enough to discuss bond distances and angles, the molecular structure of  $[\text{Fe}(\text{opo})_3]$  is depicted in Figure 20.

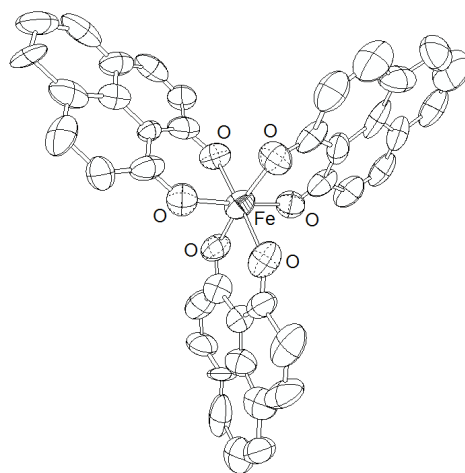


Figure 20: Molecular structure (thermal ellipsoids at 50% probability level) of  $[\text{Fe}(\text{opo})_3]$ , H atoms omitted for clarity

The iron atom in the complex  $[\text{Fe}(\text{opo})_3]$  is octahedrally coordinated, the Fe–O distances vary from 1.9737(7) Å to 2.0073(5) Å. The angles between two *trans*-located O atoms deviate from the ideal 180° (172.93(3)°, 176.18(2)° and 176.77(2)°). The other O–Fe–O angles vary between 85.88(2)° and 95.06(2)°. The bond distances and angles are very similar to those reported for  $[\text{Fe}(\text{acac})_3]$ <sup>[278]</sup>, proving the high similarity of the two ligands.

$[\text{Cu}(\text{opo})_2]$  is expected to be a square planar complex, similar to  $[\text{Cu}(\text{acac})_2]$ . Since no single crystals of  $[\text{Cu}(\text{opo})_2]$  could be obtained, the complex geometry was verified by EPR spectroscopy. Indeed, very similar spectra were obtained for the opo and acac complex (Figure 21). The complexes exhibit isotropic EPR signals with *g* values of 2.124 for  $[\text{Cu}(\text{acac})_2]$  and 2.127 for  $[\text{Cu}(\text{opo})_2]$ . The hyperfine splitting is also slightly different with  $A_{\parallel\text{Cu}} = 76$  G for  $[\text{Cu}(\text{opo})_2]$  and  $A_{\parallel\text{Cu}} = 67$  G for  $[\text{Cu}(\text{acac})_2]$ .

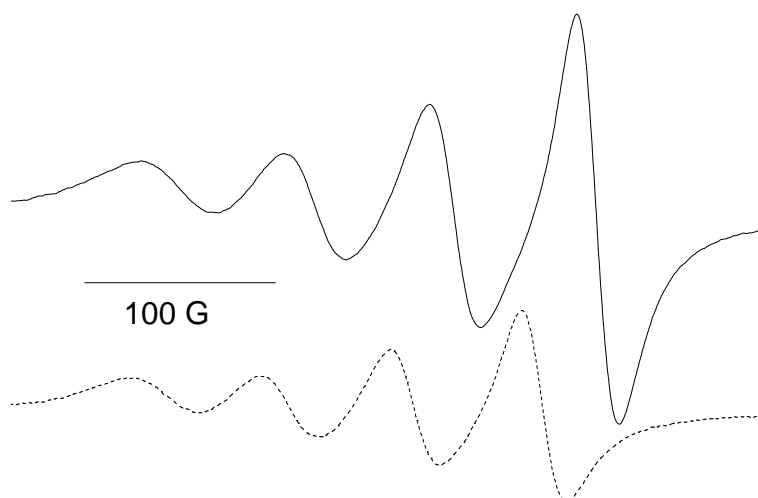


Figure 21: X-band EPR spectra of  $[\text{Cu}(\text{opo})_2]$  (solid line) and of  $[\text{Cu}(\text{acac})_2]$  (dashed line) both measured in DMF at 298 K

High similarity of the EPR signals was also observed for the two Fe<sup>III</sup> complexes, but both spectra are very broad and have isotropic line shape, thus the similarity of the two *g* values is not very indicative for similar complex geometries. [Fe(acac)<sub>3</sub>] exhibits a *g* value of 2.060, while [Fe(opo)<sub>3</sub>] exhibits a *g* value of 2.013 (both complexes were measured at 298 K in THF solution).

The diamagnetic [Zn(opo)<sub>2</sub>] complex was analysed by NMR spectroscopy to establish the opo coordination (Figure 22). Besides a high field shift of all <sup>1</sup>H signals upon coordination the hydroxy proton is missing in the complex. The shift differences of free opoH and [Zn(opo)<sub>2</sub>] (all ~ 0.2 ppm) are high for the protons located near the coordinating functions (H2,H8) and for the proton lying opposite of the oxo-functions (H5).

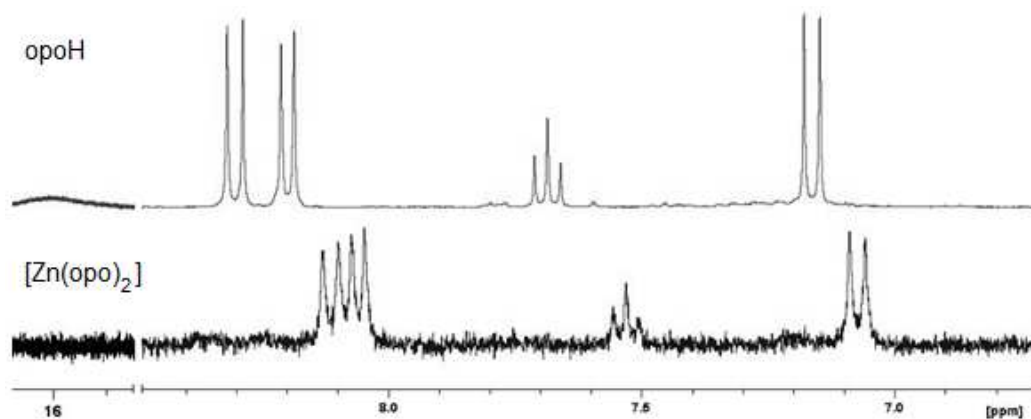


Figure 22: 300 MHz <sup>1</sup>H NMR spectra of opoH (top) and [Zn(opo)<sub>2</sub>] (bottom) measured in [D<sub>6</sub>]-acetone

The [Ni(opo)<sub>2</sub>] complex could not be obtained by the method used for the syntheses of iron, copper and zinc complexes (Scheme 27). Reactions using [Ni(acac)<sub>2</sub>]<sub>n</sub> as metal source resulted in opo compounds with unclear stoichiometry. Elemental analysis of the yellow product revealed 61.12% carbon and 3.73% hydrogen content. This lies in between the values expected for [Ni(opo)<sub>2</sub>] (69.54% C and 3.14% H) and [Ni(acac)<sub>2</sub>]<sub>n</sub> (45.56% C and 5.35% H) and does not fit to the stoichiometry of [Ni(acac)(opo)] (61.07% C and 4.27% H) as well. So it has to be concluded that the product is a crude mixture. The problems with [Ni(opo)<sub>2</sub>] synthesis might arise from the structure of the precursor complex. [Ni(acac)<sub>2</sub>] is known to exist in mononuclear form,<sup>[279]</sup> as binuclear compound,<sup>[280]</sup> in polymeric chains<sup>[281]</sup> or even as cluster compounds<sup>[282]</sup>. Such multinuclear complexes contain terminal and bridging acac ligands. Since the main driving force for the exchange reaction is assumed to be the virtual insolubility of the opo complexes and not decent enthalpy differences, bridging acac ligands

might not be replaced and reaction might thus stop half-way, leaving materials with partly exchanged ligands.

In course of this studies single crystals of the nickel precursor from methanol solutions used for the opo complex synthesis could be obtained. The polygonal green crystals were suitable for XRD; structure solution and refinement in the monoclinic space group  $C2/c$  revealed the structure of a tetranuclear complex of the formula  $[\text{Ni}_4(\text{OCH}_3)_4(\text{acac})_4(\text{CH}_3\text{OH})_4]$ . This compound was already reported by Reibenspeis *et al.* The molecular structure of the cubane like cluster is shown in Figure 23.

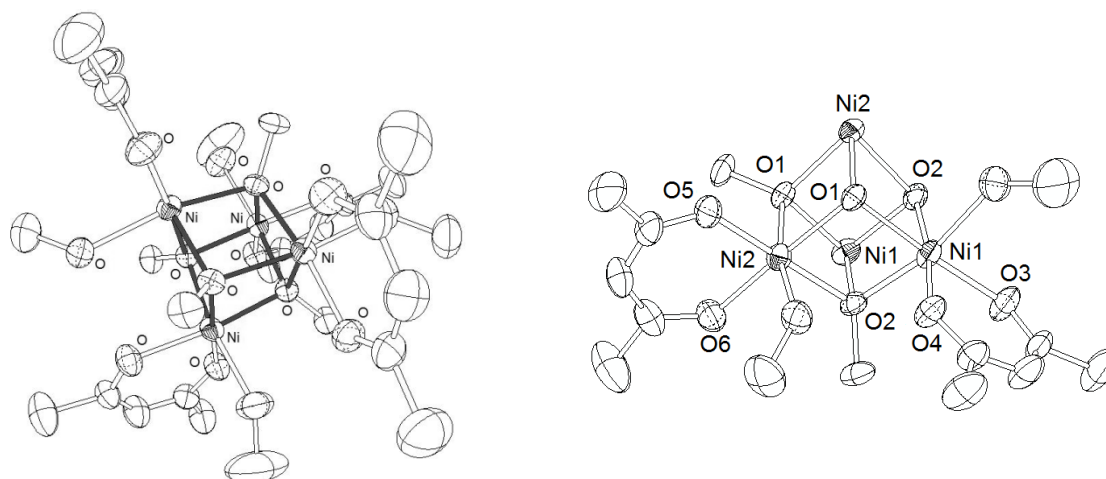


Figure 23: ORTEP-representation (50% probability level) of the Ni–O hetero-cubane cluster; left: view on the complete cluster molecule, H atoms were omitted for clarity;<sup>[283]</sup> right: hetero-cubane with detailed view on two Ni-edges atoms

$[\text{Ni}_4(\text{OCH}_3)_4(\text{acac})_4(\text{CH}_3\text{OH})_4]$  is a derivative of  $[\text{Ni}_4(\text{OCH}_3)_4(\text{dbm})_4(\text{CH}_3\text{OH})_4]_2 \cdot \text{Et}_2\text{O}$  (dbm = dibenzoylmethane) published by Gatteschi *et al.* (Table 16).<sup>[284]</sup>

Table 16: Selected distances and angles of the two cluster type compounds

	$[\text{Ni}_4(\text{OCH}_3)_4(\text{acac})_4(\text{CH}_3\text{OH})_4]$	$[\text{Ni}_4(\text{OCH}_3)_4(\text{dbm})_4(\text{CH}_3\text{OH})_4]_2 \cdot \text{Et}_2\text{O}$		$[\text{Ni}_4(\text{OCH}_3)_4(\text{acac})_4(\text{CH}_3\text{OH})_4]$	$[\text{Ni}_4(\text{OCH}_3)_4(\text{dbm})_4(\text{CH}_3\text{OH})_4]_2 \cdot \text{Et}_2\text{O}$
Ni–Ni-1	3.0645(8)	3.048(3)	Ni–O <sub>methoxide</sub> -2	2.0620(9)	2.072(9)
Ni–Ni-3	3.1146(8)	3.111(3)	Ni–O <sub>chelate</sub> -1	2.0047(9)	1.975(9)
Ni–O <sub>methanol</sub> -1	2.1137(6)	2.127(9)	Ni–O <sub>chelate</sub> -2	2.0265(7)	2.033(9)
Ni–O <sub>methanol</sub> -2	2.1452(8)	2.16(1)	Ni–O–Ni-1	80.77(1)	95.8(4)
Ni–O <sub>methoxide</sub> -1	2.0404(6)	2.02(1)	Ni–O–Ni-2	98.99(2)	100.3(4)

In contrast to  $[\text{Ni}_4(\text{OCH}_3)_4(\text{dbm})_4(\text{CH}_3\text{OH})_4]_2 \cdot \text{Et}_2\text{O}$ ,  $[\text{Ni}_4(\text{OCH}_3)_4(\text{acac})_4(\text{CH}_3\text{OH})_4]$  is highly air stable. Freshly prepared crystals of the latter compound were analysed by far infrared spectroscopy as well as crystals stored six months exposed to air (crystals became



amorphous powders after three to four months) yielding no differences of IR frequencies (Table 17).<sup>[285]</sup>

Table 17: FIR vibration frequencies for the nickel cluster and [Ni(acac)<sub>2</sub>]

cluster / cm <sup>-1</sup>	[Ni(acac) <sub>2</sub> ] / cm <sup>-1</sup>	assignment <sup>[285]</sup>
677	666	δ <sub>ringdeformation</sub> + ν(M–O)
657	-	-
573	579	ν(M–O)
564	563	ν(M–O)
449	452	δ (C–CHO) + ν(M–O)
420	427	δ (O–M–O)
337	-	-
290	-	-
250	-	-

### 3.2.3 Electrochemical properties

Figure 24 shows cyclic voltammograms of opoH measured in DMF/<sup>n</sup>Bu<sub>4</sub>NPF<sub>6</sub> at different temperatures, Table 18 collects the electrochemical data of all compounds.

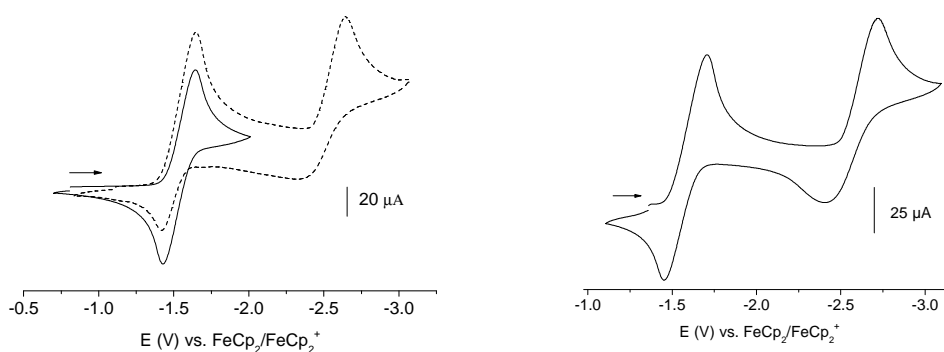


Figure 24: Cyclic voltammograms of opoH measured in DMF/<sup>n</sup>Bu<sub>4</sub>NPF<sub>6</sub> at 298 K (left) and at 273 K (right)

Table 18: Electrochemical properties of opo and its iron and copper complexes<sup>[a]</sup>

compound	$E_{1/2}(M^{n+1}/M^n)$	$E_{1/2}(1_{\text{ligand}})$	$E_{1/2}(2_{\text{ligand}})$
opoH	-	-1.5	-2.5
[Fe(opo) <sub>3</sub> ]	-1.19	-1.3	-1.6
[Fe(acac) <sub>3</sub> ]	-1.13	-1.4	-
[Cu(opo) <sub>2</sub> ]	-1.14 <sup>[b]</sup>	-1.6	-1.9
[Cu(acac) <sub>2</sub> ]	-1.19 <sup>[c]</sup>	-2.5	-
[Zn(opo) <sub>2</sub> ]	-	-1.4	-2.5
[Zn(acac) <sub>2</sub> ]	-	-1.3	-

[a] From cyclic voltammetry measured in DMF/<sup>n</sup>Bu<sub>4</sub>NPF<sub>6</sub> at 298 K with 100 mV/s scan rate; potentials in V vs. FeCp<sub>2</sub>/FeCp<sub>2</sub><sup>+</sup>

[b]  $E_{\text{pc}} = -1.4$  V

[c]  $E_{\text{pc}} = -1.6$  V

The free ligands and complexes can be reduced twice, while oxidation was not observed in the range of 0.0 to 3.0 V. The first reduction process observed for free opoH is clearly reversible, while the second reduction occurs partly reversible at 298 K and fully reversible at 273 K (Figure 24).

For the complex  $[\text{Zn}(\text{opo})_2]$  no metal centred reduction is expected ( $\text{Zn}^{\text{II}} = \text{d}^{10}$ ), thus all observed reduction processes are ligand centred. While oxidation was impossible (0.0 V to 3.0 V) two reduction processes were found. The first reduction process occurs reversible, the second is irreversible, both potentials are similar to those measured for opoH.

For  $[\text{Cu}(\text{opo})_2]$  three reductive processes were found (Figure 25), while oxidation of the complex could not be observed (0.0 to 3.0 V). The first electrochemical reduction reveals an extremely broad peak-to-peak separation and is assigned to the  $\text{Cu}^{\text{II}}/\text{Cu}^{\text{I}}$  redox couple. The redox potential  $E_{1/2}$  of about  $-1.14$  V is very low for  $\text{Cu}^{\text{II}}/\text{Cu}^{\text{I}}$ , but similar to the corresponding redox couple in  $[\text{Cu}(\text{acac})_2]$ .<sup>[286]</sup> Such a potential is indicative for a strongly stabilised  $\text{Cu}^{\text{II}}$  state (or strongly disfavoured  $\text{Cu}^{\text{I}}$  state) as expected for ligands solely providing O atoms for coordination (following the HSAB-principle). Furthermore, two ligand centred reduction waves were observed at  $-1.6$  V and at  $-1.9$  V, both reduction waves are reversible at 298 K and probably due to single reduction of each ligand.

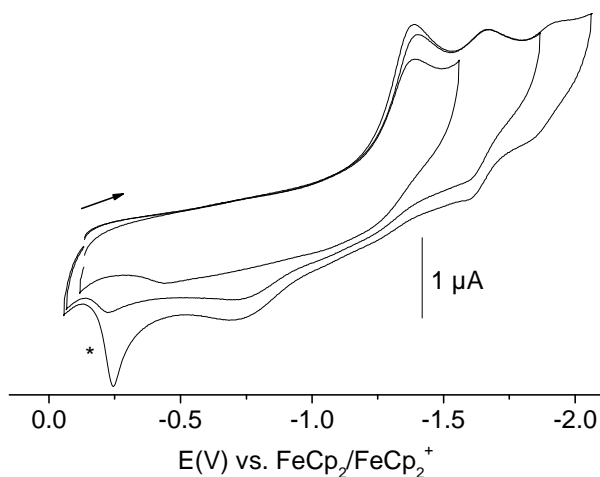


Figure 25: Cyclic voltammograms of crystalline  $[\text{Cu}(\text{opo})_2]$  dissolved in  $\text{DMF}/\text{Bu}_4\text{NPF}_6$  at 298 K, \* marks an adsorption process on the electrode

For  $[\text{Fe}(\text{opo})_3]$  again no oxidation was observed, while three reduction waves were found. The first reduction occurred fully reversible and is assigned to the  $\text{Fe}^{\text{III}}/\text{Fe}^{\text{II}}$  redox couple, since an equivalent reduction is observed for the corresponding acac complex. Further reductions occur irreversibly and ligand centred. Due to the oxidation state of  $\text{Fe}^{\text{III}}$ , the potentials of ligand centred reduction are less negative as those for opoH or  $\text{opo}^-$  in

complexes of  $M^{II}$ . Interestingly, the twofold reduced  $Fe^{II}$  species  $[Fe(opo)_3]^{3-}$  cannot be reduced further, although three opo ligands should allow a fourth reduction (one reduction process per ligand).

### 3.2.4 Absorption spectroscopy and spectroelectrochemistry

The absorption spectra of the opo compounds show typical absorptions for aromatic systems. The free ligand opoH exhibits absorptions in the range of 300 to 450 nm attributed to  $\pi-\pi^*$  transitions (Table 19). For the zinc complex, which does not exhibit charge transfer or d-d absorption bands, most of the absorption maxima were almost identical to those of opoH. This proves that the chromophore is the  $\pi$ -system of opoH (or  $opo^-$ ). For  $Cu^{II}$  most absorption bands are similar to those of opoH, while an absorption band at 481 nm is additionally observed. The absorption band is presumably due to a charge transfer. Furthermore, a very broad and weak long-wavelength absorption is observed at 655 nm, which is a typical  $Cu^{II}$  d-d transition band. This ligand field absorption is similar to that found for  $[Cu(acac)_2]$ .

The spectrum of  $[Fe(opo)_3]$  is also dominated by the  $\pi-\pi^*$  transitions of the opo ligand, however the absorption bands are markedly shifted from those of the free ligand opoH and additional bands at 484 nm and 568 nm were observed, which could both not be found for the corresponding acac complex.

The measured extinction coefficients  $\epsilon$  for opo compounds all seem to be very small, which might be due to incomplete dissolution since all the compounds exhibit extremely poor solubility.

Table 19: Absorption data of opo compounds

compound	$\lambda / \text{nm}$ ( $\epsilon / \text{Lmol}^{-1}\text{cm}^{-1}$ )	solvent
opoH	350 (1231), 393 (331), 413 (607), 428 (502), 438 (719), 451 (131)	DMF
$[Cu(opo)_2]$	294 (5907), 354 (1236), 393 (331), 414 (494), 430 (456), 439 (569), 453 (198), 481 (56), 655 (7)	DMF
$[Cu(acac)_2]$	376sh (274), 639 (56), 655 (13)	DMF
opoH	235 (950), 257 (607), 265 (567), 350 (1228), 393 (296), 414 (538), 430 (397), 439 (607)	THF
$[Fe(opo)_3]$	263sh (1155), 331 (590), 375 (907), 428 (324), 439 (350), 455 (363), 484 (372), 568 (31)	THF
$[Fe(acac)_3]$	273 (28449), 353 (4154), 435 (4193)	THF
opoH	350 (1230), 393 (333), 413 (606), 428 (504), 438 (717), 451 (133)	$CH_3OH$
$[Zn(opo)_2]$	351 (1012), 393 (239), 414 (440), 429 (348), 438 (504), 453 (67)	$CH_3OH$

To allow further assignment of absorption bands and to characterise the complex species obtained by electrochemical reduction, spectroelectrochemical measurements were carried out. Upon the first reduction ( $\text{Cu}^{\text{II}}/\text{Cu}^{\text{I}}$ ) the spectrum is almost identical to the parent spectrum (Figure 26).

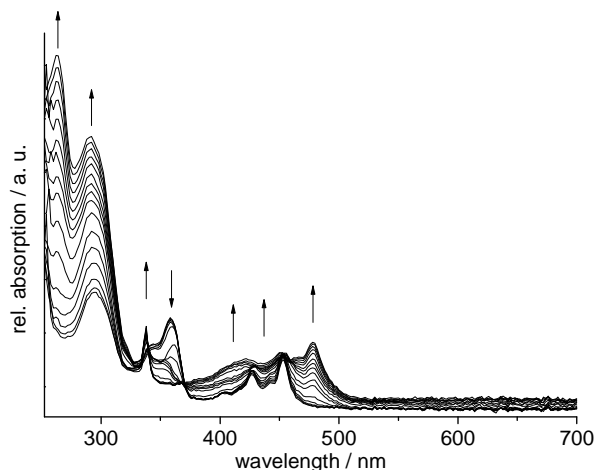


Figure 26: Absorption spectra of  $[\text{Cu}(\text{opo})_2]$  recorded during reduction at  $-2.0$  V in  $\text{DMF}/n\text{Bu}_4\text{NPF}_6$  solution

Upon further reduction (at  $-2.0$  V), the  $\pi\text{-}\pi^*$  bands are largely modified. The structured absorption band at about 350 nm is blue-shifted (to 338 nm), the strong band at 295 nm is more than doubled in intensity and the structured absorption band in the visible range is broadened and red-shifted showing the long-wavelength maximum now at 480 nm (Figure 26). Very probably these changes indicate the formation of a  $[\text{Cu}^{\text{I}}(\text{opo}^{2-\bullet})(\text{opo}^-)]$  complex. The offset of the spectra in the low-energy end (700 nm) might be due to precipitation of generated species in DMF solution, by deposition of side products at the platinum electrode or might be a very broad and weak band caused by dimerisation of radical species.<sup>[287]</sup>

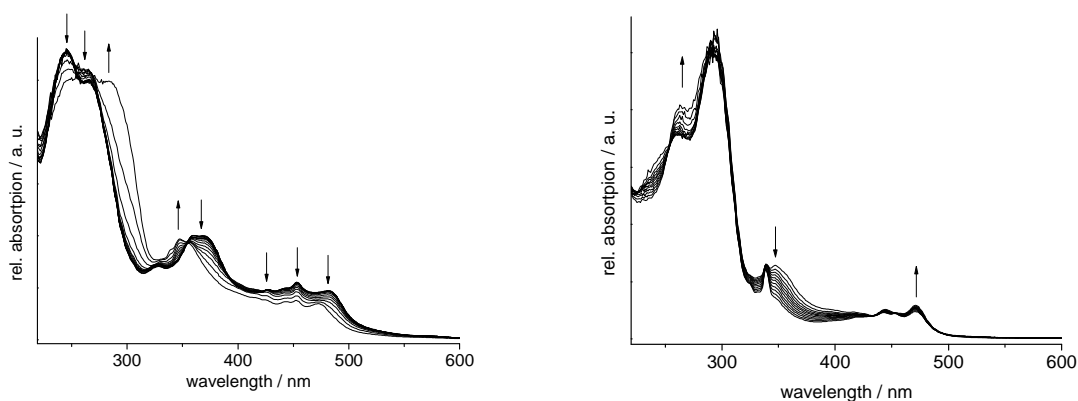


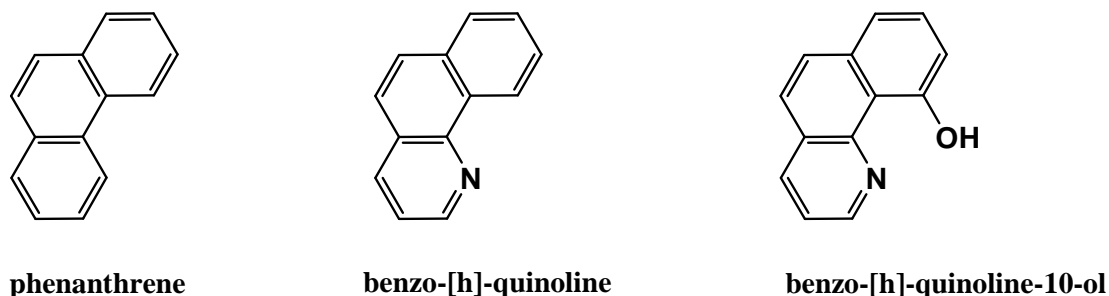
Figure 27: Absorption spectra of  $[\text{Fe}(\text{opo})_3]$  recorded during reduction at  $-1.3$  V (left) and at  $-2.5$  V (right) in  $\text{THF}/n\text{Bu}_4\text{NPF}_6$  solution

The absorption spectra of  $[\text{Fe}(\text{opo})_3]$  detected upon reduction cannot be interpreted easily. At  $-1.3$  V the compound still exhibits the typical absorption bands for opo complexes, spectral changes are found for the long-wavelength absorption band, which becomes less intense as well as the absorption band at 370 nm, while a new absorption band at 294 nm rises. Upon reduction at  $-2.5$  V these processes continue, only the band at 472 nm again increases in intensity as well as a new UV absorption band at 260 nm. After reduction to  $-2.5$  V the absorption bands of  $[\text{Fe}(\text{opo})_3]$  have largely changed without showing any new absorption in the visible range. It has to be considered that the main consequence from electrochemical reduction is complex degradation. Generation of a radical species should have been accompanied by a similar long-wavelength band as found for  $[\text{Cu}(\text{opo})_2]$ . This conclusion is further supported by electrochemical measurements, which showed at least one reversible ligand centred reduction for the copper complex, but no reversible ligand centred reduction for the iron complex.

### 3.3 Benzo-[h]-quinoline-10-ol (bqOH) complexes

#### 3.3.1 Introduction

Benzo-[h]-quinoline-10-ol (bqOH) is a derivative of benzo-[h]-quinone and generally speaking, a phenanthrene (Scheme 28). BqOH and corresponding complexes  $[\text{M}(\text{bqO})_n]$  should be able to form phenoxy radicals upon oxidation, while the aromatic scaffold might contribute to its stabilisation.

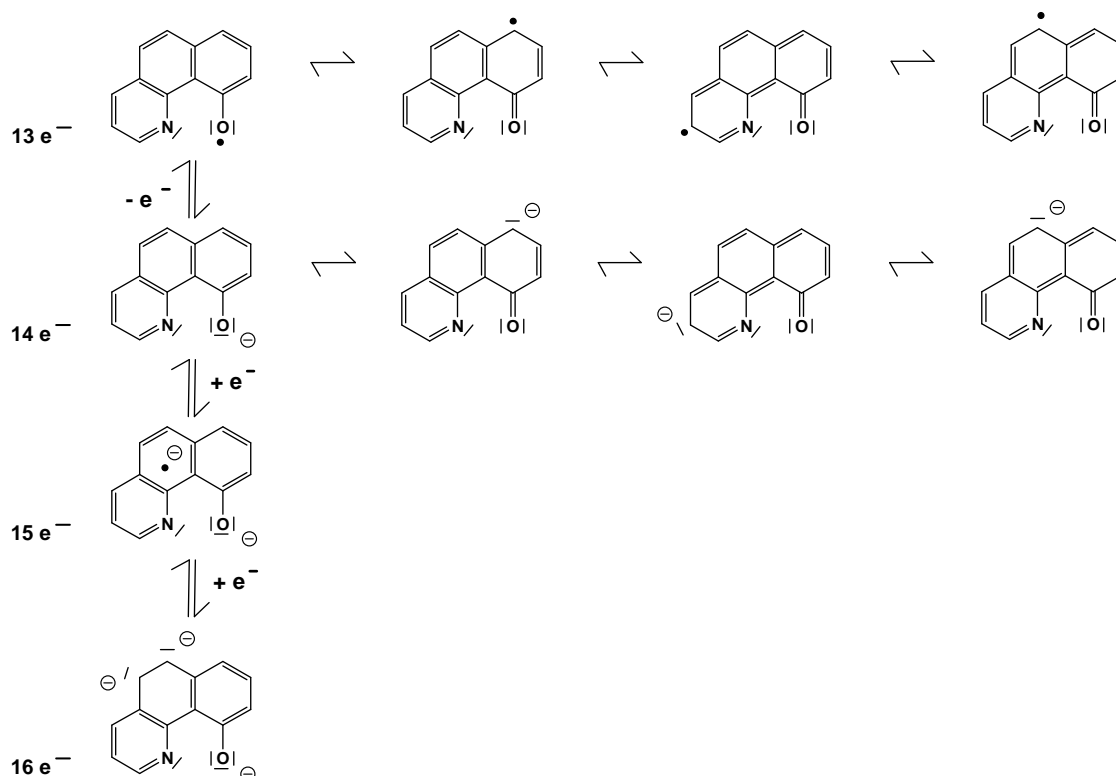


Scheme 28: Aromatic systems with phenanthrene scaffold

So far reports on the bqOH ligand and its complexes are scarce. Its  $\text{Be}^{\text{II}}$  complex<sup>[288]</sup> and

its  $\text{Zn}^{\text{II}}$  complex<sup>[289]</sup> have been used as light emitting diodes and their luminescence properties have been analysed.<sup>[288,289]</sup> Furthermore, an  $\text{Au}^{\text{III}}$  complex  $[\text{Au}(\text{bqO})_2\text{Cl}]$ <sup>[290]</sup> and a  $\text{Cu}^{\text{II}}$  complex  $[\text{Cu}(\text{bqO})_2]$ <sup>[291]</sup> are reported.

In the present study the bqOH copper complexes  $[(\text{bqO})_2\text{Cu}]$ ,  $[(\text{bqOH})\text{CuCl}_2]$  and  $[(\text{bqOH})\text{CuBr}_2]$  were synthesised and their electrochemical properties were analysed. The bqO ligand system is expected to be able to form radicals through oxidation or reduction, stabilised by aromatic delocalisation (Scheme 29).



Scheme 29: Redox states of bqO<sup>-</sup>

### 3.3.2 Synthesis of bqOH complexes

Synthesis of complexes containing bqOH (or bqO<sup>-</sup>) as a ligand is quite simple. A suitable metal source ( $\text{CuCl}_2$ ,  $\text{CuBr}_2$  or  $\text{Cu}(\text{OAc})_2$  respectively) and bqOH, both dissolved in methanol, are mixed without additional base. The products  $[\text{Cu}(\text{bqOH})\text{Cl}_2]$ ,  $[\text{Cu}(\text{bqOH})\text{Br}_2]$  and  $[\text{Cu}(\text{bqO})_2]$  are obtained as brown precipitates in moderate yields (50-70%) and show extremely poor solubility in most solvents (even if very polar solvents such as MeCN or DMF are used). Thus crystallisation of the bqOH complexes failed. Instead, the three complexes were analysed by elemental analysis, EPR spectroscopy, cyclic voltammetry, absorption

spectroscopy and spectroelectrochemical methods.

### 3.3.3 EPR spectroscopy

EPR spectra of the copper compounds were measured on solid samples at 298 K. All complexes exhibit axial spectra with  $g_{\parallel} > g_{\perp}$  and only marginal variations in  $g$  values and  $g$  anisotropy ( $\Delta g$ ). The observed  $g$  values lie in the range expected for  $\text{Cu}^{\text{II}}$  complexes (Table 20). The signal shape indicates the complex geometries to be either square planar or octahedral elongated in the solid state.

Table 20: X-band EPR data for the three bqOH complexes<sup>[a]</sup>

compound	$g_{av}$ <sup>[b]</sup>	$g_{\parallel}$	$g_{\perp}$	$\Delta g$ <sup>[c]</sup>	symmetry <sup>[d]</sup>
[Cu(bqO) <sub>2</sub> ]	2.113	2.233	2.053	0.180	SQ (or OE)
[Cu(bqOH)Cl <sub>2</sub> ]	2.112	2.229	2.053	0.176	SQ (or OE)
[Cu(bqOH)Br <sub>2</sub> ]	2.104	2.220	2.056	0.164	SQ (or OE)

[a] Spectra were measured on solid samples at 298 K

[b]  $g_{av}$  = averaged  $g$  value =  $(g_{\parallel} + 2 g_{\perp}) / 3$ ;

[c]  $\Delta g = g_{\parallel} - g_{\perp}$

[d] SQ = square planar, OE = octahedral elongated

### 3.3.4 Electrochemical properties

Electrochemical properties were analysed by cyclic voltammetry, data are summarised in Table 21 and a representative plot is shown in Figure 28. For the copper complexes the first reduction occurs reversibly around 0.2 V and can be assigned to the  $\text{Cu}^{\text{II}}/\text{Cu}^{\text{I}}$  redox couple. The potentials increase along the series of the coligands  $\text{Br}^- < \text{Cl}^- < \text{RO}^-$  and show very high potentials which lie close to the oxidation waves of the complexes. Therefore the  $\text{Cu}^{\text{II}}/\text{Cu}^{\text{I}}$  couple is detected best upon starting from the  $\text{Cu}^{\text{I}}$  side (Figure 28).

Table 21: Summary of the electrochemical data of bqOH and the three bqOH copper complexes<sup>[a]</sup>

compound	$E_{1/2}$ oxidation	$E_{1/2}$ $\text{Cu}^{\text{II}}/\text{Cu}^{\text{I}}$	$E_{pc}$ reduction
bqOH	0.63(irr) <sup>[b]</sup>	-	-1.50
[Cu(bqO) <sub>2</sub> ]	0.62	0.36	-1.13
[Cu(bqOH)Cl <sub>2</sub> ]	0.55	0.23	-1.49
[Cu(bqOH)Br <sub>2</sub> ]	0.74	0.16	-1.10

[a] From cyclic voltammetry in MeCN/<sup>n</sup>Bu<sub>4</sub>NPF<sub>6</sub> solutions; potentials in V vs. FeCp<sub>2</sub>/FeCp<sub>2</sub><sup>+</sup>

[b]  $E_{pa}$

Further reduction of the complexes occurs irreversibly at less negative potentials as observed for the free ligand. The two complexes  $[\text{Cu}(\text{bqOH})\text{Cl}_2]$  and  $[\text{Cu}(\text{bqOH})\text{Br}_2]$  show further irreversible reduction at more negative potentials. The decomposition is surely induced by halogenide abstraction upon electrochemical reduction and followed by typical subsequent reactions.<sup>[292–294]</sup> The copper complexes can be oxidised reversibly in a similar range as the free ligand.

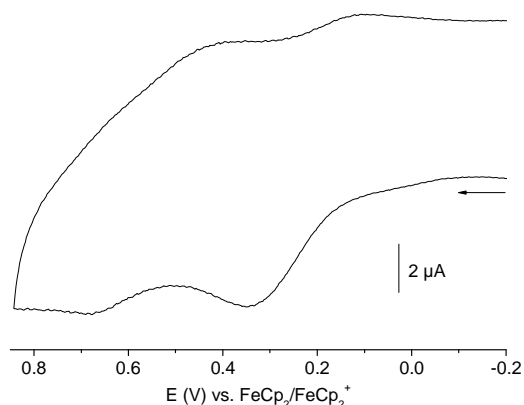


Figure 28: Cyclic voltammogram of  $[\text{Cu}(\text{bqOH})\text{Cl}_2]$  in  $\text{MeCN}/n\text{Bu}_4\text{NPF}_6$  at 298 K measured with 100 mV/s scan rate

### 3.3.5 UV/vis absorption spectroscopy

Characterisation of the copper complexes and bqOH was carried out in MeCN solution at 298 K in the range of 200 to 1000 nm, Table 22 summarises the absorption maxima.

Table 22: Absorption data of the bqOH compounds<sup>[a]</sup>

compound	$\lambda / \text{nm} (\epsilon / \text{Lmol}^{-1}\text{cm}^{-1})$
bqOH	304 (3754), 357 (5667), 369 (6382)
$[\text{Cu}(\text{bqO})_2]$	352 (4710), 371 (4603), 413 (4602)
$[\text{Cu}(\text{bqOH})\text{Cl}_2]$	354 (1868), 370 (1907), 410 (1390)
$[\text{Cu}(\text{bqOH})\text{Br}_2]$	312sh (2502), 382 (2530), 439sh (1422)

[a] Measured in MeCN at 298 K

The absorption bands for the free bqOH ligand lie in the range of 300 to 370 nm and are assigned to  $\pi\text{-}\pi^*$  transition. In the copper complexes similar  $\pi\text{-}\pi^*$  transition is observed, but complex absorption bands are shifted relative to the bands of the free ligand. Additionally, there are absorption bands at 410 to 440 nm found for the copper complexes, which are assigned to be CT absorption bands. Due to the very low solubility of the complexes no long-wavelength bands (d-d absorption bands) could be detected. The determined extinction coefficients  $\epsilon$  are



small, presumably due to the low solubility of the bqO compounds, which might have been dissolved incompletely.

To characterise the oxidised and reduced species of the parent complexes  $[\text{Cu}(\text{bqOH})\text{Cl}_2]$  and  $[\text{Cu}(\text{bqOH})\text{Br}_2]$  spectroelectrochemical measurements in  $\text{MeCN}/n\text{Bu}_4\text{NPF}_6$  solution were performed (Table 23 and Figure 29).

Table 23: Absorption data of spectroelectrochemical measurements<sup>[a]</sup>

compound	oxidation	parent ( $\text{Cu}^{\text{II}}$ )	$\text{Cu}^{\text{II}} \rightarrow \text{Cu}^{\text{I}}$
$[\text{Cu}(\text{bqOH})\text{Cl}_2]$	240, 389, 525	211, 238, 370	214, 240, 271sh
$[\text{Cu}(\text{bqOH})\text{Br}_2]$	236, 294, 325, 623	208, 244, 273, 312sh, 382	206, 239, 269sh, 309, 370,

[a] Spectra were recorded using  $\text{MeCN}/n\text{Bu}_4\text{NPF}_6$  solutions at 298 K

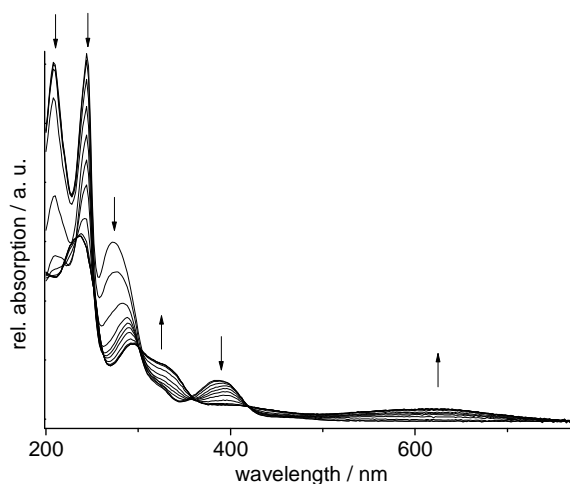


Figure 29: Absorption spectra of  $[\text{Cu}(\text{bqOH})\text{Br}_2]$  recorded upon electrochemical oxidation (+1.5 V) in  $\text{MeCN}/n\text{Bu}_4\text{NPF}_6$  solution

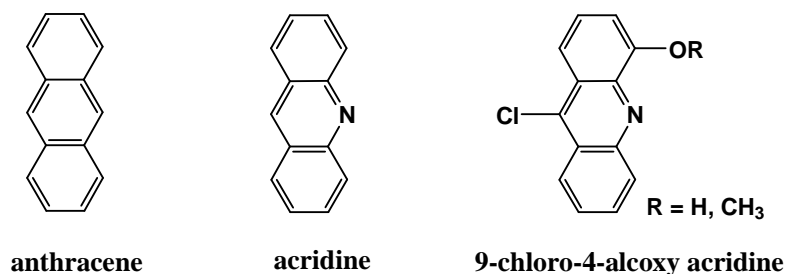
For both complexes absorption bands in the long-wavelength range, emerging upon oxidation can be assigned to copper radical LMCT and are indicative for ligand oxidation. For  $[\text{Cu}(\text{bqOH})\text{Cl}_2]$  a band at 525 nm ( $19050 \text{ cm}^{-1}$ ) is detected, while the  $[\text{Cu}(\text{bqOH})\text{Br}_2]$  complex exhibits a band at 623 nm ( $16050 \text{ cm}^{-1}$ ). The difference of  $3000 \text{ cm}^{-1}$  in the absorption maxima of both species is due to the different coligands, which influence the charge transfer energy of the ligand centred radical: The energy for the LMCT absorption band reflects the energy gap between orbitals localised at the metal ion and those localised at the ligand site. Interactions of soft acids and soft bases (following the HSAB principle) are ideal, since their orbitals lie closer than those of soft acids and hard bases. The softer halogenide (the softer *Lewis* base) is the bromido coligand and as a consequence the frontier

orbitals in this complex lie closer and the energy of the charge transfer absorption is smaller than for the chlorido coligands. The absorption band thus is markedly red-shifted.

### 3.4 Acridine complexes

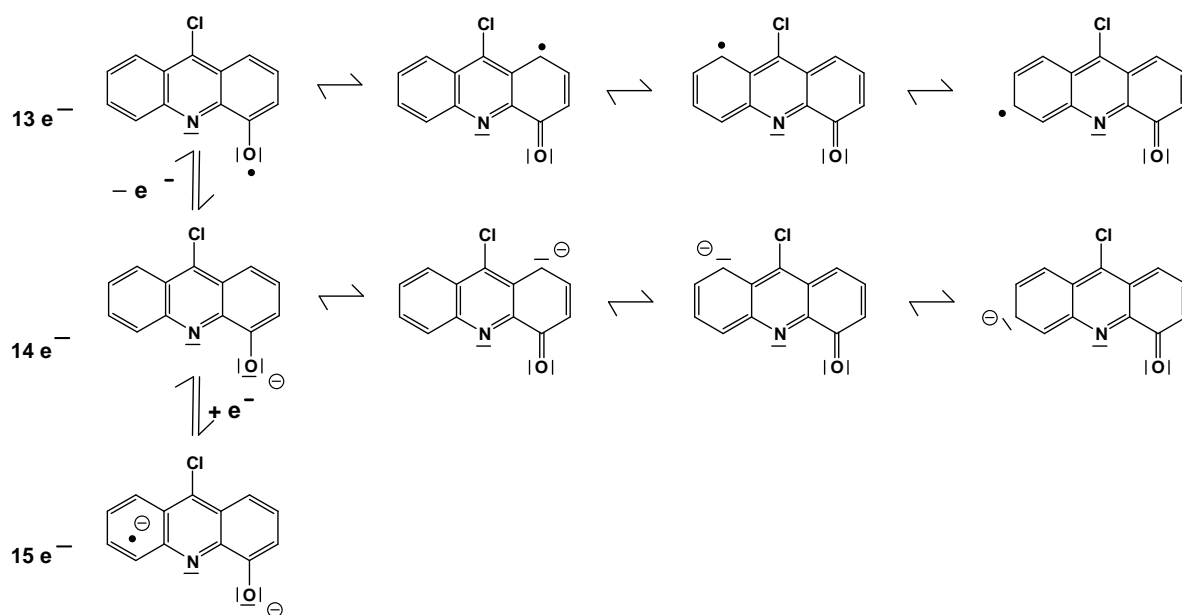
#### 3.4.1 Introduction

A third ligand type providing an aromatic scaffold for radical delocalisation is the anthracen derivative acridine (Scheme 30).



Scheme 30: Aromatic systems with phenanthrene scaffold

Complexes containing this type of ligand are expected to form radical species upon oxidation (and reduction), with the unpaired electron delocalised in the aromatic scaffold and therefore stabilised. An overview on the different species is shown in Scheme 31.

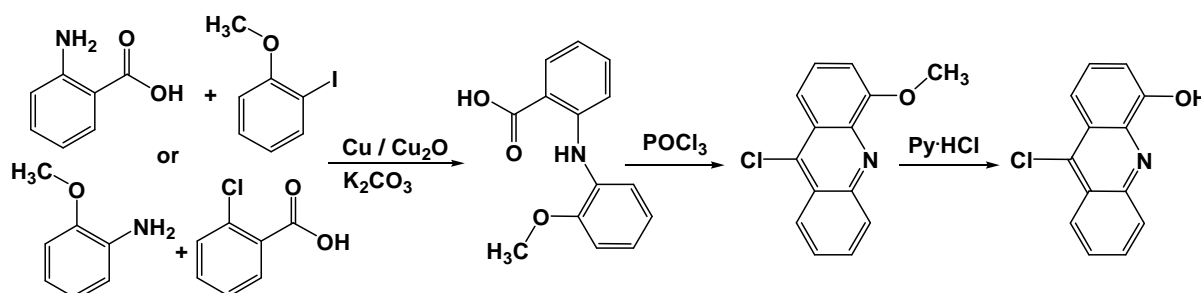


Scheme 31: Redox states of  $acrO^-$

There are reports on some symmetric acridine derivatives possessing an O,N,O donor set which were used as ligands in transition metal coordination using  $\text{Co}^{\text{II}}$ ,  $\text{Ni}^{\text{II}}$ ,  $\text{Zn}^{\text{II}}$  and  $\text{Cu}^{\text{II}}$ .<sup>[295]</sup> The asymmetric acridine derivative 9-chloro-4-methoxy acridine (acrOMe) has already been synthesised,<sup>[296]</sup> but not used as ligand, yet.

### 3.4.2 Synthesis and structure of ligands and complexes

9-chloro-4-methoxy acridine (acrOH) and 9-chloro-4-methoxy acridine (acrOMe) were synthesised by a *Jourdan-Ullmann* coupling reaction followed by a cyclisation reaction (Scheme 32).<sup>[295c,297]</sup> For the *Jourdan-Ullmann* coupling reaction two different types of starting materials can be used. Due to the chosen isolation method, which is a pH dependent precipitation the ligands were obtained in high purity but low yields (25%). The second reaction step of the synthesis is a cyclisation induced by  $\text{POCl}_3$ , leading to the 9-chloro-4-methoxy-acridine (acrOMe). AcrOMe can be transformed into the 9-chloro-4-hydroxy acridine (acrOH) by a demethoxylation using pyridinium hydrochloride.

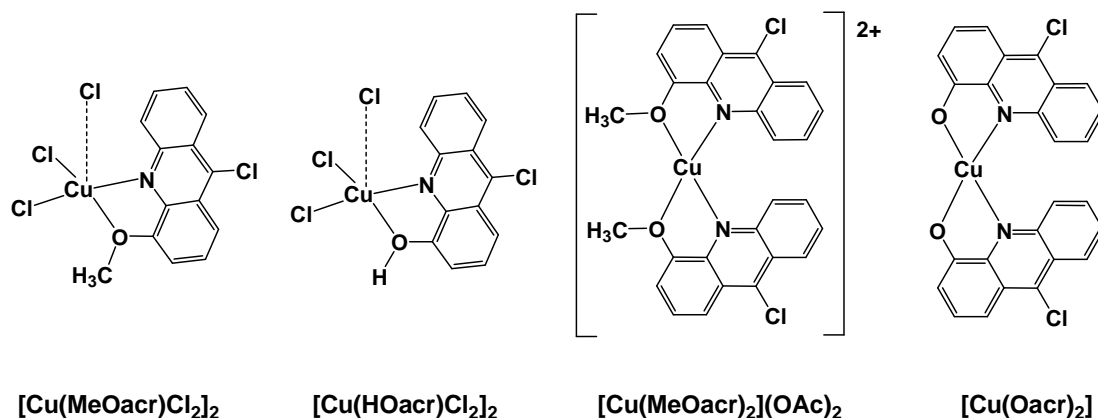


Scheme 32: Overview on the different steps of the acridine ligand synthesis

The resulting ligands acrOMe and acrOH were reacted with  $\text{CuCl}_2$  in 1:1 stoichiometry and also in 2:1 ratio with  $\text{Cu}(\text{OAc})_2$ . The resulting copper complexes were found to be  $[\text{Cu}(\text{acrOMe})\text{Cl}_2]_2$ ,  $[\text{Cu}(\text{acrOH})\text{Cl}_2]_2$ ,  $[\text{Cu}(\text{acrO})_2]$  and  $[\text{Cu}(\text{acrOMe})_2](\text{OAc})_2$ . The complexes are sparingly soluble and exhibit black ( $[\text{Cu}(\text{acrO})_2]$ ), brown ( $[\text{Cu}(\text{acrOMe})\text{Cl}_2]_2$  and  $[\text{Cu}(\text{acrOH})\text{Cl}_2]_2$ ) or green ( $[\text{Cu}(\text{acrOMe})_2](\text{OAc})_2$ ) colour. The complexes were analysed by elemental analysis and EPR spectroscopy, detailed electrochemical, spectroelectrochemical and absorption measurements were carried out as well.

In Scheme 33 the presumed coordination geometries of the mononuclear complexes or complex fragments are depicted. While the complexes containing chlorido coligands were found to be binuclear compounds, the complexes containing two acridine ligands are  $\eta^2$

coordinated. Assuming a coordination geometry similar to those of reported copper phenoxazine complexes,<sup>[298]</sup> the compounds should be square planar with tetrahedral distortion. The complexes  $[\text{Cu}(\text{acrOMe})_2](\text{OAc})_2$  and  $[\text{Cu}(\text{acrO})_2]$  shown in Scheme 33 are represented as *cis* isomers, although this geometrical information could not be obtained by the measurements performed. Regarding the high sterical demand of the acridine scaffold, it can also be assumed that both compounds possibly are *trans* isomers.

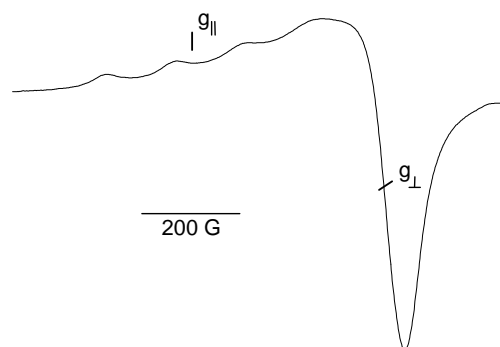


Scheme 33: Mononuclear complex units of acridine compounds with bridging ligands (dotted bonds)

### 3.4.3 EPR spectroscopy

EPR spectra of the copper complexes were measured on solid samples at 298 K and on glassy frozen MeCN solutions at 110 K. All complexes exhibit axial spectra with  $g_{\parallel} > g_{\perp}$  and no indication of a half field signal. All observed  $g$  values lie in the range expected for  $\text{Cu}^{\text{II}}$  complexes (Table 24), a closer look reveals small differences in  $g$  values and  $g$  anisotropy ( $\Delta g$ ).

The complexes  $[\text{Cu}(\text{acrOMe})\text{Cl}_2]_2$  and  $[\text{Cu}(\text{acrOH})\text{Cl}_2]_2$  in the solid state exhibit ill resolved spectra, which are presumably due to chlorido bridged dimers of square pyramidal geometry.<sup>[230,231,240]</sup> The solid sample of  $[\text{Cu}(\text{acrOMe})_2](\text{OAc})_2$  exhibits a resolved  $g_{\parallel}$  component with a coupling constant ( $A_{\parallel\text{Cu}}$ ) of 148 G (Figure 30), which is typical for mononuclear copper complexes. The corresponding  $\text{acrO}^-$  complex  $[\text{Cu}(\text{acrO})_2]_2$  does not exhibit a spectrum with hyperfine splitting, which indicates a binuclear compound. Thus, a coordination with bridging deprotonated oxido functions might be present.

Figure 30: X-band EPR spectrum of  $[\text{Cu}(\text{acrOMe})_2](\text{OAc})_2$  in the solid state at 298 KTable 24: X-band EPR data of copper complexes<sup>[a]</sup>

compound	$g_{av}$	$g_{  }$	$g_{\perp}$	$A_{  \text{Cu}}$	$\Delta g$	state / T
$[(\text{acrOMe})\text{CuCl}_2]_2$	2.188	2.301	2.131	-	0.170	solid / 298 K
$[(\text{acrOH})\text{CuCl}_2]_2$	2.083	2.240	2.005	-	0.235	solid / 298 K
$[\text{Cu}(\text{acrOMe})_2](\text{OAc})_2$	2.139	2.261	2.078	148	0.183	solid / 298 K
$[\text{Cu}(\text{acrO})_2]_2$	2.212	2.355	2.141	-	0.214	solid / 298 K
$[(\text{acrOMe})\text{CuCl}_2(\text{MeCN})_2]$	2.139	2.323	2.047	141	0.276	MeCN / 110 K
$[(\text{acrOH})\text{CuCl}_2(\text{MeCN})_2]$	2.133	2.316	2.042	147	0.274	MeCN / 110 K
$[\text{Cu}(\text{acrOMe})_2](\text{OAc})_2$	2.134	2.305	2.049	150	0.256	MeCN / 110 K
$[\text{Cu}(\text{acrO})_2(\text{MeCN})_2]$	2.115	2.272	2.036	-	0.236	MeCN / 110 K

[a]  $g_{av}$  = averaged  $g$  value =  $(g_{||} + 2 g_{\perp}) / 3$ ;  $\Delta g = g_{||} - g_{\perp}$

When dissolving the solids in MeCN and measuring the glassy frozen solutions at 110 K, axial EPR signals were observed. This indicates presence of mononuclear species, which presumably are solvent complexes  $[(\text{acrO})\text{CuCl}_2(\text{MeCN})_2]$ .<sup>[226,241–244]</sup> For the complex  $[\text{Cu}(\text{acrOMe})_2](\text{OAc})_2$ , which is already mononuclear in the solid state, incorporation of MeCN is possible and would explain the differences between spectra measured on solid samples and on MeCN solutions. The resolved coupling constants ( $A_{||\text{Cu}}$ ) lie at about 150 G for the  $g_{||}$  component and are typical for square-based pyramidal (SP), tetragonally elongated octahedral (OE) or trigonal bipyramidal (TBP) configured  $\text{Cu}^{\text{II}}$  complexes.<sup>[226,241–244]</sup>

### 3.4.4 Electrochemical properties

The free ligands and copper complexes were characterised by cyclic voltammetry (Table 25). The copper complexes all show a reversible reduction wave around 0.15 V attributed to the  $\text{Cu}^{\text{II}}/\text{Cu}^{\text{I}}$  redox couple. Markedly lower, at  $-0.31$  V, lies the corresponding potential of  $[\text{Cu}(\text{acrO})_2]$  (Figure 31). The difference from the potential of  $[\text{Cu}(\text{acrOMe})_2](\text{OAc})_2$  can be explained by the neutral charge of  $[\text{Cu}(\text{acrO})_2]$  (deprotonated ligands). Further reduction of all complexes as well as first reduction of the free ligands occurs irreversibly around  $-1.4$  V.

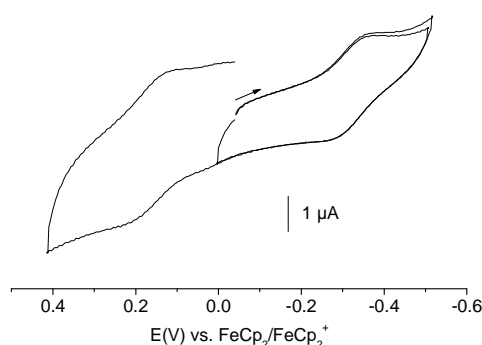


Figure 31: Cyclic voltammograms of  $[\text{Cu}(\text{acrO})_2(\text{MeCN})_2]$ , measured at 298 K with 100 mV/s scan rate in  $\text{MeCN}/n\text{Bu}_4\text{NPF}_6$  solution

Table 25: Summary of electrochemical data<sup>[a]</sup>

compound	$E_{\text{pa}}$	$E_{1/2} \text{Cu}^{\text{II}}/\text{Cu}^{\text{I}}$	$E_{\text{pc}}$
acrOMe	1.04	-	-1.44
$[\text{Cu}(\text{acrOMe})\text{Cl}_2(\text{MeCN})_2]$	1.01	0.18	-1.46
$[\text{Cu}(\text{acrOMe})_2](\text{OAc})_2$	0.76, 0.94	0.14	-1.30
acrOH	0.78, 1.30	-	-1.15
$[\text{Cu}(\text{acrOH})\text{Cl}_2(\text{MeCN})_2]$	0.54 <sup>[b]</sup> , 0.98	0.13	-1.40
$[\text{Cu}(\text{acrO})_2(\text{MeCN})_2]$	0.17 <sup>[b]</sup>	-0.31	-1.40

[a] From cyclic voltammetry in  $\text{MeCN}/n\text{Bu}_4\text{NPF}_6$  solutions; potentials in V vs.  $\text{FeCp}_2/\text{FeCp}_2^+$

[b] Reversible oxidation potential is given as  $E_{1/2}$

The oxidation properties of the different systems vary. For the complexes oxidation occurs between 0.17 V ( $[\text{Cu}(\text{acrO})_2(\text{MeCN})_2]$ ) and 1.01 V ( $[\text{Cu}(\text{acrOMe})\text{Cl}_2(\text{MeCN})_2]$ ). Since a copper centred oxidation is not expected ( $\text{Cu}^{\text{II}}/\text{Cu}^{\text{III}}$ ) this electron transfer is assigned to a ligand centred oxidation. For the free ligands acrOMe and protonated acrOH these waves were observed at markedly higher potentials, while for  $[\text{Cu}(\text{acrOH})\text{Cl}_2(\text{MeCN})_2]$  and  $[\text{Cu}(\text{acrO})_2(\text{MeCN})_2]$  these waves were reversible and at rather low potentials, the oxidation occurs irreversibly for the free ligands and complexes  $[\text{Cu}(\text{acrOMe})\text{Cl}_2(\text{MeCN})_2]$  and  $[\text{Cu}(\text{acrOMe})_2](\text{OAc})_2$ . Thus the binding situation in  $[\text{Cu}(\text{acrOH})\text{Cl}_2(\text{MeCN})_2]$  and  $[\text{Cu}(\text{acrO})_2(\text{MeCN})_2]$  strongly stabilises the generation of phenoxy radicals. This is further substantiated by UV/vis and spectroelectrochemical experiments.

### 3.4.5 UV/vis absorption spectroscopy and spectroelectrochemistry

Absorption measurements on all compounds were performed in MeCN solution. Due to the large aromatic scaffold of the acridine system, the absorption spectra of all compounds show very intense and characteristic absorption bands (Table 26) attributed to  $\pi-\pi^*$  transitions. The bands recorded for the two ligands differ slightly (red-shifted for acrOH) and

also the copper complexes reveal similar absorption maxima, but different absorption intensities, compared to their free ligands. The spectrum of  $[\text{Cu}(\text{Oacr})_2(\text{MeCN})_2]$  deviates markedly from the spectrum of  $\text{acrOH}$ , thus underlining that the ligand is deprotonated in contrast to the spectrum of  $[\text{Cu}(\text{Oacr})\text{Cl}_2(\text{MeCN})_2]$  which resembles strongly that of  $\text{acrOH}$ . For the copper complexes additional absorption bands were observed in the visible range. Their intensities are indicative for LMCT transitions.

Table 26: Absorption data of acridine ligands and complexes<sup>[a]</sup>

compound	$\lambda / \text{nm}$ ( $\epsilon / \text{Lmol}^{-1}\text{cm}^{-1}$ )
acrOMe	297 (12842), 309 (19817), 341sh (5042), 357sh (12186), 372 (20807), 392 (21627)
acrOH	299 (53240), 312 (79816), 362sh (49122), 377 (82916), 395 (84147)
$[\text{Cu}(\text{acrOMe})\text{Cl}_2(\text{MeCN})_2]$	297 (8075), 309 (10587), 344sh (5428), 360 (9348), 373 (12564), 392 (13803), 406sh (4724)
$[\text{Cu}(\text{acrOH})\text{Cl}_2(\text{MeCN})_2]$	300 (14121), 310 (15852), 358 (9755), 375 (10695), 393 (9884), 460 (4776), 534 (2975)
$[\text{Cu}(\text{acrOMe})_2](\text{OAc})_2$	297 (7566), 309 (9094), 342sh (2593), 360sh (4199), 373 (6867), 391 (7256), 407sh (290),
$[\text{Cu}(\text{acrO})_2(\text{MeCN})_2]$	272 (15179), 391 (4761), 444 (4590), 474 (5066), 511 (5506), 572 (3978), 631 (3842)

[a] Measured at 298 K in MeCN solution

Since the parent species of all complexes were successfully characterised by absorption spectroscopy, oxidised and reduced species were analysed by absorption spectroscopy as well. Therefore spectroelectrochemical measurements were carried out on samples dissolved in  $\text{MeCN}/^n\text{Bu}_4\text{NPF}_6$  solution. The obtained data are summarised in Table 27.

Table 27: Absorption data of oxidised and reduced complexes<sup>[a]</sup>

compound	oxidation	parent ( $\text{Cu}^{\text{II}}$ )	$\text{Cu}^{\text{II}} \rightarrow \text{Cu}^{\text{I}}$	reduction
acrOMe	223, 242, 269, 322, 429sh, 531	219, 252, 298, 310, 372, 392,	-	224, 263, 338, 353, 380sh, 400, 421, 444
$[\text{Cu}(\text{acrOMe})\text{Cl}_2(\text{MeCN})_2]$	218, 253, 297, 310, 340sh, 376, 393, 464	218, 253, 297, 310, 373, 393	219, 253, 297, 310, 341sh, 359sh, 376, 394	224, 262, 324sh, 338, 354, 378sh, 400sh, 420, 445
$[\text{Cu}(\text{acrOH})\text{Cl}_2(\text{MeCN})_2]$	228, 254, 308, 377, 394, 461, 544sh	254, 297, 310, 359sh, 377, 394	254, 297, 310, 359sh, 377, 394	223, 266, 337, 355, 372, 421, 445, 477sh
$[\text{Cu}(\text{acrOMe})_2](\text{OAc})_2$	235, 270, 328sh, 344, 362, 439	218, 256, 297, 309, 360sh, 378, 393	218, 255, 298, 310, 361sh, 376, 393,	224, 263, 342, 355, 400sh, 420, 443
$[\text{Cu}(\text{acrO})_2(\text{MeCN})_2]$	272, 484sh, 507, 548sh	227, 378, 603	260, 353, 415, 441sh	260, 353, 415, 441sh

[a] Spectra were recorded using  $\text{MeCN}/^n\text{Bu}_4\text{NPF}_6$  solutions at 298 K

During the reduction of  $\text{Cu}^{\text{II}}$  to  $\text{Cu}^{\text{I}}$  only slight changes (mainly in absorption intensity) of the absorption bands assigned to  $\pi$ - $\pi^*$  transition can be observed. The main difference between parent and reduced species is found in between 340 nm and 400 nm. The absorption bands in this region (three maxima and one shoulder) change their intensity and two new absorption bands (400-450 nm) appear in line with the assignment of LMCT transitions. The red shift of the long-wavelength absorption might be explained by chloride abstraction upon reduction, followed by ligand dimerisation (Figure 32).

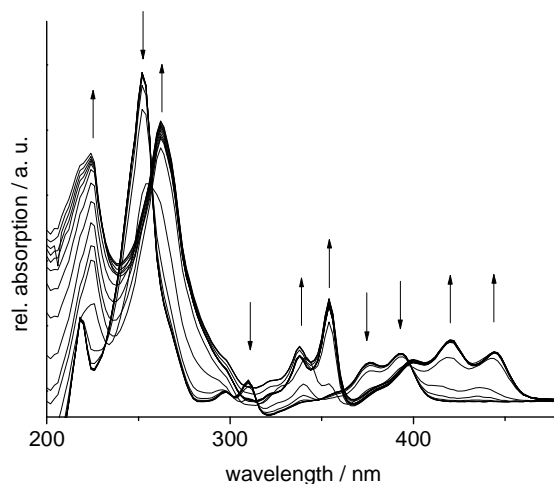


Figure 32: Absorption spectra recorded upon reductive spectroelectrochemistry ( $-2.0$  V) of  $\text{acrOMe}$  in  $\text{MeCN}/n\text{Bu}_4\text{NPF}_6$

Oxidation of the complexes also leads to an additional long-wavelength absorption band at about 450 to 500 nm, which is a broad (unresolved) band (Figure 33). The absorption band can be assigned to ligand centred oxidation generating a phenoxy radical, which is delocalised in the aromatic scaffold of the acridine system. Therefore, the charge transfer between radical and copper ion occurs at longer wavelengths as found for charge transfer between copper and unsubstituted phenoxy radicals.

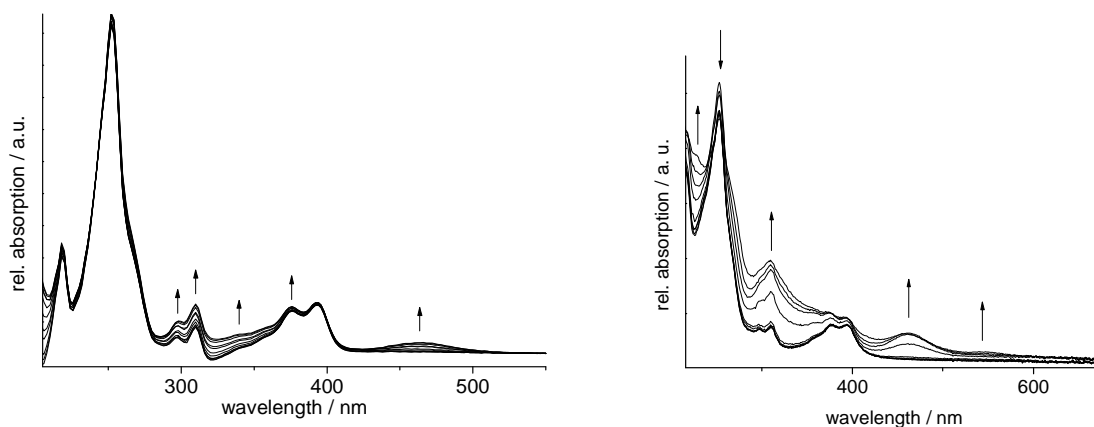


Figure 33: Absorption spectra recorded upon oxidative spectroelectrochemistry ( $+1.0$  V) of  $[\text{Cu}(\text{acrOMe})\text{Cl}_2(\text{MeCN})_2]$  (left) and  $[\text{Cu}(\text{acrOH})\text{Cl}_2(\text{MeCN})_2]$  (right) in  $\text{MeCN}/n\text{Bu}_4\text{NPF}_6$



### 3.5 Radicals in aromatic ligands - conclusions

While reduction of opo complexes is possible and goes along with radical formation as shown in detail for  $[\text{Cu}(\text{opo})_2]$ , oxidation of the opo complexes and opoH is not feasible up to very high potentials ( $> 3.0 \text{ V vs. FeCp}_2/\text{FeCp}_2^+$ ).  $[\text{Cu}(\text{opo})_2]$  therefore does not exhibit the desired physical properties for application of  $[\text{Cu}(\text{opo})_2]$  in catalytic oxidation reactions and is not suitable as GO model system.

Investigations on bqOH revealed that the complexes  $[\text{Cu}(\text{bqOH})\text{Cl}_2]$ ,  $[\text{Cu}(\text{bqOH})\text{Br}_2]$  and  $[\text{Cu}(\text{bqO})_2]$  can be oxidised. These ligand centred oxidations occur on potentials, which are typical for GO model systems and result in phenoxyl radical species as shown by spectroelectrochemical measurements. The radical species seem to be stabilised by aromatic delocalisation, as can be inferred from the energies of charge transfer absorption. While the applied coligands do not influence the electrochemical oxidation, reduction processes are strongly affected. Reduction occurs irreversibly and the coligands can be considered to influence the complex stability. E.g. the corresponding bromido complex is far less stable as can be inferred from spectroelectrochemical investigation. For the use of bqOH complexes in oxidation catalysis this instability is meaningless, since the reaction medium is not reductive. Thus bqOH and  $\text{bqO}^-$  complexes seem to be potential GO model systems and their suitability as oxidation catalysts have to be determined under reaction conditions. Therefore catalytic test reactions were performed, results are presented and discussed in Chapter 7.

Complexes of the acridine ligands acrOMe and acrOH supposedly possess strongly distorted geometries. As a result, the copper centred reduction ( $\text{Cu}^{\text{II}}/\text{Cu}^{\text{I}}$ ) is facilitated. The compounds  $[\text{Cu}(\text{acrOMe})\text{Cl}_2(\text{MeCN})_2]$ ,  $[\text{Cu}(\text{acrOMe})_2(\text{OAc})_2]$  and  $[\text{Cu}(\text{acrOH})\text{Cl}_2(\text{MeCN})_2]$  have a copper potential lying around 0.1 V (the  $\text{Cu}^{\text{II}}$  state is disfavoured, eventually due to a nearly tetrahedral ligand field), while in case of  $[\text{Cu}(\text{acrO})_2(\text{MeCN})_2]$  the copper potential lies at  $-0.3 \text{ V}$ , which clearly indicates a disfavoured  $\text{Cu}^{\text{I}}$  state (presumably due to the two negatively charged acridine ligands). Nevertheless, all copper potentials lie in the relevant range for GO model systems. A ligand centred oxidation process can be observed for all complexes at rather low potential (below 1.0 V). Again the  $[\text{Cu}(\text{acrO})_2(\text{MeCN})_2]$  complex earns special focus, since it exhibits the lowest acridinyl generation potential (below 0.2 V). Therefore  $[\text{Cu}(\text{acrO})_2(\text{MeCN})_2]$  settles among highly efficient GO model catalysts. Additional spectroelectrochemical investigations revealed that the radical, generated upon oxidation, is delocalised in the aromatic scaffold. This should result in a remarkable stabilisation of the radical species. The acridine complexes thus also seem to be potential GO model systems and

their suitability as oxidation catalysts has to be investigated under catalytic conditions. Test reactions using *acrOMe* and *acrOH* were performed and the results are presented and discussed in Chapter 7.

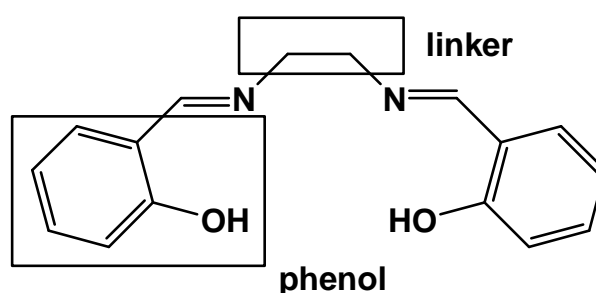
The results on *bqOH* and *acrOMe* as well as *acrOH* verify that aromatic stabilisation of phenoxyl radicals in copper complexes is possible. The results suggest that aromatic delocalisation (studied for systems containing three aromatic six-membered rings) has almost the same influence on the physical properties of phenoxyl radicals as the established *ortho* and *para* substituted systems. Interestingly, not all aromatic scaffolds exhibit the same stabilisation effect. This has to be inferred from the electrochemical potentials of the ligand oxidation as well as from the reversibility of the oxidation processes. The most efficient aromatic system seems to be the linear acridine scaffold, followed by the benzo-[h]-quinoline, while the phenalenone system exhibits almost no positive effect.

First of all, this means that the state of annulation determines the stabilising effect. High annulated systems (phenalene) are less effective than medium (phenanthrene) or low annulated (acridine) systems. To find a reason for this astonishing fact, one might meet with the differing ionisation potentials of the aromatic systems. The ionisation potential of anthracene is the lowest at 7.43 eV<sup>[299]</sup>, while the ionisation potentials of phenanthrene and phenalenone are pretty similar (8.19 eV<sup>[299]</sup> vs. 8.20 eV<sup>[300]</sup>). Hence, it has to be concluded that the ionisation potential does not explain the extraordinary electrochemical behaviour of *opoH* and its complexes. Electrochemical studies on phenalenine systems (e.g. 1,2-bis-(phenalen-1-ylidene)ethene) show that these close derivatives can be oxidised in the same range as phenanthrenes (0.51 V), which makes the lacking oxidation of *opo* systems even more puzzling.<sup>[301]</sup>

## 4.0 Copper complexes with salen type ligands (N<sub>2</sub>O<sub>2</sub> donor set)

### 4.1 Introduction

Salen (2,2'-Ethylenebis(nitrilomethylidene)diphenol) (Scheme 34) and salen type ligands are known to be highly suitable for the synthesis of transition metal complexes. Many of them have been studied with regard to their catalytic properties, especially in oxidation catalysis. Therefore it is not surprising that copper complexes bearing salen type ligands have already been used in oxidation catalysis similar to Galactose Oxidase (GO).<sup>[84,137–140,302]</sup> Some general conclusions have been drawn from these investigations:

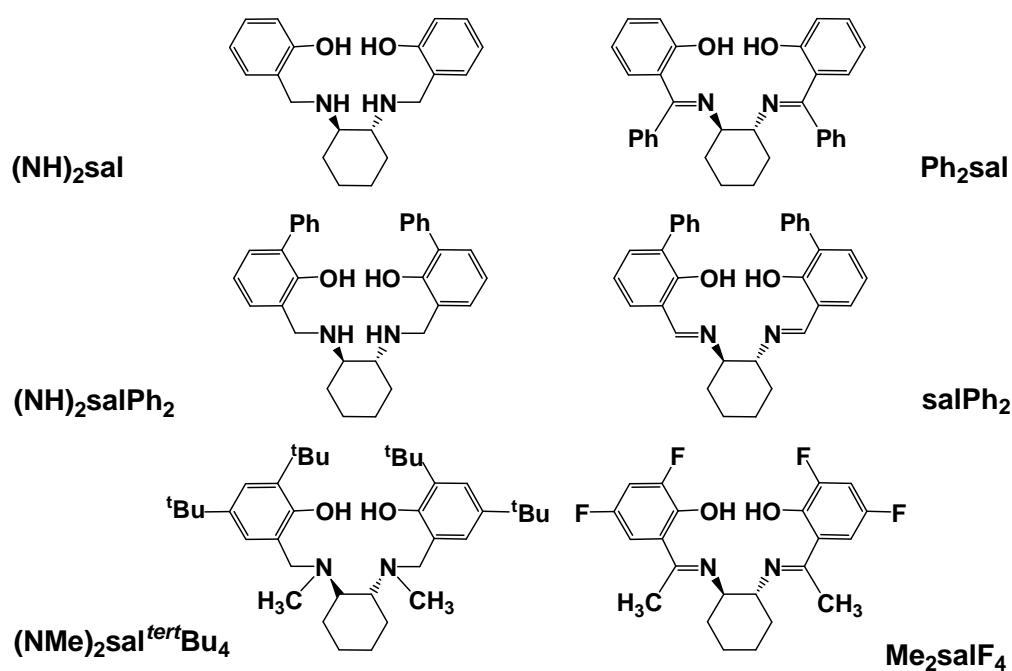


Scheme 34: Salen (2,2'-Ethylenebis(nitrilomethylidene)diphenol)

1. The coordination geometry provided by salen type ligands varies from square planar to tetrahedral, depending on the flexibility of the linker (Scheme 34).
2. Salen type complexes form phenoxyl radicals upon oxidation. In principle, most copper salen type complexes are able to form even two phenoxyl radicals. The monoradical species is EPR silent (coupling of the unpaired electron of the radical site to d<sup>9</sup> Cu<sup>II</sup>) while the biradical species exhibits a signal corresponding to an organic radical.<sup>[137,258]</sup>
3. Salen type ligands bearing amine instead of imine functions (sometimes referred to as “reduced” salen ligands or “salan” ligands) are more easily oxidised, but the radical species show less intense charge transfer absorption bands.<sup>[71]</sup>
4. Some copper salen type complexes have been found to be highly active (turn over number of 1300 at 295 K in 20 h)<sup>[84,302]</sup> in catalytic alcohol oxidation, even oxidation of non activated alcohols such as methanol<sup>[148,303]</sup> is possible.

The salen type complexes reported so far contain *ortho*- and *para*-substituted phenol moieties and thus stabilise the generated phenoxyl radicals. Non-stabilised radical species have been examined in benzyl alcohol oxidation and have been reported to lack any activity.<sup>[84]</sup> The influence of different linkers and their varying flexibility has not been considered in this context, although it is known that the linker affects the complex geometry. Hence it influences the coupling between the unpaired electrons of the copper ion and the radical and therefore the catalytic properties of the complexes.

In this work copper complexes of chiral salen type ligands (all *R,R*) were examined (Scheme 35). They differ concerning the *ortho* and *para* positioned substituents and the character of the N-atom (imine; sec. amine; tert. amine) while in each case cyclohexane is the linking group. The sp<sup>2</sup> carbon atom of the imine function is furthermore modified by substituents with varying sterical demand: an H atom, a methyl group or a phenyl group.



Scheme 35: Applied salen type ligands<sup>[304]</sup>

The phenol cores are substituted with either phenyl groups, fluorine atoms or *tert*butyl groups. Fluorine atoms and alkyl groups are expected to cause stabilisation by their electron donating ability (fluorine possesses a +M and a -I effect), while the stabilising ability of phenyl groups is unequivocal, since a +I and a -M effect is attributed to this group. The salen type ligands applied in this thesis (Scheme 35) have been synthesised by Thomas Günther working in the group of Prof. Dr. A. Berkessel (Institute of Organic Chemistry, University of Cologne).<sup>[304]</sup>

## 4.2 Synthesis and structure of the copper complexes

Complex synthesis was carried out using the standard procedure reported for copper salen complexes using Cu(OAc)<sub>2</sub> as metal source (1:1 stoichiometry) in methanol solution. The complexes [((NMe)<sub>2</sub>sal<sup>tert</sup>Bu<sub>4</sub>)Cu] (green), [((NH)<sub>2</sub>sal)Cu] (brown), [((NH)<sub>2</sub>salPh<sub>2</sub>)Cu] (green), [(Me<sub>2</sub>salF<sub>4</sub>)Cu] (green), [(Ph<sub>2</sub>sal)Cu] (brown) and [(salPh<sub>2</sub>)Cu] (off-white) were synthesised in high to moderate yields (79% to 33%) and in high purity as inferred from elemental analyses. All complexes were further analysed by EPR spectroscopy, absorption spectroscopy, cyclic voltammetry and spectroelectrochemical methods.

The complex [(Me<sub>2</sub>salF<sub>4</sub>)Cu] could be crystallised from methanol and single crystals suitable for XRD were obtained. The crystal structure was solved and refined in the monoclinic space group *C*2 (Figure 34, Figure 35 and Table 28). In the crystal the copper complexes are stacked along the *c* axis with Cu··Cu distances of 3.820(1) Å and 3.865(1) Å. These distances are markedly longer than a covalent Cu–Cu bond as inferred from the sum of covalent radii (2.556 Å). No intermolecular interaction such as hydrogen bridges were found in the crystal structure. The stacks leave tunnels in the structure along the *c* axis, each of them has an ellipsoid cross-section and is coated with fluorine atoms. The residual electron density found in these tunnels is due to small amounts of solvent molecules and the solvent correction tool of platon (SWAT) was used. Assignment and refinement of the solvent molecules were impossible due to statistic distribution of the molecules.

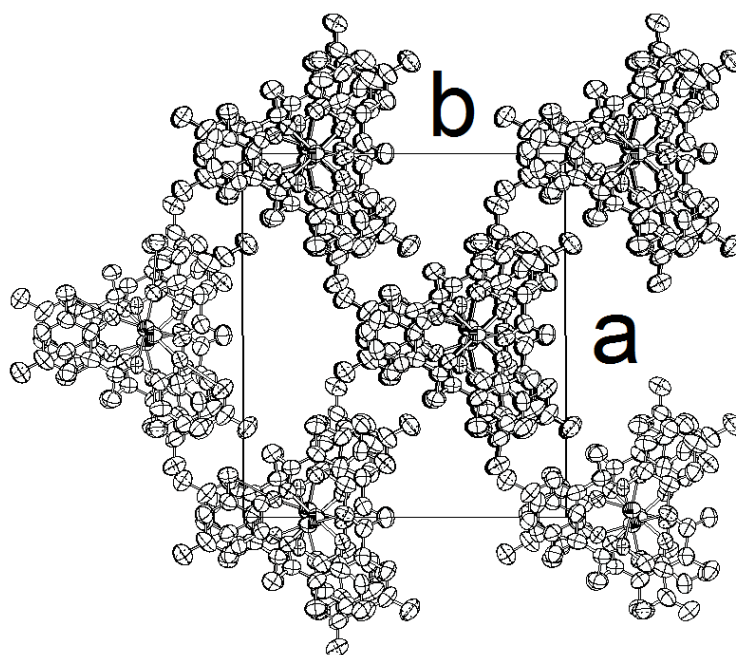


Figure 34: Packing of [(Me<sub>2</sub>salF<sub>4</sub>)Cu] in the crystal structure, H atoms are omitted for clarity

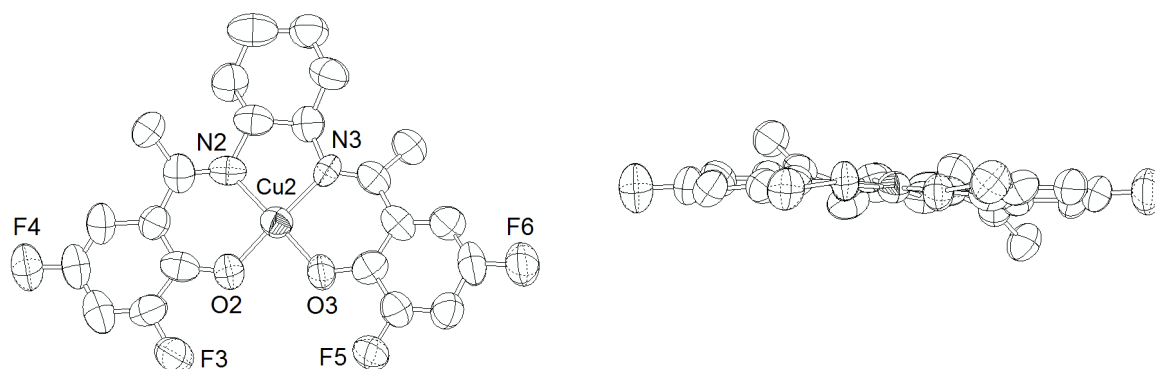
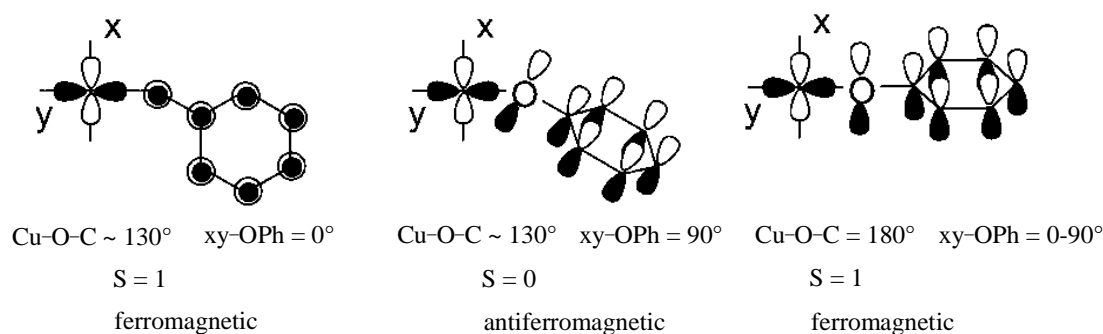


Figure 35: ORTEP representation (50% probability level) of the molecular structure of [(Me<sub>2</sub>salF<sub>4</sub>)Cu], H atoms are omitted for clarity

Table 28: Crystal structure and refinement data of [(Me<sub>2</sub>salF<sub>4</sub>)Cu]

formula	C <sub>22</sub> H <sub>20</sub> N <sub>2</sub> O <sub>2</sub> F <sub>4</sub> Cu	Flack x	-0.02(2)
f. w. /g mol <sup>-1</sup>	483.94	refl. coll.	23671
crystal system	monoclinic	data / restr. / param.	7921 / 1 / 425
space group	C2 (No. 5)	h, k, l	-24 < h < 24
crystal shape	needle		-21 < k < 21
colour	green		-13 < l < 14
a / Å	19.090(3)	goof on F <sup>2</sup>	0.610
b / Å	16.624(3)	R <sub>int</sub>	0.0945
c / Å	11.362(2)	final R indices	R1 = 0.1387
β / °	101.06(1)	[I > 2σ(I)]	wR2 = 0.0477
volume / Å <sup>3</sup> , Z	3539(1) / 6	R indices (all data)	R1 = 0.1474
F(000)	1482		wR2 = 0.1588
density / g cm <sup>-3</sup>	1.362	largest diff. p. a. h. / e Å <sup>-3</sup>	0.298 and -0.103
abs. coeff / mm <sup>-1</sup>	0.976		

It has been reported that spin-spin coupling (antiferromagnetic) between the unpaired electrons of the radical site and the copper ion is ideal if the Cu–O–C angle is found to be about 130° and the plane angle of the copper coordination plane and the phenol ring plane is about 90° (Scheme 36).<sup>[71]</sup> In [(Me<sub>2</sub>salF<sub>4</sub>)Cu] the Cu2–O3–C33 angle is found to be 127.02(1)°, while the angle between coordination plane and phenol ring is only 7.61(1)°. Thus only the first geometrical requirement for an efficient antiferromagnetic coupling is observed. Additional bond distances and angles of [(Me<sub>2</sub>salF<sub>4</sub>)Cu] are shown in Table 29.



Scheme 36: Orbital overlap between phenoxy moiety and copper ion for different Cu–O–C angles and xy-plane/phenol-ring dihedral angles<sup>[71]</sup>

Table 29: Selected distances and angles in the crystal structure of [(Me<sub>2</sub>salF<sub>4</sub>)Cu]

distances / Å		angles / °	
Cu2–N2	1.9572(4)	N2–Cu2–N3	87.432(8)
Cu2–N3	1.9505(3)	O2–Cu2–O3	84.870(8)
Cu2–O2	1.8552(3)	O2–Cu2–N2	93.738(8)
Cu2–O3	1.8316(3)	O3–Cu2–N3	94.064(8)
		Cu2–O3–C33	127.02(1)

### 4.3 EPR spectroscopy

All complexes were analysed by EPR spectroscopy at 298 K, using solid samples and MeCN solutions. Figure 36 shows a representative spectrum and Table 30 lists the obtained data. For the complexes [((NMe)<sub>2</sub>sal<sup>tert</sup>Bu<sub>4</sub>)Cu], [((NH)<sub>2</sub>sal)Cu], [((NH)<sub>2</sub>salPh<sub>2</sub>)Cu], [(Me<sub>2</sub>salF<sub>4</sub>)Cu], [(Ph<sub>2</sub>sal)Cu] and [(salPh<sub>2</sub>)Cu] the geometry of the first copper coordination sphere is square planar. The slight tetrahedral distortion of the complex can be estimated by EPR spectroscopy. Generally it is assumed that a high degree of tetrahedral distortion is accompanied with a small  $A_{\parallel\text{Cu}}$  coupling constant. Thus, regular complexes with small distortion exhibit  $A_{\parallel\text{Cu}}$  values of about 150 G, while copper enzymes (with entatic state distortion) have  $A_{\parallel\text{Cu}}$  values of about 60 G or even smaller.<sup>[1]</sup>

All compounds exhibit axial spectra with  $g_{\parallel} > g_{\perp}$ . Consequently, the "isotropic" signal for [((NH)<sub>2</sub>sal)Cu] is assigned to a non-resolved axial geometry with a small  $\Delta g$  value. All  $g$  values are very similar to each other and lie in the typical range for Cu<sup>II</sup> compounds. Compounds measured at solid state do not show a hyperfine structure, while all spectra recorded on MeCN solutions show signals with  $A_{\parallel\text{Cu}}$  values of about 90 G. This is a small copper coupling constant and a hint for tetrahedral distortion in solution. Interestingly,  $A_{\parallel}$  does not differ markedly upon varying the linker group and the substituents.

Samples containing MeCN dissolved complexes show some hyperfine structure, which is not due to <sup>63,65</sup>Cu coupling. This additional hyperfine structure was best resolved for [(Ph<sub>2</sub>sal)Cu] in MeCN solution. Hence, simulation<sup>[305]</sup> of the EPR signal was exemplarily performed on this spectrum, the result is presented in Figure 36. To simulate the spectrum,  $A_{\parallel\text{Cu}} = 86$  G and an additional <sup>14</sup>N-hyperfine structure ( $I^{14\text{N}} = 1$ ) with two slightly different coupling constants  $A_{14\text{N}} = 11.4$  and 13.8 were used. This is in line with earlier investigations on copper complexes containing N donor ligands, where the spin density at the nitrogen atoms was determined to be 14%.<sup>[306]</sup>

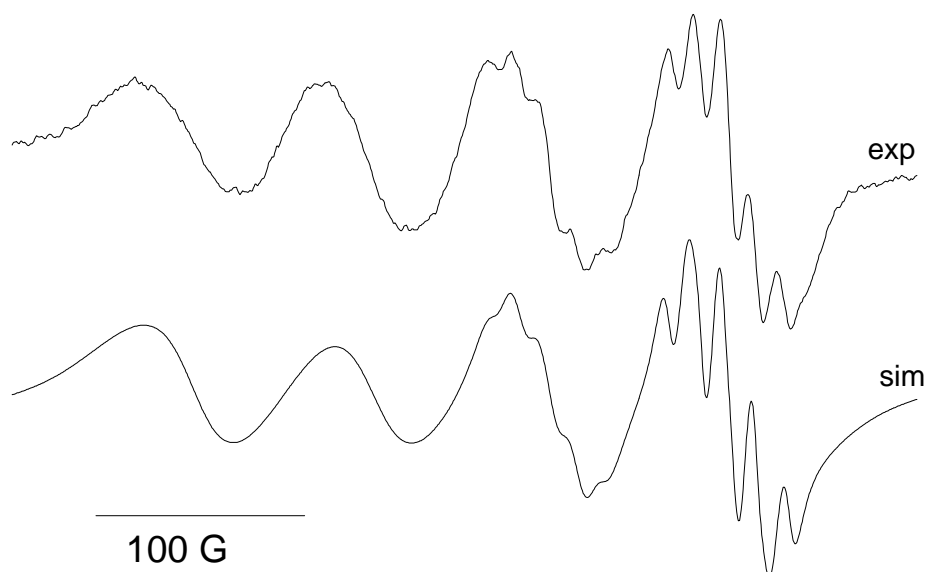
Figure 36: EPR spectrum of [(Ph<sub>2</sub>sal)Cu] in MeCN and simulation of the hyperfine structure

Table 30: X-band EPR data of the salen type complexes measured at 298 K

compound	$g_{av}$	$g_{  }$	$g_{iso}$ or $g_{\perp}$	$\Delta g$	$A_{  Cu}$	state
[((NMe) <sub>2</sub> sal <sup>tert</sup> Bu <sub>4</sub> )Cu]	2.143	2.186	2.056	0.130	-	solid
[((NMe) <sub>2</sub> sal <sup>tert</sup> Bu <sub>4</sub> )Cu]	2.135	2.020	2.097	0.115	90 G	MeCN
[(NH) <sub>2</sub> sal)Cu]	2.068	-	2.068	-	-	solid
[(NH) <sub>2</sub> sal)Cu]	2.137	2.021	2.098	0.116	87 G	MeCN
[(NH) <sub>2</sub> salPh <sub>2</sub> )Cu]	2.080	2.127	2.057	0.070	-	solid
[(NH) <sub>2</sub> salPh <sub>2</sub> )Cu]	2.039	2.130	2.053	0.077	92 G	MeCN
[(Me <sub>2</sub> salF <sub>4</sub> )Cu]	2.108	2.185	2.070	0.115	-	solid
[(Me <sub>2</sub> salF <sub>4</sub> )Cu]	2.056	2.122	2.023	0.099	83 G	MeCN
[(Ph <sub>2</sub> sal)Cu]	2.112	2.211	2.063	0.148	-	solid
[(Ph <sub>2</sub> sal)Cu]	2.053	2.130	2.015	0.115	86 G	MeCN
[(salPh <sub>2</sub> )Cu]	2.080	2.139	2.050	0.089	-	solid
[(salPh <sub>2</sub> )Cu]	2.049	2.114	2.017	0.097	86 G	MeCN

$$g_{av} = \text{averaged } g \text{ value} = (g_{||} + 2 g_{\perp}) / 3; \Delta g = g_{||} - g_{\perp}$$

#### 4.4 Electrochemical properties

Electrochemical investigations were carried out on the free ligands as well as on the copper complexes. Figure 37 shows representative samples and Table 31 lists the collected data.



Table 31: Electrochemical data of the free ligands and Cu<sup>II</sup> complexes<sup>[a]</sup>

compound	$E_{pa}$ or $E_{1/2}$	$E_{1/2}$ Cu <sup>II</sup> /Cu <sup>I</sup> ( $\Delta E_{pp}$ <sup>[b]</sup> )	$E_{pc}$ or $E_{1/2}$
(NMe) <sub>2</sub> sal <sup>tert</sup> Bu <sub>4</sub>	0.27 (p.rev) <sup>[c]</sup>	-	-1.27 (rev)
(NH) <sub>2</sub> sal	0.40 (irr)	-	-1.51 (irr)
(NH) <sub>2</sub> salPh <sub>2</sub>	0.31 (irr)	-	-1.46 (irr)
Me <sub>2</sub> salF <sub>4</sub>	0.99 (irr), 0.79 (irr)	-	-1.40 (irr)
Ph <sub>2</sub> sal	1.10 (irr), 0.84 (irr)	-	-1.37 (irr)
salPh <sub>2</sub>	0.93 (irr), 0.67 (irr)	-	-1.46 (p.rev) <sup>[c]</sup>
[(NMe) <sub>2</sub> sal <sup>tert</sup> Bu <sub>4</sub> Cu]	0.35 (rev)	0.15 (100)	-1.31 (p.rev) <sup>[c]</sup>
[(NH) <sub>2</sub> salCu]	0.91 (irr); 0.38 (irr)	0.05 (140)	-1.44 (rev)
[(NH) <sub>2</sub> salPh <sub>2</sub> Cu]	0.26 (irr)	-0.03 (190)	-1.43 (p.rev) <sup>[c]</sup>
[(Me <sub>2</sub> salF <sub>4</sub> )Cu]	0.89 (rev), 0.61 (rev)	-0.26 (890)	-1.44 (p.rev) <sup>[c]</sup>
[(Ph <sub>2</sub> sal)Cu]	0.98 (rev), 0.44 (p.rev) <sup>[c]</sup>	-0.12 (730)	-1.43 (p.rev) <sup>[c]</sup>
[(salPh <sub>2</sub> )Cu]	0.81 (irr), 0.55 (irr)	0.28 (110)	-1.32 (rev)

[a] From cyclic voltammetry measured in MeCN/<sup>n</sup>Bu<sub>4</sub>NPF<sub>6</sub> at 298 K at 100 mV/s scan rate; potentials in V vs. FeCp<sub>2</sub>/FeCp<sub>2</sub><sup>+</sup>

[b] Peak-to-peak separation  $E_{pc}-E_{pa}$  in mV

[c] Partly reversible, 0.2 < peak current ratio < 1.0

The free ligands exhibit irreversible reductions around -1.4 V except for (NMe)<sub>2</sub>sal<sup>tert</sup>Bu<sub>4</sub> (reversible) and for salPh<sub>2</sub> (partly reversible, with a peak current ratio between 0.2 and 1.0) and an irreversible oxidation in the range of +0.27 V to +0.84 V except for (NMe)<sub>2</sub>sal<sup>tert</sup>Bu<sub>4</sub> (partly reversible). The ligands Me<sub>2</sub>salF<sub>4</sub>, Ph<sub>2</sub>sal and salPh<sub>2</sub> show a second irreversible oxidation around 0.9 - 1.1 V.

The complexes exhibit redox processes at potentials similar to those observed for the free ligands, but all reductions and most of the oxidations reveal at least partial reversibility. Additional reversible reduction waves were found around 0 V and are unequivocally assigned to the Cu<sup>II</sup>/Cu<sup>I</sup> redox couple (the previously discussed redox processes were presumably ligand centred). A marked separation of the  $E_{pc}$  and the  $E_{pa}$  wave of the reduction process for [(Me<sub>2</sub>salF<sub>4</sub>)Cu] (Figure 37, right) was observed for many complexes. The Cu<sup>II</sup> oxidation state favours square planar complex geometry while the Cu<sup>I</sup> oxidation state favours a tetrahedral surrounding and thus metal centred reduction affects the coordination geometry. Salen type ligands, which provide a comparably rigid ligand scaffold, hamper the geometric rearrangement and as a result  $E_{pc}$  and  $E_{pa}$  of the reduction wave are largely separated (huge reorganisation energy). The largest separation can be observed for ligands containing imine functions, while tertiary amines or reduced salen type ligands are less rigid and giving rise to a smaller peak-to-peak separation (Figure 37, left).

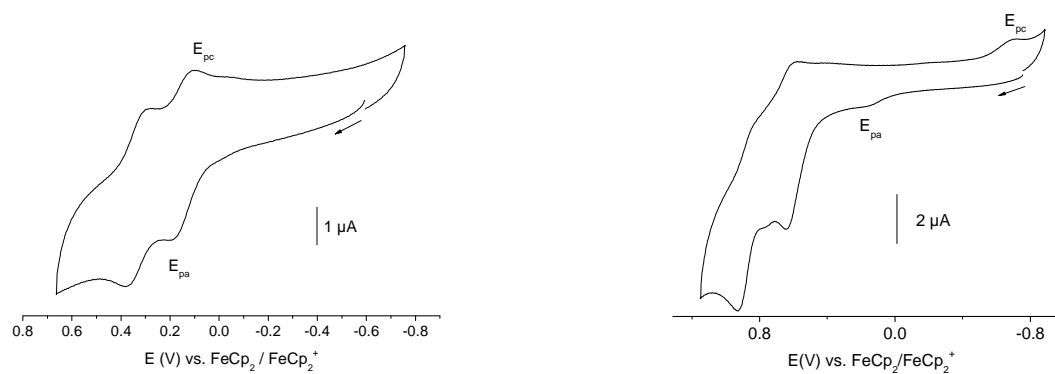


Figure 37: Cyclic voltammograms of  $[(\text{NMe})_2\text{sal}^{\text{tert}}\text{Bu}_4\text{Cu}]$  and  $[(\text{Me}_2\text{salF}_4)\text{Cu}]$  in  $\text{MeCN}/n\text{Bu}_4\text{NPF}_6$  solution at 298 K at 100 mV/s scan rate

Since this thesis puts special focus on the influence of phenoxy radical stabilisation, a detailed look on the effects of different substituents on the electrochemistry is worthwhile.  $[(\text{NMe})_2\text{sal}^{\text{tert}}\text{Bu}_4\text{Cu}]$  and  $[(\text{Me}_2\text{salF}_4)\text{Cu}]$  possess the highest degree of substitution and their ligand centred oxidation (presumably the  $[\text{PhO}]^{\bullet+}/[\text{PhO}]$  couple) occurs reversible at low potential. The complexes  $[(\text{salPh}_2)\text{Cu}]$  and  $[(\text{NH})_2\text{salPh}_2\text{Cu}]$  which solely possess *ortho*-phenyl substituents at the phenol moieties are irreversibly oxidised but also at low potential, while  $[(\text{Ph}_2\text{sal})\text{Cu}]$ , lacking substituents on the phenol moieties, is oxidised partly reversible at slightly higher potential. Thus it seems that *ortho*- and *para*-substitution facilitates oxidation, while less substitution is accompanied with decreasing reversibility of the oxidation process and increases the oxidation potential.

The metal centred reduction also varies with the ligand substitution and increases in the series  $[(\text{Me}_2\text{salF}_4)\text{Cu}] < [(\text{Ph}_2\text{sal})\text{Cu}] < [(\text{NH})_2\text{salPh}_2\text{Cu}] < [(\text{NH})_2\text{salCu}] < [(\text{NMe})_2\text{sal}^{\text{tert}}\text{Bu}_4\text{Cu}] < [(\text{salPh}_2)\text{Cu}]$ . This series nicely reflects the influence of the different substituents: F atoms on the phenol moieties withdraw electron density, the same effect (although less intense) is found for *ortho*-Ph substitution. In contrast, Ph substitution on the imine C atom leads to increased electron density. Two *tert*-butyl groups on each phenol core lead to a high  $\text{Cu}^{\text{II}}/\text{Cu}^{\text{I}}$  potential.

However, the assignment of the ligand centred oxidation to a  $[\text{PhO}]^{\bullet+}/[\text{PhO}]$  couple remains preliminary without further evidence from spectroelectrochemical experiments which will be described in the next paragraph.

#### 4.5 Absorption spectroscopy and spectroelectrochemistry

The complexes were dissolved in MeCN solution and absorption spectra were recorded from 200 nm to 800 nm (Table 32). Apart from two intense absorption bands in the UV range

of the spectra (assigned to  $\pi$ - $\pi^*$  transition) there are charge transfer absorption bands at 350 nm to 450 nm and d-d absorption bands around 600 nm. This is in agreement with previous reports.<sup>[307]</sup> Interestingly, the complexes containing ligands with imine functions generally show larger extinction coefficients than the complexes containing reduced salen type ligands or tertiary amines.

Table 32: Absorption data of the salen type copper complexes<sup>[a]</sup>

complexes	$\lambda$ / nm ( $\epsilon$ / Lmol <sup>-1</sup> cm <sup>-1</sup> )		
[((NMe) <sub>2</sub> sal <sup>tert</sup> Bu <sub>4</sub> )Cu]	255 (9695), 297 (6569)	434 (824)	623 (509)
[((NH) <sub>2</sub> sal)Cu]	246 (8941), 278 (7032)	385 (680)	595 (189)
[((NH) <sub>2</sub> salPh <sub>2</sub> )Cu]	254 (8322), 313 (9330)	394 (907)	611 (454)
[(Me <sub>2</sub> salF <sub>4</sub> )Cu]	264 (50771), 269 (45061)	362 (6268)	613 (135)
[(Ph <sub>2</sub> sal)Cu]	264 (37739)	352 (1969), 469sh (192)	616 (120)
[(salPh <sub>2</sub> )Cu]	262 (26908)	363 (14019)	572 (971)

[a] Measured in MeCN

Spectroelectrochemical measurements were carried out on all samples to support the assignment of the redox processes as well as the assignment of the electronic absorptions. The results are collected in Table 33.

Table 33: Spectroelectrochemical data<sup>[a]</sup>

compound	oxidation	parent (Cu <sup>II</sup> )	Cu <sup>II</sup> →Cu <sup>I</sup>	reduction
[((NMe) <sub>2</sub> sal <sup>tert</sup> Bu <sub>4</sub> )Cu]	297, 414	255, 297, 434, 623	252, 296, 422	235, 323, 422
[((NH) <sub>2</sub> sal)Cu]	271, 444	246, 278, 385, 595	247, 278	227, 243, 364
[((NH) <sub>2</sub> salPh <sub>2</sub> )Cu]	328, 469, 575	254, 313, 394, 611	<sup>[b]</sup>	<sup>[b]</sup>
[(Me <sub>2</sub> salF <sub>4</sub> )Cu]	305, 313, 337, 542	226, 264, 362, 613	226, 264, 362	226, 264, 362
[(Ph <sub>2</sub> sal)Cu]	303, 313, 449	264, 352, 469, 616	254, 366	356, 431sh
[(salPh <sub>2</sub> )Cu]	266, 520, 620sh	228, 262, 363, 572	228, 262, 362	236, 421

[a] Measurements in MeCN/<sup>tert</sup>Bu<sub>4</sub>NPF<sub>6</sub> solution at 298 K, all absorption bands in nm

[b] Due to the bad solubility all bands in the long-wavelength range are extremely weak

As already known from other copper complexes (Chapter 2.2) the reduction of the salen complexes (Cu<sup>II</sup> to Cu<sup>I</sup>) leads to a loss of the long-wavelength d-d band and a marked shift of charge transfer bands, while the  $\pi$ - $\pi^*$  absorption bands are far less affected. Oxidation of the complexes lead to one or more new absorption bands in the long-wavelength region, which can be assigned to charge transfer transitions in the copper phenoxyl radical species. The absorption energy of these bands are assumed to correspond to the radical stabilisation, thus the fully stabilised systems have been expected to show a radical dependent absorption band lying in between 400 nm and 500 nm, the non- and partly stabilised complexes were expected to show charge transfer bands, shifted to higher energy.

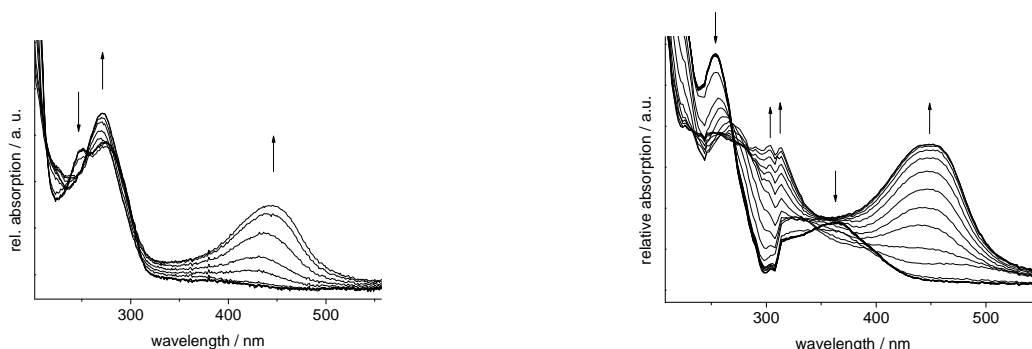


Figure 38: Absorption spectra of  $[(\text{NH})_2\text{sal})\text{Cu}]$  (left) and  $[(\text{Ph}_2\text{sal})\text{Cu}]$  (right) measured during electrochemical oxidation at 2.0 V in  $\text{MeCN}/t\text{Bu}_4\text{NPF}_6$  at 298 K

Figure 38 shows absorption spectra of the oxidised species of  $[(\text{NH})_2\text{sal})\text{Cu}]$  (left) and  $[(\text{Ph}_2\text{sal})\text{Cu}]$  (right). Although both complexes are not able to stabilise phenoxyl radicals, an intense absorption band around 450 nm (undoubtedly caused by phenoxyl radicals) is observed. In the case of  $[(\text{salPh}_2)\text{Cu}]$ , the formation of two phenoxyl radicals in a molecule is indicated by an absorption shoulder at 620 nm, which is assigned to a charge transfer between two radical sites.<sup>[71]</sup>

#### 4.6 Conclusion on the suitability of the salen type complexes as GO model systems

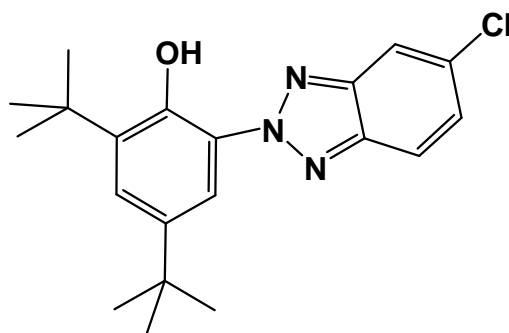
All complexes show oxidation at comparably small potentials, the smallest values lie around 0.3 V. The oxidation of  $[(\text{NMe})_2\text{sal}^{tert}\text{Bu}_4)\text{Cu}]$ ,  $[(\text{Me}_2\text{salF}_4)\text{Cu}]$  as well as  $[(\text{Ph}_2\text{sal})\text{Cu}]$  occurs fully reversible. In addition to the first reversible oxidation the complexes  $[(\text{NH})_2\text{sal})\text{Cu}]$ ,  $[(\text{Ph}_2\text{sal})\text{Cu}]$ ,  $[(\text{salPh}_2)\text{Cu}]$  and  $[(\text{NMe})_2\text{sal}^{tert}\text{Bu}_4)\text{Cu}]$  exhibit a second oxidation process at slightly higher potential. Spectroelectrochemical investigations revealed that all oxidation processes lead to phenoxyl radical species and (from their charge transfer absorption energy) these species seem to be stable. This discovery is surprising for systems such as  $[(\text{Ph}_2\text{sal})\text{Cu}]$ ,  $[(\text{salPh}_2)\text{Cu}]$ ,  $[(\text{NH})_2\text{sal})\text{Cu}]$  and  $[(\text{NH})_2\text{salPh}_2)\text{Cu}]$ , which are, according to the current opinion, non- or partly stabilised due to lacking substituents on the phenol core.

Considering their physical properties, all complexes might be suitable as GO model systems and therefore applicable in oxidation catalysis. On a first view, neither the lacking substitution nor rigidity of the linker group seems to be a limiting factor. Thus, activities of all complexes should be determined under catalytic reaction conditions. This was done using benzyl alcohol as a substrate, experiments and results are described in Chapter 7.

## 5.0 An O,N chelating triazol ligand (triazH) and its copper complex [Cu(triaz)<sub>2</sub>]

### 5.1 Introduction

The ligand 2,4-di<sup>tert</sup>butyl-6-(5-chloro-2H-benzo[d][1,2,3]triazol-2-yl)phenol (triazH) (Scheme 37) contains <sup>tert</sup>butyl groups in *ortho*- and *para*-position and offers a η<sup>2</sup>-O,N donor set. Copper complexes of this ligand have not been reported, with the exception of the binuclear, organometallic complex [Cu(triaz)<sub>μ</sub>-R]<sub>2</sub> (R = norbornadiene) which contains two Cu<sup>+</sup> ions.<sup>[308]</sup>



Scheme 37: 2,4-di<sup>tert</sup>butyl-6-(5-chloro-2H-benzo[d][1,2,3]triazol-2-yl)phenol (triazH)

The target complex for the following study was [Cu(triaz)<sub>2</sub>], which should be easily obtained from the reaction of deprotonated ligand (2 eq) and an appropriate copper source (1 eq). This complex is expected to be similar to salen type complexes (Chapter 4) since two triaz<sup>-</sup> ligands exhibit the same donor set (N<sub>2</sub>O<sub>2</sub>) as a salen type ligand. In contrast to coordination of salen type ligands, two triaz<sup>-</sup> ligands result in a more flexible complex geometry. Salen type ligands are relatively rigid (depending on the applied linking group) and form square planar complexes with slight distortion, while the complex [Cu(triaz)<sub>2</sub>] is expected to be able to obtain also tetrahedral geometry e.g. upon reduction of Cu<sup>II</sup> to Cu<sup>I</sup>. This might be of advantage for electrochemical processes and simplifies substrate coordination in catalytic reactions. Therefore [Cu(triaz)<sub>2</sub>] can be expected to possess even better catalytic abilities than salen type complexes. On the other hand stereoisomers for [Cu(triaz)<sub>2</sub>] might occur, which is impossible for salen type complexes. In the following, synthesis of [Cu(triaz)<sub>2</sub>] as well as its characterisation are described, especially regarding the electrochemical and spectroelectrochemical properties.

## 5.2 Synthesis and Structure of [Cu(triaz)<sub>2</sub>]

The triazH ligand was commercially purchased and used in complex forming reactions without further purification. Since triazH is sparingly soluble in nearly all solvents despite toluene, which is an unfavourable solvent for established copper sources (such as CuCl<sub>2</sub> or Cu(OAc)<sub>2</sub>), complex formation was carried out in a solvent mixture using MeCN/toluene (5:3). The reaction was carried out at 298 K and yielded a green powder, which was purified by recrystallisation and [Cu(triaz)<sub>2</sub>] was thus isolated in relatively low yield (43%). The completely dry solid was observed to be stable over several weeks, while remaining solvent leads to decomposition upon storage within three to four days. Single crystals of [Cu(triaz)<sub>2</sub>] were obtained from MeCN/toluene solution and analysed by XRD. [Cu(triaz)<sub>2</sub>] was further characterised by absorption spectroscopy, cyclic voltammetry and spectroelectrochemical methods.

The crystal structure of [Cu(triaz)<sub>2</sub>] was solved and refined in the triclinic space group  $P\bar{1}$  (for solution and refinement parameters see Table 34), Figure 39 shows a view on the structure along the *a* axis. In the crystal structure no hydrogen bridges are found, while channels located on the cell edges along the *a* axis are formed by  $\pi$ -stacking of neighbouring triaz-ligands (distance of the ligand planes = 3.4260(8) Å). Each channel is branched with *tert*-butyl groups, half of them posses large thermal ellipsoids, proving that these groups strongly librate. This libration is made possible by the lack of hindering contacts in the crystal packing and by the temperature applied for the measurement (298 K).

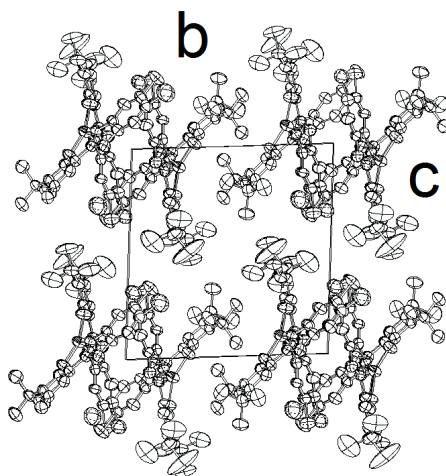
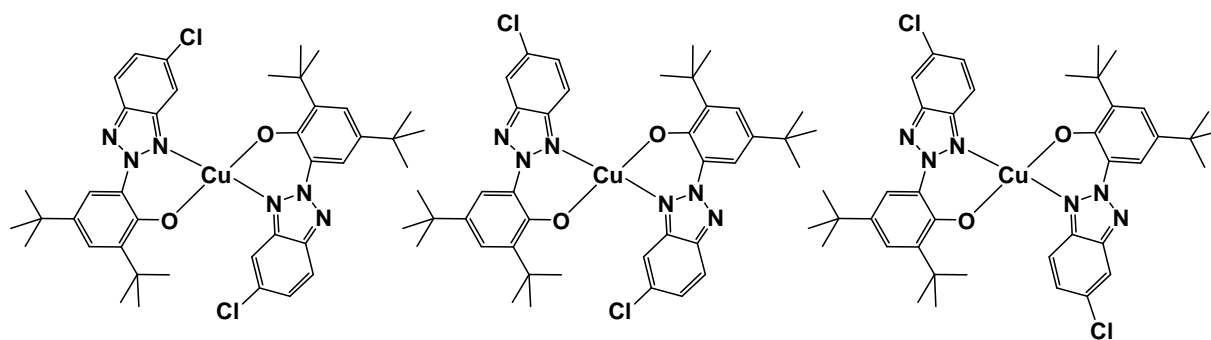


Figure 39: Crystal structure of [Cu(triaz)<sub>2</sub>], view along the *a* axis, thermal ellipsoids shown on 50% probability level, H atoms omitted for clarity

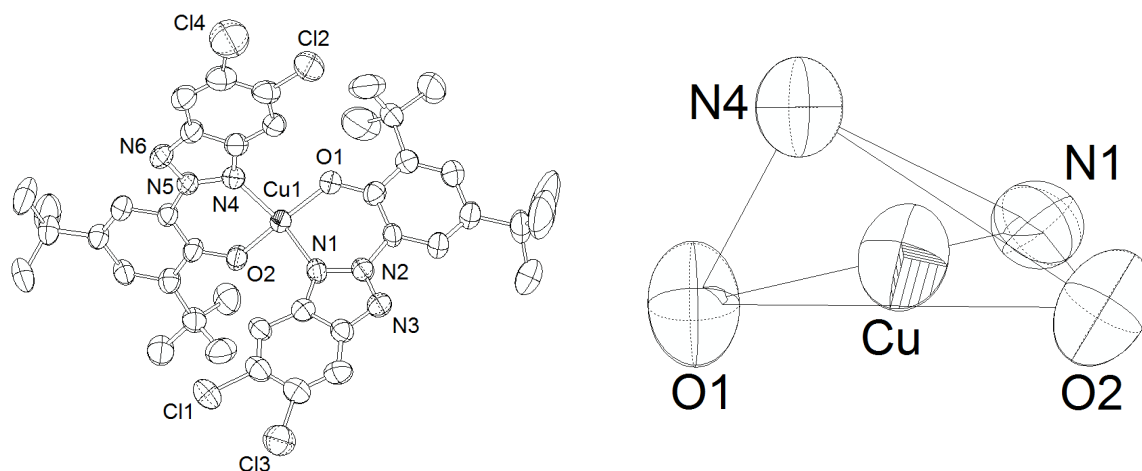
Table 34: Solution and refinement data of [Cu(triaz)<sub>2</sub>]

formula	C <sub>40</sub> H <sub>46</sub> CuN <sub>6</sub> O <sub>2</sub> Cl <sub>2</sub>	abs. coeff / mm <sup>-1</sup>	0.731
f. w. /g mol <sup>-1</sup>	777.27	refl. coll.	24040
crystal system	triclinic	data / restr. / param.	8889 / 6 / 490
crystal shape	needle	h, k, l	-14 < h < 14
colour	green		-17 < k < 17
space group	<i>P</i> $\bar{1}$ (No. 2)		-18 < l < 18
a / Å	11.238(2)	goof on F <sup>2</sup>	0.589
b / Å	13.151(2)	R <sub>int</sub>	0.1691
c / Å	13.648(2)	final R indices	0.0522
α / °	85.54(2)	[I > 2σ(I)]	0.1257
β / °	82.78(2)	R indices (all data)	0.2273
γ / °	80.88(2)		0.2093
volume / Å <sup>3</sup> , Z	1972.2(5), 2	largest diff.	0.264 and -0.402
F(000)	814	p. a. h. / e Å <sup>-3</sup>	
density / g cm <sup>-1</sup>	1.309		

Additionally, a disorder is found in the crystal structure, which is concerning the chlorine atom position (atoms are disordered by 20%). The disorder results from co-crystallisation of three [Cu(triaz)<sub>2</sub>] isomers (Scheme 38) which are formed during the complex synthesis. Isomerisation occurs, since the C–N bond between triazol and phenol subunit of the triaz ligand is freely rotatable (rotation energy seems to be low) and thus two ligand conformations are possible, leading to three different isomers.

Scheme 38: Isomers of [Cu(triaz)<sub>2</sub>]; left: isomer 1; middle isomer 2; right: isomer 3

Interestingly, the crystal mainly contains isomer 1 (only 20% of all molecules are not isomer 1 and thus are isomers 2 and isomer 3 in an unknown ratio). Two reasons can be considered for this: either isomer 1 is thermodynamically favoured and thus the main product of the complex formation, or isomer 1 is favoured for crystallisation.



Figur 40: Molecular structure of  $[\text{Cu}(\text{triaz})_2]$  thermal ellipsoids on 50% probability level, H atoms omitted for clarity; left: complete complex molecule, right: coordination polyhedron

The coordination polyhedron of  $[\text{Cu}(\text{triaz})_2]$  is strongly distorted from square planar geometry (expected for  $\text{Cu}^{\text{II}}$ ) and thus nearly tetrahedral (Figure 40). This distortion is indicated by the angles around the copper ion (Table 35): the values of  $\text{O1-Cu-N1}$  and  $\text{O2-Cu-N4}$  lie close to  $90^\circ$  (expected for a square planar geometry), while  $\text{O1-Cu-N4}$  and  $\text{O2-Cu-N1}$  are markedly larger. The angle sum (for an ideal square planar geometry  $360^\circ$ ) is  $376^\circ$  for  $[\text{Cu}(\text{triaz})_2]$ .

Table 35: Selected distances and angles of  $[\text{Cu}(\text{triaz})_2]$

distances / Å	angles / °		angles / °		
Cu1–O1	1.8606(3)	O1–Cu1–O2	157.06(2)	$\Sigma_{\text{Cu}}^{[\text{a}]}$	376.09(2)
Cu1–O2	1.8541(4)	N1–Cu1–N4	138.59(2)	phenol1–phenol2	62.29(1)
Cu1–N1	1.9588(3)	O1–Cu1–N1	90.92(2)	phenol–triaz	16.45(1)/15.51(1)
Cu1–N4	1.9862(3)	O2–Cu1–N4	91.11(1)	(O1–N4–Cu)–	46.84(1)
		O1–Cu1–N4	98.49(2)	(N1–O2–Cu)	
		O2–Cu1–N1	95.57(2)		

[a]  $\Sigma_{\text{Cu}} = (\text{N1-Cu-O2}) + (\text{O2-Cu-N4}) + (\text{N4-Cu-O1}) + (\text{O1-Cu-N1})$

### 5.3 EPR spectroscopy

The EPR spectrum of  $[\text{Cu}(\text{triaz})_2]$  was recorded at 298 K in the solid state (Figure 41). The signal shape cannot be classified unambiguously. At a first glance, the signal seems to be axial



with  $g_{\parallel} > g_{\perp}$  ( $g_{\parallel} = 2.339$ ,  $g_{\perp} = 2.074$ ,  $\Delta g = 0.265$ ,  $g_{\text{av}} = 2.162$ ) and a  $^{63,65}\text{Cu}$  coupling constant  $A_{\parallel\text{Cu}}$  of 135 G. Closer examination reveals the  $g_{\perp}$  line to be split and therefore the signal might also be rhombic ( $g_1 = 2.339$ ;  $g_2 = 2.088$ ;  $g_3 = 2.048$ ;  $\Delta g = 0.291$ ,  $g_{\text{av}} = 2.158$ ). EPR spectra which have been measured on square planar  $[\text{CuCl}_4]^{2-}$  compounds with varying tetrahedral distortion revealed that increasing distortion corresponds to increasing rhombicity of the EPR spectra.<sup>[241]</sup> Thus the EPR signal recorded on solid  $[\text{Cu}(\text{triaz})_2]$  matches very well with the coordination polyhedron found in its crystal structure.

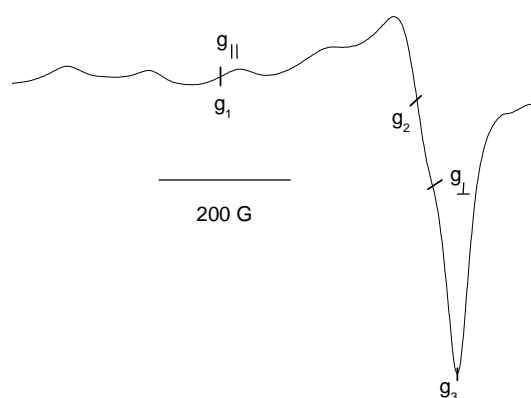


Figure 41: X-band EPR spectrum of  $[\text{Cu}(\text{triaz})_2]$  (solid sample) recorded at 298 K

#### 5.4 Cyclic voltammetry

Cyclic voltammetry was carried out on triazH and  $[\text{Cu}(\text{triaz})_2]$  in  $\text{MeCN}/\text{Bu}_4\text{NPF}_6$  solution at 298 K (Figure 42).

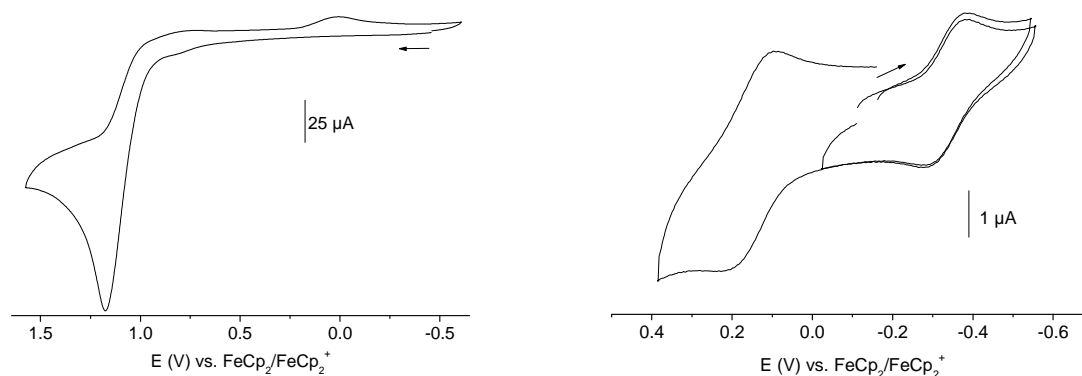


Figure 42: Cyclic voltammograms of triazH (left) and  $[\text{Cu}(\text{triaz})_2]$  (right) in  $\text{MeCN}/\text{Bu}_4\text{NPF}_6$  at 298 K at 100 mV/s scan rate; potentials in V vs.  $\text{FeCp}_2^+/\text{FeCp}_2^+$

The measurements showed that free triazH is oxidised irreversibly at  $E_{pa} = 1.2$  V, while the first reduction of the ligand occurs reversibly at  $E_{1/2} = -1.26$  V.  $[\text{Cu}(\text{triaz})_2]$  can be reduced twice, at  $E_{1/2} = -0.33$  V and  $E_{1/2} = -1.26$  V, the first reduction can be assigned to the  $\text{Cu}^{\text{II}}/\text{Cu}^{\text{I}}$  redox couple, the second reduction is ligand centred. Additionally,  $[\text{Cu}(\text{triaz})_2]$  can be oxidised reversibly at  $E_{1/2} = 0.15$  V. This oxidation is ligand centred as well and supposed to lead to a phenoxyl radical species. Inferred from the electrochemical potentials the phenoxyl radical state seems to be easily accessible, while the  $\text{Cu}^{\text{I}}$  state of the complex is clearly disfavoured. The peak separation  $\Delta E$  ( $E_{pc} - E_{pa}$ ) for the copper centred reduction of  $[\text{Cu}(\text{triaz})_2]$  is small ( $\Delta E = 0.10$  V) in comparison to the  $\Delta E$  of salen type complexes. This indicates high flexibility of  $[\text{Cu}(\text{triaz})_2]$  in forming different coordination polyhedra.

### 5.5 Absorption spectroscopy and spectroelectrochemistry

Absorption spectra were recorded in MeCN/toluene solution (Table 36) and revealed two UV absorption bands for the free triazH ligand, which can be assigned to  $\pi\text{-}\pi^*$  transition as indicated by their high extinction coefficients. These absorption bands can also be found in the  $[\text{Cu}(\text{triaz})_2]$  complex (with slightly decreased intensity) accompanied by a long-wavelength band at 647 nm. This absorption is assigned to a d-d transition and corresponds to a relatively strong ligand field with a  $t_{2g}/e_g$  separation of  $15385\text{ cm}^{-1}$  (1.91 eV).

Table 36: Absorption bands of triazH and  $[\text{Cu}(\text{triaz})_2]$ <sup>[a]</sup>

compound	$\lambda / \text{nm}$ ( $\epsilon / \text{Lmol}^{-1}\text{cm}^{-1}$ )
triazH	312 (41674), 348 (47659)
$[\text{Cu}(\text{triaz})_2]$	307 (19362), 346 (19747), 647 (241)
$[\text{Cu}(\text{triaz})_2]^{\bullet+}$	321, 404

[a] Absorption spectra measured in MeCN/toluene (5/3) solution, spectroelectrochemistry performed in MeCN/<sup>m</sup>Bu<sub>4</sub>NPF<sub>6</sub>

Spectroelectrochemical characterisation of  $[\text{Cu}(\text{triaz})_2]$  was performed in MeCN/<sup>m</sup>Bu<sub>4</sub>NPF<sub>6</sub> solution. Therefore absorption maxima of the parent species are slightly blue-shifted if compared to those recorded in MeCN/toluene solution. Upon electrochemical oxidation a new band at

404 nm appears, which is typical for charge transfer absorption of copper phenoxyl species and thus assigned to the formation of  $[\text{Cu}(\text{triaz})_2]^{\bullet+}$ . The wavelength of the absorption band is typical for alkyl stabilised phenoxyl radicals.<sup>[248]</sup>

### 5.6 Summary on the suitability of $[\text{Cu}(\text{triaz})_2]$ as a GO model system

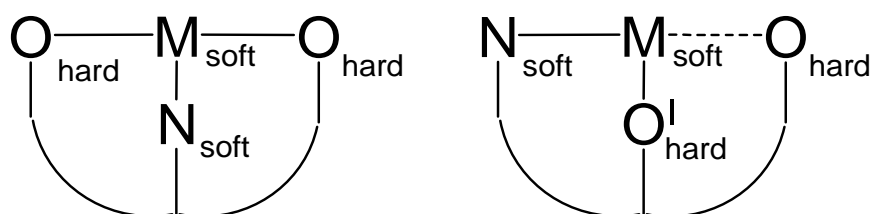
Similar to other copper complex possessing di<sup>tert</sup>butyl substituted phenol moieties, the complex  $[\text{Cu}(\text{triaz})_2]$  was expected to form  $[\text{Cu}(\text{triaz})_2]^{\bullet+}$  upon oxidation. This was confirmed by cyclic voltammetry and spectroelectrochemistry. The formation of the radical species proceeds reversibly at 0.15 V. Furthermore, the reversible  $\text{Cu}^{\text{II}}/\text{Cu}^{\text{I}}$  reduction was detected at  $-0.33$  V with small peak-to-peak separation. This is due to strong tetrahedral distortion of  $[\text{Cu}(\text{triaz})_2]$  which simplifies the geometry change upon  $\text{Cu}^{\text{II}}/\text{Cu}^{\text{I}}$  reduction. Hence  $[\text{Cu}(\text{triaz})_2]$  is a promising candidate for catalytic alcohol oxidation. Both redox couples (phenoxyl radical and copper redox couple) are slightly disfavoured compared to the corresponding redox couples in natural GO (0.01 V for the tyrosyl radical and  $-0.24$  V for the copper redox couple). Due to its spectroscopic properties,  $[\text{Cu}(\text{triaz})_2]$  seems to be the ideal system for a close examination in catalytic test reactions. A detailed study on  $[\text{Cu}(\text{triaz})_2]$  as oxidation catalyst is presented in Chapter 7.

## 6.0 Highly flexible O,O',N Ligands and their Co, Fe, Ni, Cu and Zn complexes

### 6.1 Introduction

As outlined in Chapter 2, oxido-pincer ligands usually bear an aromatic central core and two *ortho* substituents carrying various oxygen functions thus providing a tridentate O,E,O donor set where E = C, N, P or else. Most important are ligands with a central pyridine ring, which have found a number of applications e.g. in catalysis.<sup>[181,182,185,309]</sup> Typical oxido donor functions can be carboxylates<sup>[186,194,310]</sup>, carbonyl<sup>[311]</sup> or alcohol functions<sup>[312-314]</sup>. The latter are interesting, since they provide the opportunity of stepwise deprotonation upon coordination and this leads to a huge diversity of complexes and structures. An increasing tendency to deprotonation is expected with increasing hardness (HSAB) of the metal ion. Consequently, complexes of early transition metals exclusively contain the fully deprotonated ligand dianion.<sup>[315-318]</sup> Intermediate cases (partly deprotonated) were found in polynuclear manganese complexes<sup>[319-321]</sup> while the ligand usually coordinates fully protonated to late transition metals (Co – Zn, 4d and 5d metals)<sup>[200,322-327]</sup>. However, there are also exceptions from this correlation, e.g. found in  $[\text{Cu}_2(\eta^2, \mu\text{-pydimH})_2(\eta^3\text{-pydimH}_2)_2]^{2+}$ <sup>[324,328]</sup> and in  $[\text{Cu}(\text{pydimH}_2)(\text{pydimH})]^+$ <sup>[324]</sup>.

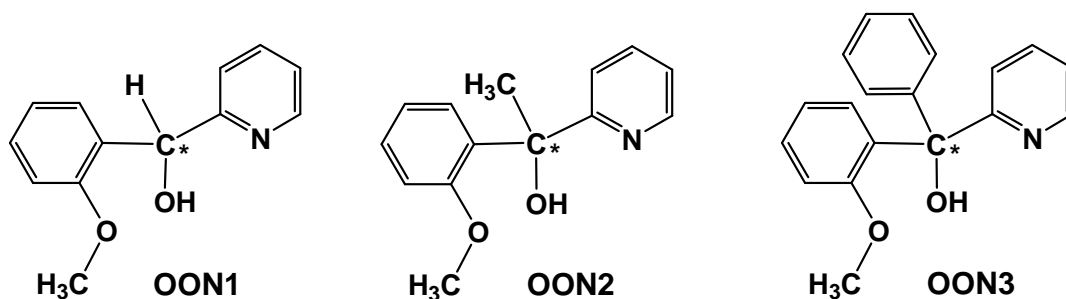
In agreement with the HSAB concept<sup>[4,329]</sup> weak bonds are observed between the O-donor functions and late transition metals like  $\text{Co}^{\text{II}}$ ,  $\text{Ni}^{\text{II}}$ ,  $\text{Cu}^{\text{II}}$  and  $\text{Zn}^{\text{II}}$ , while the metals  $\text{Pd}^{\text{II}}$  and  $\text{Pt}^{\text{II}}$  are exclusively bound via the pyridine nitrogen.<sup>[183,330,331]</sup> As a result, oxido-pincer ligands show a wealth of structural motifs including square planar (Pt, Pd), trigonal bipyramidal (Co, Ni, Zn), square pyramidal (Cu) and octahedral (Co, Ni, Cu, Zn) coordination.<sup>[183,184,332]</sup>



Scheme 39: Schematic binding situation of O,N,O oxido-pincer ligands compared to O,O',N ligands to soft transition metal ions

Most of the so far reported studies focus on symmetric oxido-pincer ligands with an O,N,O donor set. The modification of the donor atom sequence from O,N,O to O,O,N or O,O',N (Scheme 39) bears some interesting possibilities as the intrinsic non-symmetry and the option to built up hemilabile systems resulting from the *trans*-effect of the (presumably) strong N–M interaction weakening the peripheral M–O bond.

If the outer O donor is designed to be a phenoxy moiety, this allows generating weakly coordinated phenoxy moieties. Copper complexes of this type would close the gap between lacking interaction between copper ion and phenoxy radical as found for pydic-ester ligands (Chapter 2.1) and strong interaction as found for bis-phenoxido pincers, benzoquinone-, acridine- and salen type ligands (Chapters 2.2, 3 and 4).



Scheme 40: Three new chiral O,O',N pincer ligands; left: 2-(hydroxy(pyridin-2-yl)methyl)methoxyphenol (OON1), middle: 2-(1-hydroxy-1-(pyridin-2-yl)ethyl)phenol (OON2), right: 2-(hydroxy(phenyl)(pyridin-2-yl)methyl)phenol (OON3)

In this contribution three new chiral O,O',N pincer ligands were synthesised (Scheme 40). The new ligands were designed focussing on four main aspects. i) In comparison with the frequently used oxido-pincer ligands with a central pyridine core and two pendant carboxylate or methanol functions, the new ligands provide a change in donor atom sequence O,N,O  $\rightarrow$  O,O',N and an altered sequence of (expected) binding strength  $O_{\text{weak}}, N_{\text{strong}}, O_{\text{weak}} \rightarrow O_{\text{weak}}, O'_{\text{weak}}, N_{\text{strong}}$  as indicated in Scheme 39. ii) The ligands provide the possibility of tris-chelate binding, upon forming two five-membered chelate rings. In contrast to ligands containing rigid aromatic cores such as pyridine the central binding position here is far more flexible and might open the option of a  $\eta^3$ -facial binding, while pyridine centred ligands allow only  $\eta^3$ -meridional binding. The steric bulk at the central C atom increases within the series OON1 < OON2 < OON3, while the acidity of the hydroxy function is expected to decrease along the series OON3 > OON1 > OON2. iii) Only one of the two oxido donor functions can be deprotonated upon coordination, since the

second is a methoxy group. The methoxy and hydroxy functions are expected to exert approximately the same binding strength but deprotonation of the central hydroxy group will greatly enhance its coordination capacity over that of the methoxy group (creating a  $O_{\text{weak}}, O'_{\text{strong}}, N_{\text{strong}}$  binding situation). iv) The new ligands are chiral due to four different substituents at the central C atom. Thus the chiral centre is very close to the metal atom, which might be important for the transfer of chiral information to a substrate bound at the central metal atom.

The three ligands were reacted to  $Fe^{III}$ ,  $Fe^{II}$ ,  $Co^{II}$ ,  $Ni^{II}$ ,  $Cu^{II}$  and  $Zn^{II}$ . The chosen metal ions, are expected to increase in "hardness" along the series  $Cu^{II} < Ni^{II} < Co^{II} < Fe^{II} < Fe^{III}$  and also provide different preferences for feasible coordination polyhedra. The resulting metal complexes were characterised by their elemental analysis and UV/vis absorption spectroscopy, in case of the diamagnetic  $Zn^{II}$  and potentially diamagnetic  $Ni^{II}$  compounds additionally by  $^1H$  and  $^{13}C$  NMR spectroscopy. The paramagnetic  $Co^{II}$ ,  $Cu^{II}$  and  $Fe^{III}$  complexes were investigated by EPR spectroscopy, EPR measurements of the  $Co^{II}$  complexes were complemented by magnetic SQUID measurements. Structural characterisation is completed by XRD on obtained single crystals. Electrochemical experiments (cyclic voltammetry) were performed as well.

## 6.2 Ligand preparation

The ligands were synthesised by Grignard coupling reaction of 2-iodo-anisole with 2-formylpyridine (OON1), 2-acetylpyridine (OON2), or 2-benzoylpyridine (OON3) respectively. The resulting ligands were obtained as racemates and characterised by NMR and elemental analysis. Since for a first view on the coordination chemistry of the ligands the chirality is not of importance, all ligands were used as racemates for complex synthesis and characterisation. The ligands exhibit a good solubility in organic solvents and were purified by recrystallisation from acetone, upon which single crystals of OON2 and OON3 were obtained and analysed by XRD. The ligands OON2 and OON3 were found to crystallise in the triclinic space group  $P\bar{1}$ , crystal data can be found in the appendix. In the crystal of OON2 three intermolecular hydrogen bridges were found ( $O1-H100\cdots N1$  with a D $\cdots$ A distance of 2.976(2) Å,  $C13-H13\cdots O1$  with a D $\cdots$ A distance of 2.710(2) Å and  $C7-H7\cdots O2$  with a D $\cdots$ A distance of 2.985(2) Å). These interaction

can be considered to be weak electrostatic.<sup>[333]</sup> H bonds involving the phenol substituent of OON3 were not found in the crystal structure. Additionally, a rather short intramolecular O1–H $\cdots$ O2 hydrogen bridge ((O $\cdots$ H = 1.86(4) Å, D $\cdots$ A distance of 2.644(3) Å, O $\cdots$ H–O = 138(4)°) is found. Figure 44 displays the molecular structures of OON2 and OON3 including the intramolecular O1–H $\cdots$ O2 hydrogen bridge in OON3.

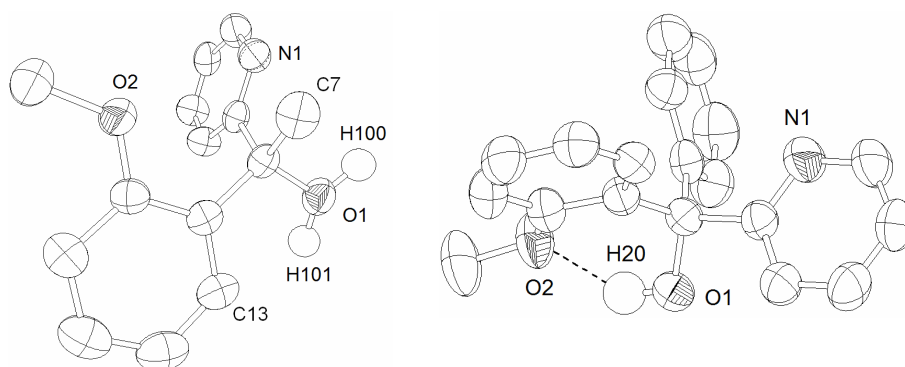


Figure 44: ORTEP representations of molecular structures of OON2 (left) and OON3 (right), 50% probability level, H atoms omitted for clarity despite those involved in the H bridge in OON3 and the disordered (50%) proton on O1 of OON2

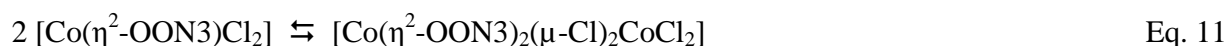
In the molecular structures of the free ligands the O,O',N binding pocket is not available. E.g. torsion angles O1–C–C–N1 of 98.9(2)° in OON2 and 149.9(2)° in OON3 show that the pyridine ring has to rotate about the C–C axis by approximately 98° or 150° respectively to allow an effective five-ring chelate coordination of the pyridine N and the hydroxo donor function. The methoxy function is also largely bent away from the hydroxy oxygen atom for OON2, while for OON3 the intramolecular hydrogen bridge brings the two oxygen atoms in perfect position for a potential chelate binding. On the other hand the interplanar angle of anisol and pyridine ring is about 39.7(1)° for OON3 and 83.31(1)° for OON2.

Summarising, the potentially coordinating sites (O,O',N) in both ligand are arranged around the central chiral C atom in a rather flexible way and the conformational changes necessary to allow tridentate coordination are probably very small.

### 6.3 Complex synthesis

The complexes were obtained by stirring the metal chloride salts with the ligands in a 1:1 ratio at 298 K in methanol for 16 h and without the use of external base. Strongly coloured

products of the general formulae  $[M^{II}(O,O',N)Cl_2]$  ( $M = Fe, Ni, Cu, Zn$ ) or  $[Fe^{III}(O,O',N)Cl_3]$  (except OON2) were obtained in high yields. Using  $Co^{II}$  as metal the complexes undergo a fast so called coordinative disproportionation following Eq. 11, thus the formed complexes possess the general formula  $[Co(O,O',N)(\mu-Cl)_2CoCl_2]$ . A similar type of reaction was already observed for several pyridine-dimethanol pincer complexes providing an O,N,O donor coordination (Eq. 12). The disproportionation of compounds containing O,N,O pincer ligands, which provide a tridentate binding mode, leads to the formation of ionic complexes. This is due to the saturation of the cobalt ion by two O,N,O donor ligands and the formation of the very stable  $[CoCl_4]^{2-}$  ion. The O,O',N ligands obviously do not prefer a tridentate binding mode (see below), hence a fusion of the resulting ions to a neutral binuclear complex seems to be thermodynamically favoured although this lowers the entropy of the system.



Using O,O',N donor ligands a coordinative disproportionation is only observed for cobalt complexes (using O,N,O donor ligands also Ni, Cu and Zn show disproportionation). On the one hand this is due to a large stabilising effect achieved for a  $d^7$  high spin system ( $Co^{II}$ ) upon formation of a  $[MCl_4]^{2-}$  ion, on the other hand this is due to the stabilisation of pentacoordinated complexes (square pyramidal or trigonal bipyramidal) in complexes of iron, copper and zinc.

While the Co, Ni, Cu and Zn compounds show good solubility in polar organic solvents such as acetone, methanol, ethanol, THF, DMF or MeCN, the  $Fe^{II}$  and  $Fe^{III}$  compounds are less soluble and despite  $[Fe(OON3)Cl_3]$  and  $[Fe(OON1)Cl_3]$  they precipitated from the methanol reaction mixture. The iron complexes therefore require strongly polar solvents such as MeCN or DMF to be redissolved. Several attempts to obtain the  $Fe^{III}$  complex  $[Fe(OON2)Cl_3]$  failed. In any case virtually insoluble orange material was obtained which gave elemental analyses far from a reasonable stoichiometry.

#### 6.4 NMR spectroscopy

From the  $Zn^{II}$  compounds ( $d^{10}$  diamagnetic) NMR spectra could be obtained, Table 37 lists selected data. Special attention was paid to the chemical shifts of the OH,  $OCH_3$  and  $H_{6_{py}}$  atoms



which best indicate coordination of the metal to the adjacent donor atoms. Since this coordination might be depending on the solvent polarity and/or the solvent's ability to act as a ligand, spectra were recorded in  $\text{CDCl}_3$  (unpolar, non-coordinating),  $[\text{D}_6]$ -acetone (polar, presumably non-coordinating),  $[\text{D}_4]$ -methanol (highly polar, potentially coordinating),  $[\text{D}_5]$ -pyridine and  $[\text{D}_7]$ -DMF (both polar, presumably coordinating).

Table 37: Selected NMR data for free OON ligands and  $\text{Zn}^{\text{II}}$  complexes<sup>[a]</sup>

in $\text{CDCl}_3$	$\delta\text{H}_{6_{\text{py}}}$	$\Delta\delta$	$\delta\text{OH}$	$\Delta\delta$	$\delta\text{OMe}$	$\Delta\delta$
OON1	8.54		5.20		3.86	
$[\text{Zn}(\text{OON1})\text{Cl}_2]$	8.71	0.17	7.30	2.10	3.75	0.11
OON2	8.49		5.12		3.56	
$[\text{Zn}(\text{OON2})\text{Cl}_2]$	8.73	0.24	6.55	1.43	3.71	0.15
OON3	8.55		5.71		3.53	
$[\text{Zn}(\text{OON3})\text{Cl}_2]$	8.74	0.19	7.72	2.01	3.81	0.28
in $[\text{D}_6]$ -acetone	$\delta\text{H}_{6_{\text{py}}}$	$\Delta\delta$	$\delta\text{OH}$	$\Delta\delta$	$\delta\text{OMe}$	$\Delta\delta$
OON1	8.50		5.33		3.83	
$[\text{Zn}(\text{OON1})\text{Cl}_2]$	8.76	0.26	8.77	3.44	3.84	0.01
OON2	8.42		5.10		3.55	
$[\text{Zn}(\text{OON2})\text{Cl}_2]$	8.70	0.28	7.94	2.84	3.49	0.06
OON3	8.46		5.67		3.49	
$[\text{Zn}(\text{OON3})\text{Cl}_2]$	8.73	0.27	8.18	2.51	3.66	0.17
in $[\text{D}_4]$ -methanol	$\delta\text{H}_{6_{\text{py}}}$	$\Delta\delta$	$\delta\text{OH}$	$\Delta\delta$	$\delta\text{OMe}$	$\Delta\delta$
OON3	8.15		5.59		<sup>[b]</sup>	-
$[\text{Zn}(\text{OON3})\text{Cl}_2]$	8.35	0.20	7.06	1.47	<sup>[b]</sup>	-
in $[\text{D}_7]$ -DMF	$\delta\text{H}_{6_{\text{py}}}$	$\Delta\delta$	$\delta\text{OH}$	$\Delta\delta$	$\delta\text{OMe}$	$\Delta\delta$
OON3	8.56		6.03		3.56	
$[\text{Zn}(\text{OON3})\text{Cl}_2]$	8.58	0.02	6.16	0.13	3.57	0.01
in $[\text{D}_5]$ -pyridine	$\delta\text{H}_{6_{\text{py}}}$	$\Delta\delta$	$\delta\text{OH}$	$\Delta\delta$	$\delta\text{OMe}$	$\Delta\delta$
OON3	8.56		5.03		3.35	
$[\text{Zn}(\text{OON3})\text{Cl}_2]$	8.56	0	5.71	0.68	3.35	0

[a] Chemical shifts  $\delta$  in ppm vs. TMS; change of the chemical shift  $\Delta\delta$  upon coordination in ppm

[b] Obscured by solvent signal

Upon coordination the  $^1\text{H}$  signals of protons adjacent to donor atoms usually exhibit a low-field shift. In  $\text{CDCl}_3$  these shifts are relatively small for the  $\text{H}_{6_{\text{py}}}$  atom and the OMe group ( $\Delta\delta = 0.1 - 0.28$  ppm) but large for the OH group (1.4 – 2.1 ppm). In  $[\text{D}_6]$ -acetone the  $\Delta\delta$  values for the

H<sub>6py</sub> and OH protons point to coordination, while the values for the OMe group for the complexes with OON1 and OON2 drop to zero (indicating non-coordination). Qualitatively the same holds for [Zn(OON3)Cl<sub>2</sub>] in [D<sub>4</sub>]-methanol, but the OMe proton signal overlaps with the signal of the solvent protons and thus cannot be studied. Importantly, the OH proton of the ligands can be unequivocally detected, thus the ligands remain protonated upon coordination. In the coordinating solvents DMF and pyridine the  $\Delta\delta$  values strongly indicate that the O,O',N ligands were replaced by solvent molecules, the shift observed for the OH proton might also be due to H bridge formation with solvent molecules.

For the Ni<sup>II</sup> complexes the <sup>1</sup>H NMR spectra show paramagnetic broadening, so 2D experiments failed and no assignments of the signals were made. As a consequence comparison of the shifts of free ligands and complexes fails. For the Ni<sup>II</sup> complexes tetrahedral or (distorted) octahedral configurations can be assumed from this behaviour. This is in contrast to recently reported Ni complexes of oxido-pincer ligands with phenolate groups [2,6-bis(2-methoxyphenyl)pyridine (LOMe<sub>2</sub>), 2,6-bis(2-hydroxyphenyl)pyridine (LOH<sub>2</sub>), 2,6-bis-(2,4-dimethoxyphenyl)pyridine (LOMe<sub>4</sub>)] which were diamagnetic, bromido bridged dimers.<sup>[332]</sup> For the Fe<sup>II</sup> complex [Fe(OON1)Cl<sub>2</sub>] bad solubility and paramagnetic impurities prevented any NMR measurements. Thus a high spin configuration can be concluded which would lead to systems with  $S = 2$  for both, octahedral or tetrahedral complex geometries.

## 6.5 Crystal and molecular structures from XRD

From the compounds [Co(OON3)<sub>2</sub>( $\mu$ -Cl)<sub>2</sub>CoCl<sub>2</sub>] $\cdot$ C<sub>3</sub>H<sub>6</sub>O, [Fe(OON1)Cl<sub>2</sub>]<sub>2</sub>, [Cu(OON1)Cl<sub>2</sub>]<sub>n</sub> and [Cu(OON3)Cl<sub>2</sub>]<sub>2</sub> single crystals were obtained and could be analysed by XRD. Details of the structures were shown in Figures 45-48 and Tables 38 and 40 summarise essential crystal and structural data.

The crystal structure of [Co(OON3)<sub>2</sub>( $\mu$ -Cl)<sub>2</sub>CoCl<sub>2</sub>] $\cdot$ C<sub>3</sub>H<sub>6</sub>O was solved and refined in the triclinic space group  $P\bar{1}$ . In the crystal structure no packing effects such as H bridges or  $\pi$ -stacking can be observed. This is mirrored by the very low density in the crystal structure, the lowest in the whole series (Table 38)

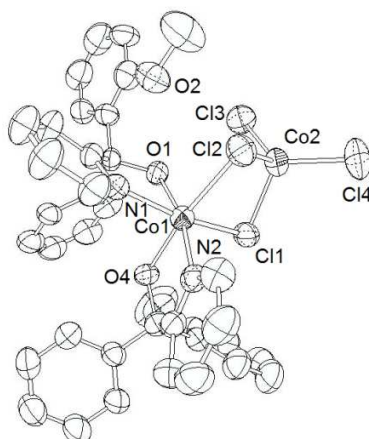


Figure 45: ORTEP representation (50% probability level) of the molecular structure of  $[\text{Co}(\text{OON3})_2(\mu\text{-Cl})_2\text{CoCl}_2]$ , H atoms and solvent molecule are omitted for clarity

The complex molecule consists of two fused cobalt centres, an octahedral  $(\text{OON3})_2\text{Co}$  fragment and a tetrahedral  $\text{CoCl}_4$  fragment. Both fragments are covalently bonded by two  $\mu\text{-Cl}$  bridges (Figure 45). The two coordination polyhedra are slightly distorted and share edges. The  $\text{Co1}-(\mu\text{-Cl})$  bonds are slightly longer (2.441(2) Å and 2.494(2) Å) than the  $\text{Co2}-(\mu\text{-Cl})$  bonds (2.305(2) Å and 2.321(2) Å) but they are still in the range of covalent bonds. The two OON3 ligands coordinate in a bidentate mode and the methoxy groups lie far away from the cobalt ions. The complex molecule contains OON3 ligands with *R* and *S* chirality, the resulting complex is achiral.

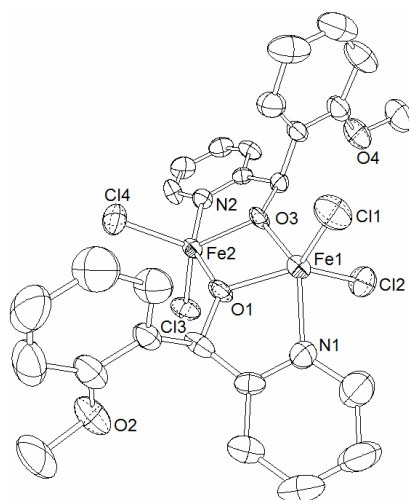
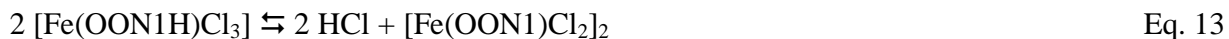


Figure 46: ORTEP representation (50% probability level) of the molecular structure of  $[\text{Fe}(\text{OON1})\text{Cl}_2]_2$ , H atoms are omitted for clarity

When recrystallising the complex  $[\text{Fe}(\text{OON1})\text{Cl}_3]$  from acetone, single crystals of the

dimeric complex  $[\text{Fe}(\text{OON1})\text{Cl}_2]_2$  were obtained (Figure 46). The compound has obviously been formed through elimination of HCl (Eq. 13)



The crystal structure was solved and refined in the triclinic space group  $P\bar{1}$  (Tables 38,40). In the crystal structure the two iron atoms are bridged by the central deprotonated oxido function of the OON1 ligand, forming a polyhedron of two edge-sharing (distorted) trigonal bipyramids with a nearly planar  $\text{Fe}_2\text{O}_2$  core (with a dihedral angle  $\text{Fe1-O1-Fe2-O2}$  of  $-9.8(2)^\circ$  and small  $\text{O-Fe-O}$  angles of about  $73.31(2)^\circ$  and  $73.12(2)^\circ$ ). The trigonal planes around  $\text{Fe}^{\text{III}}$  are formed by the two chlorido ligands and one of the bridging O atoms. The axial positions are occupied by the pyridine N atoms and the second bridging O atom, the angles  $\text{N1-Fe1-O3}$  ( $147.0(2)^\circ$ ) and  $\text{N2-Fe2-O1}$  ( $150.1(2)^\circ$ ) deviate markedly from the ideal angle of  $180^\circ$ . The methoxy function remains uncoordinated. Interestingly, the dimer is formed by two mononuclear units which contain ligands of the same chirality; one of the molecules in the unit cell possesses ligands of *R* configuration, this is depicted in Figure 46, the other molecule possesses ligands of *S* chirality, thus in the crystal structure both types of stereoisomers occur.

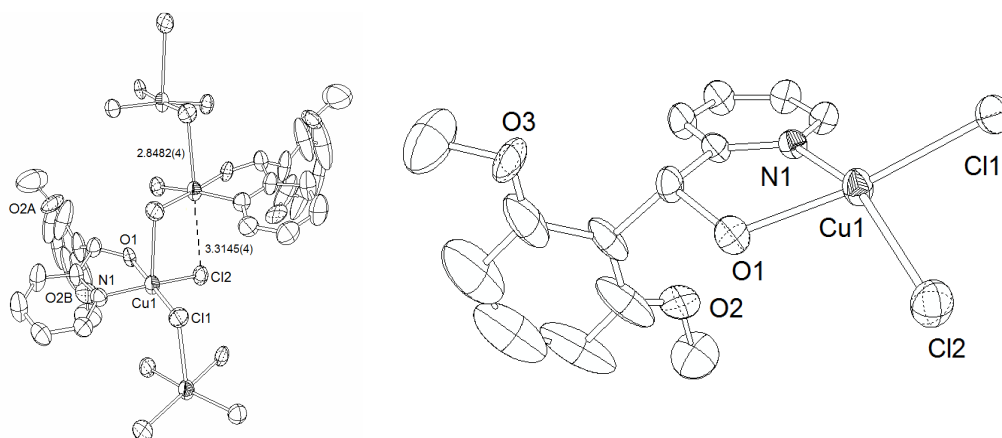


Figure 47: ORTEP representation (30% probability level) of - left: view on the polymeric chain structure of  $[\text{Cu}(\text{OON1})\text{Cl}_2]_n$ ; right: the asymmetric unit in the chain structure with the disordered anisol ring (right); H atoms are omitted for clarity

The  $\text{Cu}^{\text{II}}$  compound  $[\text{Cu}(\text{OON1})\text{Cl}_2]_n$  was crystallised from acetone and the structure was solved and refined in the monoclinic space group  $P2_1/c$  (Table 38). Essential binding parameters are summarised in Table 40, while Figure 47 gives a view on one of the polymer strands along the *c* axis and a mononuclear unit. The structure shows a one-dimensional polymer, in which

square planar coordination units consisting of  $\text{Cu}^{\text{II}}$ , the  $\eta^2\text{-N,O}$  bound ligand OON1 and two Cl ligands, were interconnected along the crystallographic  $c$  axis by rather long axial Cl–Cu bonds (using one of the Cl ligands). While the Cu–Cl bond in the apical position is 2.848(2) Å, the Cu–Cl distance opposite is 3.144(4) Å (Figure 47). Although this is a very long Cu–Cl distance, similar bond lengths<sup>[334,335]</sup> or even longer distances (about 3.5 Å)<sup>[336]</sup> have been found. The overall geometry around the Cu atom is thus square pyramidal (or asymmetrically elongated octahedral). Similar to the  $\text{Fe}^{\text{III}}$  complex, OON1 coordinates in a bidentate mode to the  $\text{CuCl}_2$  fragment and a 50% disorder of the methoxy groups was found. The OON1 ligands alternate in the chain structure so that all ligands on one side of the chain possess the same chirality.

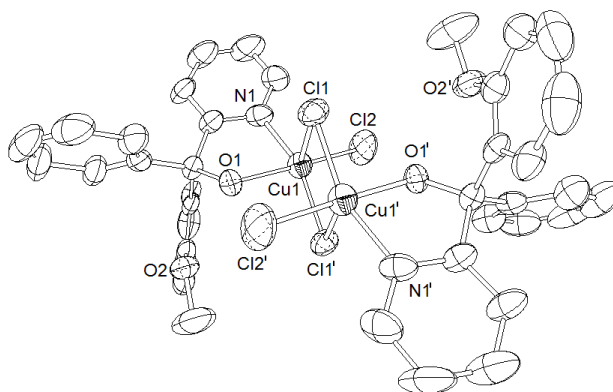


Figure 48: ORTEP representation of the molecular structure of  $[\text{Cu}(\text{OON3})\text{Cl}_2]_2$  (50% probability level); H atoms are omitted for clarity

The  $\text{Cu}^{\text{II}}$  compound  $[\text{Cu}(\text{OON3})\text{Cl}_2]_2$  was crystallised from acetone and the structure was solved and refined in the monoclinic space group  $P2_1/c$  (Tables 38,39). The structure shows a binuclear  $\mu\text{-Cl}_2$ -bridged complex entity. The crystal structure reveals a short intramolecular H bridge between O2 and H1 with a distance of 1.94(5) Å. Furthermore, intermolecular  $\pi$  stacking along the crystallographic  $a$  axis is observed for the anisol rings of neighbouring molecules. Both rings are coplanar ( $0.00(3)^\circ$ ) and exhibit a rather short distance (3.53(2) Å). In the binuclear  $[\text{Cu}(\text{OON3})\text{Cl}_2]_2$  molecules  $\text{Cu}^{\text{II}}$  (Figure 48) is coordinated by the N and O atoms of the OON3 ligand, one peripheral chlorido ligand and two bridging chlorido ligands. The resulting coordination polyhedra can be ascribed as distorted square pyramidal with the  $\mu\text{-Cl}$  (Cl1) atom in the axial positions or as distorted trigonal bipyramidal with N1 and Cl1' as axial ligands (Table 39). The two OON3 ligands which are part of the binuclear molecule reveal opposite chirality, in contrast to the iron complex but similar to the cobalt complex  $[\text{Co}(\text{OON3})_2(\mu\text{-Cl})_2\text{CoCl}_2]$ . Again, the methoxy group is non-coordinating ( $\text{Cu}\cdots\text{OMe} = 4.121(2)$  Å).

Table 38: Crystal structure and refinement data of  $[\text{Co}(\text{OON3})_2(\mu\text{-Cl})_2\text{CoCl}_2]\cdot\text{C}_3\text{H}_6\text{O}$ ,  $[\text{Fe}(\text{OON1})\text{Cl}_2]_2$ ,  $[\text{Cu}(\text{OON1})\text{Cl}_2]_n$  and  $[\text{Cu}(\text{OON3})\text{Cl}_2]_2$ 

Compound	$[\text{Co}(\text{OON3})_2(\mu\text{-Cl})_2\text{CoCl}_2]\cdot\text{C}_3\text{H}_6\text{O}$	$[\text{FeCl}_2(\text{OON1})]_2$	$[\text{CuCl}_2(\text{OON1})]_n$	$[\text{CuCl}_2(\text{OON3})]_2$
formula	$\text{C}_{41}\text{H}_{40}\text{Cl}_4\text{Co}_2\text{N}_2\text{O}_5$	$\text{C}_{26}\text{H}_{24}\text{Cl}_4\text{Fe}_2\text{N}_2\text{O}_4$	$[\text{C}_{13}\text{H}_{12}\text{Cl}_2\text{CuNO}_2]_n$	$\text{C}_{38}\text{H}_{34}\text{Cl}_4\text{Cu}_2\text{N}_2\text{O}_4$
f. w. / $\text{g mol}^{-1}$	900.41	681.98	348.68	851.59
crystal system	triclinic	triclinic	monoclinic	monoclinic
crystal shape	block	block	fraction	block
colour	blue	red	green	green
space group	$P\bar{1}$ (No. 2)	$P\bar{1}$ (No. 2)	$P2_1/c$ (No. 14)	$P2_1/c$ (No. 14)
a / $\text{Å}$	8.983(2)	9.882(5)	14.674(2)	9.073(2)
b / $\text{Å}$	12.107(3)	11.354(5)	14.407(2)	11.196(2)
c / $\text{Å}$	19.539(5)	14.259(5)	7.0563(9)	18.518(3)
$\alpha / ^\circ$	92.74(2)	79.901(5)	90	90
$\beta / ^\circ$	97.43(2)	87.670(5)	103.84(2)	100.18(2)
$\gamma / ^\circ$	94.01(2)	65.751(5)	90	90
volume / $\text{Å}^3$ , Z	2098.7(8), 2	1435.2(4), 2	1448.5(3), 4	1851.5(7), 2
F(000)	924	692	704	868
density / $\text{g cm}^{-3}$	1.425	1.58	1.60	1.53
abs. coeff / $\text{mm}^{-1}$	1.089	1.418	1.872	1.480
refl. coll.	20126	17398	13633	17774
data / restr. / param.	9100 / 0 / 493	6418 / 0 / 345	3342 / 36 / 193	4478 / 0 / 228
indices	$-11 < h < 10$ $-15 < k < 15$ $-24 < l < 25$	$-13 < h < 13$ $-13 < k < 13$ $-18 < l < 18$	$-19 < h < 19$ $-19 < k < 19$ $-8 < l < 8$	$-11 < h < 11$ $-14 < k < 14$ $-24 < l < 24$
goof on $F^2$	0.653	0.666	0.845	0.655
$R_{\text{int}}$	0.0982	0.1593	0.1464	0.2427
final R indices	R1 = 0.0477	R1 = 0.0464	R1 = 0.0467	R1 = 0.0452
$[I > 2\sigma(I)]$	wR2 = 0.0931	wR2 = 0.0692	wR2 = 0.1452	wR2 = 0.0542
R indices (all data)	R1 = 0.2007 wR2 = 0.1211	R1 = 0.1911 wR2 = 0.0692	R1 = 0.0880 wR2 = 0.0749	R1 = 0.2433 wR2 = 0.0824
largest diff. p. a. h. / $\text{e Å}^{-3}$	0.937 and -0.397	0.391 and -0.484	0.421 and -0.494	0.298 and -0.340

Table 39: Angles found for  $[\text{Cu}(\text{OON3})\text{Cl}_2]_2$  compared to angles of ideal coordination polyhedra

angles	found	TBP - ideal	TPy - ideal
O1-Cu1-Cl2	171.23(1) $^\circ$	120 $^\circ$	180 $^\circ$
N1-Cu1-Cl1'	159.28(1) $^\circ$	180 $^\circ$	180 $^\circ$
O1-Cu1-Cl1	85.42(1) $^\circ$	120 $^\circ$	90 $^\circ$
Cl1'-Cu1-Cl1	97.014(9) $^\circ$	90 $^\circ$	90 $^\circ$
Cl2-Cu1-Cl1	102.07(1) $^\circ$	120 $^\circ$	90 $^\circ$
N1-Cu1-Cl1	95.29(1) $^\circ$	90 $^\circ$	90 $^\circ$
Cl1-Cu1-Cl2	96.82(2) $^\circ$	90 $^\circ$	90 $^\circ$
Cl1'-Cu1-O1	86.668(9) $^\circ$	90 $^\circ$	90 $^\circ$
N1-Cu1-O1	77.76(1) $^\circ$	90 $^\circ$	90 $^\circ$
N1-Cu1-Cl2	96.829(9) $^\circ$	90 $^\circ$	90 $^\circ$
$\Sigma a^{[a]}$	358.06(2) $^\circ$	-	360 $^\circ$
$\Sigma b^{[b]}$	358.72(1) $^\circ$	360 $^\circ$	-

[a]  $\Sigma a = (\text{N1-Cu1-O1}) + (\text{N1-Cu1-Cl2}) + (\text{Cl1-Cu1-O1}) + (\text{Cl1-Cu1-O1})$ [b]  $\Sigma b = (\text{O1-Cu1-Cl2}) + (\text{O1-Cu1-Cl1}) + (\text{Cl2-Cu1-Cl1})$

Table 40: Selected distances and angles of  $[\text{Co}(\text{OON3})_2(\mu\text{-Cl})_2\text{CoCl}_2]\cdot\text{OC}_3\text{H}_6$ ,  $[\text{Fe}(\text{OON1})\text{Cl}_2]_2$  and  $[\text{Cu}(\text{OON1})\text{Cl}_2]_n$ 

[Fe(OON1) <sub>2</sub> Cl <sub>2</sub> ]					
distances / Å		distances / Å		angles / °	
Fe1–O1	1.951(4)	Fe1–Cl2	2.212(2)	O1–Fe1–O3	73.3(1)
Fe2–O1	1.981(3)	Fe2–Cl4	2.176(2)	O1–Fe2–O3	73.2(1)
Fe1–Cl1	2.173(2)	Fe2–N2	2.088(4)	Cl1–Fe1–Cl2	111.45(9)
Fe2–Cl3	2.223(2)	O1 <sup>...</sup> O3	2.350(1)	Cl3–Fe2–Cl4	112.79(9)
Fe1–N1	2.109(5)	Fe1 <sup>...</sup> Fe2	3.147(1)	N1–Fe1–O3	147.0(2)
Fe1–O3	1.986(3)	Fe1 <sup>...</sup> OMe	4.994(2)	N2–Fe2–O1	150.1(2)
Fe2–O3	1.965(4)	Fe2 <sup>...</sup> OMe	4.931(2)	N1–Fe1–Cl1	99.2(1)
				N2–Fe2–Cl3	95.2(1)
[Cu(OON1)Cl <sub>2</sub> ] <sub>n</sub>					
distances / Å		angles / °			
N1–Cu1	2.002(4)	O1–Cu1–N1	79.964(4)		
O1–Cu1	1.986(3)	O1–Cu1–Cl2	87.685(4)		
Cu1–Cl1	2.249(2)	O1–Cu1–Cl1	173.163(5)		
Cu1–Cl2	2.255(2)	N1–Cu1–Cl1	96.78(1)		
Cu1–(μ-Cl1)	2.848(2)	N1–Cu1–Cl2	162.4(1)		
Cu1–(μ-Cl2)	3.144(4)	(μ-Cl1)–Cu1–(μ-Cl2)	172.7(1)		
Cu1 <sup>...</sup> OMe	4.089(4)				
Co(OON3) <sub>2</sub> (μ-Cl) <sub>2</sub> CoCl <sub>2</sub> ·OC <sub>3</sub> H <sub>6</sub>					
distances / Å		distances / Å		angles / °	
Co1–Cl1	2.441(2)	Co1–N2	2.086(5)	O4–Co1–O1	93.2(1)
Co1–Cl2	2.494(2)	Co1 <sup>...</sup> Co2	3.252(8)	N2–Co1–O4	75.7(1)
Co2–Cl1	2.305(2)	Co1 <sup>...</sup> O3Me	4.362(9)	Cl2–Co1–O1	93.9(2)
Co2–Cl2	2.321(2)	Co1 <sup>...</sup> O2Me	4.035(9)	Cl1–Co1–N2	98.4(1)
Co2–Cl3	2.240(2)	Co2 <sup>...</sup> O2Me	4.252(9)	Cl1–Co1–N1	164.8(1)
Co2–Cl4	2.213(2)			Cl1–Co2–Cl2	93.87(7)
Co1–O1	2.134(5)			Cl1–Co2–Cl3	107.93(7)
Co1–O4	2.116(5)			Cl2–Co2–Cl4	117.49(7)
Co1–N1	2.109(5)			Cl3–Co2–Cl4	113.98(9)

## 6.6 EPR spectroscopy of Co<sup>II</sup>, Cu<sup>II</sup> and Fe<sup>III</sup> compounds

EPR spectroscopy has been shown to be a well suited method to analyse the coordination geometry around the paramagnetic metal ion Cu<sup>2+</sup> (d<sup>9</sup>)<sup>[241]</sup> as well as the spin states of Co<sup>II</sup> (d<sup>7</sup>) and Fe<sup>III</sup> (d<sup>5</sup>). In contrast to XRD, EPR can be applied on crystalline and amorphous solids as well as on species in solution, thus allowing detection of the coordination geometry for various physical states. From all obtained Cu<sup>II</sup> and Fe<sup>III</sup> compounds EPR measurements were carried out at 298 K (data collection in Table 41). The Co<sup>II</sup> complexes have to be measured at 4 K to freeze

spin flipping, which prevents  $\text{Co}^{\text{II}}$  complexes from exhibiting EPR signals at 298 K. Figure 49 shows three rather different EPR spectra, recorded for the amorphous material obtained from the preparation procedure  $[\text{Cu}(\text{OON1})\text{Cl}_2]$  (parent material), the recrystallised and structurally characterised binuclear complex  $[\text{Cu}(\text{OON1})\text{Cl}_2]_n$  and an acetone/THF solution of the parent material. While the spectra of the parent material  $[\text{Cu}(\text{OON1})\text{Cl}_2]$  and its solution show rhombic symmetry, the polymeric material exhibits an axial EPR signal with  $g_{\parallel} > g_{\perp}$  (Table 41).

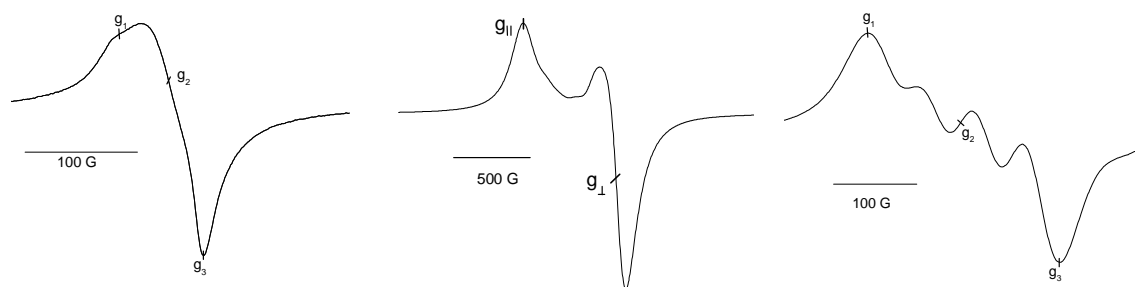


Figure 49: X-band EPR spectra of an amorphous powder of  $[\text{Cu}(\text{OON1})\text{Cl}_2]$  (left), polycrystalline powder of  $[\text{Cu}(\text{OON1})\text{Cl}_2]_n$  (middle) and  $[\text{Cu}(\text{OON1})\text{Cl}_2]$  in a 1:1 acetone/THF mixture (right); all samples measured at 298 K

The latter signal shape is in line with the elongated square pyramidal (octahedral) coordination revealed by XRD. The rhombic symmetry of the other two spectra indicates distorted square pyramidal coordination as found in the recently described complex  $[(\text{pydimH}_2)\text{CuCl}_2]$  ( $g_{\text{av}} = 2.149$ ,  $g_1 = 2.311$ ,  $g_2 = 2.094$ ,  $g_3 = 2.041$   $\Delta g = 0.270$ )<sup>[184]</sup> From the similarity of the averaged  $g$  value and the  $g$  anisotropy  $\Delta g$  of the parent compound and  $[(\text{pydimH}_2)\text{CuCl}_2]$  we conclude that in both compounds the ligand binds in a tridentate fashion. From the markedly deviating values for the parent sample in solution it can be concluded that a square pyramidal coordination sphere with a N,O bidentate binding mode is formed. A solvent molecule therefore is incorporated into the coordination sphere, in line with the findings from NMR spectroscopy of the corresponding  $\text{Zn}^{\text{II}}$  complexes.

The spectra of the iron complexes  $[\text{Fe}(\text{OON1})\text{Cl}_3]$  (parent material) and  $[\text{Fe}(\text{OON1})\text{Cl}_2]_2$  (recrystallised) are also not identical as Figure 50 shows. While the parent material exhibits an EPR signal with a  $g$  value of  $g_{\text{av}} = 2.130$  the binuclear species reveals  $g_{\text{av}} = 2.063$  but an anisotropic signal shape. Dissolving the  $\text{Fe}^{\text{III}}$  compounds in an acetone/THF mixture leads in any case to identical isotropic, narrow ( $\Delta H \sim 60$  G) EPR spectra with a  $g$  value of 2.014. So far



assignment of this species is impossible.

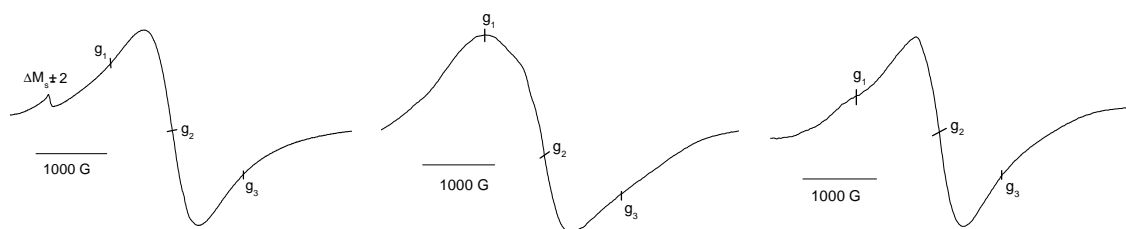


Figure 50: X-band EPR powder spectra of  $[\text{Fe}(\text{OON1})\text{Cl}_3]$  (left),  $[\text{Fe}(\text{OON1})\text{Cl}_2]_2$  (middle) and  $[\text{Fe}(\text{OON3})\text{Cl}_3]$  (right) recorded at 298 K

The cobalt compounds exhibit axial EPR signals (Figure 51) with  $g_{\parallel} < g_{\perp}$ , which are extremely broadened due to the temperature of the measurement (4 K). The  $g$  values are all very high, but in line with EPR studies on other high spin  $\text{Co}^{\text{II}}$  complexes.<sup>[337-339]</sup> EPR spectra in solution were measured in acetone (blue solution) and in methanol (red solution). Signal shape of the blue and the red species differ, especially in the  $g_{\parallel}$  range of the spectra (Table 41).

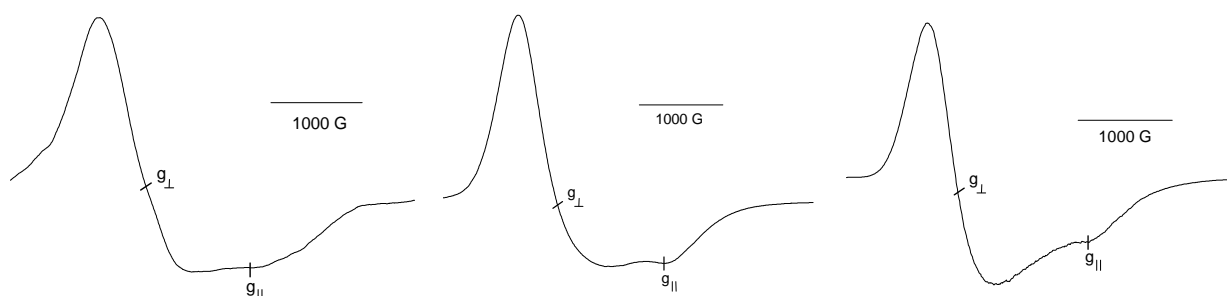


Figure 51: X-band EPR spectra of  $[\text{Co}(\text{OON2})_2(\mu\text{-Cl})_2\text{CoCl}_2]$  recorded at 4 K, left: solid sample, middle: acetone solution and right: methanol solution

By trend, the smallest  $g_{\perp}$  values are observed in the solid state and the highest values are found for methanol solutions. Furthermore, the  $g_{\perp}$  signal part becomes more intense and sharper in methanol solution. As a result the  $\Delta g$  values are small in methanol, while the  $g_{\text{av}}$  values are increased. Reference measurements of a pentacoordinated complex  $[(\text{pydotH}_2)\text{CoCl}_2]^{[183]}$  showed a signal with axial shape but higher  $g$  values and decreased signal width  $\Delta H$ . In a reference compound  $(\text{pydipH}_3)_2[\text{CoCl}_4]^{[183]}$  containing solely the tetrahedral anion  $[\text{CoCl}_4]^{2-}$ , the signal is as well very small, but the  $g$  values are similar to those observed for the O,O',N complexes. Thus some general conclusions can be drawn: the structure of all three O,O',N complexes is

magnetically (and therefore structurally) identical, the three OON complexes are not pentacoordinated in the different states and the red species cannot be assigned to an undissociated complexes of the formula [(O,O',N)CoCl<sub>2</sub>].

Table 41: X-band EPR data of Co<sup>II</sup>, Cu<sup>II</sup> and Fe<sup>III</sup> complexes<sup>[a]</sup>

sample	state	$g_{av}$	$g_I$ or $g_{  }$	$g_2$ or $g_{\perp}$	$g_3$	$\Delta g$	geometry <sup>[b]</sup>
[Cu(OON1)Cl <sub>2</sub> ]	amorphous	2.148	2.267	2.128	2.048	0.219	OE or SPy
[Cu(OON1)Cl <sub>2</sub> ] <sub>n</sub>	polycryst.	2.148	2.286	2.079	-	0.207	OE or SPy
[Cu(OON1)Cl <sub>2</sub> ]	dissolved <sup>[c]</sup>	2.128	2.207	2.128	2.050	0.157	OE
[Cu(OON2)Cl <sub>2</sub> ]	amorphous	2.145	2.247	2.134	2.053	0.194	OE or SPy
[Cu(OON2)Cl <sub>2</sub> ]	dissolved <sup>[c]</sup>	2.128	2.210	2.127	2.048	0.162	OE
[Cu(OON3)Cl <sub>2</sub> ]	amorphous	2.145	2.283	2.076	-	0.207	OE or SPy
[Cu(OON3)Cl <sub>2</sub> ]	dissolved <sup>[c]</sup>	2.131	2.209	2.130	2.054	0.155	OE
[Fe(OON1)Cl <sub>3</sub> ]	amorphous	2.130	2.871	2.024	1.495	1.376	TBP or OE
[Fe(OON1)Cl <sub>3</sub> ]	dissolved <sup>[c]</sup>	2.014	-	2.014	-	0	TBP or OE
[Fe(OON1)Cl <sub>2</sub> ] <sub>2</sub>	polycryst.	2.063	2.723	2.052	1.414	1.309	TBP
[Fe(OON1)Cl <sub>2</sub> ] <sub>2</sub>	dissolved <sup>[c]</sup>	2.014	-	2.014	-	0	TBP or OE
[Fe(OON3)Cl <sub>3</sub> ]	amorphous	2.212	3.081	2.048	1.508	1.573	TBP or OE
[Fe(OON3)Cl <sub>3</sub> ]	dissolved <sup>[c]</sup>	2.014	-	2.014	-	0	TBP or OE
[Co(OON1) <sub>2</sub> ( $\mu$ -Cl) <sub>2</sub> CoCl <sub>2</sub> ]	amorphous	3.605	4.355	2.104		2.251	Oh+Td
[Co(OON1) <sub>2</sub> ( $\mu$ -Cl) <sub>2</sub> CoCl <sub>2</sub> ]	methanol	3.642	4.356	2.215		2.141	Oh
[Co(OON1) <sub>2</sub> ( $\mu$ -Cl) <sub>2</sub> CoCl <sub>2</sub> ]	acetone	3.636	4.362	2.185		2.178	Oh+Td
[Co(OON2) <sub>2</sub> ( $\mu$ -Cl) <sub>2</sub> CoCl <sub>2</sub> ]	amorphous	3.628	4.349	2.185		2.163	Oh+Td
[Co(OON2) <sub>2</sub> ( $\mu$ -Cl) <sub>2</sub> CoCl <sub>2</sub> ]	methanol	3.667	4.359	2.283		2.076	Oh
[Co(OON2) <sub>2</sub> ( $\mu$ -Cl) <sub>2</sub> CoCl <sub>2</sub> ]	acetone	3.653	4.358	2.242		2.116	Oh+Td
[Co(OON3) <sub>2</sub> ( $\mu$ -Cl) <sub>2</sub> CoCl <sub>2</sub> ]	amorphous	3.640	4.358	2.202		2.156	Oh+Td
[Co(OON3) <sub>2</sub> ( $\mu$ -Cl) <sub>2</sub> CoCl <sub>2</sub> ]	methanol	3.666	4.359	2.278		2.082	Oh
[Co(OON3) <sub>2</sub> ( $\mu$ -Cl) <sub>2</sub> CoCl <sub>2</sub> ]	acetone	3.633	4.355	2.190		2.165	Oh+Td
[(pydotH <sub>2</sub> )CoCl <sub>2</sub> ]	amorphous	4.466	5.787	3.805		1.981	TBP
(pydipH <sub>3</sub> ) <sub>2</sub> [CoCl <sub>4</sub> ]	amorphous	3.753	4.357	2.546		1.811	Td

[a] Cu<sup>II</sup> and Fe<sup>III</sup> measured at 298 K, Co<sup>II</sup> measured at 4 K; averaged  $g$  value  $g_{av} = (g_{||} + 2 g_{\perp}) / 3$  or  $g_{av} = (g_I + g_2 + g_3) / 3$ ;  $g$  anisotropy  $\Delta g = g_{\perp} - g_{||}$  or  $\Delta g = g_I - g_3$ ;

[b] Symmetry assigned by EPR spectroscopy or XRD, SPy = square pyramidal, TBP = trigonal bipyramidal, OE = octahedral elongated, Oh = octahedral, Td = tetrahedral;

[c] Dissolved in an acetone/THF (1:1) mixture

## 6.7 Magnetic measurements

Magnetic measurements (SQUID) were performed on the cobalt complexes to ensure that the EPR signals of the high spin Co<sup>II</sup> complexes are not influenced by spin-orbit interactions (which

might be inferred from such high  $g$  values). Figure 52 shows the  $\chi$  over  $T$  plots for  $[\text{Co}(\text{OON1})_2(\mu\text{-Cl})_2\text{CoCl}_2]$  and  $(\text{pydipH}_3)_2[\text{CoCl}_4]$ .

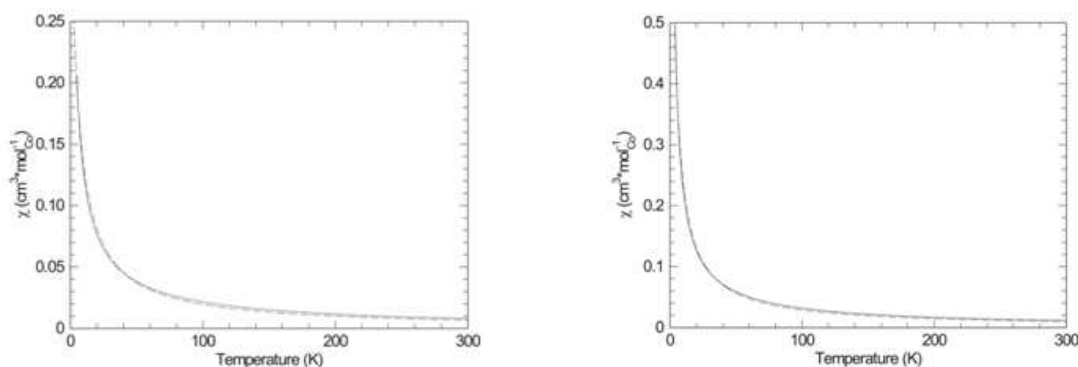


Figure 52:  $\chi$  over  $T$  plots of magnetic measurements (SQUID) performed on solid samples of  $[\text{Co}(\text{OON1})_2(\mu\text{-Cl})_2\text{CoCl}_2]$  (left) and  $(\text{pydipH}_3)_2[\text{CoCl}_4]$  (right),  $H = 0.1$  T

The measurements reveal no extraordinary magnetic behaviour. The temperature dependence of the magnetic susceptibility  $\chi$  clearly shows Curie-Weiss behaviour of the analysed materials but with different Curie-Weiss temperatures ( $-5.6$  K for  $[\text{Co}(\text{OON1})_2(\mu\text{-Cl})_2\text{CoCl}_2]$  and  $-2.4$  K for  $(\text{pydipH}_3)_2[\text{CoCl}_4]$ ) as well as different magnetic moments ( $M = 4.1 \mu_B$  for  $[\text{Co}(\text{OON1})_2(\mu\text{-Cl})_2\text{CoCl}_2]$  and  $4.9 \mu_B$  for  $(\text{pydipH}_3)_2[\text{CoCl}_4]$ ), verifying that the cobalt compounds are high spin complexes with marginal spin-orbit interactions.

## 6.8 UV/vis/NIR absorption spectroscopy

UV/vis absorption spectra were recorded in the range 200 to 1000 nm (Table 42). Due to the differences in complex solubility and stability, measurements of the Zn complexes were carried out in  $\text{CHCl}_3$  and THF, the copper complexes were measured in acetone, while iron complexes were measured in MeCN and Ni complexes in THF. The absorption of Cobalt complexes was measured in acetone (blue solution) and in methanol (red solution). Due to the different absorption properties and complex geometries cobalt complexes are discussed separately (see below).

The absorption spectra of the Zn complexes show intense absorption bands in the UV range

( $\lambda_1$ ), which can be assigned to  $\pi$ - $\pi^*$  transitions within the ligands.

Table 42: Absorption data of zinc, copper, nickel and iron complexes<sup>[a]</sup>

complex	$\lambda$ / nm; ( $\epsilon$ / Lmol <sup>-1</sup> cm <sup>-1</sup> )			solvent
	$\lambda_1$	$\lambda_2$	$\lambda_3$	
[Zn(OON1)Cl <sub>2</sub> ]	264 (5179), 281 (3130)			CHCl <sub>3</sub>
[Zn(OON2)Cl <sub>2</sub> ]	262 (5798), 279 (3041)			CHCl <sub>3</sub>
[Zn(OON3)Cl <sub>2</sub> ]	263 (6328), 270 (5548)			CHCl <sub>3</sub>
[Zn(OON1)Cl <sub>2</sub> ]	271 (12098)			THF
[Zn(OON2)Cl <sub>2</sub> ]	262 (6404), 294sh (1468)			THF
[Zn(OON3)Cl <sub>2</sub> ]	271 (12684)			THF
[Fe(OON1)Cl <sub>2</sub> ] <sub>2</sub>	242 (10737), 255 (10214)	311 (5593), 356 (4155)		MeCN
[Fe(OON1)Cl <sub>3</sub> ]	244 (16509), 261 (14954)	310 (3197), 358 (6635)		MeCN
[Fe(OON3)Cl <sub>3</sub> ]	239 (9088), 264 (8432)	311 (4385), 360 (4155)		MeCN
[Cu(OON1)Cl <sub>2</sub> ]	- <sup>[b]</sup>	379 (284) <sup>[c]</sup>	735 (25)	acetone
[Cu(OON2)Cl <sub>2</sub> ]	- <sup>[b]</sup>	379 (236) <sup>[c]</sup>	732 (19)	acetone
[Cu(OON3)Cl <sub>2</sub> ]	- <sup>[b]</sup>	385 (243) <sup>[c]</sup>	730 (24)	acetone
[Ni(OON1)Cl <sub>2</sub> ] <sub>2</sub>	228 (6660)	264 (4960)	453 (62), 545sh (24), 852 (18)	THF
[Ni(OON2)Cl <sub>2</sub> ] <sub>2</sub>	229 (10539)	263 (8961)	461 (61), 544sh (18), 866 (17)	THF
[Ni(OON3)Cl <sub>2</sub> ] <sub>2</sub>	223 (12291)	264 (13449)	456 (70), 561sh (21), 861 (22)	THF

[a] Absorption maxima  $\lambda$  / nm and extinction coefficients  $\epsilon$  / Lmol<sup>-1</sup>cm<sup>-1</sup> (in parentheses)

[b] Obscured by solvent absorptions

[c] Minor bands were found around 460 nm indicative for traces of [CuCl<sub>4</sub>]<sup>2-</sup>

All three iron complexes exhibit quite similar absorption spectra in line with the EPR experiments. Interestingly, further long-wavelength absorption bands apart from the  $\pi$ - $\pi^*$  transitions of the ligand were observed, which indicates that Fe<sup>III</sup> is still coordinated. The absorption bands below 300 nm are  $\pi$ - $\pi^*$  absorption bands, as can be seen from their extinction coefficient and from comparison with the zinc complexes. Furthermore, absorption bands around 310 nm and around 360 nm can be observed which are assigned to charge transfer transitions. The binuclear complex [Fe(OON1)Cl<sub>2</sub>]<sub>2</sub> and the mononuclear [Fe(OON1)Cl<sub>3</sub>] show nearly identical absorption properties, the deprotonation of the hydroxy function and the loss of one chlorido ligand thus seem to have no influence on the spectra.

The spectra of the copper complexes were characterised by intense absorption bands around

380 nm ( $\lambda_2$ , assigned to ligand to metal charge transfer LMCT) and very broad absorption bands around 730 nm ( $\lambda_3$ , d-d absorption bands of typical Jahn-Teller elongated  $d^9$  systems).

To assess if the structure of the complexes change under the influence of the solvent molecules (de-coordination of the individual donor atoms of O,O',N ligands) the absorption properties of  $[\text{Cu}(\text{OON}_3)\text{Cl}_2]$  in various solvents were studied. Table 43 lists the absorption maxima of the LMCT- and the d-d absorption bands in wavenumbers.

Table 43: Long-wavelength absorption maxima of  $[\text{Cu}(\text{OON}_3)\text{Cl}_2]$  in various solvents

solvent	LMCT/ $\text{cm}^{-1}$	d-d <sup>[a]</sup> / $\text{cm}^{-1}$	$E_T$ /kcal mol <sup>-1</sup> [a]
MeOH	28735	12484	55.5
EtOH	22779	12240	51.9
MeCN	26042	12821	46.0
DMF	25907	11600	43.8
acetone	25510	12987	42.2
$\text{CHCl}_3$	25510	15974	39.1
THF	25063	13106	37.4

[a] Dimroth-Reichardt parameter for the applied solvents from ref. [340]

The solvent depending Dimroth-Reichardt parameter ( $E_T$ ) correlates with the absorption energies of the LMCT absorption band, only the values for the protic solvents MeOH and EtOH do not match the series. The LMCT absorption band is shifted to longer wavelength upon using solvents with decreasing  $E_T$ , a plot of the relationship between LMCT and  $E_T$  is shown in Figure 53. The values of the d-d absorption bands do not correlate with  $E_T$ .

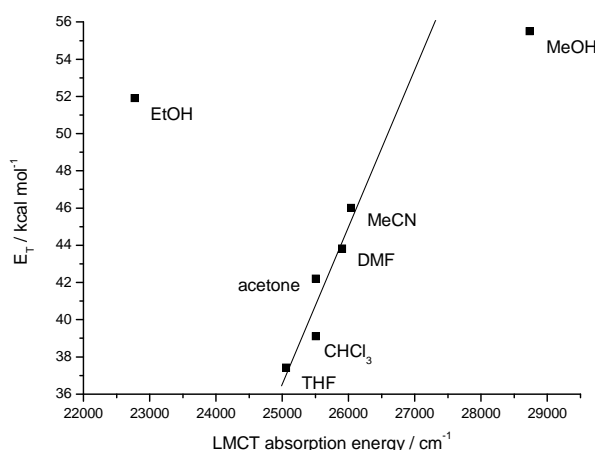


Figure 53: Plot of the Dimroth-Reichardt parameter  $E_T$  over the observed LMCT absorption energy

DMF, which is clearly the best ligand of all applied solvents, does not fit into the series of d-d absorption band changes, which seem to increase with decreasing  $E_T$ . It might therefore be stated that DMF coordinates and eventually partly replaces the O,O',N ligands, which would be in line with results of the NMR experiments performed on the zinc complexes.

Spectra of the different O,O',N cobalt complexes exhibit nearly identical absorption spectra (Figure 54, Table 44) and show solvatochromism.

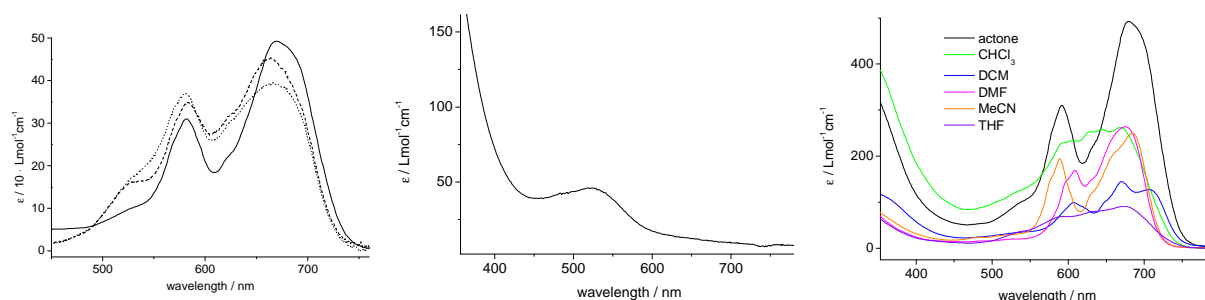


Figure 54: Absorption spectra recorded at 298 K; left: spectra recorded in acetone,  $[\text{Co}(\text{OON1})_2(\mu\text{-Cl})_2\text{CoCl}_2]$  (solid),  $[\text{Co}(\text{OON2})_2(\mu\text{-Cl})_2\text{CoCl}_2]$  (dashed) and  $[\text{Co}(\text{OON3})_2(\mu\text{-Cl})_2\text{CoCl}_2]$  (dotted); middle:  $[\text{Co}(\text{OON1})_2(\mu\text{-Cl})_2\text{CoCl}_2]$  in methanol solution; right: solvent dependence of the d-d absorption bands of  $[\text{Co}(\text{OON1})_2(\mu\text{-Cl})_2\text{CoCl}_2]$

In methanol solution the complexes exhibit a weak red colour, while solutions in DMF, MeCN, acetone, THF,  $\text{CHCl}_3$  and  $\text{CH}_2\text{Cl}_2$  are blue, Figure 54 shows spectra on various solutions of  $[\text{Co}(\text{OON1})_2(\mu\text{-Cl})_2\text{CoCl}_2]$ . The blue colour is due to absorption bands in the range of 550 nm to 750 nm, which are assigned to d-d transitions of tetrahedral  $\text{Co}^{\text{II}}$  complexes.<sup>[341]</sup> The absorption spectra of the complexes dissolved in methanol (red solutions) show maxima around 530 nm, which are very weak and typical for octahedral  $\text{Co}^{\text{II}}$  complexes.<sup>[342]</sup> Interestingly, all absorption spectra recorded on blue solutions also contain a weak shoulder in the range of 530 nm, which indicates that the spectra contain both, an octahedral and a tetrahedral cobalt ion. So it can be assumed that the binding motive of the neutral complexes is not destroyed upon dissolving  $[\text{Co}(\text{O},\text{O}',\text{N})_2(\mu\text{-Cl})_2\text{CoCl}_2]$ . These shoulders are not found in the absorption spectra recorded on  $(\text{pydipH}_3)_2[\text{CoCl}_4]$ , which solely contains a tetrahedral cobalt fragment and absorbs only in the 550 to 750 nm range with maxima at 584 nm and 685 nm.

Table 44: d-d absorption bands of the O,O',N Co<sup>II</sup> complexes

compound	geometry	$\lambda$ / nm ( $\epsilon$ / Lmol <sup>-1</sup> cm <sup>-1</sup> )	solvent
[Co(OON1) <sub>2</sub> ( $\mu$ -Cl) <sub>2</sub> CoCl <sub>2</sub> ]	Oh-Oh	525 (24)	MeOH
[Co(OON2) <sub>2</sub> ( $\mu$ -Cl) <sub>2</sub> CoCl <sub>2</sub> ]	Oh-Oh	523 (26)	MeOH
[Co(OON3) <sub>2</sub> ( $\mu$ -Cl) <sub>2</sub> CoCl <sub>2</sub> ]	Oh-Oh	523 (30)	MeOH
[Co(OON1) <sub>2</sub> ( $\mu$ -Cl) <sub>2</sub> CoCl <sub>2</sub> ]	Oh-Td	540sh (204), 591 (622), 634sh (456), 680 (970)	acetone
[Co(OON2) <sub>2</sub> ( $\mu$ -Cl) <sub>2</sub> CoCl <sub>2</sub> ]	Oh-Td	532sh (32), 583 (70), 663 (90)	acetone
[Co(OON3) <sub>2</sub> ( $\mu$ -Cl) <sub>2</sub> CoCl <sub>2</sub> ]	Oh-Td	532sh (36), 581 (74), 667 (80)	acetone
(pydipH <sub>3</sub> ) <sub>2</sub> [CoCl <sub>4</sub> ]	Td	589, 685 <sup>[343]</sup>	MeCN

The absorption bands recorded for the O,O',N Co<sup>II</sup> complexes in methanol are similar to the absorption band observed for [CoCl<sub>2</sub>(OH<sub>2</sub>)<sub>4</sub>] in water (Figure 55). [CoCl<sub>2</sub>(OH<sub>2</sub>)<sub>4</sub>] which is known to be octahedrally coordinated<sup>[342]</sup> exhibits an absorption band at 510 nm accompanied by a shoulder at 480 nm. Thus, methanol solutions of O,O',N Co<sup>II</sup> complexes presumably contain exclusively octahedral coordinated Co<sup>II</sup> ions. Unfortunately these species cannot be isolated (solidifying the compounds from methanol solution results in blue complexes, c.f. synthesis of the Co<sup>II</sup> complexes).

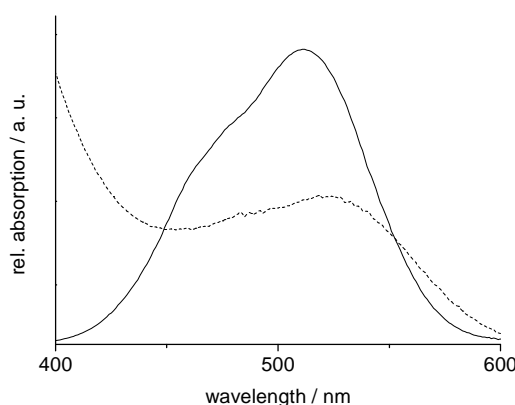


Figure 55: Absorption spectra of [CoCl<sub>2</sub>(H<sub>2</sub>O)<sub>4</sub>] (dotted) in water and [Co(OON1)<sub>2</sub>( $\mu$ -Cl)<sub>2</sub>CoCl<sub>2</sub>] dissolved in methanol (solid)

To further analyse the red complex species some titration experiments using THF and methanol as solvents were performed. Starting with [Co(OON3)<sub>2</sub>( $\mu$ -Cl)<sub>2</sub>CoCl<sub>2</sub>] in methanol solution, THF was added slowly and spectra were recorded simultaneously. The red solution turned blue upon adding THF, a retitration performed on the complex in THF/MeOH mixture adding methanol resulted in a red solution again. Figure 56 shows both titration steps upon adding THF and methanol.

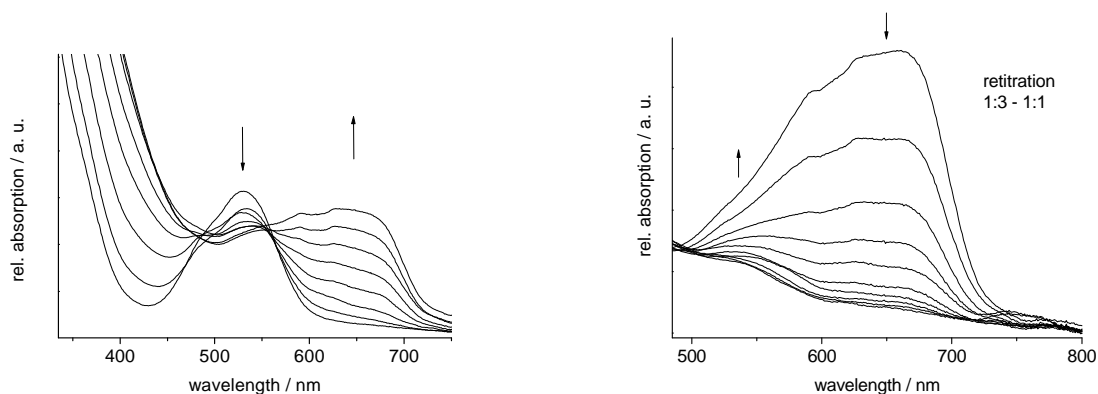
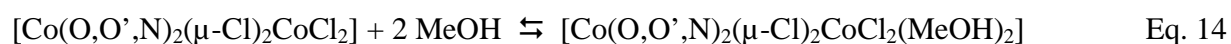


Figure 56: Absorption spectra recorded during titration of  $[\text{Co}(\text{OON3})_2(\mu\text{-Cl})_2\text{CoCl}_2]$  dissolved in methanol using THF (solvent ratio 1:3, left); during re-titration of the obtained solution using methanol (right)

The reversibility of the titration experiments clearly shows that the colour change is not caused by a decomposition reaction. The low intensity of the absorption band at 530 nm after re-titration (Figure 56, right) is due to the dilution caused by increasing volume of solvent. As a result of the described experiments the following reaction is assumed to occur in methanol solution (Eq. 14):



## 6.9 Electrochemical investigations

Electrochemical investigations were carried out on the free O,O',N ligands as well as on Cu, Fe and Ni complexes (Table 45). Surprisingly, the first reduction of OON2 and OON3 was found to be fully reversible. The O,O',N ligands were not expected to form stable radical anions. This stabilisation might be due to a similar effect which is found for triphenyl-methyl radicals and derivatives.<sup>[344]</sup> Comparison of the redox potentials shows that the residue's variation (H, CH<sub>3</sub>, Ph) highly influences the electrochemical properties of the O,O',N ligands, although the functional groups remain identical (Table 45).

For the copper complexes reversible reductions were found around 0 V which were assigned



to the  $\text{Cu}^{\text{II}}/\text{Cu}^{\text{I}}$  redox couple. The three ligands do not influence the redox potentials markedly. This is in line with the EPR experiments, which already revealed that the  $\text{Cu}^{\text{II}}$  ions in the three complexes are magnetically (and thus structurally) identical in solution (Table 41). Further reductions (ligand centred) and oxidations occur irreversibly which is a bit surprising in view of the reversible reduction of the free ligands OON2 and OON3.

The iron complexes  $[\text{Fe}(\text{OON1})\text{Cl}_3]$ , and  $[\text{Fe}(\text{OON3})\text{Cl}_3]$  show reduction waves corresponding to the  $\text{Fe}^{\text{III}}/\text{Fe}^{\text{II}}$  couple, while for the binuclear complex  $[\text{Fe}(\text{OON1})\text{Cl}_2]_2$  no metal centred reduction was detected. The oxidation wave for the  $\text{Fe}^{\text{II}}$  complex  $[\text{Fe}(\text{OON3})\text{Cl}_2]$  was found at the same potential than the reduction wave of the  $\text{Fe}^{\text{III}}$  derivative proving the full reversibility of the redox process.

The nickel complexes cannot be oxidised in a range between 0.0 and 2.0 V, while fully irreversible reduction was observed around  $-1.8$  V. This reduction is assumed to be originated by a  $\text{Ni}^{\text{II}}$  to  $\text{Ni}^{\text{I}}$  reduction followed by a splitting of the terminal chlorido ligand (see above) resulting in  $\text{Cl}^-$  and a  $\text{Ni}^{\text{II}}$  complex fragment.

Table 45: Redox potentials of the free OON ligands and the  $\text{Cu}^{\text{II}}$ ,  $\text{Fe}^{\text{II}}$ ,  $\text{Fe}^{\text{III}}$  and  $\text{Ni}^{\text{II}}$  complexes<sup>[a]</sup>

compound	$E_{\text{pa}} / \text{V}$	$E_{1/2} / \text{V}$	$E_{\text{pc}} / \text{V}$	solvent
OON1	0.46	-	-3.23	MeCN
OON2	0.55	-1.34		MeCN
OON3	1.30	-1.35		MeCN
$[\text{Cu}(\text{OON1})\text{Cl}_2]$		-0.17		THF
$[\text{Cu}(\text{OON2})\text{Cl}_2]$		-0.15		THF
$[\text{Cu}(\text{OON3})\text{Cl}_2]$		-0.10		THF
$[\text{Fe}(\text{OON1})\text{Cl}_3]$		-0.39		MeCN
$[\text{Fe}(\text{OON3})\text{Cl}_3]$		-0.30		MeCN
$[\text{Fe}(\text{OON3})\text{Cl}_2]$		-0.32		MeCN
$[\text{Ni}(\text{OON1})\text{Cl}_2]_2$			-1.78	THF
$[\text{Ni}(\text{OON2})\text{Cl}_2]_2$			-1.94	THF
$[\text{Ni}(\text{OON3})\text{Cl}_2]_2$			-1.87	THF

[a] from cyclic voltammetry in solvent/<sup>n</sup>Bu<sub>4</sub>NPF<sub>6</sub> mixtures; potentials in V vs. FeCp<sub>2</sub>/FeCp<sub>2</sub><sup>+</sup>

The electrochemical measurements of the  $\text{Co}^{\text{II}}$  complexes revealed irreversible reductions (Figure 57), while no oxidation processes were observed. The reductions take place at  $-1.5$  V and were found (at identical potential) for all three  $[\text{Co}(\text{O},\text{O}',\text{N})_2(\mu\text{-Cl})_2\text{CoCl}_2]$  complexes as well as

for  $(\text{pydipH}_3)_2[\text{CoCl}_4]$ .

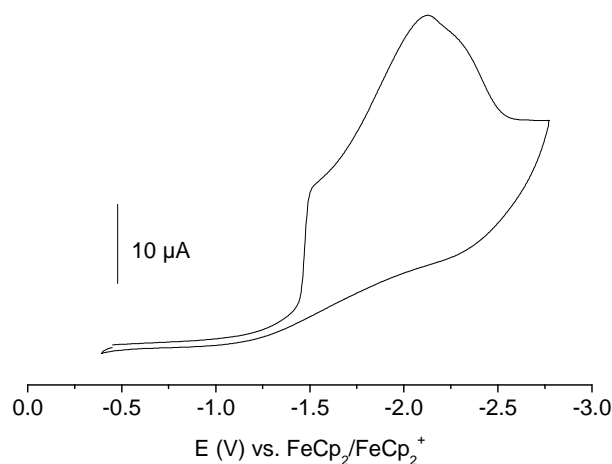


Figure 57: Cyclic voltammogram of  $[\text{Co}(\text{OON}_3)_2(\mu\text{-Cl})_2\text{CoCl}_2]$  measured in  $\text{THF}/\text{Bu}_4\text{NPF}_6$  at 298 K at  $100 \text{ mV s}^{-1}$  scan rate; potentials in V vs.  $\text{FeCp}_2/\text{FeCp}_2^+$

The irreversible reduction is assigned to a complex degradation by loss of halogenido ligands (Figure 58, right) and is thus assumed to highly influence the absorption properties of the resulting complex. Therefore spectroelectrochemical measurements were carried out in  $\text{THF}/\text{Bu}_4\text{NPF}_6$  solution at 298 K. Spectra of the reduction process are shown in Figure 58, left.

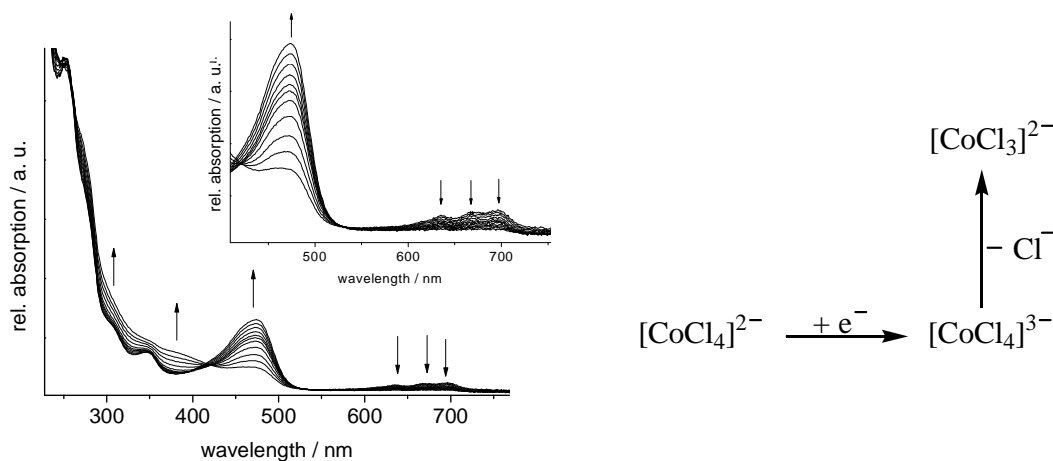


Figure 58: Absorption spectra recorded during electrochemical reduction of  $[\text{Co}(\text{OON}_3)_2(\mu\text{-Cl})_2\text{CoCl}_2]$  at  $-2.0 \text{ V}$  in  $\text{THF}/\text{Bu}_4\text{NPF}_6$  solution at 298 K (left); schematic drawing of proposed reductive complex degradation

Absorption spectra measured at  $-2.0 \text{ V}$  reveal that the d-d absorption bands which were

assigned to the tetrahedral  $\text{CoCl}_4$ -fragment (see above) vanish, while an intense absorption band at 474 nm rises. It can be concluded, that the tetrahedral complex fragment is destroyed upon reduction probably due to  $\text{Cl}^-$  cleavage. The new absorption band cannot be assigned to a specific fragment, since it even remains unclear, whether it is a charge transfer band (more likely) or a d-d band of a new octahedral  $\text{Co}^{\text{II}}$  complex and further investigations have to be carried out.

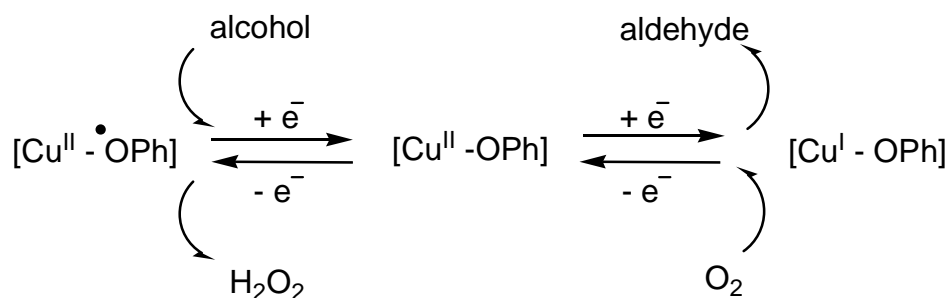
### **6.10 Conclusion on the suitability of O,O',N donor complexes as GO models**

Since the O,O',N donor ligands were found to bind in a bidentate mode, leaving in most cases the methoxy function uncoordinated, the complexes lack a well accessible  $[\text{OPh}]^{\bullet+}/[\text{OPh}]$  redox couple. Thus the copper complexes are not suitable as GO model compounds.

## 7.0 Catalytic test reactions

### 7.1 Introduction

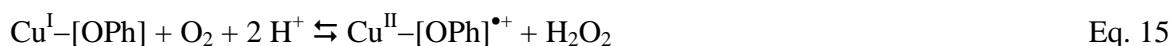
The three established catalyst states of the catalytic cycle of oxidation catalysis performed by copper phenoxyl complexes is depicted in Scheme 41.



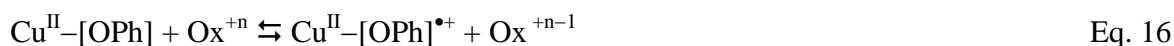
Scheme 41: Catalytic states of copper phenoxyl complexes

An important aspect is the generation of the active species  $\text{Cu}^{\text{II}}\text{-}[\text{OPh}]^{\bullet+}$  and several methods have been described in literature:

1. The catalytic cycle can be started using a  $\text{Cu}^{\text{I}}$  precursor, the active species is generated by oxidation using air oxygen<sup>[142]</sup> as described by Eq. 15:



2. Another possibility is to synthesise  $\text{Cu}^{\text{II}}$  complexes and use an oxidising agent as e.g. silver hexafluoroantimonate, tris(4-bromophenyl)ammonium hexachloroantimonate or acetyl ferricenium hexafluoroantimonate to generate copper<sup>II</sup> radical complexes<sup>[84,137]</sup> see Eq. 16:



3. A third way is to take advantage of a disproportionation reaction of copper complexes following Eq. 17:



Method 1 is a standard method, which works reliably and was also applied to generate the active enzyme from isolated apo Galactose Oxidase (GO) *in vitro*.<sup>[345]</sup> For method 2 it has to be ensured that the external oxidant does not oxidise the substrate, e.g. by previously isolating the radical complex. Isolation of copper phenoxyl radicals has been reported for complexes containing stabilising groups in *ortho*- and *para*-position at the ligands' phenol core,<sup>[84,137]</sup> but isolation is impossible if stabilising substituents are missing. Method 3 is an uncommon strategy to generate copper phenoxyl radicals. Only few studies have been carried out to investigate the requirements of such reactions and until now, this strategy has not been reported as initial step in catalytic test reactions.

Copper disproportionation reactions were previously observed for tripodal ligands as (shown in Scheme 14) dissolved in MeCN and treated with  $\text{Cu}(\text{ClO}_4)_2$ <sup>[153]</sup> or  $\text{Cu}(\text{OTf})_2$  in presence of  $\text{NEt}_3$ <sup>[130]</sup>. In these studies the reaction was described to depend on the applied coligands ( $\text{OTf}^-$  or  $\text{ClO}_4^-$  respectively). The generated  $\text{Cu}^{\text{I}}$  species cannot be characterised easily, because they are  $d^{10}$  systems and therefore EPR silent. They do not show characteristic d-d absorption bands. Furthermore, the reaction mixture also contains  $\text{Cu}^{\text{II}}$  and conclusive NMR experiments could not be performed. In an earlier study Yamauchi *et al.* were able to isolate the  $\text{Cu}^{\text{I}}$  complex in their disproportionation system, they found that the  $\text{Cu}^{\text{I}}$  species was the solvent complex  $[\text{Cu}^{\text{I}}(\text{MeCN})_4]^+$ .<sup>[153]</sup>

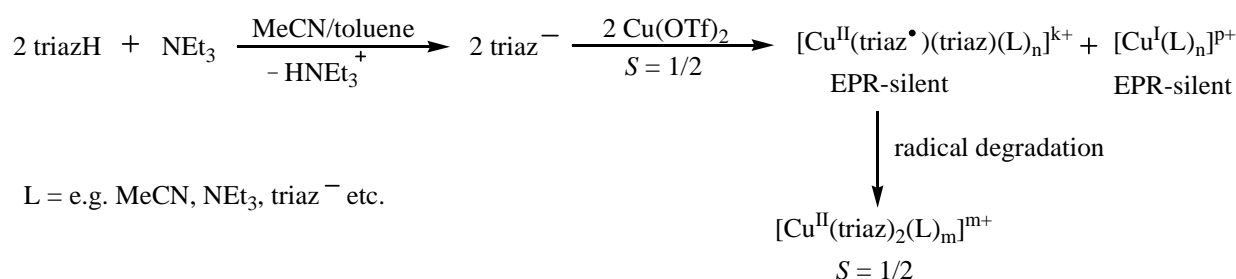
In cases which exclude a radical generation upon disproportionation (e.g. by applying a ligand which does not stabilise organic radicals) a  $\text{Cu}^{\text{II}}$  disproportionation reaction leads to the formation of  $\text{Cu}^{\text{III}}$  complex species.<sup>[154]</sup> This has been reported by Stack *et al.* who performed the reaction at 298 K under oxygen free conditions using triazamacrocyclic ligands (N,N,N,C-donor set) and  $\text{Cu}(\text{OTf})_2$  or  $\text{Cu}(\text{ClO}_4)_2$  as metal sources (Eq. 18).



In this thesis several strategies for the generation of copper phenoxyl radicals ought to be compared using the  $[\text{Cu}(\text{triaz})_2]$  complex (Chapter 5) as a test system. The generated radical species may then be applied in catalytic alcohol oxidation using the well established substrate benzyl alcohol. After optimising the conditions for the radical formation, the catalytic activity of copper complexes described in Chapters 2, 3, 4 and 5 are to be investigated in detail.

## 7.2 Phenoxy radical generation by a copper disproportionation reaction

For the chemical generation of a radical copper complex a MeCN/toluene (5:3) mixture containing the ligand triazH was prepared. To 1 mL of this solution (1 eq triazH) 1 eq NEt<sub>3</sub> was added and the mixture was stirred for five minutes. To the resulting solution varying amounts of Cu(OTf)<sub>2</sub> dissolved in MeCN were added. The reaction mixtures immediately turned brown (charge transfer absorption band at  $\lambda_{\text{max}} = 410$  nm), indicating a radical formation as visualised in Scheme 42. The resulting radical species does not show exactly the same radical dependent charge transfer absorption band as observed for isolated [Cu(triaz)<sub>2</sub>]<sup>•+</sup> ( $\lambda_{\text{max}} = 404$  nm). This indicates, that the radical complex formed upon disproportionation might contain further coligands (L = MeCN, OTf<sup>-</sup>, NEt<sub>3</sub> etc.). The radical species is therefore referred as [Cu(triaz)<sub>2</sub>(L)<sub>n</sub>]<sup>•k+</sup> in the following. At the same time, disproportionation leads to a reduced copper complex. The distinct composition of this compound is still unknown, so the complex is described by the general formula [Cu<sup>I</sup>(L)<sub>n</sub>]<sup>P+</sup>.



Scheme 42: Proposed disproportionation reaction

First disproportionation experiments were carried out at 273 K because reports on similar experiments have revealed that the radical species is more stable at lower temperature.<sup>[130,153]</sup> Furthermore, the reactions were carried out in diluted solutions (0.00025 molL<sup>-1</sup>) using varying amounts of Cu(OTf)<sub>2</sub>, spectra are shown in Figure 59 on the left. Almost no radical formation was observed (by UV/vis absorption spectroscopy) under these conditions (even if excess Cu(OTf)<sub>2</sub> was used). If the same reaction was performed at 298 K in rather concentrated solution (0.025 molL<sup>-1</sup>, Figure 59, right), radical formation was observed by an increasing absorption band at 410 nm.

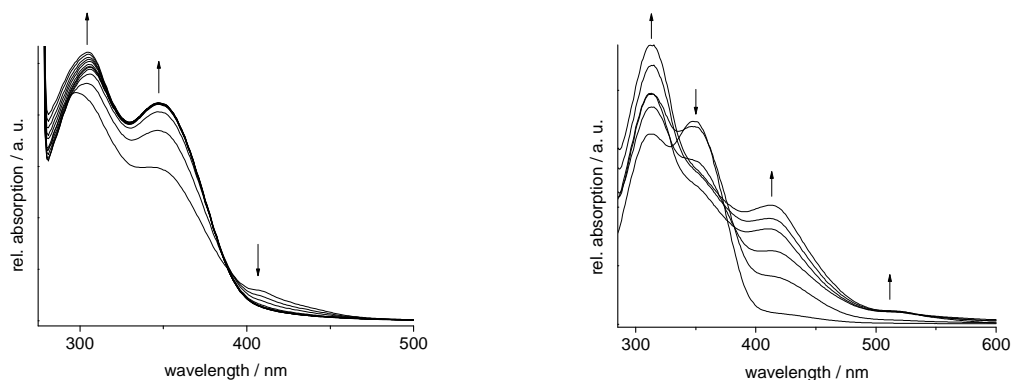


Figure 59: Absorption spectra recorded upon titration of triaz<sup>-</sup> solutions (MeCN/toluene 5:3) with varying amounts of Cu(OTf)<sub>2</sub>; left:  $c = 0.00025 \text{ molL}^{-1}$ ,  $T = 273 \text{ K}$ ; right:  $c = 0.025 \text{ molL}^{-1}$ ,  $T = 298 \text{ K}$

### 7.3 Phenoxy radical stability

To analyse the stability of the *in situ* generated  $[\text{Cu}(\text{triaz})_2(\text{L})_n]^{\bullet k+}$  species, time resolved measurements were carried out. Absorption spectroscopy was used to detect the radical degradation at low concentration ( $0.00025 \text{ molL}^{-1}$ ). The absorption intensity of the charge transfer band located at 410 nm should linearly correlate, according to the *Lambert-Beer* rule, with the concentration of the radical species (absorption =  $\epsilon \cdot c \cdot d$  with  $\epsilon$  = extinction coefficient,  $c$  = concentration,  $d$  = cuvette diameter = optical path). Thus decreasing absorption intensity is a measure for decreasing  $[\text{Cu}(\text{triaz})_2(\text{L})_n]^{\bullet k+}$  concentration. As time dependent measurements showed, the concentration of the radical complex decreases with time and after 42 h the degradation is more or less completed (Figure 60).

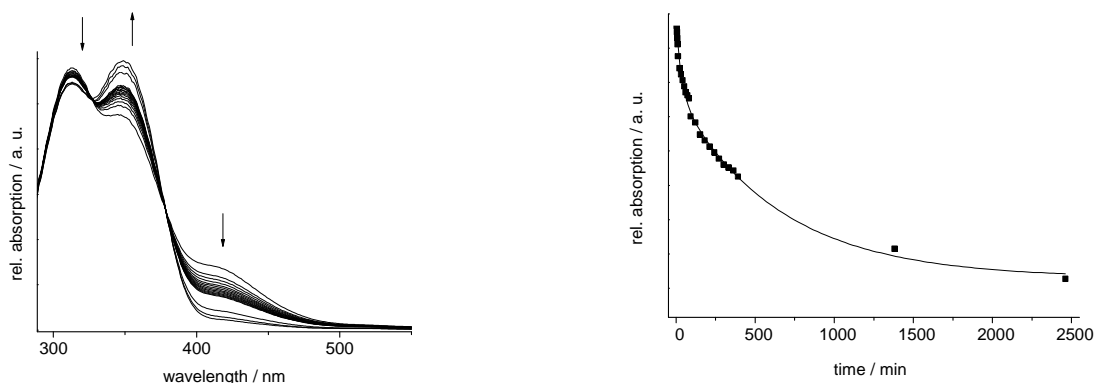


Figure 60: Absorption spectra recorded on a solution containing 2 eq triaz<sup>-</sup>, 2 eq NEt<sub>3</sub>, 1 eq Cu(OTf)<sub>2</sub> in 5:3 MeCN/toluene, measured during 42 h at 298 K; right: plot of relative intensity ( $\lambda_{\text{max}} = 410 \text{ nm}$ ) over time

A plot of the absorption intensity detected for the radical dependent charge transfer at 410 nm over time is given in Figure 60. It shows that the degradation proceeds fast during the first 60 minutes and follows a (pseudo) first order reaction kinetic. First order kinetic means that the decay (thus the stability) only depends on the concentration of the starting material, which is the radical. Upon plotting  $\ln(\text{rel. abs}/\text{rel. abs}_0)$  over time (in seconds) the reaction constant  $k$  was determined to be  $-6.13 \cdot 10^{-5} \text{ s}^{-1}$ .

Degradation might proceed by chemical reactions leading to several unknown  $\text{Cu}^{\text{II}}$  complexes, or by reduction leading to the corresponding  $[\text{Cu}(\text{triaz})_2(\text{L})_n]$  complex as shown in Scheme 42. The product of degradation is EPR active ( $S = 1/2$ ), in contrast to the  $\text{Cu}^{\text{I}}$  ( $d^{10}$ ) and the  $[\text{Cu}(\text{triaz})_2(\text{L})_n]^{\bullet k+}$  complexes. Additionally, the copper precursor should give an EPR signal if not completely consumed by coordination or disproportionation reaction leading either to  $[\text{Cu}(\text{triaz})_2(\text{L})_m]$  or to  $[\text{Cu}(\text{triaz})_2(\text{L})_n]^{\bullet k+}$ . Under the present conditions it can be assumed that the copper sources are coordinated rapidly and thus the EPR signal is not due to the precursor. The stability of the radical can be determined upon measuring the concentration of degradation products by EPR. The time dependent EPR measurements (Figure 61) were performed during 180 min at 298 K using concentrated solutions ( $0.025 \text{ molL}^{-1}$ ), which were prepared as described above.

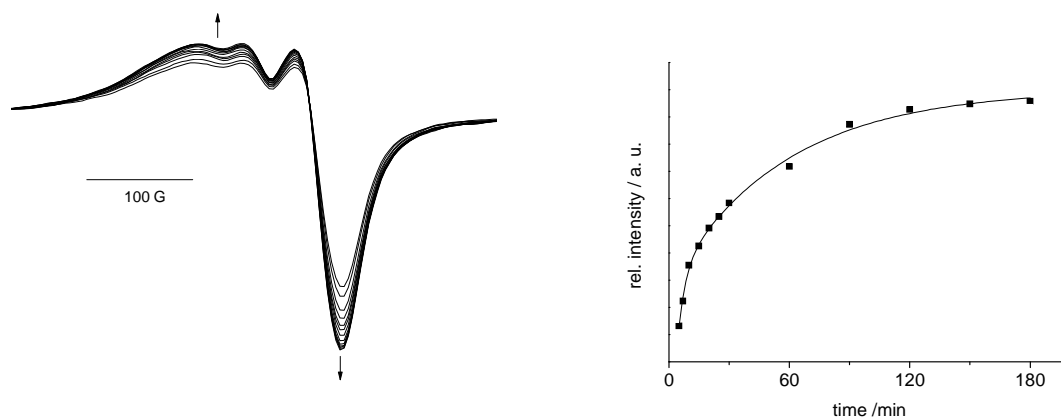


Figure 61: Left: EPR spectra recorded on a sample containing 2 eq  $\text{triaz}^-$  and 1 eq  $\text{Cu}(\text{OTf})_2$  in 5:3 MeCN/toluene at 298 K (0-60 min); right: time dependence of the signal intensity during (0-180 min)

The recorded spectra revealed increasing signal intensity with a fast signal growth during the first 20 minutes. The EPR signal clearly belongs to a copper centred unpaired electron ( $\Delta H = 300 \text{ G}$ ) and thus is assigned to a  $[\text{Cu}(\text{triaz})_2(\text{L})_m]$  complex. In general, the EPR signal intensity linearly correlates with the number of unpaired spins in the sample (one unpaired



electron per  $[\text{Cu}(\text{triaz})_2(\text{L})_m]$  complex). A plot of the signal intensity over time shows a (pseudo) first order reaction kinetic. Upon plotting  $\ln(I/I_0)$  over time (in seconds) the reaction constant  $k$  was determined to be  $5.52 \cdot 10^{-4} \text{ s}^{-1}$ . The reaction therefore proceeds approximately ten times faster at  $c = 0.025 \text{ molL}^{-1}$  compared to diluted solution ( $c = 0.000025 \text{ molL}^{-1}$ ). This is another indication of a first order kinetic.

#### 7.4 Variation of the copper source

Another question which was addressed using the triaz system is the influence of the applied copper source. Previous reports discuss the importance of the  $\text{Cu}^{\text{II}}$  salt anion for the disproportionation and stated that the radical formation depends on application of counter ions such as  $\text{OTf}^-$  and  $\text{ClO}_4^-$ .<sup>[130,153]</sup>

More likely, the radical formation relates to the redox potentials of the applied copper source (which is expected to differ only marginally) and the  $[\text{OPh}]^{*\text{+}}/[\text{OPh}]$  redox couple of the copper complex. To investigate the influence of the copper source, the afore mentioned disproportionation reaction was carried out (page 161) using  $\text{CuCl}_2$ ,  $\text{CuBr}_2$ ,  $\text{Cu}_3(\text{PO}_4)_2$ ,  $\text{Cu}(\text{C}_2\text{O}_4)$ ,  $\text{Cu}(\text{OAc})_2$ ,  $\text{Cu}(\text{OTf})_2$ ,  $\text{Cu}(\text{OTs})_2$ ,  $\text{Cu}(\text{NO}_3)_2$ ,  $\text{Cu}(\text{ClO}_4)_2$ ,  $\text{Cu}(\text{SCN})_2$  and  $[\text{Cu}(\text{MeCN})_4](\text{TFA})_2$ . Furthermore, perchlorate salts containing other cations ( $\text{Ni}(\text{ClO}_4)_2$  and  $\text{NH}_4\text{ClO}_4$ ) were used to perform a radical generation reaction. Again, the formation of the radical species was observed by absorption spectroscopy (absorption band with  $\lambda_{\text{max}} = 410 \text{ nm}$ ) and the resulting products of the decay were examined by EPR spectroscopy, spectra are presented in Figure 62.

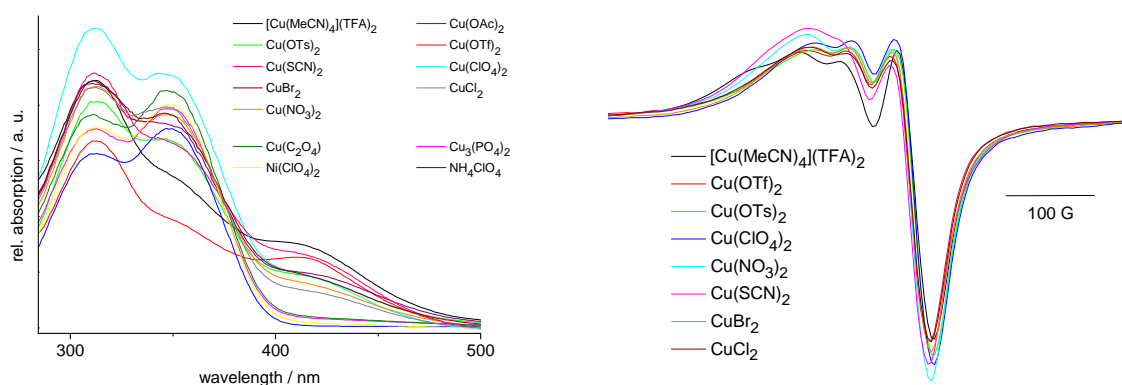


Figure 62: Absorption spectra (left) and X-band EPR spectra (right) recorded on mixtures of various  $\text{Cu}^{\text{II}}$  salts and triaz<sup>-</sup> in MeCN/toluene 5:3 at 298 K

The absorption spectra (Figure 62, left) were recorded after 5 min of reaction time and show that most of the copper salts lead to the formation of a radical species. Absorption spectroscopy showed that this is not the case for  $\text{Cu}_3(\text{PO}_4)_2$  and  $\text{Cu}(\text{C}_2\text{O}_4)$ , which might be due to the low solubility of these salts in the applied solvent mixture. Furthermore, the perchlorate salts  $\text{NH}_4\text{ClO}_4$  and  $\text{Ni}(\text{ClO}_4)_2$  did not lead to a radical formation. Thus, in our experimental setup, it seems that the disproportionation reaction is not depending on the applied copper source.

EPR spectra recorded on the degradation products  $[\text{Cu}(\text{triaz})_2(\text{L})_m]$  (Figure 62, right) exhibit axial signal shape with  $g_{\parallel} > g_{\perp}$ , which are nearly identical no matter which copper source was used. Solely the  $g_{\parallel}$  part of the spectrum varies. These variations might indicate incorporation of (some of) the anions as ligands into the coordination sphere of the  $\text{Cu}^{\text{II}}$  complexes.

### 7.5 Influences of the base

For a better understanding of the course of the disproportionation reaction (Scheme 42) also the influence of the applied base was examined. Therefore the type (a) and the amount (b) of base were modified.

The disproportionation reaction fails in the absence of base (indicated by green colour of the reaction mixture and a lacking charge transfer absorption band at  $\lambda_{\text{max}} = 410 \text{ nm}$ ). Therefore comparative experiments using different bases varying in base strength, type (primary, secondary and tertiary amines, alcoholates, acetates), sterical demand and donor abilities (coordination strength towards copper) were carried out. Reactions were performed following the already described instructions, characterisation was performed by absorption spectroscopy and spectra are shown in Figure 63.

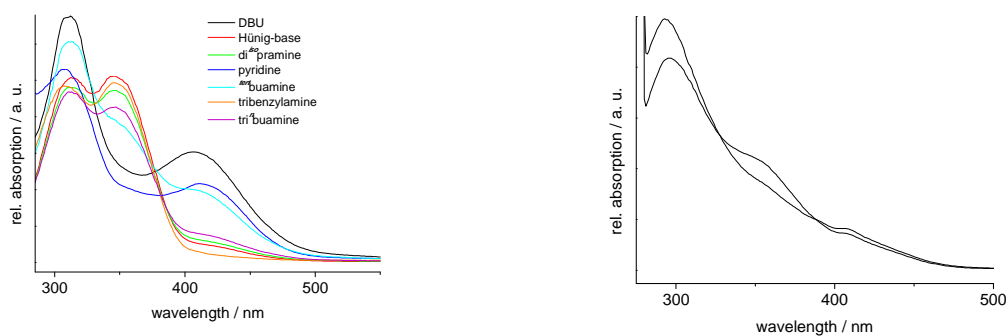


Figure 63: Absorption spectra recorded on mixtures of 2 eq triazH, 1 eq  $\text{Cu}(\text{OTf})_2$  and 0.1 eq of amine bases (left) and 0.1 eq of  $\text{KO}^{\text{tert}}\text{Bu}$  and  $\text{NaOAc}$  (right) at 298 K in MeCN/toluene 5:3

While solutions containing amine bases mostly show a charge transfer absorption band at 410 nm (with varying intensities), the absorption spectra recorded on solutions containing  $\text{KO}^{tert}\text{Bu}$  or  $\text{Na}(\text{OAc})$  show a blue shift of the UV absorption band from 311 nm to 294 nm combined with a decrease of the band around 350 nm but no radical specific absorption band around 410 nm. Thus, not any base is appropriate for application in this type of disproportionation reaction. Also,  $\text{Tri}^n\text{butylamine}$ ,  $\text{tribenzylamine}$ ,  $\text{di}^{iso}\text{propylamine}$ , Hünig-base (ethyl- $\text{di}^{iso}\text{propylamine}$ ) do not lead to marked amounts of radical species, while the bases  $\text{pyridine}$ ,  $\text{DBU}$  (1,8-diazabicyclo[5.4.0]undec-7-ene) and  $^{tert}\text{butylamine}$  can be applied with more success than  $\text{NEt}_3$  (Table 47). Hence, the ideal base seems to be strong ( $pK_a$ ) and should possess good donor abilities towards copper (qualitatively N atoms with small sterical hindrance seem to be favoured).

Table 47: Variation of the applied base

base		$pK_a$	rel. abs at $\lambda_{\text{max}} = 410 \text{ nm}$ ( $c = 2.5 \cdot 10^{-4}$ )
$\text{NaOAc}$	0.1 eq	4.76 <sup>[a]</sup>	0.4
$\text{pyridine}$	0.1 eq	5.23 <sup>[346]</sup>	1.1
$\text{tribenzylamine}$	0.1 eq	6.90 <sup>[346]</sup>	0.1
$\text{tri}^n\text{butylamine}$	0.1 eq	9.99 <sup>[346]</sup>	0.4
$\text{NEt}_3$	0.1 eq	10.62 <sup>[346]</sup>	0.50
$^{tert}\text{butylamine}$	0.1 eq	10.68 <sup>[346]</sup>	1.0
$\text{di}^{iso}\text{propylamine}$	0.1 eq	10.76 <sup>[346]</sup>	0.3
Hünig-base	0.1 eq	10.98 <sup>[346]</sup>	0.2
$\text{DBU}$	0.1 eq	13.28 <sup>[346]</sup>	1.5
$\text{KO}^{tert}\text{Bu}$	0.1 eq	18.00 <sup>[347]</sup>	0.4
$\text{NEt}_3$	0.5 eq		0.45
$\text{NEt}_3$	0.75 eq		0.41
$\text{NEt}_3$	1.0 eq		0.39
$\text{NEt}_3$	2.0 eq		0.15
$\text{NEt}_3$	5.0 eq		0.13
$\text{NEt}_3$	10.0 eq		0.02

[a]  $pK_a$  of acidic acid

This implies that the used base does not only adopt “base functionality” during the reaction, but also stabilises a copper species during the reaction (e.g. by coordination or by weak interactions). This might either be the  $\text{Cu}^{\text{II}}$  phenoxy complexes  $[\text{Cu}(\text{triaz})_2(\text{L})_n]^{\bullet k+}$  or the  $\text{Cu}^{\text{I}}$

disproportionation product  $[\text{Cu}^{\text{I}}(\text{L})_n]^{\text{P}+}$  or both. For the well working bases the absorption wavelength of the copper d-d absorption band was observed to increase along the series  $\lambda_{\text{d-d}} = 640 \text{ nm}$  (pyridine) < 732 nm (DBU) < 750 nm (*tert*-butylamine) < 758 nm ( $\text{NEt}_3$ ). These bands suggest that a  $\text{Cu}^{\text{II}}$  species (oxidised or parent species) is stabilised by the bases, with pyridine inducing the strongest ligand field and  $\text{NEt}_3$  inducing the weakest ligand field.

Besides the type of base also the amount might influence the radical generation. Therefore, the four best suited bases  $\text{NEt}_3$ , DBU, pyridine and *tert*-butylamine were chosen to perform experiments on varying the base concentrations. Figure 64 shows all four experiments, using base in substoichiometric (0.1 eq) to excess (2-10 eq) amounts.

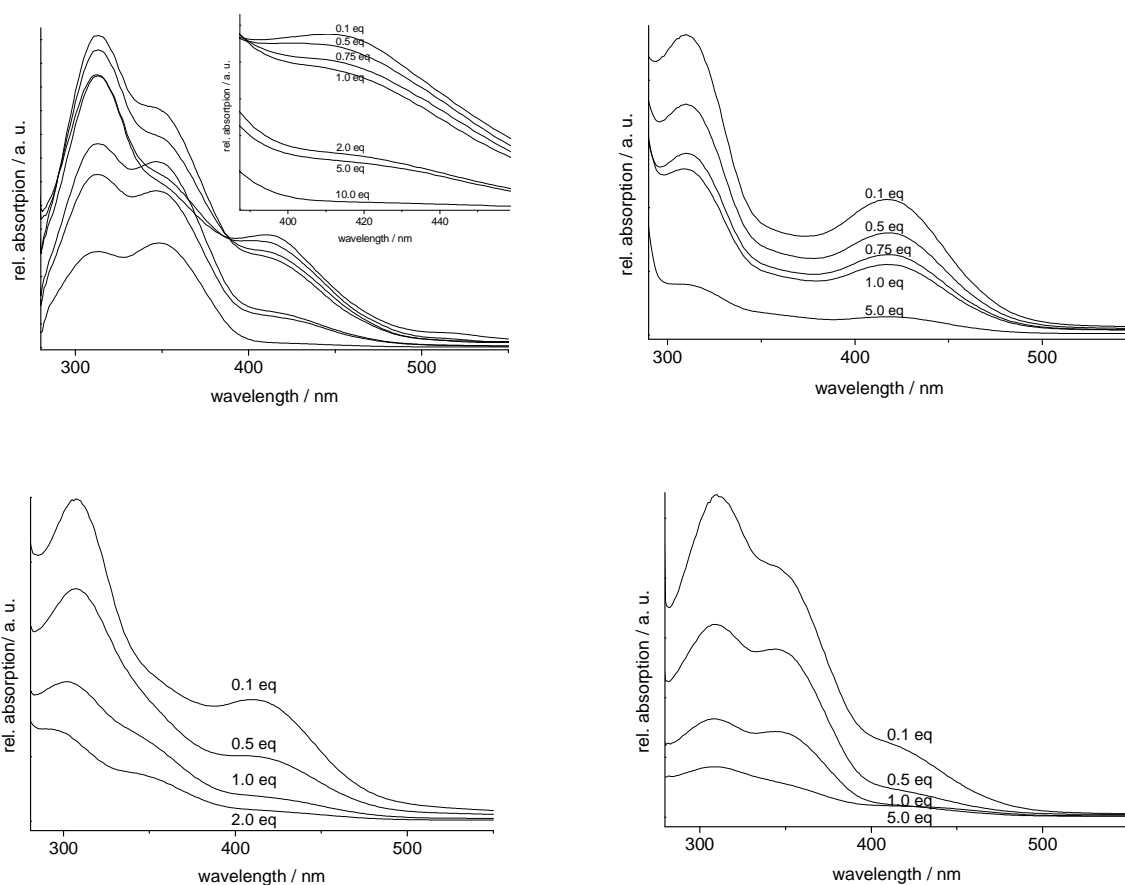


Figure 64: Absorption spectra of reaction mixtures containing 2 eq triazH and 1 eq  $\text{Cu}(\text{OTf})_2$  in MeCN/toluene 5:3 using different amounts of base,  $\text{NEt}_3$  (top, left), pyridine (top, right), DBU (bottom, left) and *tert*-butylamine (bottom, right) at 298 K

The radical is formed reliably upon adding 0.1 – 1.0 eq base, while excess of  $\text{NEt}_3$  (2.0 eq – 10.0 eq) yields almost no radical species in solution. At the same time, it is observed that

increasing amounts of base lead to the formation of precipitates. In case of  $\text{NEt}_3$  this is a dark green, insoluble material, from the pyridine solution a dark blue precipitate was isolated. The EPR spectrum of the green powder formed upon using  $\text{NEt}_3$  as base shows several overlapping  $\text{Cu}^{\text{II}}$  signals, which are assigned to different  $\text{Cu}^{\text{II}}$  ions. Presumably the green solid is an inhomogeneous polymer.

The blue material formed upon using pyridine as base shows an axial EPR signal ( $g_{\parallel} > g_{\perp}$ ) with typical shape and  $g$  values for mononuclear  $\text{Cu}^{\text{II}}$  complexes of (elongated) octahedral or square planar geometry.<sup>[215,228-231]</sup> The  $g$  value of the compound is  $g_{\parallel} = 2.126$  and  $g_{\perp} = 2.048$  (Figure 65, left). An absorption spectrum recorded on the blue substance was measured in MeCN solution (Figure 65, right). Two absorption bands were found, one at 254 nm and another at 610 nm. The latter is a typical d-d transition band for  $\text{Cu}^{\text{II}}$  complexes, possessing a strong ligand field.

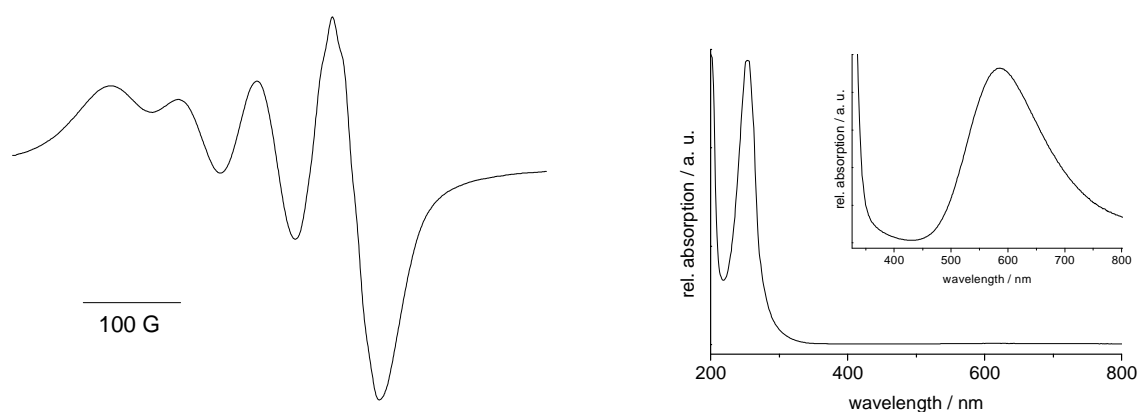


Figure 65: X-band EPR spectrum and absorption spectrum of the blue precipitate isolated from a mixture of 2 eq triazH, 1 eq  $\text{Cu}(\text{OTf})_2$  and excess pyridine in MeCN/toluene 5:3 at 298 K

The blue species could be crystallised from a mixture of 2 eq triazH, 1 eq  $\text{Cu}(\text{OTf})_2$  and excess (~10 eq) pyridine in MeCN/toluene 5:3 at 277 K. Single crystals were suitable for XRD and structure solution and refinements in the monoclinic space group  $P2_1/c$  was carried out with the results collected in Table 48. In the crystal structure (Figure 66, left) the complex  $[\text{Cu}(\text{py})_4(\text{OTf})_2]$  is co-crystallised to two pyridine molecules per unit cell. Figure 66, right shows the molecular structure of  $[\text{Cu}(\text{py})_4(\text{OTf})_2]$ , which is a Jahn-Teller elongated octahedral complex. A crystal structure of this complex has already been reported<sup>[348]</sup> (orthorhombic space group  $Pbcn$ ), but without further pyridine content in the crystal. Nevertheless the molecules in both

structures are similar and the molecular structure of  $[\text{Cu}(\text{py})_4(\text{OTf})_2]$  is therefore not further discussed.

To ensure that the blue powder obtained from the reaction mixture only contains  $[\text{Cu}(\text{py})_4(\text{OTf})_2]$  further investigations have to be carried out e.g. powder XRD or XAS. Nevertheless it seems obvious that application of excess base removes copper ions from the solvent mixture and therefore decreases the amount of triaz complexes (and thus active species) in solution.

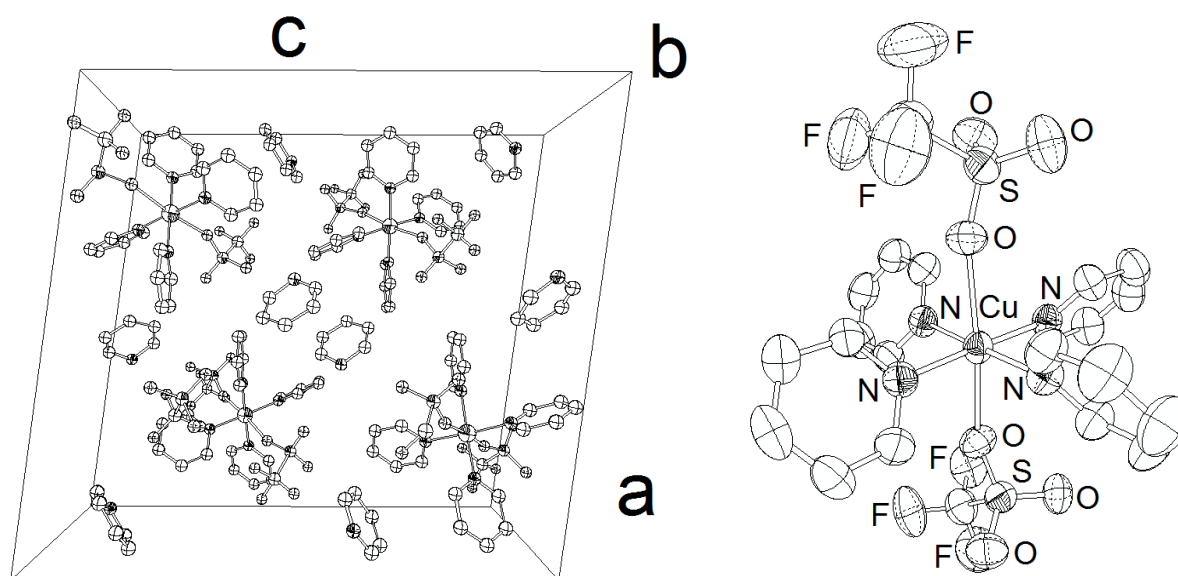


Figure 66: ORTEP representation of  $[\text{Cu}(\text{py})_4(\text{OTf})_2]$  left: unit cell content, right: molecular structure of (50% probability level), H atoms omitted for clarity

Table 48: Solution and refinement data of  $[\text{Cu}(\text{py})_4(\text{OTf})_2] \cdot 2 \text{ py}$

formula	$\text{C}_{32}\text{H}_{30}\text{CuF}_6\text{S}_2\text{N}_6\text{O}_6$	abs. coeff / $\text{mm}^{-1}$	0.767
f. w. / $\text{g mol}^{-1}$	836.28	refl. coll.	47563
crystal system	monoclinic	data / restr. / param.	8425 / 0 / 558
crystal shape	block	h, k, l	$-25 < h < 25$
colour	blue		$-10 < k < 11$
space group	$P2_1/c$ (No. 14)		$-27 < l < 26$
a / $\text{\AA}$	19.545(5)	goof on $F^2$	0.702
b / $\text{\AA}$	9.326(5)	$R_{\text{int}}$	0.1010
c / $\text{\AA}$	20.958(5)	final R indices	$R1 = 0.0388$
$\alpha / ^\circ$	90.0	$[I > 2\sigma(I)]$	$wR2 = 0.0643$
$\beta / ^\circ$	97.841(5)	R indices (all data)	$R1 = 0.1332$
$\gamma / ^\circ$	90.0		$wR2 = 0.0786$
volume / $\text{\AA}^3$ , Z	3784.0(2), 4	largest diff.	0.320 and $-0.487$
F(000)	1708	p. a. h. / $\text{e \AA}^{-3}$	
density / $\text{g cm}^{-3}$	1.468		

Another reaction parameter which is expected to affect the radical stability is the composition of the solvent mixture. Again disproportionation reactions at 298 K were performed using  $\text{Cu}(\text{OTf})_2$  and  $\text{NEt}_3$  as base. The applied solvent mixtures were varied from 0:1 (toluene/MeCN) to 1:0 (toluene/MeCN), absorption spectra of each mixture were recorded and are presented in Figure 67. This variation leads to intensity changes of the radical indicating absorption band at 410 nm. This band only occurs in solvent mixtures with at least 50% MeCN. The reason might be that solvent mixtures with very low polarity quench the radical species (such mixtures support radical degradation) and that MeCN stabilise the radical species by coordination.

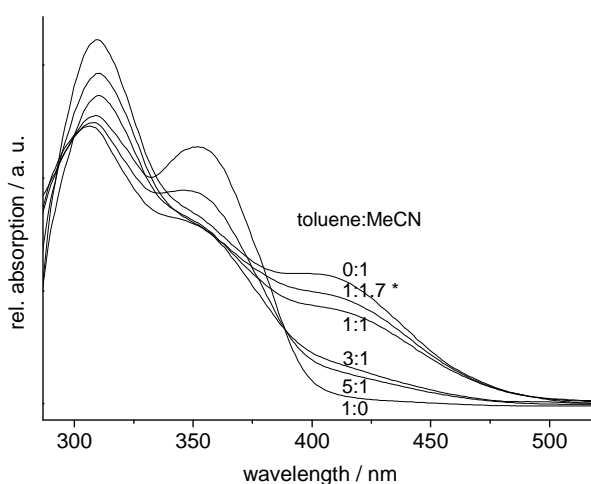


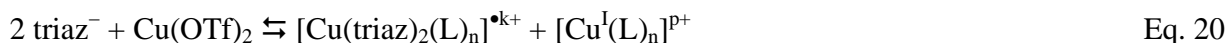
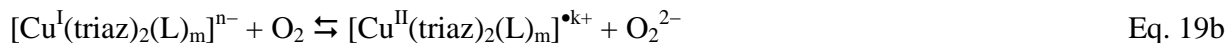
Figure 67: Absorption spectra of  $[\text{Cu}(\text{triaz})_2(\text{L})_n]^{\bullet k+}$  in various mixtures of toluene/MeCN, \* marks the 5:3 solvent mixture used according to former descriptions

To examine whether the polarity or the donor capacity of MeCN is important for radical stabilisation, polar solvents which are weaker ligands (for  $\text{Cu}^{\text{II}}$  coordination) than MeCN were used. Reactions were carried out in acetone, THF and DME (1,2-dimethoxy ethane), the radical formation was determined by absorption spectroscopy as already described. In all three cases an intense absorption band at 410 nm was still observed, verifying that the polarity of the solvent is of importance.

### 7.6 Catalytic oxidation using the phenoxy radical complex $[\text{Cu}(\text{triaz})_2(\text{L})_n]^{\bullet k+}$

A series of catalytic test reactions using benzyl alcohol and yielding benzaldehyde was

carried out to allow a comparison of two different radical generating methods (Eq. 19 and 20).



with  $\text{L} = \text{MeCN}, \text{NEt}_3$  or  $\text{OTf}^-$

The catalytic active species is the  $\text{Cu}^{\text{II}}$  radical complex  $[\text{Cu}(\text{triaz})_2(\text{L})_n]^{\bullet k+}$ . This radical is either generated as outlined in the previous paragraphs by mixing 2 eq triazH with 0.1 eq  $\text{NEt}_3$  and 2 eq  $\text{Cu}(\text{OTf})_2$  in MeCN/toluene 5:3 (Eq. 20) or by mixing 2 eq triazH, 0.1 eq  $\text{NEt}_3$  and 0.5 eq  $[(\text{Cu}(\text{OTf}))_2(\mu\text{-C}_7\text{H}_8)]$  in MeCN/toluene 5:3 (Eq. 19). After 3 minutes benzyl alcohol and NaOH (solid) were added to the mixtures (2.5%<sub>mol</sub>). Furthermore, a reference reaction was carried out using benzyl alcohol and NaOH (solid) without any catalyst. The reaction mixtures were stirred under normal atmosphere in oxygen saturated solution (solvent mixture was bubbled with pure oxygen for 5 minutes before starting the reactions). During two hours reaction time samples were taken from the reaction mixture and analysed by NMR spectroscopy. The intensity (integral) of the benzaldehyde proton was used as measure to quantify the product content of the samples. While the reaction mixture without catalyst only showed benzyl alcohol, the other mixtures were found to contain benzaldehyde. In Figure 68 a typical plot of the product concentration over the reaction time is shown.

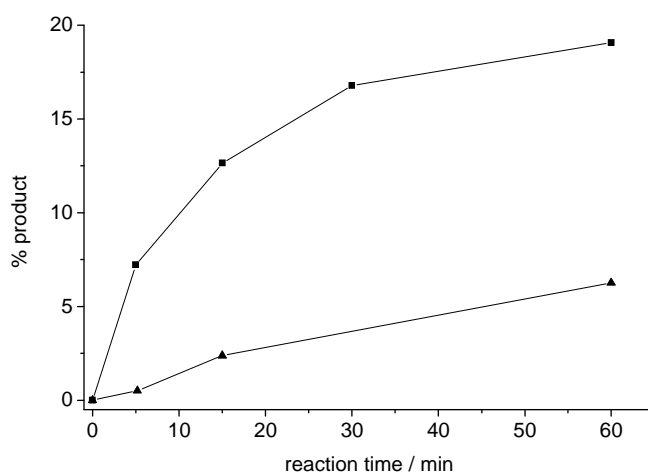


Figure 68: Plot of the benzaldehyde yield; using a  $\text{Cu}^{\text{I}}$  precatalyst (square) or the  $[\text{Cu}(\text{triaz})_2(\text{L})_n]^{\bullet n+}$  species generated in disproportionation reaction (triangle)



At a first glance the  $\text{Cu}^{\text{I}}$  method is superior to the  $\text{Cu}^{\text{II}}$  method. 2.5%<sub>mol</sub> catalyst is a comparably small amount,<sup>[349]</sup> nevertheless the oxidation yields 15% product after 30 min reaction time. Thus final product concentration is far higher (four times higher after 60 minutes reaction time). The reaction conditions seem to be not ideal for the  $\text{Cu}^{\text{I}}$  method as can be seen from the short life time of this species, which is inferred from the product concentration. After 30 min reaction time the product concentration does not increase anymore, thus the catalyst presumably was destroyed. A further indication for catalyst destruction is a green brown precipitate formed upon carrying out the reaction.

The low catalytic activity found for the  $\text{Cu}^{\text{II}}$  method (Eq. 20) might be explained best by a low concentration of active molecules. Right from the beginning the product concentration increases very slowly but constantly during the whole measurement. Thus it has to be assumed that the disproportionation reaction does not proceed quantitatively, so that the amount of active species is far lower than 2.5%<sub>mol</sub>. The life time of the radical species in this solution is higher than life time of the radical in solution formed by the  $\text{Cu}^{\text{I}}$  method. Generation of the active species is assumed to proceed quantitatively for the  $\text{Cu}^{\text{I}}$  method as shown in Eq. 19, therefore the number of catalytic cycles of the triaz catalyst was determined from this method and was calculated to be 6.8 per 30 minutes (meaning that one catalytic cycle takes 4 minutes). Presumably, a too low catalyst concentration accounts for this long period.

### 7.7 Catalytic activity of copper complexes from Chapters 2, 3 and 4

For catalytic test reactions performed on the systems presented in Chapters 2 to 4 the reaction described in the previous paragraph was used. Since the radical generation by using a  $\text{Cu}^{\text{I}}$  precatalyst was superior to the method using a disproportionation to form the active species (Chapter 7.6) further catalytic test reactions were carried out using the  $\text{Cu}^{\text{I}}$  method. Accordingly not the isolated copper complexes (which were characterised and described in former chapters) were used for catalysis but the free ligands mixed with the complex  $[(\text{Cu}(\text{OTf}))_2(\mu\text{-C}_7\text{H}_8)]$ . The substrate used in these reactions was again benzyl alcohol and catalyst concentration was enlarged (10%<sub>mol</sub>), details of the reaction parameters can be found on page 163. The product was detected by  $^1\text{H}$  NMR spectroscopy using the aldehyde proton as a measure for the reaction rate.

Samples were taken after 1 h and 17 h reaction time. Table 49 summarises the results of the catalytic test reactions.

Table 49: Overview on catalytic test reactions performed with catalysts synthesised and characterised in this study

applied ligand	from Chapter	% product after 1 h	% product after 17 h
pydicOIPh	2.1	-	-
LOMe <sub>2</sub>	2.2	-	-
LOH <sub>2</sub>	2.2	2.9 <sup>[a]</sup>	21.1 <sup>[a]</sup>
LOMe <sub>4</sub>	2.2	2.6	18.3
LOH <sub>3</sub> OMe	2.2	- <sup>[a]</sup>	- <sup>[a]</sup>
LOMe <sub>2</sub> <sup>i</sup> Pr	2.2	-	-
LOH <sub>2</sub> <sup>i</sup> Pr	2.2	-	-
bqOH	3.2	1.6 <sup>[a]</sup>	53.6 <sup>[a]</sup>
acrOMe	3.3	0.3 <sup>[a]</sup>	0.4 <sup>[a]</sup>
acrOH	3.3	6.3 <sup>[a]</sup>	6.3 <sup>[a]</sup>
(NH) <sub>2</sub> salPh <sub>2</sub>	4	25.6	67.6
Me <sub>2</sub> salF <sub>4</sub>	4	9.1	81.5
Ph <sub>2</sub> sal	4	4.8	70.0
salPh <sub>2</sub>	4	- <sup>[a]</sup>	- <sup>[a]</sup>
(NH) <sub>2</sub> sal	4	-	-
(NMe) <sub>2</sub> sal <sup>terr</sup> Bu <sub>4</sub>	4	3.3 <sup>[b]</sup>	38.8 <sup>[b]</sup>

[a] Catalyst precipitated at the beginning or during the reaction

[b] The reaction was performed with 3%<sub>mol</sub> instead of 10%<sub>mol</sub>

Table 49 summarises the amount of benzaldehyd obtained in catalytic test reactions. Obviously there are large differences in catalytic activity of the systems as inferred from the different yields ranging from 0% to 81.5%. High yields (above 50%) are only found for salen type ligands and bqOH, validating that most of the catalysts possess rather low efficiency.

Complexes containing methoxy functions generally perform catalytic oxidation similar to systems containing hydroxy functions although not all OMe systems are catalytically active. Aromatic stabilisation is a working strategy for oxidation catalysts, as the systems bqOH and acrOH show. Complexes containing these ligands were found to possess very poor solubility and even formed precipitates during the catalytic test reaction; nevertheless they were found to be active (due to remaining catalyst molecules in solution or due to heterogeneous catalysis).

The systems containing pydicOIPh, LOMe<sub>2</sub> and (NH)<sub>2</sub>sal are not substituted on the phenol cores and thus their inactivity is not surprising. Catalytic reactions performed with partly substituted systems such as LOH<sub>3</sub>OMe, LOMe<sub>2</sub><sup>i</sup>Pr, LOH<sub>2</sub><sup>i</sup>Pr and salPh<sub>2</sub> did not reveal any product formation as well. An explanation can hardly be found since other partly stabilised

systems such as  $(\text{NH})_2\text{salPh}_2$  produced high amounts of benzaldehyde and even non substituted systems such as  $\text{LOH}_2$  show catalytic activity. Furthermore, some partly substituted systems revealed very promising electrochemical properties upon spectroscopic characterisation.

Interestingly, some catalysts are nearly inactive after 1 h (no increasing product concentration after 1 h reaction time) such as  $\text{acrOMe}$  and  $\text{acrOH}$ , while other systems showed low product concentration after 1 h and very high product concentration after 17 h reaction time (e.g.  $\text{Me}_2\text{salF}_4$ ). These results lack helpful tendencies to further draw general conclusions. At least it might be very helpful to perform detailed catalytic test reactions in a more standardised way e.g. using a reaction automat.

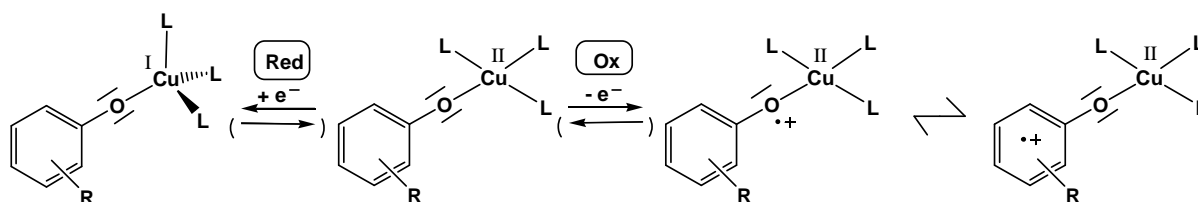
## 8.0 Summary

This thesis gives an account on the preparation and characterisation of new  $\text{Cu}^{\text{II}}$  complexes bearing bis-phenoxido pincer ligands, phenalenone-, benzoquinone-, acridine-, salen type-, O,O',N donor ligands (derivatives of (2-methoxyphenyl)(pyridin-2-yl)methanol), triazol- and pydic-ester (pydic = pyridine-2,6-dicarboxylic acid) ligands. Detailed studies using XRD, EPR and absorption spectroscopy as well as elemental analysis, allowed to identify the compositions and geometries of all complexes in the solid state and in solution. All of the ligands contain one or two phenoxy moieties, which take part in copper coordination in most cases. Solely for O,O',N donor ligands and pydic-ester ligands the phenoxy donor function were not coordinated.

The new complexes were studied in detail focusing on three aspects important for their suitability to perform oxidation catalysis especially conversion of alcohols to aldehydes (Eq. 21).



Since this reaction requires two electrons, a suitable catalyst should transfer two electrons and thus needs two (more or less coupled) redox centres. In copper phenoxyl complexes these centres correspond to the redox couples  $\text{Cu}^{\text{II}}/\text{Cu}^{\text{I}}$  and  $[\text{PhO}]^{\bullet+}/[\text{PhO}]$  (Scheme 43), a combination which is inspired by naturally occurring oxidation catalysts such as the metalloenzyme Galactose Oxidase (GO).



Scheme 43: General drawing of a copper phenoxyl complex and its phenoxyl species with two mesomeric forms

The two redox couples of each complex were studied by electrochemical methods (cyclic voltammetry and spectroelectrochemistry) focussing on three important aspects: (i) the potential and the reversibility (or rather the peak-to-peak separation) of the  $\text{Cu}^{\text{II}}/\text{Cu}^{\text{I}}$  redox process, which is closely linked to the flexibility of the copper coordination sphere; (ii) the potential and reversibility of the  $[\text{PhO}]^{\bullet+}/[\text{PhO}]$  redox couple which largely depends on the structure of the phenoxyl-ligands and (iii) the energy of the metal ( $\text{Cu}^{\text{II}}$ )-to-ligand ( $[\text{PhO}]^{\bullet+}$ )

charge transfer (LMCT) absorption band of the radical complexes, which were examined by spectroelectrochemical measurements using absorption spectroscopy as detection method. The emergence of the LMCT band (in the range 400 to 600 nm) indication for the radical generation or decay and the energy of the transition is an excellent quantitative measure for the stability of the formed radicals. Besides determination of physical properties, all complexes have been applied in catalytic test reactions using benzyl alcohol as the substrate to determine the catalytic potential of the complexes. In Figure 69 the obtained data are summarised to depict existing tendencies.

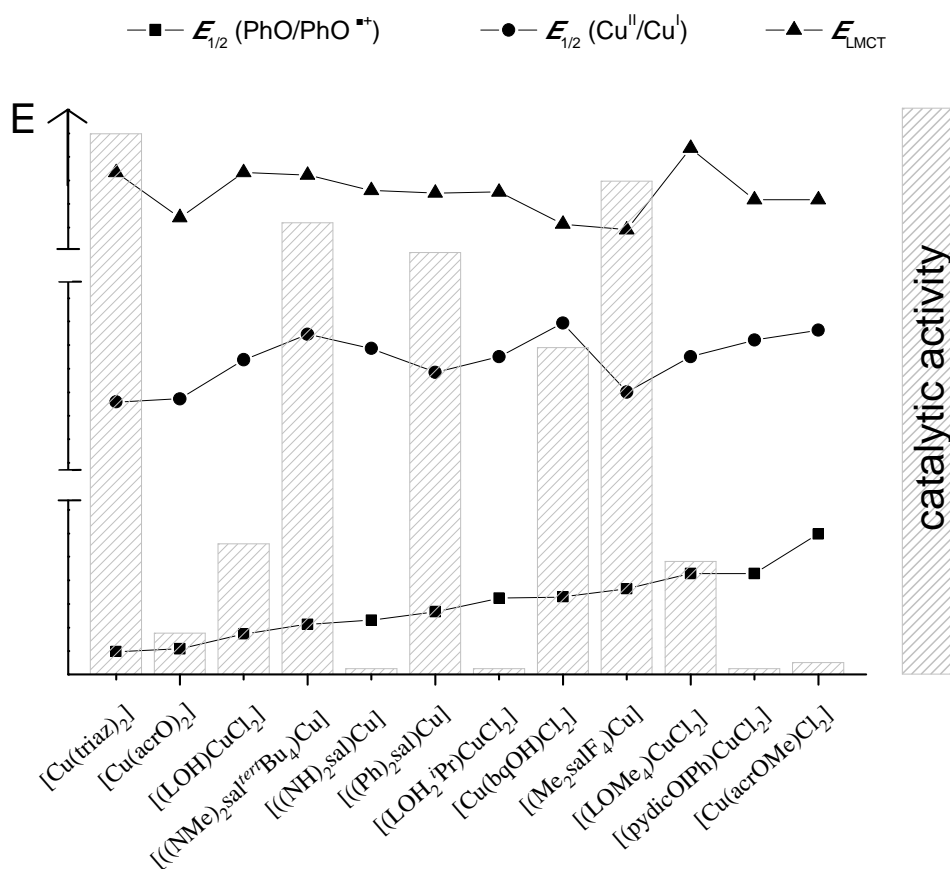


Figure 69: Plot of  $E_{1/2}([\text{PhO}]^{\bullet+}/[\text{PhO}])$  (square),  $E_{1/2}(\text{Cu}^{\text{II}}/\text{Cu}^{\text{I}})$  (circle),  $E_{\text{LMCT}}$  (triangle) and catalytic activity (bars) of selected copper complexes

The electrochemical potential for the  $\text{Cu}^{\text{II}}/\text{Cu}^{\text{I}}$  redox couple varies from 0.23 V for  $[\text{Cu}(\text{bqOH})\text{Cl}_2]$  to  $-0.33$  V for  $[\text{Cu}(\text{triaz})_2]$  and is reversible for all complexes. The potentials of ligand centred oxidation ( $[\text{OPh}]^{\bullet+}/[\text{OPh}]$ ) differ stronger from those of the  $\text{Cu}^{\text{II}}/\text{Cu}^{\text{I}}$  redox couple, they range from 1.01 V ( $[\text{Cu}(\text{acrOMe})\text{Cl}_2]$ ) and 0.15 V ( $[\text{Cu}(\text{triaz})_2]$ ). No correlation was found between both redox couples, hence  $\Delta E_{1/2}$  is low for some complexes (e.g. 0.32 V for  $[\text{Cu}(\text{bqOH})\text{Cl}_2]$ ) and high for others (e.g. 0.87 V for  $[(\text{Me}_2\text{salF}_4)\text{Cu}]$ ). In general, the stability of the electrochemically formed radicals is influenced by the potential of the  $[\text{PhO}]^{\bullet+}/[\text{PhO}]$

redox couple (the lower the more stable) and by the spin density (the higher the spin dilution or the larger the area of delocalisation, the more stable the unpaired electron). Consequently, there are two ways to stabilise the copper phenoxyl radicals, which both have been used in the present study. On one hand, substitution of the phenol core can increase the electron density and therefore lower the  $[\text{PhO}]^{\bullet+}/[\text{PhO}]$  potential. Suitable are substituents with +I effect, e.g. alkyl groups, with -I and +M effect e.g. halogens and with a +M effect, e.g. methoxy groups. On the other hand, using ligands with enlarged aromatic scaffolds leads to spin dilution by delocalisation of the unpaired electron (mesomeric forms) (e.g. in benzoquinone or acridine).

Figure 69 also shows the energy of the absorption bands assigned to the copper phenoxyl radical MLCT, which range from 371 nm (for  $[(\text{LOMe}_4)\text{CuCl}_2]$ ) to 542 nm (for  $[(\text{Me}_2\text{salF}_4)\text{Cu}]$ ). Interestingly, the tendencies found for  $E_{1/2}([\text{PhO}]^{\bullet+}/[\text{PhO}])$  and  $E_{\text{LMCT}}$  are not identical, thus the stability of the phenoxyl radicals inferred from spectroelectrochemical measurements and inferred from electrochemical measurements are not identical.

Generally, the absorption bands of the complexes containing larger aromatic scaffolds (fused aromatic rings, e.g. phenanthrenes) lie at longer wavelengths than absorptions observed for systems containing six membered rings. This indicates that the radical is stabilised by delocalisation in the aromatic  $\pi$ -system. An unexpected long absorption wavelength was found for  $[(\text{Me}_2\text{salF}_4)\text{Cu}]$ , that presumably may be ascribed to the influence of *ortho* and *para* substitution at the phenol core or to the formation of a second phenoxyl radical in the complex. Such biradical complexes show a long-wavelength absorption assigned to an inter-ligand CT between both radicals. Inter-ligand charge transfer absorption bands normally lie in the range of 500 to 650 nm and thus the absorption band at 542 nm observed for  $[(\text{Me}_2\text{salF}_4)\text{Cu}]$  might also be assigned to an inter-ligand charge transfer absorption.

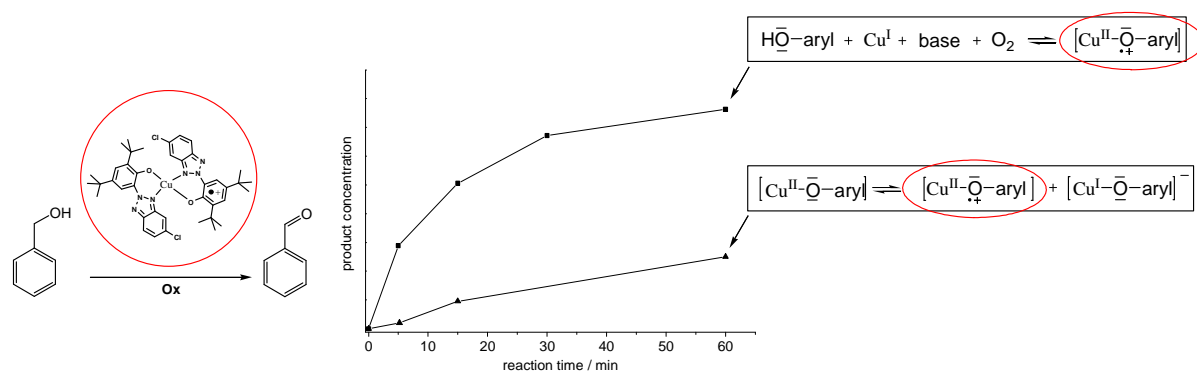


Figure 70: Catalytic benzyl alcohol oxidation using the triaz catalyst generated by two alternative methods

A study on catalytic activity was performed using benzyl alcohol as substrate and the product formation was monitored by  $^1\text{H}$  NMR spectroscopy. Detailed investigations were carried out using the triazH system (Figure 69). First experiments focused on radical generation (= generation of the catalytic active species) under reaction conditions. Two alternative strategies were compared: (1) application of a  $\text{Cu}^{\text{I}}$  precursor in the presence of  $\text{O}_2$ ; (2) application of a  $\text{Cu}^{\text{II}}$  precursor inducing a disproportionation reaction.

As shown in Figure 70, the reaction starting from a  $\text{Cu}^{\text{I}}$  precursor was more successful and yielded higher amounts of benzaldehyde than the reaction starting from  $\text{Cu}^{\text{II}}$ . It can be concluded that the disproportionation reaction leads to very low concentration of active species, whereas the use of  $\text{Cu}^{\text{I}}$  precursors results in higher concentration of radical species and therefore works more reliably. So catalytic benzyl alcohol oxidation was performed using the ligands analysed in this thesis for *in situ* generation of radical complex species by the  $\text{Cu}^{\text{I}}$  method, Figure 69 presents results of the catalytic test reactions (bares).

At first glance, the catalytic activity of the different systems does not correlate to their physical properties (e.g. electrochemical potentials for radical generation or copper reduction). From the systems with extended aromatic ligand scaffold only the bqO complex exhibits reasonable catalytic activity. The most obvious reason for the lacking catalytic activity of systems with extended aromatic ligand scaffold (although they show high radical stability) is the poor solubility of such complexes. Therefore, the activity found for the bqO system is surprising, since bqO even precipitated during the catalytic test reaction. Systems containing methoxy donor ligands turned out to be not suitable for application in catalysis. Complexes containing  $\text{Cu}-\text{OMe}$  bonds possess higher redox potentials for both redox couples  $[\text{PhO}]^{\bullet+}/[\text{PhO}]$  and  $\text{Cu}^{\text{II}}/\text{Cu}^{\text{I}}$ , than the corresponding complexes with hydroxy donor functions and the resulting catalytic activity is low. However, reasonable activity was found for the tetra-methoxylated ( $\text{LOMe}_4$ ) ligand. Salen type ligands, which have previously been shown to be suitable as oxidation catalysts, are the most efficient systems in this series. Nevertheless, none of the analysed systems are as active as established copper phenoxyl complexes.

Generally, the present investigations confirm that systems containing substituted phenol cores are more suitable for phenoxyl radical generation as well as for application in catalysis. Nevertheless, some surprising exceptions were found such as the high catalytic activity of the non-stabilised system  $[(\text{Ph}_2\text{sal})\text{Cu}]$  or the fluorine-stabilised system  $[(\text{Me}_2\text{salF}_4)\text{Cu}]$ . Thus, further investigation on partly or non-stabilised systems are useful and might lead to highly active catalysts.

## 9.0 Experimental

### 9.1 Instrumentation

NMR spectra were recorded on a Bruker Avance II 300 MHz spectrometer, using a triple resonance  $^1\text{H}$ ,  $^2\text{BB}$  inverse probe head. The unambiguous assignment of the  $^1\text{H}$  and  $^{13}\text{C}$  resonances was obtained from  $^1\text{H}$  NOESY,  $^1\text{H}$  COSY, gradient selected  $^1\text{H}$ ,  $^{13}\text{C}$  HSQC and HMBC experiments. All 2D NMR experiments were performed using standard pulse sequences from the Bruker pulse program library. Chemical shifts were relative to TMS.

UV/vis/NIR absorption spectra were measured on Varian Cary50 Scan or Shimadzu UV-3600 photo spectrometers.

UV/Vis emission spectra were recorded with a Spex FluoroMax-3.

Elemental analyses were carried out using a HEKAtech CHNS EuroEA 3000 Analyzer.

EPR spectra were recorded in the X-band on a Bruker System ELEXSYS 500E equipped with a Bruker Variable Temperature Unit ER 4131VT (500 to 100 K or an Oxford Instruments helium-cryostat (300 to 4 K); the  $g$  values were calibrated using a dpph sample. Simulation of the EPR spectra were performed using the PEST Winsim software.<sup>[305]</sup>

Electrochemical experiments were carried out in 0.1 M  $^n\text{Bu}_4\text{NPF}_6$  solutions using a three-electrode configuration (glassy carbon working electrode, Pt counter electrode, Ag/AgCl pseudo reference) and an Autolab PGSTAT30 potentiostat and function generator. The ferrocene/ferrocenium couple ( $\text{Fc}/\text{Fc}^+$ ) served as internal reference.

UV/Vis spectroelectrochemical measurements were performed with an optical transparent thin-layer electrochemical (OTTLE) cell.<sup>[350]</sup>

Magnetic Susceptibilities were measured with a SQUID magnetometer (MPMS-5S, Quantum Design) in a temperature range of 2 to 300 K at a magnetic field of  $H = 0.1$  T.

Crystal structure determinations were performed at 293(2) K (despite for  $[\text{Cu}(\text{py})_4(\text{OTf})_2]$ , which was measured at 273(2) K) using graphite-monochromatised Mo- $K_\alpha$  radiation ( $\lambda = 0.71073$  Å) on IPDS II (STOE and Cie.). The structures were solved by direct methods



using SHELX-97 and WinGX (SHELXS-97)<sup>[351]</sup> and refined by full-matrix least-squares techniques against  $F^2$  (SHELXL-97)<sup>[352]</sup>. The numerical absorption corrections (X-RED V1.22; Stoe & Cie, 2001) were performed after optimising the crystal shapes using X-SHAPE V1.06 (Stoe & Cie, 1999)<sup>[353]</sup>. The non-hydrogen atoms were refined with anisotropic displacement parameters. H atoms were included by using appropriate riding models.

Water free reactions were carried out under inert gas conditions and performed using Schlenk techniques. Solvents were dried using a MBRAUN MB SPS-800 solvent purification system.

## 9.2 Synthesis

Starting materials: The nickel complexes  $[(PPh_3)_2NiBr_2]$ ,<sup>[354]</sup>  $[(dppe)NiCl_2]$ <sup>[355]</sup> and  $[Ni(acac)_2]$ <sup>[356]</sup> were synthesised by procedures described in literature, as well as the organic components 4-Iodo-1,3-dimethoxybenzene,<sup>[357]</sup> 2-(2-methoxyphenylamino)benzoic acid (from anthranilic acid and 2-iodo-anisol)<sup>[297]</sup> and 1-hydroxidophenalenone-9 (opoH)<sup>[358]</sup>. Catalytically applied  $Cu^0$  was activated as described previously.<sup>[359]</sup>

The ligands 10-hydroxybenzo-[h]-quinoline was purchased from Across Organics and 2,4-di<sup>tert</sup>butyl-6-(5-chloro-2H-benzo[d][1,2,3]triazol-2-yl)phenol was purchased from ABCR.

**$[Cu(MeCN)_4](TFA)_2$ :** 2.0 g (15 mmol)  $CuCl_2$  (anhydrous) was dissolved in 100 mL MeCN and 20 mL trifluoroacetic acid and refluxed over night. The remaining solution was evaporated to 50 mL and the product was precipitated by cooling to 273 K as a blue powder. Yield: 4.30 g (9.5 mmol 63%). Elemental analyses: calc (for  $C_{12}H_{12}F_6N_4O_4Cu$ ;  $M = 453.78$  g mol<sup>-1</sup>) N 12.35; C 31.76; H 2.67; found: N 12.33; C 31.74; H 2.66.

**$Cu(OTs)_2$ :** 1.0 g (5.5 mmol, 1 eq)  $Cu(OAc)_2$  was dissolved in 50 mL MeCN. 3.0 g (excess) *p*-toluenesulfonic acid were dissolved in 50 mL MeCN and was added in small portions to the  $Cu(OAc)_2$  solution. 150 mL diethyl ether were added upon which a pale blue precipitate was formed. After 1 h the precipitate was filtered off and washed with diethyl ether and dried at ambient temperature. Yield: 0.69 g (1.7 mmol, 31%). Elemental analyses: calc (for  $C_{14}H_{14}S_2O_6Cu$ ;  $M = 405.93$  g mol<sup>-1</sup>) C 41.42; H 3.48; S 15.80; found: C 41.71; H 3.40; S 14.83.

**Pyridine-2,6-dicarbonyl dichloride:** 2.0 g pyridine-2,6-dicarboxylic acid (12 mmol, 1 eq) was suspended in 100 mL  $\text{SOCl}_2$ . The mixture was refluxed for 72 h at 366 K. The resulting yellow solution was evaporated under reduced pressure to yield a colourless oil. 350 mL cyclohexane were added and the mixture was cooled to 278 K. After 4 h the precipitated product was collected by filtration and dried under vacuum to yield colourless needles. Yield: 2.24 g (11 mmol, 88%). mp: 335 K. NMR (300 MHz,  $[\text{D}_6]$ -acetone):  $^1\text{H}$ : 8.55-8.41 (m, 3H,  $\text{H}_{3,4,5\text{Py}}$ ).  $^{13}\text{C}$ : 170 (2C,  $\text{C}_{\text{carbonyl}}$ ), 150 (2C,  $\text{C}_{2,6\text{Py}}$ ), 142 (1C,  $\text{C}_{4\text{Py}}$ ), 131 (2C,  $\text{C}_{3,5\text{Py}}$ ) ppm. Elemental analyses: calc (for  $\text{C}_7\text{H}_3\text{NO}_2\text{Cl}_2$ ;  $M = 204.01 \text{ g mol}^{-1}$ ) N 6.87; C 41.21; H 1.48; found: N 6.83; C 41.13; H 1.30.

**Bis(2-iodophenyl) pyridine-2,6-dicarboxylic ester (pydicOIPh):** 1.0 g (5 mmol, 1 eq) pyridine-2,6-dicarbonyl dichloride was dissolved in 20 mL dry diethyl ether. 2.3 g (10 mmol, 2 eq) of 2-iodo-phenol were dissolved in 30 mL dry diethyl ether. 10 mg 4-dimethylaminopyridine (5% $_{\text{mol}}$ ) and 0.7 mL  $\text{NEt}_3$  were added to the alcohol mixture, which was then cooled using an ice bath. The acid chloride solution was dropped slowly into the alcohol mixture and precipitation of the product started immediately. After stirring for 1 h at 273 K, 0.7 mL  $\text{NEt}_3$  were added at 298 K and the mixture was stirred for 16 h. The formed colourless precipitate was filtered off and washed with 5 mL diethyl ether. The remaining powder was dried on air to yield 2.35 g (4.1 mmol, 82%). NMR (300 MHz,  $[\text{D}_7]$ -dmf):  $^1\text{H}$ : 8.64 (d, 2H,  $\text{H}_{3,4\text{Py}}$ ), 8.47 (t, 1H,  $\text{H}_{5\text{Py}}$ ), 7.94 (d, 2H,  $\text{H}_{3\text{Ph}}$ ), 7.51 (t, 2H,  $\text{H}_{5\text{Ph}}$ ), 7.47 (d, 2H,  $\text{H}_{6\text{Ph}}$ ), 7.11 (t, 2H  $\text{H}_{4\text{Ph}}$ ) ppm. Elemental analyses: calc (for  $\text{C}_{19}\text{H}_{11}\text{NO}_4\text{I}_2$ ;  $M = 571.10 \text{ g mol}^{-1}$ ) N 2.45; C 39.96; H 1.94; found: N 2.43; C 39.89; H 1.93.

**$[(\text{pydicOIPh})\text{CuCl}_2]$ :** 100 mg (0.18 mmol, 1 eq) pydicOIPh were dissolved in 15 mL methanol. 24 mg (0.18 mmol, 1 eq)  $\text{CuCl}_2$  (anhydrous) were dissolved in 10 mL methanol and both solutions were mixed and stirred at 298 K for 16 h. The solvent was evaporated to yield a brown powder, 85 mg (0.12 mmol, 67%). Elemental analyses: calc (for  $\text{C}_{19}\text{H}_{11}\text{CuCl}_2\text{NO}_4\text{I}_2$ ;  $M = 705.56 \text{ g mol}^{-1}$ ) N 1.99; C 32.34; H 1.57; found: N 2.02; C 32.00; H 1.62.

**$[(\text{pydic})\text{Cu}(\text{OH}_2)_2]_n$ :** 100 mg (0.5 mmol, 1 eq) pyridine-2,6-dicarbonyl dichloride were dissolved in 15 mL methanol. 67 mg (0.5 mmol, 1 eq)  $\text{CuCl}_2$  (anhydrous) and 1 mL (excess)  $\text{NEt}_3$  were added and the whole mixture was stirred at 298 K for 16 h. The resulting green solution was evaporated to dryness to yield 33 mg (0.12 mmol, 24%) turquoise crystals. Elemental analyses: calc (for  $\text{C}_7\text{H}_7\text{CuNO}_6$ ;  $M = 264.68 \text{ g mol}^{-1}$ ) N 5.29; C 31.76; H 2.67; found: N 5.14; C 32.09; H 2.72.

**[Cu(OH<sub>2</sub>)<sub>6</sub>][(Cu(pydic) $\mu$ -Cl)<sub>2</sub>]:** 100 mg (0.5 mmol, 1 eq) pyridine-2,6-dicarbonyl dichloride were dissolved in 15 mL methanol. 81 mg (0.6 mmol, 1.2 eq) CuCl<sub>2</sub> (anhydrous) and 1 mL (excess) NEt<sub>3</sub> were added and the whole mixture was stirred at 298 K for 16 h. The resulting green solution was slowly evaporated to dryness to yield 21 mg (0.03 mmol, 12%) blue-green crystals. Elemental analyses: calc (for C<sub>14</sub>H<sub>18</sub>Cu<sub>3</sub>Cl<sub>2</sub>N<sub>2</sub>O<sub>14</sub>; M = 699.84 g mol<sup>-1</sup>) N 3.62; C 21.74; H 1.82; found: N 3.58; C 22.00; H 1.79.

**(HNEt<sub>3</sub>)[(pydicOMe)CuCl<sub>3</sub>]:** 100 mg (0.5 mmol, 1 eq) pyridine-2,6-dicarbonyl dichloride were dissolved in 15 mL methanol (anhydrous). 67 mg (0.5 mmol, 1 eq) CuCl<sub>2</sub> (anhydrous) were added and 1 mL (excess) NEt<sub>3</sub> (anhydrous) was added and the whole mixture was stirred at 298 K for 16 h. The resulting green solution was evaporated to dryness to yield 75 mg (0.16 mmol, 32%) green-brown crystals. Elemental analyses: calc (for C<sub>15</sub>H<sub>25</sub>CuCl<sub>3</sub>N<sub>2</sub>O<sub>4</sub>; M = 467.27 g mol<sup>-1</sup>) N 6.00; C 38.56; H 5.39; found: N 6.02; C 38.43; H 5.34.

**(HNEt<sub>3</sub>)[(pydicOPh)CuCl<sub>3</sub>]:** 200 mg (1 mmol, 1 eq) pyridine-2,6-dicarbonyl dichloride were mixed with 15 g phenol. 132 mg (1 mmol, 1 eq) CuCl<sub>2</sub> (anhydrous) were added as solid and 1 mL (excess) NEt<sub>3</sub> was added in one portion. The whole mixture was warmed up to 323 K and stirred in a big round bottom flask for 96 h. During that time the excess phenol solidified in the upper part of the flask and the product complex remained as brown oil. The oil was transferred to a new flask and cooled down to 298 K, upon which the oil solidified as brownish powder. The crude product was dissolved in acetone and slowly evaporated to dryness to yield 319 mg (0.54 mmol, 54%) of a green-yellow microcrystalline powder. Elemental analyses: calc (for C<sub>25</sub>H<sub>29</sub>CuCl<sub>3</sub>N<sub>2</sub>O<sub>4</sub>; M = 591.41 g mol<sup>-1</sup>) N 4.74; C 50.77; H 4.94; found: N 4.66; C 51.12; H 5.02.

**4-Iodo-1,3-dimethoxybenzene:** 1.38 g (10 mmol, 1 eq) 1,3-dimethoxybenzene were mixed with 1.27 g (5 mmol, 0.5 eq) I<sub>2</sub> (finely powdered) and 0.56 g (6 mmol, 0.6 eq) UHP (finely powdered). After exposing to ultrasound for 10 h, the mixture was extracted with 100 mL methyl <sup>tert</sup>butyl ether (MTBE). The organic phase was washed with aqueous Na<sub>2</sub>S<sub>2</sub>O<sub>3</sub> solution (10%) and water. After drying the organic phase using MgSO<sub>4</sub>, the solvent was removed under reduced pressure to yield 2.62 g (9.9 mmol, 99%) of a brown oil. NMR (300 MHz, CDCl<sub>3</sub>): <sup>1</sup>H:  $\delta$  = 7.60 (d, 1H, H<sub>5Ph</sub>), 6.42 (d, 1H, H<sub>2Ph</sub>), 6.31 (dd, 1H, H<sub>6Ph</sub>), 3.84 (s, 3H, H<sub>3OMe</sub>), 3.78 (s, 3H, H<sub>1OMe</sub>). <sup>13</sup>C:  $\delta$  = 161 (1C, C<sub>1Ph</sub>), 159 (1C, C<sub>3Ph</sub>), 139 (1C, C<sub>5Ph</sub>), 107 (1C, C<sub>6Ph</sub>), 99 (1C, C<sub>2Ph</sub>), 75 (1C, C<sub>4Ph</sub>), 56 (1C, C<sub>3OMe</sub>), 55 (1C, C<sub>1OMe</sub>) ppm. Elemental analyses: calc (for C<sub>8</sub>H<sub>9</sub>O<sub>2</sub>I; M = 264.06 g mol<sup>-1</sup>) C 36.39; H 3.44; found: C 36.30; H 3.45.

**2,6-Bis(2-methoxyphenyl)pyridine (LOMe<sub>2</sub>):**<sup>[232]</sup> Mp = 403 K. NMR (300 MHz, CDCl<sub>3</sub>): <sup>1</sup>H: δ = 7.93 (dd, 2H, H<sub>6Ph</sub>), 7.76 (m, 3H, H<sub>3,4,5Py</sub>), 7.36 (t, 2H, H<sub>4Ph</sub>), 7.14 (d, 2H, H<sub>3Ph</sub>), 7.07 (t, 2H, H<sub>5Ph</sub>), 3.88 (s, 6H, H<sub>OMe</sub>). <sup>13</sup>C: δ = 158 (2C, C<sub>2Ph</sub>), 155 (2C, C<sub>2,6Py</sub>), 135 (1C, C<sub>4Py</sub>), 132 (2C, C<sub>6Ph</sub>), 130 (2C, C<sub>4Ph</sub>), 123 (2C, C<sub>3,5Py</sub>), 121 (4C, C<sub>1,5Ph</sub>), 112 (2C, C<sub>3Ph</sub>), 55 (2C, C<sub>OMe</sub>) ppm. Elemental analyses: calc (for C<sub>19</sub>H<sub>17</sub>NO<sub>2</sub>; M = 291.34 g mol<sup>-1</sup>) N 4.81; C 78.33; H 5.88; found: N 4.82; C 78.33; H 5.85.

**2,6-Bis(2-hydroxyphenyl)pyridine (LOH<sub>2</sub>):**<sup>[236]</sup> Mp = 412 K. NMR (300 MHz, CDCl<sub>3</sub>): <sup>1</sup>H: δ = 9.88 (s(br), 2H, H<sub>OH</sub>), 8.00 (t, 1H, H<sub>4Py</sub>), 7.72 (d, 2H, H<sub>3,5Py</sub>), 7.69 (d, 2H, H<sub>6Ph</sub>), 7.35 (t, 2H, H<sub>4Ph</sub>), 7.05 (d, 2H, H<sub>3Ph</sub>), 7.00 (t, 2H, H<sub>5Ph</sub>). <sup>13</sup>C: δ = 156 (2C, C<sub>2Ph</sub>), 151 (2C, C<sub>2,6Py</sub>), 140 (1C, C<sub>4Py</sub>), 132 (2C, C<sub>4Ph</sub>), 128 (2C, C<sub>6Ph</sub>), 121 (2C, C<sub>1Ph</sub>), 120 (4C, C<sub>3,5Py,5Ph</sub>), 118 (2C, C<sub>3Ph</sub>) ppm. Elemental analyses: calc (for C<sub>17</sub>H<sub>13</sub>NO<sub>2</sub>; M = 263.30 g mol<sup>-1</sup>): N 5.32; C 77.55; H 4.98; found N 5.31; C 77.54; H 4.99.

**[(LOMe<sub>4</sub>)MgBr<sub>2</sub>]:** A Grignard reagent was prepared from 12.5 g (47 mmol, 2 eq) 4-iodo-1,3-dimethoxybenzene and 2.00 g (excess) magnesium in THF. The Grignard-solution was added slowly to a solution of 5.57 g (23.5 mmol, 1 eq) 2,6-dibromo-pyridine and 0.97 g (8%<sub>mol</sub>) [(dppe)NiCl<sub>2</sub>] in dry THF at 273 K. The reaction mixture was stirred for 16 h, 150 mL HCl/water (1:1) were added and the reaction product was precipitated by adding 400 mL of CH<sub>2</sub>Cl<sub>2</sub>. The bright yellow solid was filtered off and washed with small portions of cold acetone. The product was dried on air and stored in a brown glass vessel. Yield: 8.03 g (15 mmol, 63%). NMR (300 MHz, [D<sub>6</sub>]-acetone): <sup>1</sup>H: δ = 8.63 (t, 1H, H<sub>4Py</sub>), 8.29 (d, 2H, H<sub>3,5Py</sub>), 8.01 (d, 2H, H<sub>6Ph</sub>), 6.93 (d, 2H, H<sub>5Ph</sub>), 6.87 (dd, 2H, H<sub>3Ph</sub>), 4.19 (s, 6H, H<sub>2OMe</sub>), 3.88 (s, 6H, H<sub>4OMe</sub>). <sup>13</sup>C: δ = 167 (2C, C<sub>4Ph</sub>), 161 (2C, C<sub>2Ph</sub>), 151 (2C, C<sub>2,6Py</sub>), 146 (1C, C<sub>4Py</sub>), 133 (2C, C<sub>3Ph</sub>), 123 (2C, C<sub>3,5Py</sub>), 108 (2C, C<sub>6Ph</sub>), 101 (2C, C<sub>1Ph</sub>), 100 (2C, C<sub>5Ph</sub>), 57 (4C, C<sub>2,4OMe</sub>) ppm. Elemental analyses: calc (for C<sub>21</sub>H<sub>21</sub>NO<sub>4</sub>MgBr<sub>2</sub>; M = 535.52 g mol<sup>-1</sup>): N 2.62; C 47.10; H 3.95; found: N 2.61; C 47.13; H 4.02.

**2,6-Bis(2,4-dimethoxyphenyl)pyridine (LOMe<sub>4</sub>):** 3.0 g (5.2 mmol, 1 eq) of [(LOMe<sub>4</sub>)MgBr<sub>2</sub>] were suspended in ethyl acetate and an aqueous solution of 1.0 g Kryptofix® (2.2.2) is added until all starting material has dissolved. Then the phases were separated and the organic phase was subsequently washed with two small portions of Kryptofix solution. After final phase separation the organic phase was dried over anhydrous Na(OAc). After filtration the solvent was removed under vacuum leaving a yellow-orange solid. Yield: 1.57 g (4.5 mmol, 87%). NMR (300 MHz, [D<sub>6</sub>]-acetone): <sup>1</sup>H: δ = 8.01 (d, 2H,

H<sub>6Ph</sub>), 7.79 (d, 2H, H<sub>3,5Py</sub>), 7.69 (t, 1H, H<sub>4Py</sub>), 6.68 (m, 4H, H<sub>5,6Ph</sub>), 3.91 (s, 6H, H<sub>2OMe</sub>), 3.87 (s, 6H, H<sub>4OMe</sub>). <sup>13</sup>C:  $\delta$  = 163 (2C, C<sub>4Ph</sub>), 160 (2C, C<sub>2Ph</sub>), 156 (2C, C<sub>2,6Py</sub>), 135 (1C, C<sub>4Py</sub>), 132 (2C, C<sub>6Ph</sub>), 135 (2C, C<sub>3,5Py</sub>), 105 (2C, C<sub>5Ph</sub>), 102 (2C, C<sub>1Ph</sub>), 98 (2C, C<sub>3Ph</sub>), 55 (4C, C<sub>2,4OMe</sub>) ppm. Elemental analyses: calc (for C<sub>21</sub>H<sub>21</sub>NO<sub>4</sub>; M = 351.41 g mol<sup>-1</sup>): N 3.99; C 71.78; H 6.02; found: N 4.00; C 71.63; H 6.05.

**2,6-(2,2',4-tri-hydroxy-4'-methoxyphenyl)pyridine (LOH<sub>3</sub>OMe):** 300 mg (0.85 mmol, 1 eq) LOMe<sub>4</sub> were mixed with 6.00 g (excess) pyridinium hydrochloride and heated up to 463 K for 1 h. After cooling the mixture to 298 K, 100 mL aqua dest. were added and the suspension was exposed to ultrasound for 2 h. The remaining suspension was extracted three times with CH<sub>2</sub>Cl<sub>2</sub>. The organic phase was neutralised with aqueous Na<sub>2</sub>CO<sub>3</sub> solution and washed with water. (During this process the organic phase turns from brown to yellow.) The aqueous phases were re-extracted with CH<sub>2</sub>Cl<sub>2</sub> and the combined organic phases were dried over MgSO<sub>4</sub>. The solvent was removed under vacuum to yield 160 mg (0.52 mmol, 61%) of a brownish solid. NMR (300 MHz, [D<sub>6</sub>]-acetone): <sup>1</sup>H:  $\delta$  = 7.91 (t, 1H, H<sub>4Ph</sub>), 7.83 (d, 2H, H<sub>3,5Py</sub>), 7.78 (d, 1H, H<sub>6Ph</sub>), 7.70 (d, 1H, H<sub>6Ph</sub>), 6.55 (s, 1H, H<sub>3'Ph</sub>), 6.51 (m, 2H, H<sub>3,5Ph</sub>), 3.83 (s, 3H, H<sub>4'OMe</sub>). Elemental analyses: calc (for C<sub>18</sub>H<sub>15</sub>NO<sub>4</sub>; M = 309.32 g mol<sup>-1</sup>): N 4.53; C 69.89; H 4.89; found: N 4.48; C 69.07; H 4.99.

**2,6-bis(5-<sup>iso</sup>propyl-2-methoxyphenyl)pyridine (LOMe<sub>2</sub><sup>i</sup>Pr):** 300 mg (1.29 mmol, 1 eq) 2,6-dibromo pyridine were dissolved in 15 mL degassed DME. To this mixture 225 mg (15%<sub>mol</sub>) [Pd(PPh<sub>3</sub>)<sub>4</sub>] were added and the suspension was warmed on a water bath until a clear solution was formed. 500 mg (2.58 mmol, 2 eq) 5-<sup>iso</sup>propyl-2-methoxyphenylboronic acid and 300 mg (2.58 mmol, 2 eq) KO<sup>tert</sup>Bu were added. The reaction mixture was heated to reflux for 1 h, after cooling to 298 K the mixture was filtered over celite and the filter cake was washed with 50 mL CH<sub>2</sub>Cl<sub>2</sub>. A fine colourless solid precipitated and after filtering again the solution was evaporated to dryness to yield a yellow oil, which was purified by column chromatography (eluent: cyclohexane/ethylacetate 6:1, R<sub>f</sub> = 0.725). Yield: 408 mg (1.1 mmol, 84%). NMR (300 MHz, CD<sub>2</sub>Cl<sub>2</sub>): <sup>1</sup>H:  $\delta$  = 7.73 (m, 5H, H<sub>3,4,5Py,5Ph</sub>), 7.25 (d, 2H, H<sub>3Ph</sub>), 6.98 (d, 2H, H<sub>2Ph</sub>), 3.86 (s, 6H, H<sub>OMe</sub>), 2.95 (q, 2H, H<sub>2propyl</sub>), 1.27 (d, 12H, H<sub>1,3propyl</sub>). <sup>13</sup>C:  $\delta$  = 155 (4C, C<sub>2,6Py,1Ph</sub>), 141 (2C, C<sub>4Ph</sub>), 135 (1C, C<sub>4Py</sub>), 130 (2C, C<sub>5Ph</sub>), 128 (2C, C<sub>3Ph</sub>), 124 (2C, C<sub>3,5Py</sub>), 123 (2C, C<sub>6Ph</sub>), 112 (2C, C<sub>2Ph</sub>), 56 (2C, C<sub>OMe</sub>), 33 (2C, C<sub>2propyl</sub>), 24 (4C, C<sub>1,3propyl</sub>) ppm. Elemental analyses: calc (for C<sub>25</sub>H<sub>29</sub>NO<sub>2</sub>; 375.50 g mol<sup>-1</sup>): N 3.73; C 79.96; H 7.78; found: C 80.25; H 7.77; N 3.65.

**2,6-bis(5-<sup>iso</sup>propyl-2-hydroxyphenyl)pyridine (LOH<sub>2</sub><sup>i</sup>Pr):** 700 mg (1.86 mmol, 1 eq) 2,6-bis(5-<sup>i</sup>propyl-2-methoxyphenyl)pyridine were mixed with 12.0 g (excess) pyridinium hydrochloride and the mixture was heated up to 403 K for 1.5 h. The solidified pyridinium hydrochloride was dissolved in 200 mL aqua dest. by ultra sonic treatment. The resulting suspension was extracted three times with 50 mL CH<sub>2</sub>Cl<sub>2</sub> each. The collected organic phases were dried over MgSO<sub>4</sub> and the solvent was removed under vacuum to result a yellow powder. Yield: 430 mg (1.24 mmol, 67%). NMR (300 MHz, [D<sub>6</sub>]-acetone): <sup>1</sup>H: δ = 8.03 (m, 3H, H<sub>3,4,5Py</sub>), 7.75 (d, 2H, H<sub>6Ph</sub>), 7.21 (d, 2H, H<sub>4Ph</sub>), 6.98 (d, 2H, H<sub>3Ph</sub>), 2.95 (q, 2H, H<sub>2propyl</sub>), 1.28 (d, 12H, H<sub>1,3propyl</sub>). <sup>13</sup>C: δ = 156 (2C, C<sub>2,6Py,1Ph</sub>), 140 (2C, C<sub>5Ph</sub>), 138 (1C, C<sub>4Py</sub>), 129 (2C, C<sub>3Ph</sub>), 126 (2C, C<sub>4Ph</sub>), 122 (2C C<sub>6Ph</sub>), 120 (2C, C<sub>3,5Py</sub>), 117 (2C, C<sub>2Ph</sub>), 33 (2C, C<sub>2propyl</sub>), 24 (4C, C<sub>1,3propyl</sub>) ppm. Elemental analyses: calc (for C<sub>23</sub>H<sub>25</sub>NO<sub>2</sub>; M = 347.45 g mol<sup>-1</sup>): N 4.03; C 79.51; H 7.25; found: N 4.09; C 78.63; H 7.16.

**[(LOMe<sub>2</sub>)CuCl<sub>2</sub>]<sub>2</sub>:** 200 mg (0.69 mmol, 1 eq) LOMe<sub>2</sub> and 92 mg (0.69 mmol, 1 eq) CuCl<sub>2</sub> (anhydrous) were dissolved in 5 mL methanol each, both solutions were combined and the mixture was stirred at 298 K for 16 h. The solvent was removed under vacuum and the remaining orange-brown solid was washed with a small portion cold acetone and dried on air. Yield: 210 mg (0.49 mmol, 71%). Elemental analyses: calc (for C<sub>19</sub>H<sub>17</sub>NO<sub>2</sub>CuCl<sub>2</sub>; M = 425.80 g mol<sup>-1</sup>): N 3.29; C 53.60; H 4.02; found: N 3.30; C 53.57; H 4.00.

**[(LOH<sub>2</sub>)CuCl<sub>2</sub>]<sub>2</sub>:** 0.20 g (0.76 mmol, 1 eq) LOH<sub>2</sub> and 0.10 g (0.76 mmol, 1 eq) CuCl<sub>2</sub> (anhydrous) were dissolved in 5 mL methanol each. Both solutions were combined and stirred at 298 K for 12 h. After removing the solvent under vacuum a black solid was obtained. Yield: 211 mg (53 mmol, 70%). Elemental analyses: calc (for C<sub>17</sub>H<sub>13</sub>NO<sub>2</sub>CuCl<sub>2</sub>; M = 397.75 g mol<sup>-1</sup>): N 3.52; C 51.34; H 3.29; found: N 3.51; C 51.28; H 3.29.

**[(LOH)CuCl]<sub>2</sub>:** 50 mg (0.13 mmol, 1 eq) of [(LOH<sub>2</sub>)CuCl<sub>2</sub>] were dissolved in 7 mL methanol and 0.5 mL (excess) NEt<sub>3</sub> were added. A green-brown solid immediately precipitated and was filtered off. Yield: 35 mg (9.7, 75%). Elemental analyses: calc (for C<sub>17</sub>H<sub>12</sub>NO<sub>2</sub>CuCl; M = 361.29 g mol<sup>-1</sup>): N 3.88; C 56.52; H 3.35; found: N 3.89; C 56.52; H 3.38.

**[(LOMe<sub>2</sub><sup>i</sup>Pr)CuCl<sub>2</sub>]:** 100 mg (0.27 mmol, 1 eq) LOMe<sub>2</sub><sup>i</sup>Pr were dissolved in 5 mL methanol. 36 mg (0.27 mmol, 1 eq) anhydrous CuCl<sub>2</sub> were separately dissolved in 5 mL methanol. Both solutions were combined and stirred at 298 K over night. Evaporation of the solvent yielded 104 mg (0.20 mmol, 74%) of an orange powder. Elemental analyses: calc (for

$C_{25}H_{29}NO_2CuCl_2$ ;  $M = 509.96 \text{ g mol}^{-1}$ : N 2.75; C 58.88; H 5.73; found: N 2.81; C 58.63; H 5.66.

**[(LOMe<sup>*i*</sup>Pr)Cu(TFA)<sub>2</sub>]:** 100 mg (0.27 mmol, 1 eq) LOMe<sup>*i*</sup>Pr were dissolved in 5 mL methanol. 167 mg (0.27 mmol, 1 eq) [Cu(MeCN)<sub>4</sub>](TFA)<sub>2</sub> were dissolved in 10 mL methanol each. Both solutions were combined and stirred at 298 K for 12 h. Evaporation of the solvent yielded 185 mg (0.25 mmol, 93%) of an orange powder. Elemental analyses: calc (for  $C_{29}H_{29}NO_6CuF_6Cl_2$ ;  $M = 735.99 \text{ g mol}^{-1}$ ): N 1.90; C 47.33; H 3.97; found: N 1.87; C 47.89; H 3.82.

**[(LOH<sup>*i*</sup>Pr)CuCl<sub>2</sub>]<sub>2</sub>:** 50 mg (0.14 mmol, 1 eq) LOH<sup>*i*</sup>Pr and 19 mg (0.14 mmol, 1 eq) CuCl<sub>2</sub> (anhydrous) were dissolved separately in 5 mL methanol. Both solutions were combined and stirred at 298 K for 2 d. Evaporation of the solvent yielded a brown solid, which was washed with a small amount of cold acetone and dried on air. Yield: 53 mg (0.06 mmol, 43%). Elemental analyses: calc (for  $C_{46}H_{50}N_2O_4Cu_2Cl_4$ ;  $M = 963.80 \text{ g mol}^{-1}$ ): N 2.91; C 57.32; H 5.23; found N 2.94; C 57.61; H 5.19.

**[(LOH<sup>*i*</sup>Pr)<sub>2</sub>Cu]:** 50 mg (0.14 mmol, 2 eq) LOH<sup>*i*</sup>Pr and 89 mg (0.14 mmol, 2 eq) [Cu(MeCN)<sub>4</sub>](TFA)<sub>2</sub> were dissolved in 5 mL methanol each. Both solutions were combined and stirred at 298 K. After a few minutes an olive-green precipitate was formed, which was filtered off after 10 h and was washed with further 5 mL methanol and dried on air. Yield: 55 mg (0.07 mmol, 99%). Elemental analyses: calc (for  $C_{46}H_{48}N_2O_4Cu$ ;  $M = 756.43 \text{ g mol}^{-1}$ ): N 3.70; C 73.04; H 6.40; found: N 3.71; C 70.77; H 6.40.

**[(LOMe<sub>4</sub>)CuCl<sub>2</sub>]<sub>2</sub>:** 0.20 g (0.58 mmol, 1 eq) LOMe<sub>4</sub> and 78 mg (0.58 mmol, 1 eq) CuCl<sub>2</sub> (anhydrous) were dissolved in 5 mL methanol each. Both solutions were combined and stirred at 298 K for 2 d. Evaporation of the solvent yielded a brown solid, which was washed with small portions of cold acetone and dried on air. Yield: 190 mg (0.39 mmol, 78%). Elemental analyses: calc (for  $C_{21}H_{21}NO_4CuCl_2$ ;  $M = 485.86 \text{ g mol}^{-1}$ ): N 2.88; C 51.91; H 4.36; found: N 2.88; C 51.89; H 4.33.

**[(LOMe<sub>4</sub>)Cu(TFA)<sub>2</sub>]:** 179 mg (0.29 mmol, 1.5 eq) [Cu(MeCN)<sub>4</sub>](TFA)<sub>2</sub> and 100 mg (0.19 mmol, 1 eq) [(LOMe<sub>4</sub>)MgBr<sub>2</sub>] were mixed as solids and dissolved in 15 mL MeCN. The green solution was stirred for 6 h at 298 K and the solvent was removed under vacuum to yield a dark green solid. Yield: 103 mg (84%). Elemental analyses: calc (for  $C_{25}H_{21}NO_8CuF_6$ ;  $M = 641.00 \text{ g mol}^{-1}$ ): N 2.19; C 46.84; H 3.30; found: N 2.20; C 46.82; H 3.33.

**[(LOH<sub>3</sub>OMe)Cu(TFA)<sub>2</sub>]:** 130 mg (0.42 mmol, 1 eq) LOH<sub>3</sub>OMe were dissolved in 5 mL methanol. In additional 5 mL methanol 258 mg [Cu(MeCN)<sub>4</sub>](TFA)<sub>2</sub> were dissolved and both solutions were mixed and stirred 6 h at 298 K. The resulting solution was evaporated to dryness and the remaining solid was washed with cold acetone to yield 60 mg (0.13 mmol, 31%) of a green-brown solid. Elemental analyses: calc (for C<sub>22</sub>H<sub>21</sub>NO<sub>7</sub>Cu; M = 474.95 g mol<sup>-1</sup>): N 2.95; C 55.63; H 4.46; found: N 2.92; C 55.72; H 4.39.

**[(LOMe<sub>2</sub>)NiBr<sub>2</sub>]<sub>2</sub>:** 85 mg (0.29 mmol, 1 eq) of LOMe<sub>2</sub> were dissolved in 7 mL methanol. A methanol solution of 215 mg (0.29 mmol, 1 eq) [(PPh<sub>3</sub>)<sub>2</sub>NiBr<sub>2</sub>] (7 mL) was added in one portion and the resulting mixture was stirred for 6 h at 298 K. The solvent was removed under vacuum and the remaining turquoise solid was washed with several portions of heptane, pentane and cold acetone, the remaining solid was dried on air. Yield: 66 mg (0.13 mmol, 45%). NMR (300 MHz, [D<sub>6</sub>]-acetone): <sup>1</sup>H: δ = 8.52 (t, 1H, H<sub>4Py</sub>), 8.30 (d, 2H, H<sub>3,5Py</sub>), 8.04 (d, 2H, H<sub>6Ph</sub>), 7.59 (t, 2H, H<sub>4Ph</sub>), 7.35 (t, 2H, H<sub>5Ph</sub>), 7.22 (d, 2H, H<sub>3Ph</sub>), 4.10 (s(br), 6H, H<sub>OMe</sub>) ppm. Elemental analyses: calc (for C<sub>19</sub>H<sub>17</sub>NO<sub>2</sub>NiBr<sub>2</sub>; M = 509.86 g mol<sup>-1</sup>): N 2.75; C 44.76; H 3.36; found: N 2.74; C 44.75; H 3.35.

**[(LOH<sub>2</sub>)NiBr<sub>2</sub>]<sub>2</sub>:** 75 mg (0.30 mmol, 1 eq) of LOH<sub>2</sub> were dissolved in 7 mL methanol. A methanol solution of 223 mg (0.30 mmol, 1 eq) [(PPh<sub>3</sub>)<sub>2</sub>NiBr<sub>2</sub>] (7 mL) was added in one portion and the resulting mixture was stirred for 6 h at 298 K. The solvent was removed under vacuum and the remaining green solid was washed with several portions of heptane, pentane and cold acetone, the remaining solid was dried on air. Yield: 67 mg (0.14, 47%). NMR (300 MHz, [D<sub>6</sub>]-acetone): <sup>1</sup>H: δ = 11.67 (s(br), 2H, H<sub>OH</sub>), 8.00 (m, 3H, H<sub>3,4,5Py</sub>), 7.86 (dd, 2H, H<sub>6Ph</sub>), 7.32 (t, 2H, H<sub>4Ph</sub>), 7.00 (m, 2H, H<sub>3,5Ph</sub>) ppm. Elemental analyses: calc (for C<sub>17</sub>H<sub>13</sub>NO<sub>2</sub>NiBr<sub>2</sub>; M = 481.81 g mol<sup>-1</sup>): N 2.91; C 42.38; H 2.72; found: N 2.88; C 42.36; H 2.75.

**[(LOMe<sub>4</sub>)NiBr<sub>2</sub>]<sub>2</sub>:** 100 mg (0.19 mmol, 1 eq) of [(LOMe<sub>4</sub>)MgBr<sub>2</sub>] were dissolved in 7 mL methanol. A methanol solution of 215 mg (0.29 mmol, 1.5 eq) [(PPh<sub>3</sub>)<sub>2</sub>NiBr<sub>2</sub>] (7 mL) was added in one portion and the resulting mixture was stirred for 6 h at 298 K. The solvent was removed under vacuum and the remaining green solid was washed with several portions of heptane, pentane and cold acetone, the remaining solid was dried on air. Yield: 83 mg (0.15, 79%). NMR (300 MHz, [D<sub>6</sub>]-acetone): <sup>1</sup>H: δ = 8.94 (t, 1H, H<sub>4Py</sub>), 8.55 (d, 2H, H<sub>3,5Py</sub>), 8.18 (d, 2H, H<sub>6Ph</sub>), 7.04 (d, 2H, H<sub>5Ph</sub>), 7.00 (d, 2H, H<sub>6Ph</sub>), 4.40 (s, 6H, H<sub>2OMe</sub>), 4.05 (s, 6H, H<sub>4OMe</sub>) ppm. Elemental analyses: calc (for C<sub>21</sub>H<sub>21</sub>NO<sub>4</sub>NiBr<sub>2</sub>; M = 569.92 g mol<sup>-1</sup>): N 2.46; C 44.26; H



3.71; found N 2.48; C 44.26; H 3.70.

**[(LOMe<sup>*i*</sup>Pr)NiBr<sub>2</sub>]<sub>2</sub>**: 100 mg (0.27 mmol, 1 eq) of LOMe<sup>*i*</sup>Pr were dissolved in 7 mL methanol. A methanol solution of 215 mg (0.29 mmol, 1.1 eq) [(PPh<sub>3</sub>)<sub>2</sub>NiBr<sub>2</sub>] (7 mL) was added in one portion and the resulting mixture was stirred for 6 h at 298 K. The solvent was removed under vacuum and the remaining green solid was washed with a small portion of heptane, pentane and cold acetone, the remaining solid was dried on air. Yield: 143 mg (0.12 mmol, 88%). NMR (300 MHz, [D<sub>6</sub>]-acetone): <sup>1</sup>H: δ = 14.65; 9.44; 8.15; 7.93; 7.41; 3.88; 3.56; 1.57 ppm. Elemental analyses: calc (for C<sub>50</sub>H<sub>58</sub>N<sub>2</sub>O<sub>4</sub>Ni<sub>2</sub>Br<sub>4</sub>; M = 1188.01 g mol<sup>-1</sup>): C 50.55, H 4.92, N 2.36; found C 51.29, H 4.80, N 2.39.

**[(LOH<sub>2</sub><sup>*i*</sup>Pr)NiBr<sub>2</sub>]<sub>2</sub>**: 100 mg (0.29 mmol, 1 eq) of LOH<sup>*i*</sup>Pr were dissolved in 7 mL methanol. A methanol solution of 215 mg (0.29 mmol, 1 eq) [(PPh<sub>3</sub>)<sub>2</sub>NiBr<sub>2</sub>] (7 mL) was added in one portion and the resulting mixture was stirred for 6 h at 298 K. The solvent was removed under vacuum and the remaining green solid was washed with a small portion of heptane, pentane and cold acetone, the remaining solid was dried on air. Yield: 130 mg (0.12 mmol, 79%). NMR (300 MHz, [D<sub>6</sub>]-acetone): <sup>1</sup>H: δ = 8.54 (t, 1H, H<sub>4Py</sub>), 8.25 (d, 2H, H<sub>3,5Py</sub>), 7.89 (d, 2H, H<sub>6Ph</sub>), 7.25 (d, 2H, H<sub>4Ph</sub>), 6.91 (d, 2H, H<sub>3Ph</sub>); 3.03 (q, 2H, H<sub>iPr</sub>); 1.35 (d, 12H, H<sub>1,3propyl</sub>) ppm. Elemental analyses: calc (for C<sub>46</sub>H<sub>50</sub>N<sub>2</sub>O<sub>4</sub>Ni<sub>2</sub>Br<sub>4</sub>; M = 1131.90 g mol<sup>-1</sup>): C 48.81, H 4.45, N 2.47; found C 47.63, H 4.61, N 2.38.

**[Cu(opo)<sub>2</sub>]**: 0.50 g (1.9 mmol, 1 eq) [Cu(acac)<sub>2</sub>] were dissolved in methanol and a suspension of 0.65 g (3.8 mmol, 2 eq) opoH in methanol were added. The mixture was stirred at 298 K for 16 h and the formed precipitate was filtered off and washed with acetone to yield 0.82 mg (1.8 mmol, 98%) of a brown solid. Elemental analyses: calc (for C<sub>26</sub>H<sub>14</sub>O<sub>4</sub>Cu; M = 453.93 g mol<sup>-1</sup>) C 68.79; H 3.11; found: C 68.32; H 3.03.

**[Fe(opo)<sub>3</sub>]**: 200 mg (0.57 mmol, 1 eq) [Fe(acac)<sub>3</sub>] were dissolved in methanol and a suspension of 294 mg (1.71 mmol, 3 eq) opoH in methanol were added. The mixture was stirred at 298 K for 16 h and the formed precipitate was filtered off and washed with acetone to yield 288 mg (0.45 mmol, 78%) of a dark red solid. Elemental analyses: calc (for C<sub>39</sub>H<sub>21</sub>O<sub>6</sub>Fe; M = 641.43 g mol<sup>-1</sup>) C 73.03; H 3.30; found: C 72.39; H 3.33.

**[Zn(opo)<sub>2</sub>]**: 200 mg (0.76 mmol, 1 eq) [Zn(acac)<sub>2</sub>] were suspended in methanol and a suspension of 261 mg (1.52 mmol, 2 eq) opoH in methanol were added. The mixture was stirred at 298 K for 4 h and the formed voluminous precipitate was filtered off and washed

with acetone to yield 283 mg (0.62 mmol, 81%) of a yellow solid. NMR (300 MHz, [D<sub>7</sub>]-dmf): <sup>1</sup>H: δ = 8.13 (d, 2H, H<sub>2,8</sub>), 8.07 (d, 2H, H<sub>3,7</sub>), 7.52 (t, 1H, H<sub>5</sub>), 7.09 (d, 2H, H<sub>4,6</sub>) ppm. Elemental analyses: calc (for C<sub>26</sub>H<sub>14</sub>O<sub>4</sub>Zn; M = 455.78 g mol<sup>-1</sup>) C 68.52; H 3.10; found: C 69.07; H 3.15.

**Reaction of opoH with “[Ni(acac)<sub>2</sub>]”:** 200 mg (0.68 mmol, 1 eq) “[Ni(acac)<sub>2</sub>]” were dissolved in methanol and a suspension of 234 mg (1.36 mmol, 2 eq) opoH in methanol were added. The mixture was stirred over night and the formed precipitate was filtered off and washed with acetone to yield 305 mg of a yellow-brown solid. Elemental analyses found: C 61.12; H 3.73.

**[Cu(bqOH)Cl<sub>2</sub>]:** 100 mg (0.51 mmol, 1 eq) bqOH dissolved in 5 mL methanol and 69 mg (0.51 mmol, 1 eq) CuCl<sub>2</sub> (anhydrous) dissolved in 10 mL methanol were mixed and stirred at 298 K for 10 h. The formed brown precipitate was filtered off and washed with acetone to yield 90 mg (0.27 mmol, 53%). Elemental analyses: calc (for C<sub>13</sub>H<sub>9</sub>Cl<sub>2</sub>CuON; M = 329.67 g mol<sup>-1</sup>) N 4.25; C 47.36; H 2.75; found: N 4.09; C 49.15; H 2.87.

**[Cu(bqOH)Br<sub>2</sub>]:** 100 mg (0.51 mmol, 1 eq) bqOH dissolved in 5 mL methanol and 115 mg (0.51 mmol, 1 eq) CuBr<sub>2</sub> (anhydrous) dissolved in 10 mL methanol were mixed and stirred at 298 K for 10 h. The formed brown precipitate was filtered off and washed with acetone to yield 130 mg (0.31 mmol, 61%). Elemental analyses: calc (for C<sub>13</sub>H<sub>9</sub>Br<sub>2</sub>CuON; M = 418.57 g mol<sup>-1</sup>) N 3.35; C 37.30; H 2.17; found: N 3.45; C 35.60; H 2.21.

**[Cu(bqO)<sub>2</sub>]:** 100 mg (0.51 mmol, 1 eq) bqOH dissolved in 5 mL methanol and 48 mg (0.26 mmol, 0.5 eq) Cu(OAc)<sub>2</sub> dissolved in 10 mL methanol were mixed and stirred at 298 K for 10 h. The formed brown precipitate was filtered off and washed with acetone to yield 87 mg (0.19 mmol, 73%). Elemental analyses: calc (for C<sub>26</sub>H<sub>16</sub>O<sub>2</sub>N<sub>2</sub>Cu; M = 451.96 g mol<sup>-1</sup>) N 6.20; C 69.09; H 3.57; found: N 6.38; C 67.19; H 3.41.

**9-Chloro-4-methoxy-acridine (acrOMe):** 4.16 g (20 mmol, 1 eq) 2-(2-methoxyphenyl-amino)benzoic acid were mixed with 40 mL POCl<sub>3</sub> (excess). The mixture was heated up to 398 K for 3 h and cooled down to 298 K again. The POCl<sub>3</sub> was removed under vacuum and the remaining oil was mixed with concentrated ammonia solution. 200 mL chloroform was added and the aqueous phase was extracted three times. The collected organic phases were dried over MgSO<sub>4</sub> and the solvent was removed under vacuum. 3.23 g (13 mmol, 65 %) The product was obtained as a yellow solid. NMR (300 MHz, [D<sub>6</sub>]-acetone): <sup>1</sup>H: δ = 8.44 (d, 1H,

H<sub>8</sub>), 8.27 (d, 1H, H<sub>5</sub>); 7.98 (d, 1H, H<sub>1</sub>), 7.91 (t, 1H, H<sub>6</sub>), 7.78 (t, 1H, H<sub>7</sub>), 7.66 (t, 1H, H<sub>2</sub>), 7.25 (d, 1H, H<sub>3</sub>) 4.11 (s, 3H, H<sub>OMe</sub>). <sup>13</sup>C:  $\delta$  = 158 (1C, C<sub>4</sub>), 144 (1C, C<sub>9</sub>), 129 (1C, C<sub>5a</sub>), 132 (1C, C<sub>8a</sub>), 132 (1C, C<sub>4a</sub>), 131 (1C, C<sub>6</sub>), 131 (1C, C<sub>5</sub>), 128 (1C, C<sub>7</sub>), 128 (1C, C<sub>2</sub>), 127 (1C, C<sub>1a</sub>), 125 (1C, C<sub>8</sub>), 116 (1C, C<sub>1</sub>), 109 (1C, C<sub>3</sub>), 56 (1C, C<sub>OMe</sub>) ppm. Elemental analyses: calc (for C<sub>14</sub>H<sub>10</sub>ONCl; M = 243.05 g mol<sup>-1</sup>) N 5.75; C 69.00; H 4.14; found: N 5.80; C 70.78; H 4.29.

**9-Chloro-4-hydroxy-acridine (acrOH):** 0.50 g (2.0 mmol, 1 eq) 9-Chloro-4-methoxy-acridine were mixed with 10.0 g (excess) pyridinium hydrochloride and heated up to 423 K for 1 h. The resulting black liquid was cooled to 298 K and 150 mL aqua dest. were added. The mixture was given to the ultra sonic bath for 1 h and the resulting yellow suspension was filtered. The collected precipitate was washed with three portions (20 mL) of hot water to remove the remaining pyridine and with a small portion of acetone (5 mL). The solid was dried in vacuum to yield 0.40 g (1.7 mmol, 85%) of a yellow powder. NMR (300 MHz, [D<sub>6</sub>]-acetone): <sup>1</sup>H:  $\delta$  = 9.55 (s, 1H, OH), 9.34 (d, 1H, H<sub>5</sub>), 7.86 (t, 2H, H<sub>1,8</sub>); 7.69 (t, 1H, H<sub>6</sub>), 7.25 (t, 1H, H<sub>7</sub>), 7.20 (d, 1H, H<sub>3</sub>), 7.06 (t, 1H, H<sub>2</sub>). <sup>13</sup>C:  $\delta$  = 177 (1C, C<sub>4</sub>), 145 (1C, C<sub>9</sub>), 141 (1C, C<sub>5a</sub>), 137 (1C, C<sub>8a</sub>), 134 (1C, C<sub>6</sub>), 132 (1C, C<sub>4a</sub>), 127 (1C, C<sub>5</sub>), 125 (1C, C<sub>1a</sub>), 122 (1C, C<sub>7</sub>), 121 (1C, C<sub>2</sub>), 120 (1C, C<sub>8</sub>), 117 (1C, C<sub>3</sub>), 116 (1C, C<sub>1</sub>) ppm. Elemental analyses: calc (for C<sub>13</sub>H<sub>8</sub>ONCl; M = 229.66 g mol<sup>-1</sup>) N 6.10; C 67.99; H 3.51; found: N 6.13; C 68.20; H 3.58.

**[(acrOMe)CuCl<sub>2</sub>]<sub>2</sub>:** 106 mg (0.43 mmol, 1 eq) acrOMe and 58 mg (0.43 mmol, 1 eq) CuCl<sub>2</sub> (anhydrous) were dissolved in 10 mL methanol each and both solutions were mixed together. After stirring at 298 K for 14 h and the solvent was removed under vacuum to yield 120 mg (0.32 mmol, 74%) of a brown solid. Elemental analyses: calc (for C<sub>28</sub>H<sub>20</sub>O<sub>2</sub>N<sub>2</sub>Cl<sub>6</sub>Cu<sub>2</sub>; M = 756.28 g mol<sup>-1</sup>) N 3.70; C 44.47; H 2.67; found: N 3.87; C 43.75; H 2.55.

**[(acrOH)CuCl<sub>2</sub>]<sub>2</sub>:** 100 mg (0.41 mmol, 1 eq) acrOH and 55 mg (0.41 mmol, 1 eq) CuCl<sub>2</sub> (anhydrous) were dissolved in 10 mL methanol each and both solutions were mixed together. The reaction mixture was stirred for 14 h at 298 K. The solvent was removed under vacuum and the remaining powder was washed several times with acetone to yield 142 mg (0.39 mmol, 95%) of a red brown solid. Elemental analyses: calc (for C<sub>26</sub>H<sub>16</sub>Cl<sub>6</sub>O<sub>2</sub>N<sub>2</sub>Cu<sub>2</sub>; M = 728.22 g mol<sup>-1</sup>) N 3.85; C 42.88; H 2.21; found: N 3.72; C 43.50; H 2.24.

**[Cu(acrOMe)<sub>2</sub>](OAc)<sub>2</sub>:** 101 mg (0.41 mmol, 2 eq) of the acrOMe ligand were dissolved in 10 mL methanol and mixed with a solution of 34 mg (0.21 mmol, 1 eq) Cu(OAc)<sub>2</sub> in methanol. After stirring at 298 K for 14 h the solvent was removed under vacuum to yield 104 mg (0.16 mmol, 76%) of a brown solid. Elemental analyses: calc (for C<sub>32</sub>H<sub>26</sub>Cl<sub>2</sub>CuO<sub>5</sub>N<sub>2</sub>;

$M = 653.01 \text{ g mol}^{-1}$ ) N 4.29; C 58.86; H 4.01; found: N 4.18; C 58.52; H 4.05.

**[Cu(acrO)<sub>2</sub>]:** 100 mg (0.41 mmol, 2 eq) acrOH were dissolved in 10 mL methanol. 75 mg (0.21 mmol, 1 eq) Cu(OAc)<sub>2</sub> were dissolved in 10 mL methanol each, both solutions were combined and stirred for 14 h at 298 K. The solvent was removed under vacuum until a suspension was formed (~5 mL remaining) and the black solid was filtered off and washed with acetone to yield 52 mg (0.1 mmol, 48%) of a black solid which exhibits red-violet colour in solution. Elemental analyses: calc (for C<sub>26</sub>H<sub>14</sub>Cl<sub>2</sub>CuO<sub>2</sub>N<sub>2</sub>; M = 520.85 g mol<sup>-1</sup>) C 59.96; H 2.71; N 5.38; found: C 59.92; H 2.82; N 5.38.

**General Procedure for the synthesis of salen type complex:** 1 eq Ligand and 1 eq Cu(OAc)<sub>2</sub> were dissolved in methanol and both solutions were mixed at 298 K. The mixture was stirred at 298 K for 16 h. While [(NH<sub>2</sub>)salPh<sub>2</sub>)Cu] and [(salPh<sub>2</sub>)Cu] precipitated and were filtered off and washed with small portions of methanol, all other complexes were isolated by removing the solvent under vacuum and recrystallisation from acetone solution.

**[((NMe<sub>2</sub>)sal<sup>tert</sup>Bu<sub>4</sub>)Cu]:** 58 mg (0.1 mmol, 1 eq) (NMe<sub>2</sub>)sal<sup>tert</sup>Bu<sub>4</sub> and 18 mg (0.1 mmol, 1 eq) Cu(OAc)<sub>2</sub> were reacted. Yield: 24 mg (0.04 mmol, 40%) of dark green needle shaped crystals. Elemental analyses: calc (for C<sub>38</sub>H<sub>60</sub>CuO<sub>2</sub>N<sub>2</sub>; M = 640.44 g mol<sup>-1</sup>) N 4.37; C 71.26; H 9.44; found: N 4.24; C 72.23; H 9.57.

**[((NH)<sub>2</sub>sal)Cu]:** 30 mg (0.1 mmol, 1 eq) (NH)<sub>2</sub>sal and 18 mg (0.1 mmol, 1 eq) Cu(OAc)<sub>2</sub> were reacted. Yield: 25 mg (0.07 mmol, 70%) reddish-brown crystalline needles. Elemental analyses: calc (for C<sub>18</sub>H<sub>20</sub>CuO<sub>2</sub>N<sub>2</sub>; M = 359.91 g mol<sup>-1</sup>) N 7.78; C 60.07; H 5.60; found: N 7.99; C 62.02; H 5.64.

**[((NH<sub>2</sub>)salPh<sub>2</sub>)Cu]:** 100 mg (0.2 mmol, 1 eq) (NH<sub>2</sub>)salPh<sub>2</sub> and 38 mg (0.2 mmol, 1 eq) Cu(OAc)<sub>2</sub> were reacted. Yield: 45 mg (0.08 mmol, 40%) blue-green powder. Elemental analyses: calc (for C<sub>32</sub>H<sub>32</sub>CuO<sub>2</sub>N<sub>2</sub>; M = 540.15 g mol<sup>-1</sup>) N 5.19; C 71.15; H 5.97; found: N 5.22; C 71.32; H 5.89.

**[(Me<sub>2</sub>salF<sub>4</sub>)Cu]:** 40 mg (0.1 mmol, 1 eq) Me<sub>2</sub>salF<sub>4</sub> and 17 mg (0.1 mmol, 1 eq) Cu(OAc)<sub>2</sub> were reacted. Yield: 36 mg (0.075 mmol, 75%) dark green crystals. Elemental analyses: calc (for C<sub>22</sub>H<sub>20</sub>CuO<sub>2</sub>N<sub>2</sub>F<sub>4</sub>; M = 483.94 g mol<sup>-1</sup>) C 54.60; H 4.17; N 5.79; found: C 54.62; H 4.14; N 5.77.

**[(Ph<sub>2</sub>sal)Cu]:** 55 mg (0.12 mmol, 1 eq) Ph<sub>2</sub>sal and 21 mg (0.12 mmol, 1 eq) Cu(OAc)<sub>2</sub> were

reacted. Yield: 20 mg (0.04 mmol, 33%) brown amorphous powder. Elemental analyses: calc (for  $C_{32}H_{28}CuO_2N_2$ ;  $M = 536.12 \text{ g mol}^{-1}$ ) N 5.23; C 71.69; H 5.26; found: N 5.34; C 72.01; H 5.20.

**[(salPh<sub>2</sub>)Cu]:** 100 mg (0.21 mmol, 1 eq) salPh<sub>2</sub> and 38 mg (0.21 mmol, 1 eq) Cu(OAc)<sub>2</sub> were reacted. Yield: 86 mg (0.16 mmol, 79%) light brown powder. Elemental analyses: calc (for  $C_{32}H_{28}CuO_2N_2$ ;  $M = 536.12 \text{ g mol}^{-1}$ ) N 5.23; C 71.69; H 5.26; found: N 5.30; C 71.52; H 5.28;.

**2-(methoxy(pyridin-2-yl)methyl)phenol (OON1):** 0.41 g (17.02 mmol, 2 eq) magnesium were suspended in 20 mL dry diethyl ether. 1.67 mL (3.0 g, 12.77 mmol, 1.5 eq) 2-iodomethoxybenzene in 20 mL dry diethyl ether were added slowly. The reaction mixture was warmed to 348 K until it was brown and turbid (~45 min). 0.91 g (8.5 mmol, 1 eq) pyridin-2-carboxaldehyde were added drop by drop and the mixture became orange. After stirring for 16 h, the reaction was quenched with 50 mL water. The phases were separated, the aqueous phase was extracted with diethyl ether and dried over Na<sub>2</sub>SO<sub>4</sub>. The solvent was removed under vacuum and the remaining solid was washed with acetone to yield 0.95 g (4.4 mmol, 52%) of an off-white powder. NMR (300 MHz, [D<sub>6</sub>]-acetone): <sup>1</sup>H: 8.50 (d, 1H, H<sub>6Py</sub>), 7.69 (t, 1H, H<sub>4Py</sub>), 7.40 (t, 2H, H<sub>4,6Ph</sub>), 7.22 (m, 2H, H<sub>3,5Py</sub>), 6.98 (d, 1H, H<sub>3Ph</sub>), 6.92 (t, 1H, H<sub>5Ph</sub>), 6.20 (s, 1H, H<sub>methanol</sub>), 5.33 (s, 1H, H<sub>OH</sub>) 3.83 (s, 3H, H<sub>OMe</sub>). <sup>13</sup>C: 162 (1C, C<sub>2Py</sub>), 157 (1C, C<sub>2Ph</sub>), 148 (1C, C<sub>6Py</sub>), 137 (1C, C<sub>4Py</sub>), 132 (1C, C<sub>1Ph</sub>), 128 (1C, C<sub>3Py</sub>), 127 (1C, C<sub>6Ph</sub>), 122 (1C, C<sub>5Py</sub>), 121 (1C, C<sub>4Ph</sub>), 120 (1C, C<sub>5Ph</sub>), 110 (1C, C<sub>3Ph</sub>), 69 (1C, C<sub>methanol</sub>), 55 (1C, C<sub>OMe</sub>) ppm. Elemental Analysis: calc (for  $C_{13}H_{13}O_2N$ ;  $M = 215.25 \text{ g mol}^{-1}$ ) C 72.54; H 6.09; N 6.51. found: C 73.45; H 6.04; N 6.46.

**2-(methoxy(pyridin-2-yl)ethyl)phenol (OON2):** 2.8 mL 2-iodo methoxybenzene (5.00 g, 21 mmol, 1 eq) and 0.61 g (25 mmol, 1.2 eq) magnesium were reacted in dry THF to give the Grignard compound. 2.8 mL (2.54 g 21 mmol, 1 eq) 2-acetylpyridine were dropped into the mixture and the reaction mixture was stirred for 12 h at 298 K. 100 mL water were added and the resulting phases were separated. The aqueous phase was extracted with diethyl ether, the combined organic solutions were dried over Na<sub>2</sub>SO<sub>4</sub> and the solvent was removed under vacuum to yield a brown oil. During 3 d colourless crystals were formed which were separated by filtration. Yield: 3.0 g (13 mmol, 64%) NMR (300 MHz, [D<sub>6</sub>]-acetone): <sup>1</sup>H: 8.42 (d, 1H, H<sub>6Py</sub>), 7.71 (t, 1H, H<sub>4Py</sub>), 7.65 (d, 1H, H<sub>3Py</sub>), 7.53 (d, 1H, H<sub>6Ph</sub>), 7.23 (t, 1H, H<sub>4Ph</sub>), 7.18 (t, 1H, H<sub>5Py</sub>), 6.96 (t, 1H, H<sub>5Ph</sub>), 6.90 (d, 1H, H<sub>3Ph</sub>), 5.09 (s, 1H, H<sub>OH</sub>), 3.55 (s, 3H, H<sub>OMe</sub>), 1.86

(s, 3H, H<sub>Me</sub>). <sup>13</sup>C: 168 (1C, C<sub>1Ph</sub>), 158 (1C, C<sub>2Py</sub>), 148 (1C, C<sub>2Ph</sub>), 147 (1C, C<sub>6Py</sub>), 136 (1C, C<sub>4Py</sub>), 128 (1C, C<sub>4Ph</sub>), 127 (1C, C<sub>3Py</sub>), 121 (1C, C<sub>5Py</sub>), 120 (2C, C<sub>5,6Ph</sub>), 112 (1C, C<sub>3Ph</sub>), 76 (1C, C<sub>OH</sub>), 55 (1C, C<sub>OMe</sub>), 28 (1C, C<sub>Me</sub>) ppm. Elemental Analysis: calc (for C<sub>14</sub>H<sub>15</sub>O<sub>2</sub>N; M = 229.27 g mol<sup>-1</sup>) N 6.11; C 73.34; H 6.59; found: N 6.06; C 73.23; H 6.54.

**2-(methoxy(pyridin-2-yl)benzyl)phenol (OON3):** 2.78 mL 2-iodo methoxybenzene (5.0 g, 21 mmol, 1 eq) and 612 mg (25 mmol, 1.2 eq) magnesium were reacted in dry THF to yield the Grignard component. To the stirred reaction mixture a THF solution of 3.84 g (21 mmol, 1 eq) benzoylpyridine was added slowly. The reaction mixture was stirred for 14 h at 298 K. Water was added and the resulting phases were separated. The aqueous phase was washed with diethyl ether, the collected organic phases were dried over Na<sub>2</sub>SO<sub>4</sub> and the solvent was removed under vacuum. The crude product, a colourless solid, was recrystallised from acetone to yield 5.4 g (15 mmol, 72%) of colourless crystals. NMR (300 MHz, [D<sub>6</sub>]-acetone): <sup>1</sup>H: 8.46 (d, 1H, H<sub>6Py</sub>), 7.76 (t, 1H, H<sub>4Py</sub>), 7.59 (d, 1H, H<sub>3Py</sub>), 7.39 (d, 2H, H<sub>2,6Bnz</sub>), 7.27 (m, 5H, H<sub>3,4,5Bnz,4Ph,5Py</sub>), 6.85 (t, 1H, H<sub>5Ph</sub>), 6.99 (d, 1H, H<sub>3Ph</sub>), 6.95 (d, 1H, H<sub>6Ph</sub>), 5.67 (s, 1H, H<sub>OH</sub>), 3.49 (s, 3H, H<sub>OMe</sub>). <sup>13</sup>C: 167 (1C, C<sub>Py2</sub>), 159 (1C, C<sub>1Ph</sub>), 147 (1C, C<sub>1Bnz</sub>), 148 (1C, C<sub>6Py</sub>), 137 (1C, C<sub>4Py</sub>), 130 (1C, C<sub>6Ph</sub>), 128 (3C, C<sub>2,6Bnz,4Ph</sub>), 127 (3C, C<sub>3,4,5Bnz</sub>), 123 (2C, C<sub>3,5Py</sub>), 121 (1C, C<sub>5Ph</sub>), 121 (1C, C<sub>1Ph</sub>), 113 (1C, C<sub>3Ph</sub>), 82 (1C, C<sub>OH</sub>), 56 (1C, C<sub>OMe</sub>) ppm. Elemental Analysis: calc (for C<sub>19</sub>H<sub>17</sub>O<sub>2</sub>N; M = 365.57 g mol<sup>-1</sup>) N 4.81; C 78.33; H 5.88; found: N 5.01; C 78.14; H 6.01.

**General procedure for complex formation reactions:** 1 eq O,O',N-ligand was dissolved in methanol and 1 eq metal precursor dissolved in MeOH/acetone (1:1) were added. The mixture was stirred at 298 K for 14 h. The solvent was removed under reduced pressure and the remaining solids were washed with cold acetone.

**[ZnCl<sub>2</sub>(OON1)]:** 100 mg (0.46 mmol, 1 eq) of OON1 were reacted with 79 mg (0.46 mmol, 1 eq) ZnCl<sub>2</sub> (anhydrous) to yield 160 mg (0.45 mmol, 97%) of a colourless powder. NMR (300 MHz, [D<sub>6</sub>]-acetone): <sup>1</sup>H: 8.77 (s, 1H, H<sub>OH</sub>), 8.76 (d, 1H, H<sub>6Py</sub>), 8.12 (t, 1H, H<sub>4Py</sub>), 7.71 (t, 1H, H<sub>5Py</sub>), 7.48 (d, 1H, H<sub>6Ph</sub>), 7.48 (d, 1H, H<sub>3Py</sub>), 7.39 (t, 1H, H<sub>4Ph</sub>), 7.11 (d, 1H, H<sub>3Ph</sub>), 6.97 (t, 1H, H<sub>5Ph</sub>), 6.75 (s, 1H, H<sub>methanol</sub>), 3.84 (s, 3H, H<sub>OMe</sub>). Elemental Analysis: calc (for C<sub>13</sub>H<sub>13</sub>O<sub>2</sub>NCl<sub>2</sub>Zn; M = 351.54 g mol<sup>-1</sup>) N 3.98; C 44.42; H 3.73; found: N 3.81; C 43.20; H 3.71.

**[ZnCl<sub>2</sub>(OON2)]:** 100 mg (0.44 mmol, 1) eq OON2 and 59 mg (0.44 mmol, 1 eq) ZnCl<sub>2</sub> (anhydrous) were reacted to yield 101 mg (0.28 mmol, 64%) of a colourless powder. NMR

(300 MHz, [D<sub>6</sub>]-acetone): <sup>1</sup>H: 8.70 (d, 1H, H<sub>6Py</sub>), 8.02 (t, 1H, H<sub>4Py</sub>), 7.94 (s(br), 1H, H<sub>OH</sub>), 7.76 (d, 1H, H<sub>6Ph</sub>), 7.63 (t, 1H, H<sub>5Py</sub>), 7.23 (d, 1H, H<sub>3Py</sub>), 7.43 (t, 1H, H<sub>4Ph</sub>), 7.08 (t, 1H, H<sub>5Ph</sub>), 6.99 (d, 1H, H<sub>3Ph</sub>), 3.49 (s, 3H, H<sub>OMe</sub>), 2.08 (s, 3H, H<sub>Me</sub>). Elemental Analysis: calc (for C<sub>14</sub>H<sub>15</sub>O<sub>2</sub>NCl<sub>2</sub>Zn; M = 365.57 g mol<sup>-1</sup>) N 3.83; C 46.00; H 4.14; found: N 3.90; C 44.91; H 4.23.

**[ZnCl<sub>2</sub>(OON3)]**: 100 mg (0.34 mmol, 1 eq) OON3 and 46 mg (0.34 mmol, 1 eq) ZnCl<sub>2</sub> (anh.) were reacted to yield 104 mg (0.24 mmol, 71%) of a colourless powder. NMR (300 MHz, [D<sub>6</sub>]-acetone): <sup>1</sup>H: 8.73 (d, 1H, H<sub>6Py</sub>), 8.07 (t, 1H, H<sub>4Py</sub>), 7.65 (t, 1H, H<sub>5Py</sub>), 7.43 (t, 1H, H<sub>4Ph</sub>), 7.34 (m, 6H, H<sub>2,3,4,5,6Bnz</sub>), 7.14 (m, 2H, H<sub>5,6Ph</sub>), 6.91 (d, 1H, H<sub>3Ph</sub>), 6.72 (s, 1H, H<sub>OH</sub>), 3.66 (s, 3H, H<sub>OMe</sub>). Elemental Analysis: calc (for C<sub>19</sub>H<sub>17</sub>O<sub>2</sub>NCl<sub>2</sub>Zn; M = 427.64 g mol<sup>-1</sup>) N 3.28; C 53.36; H 4.01; found: N 3.15; C 52.09; H 4.04.

**[CuCl<sub>2</sub>(OON1)]**: 220 mg (1.00 mmol, 1 eq) OON1 were reacted with 138 mg (1.00 mmol, 1 eq) CuCl<sub>2</sub> (anhydrous) to yield 283 mg (0.81 mmol, 81%) of a green solid. Elemental Analysis: calc (for C<sub>13</sub>H<sub>13</sub>O<sub>2</sub>NCl<sub>2</sub>Cu; M = 349.70 g mol<sup>-1</sup>) N 4.01; C 44.65; H 3.75; found: N 3.88; C 45.21; H 3.89.

**[CuCl<sub>2</sub>(OON2)]**: 100 mg (0.44 mmol, 1 eq) OON2 were reacted with 59 mg (0.44 mmol, 1 eq) CuCl<sub>2</sub> (anhydrous) to yield 107 mg (0.29 mmol, 66%) of a green solid. Elemental Analysis: calc (for C<sub>14</sub>H<sub>15</sub>O<sub>2</sub>NCl<sub>2</sub>Cu; M = 363.73 g mol<sup>-1</sup>) N 3.85; C 46.23; H 4.16; found: N 3.97; C 47.92; H 4.26.

**[CuCl<sub>2</sub>(OON3)]**: 100 mg (0.34 mmol, 1 eq) OON3 were reacted with 46 mg (0.34 mmol, 1 eq) CuCl<sub>2</sub> (anhydrous) to yield 103 mg (0.24 mmol, 71%) of a green solid. Elemental Analysis: calc (for C<sub>19</sub>H<sub>16</sub>O<sub>2</sub>NCl<sub>2</sub>Cu; M = 424.79 g mol<sup>-1</sup>) N 3.30; C 53.72; H 3.80; found: N 3.27; C 52.99; H 3.73.

**[Co(OON1)<sub>2</sub>(μ-Cl)<sub>2</sub>CoCl<sub>2</sub>]**: 0.33 mg (1.5 mmol, 1 eq) OON1 were reacted with 357 mg (1.5 mmol, 1 eq) CoCl<sub>2</sub>·6 H<sub>2</sub>O to yield 510 mg (1.48 mmol, 99%) of a blue solid. Elemental Analysis: calc (for C<sub>26</sub>H<sub>26</sub>O<sub>4</sub>N<sub>2</sub>Cl<sub>4</sub>Co<sub>2</sub>; M = 690.18 g mol<sup>-1</sup>) N 4.06; C 45.25; H 3.80; found: N 3.97; C 44.32; H 3.94.

**[Co(OON2)<sub>2</sub>(μ-Cl)<sub>2</sub>CoCl<sub>2</sub>]**: 100 mg (0.44 mmol, 1 eq) OON2 were reacted with 107 mg (0.44 mmol, 1 eq) CoCl<sub>2</sub>·6 H<sub>2</sub>O to yield 111 mg (0.31 mmol, 70%) of a blue solid. Elemental Analysis: calc (for C<sub>28</sub>H<sub>30</sub>O<sub>4</sub>N<sub>2</sub>Cl<sub>4</sub>Co<sub>2</sub>; M = 718.22 g mol<sup>-1</sup>) N 3.90; C 46.82; H 4.21; found: N 3.89; C 45.71; H 4.37.

**[Co(OON3)<sub>2</sub>(μ-Cl)<sub>2</sub>CoCl<sub>2</sub>]**: 100 mg (0.34 mmol, 1 eq) OON3 were reacted with 81 mg (34 mmol, 1 eq) CoCl<sub>2</sub>·6 H<sub>2</sub>O to yield 133 mg (0.32, 94%) of a blue solid. Elemental Analysis: calc (for C<sub>38</sub>H<sub>34</sub>O<sub>4</sub>N<sub>2</sub>Cl<sub>4</sub>Co<sub>2</sub>; M = 842.36 g mol<sup>-1</sup>) N 3.33; C 54.18; H 4.07; found: N 3.24; C 52.26; H 4.18.

**[FeCl<sub>3</sub>(OON1)]**: 100 mg (0.46 mmol, 1 eq) OON1 were reacted with 92 mg (0.46 mmol, 1 eq) FeCl<sub>3</sub>·6 H<sub>2</sub>O to yield 157 mg (0.42 mmol, 91%) of a dark red solid. Elemental Analysis: calc (for C<sub>13</sub>H<sub>13</sub>O<sub>2</sub>NCl<sub>3</sub>Fe; M = 377.45 g mol<sup>-1</sup>) N 3.71; C 41.37; H 3.47; found: N 3.84; C 42.67; H 3.56.

**[FeCl<sub>2</sub>(OON1)]<sub>2</sub>**: 50 mg (0.13 mmol, 2 eq) [FeCl<sub>3</sub>(OON1)] were dissolved in acetone and stirred for 60 h. A dark red precipitate was formed and filtered off. After washing with acetone 37 mg (0.05 mmol, 92%) were obtained. Analysis: calc (for C<sub>26</sub>H<sub>24</sub>O<sub>4</sub>N<sub>2</sub>Cl<sub>6</sub>Fe<sub>2</sub>; M = 681.98 g mol<sup>-1</sup>) N 3.55; C 45.79; H 4.11; found: N 4.06; C 44.68; H 3.46.

**[FeCl<sub>x</sub>(OON2)]<sub>y</sub>**: 170 mg (0.74 mmol, 1 eq) OON2 were reacted with 148 mg (0.74 mmol, 1 eq) FeCl<sub>3</sub>·6 H<sub>2</sub>O to yield 253 mg of a bright orange solid. The product is an asymmetric polymer with more than one Fe<sup>III</sup> species, the exact stoichiometry of this compound could not be determined. Elemental Analysis found: N 3.07; C 49.66; H 3.75.

**[FeCl<sub>2</sub>(OON3)]**: 97 mg (0.33 mmol, 1 eq) OON3 and 66 mg (0.33 mmol, 1 eq) FeCl<sub>2</sub>·4 H<sub>2</sub>O were dissolved in 5 mL methanol each. Both solutions were combined and stirred for 6 h at 298 K. The solvent of the resulting orange-brown solution was removed under vacuum to yield 83 mg (0.20 mmol, 61%) of a brown powder. Elemental Analysis: calc (for C<sub>19</sub>H<sub>17</sub>O<sub>2</sub>NCl<sub>2</sub>Fe; M = 418.09 g mol<sup>-1</sup>) N 3.35; C 54.58; H 4.10; found: N 3.45; C 53.88; H 3.92.

**[FeCl<sub>3</sub>(OON3)]**: 100 mg (0.34 mmol, 1 eq) OON3 were reacted with 68 mg (0.34 mmol, 1 eq) FeCl<sub>3</sub>·6 H<sub>2</sub>O to yield 124 mg (0.27 mmol, 79%) of a brown-red solid. Elemental Analysis: calc (for C<sub>19</sub>H<sub>17</sub>O<sub>2</sub>NCl<sub>3</sub>Fe; M = 453.55 g mol<sup>-1</sup>) N 3.09; C 50.32; H 3.78; found: N 3.07; C 49.66; H 3.75.

**[NiCl<sub>2</sub>(OON1)]**: 100 mg (0.46 mmol, 1 eq) OON1 were reacted with 110 mg (0.46 mmol, 1 eq) NiCl<sub>2</sub>·6 H<sub>2</sub>O to yield 60 mg (0.17 mmol, 37%) of a green solid. NMR (300 MHz, [D<sub>6</sub>]-acetone): <sup>1</sup>H: 11.46; 7.70; 7.46; 7.20; 6.94; 6.80; 5.38; 4.80; 4.28; 3.83 ppm. Elemental Analysis: calc (for C<sub>13</sub>H<sub>13</sub>O<sub>2</sub>NCl<sub>2</sub>Ni; M = 344.85 g mol<sup>-1</sup>) N 4.06; C 45.28; H 3.80; found: N



3.88; C 43.72; H 3.98.

**[NiCl<sub>2</sub>(OON2)]:** 100 mg (0.43 mmol, 1 eq) OON2 were reacted with 102 mg (0.43 mmol, 1 eq) NiCl<sub>2</sub>·6 H<sub>2</sub>O to yield 74 mg (0.21 mmol, 49%) of a green solid. NMR (300 MHz, [D<sub>6</sub>]-acetone): <sup>1</sup>H: 15.49; 13.27; 8.42; 7.51; 6.95; 5.52; 4.49; 2.00 ppm. Elemental Analysis: calc (for C<sub>14</sub>H<sub>15</sub>O<sub>2</sub>NCl<sub>2</sub>Ni; M = 356.98 g mol<sup>-1</sup>) N 3.90; C 46.85; H 4.21; found: N 4.09; C 44.52; H 4.05.

**[NiCl<sub>2</sub>(OON3)]:** 100 mg (0.34 mmol, 1 eq) OON3 were reacted with 82 mg (0.34 mmol, 1 eq) NiCl<sub>2</sub>·6 H<sub>2</sub>O to yield 84 mg (0.20 mmol, 59%) of a green solid. NMR (300 MHz, [D<sub>6</sub>]-acetone): <sup>1</sup>H: 14.10; 8.12; 7.47; 6.93; 4.60; 3.54 ppm. Elemental Analysis: calc (for C<sub>19</sub>H<sub>17</sub>O<sub>2</sub>NCl<sub>2</sub>Ni; M = 420.94 g mol<sup>-1</sup>) N 3.33; C 54.21; H 4.07; found: N 3.39; C 52.85; H 4.24.

**[Cu(triaz)<sub>2</sub>]:** 90 mg (0.25 mmol, 2 eq) triazH dissolved in 10 mL of a 5:3 solution MeCN/toluene were mixed with 0.350 mL (0.25 mmol, 2 eq) NEt<sub>3</sub>. After stirring for 5 minutes a solution of 480 mg (0.13 mmol, 1 eq) Cu(OTf)<sub>2</sub> in 1 mL MeCN were added in one portion and the resulting dark brown solution was slowly evaporated to dryness at 298 K to yield 47 mg (0.06 mmol, 43%) of green-brown crystals. Elemental analyses: calc (for C<sub>40</sub>H<sub>46</sub>N<sub>6</sub>O<sub>2</sub>Cl<sub>2</sub>Cu; M = 777.27 g mol<sup>-1</sup>) N 10.81; C 61.81; H 5.97; found: N 10.69; C 60.74; H 5.88.

**[Cu(py)<sub>4</sub>(OTf)<sub>2</sub>]:** 100 mg (0.27 mmol, 1 eq) Cu(OTf)<sub>2</sub> were mixed in 2 mL MeCN. 79 mg (1.1 mmol, 4 eq) pyridine were added in one portion and the solution was stirred 10 minutes. The solvent was removed by evaporation to yield 178 mg (0.27 mmol, 100%) dark blue crystals. Elemental analyses: calc (for C<sub>22</sub>H<sub>20</sub>F<sub>6</sub>N<sub>4</sub>O<sub>5</sub>S<sub>2</sub>Cu; M = 662.08 g mol<sup>-1</sup>) N 8.46; C 39.91; H 3.04; S 9.69; found: N 8.56; C 39.95; H 3.08; S 9.42.

### 9.3 Disproportionation Experiments

A solution of 358 mg (1 mmol) free ligand in 40 mL of a 5:3 solution of MeCN/toluene was prepared.

**Different metal salts:** 1 mL of the ligand solution (containing 0.025 mmol ligand) were mixed with 1 eq (0.025 mmol) NEt<sub>3</sub>. The mixture was stirred for five minutes at 298 K and

then the MeCN dissolved metal salt was added in one portion (in case of copper oxalate and copper phosphate a suspension was used). Spectra were measured immediately after the solution turned red-brown or at latest five minutes after mixing all components.

**Different amounts of Cu(OTf)<sub>2</sub> - 298 K, dilute:** 1 mL of the ligand solution (containing 0.025 mmol ligand) were mixed with 1 eq (0.025 mmol) NEt<sub>3</sub>. The mixture was stirred for five minutes at 298 K. The solution was diluted (0.00025 mmol) and the first spectrum was measured. The MeCN-dissolved Cu(OTf)<sub>2</sub> were added in several small portions directly into the cuvette followed by vigorously shaking. Spectra were measured immediately after adding the Cu(OTf)<sub>2</sub> solutions.

**Different amounts of Cu(OTf)<sub>2</sub> – 273 K, concentrated:** 1 mL of the ligand solution (containing 0.025 mmol ligand) were mixed with 0.025 mmol (1.0 eq) NEt<sub>3</sub>. The mixture was cooled to 273 K on an water/ice bath. 0.0125 mmol (0.5 eq) Cu(OTf)<sub>2</sub> dissolved in 0.2 mL MeCN were as well cooled to 273 K, both solutions were combined. The solvent for dilution (to achieve the appropriate concentration for absorption spectroscopy) was either 273 K cold. The spectra were measured immediately after dilution and with rapid scan velocity, since no temperature controlling device for the absorption spectrometer was available.

**Different bases:** 1 mL of the ligand solution (containing 0.025 mmol ligand) were mixed with 0.025 mmol (1.0 eq) of the chosen base (solids were dissolved in small portions of MeCN previously). The mixture was stirred for five minutes at 298 K and then 0.0125 mmol Cu(OTf)<sub>2</sub> dissolved in 0.2 mL MeCN were added in one portion to the ligand solution. Spectra were recorded after three minutes reaction time.

**Different amounts of base:** 1 mL of the ligand solution (containing 0.025 mmol ligand) were mixed with varying amounts of base (0.1–10 eq). The mixture was stirred for five minutes at 298 K and then 0.0125 mmol (0.5 eq) Cu(OTf)<sub>2</sub> dissolved in 0.2 mL MeCN were added in one portion to the ligand solution. Spectra were recorded after three minutes reaction time.

**Varying solvent polarity:** 1 mL of the ligand solution (containing 0.025 mmol ligand) were mixed with 0.025 mmol (1.0 eq) NEt<sub>3</sub>, the mixture was stirred for five minutes at 298 K. The different mixtures of MeCN/toluene (0:1–1:0) were prepared separately. Then 0.0125 mmol (0.5 eq) Cu(OTf)<sub>2</sub> were dissolved in 0.2 mL MeCN and added in one portion to the ligand solution. 15 µL radical containing solution (indicated by its dark brown colour) were mixed

with 3 mL of the prepared solvent (mixture) and the absorption spectra were recorded after 3 minutes.

**Catalytic test reactions on the triaz system: Reference:** 1.0 g benzyl alcohol were mixed with 1 eq powdered NaOH and was stirred vigorously. **Cu<sup>I</sup>-method:** 1.0 g benzyl alcohol was mixed with 1 eq powdered NaOH. A solution of 0.5 eq [(Cu(OTf)<sub>2</sub>(μ-C<sub>7</sub>H<sub>8</sub>))] with 2.0 eq triazH and 0.1 eq NEt<sub>3</sub> in O<sub>2</sub> saturated MeCN/toluene (5:3) was prepared. The catalyst mixture was added to the benzyl alcohol/NaOH mixture (2.5%<sub>mol</sub> catalyst). **Cu<sup>II</sup>-method:** A mixture of 2 eq triazH with 0.1 eq NEt<sub>3</sub> and 2 eq Cu(OTf)<sub>2</sub> in MeCN/toluene 5:3 (O<sub>2</sub> saturated) was prepared. 1.0 mg benzyl alcohol was mixed with 1 eq powdered NaOH and was stirred vigorously. The freshly prepared catalysts mixture (after 3 to 5 minutes) was added to the benzyl alcohol mixture (2.5%<sub>mol</sub>). **Detection:** While all reaction mixtures were stirred at 298 K, samples of the reaction mixture were taken, mixed with CD<sub>2</sub>Cl<sub>2</sub> upon which a green-brown precipitate was formed. The remaining solution was isolated and submitted to NMR spectroscopic analysis. <sup>1</sup>H spectra (300 MHz) were recorded and product yields were determined by integration of the aldehyde proton.

**Catalytic test reactions on various systems:** A solution of 0.5 eq [(Cu(OTf)<sub>2</sub>(μ-C<sub>7</sub>H<sub>8</sub>))] with 2.0 eq ligand in pure MeCN was prepared. 1.0 g benzyl alcohol was mixed with 1 eq powdered NaOH. Both mixtures were combined and vigorously stirred at 298 K. Samples of the reaction mixtures were taken, mixed with CD<sub>2</sub>Cl<sub>2</sub> upon which a green-brown precipitate was formed. The remaining solution was isolated and submitted to NMR spectroscopic analysis. <sup>1</sup>H spectra (300 MHz) were recorded and product yields were determined by integration of the aldehyde proton.

## 10.0 Literature

1. R. H. Holm, P. Kennepohl, E. I. Solomon, *Chem. Rev.* **1996**, 96, 2239–2314.
2. D. E. Fenton, *Biocoordination Chemistry*, in Oxford Chemistry Primers, 25, 1<sup>st</sup> ed. Oxford University Press, New York, **1995**.
3. W. Kaim, B. Schwederski, *Bioanorganische Chemie*, 3<sup>ed</sup> ed. Teubner Verlag, Wiesbaden, **2005**.
4. (a) R. G. Person, *J. Am. Chem. Soc.* **1963**, 85, 3533–3539; (b) R. G. Pearson, *Inorg. Chem.* **1988**, 27, 734–740.
5. J. J. R. Fraústo da Silva, R. J. P. Williams, *The biological chemistry of the elements*, 2<sup>nd</sup> ed. Oxford University Press, New York, **2001**.
6. B. G. Malmström, *Eur. J. Biochem.* **1994**, 223, 711–718.
7. B. L. Vallee, R. J. P. Williams, *Proc. Natl. Acad. Sci. U.S.A.* **1968**, 59, 498–505.
8. R. J. P. Williams, *Eur. J. Biochem.* **1995**, 234, 363–381; (b) R. J. P. Williams, *J. Mol. Catalysis* **1986**, 1–7.
9. (a) R. Lumry, H. Eyring, *J. Phys. Chem.* **1954**, 58, 110–120; (b) D. E. Hansen, R. T. Rainers, *J. Chem. Educ.* **1990**, 67, 483–483; (c) A. Haim, *J. Chem. Educ.* **1989**, 66, 935–947.
10. M. Fontecave, J.-L. Pierre, *Bull. Chim. Soc. Fr.* **1993**, 130, 77–85.
11. W. Kaim, *Dalton Trans.* **2003**, 761–768.
12. N. G. Connelly, W. E. Geiger, *Chem. Rev.* **1996**, 96, 877–910.
13. C. E. Ruggiero, S. M. Carrier, W. E. Antholine, J. W. Whittaker, C. J. Cramer, W. B. Tolman, *J. Am. Chem. Soc.* **1993**, 115, 11285–11298.
14. N. Ito, S. E. V. Phillips, C. Stevens, Z. B. Ogel, M. J. McPherson, J. N. Keen, K. D. S. Yadav, P. F. Knowles, *Faraday Discuss. Chem. Soc.* **1993**, 93, 75–84.
15. N. Ito, S. E. V. Phillips, C. Stevens, Z. B. Ogel, M. J. McPherson, J. N. Keen, K. D. S. Yadav, P. F. Knowles, *Nature* **1991**, 350, 87–90.
16. P. F. Knowles, N. Ito in *Perspectives on Bioinorganic Chemistry*, Vol. 2 (Editor: R. W. Hay, J. R. Dilworth, K. B. Nolan), Jai Press, London, **1993**.
17. N. Ito, S. E. V. Phillips, K. D. S. Yadav, P. F. Knowles, *J. Mol. Biol.* **1994**, 238, 794–814.
18. J. W. Whittaker in *Metal Ions in Biological Systems*, Vol. 30, (Editor: H. Sigel, A. Sigel), Dekker, New York, **1994**.
19. M. Moscherosch, J. S. Field, W. Kaim, S. Kohlmann, M. Krejcik, *J. Chem. Soc. Dalton Trans.* **1993**, 211–216.
20. G. Speiser, S. Tisza, Z. Tyeklar, C. W. Lange, C. G. Pierpont, *Inorg. Chem.* **1994**, 33, 2041–2045.
21. G. A. Razuvaev, V. K. Cherkasov, G. A. Abakumov, *J. Organomet. Chem.* **1978**, 160, 361–371.
22. R. M. Buchanan, C. Wilson-Blumenberg, C. Trapp, S. K. Larsen, D. L. Greene, C. G. Pierpont, *Inorg. Chem.* **1986**, 25, 3070–3076.
23. J. Rall, W. Kaim, *J. Chem. Soc. Faraday Trans.* **1994**, 90, 2905–2908.
24. D. M. Dooley, M. A. McGuirl, D. E. Brown, P. N. Turowski, W. S. McIntire, P. F. Knowles, *Nature* **1991**, 349, 262–264.
25. D. M. Dooley, W. S. McIntire, M. A. McGuirl, C. E. Cote, J. L. Bates, *J. Am. Chem. Soc.* **1990**, 112, 2782–2789.
26. M. Harata, K. Jitsukawa, H. Masuda, H. Einaga, *J. Am. Chem. Soc.* **1994**, 116, 10817–10818.

27. K. Fujisawa, M. Tanaka, Y. Moro-oka, N. Kitajima, *J. Am. Chem. Soc.* **1994**, 116, 12079–12080.
28. M. Mahroof-Tahir, K. D. Karlin, *J. Am. Chem. Soc.* **1992**, 114, 7599–7601.
29. W. Kaim, S. Kohlmann, *Inorg. Chem.* **1987**, 26, 1469–1470.
30. W. Kaim, M. Moscherosch, *J. Chem. Soc. Faraday Trans.* **1991**, 87, 3185–3187.
31. W. Kaim, M. Moscherosch, S. Kohlmann, J. S. Field, D. Fenske, in *The Chemistry of the Copper and Zinc Triads* (Editor: A. J. Welch, S. K. Chapman) RCS, Cambridge **1993**.
32. (a) E.-I. Ochiai, *Origins of Life* **1978**, 9, 81–91; (b) M. G. Schwendinger, R. Tauler, S. Saetia, K. R. Liedl, R. T. Kroemer, B. M. Rode, *Inorg. Chim. Acta* **1995**, 228, 207–214.
33. R. J. P. Williams in *The Chemistry of Copper and Zinc Triads*, (Editor: A. J. Welch, S. K. Chapman), RCS, Cambridge, **1993**.
34. (a) E.-I. Ochiai, *J. Chem. Educ.* **1986**, 63, 942–944; (b) R. J. P. Williams, *Chem. Scr.* **1986**, 26, 515; (c) C. J. Allégre, S. H. Schneider, *Sci. Am.* **1994**, 271, 44–51.
35. E. I. Solomon, U. M. Sundaram, T. E. Machonkin, *Chem. Rev.* **1996**, 96, 2563–2605.
36. W. Kaim, J. Rall, *Angew. Chem.* **1996**, 108, 47–64.
37. L. M. Mirica, X. Ottenwaelder, T. D. P. Stack, *Chem. Rev.* **2004**, 104, 1013–1045.
38. E. I. Solomon, P. Chen, M. Metz, S.-K. Lee, A. E. Palmer, *Angew. Chem.* **2001**, 113, 4702–4724.
39. G. E. Norris, B. F. Anderson, E. N. Baker, *J. Am. Chem. Soc.* **1986**, 108, 2784–2785.
40. J. M. Guss, H. D. Bartunik, H. C. Freeman, *Acta Cryst. B48* **1992**, 790–811.
41. E. I. Solomon, M. J. Baldwin, M. D. Lowery, *Chem. Rev.* **1992**, 92, 521–542.
42. K. P. Butin, E. K. Beloglazkina, N. V. Zyk, *Russ. Chem. Rev.* **2005**, 74, 6, 531–553.
43. M. M. Werst, C. E. Davoust, B. M. Hoffman, *J. Am. Chem. Soc.* **1991**, 113, 1533–1538.
44. W. E. B. Shepard, B. F. Anderson, D. A. Lewandowski, G. E. Norris, D. N. Baker, *J. Am. Chem. Soc.* **1990**, 112, 7817–7819.
45. S. T. Prigge, A. S. Kolhekar, B. A. Eipper, R. E. Mains, L. M. Amzel, *Science* **1997**, 278, 1300–1305.
46. S. T. Prigge, A. S. Kolhekar, B. A. Eipper, R. E. Mains, L. M. Amzel, *Nat. Struct. Biol.* **1999**, 6, 976–983.
47. J. P. Klinman, *Chem. Rev.* **1996**, 96, 2541–2562.
48. S. Jaron, N. J. Blackburn, *Biochemistry* **1999**, 38, 15086–15096.
49. V. Ducros, A. M. Brzozowski, K. S. Wilson, S. H. Brown, P. Østergaard, P. Schneider, D. S. Yaver, A. H. Pedersen, G. J. Davies, *Nat. Struct. Biol.* **1998**, 5, 310–316.
50. I. Zaitseva, V. Zaitsev, G. Card, K. Moshov, B. Bax, A. Ralph, P. Lindley, *J. Biol. Inorg. Chem.* **1996**, 1, 15–23.
51. A. Messerschmidt, R. Ladenstein, R. Huber, M. Bolognesi, L. Avigliano, R. Petruzzelli, A. Rossi, A. Finazzi-Agro, *J. Mol. Biol.* **1992**, 224, 179–205.
52. A. Messerschmidt, H. Luecke, R. Huher, *J. Mol. Biol.* **1993**, 230, 997–1014.
53. H. Beinert, *Chem. Scr.* **28A** **1988**, 35–40.
54. G. Buse, *Naturwiss. Rundschau* **1986**, 39, 518–611.
55. G. T. Babcock, M. Wikström, *Nature* **1992**, 356, 301–309.
56. G. C. M. Steffens, T. Soulimane, G. Wolff, G. Buse, *Eur. J. Biochem.* **1993**, 213, 1149–1157.
57. G. Henkel, A. Müller, S. Weissgräber, G. Buse, T. Soulimane, G. C. M. Steffens, H.-F. Nolting, *Angew. Chem.* **1995**, 107, 1615–1619; *Angew Chem. Int. Ed.* **1995**, 35, 1488–1492.
58. (a) T. Tsukihara, H. Aoyama, E. Ydmashita, T. Tomizaki, H. Yamaguchi, K. Shinzawa-Itōh, R. Nakashima, R. Yaono, S. Yoshikawa, *Science* **1995**, 269, 1069–1074; (b) S. Iwata, C. Ostermeier, B. Ludwig, H. Michel, *Nature* **1995**, 376, 660–669.
59. S. Han, Y. Ching, D. L. Rousseau, *Nature* **1990**, 348, 89–90.

60. J. A. Tainer, E. D. Getzoff, J. S. Richardson, D. C. Richardson, *Nature (London)*, **1983**, 306, 284–287.
61. (a) A. Girtner, U. Weser, *Top. Curr. Chem.* **1986**, 132, 1–61; (b) A. E. G. Cass in *Metalloproteins, Part 1* (Editor: P. Harrison), VCH, Weinheim, **1985**, 121–156; (c) I. Fridovich, *J. Biol. Chem.* **1989**, 264, 7761–7764.
62. (a) W. C. Stallings, K. A. Patridge, R. K. Strong, M. L. Ludwig, *J. Biol. Chem.* **1985**, 260, 16424–16432; (b) G. E. O. Borgstahl, H. E. Parge, M. J. Hickey, W. F. Beyer, Jr., R. A. Hallewell, J. A. Tainer, *CeN* **1992**, 71, 107–118.
63. U. Weser, *Forschung - Mitteilungen der DFG* **1994**, 4, 11–13.
64. J.-L. Pierre, P. Chautemps, S. Refaif, C. Beguin, A. E. Marzouki, G. Serratrice, E. Saint-Aman, P. Rey, *J. Am. Chem. Soc.* **1995**, 117, 1965–1973.
65. I. Bertini, L. Banci, M. Piccioli, C. Luchinat, *Coord. Chem. Rev.* **1990**, 100, 67–103.
66. E. D. Getzoff, D. E. Cahelli, C. L. Fisher, H. E. Parge, M. S. Viezzoli, L. Banci, R. A. Hallewell, *Nature (London)* **1992**, 358, 347–351.
67. J. Z. Pedersen, A. Finazzi-Agró, *FEBS Lett.* **1993**, 325, 53–58.
68. S. M. Janes, D. Mu, D. Wemmes, A. J. Smith, S. Kaus, S. Maltby, A. L. Burlingame, J. P. Klinman, *Science* **1990**, 248, 981–987.
69. (a) W. S. McIntire, *FASEB J.* **1994**, 8, 513–521; (b) J. A. Duine, *Eur. J. Biochem.* **1991**, 200, 271–284.
70. (a) L. Cleveland, R. E. Coffman, P. Coon, L. Davis, *Biochemistry* **1975**, 14, 1108–1115; (b) Z. B. Ögel, D. Brayford, M. J. McPherson, *Mycol. Res.* **1994**, 98, 474–480.
71. F. Thomas, *Eur. J. Inorg. Chem.* **2007**, 2379–2404.
72. J. W. Whittaker, *Chem. Rev.* **2003**, 103, 6, 2347–2364.
73. M. M. Whittaker, J. W. Whittaker, *Biochemistry* **2001**, 40, 7140–7148.
74. M. Fontecave, J.-L. Pierre, *Coord. Chem. Rev.* **1998**, 170, 125–140.
75. S. G. Minasian, M. M. Whittaker, J. W. Whittaker, *Biochemistry* **2004**, 43, 13683–13693.
76. R. M. Wachter, B. P. Branchaud, *J. Am. Chem. Soc.* **1996**, 118, 2782–2789.
77. R. M. Wachter, B. P. Branchaud, *Biochemistry* **1996**, 35, 14425–14435.
78. R. M. Wachter, M. P. Montague-Smith, B. P. Branchaud, *J. Am. Chem. Soc.* **1997**, 119, 7743–7749.
79. F. Himo, L. A. Eriksson, F. Maseras, P. E. M. Siegbahn, *J. Am. Chem. Soc.* **2000**, 122, 8031–8036.
80. M. M. Whittaker, J. W. Whittaker, *Biophys. J.* **1993**, 64, 762–772.
81. (a) M. P. Reynolds, A. J. Baron, C. W. Wilmot, E. Vinecombe, C. Stevens, S. E. V. Phillips, P. F. Knowles, M. J. McPherson, *J. Biol. Inorg. Chem.* **1997**, 327–335; (b) Y. K. Lee, M. M. Whittaker, J. W. Whittaker, *Biochemistry* **2008**, 47, 6637–6649.
82. R. M. Wachter, B. P. Branchaud, *Biochim. Biophys. Acta* **1998**, 43–54.
83. M. M. Whittaker, J. W. Whittaker, *J. Biol. Chem.* **1988**, 263, 6074–6080.
84. Y. Wang, T. D. P. Stack, *J. Am. Chem. Soc.* **1996**, 118, 13097–13098.
85. Y. Wang, J. L. DuBois, B. Hedman, K. O. Hodgson, T. D. P. Stack, *Science* **1998**, 279, 537–540.
86. U. Rothlisberger, P. Carloni, *Int. J. Quantum Chem.* **1999**, 73, 209–218.
87. (a) This observed potential is markedly lower than the potentials for free tyrosine (0.53 V vs. FeCp<sub>2</sub>/FeCp<sub>2</sub><sup>+</sup>) or tyrosine in other enzymatic systems (0.46–0.60 V vs. FeCp<sub>2</sub>/FeCp<sub>2</sub><sup>+</sup>). (b) A. Harriman, *J. Phys. Chem.* **1987**, 91, 6102–6104; A. Boussac, A. L. Eteinne, *Biochim. Biophys. Acta* **1984**, 766, 576–581.
88. (a) The published redox potential of GO are all referred to NHE in water For comparison with synthetic models these values are converted to FeCp<sub>2</sub>/FeCp<sub>2</sub><sup>+</sup> corrected values. The potential for FeCp<sub>2</sub>/FeCp<sub>2</sub><sup>+</sup> vs. NHE in water is 0.400 ± 0.007 V. Since the redox potential is nearly not influenced by the solvent, the different electrolytes and

- their ionic strange can be neglected. (b) M. Jonsson, A. Houmam, G. Jocys, D. D. M. Wayner, *J. Chem. Soc. Perkin Trans. 2* **1999**, 425–429.
89. S. Itoh, S. Takayama, R. Arakawa, A. Furuta, M. Komatsu, A. Ishida, S. Takamuku, S. Fukuzumi, *Inorg. Chem.* **1997**, 36, 1407–1416.
  90. M. S. Rogers, A. J. Baron, M. J. McPherson, P. F. Knowles, D. M. Dooley, *J. Am. Chem. Soc.* **2000**, 122, 990–991.
  91. M. S. Rogers, D. M. Dooley, *Current Opinion in Chemical Biology* **2003**, 7, 189–196.
  92. S. J. Firbank, M. S. Rogers, C. M. Wilmot, D. M. Dooley, M. A. Halcrow, P. F. Knowles, M. J. McPherson, S. E. V. Phillips, *Proc. Natl. Acad. Sci. USA* **2001**, 98, 12932–12937.
  93. M. M. Whittaker, Y.-Y. Chuang, J. W. Whittaker, *J. Am. Chem. Soc.* **1993**, 115, 10029–10035.
  94. M. M. Whittaker, W. R. Duncan, J. W. Whittaker, *Inorg. Chem.* **1996**, 35, 382–386.
  95. D. Zurita, C. Scheer, J.-L. Pierre, E. Saint-Aman, *J. Chem. Soc. Dalton Trans.* **1996**, 4331–4336.
  96. D. Zurita, I. Gautier-Luneau, S. Ménage, J.-L. Pierre, E. Saint-Aman, *J. Biol. Inorg. Chem.* **1997**, 2, 46–55.
  97. D. Zurita, S. Ménage, J.-L. Pierre, E. Saint-Aman, *New J. Chem.* **1997**, 21, 1001–1006.
  98. M. A. Halcrow, L. M. L. Chia, X. Liu, E. J. L. McInnes, L. J. Yellowlees, F. E. Mabbs, J. E. Davies, *Chem. Commun.* **1998**, 2465–2466.
  99. M. A. Halcrow, L. M. L. Chia, X. Liu, E. J. L. McInnes, L. J. Yellowlees, F. E. Mabbs, I. J. Scowen, M. McPartlin, J. E. Davies, *J. Chem. Soc. Dalton Trans.* **1999**, 1753–1762.
  100. J. A. Halfen, B. A. Jazdzewski, S. Mahapatra, L. M. Berreau, E. C. Wilkinson, L. Que Jr., W. B. Tolman, *J. Am. Chem. Soc.* **1997**, 119, 8217–8227.
  101. J. Stubbe, W. A. van der Donk, *Chem. Rev.* **1998**, 98, 705–762.
  102. J. M. Johnson, H. B. Halsall, W. R. Heineman, *Biochemistry* **1985**, 24, 1579–1585.
  103. M. A. Halcrow, E. J. L. McInnes, F. E. Mabbs, I. J. Scowen, M. McPartlin, H. R. Powell, J. E. Davies, *J. Chem. Soc. Dalton Trans.* **1997**, 4025–4035.
  104. M. A. Halcrow, N. L. Cromhout, P. R. Raithby, *Polyhedron* **1997**, 16, 4257–4264.
  105. X. Liu, L. M. L. Chia, C. A. Kilner, L. J. Yellowlees, M. Thornton-Pett, S. Trofimenko, M. A. Halcrow, *Chem. Commun.* **2000**, 1947–1948.
  106. A. J. Baron, C. Stevens, C. M. Wilmot, P. F. Knowles, S. E. V. Phillips, M. J. McPherson, *Biochem. Soc. Trans.* **1993**, 21, 319S.
  107. M. J. McPherson, C. Stevens, A. J. Baron, Z. B. Ogel, K. Seneviratne, C. M. Wilmot, N. Ito, I. Brocklebank, S. E. V. Phillips, P. F. Knowles, *Biochem. Soc. Trans.* **1993**, 21, 752–756.
  108. A. J. Baron, C. Stevens, C. M. Wilmot, K. D. Seneviratne, V. Blakeley, D. M. Dooley, S. E. V. Phillips, P. F. Knowles, M. J. McPherson, *J. Biol. Chem.* **1994**, 269, 25095–25105.
  109. S. Itoh, M. Taki, S. Fukuzumi, *Coord. Chem. Rev.* **2000**, 198, 3–20.
  110. D. Rokhsana, D. M. Dooley, R. K. Szilagy, *J. Am. Chem. Soc.* **2006**, 128, 15550–15551.
  111. M. S. Rogers, E. M. Tyler, N. Akyumani, C. R. Kurtis, R. K. Spooner, S. E. Deacon, S. Tamber, S. J. Firbank, K. Mahmoud, P. F. Knowles, S. E. V. Phillips, M. J. McPherson, D. M. Dooley, *Biochemistry* **2007**, 46, 4606–4618.
  112. R. Amorati, F. Catarzi, S. Menichetti, G. F. Pedulli, C. Viglianisi *J. Am. Chem. Soc.* **2008**, 130, 237–244.
  113. K. Yamato, T. Inada, M. Doe, A. Ichimura, T. Takui, Y. Kojima, T. Kikunaga, N. Yanagihara, T. Onaka, S. Yano, *Bull. Chem. Soc. Jpn.* **2000**, 73, 903–912.
  114. A. Berkessel, M. Doucet, S. Bulat, K. Glaubitz, *Biol. Chem.* **2005**, 386, 1035–1041.

115. A. Philibert, F. Thomas, C. Philouze, S. Hamman, E. Saint-Aman, J. L. Pierre, *Chem. Eur. J.* **2003**, 9, 3803–3812.
116. K. D. Karlin, B. I. Cohen, J. C. Hayes, A. Farooq, J. Zubieta, *Inorg. Chem.* **1987**, 26, 147–153.
117. (a) K. Bowden, I. M. Heilbron, E. R. H. Jones, B. C. L. Weedon, *J. Chem. Soc.* **1946**, 39–45; (b) E. J. Corey, J. W. Suggs, *Tetrahedron Lett.* **1975**, 16, 2647–2650.
118. S. L. Huang, K. Omura, D. Swern, *J. Org. Chem.* **1976**, 41, 3329–3331.
119. S. V. Ley, J. Norman, W. P. Griffith, S. P. Marsden, *Synthesis* **1994**, 6, 639–666.
120. D. B. Dess, J. C. Martin, *J. Org. Chem.* **1983**, 48, 4155–4156.
121. *The 12 Principles of Green Chemistry*, United States Environmental Protection Agency, 2006, <http://epa.gov/greenchemistry/pubs/principles.html>.
122. S. S. Stahl, *Angew. Chem.* **2004**, 116, 3480–3501.
123. A search for patents in scifinder®, CAS, on 28.05.2010 resulted 2769 hits on “catalytic alcohol oxidation”.
124. M. Vaidyanathan, R. Viswanathan, M. Palaniandavar, T. Balasubramanian, P. Prabhakaran, P. Muthiah, *Inorg. Chem.* **1998**, 37, 25, 6418–6427.
125. C. Ochs, F. E. Hahn, R. Fröhlich, *Eur. J. Inorg. Chem.* **2001**, 2427–2436.
126. M. Vaidyanathan, M. Palaniandavar, R. S. Gopalan, *Inor. Chim. Acta* **2001**, 324, 241–251.
127. Y. Shimazaki, S. Huth, S. Hirota, O. Yamauchi, *Inor. Chim. Acta* **2002**, 331, 168–170.
128. M. Taki, H. Hattori, T. Osako, S. Nagatomo, M. Shiro, T. Kitagawa, S. Itoh, *Inorg. Chim. Acta* **2004**, 357, 3369–3381.
129. F. Michel, F. Thomas, S. Hamman, C. Philouze, E. Saint-Aman, J.-L. Pierre, *Eur. J. Inorg. Chem.* **2006**, 3684–3696.
130. F. Michel, F. Thomas, S. Hamman, E. Saint-Aman, C. Bucher, J.-L. Pierre, *Chem. Eur. J.* **2004**, 10, 4115–4125.
131. (a) Y. Shimazaki, S. Huth, A. Odani, O. Yamauchi, *Angew. Chem.* **2000**, 112, 9, 1732–1735; (b) A. John, M. M. Shaikh, P. Ghosh, *Dalton Trans.* **2008**, 2815–2824.
132. a) A. Sokolowski, H. Leutbecher, T. Weyhermüller, R. Schnepf, E. Bothe, E. Bill, P. Hildebrandt, K. Wieghardt, *J. Biol. Inorg. Chem.* **1997**, 2, 444–453.
133. B. A. Jazdzewski, A. M. Reynolds, P. L. Holland, V. G. Young Jr., S. Kaderli, A. D. Zuberbühler, W. B. Tolman, *J. Biol. Inorg. Chem.* **2003**, 8, 381–393.
134. J. Müller, T. Weyhermüller, E. Bill, P. Hildebrandt, L. Ould-Moussa, T. Glaser, K. Wieghardt, *Angew. Chem.* **1998**, 110, 637–640; *Angew. Chem. Int. Ed.* **1998**, 37, 616–619.
135. J. A. Halfen, V. G. Young Jr., W. B. Tolman, *Angew. Chem.* **1998**, 108, 1832–1835; *Angew. Chem. Int. Ed.* **1996**, 35, 1687–1690.
136. E. Bill, J. Müller, T. Weyhermüller, K. Wieghardt, *Inorg. Chem.* **1999**, 38, 5795–5802.
137. R. C. Pratt, T. D. P. Stack, *Inorg. Chem.* **2005**, 44, 2367–2375.
138. C. Mukherjee, T. Weyhermüller, E. Bothe, P. Chaudhuri, *Inorg. Chem.* **2008**, 47, 11620–11632.
139. P. Chaudhuri, M. Hess, J. Müller, K. Hildenbrand, E. Bill, T. Weyhermüller, K. Wieghardt, *J. Am. Chem. Soc.* **1999**, 121, 9599–9610.
140. M. Königsmann, N. Donati, D. Stein, H. Schönberg, J. Harmer, A. Sreekanth, H. Grützmacher, *Angew. Chem.* **2007**, 119, 3637–3640.
141. P. Chaudhuri, M. Hess, T. Weyhermüller, K. Wieghardt, *Angew. Chem.* **1999**, 111, 1165–1168.
142. P. Chaudhuri, M. Hess, U. Flörke, K. Wieghardt, *Angew. Chem.* **1998**, 110, 2340–2343.
143. P. Gamez, I. A. Koval, J. Reedijk, *Dalton Trans.* **2004**, 4079–4088.
144. C. Mukherjee, U. Pieper, E. Bothe, V. Bachler, E. Bill, T. Weyhermüller, P. Chaudhuri, *Inorg. Chem.* **2008**, 47, 8943–8956.



145. L. Benisvy, A. J. Blake, D. Collison, E. Stephen Davies, C. D. Garner, E. J. L. McInnes, J. McMaster, G. Whittaker, C. Wilson, *Dalton Trans.* **2003**, 1975–1985.
146. M. A. Halcrow, *Heteroatom Chemistry* **2002**, 13, 494–500.
147. T. Osako, Y. Ueno, Y. Tachi, S. Itoh, *Inorg. Chem.* **2004**, 43, 6516–6518.
148. F. Thomas, O. Jarjayes, C. Duboc, C. Philouze, E. Saint-Aman, J.-L. Pierre, *Dalton Trans.* **2004**, 2662–2669.
149. F. Michel, S. Torelli, F. Thomas, C. Duboc, C. Philouze, C. Belle, S. Hamman, E. Saint-Aman, J. L. Pierre, *Angew. Chem.* **2005**, 117, 442–445; *Angew. Chem. Int. Ed.* **2005**, 44, 438–441.
150. Z. Lu, J. Sánchez Costa, O. Roubeau, I. Mutikainen, U. Turpeinen, S. J. Teat, P. Gamez, J. Reedijk, *Dalton Trans.* **2008**, 3567–3573.
151. P. Gamez, I. W. C. E. Arends, J. Reedijk, R. A. Sheldon, *Chem. Commun.* **2003**, 2414–2415.
152. Ligands are similar to salen type ligands and bear a N<sub>2</sub>O<sub>2</sub> donor set but in contrast to salen they possess a diaminobiphenyl backbone.
153. Y. Shimazaki, S. Huth, A. Odani, O. Yamauchi, *Angew. Chem. Int. Ed.* **2000**, 39, 1666–1669.
154. X. Ribas, D. A. Jackson, B. Donnadieu, J. Mahia, T. Parella, R. Xifra, B. Hedman, K. O. Hodgson, A. Llobet, T. D. P. Stack, *Angew. Chem.* **2002**, 114, 3117–3120; *Angew. Chem. Int. Ed.* **2002**, 41, 2991–2994.
155. J. Stubbe, *Annu. Rev. Biochem.* **1989**, 58, 257–285.
156. B. Barry, M. K. El-Deeb, P. O. Sandusky, G. T. Babcock, *J. Biol. Chem.* **1990**, 265, 20139–20143.
157. W. L. Smith, T. E. Eling, R. J. Kulmacz, L. J. Mamett, A.-L. Tsai, *Biochemistry* **1992**, 31, 3–7.
158. R. Karthien, R. Dietz, W. Nastainczyk, H. H. Ruf, *Eur. J. Biochem.* **1988**, 171, 313–320.
159. X. Liu, E. J. L. McInnes, C. A. Kilner, M. Thornton-Pett, M. A. Halcrow, *Polyhedron* **2001**, 20, 2889–2900.
160. X. Liu, S. A. Barrett, C. A. Kilner, M. Thornton-Pett, M. A. Halcrow, *Tetrahedron* **2002**, 58, 603–611.
161. R. C. Pratt, L. M. Mirica, T. D. P. Stack, *Inorg. Chem.* **2004**, 43, 8030–8039.
162. T. Kruse, T. Weyhermüller, K. Wieghardt, *Inorg. Chim. Acta* **2002**, 331, 81–89.
163. P. Chaudhuri, M. Hess, U. Flörke, K. Wieghardt *Angew. Chem. Int. Ed.* **1998**, 37, 2217–2220.
164. T. Kruse, Dissertation, *Übergangsmetallkomplexe neuer Thioether-Phenolatliganden Synthese, Strukturen und Eigenschaften*, Ruhr Universität Bochum, **2001**.
165. E. R. Altwicker, *Chem. Rev.* **1967**, 67, 475–531.
166. R. G. Hicks, *Org. Biomol. Chem.* **2007**, 5, 1321–1338.
167. S. Itoh, M. Taki, S. Takayama, S. Nagatomo, T. Kitagawa, N. Sakurada, R. Arakawa, S. Fukuzumi, *Angew. Chem. Int. Ed.* **1999**, 38, 2774–2776.
168. M. Taki, H. Kumei, S. Itoh, S. Fukuzumi, *J. Inorg. Biochem.* **2000**, 78, 1–5.
169. F. Thomas, G. Gellon, I. Gautier-Luneau, E. Saint-Aman, J.-L. Pierre, *Angew. Chem. Int. Ed.* **2002**, 41, 3047–3050.
170. E. Zueva, P. H. Walton, J. E. McGrady, *Dalton Trans.* **2006**, 1, 159–167.
171. H. Zipse, *Top. Curr. Chem.* **2006**, 263, 163–189.
172. F. G. Bordwell, T. Y. Lynch, *J. Am. Chem. Soc.* **1989**, 111, 7558–7562.
173. (a) T. Vreven, K. Morokuma, *J. Chem. Phys.* **1999**, 111, 8799–8803; (b) A. Fatthai, S. R. Kass, *J. Org. Chem.* **2004**, 69, 9176–9183.
174. G. P. F. Wood, D. Moran, R. Jacob, L. Radom, *J. Phys. Chem. A* **2005**, 109, 6318–6325.

175. H. G. Viehe, Z. Janousek, R. Mereny, L. Stella, *Acc. Chem. Res.* **1985**, 18, 148–154.
176. R. Sustmann, H. G. Korth, *Adv. Phys. Org. Chem.* **1990**, 26, 131–178.
177. F. G. Bordwell, X. M. Zhang, M. S. Alnajjar, *J. Am. Chem. Soc.* **1992**, 114, 7623–7629.
178. F. Himo, *Chem. Phys. Lett.* **2001**, 328, 270–276.
179. M. Jonsson, D. D. M. Wayner, D. A. Armstrong, D. Yu, A. Rauke *J. Chem. Soc. Perkin Trans. 2* **1998**, 1967–1972.
180. W. Kaim, A. Klein, *Spectroelectrochemistry*, RCS Publishing, Cambridge, UK, **2008**.
181. J. T. Singleton, *Tetrahedron* **2003**, 59, 1837–1857.
182. G. van Koten, M. Albrecht, *Angew. Chem. Int. Ed.* **2001**, 40, 3750–3781.
183. A. Klein, S. Elmas, K. Butsch, *Eur. J. Inorg. Chem.* **2009**, 2271–2281.
184. A. Klein, K. Butsch, S. Elmas, D. Heift, S. Nitsche, I. Schlipf, H. Bertagnolli, *Eur. J. Inorg. Chem.* **2010**, manuscript submitted.
185. M. E. van der Boom, D. Milstein, *Chem. Rev.* **2003**, 103, 1759–1792.
186. P. A. Brayshaw, J.-C. G. Bünzli, P. Froidevaux, J. M. Harrowfield, Y. Kim, A. N. Sobolevt, *Inorg. Chem.* **1995**, 34, 2068–2076.
187. E. Furet, K. Costuas, P. Rabiller, O. Maury, *J. Am. Chem. Soc.* **2008**, 130, 2180–2183.
188. M. L. Cable, J. P. Kirby, K. Sorasaene, H. B. Gray, A. Ponce, *J. Am. Chem. Soc.* **2007**, 129, 1474–1475.
189. H. Katada, H. Seino, Y. Mizobe, J. Sumaoka, M. Komiyama, *J. Biol. Inorg. Chem.* **2008**, 13, 249–255.
190. M. Chatterjee, M. Maji, S. Ghosh, T. C. W. Mak, *J. Chem. Soc. Dalton Trans.* **1998**, 3641–3645.
191. M. Aureliano, F. Henao, T. Tiago, R. O. Duarte, J. J. G. Moura, B. Baruah, D. C. Crans, *Inorg. Chem.* **2008**, 47, 5677–5684.
192. K. J. Ooms, S. E. Bolte, J. J. Smee, B. Baruah, D. C. Crans, T. Polenova, *Inorg. Chem.* **2007**, 46, 9285–9293.
193. B. Bitterlich, G. Anilkumar, F. G. Gelalcha, B. Spilker, A. Grotevendt, R. Jackstell, M. K. Tse, M. Beller, *Chem. Asian J.* **2007**, 2, 521–529.
194. J. A. Thich, C. C. Ou, D. Powers, B. Vasiliou, D. Mastropaolo, J. A. Potenza, H. J. Schugar, *J. Am. Chem. Soc.* **1976**, 1425–1433.
195. M. K. Tse, M. Klawonn, S. Bhor, C. Döbler, G. Anilkumar, H. Hugl, W. Mägerlein, M. Beller, *Org. Lett.* **2005**, 7, 6, 987–990.
196. H. Nishiyama, T. Shimada, H. Itoh, H. Sugiyama, Y. Motoyama, *Chem. Commun.* **1997**, 1863–1864.
197. S. M. Couchman, J. M. Dominguez-Vera, J. C. Jeffery, C. A. McKee, S. Nevitt, M. Pohlman, C. M. White, M. D. Ward, *Polyhedron* **1998**, 17, 3541–3550.
198. M. V. Kirillova, M. F. C. Guedes da Silva, A. M. Kirillov, J. J. R. Fraústo da Silva, A. J. L. Pombeiro, *Inorg. Chim. Acta* **2007**, 360, 506–512.
199. Y. Liu, J.-M. Dou, D. Wang, X.-X. Zhang, L. Zhou, *Acta Cryst. Sect. E*, **2006**, m2208–m2209.
200. M. Koman, M. Melník, J. Moncol, *Inorg. Chem. Comm.* **2000**, 3, 262–266.
201. D. Chatterjee, A. Mitra, A. Sengupta, S. Basak, *Inorg. Chim. Acta* **2005**, 358, 2900–2908.
202. X.-Y. Zhou, N. M. Kostić, *Inorg. Chem.* **1988**, 27, 4402–4408.
203. D. M. L. Goodgame, T. E. Müller, D. J. Williams, *Polyhedron* **1995**, 14, 2557–2559.
204. Z.-S. Bai, Z.-P. Qi, Y. Lu, Q. Yuan, W.-Y. Sun, *Crystal Growth & Design* **2008**, 8, 1924–1931.
205. C. Xie, Z. Zhang, X. Wang, X. Liu, G. Shen, R. Wang, D. Shen, *J. Coord. Chem.* **2004**, 57, 1173–1178.
206. M. K. Tse, S. Bhor, M. Klawonn, C. Döbler, M. Beller, *Tetrahedron Lett.* **2003**, 44, 7479–7483.

207. S. Bhor, M. K. Tse, M. Klawonn, C. Döbler, W. Mägerlein, M. Beller, *Adv. Synth. Catal.* **2004**, 346, 263–267.
208. M. Klawonn, M. K. Tse, S. Bhor, C. Döbler, M. Beller, *J. Mol. Catal. A* **2004**, 218, 13–19.
209. M. K. Tse, C. Döbler, S. Bhor, M. Klawonn, W. Mägerlein, H. Hugl, M. Beller, *Angew. Chem. Int. Ed.* **2004**, 43, 5255–5260.
210. S. Bhor, G. Anilkumar, M. K. Tse, M. Klawonn, C. Döbler, B. Bitterlich, A. Grotevendt, M. Beller, *Org. Lett.* **2005**, 7, 3393–3396.
211. G. Anilkumar, S. Bhor, M. K. Tse, M. Klawonn, B. Bitterlich, M. Beller, *Tetrahedron Asym.* **2005**, 16, 3536–3561.
212. F. Shi, M. K. Tse, M. Beller, *Chem. Asian J.* **2007**, 2, 411–415.
213. V. W. Manner, A. G. DiPasquale, J. M. Mayer, *J. Am. Chem. Soc.* **2008**, 130, 7210–7211.
214. J.-Y. Huang, W. Xu, *Acta Cryst. Sect. E. Struct. Rep. Online* **2006**, 62, o2653.
215. P. Kapoor, A. Pathak, R. Kapoor, P. Venugopalan, M. Corbella, M. Rodriguez, J. Robles, A. Llobet, *Inorg. Chem.* **2002**, 41, 6153–6160.
216. C. Platas-Iglesias, C. Piguet, N. André, J.-C. G. Bünzli, *J. Chem. Soc. Dalton Trans.* **2001**, 3084–3091.
217. G. Müller, B. Schmidt, J. Jiricek, G. Hopfgartner, J. P. Riehl, J.-C. G. Bünzli, C. Piguet, *J. Chem. Soc. Dalton Trans.* **2001**, 2655–2662.
218. P. Espinet, E. García-Orodea, J. A. Miguel, *Inorg. Chem.* **2000**, 39, 3645–3651.
219. W. Rasshoffer, V. M. Müller, F. Vögtle, *Chem. Ber.* **1979**, 112, 2096–2093.
220. A. M. Kirillov, M. Haukka, M. F. C. Guedes da Silva, A. J. L. Pombeiro, *Eur. J. Inorg. Chem.* **2007**, 1556–1565.
221. J.-M. Senegas, G. Bernardinelli, D. Imbert, J.-C. G. Bünzli, P.-Y. Morgantini, J. Weber, C. Piguet, *Inorg. Chem.* **2003**, 42, 4680–4695.
222. R. Birk, U. Grossmann, H. U. Hund, H. J. Berke, *Organomet. Chem.* **1988**, 345, 321–329.
223. T. Yoshida, T. Okano, T. Otsuka, I. Miura, T. Kubota, K. Kafuku, K. Nakatsu, *Inorg. Chim. Acta* **1985**, 100, 7–16.
224. P. Kapoor, A. Pathak, P. Kaur, P. Venugopalan, R. Kapoor, *Trans. Met. Chem.* **2004**, 29, 251–258.
225. M. B. Cingi, A. C. Villa, C. Gastini, M. Nardelli, *Gazz. Chim. Ital.* **1971**, 101, 825–832.
226. T. Glowiak, I. Podgórska, *Inorg. Chim. Acta* **1986**, 125, 83–88.
227. P. H. Rieger, *Electron Spin Resonance – Analysis and Interpretation*, RCS Publishing, Cambridge, **2007**.
228. B. J. Hathaway, D. E. Billing, *Coord. Chem. Rev.* **1970**, 5, 143–207.
229. I. A. Koval, M. Sgobba, M. Huisman, M. Lüken, E. Saint-Aman, P. Gamez, B. Krebs, J. Reedijk, *Inorg. Chim. Acta* **2006**, 359, 4071–4078.
230. S. Thakurta, P. Roy, G. Rosair, C. J. Gómez-García, E. Garribba, S. Mitra, *Polyhedron* **2009**, 28, 695–702.
231. F. Yraola, F. Albericio, M. Corbella, M. Royo, *Inorg. Chim. Acta* **2008**, 361, 2455–2461.
232. A. M. S. Silva, L. M. P. M. Almeida, J. A. S. Cavaleiro, C. Foces-Foces, A. L. Llamas-Saiz, C. Fontenas, N. Jagerovic, J. Elguero, *Tetrahedron* **1997**, 53, 11645–11658.
233. E. Ludwig, U. Schilde, E. Uhlemann, H. Hartl, I. Brüdgam, *Z. Anorg. Allg. Chem.* **1996**, 622, 701–706.
234. B. A. Sweetman, H. Müller-Bunz, P. J. Guiry, *Tetrahedron Lett.* **2005**, 46, 4643–4646.
235. V. Y. Sosnovskikh, B. I. Usachev, A. Y. Sizov, M. A. Barabanov, *Synthesis* **2004**, 6, 942–948.

236. H.-Y. Zhang, K.-Q. Ye, J.-Y. Zhang, Y. Liu, Y. Wang, *Inorg. Chem.* **2006**, 45, 1745–1753.
237. H. V. K. Diyabalanage, K. Ganguly, D. S. Ehler, G. E. Collis, B. L. Scott, A. Chaudhary, A. K. Burrell, T. M. McCleskey, *Angew. Chem. Int. Ed.* **2008**, 47, 7332–7334.
238. S. Steinhäuser, U. Heinz, J. Sander, K. Hegetschweiler, *Z. Anorg. Allg. Chem.* **2004**, 630, 1829–1838.
239. The molecule LOMe<sub>4</sub> exhibits scaffold chirality in the solid state, which is typical for tri-aryl molecules.
240. A. Bencini, D. Gatteschi, *Inorg. Chim. Acta* **1978**, 31, 11–18.
241. D. Reinen, C. Friebel, *Inorg. Chem.* **1984**, 23, 791–798.
242. N. Wei, N. N. Murthy, K. D. Karlin, *Inorg. Chem.* **1994**, 33, 6093–6100.
243. G. Kokoszka, K. D. Karlin, F. Padula, J. Baranowski, C. Goldstein, *Inorg. Chem.* **1984**, 4378–4380.
244. A. W. Addison, H. M. J. Hendriksen, J. Reedijk, L. K. Thompson, *Inorg. Chem.* **1981**, 20, 103–110.
245. Potential of the Cu<sup>II</sup>/Cu<sup>I</sup> redox couple in this compound could not be determined. Presumably the reduction wave is extremely broadened by geometry changes upon reduction. In contrast to the other complexes this change might be hindered anyhow and thus slowed down.
246. C. Furlani, *Coord. Chem. Rev.* **1968**, 3, 141–167.
247. S. E. Manahan, R. T. Iwamoto, *Inorg. Chem.* **1965**, 4, 1409–1413.
248. M. R. Ganapathi, R. Hermann, S. Naumov, O. Brede, *Phys. Chem. Chem. Phys.* **2000**, 2, 4947–4955.
249. A. Jansc , Z. Paksi, N. Jakab, B. Gyurcsik, A. Rockenbauer, T. Gajda, *Dalton Trans.* **2005**, 3187–3194.
250. Z. Paksi, A. Jansc , F. Pacello, N. Nagy, A. Battistone, T. Gajda, *J. Inorg. Biochem.* **2008**, 102, 1700–1710.
251. A. P rez-Cadenas, L. Godino-Salido, R. L pez-Garz n, P. Arranz-Mascar s, D. Guti rrez-Valero, R. Cuesta-Martos, *Trans. Met. Chem.* **2001**, 26, 581–587.
252. E. Bosch, P. Bou, H. Allemann, M. Ros s, *Anal. Chem.* **1996**, 68, 3651–3657.
253. R. C. Pratt, T. D. P. Stack, *J. Am. Chem. Soc.* **2003**, 125, 8716–8717.
254. M. J. S. Dewar, *J. Am. Chem. Soc.* **1952**, 74, 3353–3354.
255. (a) A. T. Balaban, *Rouv. Chim.* **1971**, 16, 725–737; (b) A. T. Balaban, M. T. Caprois, N. Negoita, R. Baican, *Tetrahedron* **1977**, 33, 2249–2253.
256. R. W. Baldock, P. Hudson, A. R. Katritzky, F. J. Soti, *Chem. Soc., Perkin Trans. 1* **1974**, 1422–1427.
257. D. H. Reid, *Tetrahedron* **1958**, 3, 339–352.
258. B. P. Sogo, M. Nakazaki and M. Calvin, *J. Chem. Phys.* **1957**, 26, 1343–1345.
259. (a) A. R. Forrester, J. M. Hay, R. H. Thomson, *Organic Chemistry of Stable Free Radicals*, Academic Press, London, **1968**; (b) G. E. Jeromin, *Tetrahedron Lett.* **2001**, 42, 1863–1865.
260. C. W. M. Kay, R. Bittl, A. Bacher, G. Richter, S. Weber, *J. Am. Chem. Soc.* **2005**, 127, 10780–10781.
261. F. Bordwell, X.-M. Zhang, *Acc. Chem. Res.* **1993**, 26, 510–517.
262. M. D. Ward, J. A. McCleverty *J. Chem. Soc., Dalton Trans.* **2002**, 275–288.
263. C. F. Koelsch, J. A. Antes, *J. Org. Chem.* **1941**, 6, 558–565.
264. (a) K. L. Kunze, J. R. de la Vega, *J. Am. Chem. Soc.* **1984**, 106, 6528–6537; (b) D. Kuwahara, H. Koyano, T. Manaka, H. Nakamura, T. Mochida, T. Sugawara, *J. Phys. Chem. A* **2006**, 110, 13731–13735; (c) C. Engdahl, A. Gogoll, U. Edlund, *Magn. Reson.*

- Chem.* **1991**, 29, 54–62; (d) L. M. Jackman, J. C. Trewella, R. C. Haddon, *J. Am. Chem. Soc.* **1980**, 2519–2525, (e) D.-P. Wang, S.-G. Chen, D.-Z. Chen, *J. Photochem. Photobiol. A* **2004**, 162, 407–414; (f) R. Rossetti, R. Rayford, R. C. Haddon, L. E. Brus, *J. Am. Chem. Soc.* **1981**, 103, 4303–4307; (g) J. Rodríguez, *J. Comput. Chem.* **1994**, 15, 183–189; (h) H. Nakai, K. Sodeyama, *J. Mol. Struct. (Theochem.)* **2003**, 637, 27–35; (i) C. Müller, J. Schroeder, J. Troe, *J. Phys. Chem. B* **2006**, 110, 19820–19832; (j) C. Svensson, S. C. Abrahams, J. L. Bernstein, R. C. Haddon, *J. Am. Chem. Soc.* **1979**, 101, 5759–5764; (k) H. Nakai, K. Sodeyama, *Chem. Phys. Lett.* **2002**, 365, 203–210; (l) A. Kovács, V. Izvekov, K. Zauer, K. Ohta, *J. Phys. Chem. A* **2001**, 105, 5000–5009.
265. (a) R. Rossetti, R. C. Haddon, L. E. Brus, *J. Am. Chem. Soc.* **1980**, 102, 6913–6916; (b) R. Wehrich, M. H. Limage, S. F. Parker, F. Fillaux, *J. Mol. Struct.* **2004**, 700, 147–149.
266. X. Chi, M. E. Itkis, F. S. Tham, R. T. Oakley, A. W. Corders, R. C. Haddon, *Int. J. Quantum Chem.* **2003**, 95, 853–865;
267. X. Chi, M. E. Itkis, K. Kirschbaum, A. A. Pinkerton, R. T. Oakley, A. W. Cordes, R. C. Haddon, *J. Am. Chem. Soc.* **2001**, 123, 4041–4048;
268. S. K. Pal, M. E. Itkis, F. S. Tham, R. W. Reed, R. T. Oakley, B. Donnadiou, R. C. Haddon, *J. Am. Chem. Soc.* **2007**, 129, 7163–7174;
269. R. S. Brown, A. Tse, T. Nakashima, R. C. Haddon, *J. Am. Chem. Soc.* **1979**, 101, 3157–3162.
270. R. C. Haddon, S. V. Chichester, J. H. Marshall, *Tetrahedron* **1986**, 42, 6293–6300.
271. S. K. Pal, F. S. Tham, R. W. Reed, R. T. Oakley, R. C. Haddon, *Polyhedron* **2005**, 24, 2076–2083.
272. R. Van Deun, P. Nockemann, P. Fias, K. Van Hecke, L. Van Meervelt, K. Binnemans, *Chem. Commun.* **2005**, 590–592.
273. R. Van Deun, P. Fias, P. Nockemann, K. Van Hecke, L. Van Meervelt, K. Binnemans, *Inorg. Chem.* **2006**, 45, 10416–10418.
274. R. Neidlein, Z. Behzadi, *Chemiker-Zeitung* **1976**, 100, 388–389.
275. T. Mochida, R. Torigoe, T. Koinuma, C. Asano, T. Satou, K. Koike, T. Nikaido, *Eur. J. Inorg. Chem.* **2006**, 558–565.
276. S. K. Mandal, S. Samanta, M. E. Itkis, D. W. Jensen, R. W. Reed, R. T. Oakley, F. S. Tham, B. Donnadiou, R. C. Haddon, *J. Am. Chem. Soc.* **2006**, 128, 1982–1994.
277. *Gmelins Handbuch der anorganischen Chemie*, Verlag Chemie, Weinheim, **1975**, p. 152 .
278. J. Iball, C. H. Morgan, *Acta Cryst.* **1967**, 23, 239–244.
279. H. Montgomery, E. C. Lingafaelter, *Acta Cryst.* **1964**, 17, 1481–1482.
280. A. A. Tahir, M. Hamid, M. Zeller, M. Mazhar, A. D. Hunter, *Acta Cryst. Sect E, Struct. Rep. Online* **2007**, 64, m272.
281. G. J. Bullen, R. Mason, P. Pauling, *Inorg. Chem.* **1965**, 4, 456–462.
282. V. G. Kessler, G. I. Spijksma, G. A. Seisenbaeva, S. Hakansson, D. H. A. Blank, H. J. M. Bouvmeester, *J. Sol-Gel Sci. Technol.* **2006**, 40, 163–179.
283. M. Darensbourg, R. M. Buonomo, J. H. Reibenspies, *Z. Kristallogr.* **1995**, 210, 469–451.
284. M. S. El Fallah, E. Rentschler, A. Caneschi, D. Gatteschi, *Inorg. Chim. Acta* **1996**, 231–235.
285. (a) S. Pinkas, B. L. Silver, I. Laulich, *J. Chem. Phys.* **1967**, 46, 1506–1511; (b) G. T. Behnke, K. Nakamoto, *Inorg. Chem.* **1967**, 6, 433–440; (c) G. T. Behnke, K. Nakamoto, *Inorg. Chem.* **1967**, 6, 440–445.
286. J. P. Muena, M. Villagra, N. J. Costamagna, M. J. Aguirre, *J. Coord. Chem.* **2008**, 61, 479–489.
287. D. Small, V. Zaitsev, Y. Jung, S. V. Rosokha, M. Head-Gordon, J. K. Kochi, *J. Am. Chem. Soc.* **2004**, 126, 13850–13858.

288. (a) C.-C. Lee, S.-W. Liu, Y.-T. Chung, *J. Phys. D: Appl. Phys.* **2010**, 43, 1–7; (b) T. Tsuboi, W. S. Jeon, J. H. Kwon, *Optical Materials* **2009**, 31, 1755–1758; (c) C.-H. Kuo, K.-C. Peng, L.-C. Kuo, K.-H. Yang, J.-H. Lee, M.-K. Leung, K.-H. Hsieh, *Chem. Mater.* **2006**, 18, 4121–4129.
289. (a) S.-H. Jang, J.-W. Park, *Mol. Cryst. Liq. Cryst.* **2007**, 471, 269–277; (b) Z. Guo, Z. Dong, R. Zhu, S. Jin, B. Liu, *Spectrochim. Acta Part A* **2007**, 68, 337–340.
290. T. Inazu, *J. Am. Chem. Soc.* **1966**, 39, 1065–1066.
291. D. Jakubke, *Chem. Ber.* **1957**, 6–10.
292. A. Klein, A. Kaiser, B. Sarkar, M. Wanner, J. Fiedler, *Eur. J. Inorg. Chem.* **2007**, 965–976.
293. T. Scheiring, J. Fiedler, W. Kaim, *Organometallics* **2001**, 20, 1437–1441.
294. R. J. Forster, L. R. Faulkner, *Langmuir* **1995**, 11, 1014–1023.
295. (a) A. Corsini, E. J. Billo, *J. Inorg. Nucl. Chem.* **1970**, 32, 1241–1247; (b) A. Corsini, E. J. Billo, *J. Inorg. Nucl. Chem.* **1970**, 32, 1249–1255; (c) P. Huszthy, Z. Köntös, B. Vermes, Á. Pintér, *Tetrahedron* **2001**, 57, 4967–4975.
296. K. Gleu, S. Nitzsche, *Journal fuer Praktische Chemie* **1939**, 153, 200–224.
297. C. Wolf, S. Liu, X. Mei, A. T. August, M. D. Casimir, *J. Org. Chem.* **2006**, 71, 3270–3273.
298. G. Speiser, A. M. Whalen, J. Csihony, C. G. Pierpont, *Inorg. Chem.* **1995**, 34, 1355–1360.
299. E. Cavalieri, E. Rogan, *Environmental Health Perspectives* **1985**, 64, 69–84.
300. F. Carnovale, T. H. Gan, J. B. Peel, K.-D. Franz, *Tetrahedron* **1979**, 35, 129–133.
301. K. Nakasuji, K. Yoshida, I. Murata, *Chem. Lett.* **1982**, 969–970.
302. N. Katajima, K. Whang, Y. Moro-Oka, A. Uchida, Y. Sasada, *J. Chem. Soc. Chem. Commun.* **1986**, 1504–1505.
303. E. Saint-Aman, S. Ménage, J.-L. Pierre, E. Defrancq, G. Gellon, *New. J. Chem.* **1998**, 22, 393–394.
304. T. Günther, *Dissertation*, Universität zu Köln, **2011**.
305. D. R. Duling, PEST Winsim. *J. Magn. Reson. B* **1994**, 104, 105–110.
306. A. Rodenstein, D. Creutzburg, P. Schmiedel, J. Griebel, L. Hennig, R. Kirmse, *Z. Anorg. Allg. Chem.* **2008**, 634, 2811–2818.
307. J. Tedim, S. Patrício, R. Bessada, R. Morais, C. Sousa, M. B. Marques, C. Freire, *Eur. J. Inorg. Chem.* **2006**, 3425–3433.
308. F. Franceschi, M. Guardigli, E. Solari, C. Floriani, A. Chiesi-Villa, C. Rizzoli, *Inorg. Chem.* **1997**, 36, 4099–4107.
309. J. M. Hawkins, K. B. Sharpless, *Tetrahedron Lett.* **1987**, 28, 2825–2828.
310. F. Renaud, C. Piguet, G. Bernardinelli, J.-C. G. Bünzli, G. Hopfgartner, *J. Am. Chem. Soc.* **1999**, 121, 9326–9342.
311. R. Castarlenas, M. A. Esteruelas, E. Onate, *Organometallics* **2007**, 26, 3082–3084.
312. M. Melnik, C. E. Holloway, *J. Coord. Chem.* **1999**, 49, 69–73.
313. R. M. Gauvin, J. A. Osborn, J. Kress, *Organometallics* **2000**, 19, 2944–2946.
314. E. Gómez, V. Santes, V. de la Luz, N. Farfán, *J. Organomet. Chem.* **2001**, 622, 54–60.
315. K. V. Zaitsev, M. V. Bermeshev, S. S. Karlov, Y. F. Oprunenko, A. V. Churakov, J. A. K. Howard, G. S. Zaitseva, *Inorg. Chim. Acta* **2007**, 360, 2507–2512.
316. R. Fandos, B. Gallego, A. Otero, A. Rodriguez, M. J. Ruiz, P. Terreros, C. Pastor, *Organometallics* **2007**, 26, 2896–2903.
317. R. J. Fites, A. T. Yeager, T. L. Sarvela, W. A. Howard, G. Zhu, K. Pang, *Inorg. Chim. Acta* **2006**, 359, 248–256.
318. J. M. Berg, R. H. Holm, *Inorg. Chem.* **1983**, 22, 1768–1771.
319. C. Boskovic, W. Wernsdorfer, K. Folting, J. C. Huffman, D. N. Hendrickson, G. Christou, *Inorg. Chem.* **2002**, 41, 5107–5118.

320. J. Yoo, E. K. Brechin, A. Yamaguchi, M. Nakano, J. C. Huffman, A. L. Maniero, L.-C. Brunel, K. Awaga, H. Ishimoto, G. Christou, D. N. Hendrickson, *Inorg. Chem.* **2000**, 39, 3615–3623.
321. E. K. Brechin, J. Yoo, M. Nakano, J. C. Huffman, D. N. Hendrickson, G. Christou, *Chem. Commun.* **1999**, 783–784.
322. V. T. Yilmaz, S. Guney, O. Andac, W. T. A. Harrison, *J. Coord. Chem.* **2003**, 56, 21–32.
323. O. Andac, S. Guney, Y. Topcu, V. T. Yilmaz, W. T. A. Harrison, *Acta Cryst. Sect. C* **2002**, 58, m17–m20.
324. (a) S. Winter, W. Seichter, E. Weber, *J. Coord. Chem.* **2004**, 57, 997–1014; (b) S. Winter, W. Seichter, E. Weber, *Z. Anorg. Allg. Chem.* **2004**, 630, 434–442.
325. M. Koman, M. Melnik, *Polyhedron* **1997**, 16, 2721–2726.
326. M. Melnik, M. Koman, L. Macaskova, T. Glowiak, R. Grobelny, J. Mrozinsky, *J. Coord. Chem.* **1998**, 43, 159–167.
327. M. Melnik, C. E. Holloway, *J. Coord. Chem.* **1999**, 49, 69–73.
328. A. K. Gupta, J. Kim, *Acta Crystallogr. Sect. C* **2003**, 59, m262–m264.
329. J. A. Davies, F. R. Hartley, *Chem. Rev.* **1981**, 81, 79–90.
330. T. Kawato, H. Koyama, H. Kanatomi, Y. Muramoto, *Inorg. Chim. Acta* **1991**, 183, 107–112.
331. F. D. Rochon, A. L. Beauchamp, C. Bensimon, *Can. J. Chem.* **1996**, 74, 2121–2130.
332. A. Klein, K. Butsch, J. Neudörfl, *Inorg. Chim. Acta* **2010**, doi:10.1016/j.ica.2010.06.011.
333. T. Steiner, *Angew. Chem.* **2002**, 114, 50–80; *Angew. Chem. Int. Ed.* **2002**, 41, 48–76.
334. J. C. Wilson, P. D. Verweij, W. L. Driessen, J. Reedijk, *Inorg. Chim. Acta* **1992**, 192, 219–225.
335. G. J. A. A. Koolhaas, W. L. Driessen, P. J. Van Koningsbruggen, J. Reedijk, A. L. Spek, *J. Chem. Soc. Dalton Trans.* **1993**, 3803–3807.
336. C.-D. Zhang, S.-X. Liu, C.-Y. Sun, F.-J. Ma, Z.-M. Su, *Cryst. Growth Des.* **2009**, 9, 3655–3660.
337. K. Fukui, H. Ohya-Nishiguchi, N. Hirota, K. Aoyagi, H. Ogoshi, *Chem. Phys. Lett.* **1987**, 140, 15–19.
338. (a) A. Bencini, C. Benelli, D. Gatteschi, C. Zanchini, *Inorg. Chem.* **1980**, 19, 1301–1304; (b) A. Bencini, C. Benelli, D. Gatteschi, C. Zanchini, *Inorg. Chem.* **1980**, 19, 3027–3030.
339. I. Morgenstern-Badarau, *Inorg. Chem.* **1984**, 23, 2725–2727.
340. C. Reichardt, *Angew. Chem.* **1965**, 1, 30–40.
341. (a) K. Kojima, J. Matsuda, *Bull. Chem. Soc. Jpn.* **1986**, 59, 859–863; (b) L. I. Katzin, E. Gebert, *J. Am. Chem. Soc.* **1950**, 72, 5464–5471.
342. D. D. Radanović, U. Rychlewska, M. I. Djuran, N. S. Drašković, M. M. Vasojević, I. M. Hodžić, *Polyhedron* **2003**, 22, 2745–2753.
343. S. Elmas, *Neuartige Komplexe von Oxo-Pincer-Liganden mit späten Übergangsmetallen*, Universität zu Köln, **2009**.
344. N. I. Tzerpos, A. K. Zarkadis, R. P. Kreher, L. Repas, M. Lehnig, *J. Chem. Soc., Perkin Trans. 2* **1995**, 755–761.
345. M. M. Whittaker, J. W. Whittaker, *J. Biol. Chem.* **2003**, 278, 22090–22101.
346. Substance details found under “Substance details” in SciFinder®, CAS.
347. R. L. Meline, R. L. Elsenbaum, *J. Chem. Soc., Perkin Trans. 1* **1998**, 2467–2469.
348. J. S. Haynes, S. J. Rettig, J. R. Sams, J. Trotter, R. C. Thompson, *Inorg. Chem.* **1988**, 24, 1237–1241.
349. For *in situ* generation of catalytic active species normally 5 to 10%<sub>mol</sub> catalyst are applied.

350. M. Krejčík, M. Daňek, F. Hartl, *J. Electroanal. Chem.* **1991**, 317, 179–187.
351. (a) G. M. Sheldrick, *Acta Cryst. A* **2008** 112–122 G. M. Sheldrick, SHELX-97, Programs for Crystal Structure Analysis, Göttingen, **1997**; (b) L. J. Farrugia, *J. Appl. Cryst.* **1999**, 32, 837–838.
352. G. M. Sheldrick, SHELXL-97. Program for the Refinement of Crystal Structures. Universität Göttingen, **1997**.
353. (a) STOE X-RED, Data Reduction Program, Version 1.22/Windows, STOE & Cie, Darmstadt, **2001**; (b) STOE X-SHAPE, Crystal Optimisation for Numerical Absorption Correction, Version 1.06/Windows, STOE & Cie, Darmstadt, **1999**.
354. J. Chatt, B. L. Shaw, *J. Chem. Soc.* **1960**, 4, 1718–1729.
355. K. Matsumoto, N. Kotoku, T. Shizuka, R. Tanaka, S. Okeya, *Inorg. Chim. Acta* **2001**, 321, 167–170.
356. K. Nakamoto, P. J. McCarthy, A. Ruby, A. E. Martell, *J. Am. Chem. Soc.* **1961**, 83, 1066–1072.
357. J. Pavlinac, M. Zupan, S. Stavber, *Org. Biomol. Chem.* **2007**, 5, 699–707.
358. R. C. Haddon, R. Rayford, A. M. Hirani, *J. Org. Chem.* **1981**, 46, 4587–4588.
359. G. Radau, R. Büllsbach, P. Pachaly, *Tetrahedron* **1996**, 52, 14735–14744.



# 11.0 Appendix

Table A1: Crystal data and structure refinement for pydicOIPh

empirical formula	$C_{19}H_{11}I_2NO_4$	
formula weight	571.09	
temperature	293(2) K	
wavelength	0.71073 Å	
crystal system	orthorhombic	
space group	<i>Pbca</i> (No. 61)	
unit cell dimensions	a = 13.520(5) Å	$\alpha = 90^\circ$
	b = 14.455(5) Å	$\beta = 90^\circ$
	c = 19.496(5) Å	$\gamma = 90^\circ$
volume	3810(2) Å <sup>3</sup>	
Z	8	
density (calculated)	1.991 g cm <sup>-3</sup>	
absorption coefficient	3.325 mm <sup>-1</sup>	
F(000)	2160	
crystal size	0.5 x 0.6 x 1.0 mm <sup>3</sup>	
theta range for data collection	2.31 to 28.21°	
index ranges	-17 < h < 17, -19 < k < 19, -25 < l < 25	
reflections collected	34795	
independent reflections	4654 [R(int) = 0.0939]	
data / restraints / parameters	4654 / 0 / 235	
Goodness-of-fit on F <sup>2</sup>	0.856	
final R indices [I > 2σ(I)]	R1 = 0.0338, wR2 = 0.0431	
R indices (all data)	R1 = 0.1284, wR2 = 0.0514	
largest diff. peak and hole	0.577 and -0.568 e.Å <sup>-3</sup>	

Table A2: Atomic coordinates ( $\times 10^4$ ) and equivalent isotropic displacement parameters (Å<sup>2</sup> × 10<sup>3</sup>) for pydicOIPh. U(eq) is defined as one third of the trace of the orthogonalized U<sup>ij</sup> tensor.

	x	y	z	U(eq)
I(1)	5812(1)	3443(1)	-1589(1)	80(1)
I(2)	4140(1)	-890(1)	2769(1)	82(1)
O(1)	5614(2)	3615(2)	22(1)	46(1)
O(2)	7049(2)	2898(2)	236(2)	50(1)
O(3)	5517(2)	-786(2)	1460(1)	48(1)
O(4)	6804(2)	139(2)	1689(2)	68(1)
N(1)	5991(2)	1449(2)	802(2)	36(1)
C(1)	6141(3)	4385(3)	-222(2)	40(1)
C(2)	6294(3)	4461(3)	-929(3)	48(1)

C(3)	6776(3)	5256(3)	-1164(3)	58(1)
C(4)	7095(3)	5916(4)	-705(3)	67(2)
C(5)	6940(3)	5817(4)	-19(3)	63(1)
C(6)	6457(3)	5057(3)	226(3)	54(1)
C(7)	6168(3)	2880(3)	222(2)	37(1)
C(8)	5535(3)	2079(3)	413(2)	33(1)
C(9)	4566(3)	1983(3)	192(2)	42(1)
C(10)	4048(3)	1198(3)	377(2)	49(1)
C(11)	4512(3)	542(3)	774(2)	44(1)
C(12)	5475(3)	689(3)	975(2)	34(1)
C(13)	6034(3)	12(3)	1419(2)	41(1)
C(14)	5884(3)	-1479(3)	1890(2)	40(1)
C(15)	6658(3)	-2011(3)	1684(3)	52(1)
C(16)	6967(4)	-2751(4)	2086(3)	65(2)
C(17)	6489(4)	-2932(4)	2695(3)	73(2)
C(18)	5707(4)	-2399(3)	2889(2)	66(2)
C(19)	5372(3)	-1652(3)	2496(2)	50(1)

Table A3: Bond lengths [ $\text{\AA}$ ] and angles [ $^\circ$ ] for PydicOIPh

I(1)–C(2)	2.059(5)	C(7)–C(8)	1.488(5)
I(2)–C(19)	2.066(5)	C(8)–C(9)	1.386(5)
O(1)–C(7)	1.356(5)	C(9)–C(10)	1.382(5)
O(1)–C(1)	1.405(5)	C(9)–H(9)	0.9300
O(2)–C(7)	1.192(4)	C(10)–C(11)	1.376(5)
O(3)–C(13)	1.352(5)	C(10)–H(10)	0.9300
O(3)–C(14)	1.396(4)	C(11)–C(12)	1.375(5)
O(4)–C(13)	1.181(5)	C(11)–H(11)	0.9300
N(1)–C(8)	1.337(5)	C(12)–C(13)	1.509(5)
N(1)–C(12)	1.345(5)	C(14)–C(19)	1.392(5)
C(1)–C(2)	1.398(6)	C(14)–C(15)	1.359(6)
C(1)–C(6)	1.375(6)	C(15)–C(16)	1.389(6)
C(2)–C(3)	1.399(6)	C(15)–H(15)	0.9300
C(3)–C(4)	1.378(7)	C(16)–C(17)	1.377(7)
C(3)–H(3)	0.9300	C(16)–H(16)	0.9300
C(4)–C(5)	1.361(7)	C(17)–C(18)	1.362(7)
C(4)–H(4)	0.9300	C(17)–H(17)	0.9300
C(5)–C(6)	1.364(6)	C(18)–C(19)	1.401(6)
C(5)–H(5)	0.9300	C(18)–H(18)	0.9300
C(6)–H(6)	0.9300		
C(7)–O(1)–C(1)	116.0(3)	C(11)–C(10)–C(9)	118.8(4)
C(13)–O(3)–C(14)	117.7(3)	C(11)–C(10)–H(10)	120.6
C(8)–N(1)–C(12)	117.3(3)	C(9)–C(10)–H(10)	120.6
C(2)–C(1)–C(6)	121.7(4)	C(10)–C(11)–C(12)	119.0(4)
C(2)–C(1)–O(1)	118.1(4)	C(10)–C(11)–H(11)	120.5
C(6)–C(1)–O(1)	120.2(4)	C(12)–C(11)–H(11)	120.5
C(1)–C(2)–C(3)	117.1(4)	N(1)–C(12)–C(11)	123.1(4)
C(1)–C(2)–I(1)	120.8(3)	N(1)–C(12)–C(13)	114.4(4)
C(3)–C(2)–I(1)	122.0(4)	C(11)–C(12)–C(13)	122.5(4)
C(4)–C(3)–C(2)	120.1(5)	O(4)–C(13)–O(3)	124.2(4)

C(4)–C(3)–H(3)	119.9	O(4)–C(13)–C(12)	126.6(4)
C(2)–C(3)–H(3)	119.9	O(3)–C(13)–C(12)	109.2(4)
C(3)–C(4)–C(5)	121.2(5)	C(19)–C(14)–C(15)	122.1(4)
C(3)–C(4)–H(4)	119.4	C(19)–C(14)–O(3)	117.5(4)
C(5)–C(4)–H(4)	119.4	C(15)–C(14)–O(3)	120.1(4)
C(4)–C(5)–C(6)	120.1(5)	C(14)–C(15)–C(16)	120.1(5)
C(4)–C(5)–H(5)	119.9	C(14)–C(15)–H(15)	120.0
C(6)–C(5)–H(5)	119.9	C(16)–C(15)–H(15)	120.0
C(5)–C(6)–C(1)	119.7(5)	C(17)–C(16)–C(15)	119.4(5)
C(5)–C(6)–H(6)	120.2	C(17)–C(16)–H(16)	120.3
C(1)–C(6)–H(6)	120.2	C(15)–C(16)–H(16)	120.3
O(2)–C(7)–O(1)	122.8(4)	C(18)–C(17)–C(16)	119.8(5)
O(2)–C(7)–C(8)	125.8(4)	C(18)–C(17)–H(17)	120.1
O(1)–C(7)–C(8)	111.3(3)	C(16)–C(17)–H(17)	120.1
N(1)–C(8)–C(9)	123.0(4)	C(17)–C(18)–C(19)	122.3(5)
N(1)–C(8)–C(7)	114.0(3)	C(17)–C(18)–H(18)	118.8
C(9)–C(8)–C(7)	122.9(4)	C(19)–C(18)–H(18)	118.8
C(10)–C(9)–C(8)	118.7(4)	C(14)–C(19)–C(18)	116.3(4)
C(10)–C(9)–H(9)	120.7	C(14)–C(19)–I(2)	121.6(3)
C(8)–C(9)–H(9)	120.7	C(18)–C(19)–I(2)	122.1(4)

Table A4: Anisotropic displacement parameters ( $\text{\AA}^2 \times 10^3$ ) for pydicOIPh. The anisotropic displacement factor exponent takes the form:  $-2p^2 [ h^2 a^* U^{11} + \dots + 2 h k a^* b^* U^{12} ]$

	U11	U22	U33	U23	U13	U12
I(1)	89(1)	81(1)	70(1)	-17(1)	-3(1)	-18(1)
I(2)	78(1)	88(1)	80(1)	-19(1)	24(1)	2(1)
O(1)	35(2)	35(2)	68(2)	11(2)	-1(1)	-1(2)
O(2)	32(2)	43(2)	74(2)	18(2)	2(2)	-1(2)
O(3)	47(2)	43(2)	54(2)	17(2)	-7(1)	-11(2)
O(4)	60(2)	44(2)	99(3)	24(2)	-31(2)	-18(2)
N(1)	29(2)	37(2)	42(2)	-1(2)	1(2)	3(2)
C(1)	30(3)	32(3)	57(3)	6(2)	-5(2)	3(2)
C(2)	34(3)	38(3)	72(4)	17(2)	-10(2)	-3(2)
C(3)	45(3)	52(3)	78(4)	23(3)	0(3)	-9(3)
C(4)	46(3)	35(3)	120(5)	14(4)	-19(3)	-7(3)
C(5)	54(3)	41(3)	92(4)	-2(3)	-23(3)	-1(3)
C(6)	52(3)	43(3)	69(4)	2(3)	-9(3)	9(3)
C(7)	41(3)	35(3)	36(3)	2(2)	-1(2)	1(2)
C(8)	31(3)	32(2)	37(2)	-1(2)	-2(2)	3(2)
C(9)	42(3)	40(3)	44(3)	7(2)	-4(2)	-2(2)
C(10)	37(3)	49(3)	62(3)	10(2)	-12(3)	-8(3)
C(11)	37(3)	45(3)	51(3)	8(2)	3(2)	-8(2)
C(12)	31(2)	31(3)	39(2)	2(2)	5(2)	-1(2)
C(13)	37(3)	41(3)	45(3)	-1(2)	3(2)	-4(2)
C(14)	41(2)	36(2)	42(2)	9(2)	-1(2)	-2(3)
C(15)	37(3)	60(3)	59(3)	11(3)	5(2)	-8(3)
C(16)	52(3)	59(4)	84(5)	6(3)	-4(3)	8(3)
C(17)	74(4)	64(4)	80(5)	23(3)	-14(4)	0(3)

C(18)	80(4)	70(4)	48(3)	18(3)	-2(3)	-10(4)
C(19)	59(3)	47(3)	44(3)	-1(2)	-1(2)	-13(3)

Table A5: Crystal data and structure refinement for  $[\text{Cu}(\text{OH}_2)_6][(\text{Cu}(\text{pydic})(\mu\text{-Cl})_2)]$ 

empirical formula	$\text{C}_{14}\text{H}_{18}\text{Cl}_2\text{Cu}_3\text{N}_2\text{O}_{14}$	
formula weight	671.73	
temperature	293(2) K	
wavelength	0.71073 Å	
crystal system	triclinic	
space group	$P\bar{1}$ (No. 2)	
unit cell dimensions	$a = 8.185(3)$ Å	$\alpha = 69.01(3)^\circ$
	$b = 9.500(3)$ Å	$\beta = 66.97(3)^\circ$
	$c = 9.682(2)$ Å	$\gamma = 89.04(4)^\circ$
volume	$640.2(3)$ Å <sup>3</sup>	
Z	1	
density (calculated)	$1.742$ gcm <sup>-3</sup>	
absorption coefficient	$2.737$ mm <sup>-1</sup>	
F(000)	329	
crystal size	0.2 x 0.2 x 2.0 mm <sup>3</sup>	
theta range for data collection	2.32 to 28.21°	
index ranges	-10 < h < 10, -12 < k < 12, -12 < l < 12	
reflections collected	7673	
independent reflections	2846 [R(int) = 0.0594]	
data / restraints / parameters	2846 / 0 / 160	
Goodness-of-fit on F <sup>2</sup>	0.902	
final R indices [I > 2σ(I)]	R1 = 0.0533, wR2 = 0.1322	
R indices (all data)	R1 = 0.0937, wR2 = 0.1499	
largest diff. peak and hole	1.710 and -1.147 e.Å <sup>-3</sup>	

Table A6: Atomic coordinates ( $\times 10^4$ ) and equivalent isotropic displacement parameters (Å<sup>2</sup> $\times 10^3$ ) for  $[\text{Cu}(\text{OH}_2)_6][(\text{Cu}(\text{pydic})(\mu\text{-Cl})_2)]$ . U(eq) is defined as one third of the trace of the orthogonalized  $U^{ij}$  tensor.

	x	y	z	U(eq)
Cu(1)	6574(1)	4379(1)	792(1)	25(1)
Cu(2)	0	0	5000	39(1)
Cl(1)	6058(2)	3863(2)	-1065(2)	31(1)
O(1)	8602(6)	6158(5)	-734(4)	29(1)
O(2)	4956(6)	2605(5)	2863(5)	30(1)
O(3)	10536(7)	7836(6)	-744(5)	48(1)
O(4)	4160(7)	1639(6)	5560(5)	41(1)
O(5)	1401(8)	2059(7)	3621(6)	53(2)

O(6)	8327(7)	498(6)	3944(5)	41(1)
N(1)	7315(7)	4728(6)	2318(5)	22(1)
C(1)	5108(9)	2562(8)	4171(6)	29(2)
C(2)	6481(8)	3796(7)	3884(6)	23(1)
C(3)	6894(9)	4064(8)	5029(7)	29(2)
C(4)	8138(9)	5333(9)	4506(7)	35(2)
C(5)	9006(9)	6291(8)	2864(8)	32(2)
C(6)	8545(8)	5918(8)	1780(7)	25(1)
C(7)	9325(8)	6761(8)	-56(7)	26(1)
O(11)	2290(40)	-497(11)	2544(16)	177(13)

Table A7: Bond lengths [ $\text{\AA}$ ] and angles [ $^\circ$ ] for  $[\text{Cu}(\text{OH}_2)_6][(\text{Cu}(\text{pydic})(\mu\text{-Cl})_2)]$ 

Cu(1)–N(1)	1.928(4)	O(4)–C(1)	1.242(7)
Cu(1)–O(2)	2.047(4)	O(6)–Cu(2)#5	1.968(5)
Cu(1)–O(1)	2.045(5)	N(1)–C(6)	1.331(8)
Cu(1)–Cl(1)	2.210(2)	N(1)–C(2)	1.341(7)
Cu(1)–Cl(1)#1	2.693(2)	C(1)–C(2)	1.510(9)
Cu(2)–O(6)#2	1.968(5)	C(2)–C(3)	1.381(8)
Cu(2)–O(6)#3	1.968(5)	C(3)–C(4)	1.40(1)
Cu(2)–O(5)	1.983(6)	C(3)–H(3)	0.9300
Cu(2)–O(5)#4	1.983(6)	C(4)–C(5)	1.401(9)
Cl(1)–Cu(1)#1	2.693(2)	C(4)–H(4)	0.9300
O(1)–C(7)	1.302(7)	C(5)–C(6)	1.396(8)
O(2)–C(1)	1.307(7)	C(5)–H(5)	0.9300
O(3)–C(7)	1.224(8)	C(6)–C(7)	1.522(8)
N(1)–Cu(1)–O(2)	80.8(2)	O(4)–C(1)–O(2)	123.8(6)
N(1)–Cu(1)–O(1)	79.2(2)	O(4)–C(1)–C(2)	121.5(5)
O(2)–Cu(1)–O(1)	159.5(2)	O(2)–C(1)–C(2)	114.6(5)
N(1)–Cu(1)–Cl(1)	172.6(2)	N(1)–C(2)–C(3)	119.4(6)
O(2)–Cu(1)–Cl(1)	101.0(2)	N(1)–C(2)–C(1)	113.0(5)
O(1)–Cu(1)–Cl(1)	98.3(2)	C(3)–C(2)–C(1)	127.6(5)
N(1)–Cu(1)–Cl(1)#1	96.9(2)	C(2)–C(3)–C(4)	118.1(6)
O(2)–Cu(1)–Cl(1)#1	92.0(2)	C(2)–C(3)–H(3)	120.9
O(1)–Cu(1)–Cl(1)#1	94.8(2)	C(4)–C(3)–H(3)	120.9
Cl(1)–Cu(1)–Cl(1)#1	90.26(6)	C(5)–C(4)–C(3)	121.8(6)
O(6)#2–Cu(2)–O(6)#3	180.0	C(5)–C(4)–H(4)	119.1
O(6)#2–Cu(2)–O(5)	90.0(2)	C(3)–C(4)–H(4)	119.1
O(6)#3–Cu(2)–O(5)	90.0(2)	C(4)–C(5)–C(6)	116.4(6)
O(6)#2–Cu(2)–O(5)#4	90.0(2)	C(4)–C(5)–H(5)	121.8
O(6)#3–Cu(2)–O(5)#4	90.0(2)	C(6)–C(5)–H(5)	121.8
O(5)–Cu(2)–O(5)#4	180.0	N(1)–C(6)–C(5)	120.5(6)
Cu(1)–Cl(1)–Cu(1)#1	89.74(6)	N(1)–C(6)–C(7)	113.2(5)
C(7)–O(1)–Cu(1)	116.6(4)	C(5)–C(6)–C(7)	126.2(6)
C(1)–O(2)–Cu(1)	114.0(4)	O(3)–C(7)–O(1)	126.9(5)
C(6)–N(1)–C(2)	123.7(5)	O(3)–C(7)–C(6)	121.1(5)
C(6)–N(1)–Cu(1)	118.6(4)	O(1)–C(7)–C(6)	112.0(6)
C(2)–N(1)–Cu(1)	117.6(4)		

Symmetry transformations used to generate equivalent atoms: #1  $-x+1, -y+1, -z$  #2  $-x+1, -y, -z+1$  #3  $x-1, y, z$  #4  $-x, -y, -z+1$  #5  $x+1, y, z$

Table A8: Anisotropic displacement parameters ( $\text{\AA}^2 \times 10^3$ ) for  $[\text{Cu}(\text{OH}_2)_6][(\text{Cu}(\text{pydic})(\mu\text{-Cl})_2)]$ . The anisotropic displacement factor exponent takes the form:  $-2p^2[h^2a^*2U^{11} + \dots + 2hk a^* b^* U^{12}]$

	U <sup>11</sup>	U <sup>22</sup>	U <sup>33</sup>	U <sup>23</sup>	U <sup>13</sup>	U <sup>12</sup>
Cu(1)	26(1)	31(1)	15(1)	-6(1)	-10(1)	-6(1)
Cu(2)	29(1)	28(1)	50(1)	1(1)	-19(1)	-8(1)
Cl(1)	39(1)	37(1)	25(1)	-17(1)	-18(1)	7(1)
O(1)	31(2)	30(3)	17(2)	-2(2)	-8(2)	-9(2)
O(2)	37(3)	31(3)	19(2)	-3(2)	-13(2)	-9(2)
O(3)	50(3)	46(4)	28(2)	1(2)	-10(2)	-31(3)
O(4)	46(3)	46(3)	20(2)	2(2)	-14(2)	-16(3)
O(5)	54(3)	53(4)	35(3)	9(3)	-24(2)	-23(3)
O(6)	36(3)	41(3)	30(2)	3(2)	-13(2)	-11(3)
N(1)	23(3)	24(3)	19(2)	-6(2)	-10(2)	-3(2)
C(1)	32(3)	34(4)	14(3)	-1(3)	-10(2)	-3(3)
C(2)	24(3)	25(4)	17(3)	-4(2)	-8(2)	0(3)
C(3)	31(3)	37(4)	19(3)	-8(3)	-12(3)	2(3)
C(4)	39(4)	49(5)	26(3)	-18(3)	-19(3)	1(4)
C(5)	31(4)	37(4)	32(3)	-16(3)	-13(3)	-5(3)
C(6)	25(3)	28(4)	24(3)	-9(3)	-11(2)	-1(3)
C(7)	22(3)	33(4)	21(3)	-6(3)	-9(2)	3(3)
O(11)	530(40)	6(5)	78(9)	-13(6)	-204(18)	32(12)

Table A9: Crystal data and structure refinement for  $(\text{HNEt}_3)[(\text{pydicOMe})\text{CuCl}_3]$

empirical formula	$\text{C}_{15}\text{H}_{25}\text{Cl}_3\text{CuN}_2\text{O}_4$	
formula weight	467.26	
temperature	293(2) K	
wavelength	0.71073 $\text{\AA}$	
crystal system	triclinic	
space group	$P\bar{1}$ (No. 2)	
unit cell dimensions	$a = 7.706(5) \text{\AA}$ $b = 10.274(5) \text{\AA}$ $c = 13.666(5) \text{\AA}$	$\alpha = 93.846(5)^\circ$ $\beta = 92.271(5)^\circ$ $\gamma = 107.216(5)^\circ$
volume	1029.1(9) $\text{\AA}^3$	
Z	2	
density (calculated)	1.508 $\text{gcm}^{-3}$	
absorption coefficient	1.471 $\text{mm}^{-1}$	
F(000)	482	
crystal size	0.3 x 0.4 x 0.6 $\text{mm}^3$	
theta range for data collection	2.46 to 28.16 $^\circ$ .	
index ranges	$-9 < h < 10$ $-13 < k < 13$ $-18 < l < 18$	
reflections collected	12430	
independent reflections	4602 [R(int) = 0.1262]	
data / restraints / parameters	4602 / 0 / 235	

Goodness-of-fit on F <sup>2</sup>	0.675
final R indices [I>2sigma(I)]	R1 = 0.0397, wR2 = 0.0544
R indices (all data)	R1 = 0.1468, wR2 = 0.0720
largest diff. peak and hole	0.361 and -0.313 e.Å <sup>-3</sup>

Table A10: Atomic coordinates ( x 10<sup>4</sup>) and equivalent isotropic displacement parameters (Å<sup>2</sup> x 10<sup>3</sup>) for (HNEt<sub>3</sub>)[(pydicOMe)CuCl<sub>3</sub>]. U(eq) is defined as one third of the trace of the orthogonalized U<sup>ij</sup> tensor.

	x	y	z	U(eq)
Cu(1)	11512(1)	3144(1)	2473(1)	34(1)
Cl(1)	9771(2)	885(1)	2423(1)	50(1)
Cl(2)	13549(2)	2627(1)	1499(1)	46(1)
Cl(3)	13088(2)	5441(1)	2703(1)	50(1)
O(1)	12367(4)	2834(3)	4247(2)	44(1)
O(2)	9293(5)	3792(3)	1363(2)	62(1)
O(3)	10703(5)	2311(4)	5551(2)	66(1)
O(4)	7632(4)	5202(3)	1654(2)	54(1)
N(1)	9583(5)	3558(3)	3347(3)	33(1)
N(2)	13087(5)	-550(4)	1898(3)	36(1)
C(1)	11031(6)	2770(4)	4669(3)	38(1)
C(2)	9508(6)	3262(4)	4285(3)	34(1)
C(3)	8144(6)	3462(4)	4868(3)	43(1)
C(4)	6867(7)	3977(5)	4470(4)	51(1)
C(5)	6942(6)	4292(4)	3500(4)	46(1)
C(6)	8328(6)	4067(4)	2965(3)	35(1)
C(7)	8479(6)	4334(4)	1904(4)	42(1)
C(8)	7488(8)	5364(5)	608(4)	75(2)
C(9)	12178(9)	1896(7)	6030(4)	94(2)
C(10)	13157(7)	-863(5)	2952(3)	55(1)
C(11)	14478(9)	270(6)	3587(4)	89(2)
C(12)	14865(6)	-311(4)	1434(3)	41(1)
C(13)	15479(7)	-1556(5)	1271(4)	64(2)
C(14)	11536(6)	-1602(5)	1330(3)	49(1)
C(15)	11290(8)	-1243(5)	307(4)	74(2)

Table A11: Bond lengths [Å] and angles [°] for (HNEt<sub>3</sub>)[(pydicOMe)CuCl<sub>3</sub>]

Cu(1)–N(1)	2.065(4)	C(8)–H(8A)	0.9600
Cu(1)–Cl(2)	2.255(2)	C(8)–H(8B)	0.9600
Cu(1)–Cl(3)	2.305(2)	C(8)–H(8C)	0.9600
Cu(1)–Cl(1)	2.306(2)	C(9)–H(9A)	0.9600
O(1)–C(1)	1.187(5)	C(9)–H(9B)	0.9600
O(2)–C(7)	1.200(5)	C(9)–H(9C)	0.9600
O(3)–C(1)	1.330(5)	C(10)–C(11)	1.496(7)
O(3)–C(9)	1.472(6)	C(10)–H(10A)	0.9700
O(4)–C(7)	1.306(5)	C(10)–H(10B)	0.9700
O(4)–C(8)	1.453(5)	C(11)–H(11A)	0.9600
N(1)–C(6)	1.334(5)	C(11)–H(11B)	0.9600
N(1)–C(2)	1.336(5)	C(11)–H(11C)	0.9600

N(2)–C(12)	1.493(5)	C(12)–C(13)	1.497(6)
N(2)–C(10)	1.499(5)	C(12)–H(12A)	0.9700
N(2)–C(14)	1.500(6)	C(12)–H(12B)	0.9700
N(2)–H(22)	0.90(4)	C(13)–H(13A)	0.9600
C(1)–C(2)	1.499(6)	C(13)–H(13B)	0.9600
C(2)–C(3)	1.398(5)	C(13)–H(13C)	0.9600
C(3)–C(4)	1.360(7)	C(14)–C(15)	1.489(6)
C(3)–H(3)	0.9300	C(14)–H(14A)	0.9700
C(4)–C(5)	1.385(6)	C(14)–H(14B)	0.9700
C(4)–H(4)	0.9300	C(15)–H(15A)	0.9600
C(5)–C(6)	1.384(6)	C(15)–H(15B)	0.9600
C(5)–H(5)	0.9300	C(15)–H(15C)	0.9600
C(6)–C(7)	1.495(6)		
N(1)–Cu(1)–Cl(2)	178.1(2)	H(8B)–C(8)–H(8C)	109.5
N(1)–Cu(1)–Cl(3)	87.3(1)	O(3)–C(9)–H(9A)	109.5
Cl(2)–Cu(1)–Cl(3)	94.45(6)	O(3)–C(9)–H(9B)	109.5
N(1)–Cu(1)–Cl(1)	86.1(1)	H(9A)–C(9)–H(9B)	109.5
Cl(2)–Cu(1)–Cl(1)	92.11(6)	O(3)–C(9)–H(9C)	109.5
Cl(3)–Cu(1)–Cl(1)	172.87(6)	H(9A)–C(9)–H(9C)	109.5
C(1)–O(3)–C(9)	115.3(4)	H(9B)–C(9)–H(9C)	109.5
C(7)–O(4)–C(8)	115.7(4)	C(11)–C(10)–N(2)	112.4(4)
C(6)–N(1)–C(2)	118.8(4)	C(11)–C(10)–H(10A)	109.1
C(6)–N(1)–Cu(1)	119.9(3)	N(2)–C(10)–H(10A)	109.1
C(2)–N(1)–Cu(1)	121.1(3)	C(11)–C(10)–H(10B)	109.1
C(12)–N(2)–C(10)	113.9(4)	N(2)–C(10)–H(10B)	109.1
C(12)–N(2)–C(14)	113.9(3)	H(10A)–C(10)–H(10B)	107.9
C(10)–N(2)–C(14)	110.1(3)	C(10)–C(11)–H(11A)	109.5
C(12)–N(2)–H(22)	109(2)	C(10)–C(11)–H(11B)	109.5
C(10)–N(2)–H(22)	104(2)	H(11A)–C(11)–H(11B)	109.5
C(14)–N(2)–H(22)	105(3)	C(10)–C(11)–H(11C)	109.5
O(1)–C(1)–O(3)	125.5(5)	H(11A)–C(11)–H(11C)	109.5
O(1)–C(1)–C(2)	123.7(4)	H(11B)–C(11)–H(11C)	109.5
O(3)–C(1)–C(2)	110.8(4)	N(2)–C(12)–C(13)	114.7(4)
N(1)–C(2)–C(3)	121.7(5)	N(2)–C(12)–H(12A)	108.6
N(1)–C(2)–C(1)	115.2(4)	C(13)–C(12)–H(12A)	108.6
C(3)–C(2)–C(1)	123.1(4)	N(2)–C(12)–H(12B)	108.6
C(4)–C(3)–C(2)	119.0(5)	C(13)–C(12)–H(12B)	108.6
C(4)–C(3)–H(3)	120.5	H(12A)–C(12)–H(12B)	107.6
C(2)–C(3)–H(3)	120.5	C(12)–C(13)–H(13A)	109.5
C(3)–C(4)–C(5)	119.6(4)	C(12)–C(13)–H(13B)	109.5
C(3)–C(4)–H(4)	120.2	H(13A)–C(13)–H(13B)	109.5
C(5)–C(4)–H(4)	120.2	C(12)–C(13)–H(13C)	109.5
C(6)–C(5)–C(4)	118.4(5)	H(13A)–C(13)–H(13C)	109.5
C(6)–C(5)–H(5)	120.8	H(13B)–C(13)–H(13C)	109.5
C(4)–C(5)–H(5)	120.8	C(15)–C(14)–N(2)	111.8(4)
N(1)–C(6)–C(5)	122.5(4)	C(15)–C(14)–H(14A)	109.3
N(1)–C(6)–C(7)	115.5(4)	N(2)–C(14)–H(14A)	109.3
C(5)–C(6)–C(7)	122.0(5)	C(15)–C(14)–H(14B)	109.3
O(2)–C(7)–O(4)	125.2(5)	N(2)–C(14)–H(14B)	109.3
O(2)–C(7)–C(6)	122.3(5)	H(14A)–C(14)–H(14B)	107.9
O(4)–C(7)–C(6)	112.4(4)	C(14)–C(15)–H(15A)	109.5



O(4)–C(8)–H(8A)	109.5	C(14)–C(15)–H(15B)	109.5
O(4)–C(8)–H(8B)	109.5	H(15A)–C(15)–H(15B)	109.5
H(8A)–C(8)–H(8B)	109.5	C(14)–C(15)–H(15C)	109.5
O(4)–C(8)–H(8C)	109.5	H(15A)–C(15)–H(15C)	109.5
H(8A)–C(8)–H(8C)	109.5	H(15B)–C(15)–H(15C)	109.5

Table A12: Anisotropic displacement parameters ( $\text{\AA}^2 \times 10^3$ ) for  $(\text{HNEt}_3)[(\text{pydicOMe})\text{CuCl}_3]$ . The anisotropic displacement factor exponent takes the form:  $-2p^2[h^2a^*2U^{11} + \dots + 2hk a^* b^* U^{12}]$

	U11	U22	U33	U23	U13	U12
Cu(1)	35(1)	32(1)	37(1)	3(1)	5(1)	15(1)
Cl(1)	44(1)	33(1)	70(1)	0(1)	10(1)	8(1)
Cl(2)	49(1)	40(1)	52(1)	4(1)	19(1)	16(1)
Cl(3)	47(1)	32(1)	74(1)	7(1)	15(1)	14(1)
O(1)	37(2)	61(2)	41(2)	11(2)	5(2)	23(2)
O(2)	88(3)	72(2)	45(2)	7(2)	-4(2)	54(2)
O(3)	61(3)	101(3)	52(2)	43(2)	18(2)	37(2)
O(4)	48(2)	52(2)	72(3)	17(2)	-7(2)	26(2)
N(1)	32(2)	29(2)	35(2)	2(2)	-1(2)	7(2)
N(2)	49(3)	26(2)	35(2)	0(2)	2(2)	14(2)
C(1)	38(3)	37(3)	37(3)	9(2)	2(2)	6(2)
C(2)	29(3)	28(2)	41(3)	0(2)	0(2)	5(2)
C(3)	35(3)	46(3)	46(3)	-5(2)	9(2)	11(2)
C(4)	33(3)	45(3)	73(4)	-12(3)	15(3)	13(3)
C(5)	31(3)	40(3)	67(4)	-7(3)	-2(3)	14(2)
C(6)	32(3)	28(2)	43(3)	-8(2)	-7(2)	11(2)
C(7)	30(3)	30(3)	62(4)	-6(2)	-9(2)	5(2)
C(8)	72(4)	71(4)	85(5)	28(3)	-24(3)	26(3)
C(9)	91(5)	140(6)	76(5)	68(4)	10(4)	57(5)
C(10)	76(4)	63(3)	41(3)	12(3)	13(3)	39(3)
C(11)	136(6)	104(5)	43(4)	-16(3)	-25(4)	68(5)
C(12)	40(3)	40(3)	43(3)	5(2)	9(2)	9(2)
C(13)	54(4)	57(3)	82(4)	0(3)	18(3)	19(3)
C(14)	45(3)	41(3)	56(3)	-6(2)	2(3)	10(2)
C(15)	79(4)	62(4)	68(4)	-13(3)	-28(3)	10(3)

Table A13: Crystal data and structure refinement for  $\text{LOMe}_2$

empirical formula	$\text{C}_{19}\text{H}_{17}\text{NO}_2$	
formula weight	582.67	
temperature	293(2) K	
wavelength	0.71073 $\text{\AA}$	
crystal system	monoclinic	
space group	$Cc$ (No. 9)	
unit cell dimensions	$a = 10.967(2) \text{\AA}$	$\alpha = 90^\circ$
	$b = 22.772(6) \text{\AA}$	$\beta = 120.00(1)^\circ$
	$c = 7.160(2) \text{\AA}$	$\gamma = 90^\circ$
volume	$1548.7(6) \text{\AA}^3$	
Z	2	

density (calculated)	1.250 gcm <sup>-1</sup>
absorption coefficient	0.081 mm <sup>-1</sup>
F(000)	616
crystal size	0.2 x 0.2 x 0.5 mm <sup>3</sup>
theta range for data collection	1.79 to 27.30°.
index ranges	-14 < h < 14 -29 < k < 29 -8 < l < 9
reflections collected	9221
independent reflections	5783 [R(int) = 0.0401]
data / restraints / parameters	5783 / 3 / 534
Goodness-of-fit on F <sup>2</sup>	0.752
final R indices [I>2sigma(I)]	R1 = 0.0297, wR2 = 0.0455
R indices (all data)	R1 = 0.0890, wR2 = 0.0546
absolute structure parameter	-0.1(9)
extinction coefficient	0.0112(4)
largest diff. peak and hole	0.106 and -0.097 e.Å <sup>-3</sup>

Table A14: Atomic coordinates ( x 10<sup>4</sup>) and equivalent isotropic displacement parameters (Å<sup>2</sup>x 10<sup>3</sup>) for LOMe<sub>2</sub>. U(eq) is defined as one third of the trace of the orthogonalized U<sup>ij</sup> tensor.

	x	y	z	U(eq)
O(1)	-9795(2)	3232(1)	-3282(3)	66(1)
O(2)	-4124(2)	997(1)	-946(4)	81(1)
O(3)	-9793(2)	2628(1)	-8286(3)	66(1)
O(4)	-4123(2)	4865(1)	-5946(4)	82(1)
N(1)	-7627(2)	1870(1)	-3473(3)	46(1)
N(2)	-7624(2)	3992(1)	-8475(3)	46(1)
C(007)	-8070(2)	2236(1)	-2467(4)	45(1)
C(008)	-8076(2)	3623(1)	-7475(4)	45(1)
C(009)	-6233(2)	4017(1)	-7764(4)	47(1)
C(010)	-5822(2)	1470(1)	-4065(5)	51(1)
C(011)	-10463(3)	3156(1)	-8700(4)	51(1)
C(012)	-6230(2)	1845(1)	-2763(4)	47(1)
C(013)	-5822(2)	4390(1)	-9071(5)	51(1)
C(014)	-9619(2)	2209(1)	-3288(4)	49(1)
C(015)	-10466(3)	2702(1)	-3699(4)	52(1)
C(016)	-10268(3)	1660(1)	-3713(5)	62(1)
C(017)	-9621(2)	3653(1)	-8291(4)	48(1)
C(018)	-11910(3)	3220(2)	-9499(5)	64(1)
C(019)	-4760(3)	4816(1)	-8135(5)	61(1)
C(020)	-5260(3)	2178(1)	-1024(5)	55(1)
C(021)	-10270(3)	4200(1)	-8721(5)	61(1)
C(022)	-11907(3)	2642(2)	-4498(5)	65(1)
C(023)	-5740(3)	3299(1)	-5057(5)	59(1)
C(024)	-7166(3)	2592(1)	-791(5)	54(1)
C(025)	-4459(4)	5160(1)	-9479(7)	73(1)
C(026)	-4451(3)	702(1)	-4453(7)	72(1)
C(027)	-5258(3)	3686(1)	-6014(5)	56(1)

C(028)	-10629(4)	2107(2)	-8791(7)	73(1)
C(029)	-7163(3)	3266(1)	-5787(5)	55(1)
C(030)	-5741(3)	2560(1)	-49(5)	58(1)
C(031)	-10616(4)	3756(2)	-3794(7)	75(1)
C(032)	-12506(3)	3775(2)	-9891(5)	71(1)
C(033)	-6530(3)	1543(1)	-6298(5)	60(1)
C(034)	-4758(3)	1045(1)	-3141(5)	63(1)
C(035)	-6521(3)	4319(1)	-11292(5)	59(1)
C(036)	-11685(3)	4266(1)	-9485(5)	70(1)
C(037)	-12498(3)	2084(2)	-4887(5)	74(1)
C(038)	-11689(3)	1593(1)	-4495(5)	70(1)
C(039)	-6198(3)	4654(1)	-12606(6)	70(1)
C(040)	-6200(3)	1207(1)	-7614(6)	71(1)
C(041)	-5160(4)	5074(1)	-11647(7)	79(1)
C(042)	-5153(4)	785(1)	-6646(7)	77(1)
C(043)	-2966(5)	594(2)	143(9)	109(1)
C(044)	-2962(6)	5267(2)	-4864(10)	110(2)

Table A15: Bond lengths [ $\text{\AA}$ ] and angles [ $^\circ$ ] for LOMe<sub>2</sub>.

O(1)–C(015)	1.366(3)	C(013)–C(035)	1.387(4)
O(1)–C(031)	1.429(3)	C(013)–C(019)	1.403(3)
O(2)–C(034)	1.368(3)	C(014)–C(015)	1.392(3)
O(2)–C(043)	1.440(4)	C(014)–C(016)	1.394(3)
O(3)–C(011)	1.364(3)	C(015)–C(022)	1.392(4)
O(3)–C(028)	1.431(4)	C(016)–C(038)	1.376(4)
O(4)–C(019)	1.364(3)	C(017)–C(021)	1.391(3)
O(4)–C(044)	1.440(4)	C(018)–C(032)	1.384(4)
N(1)–C(007)	1.342(3)	C(019)–C(025)	1.402(4)
N(1)–C(012)	1.353(3)	C(020)–C(030)	1.375(4)
N(2)–C(009)	1.346(3)	C(021)–C(036)	1.371(4)
N(2)–C(008)	1.348(3)	C(022)–C(037)	1.390(4)
C(007)–C(024)	1.376(3)	C(023)–C(027)	1.374(4)
C(007)–C(014)	1.496(3)	C(023)–C(029)	1.378(3)
C(008)–C(029)	1.384(3)	C(024)–C(030)	1.378(3)
C(008)–C(017)	1.493(3)	C(025)–C(041)	1.359(5)
C(009)–C(027)	1.393(3)	C(026)–C(042)	1.373(5)
C(009)–C(013)	1.490(3)	C(026)–C(034)	1.388(4)
C(010)–C(033)	1.395(4)	C(032)–C(036)	1.372(4)
C(010)–C(034)	1.401(3)	C(033)–C(040)	1.396(4)
C(010)–C(012)	1.488(3)	C(035)–C(039)	1.388(4)
C(011)–C(017)	1.396(3)	C(037)–C(038)	1.367(4)
C(011)–C(018)	1.399(3)	C(039)–C(041)	1.380(5)
C(012)–C(020)	1.390(3)	C(040)–C(042)	1.386(5)
C(015)–O(1)–C(031)	118.7(3)	C(022)–C(015)–C(014)	120.6(3)
C(034)–O(2)–C(043)	118.5(3)	C(038)–C(016)–C(014)	122.6(3)
C(011)–O(3)–C(028)	118.0(2)	C(021)–C(017)–C(011)	117.9(2)
C(019)–O(4)–C(044)	118.5(3)	C(021)–C(017)–C(008)	118.9(2)
C(007)–N(1)–C(012)	118.0(2)	C(011)–C(017)–C(008)	123.2(2)
C(009)–N(2)–C(008)	118.2(2)	C(032)–C(018)–C(011)	120.1(3)

N(1)–C(007)–C(024)	122.6(2)	O(4)–C(019)–C(025)	125.6(3)
N(1)–C(007)–C(014)	114.1(2)	O(4)–C(019)–C(013)	115.5(3)
C(024)–C(007)–C(014)	123.3(2)	C(025)–C(019)–C(013)	118.8(3)
N(2)–C(008)–C(029)	122.2(2)	C(030)–C(020)–C(012)	119.0(2)
N(2)–C(008)–C(017)	114.2(2)	C(036)–C(021)–C(017)	122.5(3)
C(029)–C(008)–C(017)	123.5(2)	C(037)–C(022)–C(015)	119.4(3)
N(2)–C(009)–C(027)	122.2(2)	C(027)–C(023)–C(029)	119.4(3)
N(2)–C(009)–C(013)	115.3(2)	C(007)–C(024)–C(030)	119.2(3)
C(027)–C(009)–C(013)	122.4(2)	C(041)–C(025)–C(019)	120.8(3)
C(033)–C(010)–C(034)	118.6(3)	C(042)–C(026)–C(034)	120.6(3)
C(033)–C(010)–C(012)	118.7(2)	C(023)–C(027)–C(009)	118.8(2)
C(034)–C(010)–C(012)	122.7(3)	C(023)–C(029)–C(008)	119.1(3)
O(3)–C(011)–C(017)	116.2(2)	C(020)–C(030)–C(024)	119.2(3)
O(3)–C(011)–C(018)	124.0(2)	C(036)–C(032)–C(018)	120.5(3)
C(017)–C(011)–C(018)	119.8(2)	C(010)–C(033)–C(040)	121.6(3)
N(1)–C(012)–C(020)	121.9(2)	O(2)–C(034)–C(026)	125.2(3)
N(1)–C(012)–C(010)	115.3(2)	O(2)–C(034)–C(010)	115.0(2)
C(020)–C(012)–C(010)	122.7(2)	C(026)–C(034)–C(010)	119.7(3)
C(035)–C(013)–C(019)	118.6(3)	C(013)–C(035)–C(039)	122.1(3)
C(035)–C(013)–C(009)	119.1(2)	C(021)–C(036)–C(032)	119.2(3)
C(019)–C(013)–C(009)	122.2(3)	C(038)–C(037)–C(022)	121.1(3)
C(015)–C(014)–C(016)	117.6(2)	C(037)–C(038)–C(016)	118.7(3)
C(015)–C(014)–C(007)	123.8(2)	C(041)–C(039)–C(035)	118.1(4)
C(016)–C(014)–C(007)	118.6(2)	C(042)–C(040)–C(033)	118.1(4)
O(1)–C(015)–C(022)	123.6(2)	C(025)–C(041)–C(039)	121.5(3)
O(1)–C(015)–C(014)	115.9(2)	C(026)–C(042)–C(040)	121.3(3)

Table A16: Anisotropic displacement parameters ( $\text{\AA}^2 \times 10^3$ ) for LOMe2. The anisotropic displacement factor exponent takes the form:  $-2p^2[ h^2 a^* 2U^{11} + \dots + 2 h k a^* b^* U^{12} ]$

	U <sup>11</sup>	U <sup>22</sup>	U <sup>33</sup>	U <sup>23</sup>	U <sup>13</sup>	U <sup>12</sup>
O(1)	57(1)	49(1)	84(2)	1(1)	30(1)	13(1)
O(2)	79(1)	74(1)	92(2)	12(1)	43(1)	37(1)
O(3)	58(1)	50(1)	83(2)	-2(1)	30(1)	-12(1)
O(4)	77(1)	76(1)	92(2)	-12(1)	43(1)	-37(1)
N(1)	43(1)	41(1)	56(1)	1(1)	26(1)	2(1)
N(2)	41(1)	42(1)	60(1)	-1(1)	28(1)	-2(1)
C(007)	43(1)	41(1)	50(2)	0(1)	24(1)	5(1)
C(008)	44(1)	41(1)	54(2)	-2(1)	27(1)	-4(1)
C(009)	43(2)	38(1)	66(2)	0(1)	31(1)	-1(1)
C(010)	43(1)	42(2)	72(2)	-4(1)	33(2)	-2(1)
C(011)	49(2)	52(2)	54(2)	-2(1)	26(1)	-4(1)
C(012)	43(2)	36(1)	64(2)	4(1)	29(1)	1(1)
C(013)	48(1)	40(1)	73(2)	3(1)	36(2)	3(1)
C(014)	43(1)	49(2)	60(2)	-1(1)	30(1)	1(1)
C(015)	47(2)	53(2)	57(2)	3(1)	25(1)	6(1)
C(016)	53(2)	59(2)	78(2)	1(2)	36(2)	1(1)
C(017)	44(1)	47(2)	57(2)	-1(1)	28(1)	-2(1)
C(018)	45(2)	81(2)	64(2)	-5(2)	25(2)	-16(2)
C(019)	52(2)	57(2)	84(3)	2(2)	41(2)	-1(1)

C(020)	43(2)	50(2)	69(2)	2(1)	26(2)	4(1)
C(021)	51(2)	60(2)	77(2)	3(2)	36(2)	1(2)
C(022)	45(2)	83(2)	64(2)	4(2)	26(2)	15(2)
C(023)	48(2)	51(2)	68(2)	11(2)	21(2)	1(1)
C(024)	52(2)	52(2)	56(2)	-2(1)	26(2)	7(1)
C(025)	65(2)	55(2)	120(3)	7(2)	62(2)	-5(2)
C(026)	62(2)	57(2)	117(3)	-7(2)	60(2)	6(2)
C(027)	44(2)	49(2)	71(2)	2(1)	25(2)	-1(1)
C(028)	77(2)	55(2)	71(3)	0(2)	25(2)	-20(2)
C(029)	50(2)	54(2)	59(2)	5(2)	26(2)	-7(1)
C(030)	48(2)	47(2)	70(2)	-8(1)	22(2)	-1(1)
C(031)	78(2)	58(2)	79(3)	4(2)	32(2)	27(2)
C(032)	46(2)	96(3)	71(2)	-2(2)	28(2)	3(2)
C(033)	59(2)	52(2)	76(2)	-8(2)	40(2)	-8(1)
C(034)	52(2)	56(2)	88(3)	-2(2)	41(2)	4(1)
C(035)	63(2)	51(2)	74(2)	7(2)	42(2)	7(1)
C(036)	50(2)	77(2)	83(2)	-4(2)	34(2)	9(2)
C(037)	47(2)	98(3)	73(2)	5(2)	28(2)	-6(2)
C(038)	51(2)	75(2)	85(2)	-2(2)	34(2)	-9(2)
C(039)	79(2)	58(2)	89(3)	13(2)	55(2)	10(2)
C(040)	80(2)	63(2)	88(3)	-14(2)	56(2)	-10(2)
C(041)	89(3)	68(2)	108(3)	25(2)	70(3)	17(2)
C(042)	85(2)	63(2)	109(3)	-24(2)	67(2)	-14(2)
C(043)	99(3)	112(3)	110(4)	24(3)	48(3)	57(3)
C(044)	104(3)	113(4)	111(4)	-29(3)	52(3)	-60(3)

Table A17: Crystal data and structure refinement for LOMe<sub>4</sub>

empirical formula	C <sub>21</sub> H <sub>21</sub> NO <sub>4</sub>	
formula weight	351.39	
temperature	298(2) K	
wavelength	0.71073 Å	
crystal system	orthorhombic	
space group	<i>P</i> 2 <sub>1</sub> 2 <sub>1</sub> 2 <sub>1</sub>	
unit cell dimensions	a = 7.043(1) Å	α = 90°
	b = 14.222(3) Å	β = 90°
	c = 18.580(4) Å	γ = 90°
Volume	1861.1(6) Å <sup>3</sup>	
Z	4	
density (calculated)	1.254 gcm <sup>-3</sup>	
absorption coefficient	0.087 mm <sup>-1</sup>	
F(000)	744	
crystal size	0.4 x 0.5 x 0.7 mm <sup>3</sup>	
theta range for data collection	1.80 to 27.00°	
index ranges	-7 < h < 8	
	-18 < k < 18	
	-23 < l < 23	
reflections collected	29269	
independent reflections	2326 [R(int) = 0.1248]	
data / restraints / parameters	2326 / 0 / 249	

Flack x	-1.6441
Goodness-of-fit on $F^2$	0.755
final R indices [ $I > 2\sigma(I)$ ]	R1 = 0.0349, wR2 = 0.0595
R indices (all data)	R1 = 0.1147, wR2 = 0.0738
absolute structure parameter	-1.6(19)
largest diff. peak and hole	0.106 and -0.134 e.Å <sup>-3</sup>

Table A18: Atomic coordinates ( $\times 10^4$ ) and equivalent isotropic displacement parameters ( $\text{Å}^2 \times 10^3$ ) for LOMe<sub>4</sub>. U(eq) is defined as one third of the trace of the orthogonalized  $U^{ij}$  tensor.

	x	y	z	U(eq)
O(1)	7589(4)	4631(2)	2750(1)	88(1)
O(2)	1933(4)	6271(2)	3495(1)	90(1)
O(3)	7572(4)	-341(2)	3440(1)	83(1)
O(4)	2181(4)	-1631(2)	4589(1)	94(1)
N(1)	5809(4)	2298(2)	3836(1)	61(1)
C(1)	5947(5)	4704(2)	3151(2)	65(1)
C(2)	4747(5)	5472(2)	3096(2)	68(1)
C(3)	3150(5)	5512(2)	3514(2)	66(1)
C(5)	2699(5)	4792(2)	3988(2)	69(1)
C(6)	3886(5)	4025(2)	4019(2)	65(1)
C(7)	5546(5)	3952(2)	3610(2)	59(1)
C(8)	6768(5)	3103(2)	3696(2)	62(1)
C(9)	6795(5)	1504(2)	3962(2)	62(1)
C(10)	5630(5)	668(2)	4132(2)	58(1)
C(11)	6007(5)	-240(2)	3873(2)	65(1)
C(12)	7826(6)	-1225(2)	3076(2)	104(1)
C(13)	4816(5)	-982(2)	4037(2)	74(1)
C(14)	3239(5)	-840(2)	4467(2)	69(1)
C(15)	501(6)	-1540(3)	5007(2)	114(2)
C(16)	2827(5)	35(2)	4741(2)	65(1)
C(17)	4022(5)	771(2)	4557(2)	61(1)
C(18)	8768(5)	1490(3)	3948(2)	71(1)
C(19)	9734(5)	2313(3)	3810(2)	77(1)
C(20)	8736(5)	3124(3)	3673(2)	72(1)
C(21)	8154(5)	5430(3)	2332(2)	98(1)
C(4)	2248(8)	7022(3)	3037(3)	104(2)
C(4A)	490(20)	6371(9)	3910(8)	77(4)

Table A19: Bond lengths [ $\text{Å}$ ] and angles [ $^\circ$ ] for LOMe<sub>4</sub>

O(1)–C(1)	1.379(4)	C(12)–H(12A)	0.9600
O(1)–C(21)	1.433(3)	C(12)–H(12B)	0.9600
O(2)–C(4A)	1.283(1)	C(12)–H(12C)	0.9600
O(2)–C(3)	1.378(4)	C(13)–C(14)	1.384(4)
O(2)–C(4)	1.384(5)	C(13)–H(13)	0.9300
O(3)–C(11)	1.372(4)	C(14)–C(16)	1.376(4)
O(3)–C(12)	1.439(3)	C(15)–H(15A)	0.9600
O(4)–C(14)	1.368(4)	C(15)–H(15B)	0.9600

O(4)–C(15)	1.421(4)	C(15)–H(15C)	0.9600
N(1)–C(9)	1.347(3)	C(16)–C(17)	1.385(4)
N(1)–C(8)	1.354(4)	C(16)–H(16)	0.9300
C(1)–C(2)	1.386(4)	C(17)–H(17)	0.9300
C(1)–C(7)	1.398(4)	C(18)–C(19)	1.378(5)
C(2)–C(3)	1.368(4)	C(18)–H(18)	0.9300
C(2)–H(2)	0.9300	C(19)–C(20)	1.374(5)
C(3)–C(5)	1.387(4)	C(19)–H(19)	0.9300
C(5)–C(6)	1.375(4)	C(20)–H(20)	0.9300
C(5)–H(5)	0.9300	C(21)–H(21A)	0.9600
C(6)–C(7)	1.398(4)	C(21)–H(21B)	0.9600
C(6)–H(6)	0.9300	C(21)–H(21C)	0.9600
C(7)–C(8)	1.491(4)	C(4)–H(4A)	0.9600
C(8)–C(20)	1.387(4)	C(4)–H(4B)	0.9600
C(9)–C(18)	1.390(4)	C(4)–H(4C)	0.9600
C(9)–C(10)	1.479(4)	C(4A)–H(4D)	0.9600
C(10)–C(17)	1.389(4)	C(4A)–H(4E)	0.9600
C(10)–C(11)	1.403(4)	C(4A)–H(4F)	0.9600
C(11)–C(13)	1.381(5)		
C(1)–O(1)–C(21)	117.8(3)	C(11)–C(13)–H(13)	119.9
C(4A)–O(2)–C(3)	124.3(7)	C(14)–C(13)–H(13)	119.9
C(4A)–O(2)–C(4)	114.2(7)	O(4)–C(14)–C(16)	124.6(3)
C(3)–O(2)–C(4)	121.4(4)	O(4)–C(14)–C(13)	114.4(3)
C(11)–O(3)–C(12)	117.8(3)	C(16)–C(14)–C(13)	121.0(3)
C(14)–O(4)–C(15)	117.9(3)	O(4)–C(15)–H(15A)	109.5
C(9)–N(1)–C(8)	119.1(3)	O(4)–C(15)–H(15B)	109.5
O(1)–C(1)–C(2)	122.1(3)	H(15A)–C(15)–H(15B)	109.5
O(1)–C(1)–C(7)	116.2(3)	O(4)–C(15)–H(15C)	109.5
C(2)–C(1)–C(7)	121.7(3)	H(15A)–C(15)–H(15C)	109.5
C(3)–C(2)–C(1)	119.5(3)	H(15B)–C(15)–H(15C)	109.5
C(3)–C(2)–H(2)	120.2	C(14)–C(16)–C(17)	117.7(3)
C(1)–C(2)–H(2)	120.2	C(14)–C(16)–H(16)	121.2
C(2)–C(3)–O(2)	121.9(3)	C(17)–C(16)–H(16)	121.2
C(2)–C(3)–C(5)	121.2(3)	C(16)–C(17)–C(10)	123.8(3)
O(2)–C(3)–C(5)	116.8(3)	C(16)–C(17)–H(17)	118.1
C(6)–C(5)–C(3)	118.2(3)	C(10)–C(17)–H(17)	118.1
C(6)–C(5)–H(5)	120.9	C(19)–C(18)–C(9)	119.0(4)
C(3)–C(5)–H(5)	120.9	C(19)–C(18)–H(18)	120.5
C(5)–C(6)–C(7)	123.1(3)	C(9)–C(18)–H(18)	120.5
C(5)–C(6)–H(6)	118.5	C(20)–C(19)–C(18)	119.7(3)
C(7)–C(6)–H(6)	118.5	C(20)–C(19)–H(19)	120.2
C(1)–C(7)–C(6)	116.3(3)	C(18)–C(19)–H(19)	120.2
C(1)–C(7)–C(8)	124.6(3)	C(19)–C(20)–C(8)	119.2(4)
C(6)–C(7)–C(8)	119.1(3)	C(19)–C(20)–H(20)	120.4
N(1)–C(8)–C(20)	121.5(3)	C(8)–C(20)–H(20)	120.4
N(1)–C(8)–C(7)	114.6(3)	O(1)–C(21)–H(21A)	109.5
C(20)–C(8)–C(7)	123.8(3)	O(1)–C(21)–H(21B)	109.5
N(1)–C(9)–C(18)	121.6(4)	H(21A)–C(21)–H(21B)	109.5
N(1)–C(9)–C(10)	115.2(3)	O(1)–C(21)–H(21C)	109.5
C(18)–C(9)–C(10)	123.2(4)	H(21A)–C(21)–H(21C)	109.5
C(17)–C(10)–C(11)	116.5(3)	H(21B)–C(21)–H(21C)	109.5

C(17)–C(10)–C(9)	119.3(3)	O(2)–C(4)–H(4A)	109.5
C(11)–C(10)–C(9)	124.2(3)	O(2)–C(4)–H(4B)	109.5
O(3)–C(11)–C(13)	122.5(3)	H(4A)–C(4)–H(4B)	109.5
O(3)–C(11)–C(10)	116.7(3)	O(2)–C(4)–H(4C)	109.5
C(13)–C(11)–C(10)	120.8(3)	H(4A)–C(4)–H(4C)	109.5
O(3)–C(12)–H(12A)	109.5	H(4B)–C(4)–H(4C)	109.5
O(3)–C(12)–H(12B)	109.5	O(2)–C(4A)–H(4D)	109.5
H(12A)–C(12)–H(12B)	109.5	O(2)–C(4A)–H(4E)	109.5
O(3)–C(12)–H(12C)	109.5	H(4D)–C(4A)–H(4E)	109.5
H(12A)–C(12)–H(12C)	109.5	O(2)–C(4A)–H(4F)	109.5
H(12B)–C(12)–H(12C)	109.5	H(4D)–C(4A)–H(4F)	109.5
C(11)–C(13)–C(14)	120.2(3)	H(4E)–C(4A)–H(4F)	109.5

Table A20: Anisotropic displacement parameters ( $\text{\AA}^2 \times 10^3$ ) for LOMe<sub>4</sub>. The anisotropic displacement factor exponent takes the form:  $-2p^2 [ h^2 a^* 2U^{11} + \dots + 2 h k a^* b^* U^{12} ]$

	U <sup>11</sup>	U <sup>22</sup>	U <sup>33</sup>	U <sup>23</sup>	U <sup>13</sup>	U <sup>12</sup>
O(1)	80(2)	94(2)	90(2)	21(1)	31(2)	7(2)
O(2)	99(2)	71(2)	99(2)	10(2)	7(2)	9(2)
O(3)	82(2)	74(2)	94(2)	-6(1)	32(2)	16(2)
O(4)	103(2)	66(2)	112(2)	7(1)	32(2)	-6(2)
N(1)	58(2)	64(2)	61(2)	-1(1)	0(2)	0(2)
C(1)	62(2)	66(2)	66(2)	-2(2)	12(2)	-5(2)
C(2)	71(3)	64(2)	69(2)	5(2)	8(2)	-7(2)
C(3)	67(2)	59(2)	73(2)	-4(2)	3(2)	-1(2)
C(5)	65(2)	65(2)	77(2)	0(2)	10(2)	-3(2)
C(6)	64(2)	61(2)	68(2)	1(2)	5(2)	-12(2)
C(7)	60(2)	55(2)	61(2)	-1(2)	1(2)	-7(2)
C(8)	63(2)	64(2)	60(2)	-1(2)	0(2)	-5(2)
C(9)	61(2)	67(2)	57(2)	-3(2)	-1(2)	10(2)
C(10)	56(2)	54(2)	62(2)	1(2)	-1(2)	8(2)
C(11)	66(2)	67(2)	64(2)	5(2)	12(2)	12(2)
C(12)	124(4)	80(3)	109(3)	-14(2)	42(3)	30(3)
C(13)	87(3)	55(2)	80(2)	4(2)	14(2)	22(2)
C(14)	78(3)	60(2)	70(2)	10(2)	13(2)	4(2)
C(15)	98(3)	105(3)	139(4)	19(3)	37(3)	-18(3)
C(16)	65(2)	67(2)	64(2)	1(2)	10(2)	12(2)
C(17)	61(2)	65(2)	58(2)	-2(2)	2(2)	12(2)
C(18)	59(2)	81(3)	74(3)	-4(2)	-4(2)	12(2)
C(19)	53(2)	94(3)	84(3)	-9(2)	-7(2)	-5(2)
C(20)	57(2)	78(3)	79(3)	-7(2)	-4(2)	-11(2)
C(21)	83(3)	119(3)	93(3)	35(3)	21(2)	-7(3)
C(4)	120(5)	87(4)	104(4)	12(3)	-4(4)	9(4)
C(4A)	65(10)	69(9)	97(11)	2(8)	23(10)	22(8)

Table A21: Crystal data and structure refinement for [Fe(opo)<sub>3</sub>]

empirical formula	C <sub>39</sub> H <sub>21</sub> FeO <sub>6</sub>
formula weight	641.41



temperature	293(2) K	
wavelength	0.71073 Å	
crystal system	triclinic	
space group	$P\bar{1}$ (No. 2)	
unit cell dimensions	a = 13.282(3) Å b = 16.451(3) Å c = 25.214(4) Å	$\alpha = 98.47(2)^\circ$ $\beta = 103.63(2)^\circ$ $\gamma = 112.28(2)^\circ$
volume	4779(2) Å <sup>3</sup>	
Z	6	
density (calculated)	1.337 gcm <sup>-1</sup>	
absorption coefficient	0.521 mm <sup>-1</sup>	
F(000)	1974	
crystal size	0.4 x 0.4 x 0.6 mm <sup>3</sup>	
theta range for data collection	2.49 to 28.21°	
index ranges	-17 < h < 17 -21 < k < 21 -32 < l < 33	
reflections collected	46307	
independent reflections	21537 [R(int) = 0.3605]	
data / restraints / parameters	21537 / 0 / 1243	
Goodness-of-fit on F <sup>2</sup>	0.630	
final R indices [I > 2σ(I)]	R1 = 0.0965, wR2 = 0.2491	
R indices (all data)	R1 = 0.4443, wR2 = 0.3747	
largest diff. peak and hole	1.620 and -0.492 e.Å <sup>-3</sup>	

Table A22: Atomic coordinates ( $\times 10^4$ ) and equivalent isotropic displacement parameters (Å<sup>2</sup> $\times 10^3$ ) for [Fe(opo)<sub>3</sub>]. U(eq) is defined as one third of the trace of the orthogonalized U<sup>ij</sup> tensor.

	x	y	z	U(eq)
Fe(1)	11397(2)	-442(2)	2714(1)	67(1)
Fe(2)	9081(2)	2386(2)	1295(1)	80(1)
Fe(3)	6914(2)	4629(2)	3832(1)	80(1)
O(1)	11261(10)	195(8)	3392(5)	86(4)
O(2)	10120(10)	-219(7)	2272(5)	73(3)
O(3)	12617(9)	660(6)	2648(5)	69(3)
O(4)	11464(9)	-1106(7)	2012(5)	76(3)
O(5)	12618(9)	-706(8)	3172(5)	86(4)
O(6)	10302(8)	-1622(8)	2762(5)	69(3)
O(7)	10309(9)	2240(8)	1839(6)	82(4)
O(8)	8450(9)	2495(8)	1930(6)	78(3)
O(9)	9996(10)	3733(8)	1520(5)	84(4)
O(10)	7841(10)	2594(9)	787(5)	87(4)
O(11)	9787(9)	2268(10)	686(6)	86(4)
O(12)	8097(10)	1069(9)	979(6)	84(4)
O(13)	6358(10)	3320(8)	3842(5)	77(3)
O(14)	6721(10)	4858(7)	4583(5)	79(3)
O(15)	5329(10)	4448(8)	3494(5)	76(4)

O(16)	6960(10)	4306(8)	3040(6)	87(4)
O(17)	7441(11)	5940(8)	3863(5)	86(4)
O(18)	8519(11)	4885(9)	4143(5)	87(4)
C(1)	9423(16)	27(11)	2457(10)	68(5)
C(2)	8543(18)	50(11)	2019(9)	85(6)
C(3)	7709(19)	244(15)	2134(13)	113(8)
C(4)	7650(20)	415(12)	2702(15)	106(8)
C(5)	6730(20)	557(16)	2861(16)	134(11)
C(6)	6810(40)	680(20)	3431(19)	155(15)
C(7)	7690(30)	730(20)	3840(16)	153(13)
C(8)	8610(30)	632(14)	3733(17)	118(11)
C(9)	9590(30)	689(17)	4152(12)	134(11)
C(10)	10410(20)	576(14)	4004(13)	118(10)
C(11)	10436(19)	311(11)	3459(9)	65(5)
C(12)	9464(17)	232(10)	3026(11)	71(5)
C(13)	8554(17)	415(12)	3152(12)	89(7)
C(14)	13236(12)	733(11)	2334(8)	57(4)
C(15)	14150(15)	1637(11)	2439(7)	70(5)
C(16)	14876(17)	1811(13)	2131(10)	84(6)
C(17)	14722(17)	1142(19)	1703(11)	79(7)
C(18)	15500(40)	1420(30)	1441(14)	220(30)
C(19)	15421(14)	900(20)	1069(16)	169(16)
C(20)	14500(20)	-184(18)	759(7)	118(9)
C(21)	13740(15)	-426(13)	1081(8)	64(5)
C(22)	12844(16)	-1284(15)	961(7)	81(6)
C(23)	12120(14)	-1490(12)	1288(9)	75(5)
C(24)	12227(14)	-825(12)	1745(8)	64(5)
C(25)	13119(12)	52(10)	1878(7)	50(4)
C(26)	13823(12)	213(12)	1527(8)	57(5)
C(27)	12575(16)	-1524(13)	3215(8)	76(5)
C(28)	13655(15)	-1520(12)	3411(9)	92(7)
C(29)	13703(17)	-2299(15)	3451(9)	100(7)
C(30)	12701(18)	-3102(12)	3362(8)	80(6)
C(31)	12789(18)	-3893(17)	3450(10)	108(7)
C(32)	11830(30)	-4691(16)	3355(10)	108(8)
C(33)	10760(20)	-4708(14)	3184(9)	103(7)
C(34)	10654(17)	-3886(13)	3092(7)	69(5)
C(35)	9598(17)	-3872(12)	2924(8)	82(6)
C(36)	9479(13)	-3139(12)	2791(7)	69(5)
C(37)	10482(14)	-2282(12)	2870(7)	65(5)
C(38)	11543(13)	-2313(11)	3087(7)	57(4)
C(39)	11669(16)	-3092(12)	3180(7)	63(5)
C(40)	10544(17)	2325(11)	2379(9)	76(6)
C(41)	11530(14)	2177(11)	2655(8)	64(5)
C(42)	11888(14)	2343(12)	3225(9)	83(6)
C(43)	11327(19)	2645(10)	3576(10)	75(6)
C(44)	11761(17)	2823(13)	4155(8)	85(6)
C(45)	11210(20)	3089(13)	4471(9)	102(7)
C(46)	10170(20)	3128(13)	4201(14)	104(8)
C(47)	9730(20)	2967(12)	3629(10)	79(6)
C(48)	8700(20)	3003(11)	3365(11)	84(6)
C(49)	8287(16)	2839(12)	2812(10)	77(6)

C(50)	8897(17)	2646(11)	2477(10)	77(5)
C(51)	9959(13)	2571(9)	2705(7)	44(4)
C(52)	10310(15)	2727(10)	3285(8)	58(5)
C(53)	9696(13)	4334(15)	1429(7)	67(5)
C(54)	10466(17)	5297(18)	1729(8)	95(7)
C(55)	10252(18)	6068(18)	1690(9)	109(8)
C(56)	9260(20)	5960(15)	1297(10)	96(7)
C(57)	8910(30)	6701(15)	1219(12)	124(9)
C(58)	7880(30)	6540(20)	846(12)	140(11)
C(59)	7180(20)	5700(20)	545(10)	113(8)
C(60)	7400(20)	4902(18)	593(10)	94(7)
C(61)	6566(18)	3970(20)	252(8)	99(7)
C(62)	6771(16)	3235(17)	321(8)	96(7)
C(63)	7773(15)	3308(16)	745(8)	79(6)
C(64)	8627(17)	4217(14)	1039(8)	78(6)
C(65)	8410(17)	5044(18)	1003(8)	87(7)
C(66)	9525(16)	1554(16)	274(8)	72(5)
C(67)	10189(15)	1690(18)	-123(10)	98(7)
C(68)	9960(20)	970(20)	-536(9)	97(7)
C(69)	9125(19)	119(17)	-642(10)	83(6)
C(70)	8990(20)	-560(20)	-1073(9)	85(6)
C(71)	8130(20)	-1390(20)	-1180(10)	111(8)
C(72)	7460(17)	-1531(19)	-810(12)	109(9)
C(73)	7710(30)	-800(20)	-372(10)	106(10)
C(74)	7016(18)	-1040(13)	-22(11)	96(7)
C(75)	7159(17)	-408(18)	420(9)	98(7)
C(76)	8007(14)	484(13)	547(9)	71(5)
C(77)	8659(14)	695(14)	176(8)	62(5)
C(78)	8505(17)	54(17)	-261(10)	77(6)
C(79)	5677(14)	2935(13)	4101(9)	70(5)
C(80)	5059(18)	1952(15)	3906(8)	85(6)
C(81)	4363(18)	1471(14)	4180(12)	103(7)
C(82)	4206(18)	1887(18)	4640(11)	88(6)
C(83)	3470(20)	1360(20)	4878(15)	141(11)
C(84)	3280(20)	1740(20)	5359(16)	142(12)
C(85)	3836(18)	2660(20)	5549(10)	118(8)
C(86)	4604(15)	3244(15)	5302(9)	75(5)
C(87)	5208(16)	4239(14)	5541(8)	78(5)
C(88)	5928(15)	4703(12)	5305(7)	64(5)
C(89)	6086(14)	4328(12)	4804(8)	63(5)
C(90)	5510(13)	3359(12)	4564(8)	58(4)
C(91)	4754(16)	2842(15)	4843(9)	71(5)
C(92)	4762(15)	4333(10)	2975(10)	67(5)
C(93)	3658(15)	4300(11)	2889(9)	71(5)
C(94)	3004(19)	4187(12)	2358(11)	96(7)
C(95)	3346(15)	4118(12)	1889(10)	85(6)
C(96)	2718(18)	3990(15)	1310(12)	114(8)
C(97)	3180(20)	3970(19)	867(12)	150(11)
C(98)	4230(20)	3986(16)	962(10)	121(8)
C(99)	4884(16)	4072(13)	1495(10)	89(6)
C(100)	6024(17)	4086(13)	1578(9)	91(6)
C(101)	6680(15)	4147(12)	2102(8)	75(5)

C(102)	6255(15)	4247(11)	2557(8)	66(5)
C(103)	5157(13)	4253(10)	2512(8)	55(4)
C(104)	4474(15)	4153(12)	1950(9)	76(5)
C(105)	8489(18)	6594(15)	4015(8)	77(5)
C(106)	8584(17)	7476(13)	3926(8)	79(6)
C(107)	9607(18)	8169(13)	4064(8)	85(6)
C(108)	10645(18)	8099(15)	4287(8)	81(6)
C(109)	11730(20)	8822(15)	4416(10)	116(8)
C(110)	12690(20)	8741(17)	4620(10)	133(10)
C(111)	12626(17)	7917(17)	4710(9)	102(7)
C(112)	11602(16)	7200(15)	4606(7)	74(5)
C(113)	11551(19)	6325(18)	4692(8)	96(7)
C(114)	10514(19)	5586(15)	4514(8)	88(6)
C(115)	9414(18)	5596(14)	4278(7)	65(5)
C(116)	9504(14)	6477(13)	4239(7)	62(5)
C(117)	10587(16)	7279(13)	4389(7)	69(5)

Table A23: Bond lengths [ $\text{\AA}$ ] and angles [ $^\circ$ ] for  $[\text{Fe}(\text{opo})_3]$ 

Fe(1)–O(1)	1.95(1)	C(43)–C(52)	1.44(2)
Fe(1)–O(4)	1.98(1)	C(44)–C(45)	1.33(3)
Fe(1)–O(6)	1.98(1)	C(45)–C(46)	1.43(3)
Fe(1)–O(3)	1.98(1)	C(46)–C(47)	1.37(3)
Fe(1)–O(5)	1.99(1)	C(47)–C(52)	1.39(2)
Fe(1)–O(2)	1.99(1)	C(47)–C(48)	1.40(3)
Fe(2)–O(12)	1.97(1)	C(48)–C(49)	1.32(2)
Fe(2)–O(7)	1.98(1)	C(49)–C(50)	1.38(2)
Fe(2)–O(8)	1.99(1)	C(50)–C(51)	1.45(2)
Fe(2)–O(9)	1.99(1)	C(51)–C(52)	1.38(2)
Fe(2)–O(11)	2.00(1)	C(53)–C(64)	1.45(2)
Fe(2)–O(10)	2.01(1)	C(53)–C(54)	1.48(3)
Fe(3)–O(18)	1.94(1)	C(54)–C(55)	1.41(3)
Fe(3)–O(15)	1.96(1)	C(55)–C(56)	1.39(3)
Fe(3)–O(14)	1.97(1)	C(56)–C(65)	1.44(3)
Fe(3)–O(17)	1.98(1)	C(56)–C(57)	1.48(3)
Fe(3)–O(13)	2.00(1)	C(57)–C(58)	1.37(3)
Fe(3)–O(16)	2.01(1)	C(58)–C(59)	1.32(3)
O(1)–C(11)	1.23(2)	C(59)–C(60)	1.46(3)
O(2)–C(1)	1.29(2)	C(60)–C(65)	1.40(3)
O(3)–C(14)	1.26(2)	C(60)–C(61)	1.48(3)
O(4)–C(24)	1.36(2)	C(61)–C(62)	1.36(3)
O(5)–C(27)	1.35(2)	C(62)–C(63)	1.45(3)
O(6)–C(37)	1.25(2)	C(63)–C(64)	1.44(2)
O(7)–C(40)	1.30(2)	C(64)–C(65)	1.50(3)
O(8)–C(50)	1.31(2)	C(66)–C(77)	1.38(2)
O(9)–C(53)	1.23(2)	C(66)–C(67)	1.47(2)
O(10)–C(63)	1.23(2)	C(67)–C(68)	1.34(3)
O(11)–C(66)	1.32(2)	C(68)–C(69)	1.35(3)
O(12)–C(76)	1.29(2)	C(69)–C(70)	1.36(3)
O(13)–C(79)	1.27(2)	C(69)–C(78)	1.40(3)
O(14)–C(89)	1.26(2)	C(70)–C(71)	1.35(3)

O(15)–C(92)	1.29(2)	C(71)–C(72)	1.42(3)
O(16)–C(102)	1.31(2)	C(72)–C(73)	1.39(3)
O(17)–C(105)	1.32(2)	C(73)–C(78)	1.33(3)
O(18)–C(115)	1.24(2)	C(73)–C(74)	1.41(3)
C(1)–C(12)	1.41(2)	C(74)–C(75)	1.33(3)
C(1)–C(2)	1.42(2)	C(75)–C(76)	1.40(2)
C(2)–C(3)	1.34(2)	C(76)–C(77)	1.41(2)
C(3)–C(4)	1.44(3)	C(77)–C(78)	1.33(2)
C(4)–C(13)	1.44(3)	C(79)–C(90)	1.38(2)
C(4)–C(5)	1.46(3)	C(79)–C(80)	1.45(2)
C(5)–C(6)	1.40(4)	C(80)–C(81)	1.37(3)
C(6)–C(7)	1.33(4)	C(81)–C(82)	1.36(3)
C(7)–C(8)	1.37(4)	C(82)–C(83)	1.36(3)
C(8)–C(9)	1.43(3)	C(82)–C(91)	1.41(3)
C(8)–C(13)	1.43(3)	C(83)–C(84)	1.40(4)
C(9)–C(10)	1.31(3)	C(84)–C(85)	1.36(3)
C(10)–C(11)	1.39(3)	C(85)–C(86)	1.44(3)
C(11)–C(12)	1.43(3)	C(86)–C(91)	1.34(2)
C(12)–C(13)	1.44(2)	C(86)–C(87)	1.47(2)
C(14)–C(25)	1.42(2)	C(87)–C(88)	1.30(2)
C(14)–C(15)	1.46(2)	C(88)–C(89)	1.42(2)
C(15)–C(16)	1.35(2)	C(89)–C(90)	1.44(2)
C(16)–C(17)	1.34(3)	C(90)–C(91)	1.44(2)
C(17)–C(18)	1.33(5)	C(92)–C(103)	1.40(2)
C(17)–C(26)	1.46(3)	C(92)–C(93)	1.41(2)
C(18)–C(19)	1.13(5)	C(93)–C(94)	1.36(2)
C(19)–C(20)	1.67(4)	C(94)–C(95)	1.37(2)
C(20)–C(21)	1.42(2)	C(95)–C(96)	1.44(3)
C(21)–C(26)	1.37(2)	C(95)–C(104)	1.45(2)
C(21)–C(22)	1.39(2)	C(96)–C(97)	1.39(3)
C(22)–C(23)	1.39(2)	C(97)–C(98)	1.35(3)
C(23)–C(24)	1.41(2)	C(98)–C(99)	1.37(3)
C(24)–C(25)	1.40(2)	C(99)–C(104)	1.39(2)
C(25)–C(26)	1.41(2)	C(99)–C(100)	1.47(2)
C(27)–C(28)	1.40(2)	C(100)–C(101)	1.37(2)
C(27)–C(38)	1.41(2)	C(101)–C(102)	1.41(2)
C(28)–C(29)	1.33(2)	C(102)–C(103)	1.44(2)
C(29)–C(30)	1.42(2)	C(103)–C(104)	1.44(2)
C(30)–C(39)	1.35(2)	C(105)–C(116)	1.43(2)
C(30)–C(31)	1.39(2)	C(105)–C(106)	1.46(2)
C(31)–C(32)	1.38(3)	C(106)–C(107)	1.32(2)
C(32)–C(33)	1.38(3)	C(107)–C(108)	1.41(2)
C(33)–C(34)	1.46(2)	C(108)–C(117)	1.39(2)
C(34)–C(35)	1.38(2)	C(108)–C(109)	1.40(2)
C(34)–C(39)	1.42(2)	C(109)–C(110)	1.32(3)
C(35)–C(36)	1.35(2)	C(110)–C(111)	1.38(3)
C(36)–C(37)	1.47(2)	C(111)–C(112)	1.35(2)
C(37)–C(38)	1.41(2)	C(112)–C(117)	1.39(2)
C(38)–C(39)	1.40(2)	C(112)–C(113)	1.47(2)
C(40)–C(51)	1.37(2)	C(113)–C(114)	1.36(2)
C(40)–C(41)	1.46(2)	C(114)–C(115)	1.45(2)
C(41)–C(42)	1.35(2)	C(115)–C(116)	1.43(2)

C(42)–C(43)	1.43(2)	C(116)–C(117)	1.45(2)
C(43)–C(44)	1.38(2)		
O(1)–Fe(1)–O(4)	177.6(5)	C(44)–C(43)–C(52)	124.4(18)
O(1)–Fe(1)–O(6)	90.9(5)	C(42)–C(43)–C(52)	116.0(18)
O(4)–Fe(1)–O(6)	87.9(5)	C(45)–C(44)–C(43)	118(2)
O(1)–Fe(1)–O(3)	94.3(5)	C(44)–C(45)–C(46)	119(2)
O(4)–Fe(1)–O(3)	87.2(4)	C(47)–C(46)–C(45)	123(2)
O(6)–Fe(1)–O(3)	172.7(5)	C(46)–C(47)–C(52)	120(2)
O(1)–Fe(1)–O(5)	91.8(5)	C(46)–C(47)–C(48)	123(2)
O(4)–Fe(1)–O(5)	90.3(5)	C(52)–C(47)–C(48)	118(2)
O(6)–Fe(1)–O(5)	86.1(4)	C(49)–C(48)–C(47)	122.4(18)
O(3)–Fe(1)–O(5)	88.5(5)	C(48)–C(49)–C(50)	119(2)
O(1)–Fe(1)–O(2)	87.0(5)	O(8)–C(50)–C(49)	117(2)
O(4)–Fe(1)–O(2)	90.9(5)	O(8)–C(50)–C(51)	120(2)
O(6)–Fe(1)–O(2)	91.2(4)	C(49)–C(50)–C(51)	123(2)
O(3)–Fe(1)–O(2)	94.2(4)	C(40)–C(51)–C(52)	122(2)
O(5)–Fe(1)–O(2)	177.1(5)	C(40)–C(51)–C(50)	124(2)
O(12)–Fe(2)–O(7)	95.1(5)	C(52)–C(51)–C(50)	114(2)
O(12)–Fe(2)–O(8)	94.4(5)	C(51)–C(52)–C(47)	124(2)
O(7)–Fe(2)–O(8)	86.0(5)	C(51)–C(52)–C(43)	121(2)
O(12)–Fe(2)–O(9)	172.9(5)	C(47)–C(52)–C(43)	115(2)
O(7)–Fe(2)–O(9)	91.0(5)	O(9)–C(53)–C(64)	127(2)
O(8)–Fe(2)–O(9)	89.6(5)	O(9)–C(53)–C(54)	120(2)
O(12)–Fe(2)–O(11)	85.9(5)	C(64)–C(53)–C(54)	113(2)
O(7)–Fe(2)–O(11)	90.7(5)	C(55)–C(54)–C(53)	128(2)
O(8)–Fe(2)–O(11)	176.8(5)	C(56)–C(55)–C(54)	119(2)
O(9)–Fe(2)–O(11)	90.4(5)	C(55)–C(56)–C(65)	118(2)
O(12)–Fe(2)–O(10)	87.4(5)	C(55)–C(56)–C(57)	125(2)
O(7)–Fe(2)–O(10)	176.2(6)	C(65)–C(56)–C(57)	117(2)
O(8)–Fe(2)–O(10)	90.9(5)	C(58)–C(57)–C(56)	122(3)
O(9)–Fe(2)–O(10)	86.7(5)	C(59)–C(58)–C(57)	119(3)
O(11)–Fe(2)–O(10)	92.3(5)	C(58)–C(59)–C(60)	125(2)
O(18)–Fe(3)–O(15)	175.7(5)	C(65)–C(60)–C(59)	117(2)
O(18)–Fe(3)–O(14)	93.5(5)	C(65)–C(60)–C(61)	120(2)
O(15)–Fe(3)–O(14)	88.5(5)	C(59)–C(60)–C(61)	122(2)
O(18)–Fe(3)–O(17)	87.2(5)	C(62)–C(61)–C(60)	121(2)
O(15)–Fe(3)–O(17)	88.9(5)	C(61)–C(62)–C(63)	123(2)
O(14)–Fe(3)–O(17)	90.3(5)	O(10)–C(63)–C(64)	127(2)
O(18)–Fe(3)–O(13)	93.4(5)	O(10)–C(63)–C(62)	117(2)
O(15)–Fe(3)–O(13)	90.5(5)	C(64)–C(63)–C(62)	116(2)
O(14)–Fe(3)–O(13)	86.3(5)	C(63)–C(64)–C(53)	118(2)
O(17)–Fe(3)–O(13)	176.6(5)	C(63)–C(64)–C(65)	123(2)
O(18)–Fe(3)–O(16)	90.9(5)	C(53)–C(64)–C(65)	119(2)
O(15)–Fe(3)–O(16)	87.4(5)	C(60)–C(65)–C(56)	120(2)
O(14)–Fe(3)–O(16)	174.7(5)	C(60)–C(65)–C(64)	116(2)
O(17)–Fe(3)–O(16)	92.9(5)	C(56)–C(65)–C(64)	123(2)
O(13)–Fe(3)–O(16)	90.5(5)	O(11)–C(66)–C(77)	126(2)
C(11)–O(1)–Fe(1)	129(1)	O(11)–C(66)–C(67)	117(2)
C(1)–O(2)–Fe(1)	128(1)	C(77)–C(66)–C(67)	117(2)
C(14)–O(3)–Fe(1)	130(1)	C(68)–C(67)–C(66)	118(2)
C(24)–O(4)–Fe(1)	129(1)	C(67)–C(68)–C(69)	126(2)

C(27)–O(5)–Fe(1)	130(1)	C(68)–C(69)–C(70)	120(3)
C(37)–O(6)–Fe(1)	129(1)	C(68)–C(69)–C(78)	112(2)
C(40)–O(7)–Fe(2)	131(1)	C(70)–C(69)–C(78)	128(2)
C(50)–O(8)–Fe(2)	132(1)	C(71)–C(70)–C(69)	119(2)
C(53)–O(9)–Fe(2)	130(1)	C(70)–C(71)–C(72)	118(2)
C(63)–O(10)–Fe(2)	130(1)	C(73)–C(72)–C(71)	118(2)
C(66)–O(11)–Fe(2)	130(1)	C(78)–C(73)–C(72)	127(3)
C(76)–O(12)–Fe(2)	132(1)	C(78)–C(73)–C(74)	121(2)
C(79)–O(13)–Fe(3)	125(1)	C(72)–C(73)–C(74)	112(3)
C(89)–O(14)–Fe(3)	130(1)	C(75)–C(74)–C(73)	119(2)
C(92)–O(15)–Fe(3)	130(1)	C(74)–C(75)–C(76)	121(2)
C(102)–O(16)–Fe(3)	130(1)	O(12)–C(76)–C(75)	118(2)
C(105)–O(17)–Fe(3)	130(1)	O(12)–C(76)–C(77)	125(2)
C(115)–O(18)–Fe(3)	132(1)	C(75)–C(76)–C(77)	118(2)
O(2)–C(1)–C(12)	126(2)	C(78)–C(77)–C(66)	118(2)
O(2)–C(1)–C(2)	113(2)	C(78)–C(77)–C(76)	121(2)
C(12)–C(1)–C(2)	121(2)	C(66)–C(77)–C(76)	122(2)
C(3)–C(2)–C(1)	121(2)	C(77)–C(78)–C(73)	121(2)
C(2)–C(3)–C(4)	122(2)	C(77)–C(78)–C(69)	128(2)
C(13)–C(4)–C(3)	118(2)	C(73)–C(78)–C(69)	110(2)
C(13)–C(4)–C(5)	116(3)	O(13)–C(79)–C(90)	126(2)
C(3)–C(4)–C(5)	125(3)	O(13)–C(79)–C(80)	117(2)
C(6)–C(5)–C(4)	117(3)	C(90)–C(79)–C(80)	117(2)
C(7)–C(6)–C(5)	124(4)	C(81)–C(80)–C(79)	121(2)
C(6)–C(7)–C(8)	122(4)	C(82)–C(81)–C(80)	122(2)
C(7)–C(8)–C(9)	125(4)	C(83)–C(82)–C(81)	118(3)
C(7)–C(8)–C(13)	117(3)	C(83)–C(82)–C(91)	122(2)
C(9)–C(8)–C(13)	118(2)	C(81)–C(82)–C(91)	120(2)
C(10)–C(9)–C(8)	120(3)	C(82)–C(83)–C(84)	122(3)
C(9)–C(10)–C(11)	128(3)	C(85)–C(84)–C(83)	115(3)
O(1)–C(11)–C(10)	120(2)	C(84)–C(85)–C(86)	125(3)
O(1)–C(11)–C(12)	127(2)	C(91)–C(86)–C(85)	117(2)
C(10)–C(11)–C(12)	114(2)	C(91)–C(86)–C(87)	121(2)
C(1)–C(12)–C(11)	119(2)	C(85)–C(86)–C(87)	122(2)
C(1)–C(12)–C(13)	118(2)	C(88)–C(87)–C(86)	118(2)
C(11)–C(12)–C(13)	122(2)	C(87)–C(88)–C(89)	124(2)
C(8)–C(13)–C(4)	122(2)	O(14)–C(89)–C(88)	119(2)
C(8)–C(13)–C(12)	118(2)	O(14)–C(89)–C(90)	122(2)
C(4)–C(13)–C(12)	120(2)	C(88)–C(89)–C(90)	119(2)
O(3)–C(14)–C(25)	128(2)	C(79)–C(90)–C(89)	122(2)
O(3)–C(14)–C(15)	116(2)	C(79)–C(90)–C(91)	121(2)
C(25)–C(14)–C(15)	117(2)	C(89)–C(90)–C(91)	116(2)
C(16)–C(15)–C(14)	122(2)	C(86)–C(91)–C(82)	119(2)
C(17)–C(16)–C(15)	119(2)	C(86)–C(91)–C(90)	122(2)
C(18)–C(17)–C(16)	112(3)	C(82)–C(91)–C(90)	119(2)
C(18)–C(17)–C(26)	122(3)	O(15)–C(92)–C(103)	126(2)
C(16)–C(17)–C(26)	126(2)	O(15)–C(92)–C(93)	115(2)
C(19)–C(18)–C(17)	116(5)	C(103)–C(92)–C(93)	119(2)
C(18)–C(19)–C(20)	133(3)	C(94)–C(93)–C(92)	119(2)
C(21)–C(20)–C(19)	106(2)	C(93)–C(94)–C(95)	125(2)
C(26)–C(21)–C(22)	115(2)	C(94)–C(95)–C(96)	129(2)
C(26)–C(21)–C(20)	121(2)	C(94)–C(95)–C(104)	119(2)

C(22)–C(21)–C(20)	124(2)	C(96)–C(95)–C(104)	112(2)
C(23)–C(22)–C(21)	122(2)	C(97)–C(96)–C(95)	124(2)
C(22)–C(23)–C(24)	121(2)	C(98)–C(97)–C(96)	120(2)
O(4)–C(24)–C(25)	127(2)	C(97)–C(98)–C(99)	121(2)
O(4)–C(24)–C(23)	115(2)	C(98)–C(99)–C(104)	120(2)
C(25)–C(24)–C(23)	118(2)	C(98)–C(99)–C(100)	119(2)
C(24)–C(25)–C(26)	117(2)	C(104)–C(99)–C(100)	121(2)
C(24)–C(25)–C(14)	119(2)	C(101)–C(100)–C(99)	120(2)
C(26)–C(25)–C(14)	124(2)	C(100)–C(101)–C(102)	118(2)
C(21)–C(26)–C(25)	126(2)	O(16)–C(102)–C(101)	113(2)
C(21)–C(26)–C(17)	122(2)	O(16)–C(102)–C(103)	122(2)
C(25)–C(26)–C(17)	113(2)	C(101)–C(102)–C(103)	125(2)
O(5)–C(27)–C(28)	114(2)	C(92)–C(103)–C(102)	123(2)
O(5)–C(27)–C(38)	124(2)	C(92)–C(103)–C(104)	122(2)
C(28)–C(27)–C(38)	123(2)	C(102)–C(103)–C(104)	115(2)
C(29)–C(28)–C(27)	118(2)	C(99)–C(104)–C(103)	121(2)
C(28)–C(29)–C(30)	122(2)	C(99)–C(104)–C(95)	123(2)
C(39)–C(30)–C(31)	121(2)	C(103)–C(104)–C(95)	116(2)
C(39)–C(30)–C(29)	119(2)	O(17)–C(105)–C(116)	124(2)
C(31)–C(30)–C(29)	120(2)	O(17)–C(105)–C(106)	116(2)
C(32)–C(31)–C(30)	122(2)	C(116)–C(105)–C(106)	120(2)
C(31)–C(32)–C(33)	119(2)	C(107)–C(106)–C(105)	120(2)
C(32)–C(33)–C(34)	119(2)	C(106)–C(107)–C(108)	123(2)
C(35)–C(34)–C(39)	120(2)	C(117)–C(108)–C(109)	118(2)
C(35)–C(34)–C(33)	121(2)	C(117)–C(108)–C(107)	119(2)
C(39)–C(34)–C(33)	119(2)	C(109)–C(108)–C(107)	123(2)
C(36)–C(35)–C(34)	122(2)	C(110)–C(109)–C(108)	122(2)
C(35)–C(36)–C(37)	122(2)	C(109)–C(110)–C(111)	119(2)
O(6)–C(37)–C(38)	128(2)	C(112)–C(111)–C(110)	121(2)
O(6)–C(37)–C(36)	118(2)	C(111)–C(112)–C(117)	120(2)
C(38)–C(37)–C(36)	114(2)	C(111)–C(112)–C(113)	121(2)
C(39)–C(38)–C(37)	125(2)	C(117)–C(112)–C(113)	120(2)
C(39)–C(38)–C(27)	115(2)	C(114)–C(113)–C(112)	119(2)
C(37)–C(38)–C(27)	112(2)	C(113)–C(114)–C(115)	125(2)
C(30)–C(39)–C(38)	123(2)	O(18)–C(115)–C(116)	127(2)
C(30)–C(39)–C(34)	120(2)	O(18)–C(115)–C(114)	120(2)
C(38)–C(39)–C(34)	117(2)	C(116)–C(115)–C(114)	113(2)
O(7)–C(40)–C(51)	125(2)	C(115)–C(116)–C(105)	120(2)
O(7)–C(40)–C(41)	117(2)	C(115)–C(116)–C(117)	124(2)
C(51)–C(40)–C(41)	119(2)	C(105)–C(116)–C(117)	116(2)
C(42)–C(41)–C(40)	119(2)	C(108)–C(117)–C(112)	119(2)
C(41)–C(42)–C(43)	123(2)	C(108)–C(117)–C(116)	122(2)
C(44)–C(43)–C(42)	120(2)	C(112)–C(117)–C(116)	119(2)

Table A24: Anisotropic displacement parameters ( $\text{\AA}^2 \times 10^3$ ) for  $[\text{Fe}(\text{opo})_3]$ . The anisotropic displacement factor exponent takes the form:  $-2p^2 [h^2 a^*{}^2 U^{11} + \dots + 2 h k a^* b^* U^{12}]$

	U <sup>11</sup>	U <sup>22</sup>	U <sup>33</sup>	U <sup>23</sup>	U <sup>13</sup>	U <sup>12</sup>
Fe(1)	64(2)	59(2)	75(2)	15(2)	26(1)	23(1)



Fe(2)	71(2)	99(2)	66(2)	20(2)	25(2)	33(2)
Fe(3)	88(2)	91(2)	71(2)	26(2)	20(2)	51(2)
O(1)	70(8)	112(10)	92(10)	26(8)	43(8)	46(8)
O(2)	77(8)	76(8)	76(9)	28(7)	24(7)	40(7)
O(3)	77(8)	47(7)	89(9)	11(7)	43(7)	24(6)
O(4)	53(7)	60(7)	93(10)	3(7)	19(7)	9(6)
O(5)	65(8)	65(8)	108(11)	18(8)	29(7)	9(7)
O(6)	55(7)	62(7)	91(10)	28(7)	19(6)	25(6)
O(7)	86(8)	117(10)	88(11)	48(9)	57(8)	68(8)
O(8)	58(7)	97(9)	73(10)	6(8)	19(7)	36(7)
O(9)	69(8)	79(9)	97(11)	16(8)	9(7)	35(7)
O(10)	90(9)	71(9)	82(11)	12(8)	17(7)	24(8)
O(11)	63(8)	123(11)	78(10)	37(9)	29(7)	39(8)
O(12)	92(9)	85(9)	68(10)	19(8)	36(8)	26(8)
O(13)	86(8)	79(8)	67(9)	9(7)	22(7)	42(7)
O(14)	110(9)	52(7)	80(10)	15(7)	33(8)	40(7)
O(15)	84(9)	92(9)	75(10)	38(8)	33(8)	52(7)
O(16)	73(8)	120(10)	69(10)	19(8)	15(7)	48(7)
O(17)	91(9)	75(9)	108(11)	42(8)	27(8)	48(8)
O(18)	80(9)	71(9)	94(11)	22(8)	4(7)	30(7)
C(1)	66(13)	51(11)	96(18)	34(12)	27(13)	26(9)
C(2)	86(14)	71(13)	103(18)	27(12)	36(14)	33(11)
C(3)	83(16)	118(19)	160(30)	60(20)	32(18)	66(14)
C(4)	91(18)	41(12)	200(30)	46(16)	50(20)	37(11)
C(5)	106(18)	112(19)	250(40)	90(20)	80(20)	82(16)
C(6)	210(40)	100(20)	230(50)	60(30)	160(40)	90(20)
C(7)	220(40)	110(20)	180(40)	80(20)	120(30)	80(30)
C(8)	160(30)	62(13)	190(30)	22(18)	150(30)	62(16)
C(9)	140(30)	110(20)	100(20)	27(18)	20(20)	12(19)
C(10)	110(20)	80(16)	190(30)	45(19)	90(20)	41(14)
C(11)	85(16)	51(11)	52(14)	18(11)	23(13)	19(11)
C(12)	84(14)	45(10)	104(19)	18(12)	65(15)	28(10)
C(13)	68(14)	59(13)	160(20)	46(15)	38(16)	38(11)
C(14)	36(9)	58(12)	63(13)	2(11)	6(9)	17(9)
C(15)	81(12)	57(12)	67(14)	14(11)	30(11)	20(10)
C(16)	100(16)	50(12)	83(18)	16(13)	20(13)	18(11)
C(17)	76(14)	116(19)	74(18)	47(16)	52(13)	47(14)
C(18)	340(60)	250(50)	90(30)	-50(30)	-20(30)	230(50)
C(19)	13(9)	220(30)	280(40)	220(30)	44(15)	4(14)
C(20)	150(20)	250(30)	40(13)	47(17)	59(14)	150(20)
C(21)	60(12)	68(13)	59(14)	-3(11)	8(10)	34(11)
C(22)	79(13)	113(17)	39(12)	-18(12)	8(11)	51(13)
C(23)	63(12)	59(12)	98(17)	17(13)	25(12)	22(10)
C(24)	59(12)	65(13)	53(13)	-5(11)	4(10)	28(11)
C(25)	44(9)	35(9)	67(13)	12(10)	21(9)	12(8)
C(26)	33(9)	58(11)	81(14)	34(11)	24(9)	13(9)
C(27)	65(13)	71(14)	90(15)	22(12)	23(11)	29(11)
C(28)	48(12)	47(12)	160(20)	20(13)	20(12)	10(9)
C(29)	74(14)	79(15)	140(20)	9(15)	31(13)	31(13)
C(30)	87(15)	48(12)	110(18)	27(12)	20(12)	39(12)
C(31)	76(15)	101(18)	150(20)	34(16)	26(14)	43(14)
C(32)	140(20)	87(18)	140(20)	43(16)	65(18)	81(18)

C(33)	150(20)	80(16)	93(18)	23(13)	57(16)	57(15)
C(34)	70(13)	78(14)	70(14)	20(11)	34(11)	36(12)
C(35)	92(16)	65(13)	94(16)	34(12)	62(13)	15(11)
C(36)	46(10)	74(13)	74(14)	24(11)	16(9)	12(10)
C(37)	57(12)	73(13)	79(14)	23(11)	34(10)	35(11)
C(38)	35(9)	52(11)	71(13)	9(10)	11(8)	9(9)
C(39)	69(13)	59(12)	77(14)	29(11)	29(10)	36(11)
C(40)	107(16)	54(11)	55(15)	8(11)	43(13)	13(11)
C(41)	52(10)	73(12)	76(16)	27(12)	20(10)	34(9)
C(42)	45(11)	76(13)	73(16)	20(12)	-22(10)	-6(9)
C(43)	100(16)	39(10)	94(19)	21(12)	60(15)	17(10)
C(44)	113(16)	98(15)	19(13)	-11(12)	4(11)	40(12)
C(45)	150(20)	77(15)	56(16)	-14(12)	29(16)	34(15)
C(46)	150(20)	64(14)	150(30)	32(16)	90(20)	62(15)
C(47)	99(17)	71(14)	59(16)	4(13)	41(14)	22(12)
C(48)	101(17)	59(12)	130(20)	29(14)	85(16)	40(12)
C(49)	91(14)	93(15)	74(16)	18(14)	47(14)	55(12)
C(50)	85(15)	54(11)	75(17)	-3(12)	29(13)	16(10)
C(51)	51(10)	43(9)	36(11)	9(9)	18(9)	15(8)
C(52)	56(11)	50(10)	67(14)	13(10)	41(11)	10(9)
C(53)	29(9)	102(17)	37(11)	13(12)	-2(8)	4(11)
C(54)	69(14)	130(20)	73(16)	34(16)	10(11)	35(16)
C(55)	60(15)	130(20)	87(18)	24(16)	4(13)	0(14)
C(56)	90(16)	61(14)	93(19)	-10(14)	35(14)	-7(14)
C(57)	180(30)	72(16)	150(30)	43(17)	110(20)	39(18)
C(58)	120(20)	170(30)	90(20)	50(20)	-28(16)	60(20)
C(59)	108(19)	180(30)	64(18)	60(20)	17(14)	70(20)
C(60)	104(18)	120(20)	72(17)	59(17)	31(14)	46(17)
C(61)	88(16)	170(30)	51(15)	49(18)	15(12)	60(19)
C(62)	58(13)	140(20)	62(15)	25(15)	1(11)	28(13)
C(63)	58(12)	82(15)	48(13)	5(13)	13(10)	-15(12)
C(64)	96(16)	88(15)	72(15)	47(13)	41(13)	44(14)
C(65)	69(13)	170(20)	52(13)	66(16)	31(11)	67(16)
C(66)	74(13)	105(17)	50(14)	18(13)	24(12)	52(14)
C(67)	59(12)	160(20)	66(17)	42(18)	7(12)	44(14)
C(68)	98(18)	170(30)	32(15)	6(16)	8(13)	78(19)
C(69)	67(14)	92(18)	72(19)	-3(16)	-5(13)	40(14)
C(70)	95(16)	130(20)	55(16)	18(16)	31(13)	70(16)
C(71)	120(20)	140(20)	75(18)	19(18)	1(17)	83(19)
C(72)	73(14)	160(30)	120(20)	100(20)	31(16)	57(15)
C(73)	170(30)	170(30)	49(17)	11(19)	41(18)	150(30)
C(74)	117(17)	61(13)	90(20)	-11(14)	23(15)	41(12)
C(75)	80(14)	140(20)	86(18)	38(17)	48(13)	44(16)
C(76)	41(10)	63(13)	76(16)	9(12)	5(11)	1(10)
C(77)	50(11)	59(12)	61(14)	10(12)	17(10)	9(10)
C(78)	65(13)	71(15)	77(19)	-3(15)	11(13)	27(12)
C(79)	52(11)	60(13)	83(16)	8(12)	16(11)	17(10)
C(80)	87(15)	89(17)	66(15)	-7(13)	2(12)	48(13)
C(81)	79(15)	62(14)	130(20)	14(16)	-10(15)	23(12)
C(82)	70(15)	110(20)	89(19)	7(17)	16(14)	56(15)
C(83)	80(18)	170(30)	210(40)	70(30)	50(20)	74(19)
C(84)	79(17)	100(20)	250(40)	70(20)	60(20)	26(16)

C(85)	69(14)	180(30)	120(20)	40(20)	50(15)	61(17)
C(86)	59(12)	96(17)	85(17)	32(15)	18(12)	49(12)
C(87)	94(14)	88(16)	69(14)	21(13)	20(12)	60(13)
C(88)	88(13)	67(12)	47(13)	9(11)	33(11)	39(10)
C(89)	72(12)	53(12)	63(14)	18(11)	11(10)	32(10)
C(90)	50(10)	67(13)	60(13)	-2(11)	12(10)	37(10)
C(91)	72(13)	72(15)	64(15)	-4(13)	8(12)	42(12)
C(92)	62(12)	47(10)	120(20)	48(12)	47(13)	34(9)
C(93)	72(13)	67(12)	56(14)	8(11)	16(11)	19(10)
C(94)	100(17)	71(13)	130(20)	26(15)	89(18)	15(12)
C(95)	41(11)	82(14)	110(19)	43(13)	6(12)	8(9)
C(96)	73(15)	125(19)	120(20)	45(18)	-3(16)	37(13)
C(97)	90(20)	200(30)	100(20)	70(20)	4(17)	10(18)
C(98)	67(15)	160(20)	85(19)	33(16)	-7(14)	13(14)
C(99)	52(13)	92(15)	82(17)	34(13)	-3(13)	0(10)
C(100)	81(15)	109(16)	86(17)	39(14)	52(13)	23(12)
C(101)	68(12)	97(14)	47(13)	23(12)	17(11)	23(10)
C(102)	61(12)	81(13)	62(14)	32(11)	30(11)	24(10)
C(103)	50(10)	53(10)	73(14)	29(10)	28(10)	24(8)
C(104)	54(12)	92(14)	73(15)	47(12)	9(11)	21(10)
C(105)	90(15)	104(17)	53(13)	26(12)	45(12)	43(14)
C(106)	93(15)	74(13)	105(17)	49(13)	52(13)	50(13)
C(107)	97(15)	70(14)	122(18)	60(13)	49(14)	49(13)
C(108)	90(16)	89(16)	80(15)	20(13)	22(12)	58(14)
C(109)	84(16)	78(16)	130(20)	17(14)	-10(14)	5(14)
C(110)	81(17)	120(20)	140(20)	66(18)	-26(14)	3(15)
C(111)	57(13)	121(19)	102(18)	37(15)	6(11)	19(14)
C(112)	67(13)	110(17)	59(13)	22(12)	23(10)	49(14)
C(113)	90(17)	150(20)	68(15)	29(15)	19(13)	82(16)
C(114)	89(15)	121(18)	72(15)	42(14)	13(12)	65(15)
C(115)	96(15)	69(13)	50(13)	20(11)	18(11)	56(12)
C(116)	54(11)	92(15)	59(12)	33(11)	26(9)	43(11)
C(117)	75(14)	84(14)	63(13)	26(11)	14(10)	51(12)

Table A25: Crystal data and structure refinement for [(Me<sub>2</sub>salF<sub>4</sub>)Cu]

empirical formula	C <sub>22</sub> H <sub>20</sub> CuF <sub>4</sub> N <sub>2</sub> O <sub>2</sub>	
formula weight	483.94	
temperature	293(2) K	
wavelength	0.71073 Å	
crystal system	monoclinic	
space group	C2 (No. 5)	
unit cell dimensions	a = 19.090(3) Å b = 16.624(3) Å c = 11.362(2) Å	α = 90° β = 101.06(1)° γ = 90°
volume	3539(1) Å <sup>3</sup>	
Z	6	
density (calculated)	1.362 gcm <sup>-3</sup>	
absorption coefficient	0.976 mm <sup>-1</sup>	
F(000)	1482	

crystal size	0.1 x 0.2 x 0.5 mm <sup>3</sup>
theta range for data collection	1.64 to 27.41°
index ranges	-24 < h < 24 -21 < k < 21 -13 < l < 14
reflections collected	23671
independent reflections	7921 [R(int) = 0.0945]
data / restraints / parameters	7921 / 1 / 425
Goodness-of-fit on F <sup>2</sup>	0.610
final R indices [I > 2sigma(I)]	R1 = 0.0477, wR2 = 0.1387
R indices (all data)	R1 = 0.1474, wR2 = 0.1588
absolute structure parameter	-0.02(2)
largest diff. peak and hole	0.298 and -0.103 e.Å <sup>-3</sup>

Table A26: Atomic coordinates ( x 10<sup>4</sup>) and equivalent isotropic displacement parameters (Å<sup>2</sup>x 10<sup>3</sup>) for [(Me<sub>2</sub>salF<sub>4</sub>)Cu]. U(eq) is defined as one third of the trace of the orthogonalized U<sup>ij</sup> tensor.

	x	y	z	U(eq)
Cu(1)	0	7766(1)	10000	91(1)
Cu(2)	197(1)	7992(1)	6733(1)	89(1)
O(1)	667(4)	6946(3)	10056(6)	94(2)
O(2)	1161(3)	7757(4)	7191(5)	102(2)
O(3)	496(3)	9036(4)	6661(5)	100(2)
N(1)	723(4)	8626(4)	10090(7)	89(2)
N(2)	-94(4)	6871(5)	6765(6)	91(2)
N(3)	-818(4)	8267(4)	6314(6)	86(2)
F(1)	1473(3)	5622(4)	10610(5)	127(2)
F(2)	3583(3)	7117(4)	11254(6)	155(2)
F(3)	2574(2)	7647(3)	7451(5)	128(2)
F(4)	2530(3)	4848(3)	7740(6)	144(2)
F(5)	1154(3)	10458(3)	7041(5)	115(2)
F(6)	-1016(3)	11854(3)	6225(6)	144(2)
C(1)	374(4)	9435(5)	9836(7)	85(2)
C(2)	765(5)	10145(5)	10522(8)	100(3)
C(3)	400(4)	10896(5)	10032(8)	107(3)
C(4)	1367(5)	8509(5)	9896(8)	89(2)
C(5)	1756(4)	9106(5)	9257(7)	105(2)
C(6)	1735(4)	7744(5)	10241(7)	93(2)
C(7)	1357(6)	7017(5)	10265(7)	91(2)
C(8)	1819(5)	6359(5)	10595(8)	101(2)
C(9)	2532(6)	6365(6)	10910(8)	112(3)
C(10)	2848(5)	7073(6)	10884(9)	109(3)
C(11)	2494(4)	7768(6)	10544(7)	105(3)
C(12)	-892(5)	6815(6)	6622(8)	98(3)
C(13)	-1232(5)	6063(5)	5937(9)	109(3)
C(14)	-2021(5)	6023(7)	6083(10)	135(4)
C(15)	-2413(5)	6811(6)	5757(9)	117(3)
C(16)	-2012(4)	7543(5)	6321(8)	108(3)
C(17)	-1264(5)	7555(5)	6034(8)	95(3)
C(18)	302(5)	6287(5)	7350(8)	94(3)
C(19)	13(4)	5616(5)	8000(8)	108(2)

C(20)	1079(5)	6316(5)	7406(7)	93(2)
C(21)	1451(5)	7028(6)	7373(8)	99(3)
C(22)	2209(5)	6939(6)	7476(8)	103(2)
C(23)	2569(5)	6240(7)	7607(8)	118(3)
C(24)	2176(6)	5545(6)	7648(8)	114(3)
C(25)	1464(5)	5563(5)	7559(8)	105(3)
C(26)	-1070(4)	8930(6)	5836(7)	89(2)
C(27)	-1741(4)	9036(5)	4914(7)	105(2)
C(28)	-664(4)	9713(6)	6145(7)	94(3)
C(29)	-1017(5)	10421(6)	6038(8)	102(3)
C(30)	-667(5)	11138(6)	6300(9)	114(3)
C(31)	90(5)	11184(5)	6634(8)	107(3)
C(32)	428(4)	10453(6)	6716(7)	99(2)
C(33)	92(5)	9694(6)	6508(7)	94(2)

Table A27: Bond lengths [ $\text{\AA}$ ] and angles [ $^\circ$ ] for  $[(\text{Me}_2\text{salF}_4)\text{Cu}]$ 

Cu(1)–O(1)	1.859(6)	C(6)–C(7)	1.41(1)
Cu(1)–O(1)#1	1.859(6)	C(6)–C(11)	1.42(1)
Cu(1)–N(1)#1	1.975(8)	C(7)–C(8)	1.41(1)
Cu(1)–N(1)	1.975(8)	C(8)–C(9)	1.34(1)
Cu(2)–O(3)	1.834(7)	C(9)–C(10)	1.33(1)
Cu(2)–O(2)	1.855(5)	C(10)–C(11)	1.36(1)
Cu(2)–N(3)	1.957(7)	C(12)–C(17)	1.51(1)
Cu(2)–N(2)	1.947(8)	C(12)–C(13)	1.55(1)
O(1)–C(7)	1.30(1)	C(13)–C(14)	1.55(1)
O(2)–C(21)	1.33(1)	C(14)–C(15)	1.52(1)
O(3)–C(33)	1.33(1)	C(15)–C(16)	1.51(1)
N(1)–C(4)	1.31(1)	C(16)–C(17)	1.52(1)
N(1)–C(1)	1.50(1)	C(18)–C(20)	1.47(1)
N(2)–C(18)	1.33(1)	C(18)–C(19)	1.50(1)
N(2)–C(12)	1.50(1)	C(20)–C(21)	1.95(1)
N(3)–C(26)	1.28(1)	C(20)–C(25)	1.44(1)
N(3)–C(17)	1.46(1)	C(21)–C(22)	1.44(1)
F(1)–C(8)	1.39(1)	C(22)–C(23)	1.34(1)
F(2)–C(10)	1.39(1)	C(23)–C(24)	1.39(1)
F(3)–C(22)	1.370(9)	C(24)–C(25)	1.34(1)
F(4)–C(24)	1.336(9)	C(26)–C(28)	1.52(1)
F(5)–C(32)	1.363(9)	C(26)–C(27)	1.50(1)
F(6)–C(30)	1.36(1)	C(28)–C(29)	1.35(1)
C(1)–C(2)	1.53(1)	C(28)–C(33)	1.42(1)
C(1)–C(1)#1	1.54(2)	C(29)–C(30)	1.37(1)
C(2)–C(3)	1.49(1)	C(30)–C(31)	1.42(1)
C(3)–C(3)#1	1.51(2)	C(31)–C(32)	1.37(1)
C(4)–C(6)	1.47(1)	C(32)–C(33)	1.42(1)
C(4)–C(5)	1.51(1)		
O(1)–Cu(1)–O(1)#1	85.6(4)	C(10)–C(11)–C(6)	118.3(9)
O(1)–Cu(1)–N(1)#1	178.7(3)	C(17)–C(12)–N(2)	112.3(8)
O(1)#1–Cu(1)–N(1)#1	93.5(3)	C(17)–C(12)–C(13)	108.6(7)
O(1)–Cu(1)–N(1)	93.5(3)	N(2)–C(12)–C(13)	115.0(8)

O(1)#1–Cu(1)–N(1)	178.7(3)	C(14)–C(13)–C(12)	107.7(8)
N(1)#1–Cu(1)–N(1)	87.3(4)	C(15)–C(14)–C(13)	112.4(8)
O(3)–Cu(2)–O(2)	84.9(3)	C(16)–C(15)–C(14)	113.9(8)
O(3)–Cu(2)–N(3)	94.0(3)	C(15)–C(16)–C(17)	109.8(8)
O(2)–Cu(2)–N(3)	177.5(3)	N(3)–C(17)–C(12)	111.0(6)
O(3)–Cu(2)–N(2)	177.6(3)	N(3)–C(17)–C(16)	119.8(8)
O(2)–Cu(2)–N(2)	93.7(3)	C(12)–C(17)–C(16)	106.0(7)
N(3)–Cu(2)–N(2)	87.5(3)	N(2)–C(18)–C(20)	118.1(8)
C(7)–O(1)–Cu(1)	127.1(5)	N(2)–C(18)–C(19)	124.2(9)
C(21)–O(2)–Cu(2)	126.6(5)	C(20)–C(18)–C(19)	117.7(8)
C(33)–O(3)–Cu(2)	127.3(6)	C(21)–C(20)–C(25)	119.5(9)
C(4)–N(1)–C(1)	119.8(7)	C(21)–C(20)–C(18)	122.9(8)
C(4)–N(1)–Cu(1)	123.7(6)	C(25)–C(20)–C(18)	117.5(8)
C(1)–N(1)–Cu(1)	111.0(5)	O(2)–C(21)–C(20)	125.6(8)
C(18)–N(2)–C(12)	118.5(8)	O(2)–C(21)–C(22)	119.3(8)
C(18)–N(2)–Cu(2)	124.9(6)	C(20)–C(21)–C(22)	115.0(9)
C(12)–N(2)–Cu(2)	110.1(6)	C(23)–C(22)–F(3)	119.5(9)
C(26)–N(3)–C(17)	116.7(7)	C(23)–C(22)–C(21)	125.8(9)
C(26)–N(3)–Cu(2)	125.3(6)	F(3)–C(22)–C(21)	114.7(8)
C(17)–N(3)–Cu(2)	111.9(5)	C(22)–C(23)–C(24)	117.1(9)
N(1)–C(1)–C(2)	116.0(6)	F(4)–C(24)–C(25)	121(1)
N(1)–C(1)–C(1)#1	110.5(5)	F(4)–C(24)–C(23)	117(1)
C(2)–C(1)–C(1)#1	105.1(6)	C(25)–C(24)–C(23)	121.7(9)
C(3)–C(2)–C(1)	108.1(7)	C(24)–C(25)–C(20)	120.8(9)
C(2)–C(3)–C(3)#1	114.4(6)	N(3)–C(26)–C(28)	120.4(8)
N(1)–C(4)–C(6)	120.1(8)	N(3)–C(26)–C(27)	126.7(9)
N(1)–C(4)–C(5)	123.4(8)	C(28)–C(26)–C(27)	112.9(8)
C(6)–C(4)–C(5)	116.4(8)	C(29)–C(28)–C(33)	120.4(9)
C(7)–C(6)–C(11)	121.3(8)	C(29)–C(28)–C(26)	120.1(8)
C(7)–C(6)–C(4)	121.8(7)	C(33)–C(28)–C(26)	119.4(9)
C(11)–C(6)–C(4)	116.9(8)	C(28)–C(29)–C(30)	121.6(9)
O(1)–C(7)–C(6)	125.5(8)	F(6)–C(30)–C(29)	122.3(9)
O(1)–C(7)–C(8)	122.5(8)	F(6)–C(30)–C(31)	115.5(9)
C(6)–C(7)–C(8)	112.0(9)	C(29)–C(30)–C(31)	122.2(8)
C(9)–C(8)–F(1)	117.6(9)	C(32)–C(31)–C(30)	114.3(8)
C(9)–C(8)–C(7)	128.1(9)	F(5)–C(32)–C(31)	117.0(8)
F(1)–C(8)–C(7)	114.3(8)	F(5)–C(32)–C(33)	117.1(8)
C(10)–C(9)–C(8)	116.4(9)	C(31)–C(32)–C(33)	125.9(8)
C(9)–C(10)–C(11)	123.9(8)	O(3)–C(33)–C(32)	118.6(8)
C(9)–C(10)–F(2)	118.6(8)	O(3)–C(33)–C(28)	125.9(8)
C(11)–C(10)–F(2)	117.5(9)	C(32)–C(33)–C(28)	115.5(9)

Symmetry transformations used to generate equivalent atoms: #1  $-x, y, -z+2$

Table A28: Anisotropic displacement parameters ( $\text{\AA}^2 \times 10^3$ ) for  $[(\text{Me}_2\text{salF}_4)\text{Cu}]$ . The anisotropic displacement factor exponent takes the form:  $-2p^2 [h^2 a^{*2} U^{11} + \dots + 2 h k a^* b^* U^{12}]$

	U11	U22	U33	U23	U13	U12
Cu(1)	91(1)	93(2)	89(1)	0	15(1)	0
Cu(2)	85(1)	97(1)	86(1)	0(1)	15(1)	0(1)

O(1)	98(5)	81(4)	102(4)	0(3)	18(4)	-5(3)
O(2)	99(4)	93(5)	113(4)	7(3)	22(3)	12(4)
O(3)	89(4)	89(4)	120(5)	-1(4)	12(3)	12(3)
N(1)	85(5)	86(5)	95(5)	-2(4)	16(4)	7(3)
N(2)	85(4)	112(6)	77(4)	-4(4)	17(3)	-13(4)
N(3)	99(5)	71(4)	88(4)	8(3)	22(4)	1(4)
F(1)	122(4)	118(4)	139(4)	5(3)	20(3)	26(3)
F(2)	102(4)	148(4)	212(6)	10(4)	26(4)	28(3)
F(3)	93(3)	142(5)	152(4)	20(3)	28(3)	5(3)
F(4)	137(4)	122(4)	166(5)	5(3)	13(3)	43(3)
F(5)	90(3)	110(4)	134(4)	-3(3)	-4(3)	-4(3)
F(6)	131(4)	107(4)	188(6)	-2(3)	17(4)	26(3)
C(1)	90(5)	89(6)	74(5)	0(4)	8(4)	1(4)
C(2)	106(6)	89(6)	103(6)	-1(5)	12(5)	-5(5)
C(3)	133(6)	84(5)	109(6)	-9(5)	35(6)	-8(4)
C(4)	82(6)	94(6)	90(6)	1(5)	12(4)	1(4)
C(5)	103(5)	106(6)	107(6)	0(5)	20(5)	-4(4)
C(6)	94(5)	103(6)	82(5)	-2(4)	18(4)	14(5)
C(7)	115(7)	85(6)	74(5)	-1(4)	21(5)	0(5)
C(8)	110(7)	87(6)	108(6)	8(5)	26(5)	0(5)
C(9)	112(7)	110(7)	117(7)	-2(5)	26(5)	30(6)
C(10)	86(6)	116(7)	125(8)	8(5)	20(5)	23(5)
C(11)	91(5)	122(8)	104(5)	2(5)	23(4)	2(5)
C(12)	90(6)	112(7)	89(6)	0(5)	14(5)	-18(5)
C(13)	116(7)	102(6)	104(6)	-14(5)	12(5)	-9(5)
C(14)	124(8)	167(11)	113(8)	-26(7)	16(6)	-54(7)
C(15)	102(6)	127(8)	122(7)	-2(6)	16(5)	-17(6)
C(16)	88(5)	138(8)	99(6)	14(5)	21(4)	-10(5)
C(17)	99(6)	107(7)	77(5)	-1(4)	12(4)	-7(5)
C(18)	114(7)	85(6)	79(6)	-6(5)	5(5)	9(5)
C(19)	119(6)	90(5)	114(7)	15(4)	22(5)	-2(4)
C(20)	108(7)	91(6)	80(5)	3(4)	17(4)	5(5)
C(21)	86(6)	121(8)	89(6)	-6(5)	13(4)	-6(5)
C(22)	105(6)	105(7)	98(6)	11(5)	14(5)	-7(6)
C(23)	108(7)	141(9)	105(7)	13(6)	19(5)	34(7)
C(24)	124(8)	108(7)	104(6)	12(5)	8(5)	39(6)
C(25)	115(8)	92(6)	102(6)	5(5)	7(5)	16(5)
C(26)	79(5)	111(7)	78(5)	-12(5)	16(4)	6(5)
C(27)	87(5)	120(6)	101(6)	4(5)	4(4)	7(4)
C(28)	77(5)	120(7)	84(5)	-4(5)	12(4)	2(5)
C(29)	96(6)	103(7)	104(6)	-12(5)	14(4)	9(6)
C(30)	118(7)	106(7)	117(7)	13(5)	20(5)	36(6)
C(31)	115(7)	97(6)	106(6)	12(5)	11(5)	5(5)
C(32)	86(6)	108(7)	97(6)	1(5)	4(4)	0(5)
C(33)	100(6)	100(6)	81(5)	-7(4)	14(4)	-6(5)

Table A29: Crystal data and structure refinement for [Cu(triaz)<sub>2</sub>]

empirical formula	C <sub>40</sub> H <sub>46</sub> Cl <sub>2</sub> CuN <sub>6</sub> O <sub>2</sub>
formula weight	777.27
temperature	293(2) K
wavelength	0.71073 Å

crystal system	triclinic	
space group	$P\bar{1}$ (No. 2)	
unit cell dimensions	a = 11.238(2) Å b = 13.151(2) Å c = 13.648(2) Å	$\alpha = 85.54(2)^\circ$ $\beta = 82.78(2)^\circ$ $\gamma = 80.88(2)^\circ$
volume	1972.2(5) Å <sup>3</sup>	
Z	2	
density (calculated)	1.309 gcm <sup>-1</sup>	
absorption coefficient	0.731 mm <sup>-1</sup>	
F(000)	814	
crystal size	0.2 x 0.2 x 0.4 mm <sup>3</sup>	
theta range for data collection	2.52 to 28.20°.	
index ranges	-14 < h < 14 -17 < k < 17 -18 < l < 18	
reflections collected	24040	
independent reflections	8889 [R(int) = 0.1691]	
data / restraints / parameters	8889 / 6 / 490	
Goodness-of-fit on F <sup>2</sup>	0.598	
final R indices [I > 2sigma(I)]	R1 = 0.0522, wR2 = 0.1257	
R indices (all data)	R1 = 0.2273, wR2 = 0.2093	
largest diff. peak and hole	0.264 and -0.402 e.Å <sup>-3</sup>	

Table A30: Atomic coordinates (  $\times 10^4$ ) and equivalent isotropic displacement parameters (Å<sup>2</sup> $\times 10^3$ ) for [Cu(triaz)<sub>2</sub>]. U(eq) is defined as one third of the trace of the orthogonalized U<sup>ij</sup> tensor.

	x	y	z	U(eq)
Cu(1)	2072(1)	2348(1)	9089(1)	54(1)
Cl(1)	276(3)	917(3)	13271(2)	87(1)
Cl(2)	4915(3)	-1085(2)	6631(2)	86(1)
Cl(3)	-1841(12)	268(10)	13171(9)	93(4)
Cl(4)	6954(15)	-1559(14)	7345(14)	134(6)
O(1)	1924(4)	2158(4)	7775(3)	64(2)
O(2)	2077(4)	3074(4)	10199(4)	60(1)
N(1)	512(5)	1872(4)	9517(4)	48(1)
N(2)	-273(5)	1650(4)	8908(4)	48(1)
N(3)	-1189(5)	1191(5)	9355(4)	56(2)
N(4)	3829(5)	1820(5)	9082(4)	50(2)
N(5)	4526(5)	2017(4)	9777(4)	46(1)
N(6)	5592(5)	1403(5)	9771(4)	54(2)
C(1)	5592(6)	760(6)	9043(5)	52(2)
C(2)	6469(7)	-57(6)	8712(6)	62(2)
C(3)	6235(7)	-605(7)	7963(6)	69(2)
C(4)	5120(7)	-344(6)	7539(6)	62(2)
C(5)	4255(6)	456(6)	7848(5)	57(2)
C(6)	4507(6)	1011(6)	8617(5)	49(2)
C(7)	2993(5)	3297(5)	10633(5)	46(2)
C(8)	2744(6)	4078(5)	11346(5)	49(2)



C(9)	3708(6)	4289(5)	11791(5)	50(2)
C(10)	4910(6)	3814(6)	11606(5)	49(2)
C(11)	5131(6)	3061(6)	10925(5)	49(2)
C(12)	4193(6)	2823(5)	10448(5)	44(2)
C(13)	1473(6)	4711(6)	11572(5)	56(2)
C(14)	1191(8)	5417(7)	10648(6)	80(3)
C(15)	481(7)	4023(7)	11841(7)	80(3)
C(16)	1420(7)	5390(7)	12434(6)	76(2)
C(17)	5892(7)	4152(6)	12122(6)	62(2)
C(18)	5491(9)	4208(8)	13233(6)	89(3)
C(19)	6110(9)	5229(8)	11675(8)	101(3)
C(20)	7075(7)	3388(8)	11989(8)	95(3)
C(21)	-996(6)	1101(6)	10316(5)	50(2)
C(22)	-1673(7)	663(6)	11147(6)	66(2)
C(23)	-1266(7)	626(6)	12032(6)	64(2)
C(24)	-186(7)	1036(6)	12126(5)	60(2)
C(25)	489(6)	1486(6)	11351(5)	51(2)
C(26)	52(6)	1511(5)	10427(5)	46(2)
C(27)	916(6)	2170(6)	7356(5)	50(2)
C(28)	900(6)	2458(6)	6324(5)	55(2)
C(29)	-152(6)	2426(6)	5910(6)	61(2)
C(30)	-1235(6)	2168(6)	6427(6)	58(2)
C(31)	-1207(6)	1908(6)	7422(5)	54(2)
C(32)	-177(6)	1914(5)	7867(5)	46(2)
C(33)	2015(7)	2806(7)	5693(5)	67(2)
C(34)	2300(12)	3769(11)	6098(9)	143(6)
C(35)	3107(8)	1978(11)	5678(8)	129(5)
C(36)	1784(9)	3078(10)	4638(6)	115(4)
C(37)	-2374(8)	2212(8)	5919(6)	79(3)
C(38)	-2413(14)	2931(17)	5061(14)	259(13)
C(39)	-2405(12)	1134(13)	5601(12)	176(7)
C(40)	-3512(9)	2407(13)	6640(9)	152(6)

Table A31: Bond lengths [ $\text{\AA}$ ] and angles [ $^\circ$ ] for  $[\text{Cu}(\text{triaz})_2]$ 

Cu(1)–O(2)	1.854(5)	C(9)–C(10)	1.396(9)
Cu(1)–O(1)	1.861(5)	C(10)–C(11)	1.38(1)
Cu(1)–N(1)	1.959(5)	C(10)–C(17)	1.520(9)
Cu(1)–N(4)	1.986(6)	C(11)–C(12)	1.393(8)
Cl(1)–C(24)	1.696(8)	C(13)–C(16)	1.52(1)
Cl(2)–C(4)	1.694(8)	C(13)–C(15)	1.54(1)
Cl(3)–C(23)	1.67(1)	C(13)–C(14)	1.54(1)
Cl(4)–C(3)	1.62(2)	C(17)–C(18)	1.53(1)
O(1)–C(27)	1.330(8)	C(17)–C(20)	1.54(1)
O(2)–C(7)	1.331(7)	C(17)–C(19)	1.54(1)
N(1)–C(26)	1.364(8)	C(21)–C(26)	1.399(9)
N(1)–N(2)	1.364(7)	C(21)–C(22)	1.420(9)
N(2)–N(3)	1.334(7)	C(22)–C(23)	1.34(1)
N(2)–C(32)	1.430(8)	C(23)–C(24)	1.43(1)
N(3)–C(21)	1.350(8)	C(24)–C(25)	1.374(9)
N(4)–C(6)	1.357(9)	C(25)–C(26)	1.406(9)

N(4)–N(5)	1.367(7)	C(27)–C(32)	1.410(9)
N(5)–N(6)	1.334(7)	C(27)–C(28)	1.433(1)
N(5)–C(12)	1.429(8)	C(28)–C(29)	1.380(9)
N(6)–C(1)	1.354(9)	C(28)–C(33)	1.539(9)
C(1)–C(6)	1.398(9)	C(29)–C(30)	1.405(9)
C(1)–C(2)	1.40(1)	C(30)–C(31)	1.38(1)
C(2)–C(3)	1.37(1)	C(30)–C(37)	1.52(1)
C(3)–C(4)	1.43(1)	C(31)–C(32)	1.375(8)
C(4)–C(5)	1.37(1)	C(33)–C(36)	1.50(1)
C(5)–C(6)	1.405(9)	C(33)–C(35)	1.51(1)
C(7)–C(12)	1.394(9)	C(33)–C(34)	1.51(1)
C(7)–C(8)	1.44(1)	C(37)–C(38)	1.45(1)
C(8)–C(9)	1.382(9)	C(37)–C(40)	1.51(1)
C(8)–C(13)	1.54(1)	C(37)–C(39)	1.52(2)
O(2)–Cu(1)–O(1)	157.1(2)	C(16)–C(13)–C(14)	108.1(7)
O(2)–Cu(1)–N(1)	95.6(2)	C(15)–C(13)–C(14)	109.5(7)
O(1)–Cu(1)–N(1)	90.9(2)	C(16)–C(13)–C(8)	111.6(6)
O(2)–Cu(1)–N(4)	91.1(2)	C(15)–C(13)–C(8)	112.4(6)
O(1)–Cu(1)–N(4)	98.5(2)	C(14)–C(13)–C(8)	108.1(6)
N(1)–Cu(1)–N(4)	138.6(2)	C(10)–C(17)–C(18)	110.4(6)
C(27)–O(1)–Cu(1)	128.2(4)	C(10)–C(17)–C(20)	111.2(7)
C(7)–O(2)–Cu(1)	130.9(4)	C(18)–C(17)–C(20)	107.8(7)
C(26)–N(1)–N(2)	103.3(5)	C(10)–C(17)–C(19)	108.1(7)
C(26)–N(1)–Cu(1)	130.1(4)	C(18)–C(17)–C(19)	109.4(8)
N(2)–N(1)–Cu(1)	125.6(4)	C(20)–C(17)–C(19)	109.9(7)
N(3)–N(2)–N(1)	115.2(5)	N(3)–C(21)–C(26)	109.8(6)
N(3)–N(2)–C(32)	120.9(5)	N(3)–C(21)–C(22)	129.5(6)
N(1)–N(2)–C(32)	123.9(5)	C(26)–C(21)–C(22)	120.7(6)
N(2)–N(3)–C(21)	103.7(5)	C(23)–C(22)–C(21)	118.4(7)
C(6)–N(4)–N(5)	103.9(5)	C(22)–C(23)–C(24)	120.0(7)
C(6)–N(4)–Cu(1)	129.3(4)	C(22)–C(23)–Cl(3)	132.8(8)
N(5)–N(4)–Cu(1)	124.5(4)	C(24)–C(23)–Cl(3)	107.0(7)
N(6)–N(5)–N(4)	114.4(5)	C(25)–C(24)–C(23)	124.0(7)
N(6)–N(5)–C(12)	121.0(5)	C(25)–C(24)–Cl(1)	119.8(6)
N(4)–N(5)–C(12)	124.6(5)	C(23)–C(24)–Cl(1)	116.3(6)
N(5)–N(6)–C(1)	104.2(6)	C(24)–C(25)–C(26)	115.2(6)
N(6)–C(1)–C(6)	109.3(7)	N(1)–C(26)–C(21)	108.0(6)
N(6)–C(1)–C(2)	129.8(7)	N(1)–C(26)–C(25)	130.2(6)
C(6)–C(1)–C(2)	120.8(7)	C(21)–C(26)–C(25)	121.7(6)
C(3)–C(2)–C(1)	118.2(7)	O(1)–C(27)–C(32)	124.0(6)
C(2)–C(3)–C(4)	120.4(8)	O(1)–C(27)–C(28)	119.8(6)
C(2)–C(3)–Cl(4)	135.7(10)	C(32)–C(27)–C(28)	116.1(6)
C(4)–C(3)–Cl(4)	103.9(9)	C(29)–C(28)–C(27)	118.0(6)
C(5)–C(4)–C(3)	122.2(7)	C(29)–C(28)–C(33)	120.8(7)
C(5)–C(4)–Cl(2)	121.4(7)	C(27)–C(28)–C(33)	121.2(6)
C(3)–C(4)–Cl(2)	116.4(7)	C(28)–C(29)–C(30)	125.3(7)
C(4)–C(5)–C(6)	116.8(7)	C(31)–C(30)–C(29)	115.8(6)
N(4)–C(6)–C(1)	108.2(6)	C(31)–C(30)–C(37)	122.6(6)
N(4)–C(6)–C(5)	130.2(7)	C(29)–C(30)–C(37)	121.6(7)
C(1)–C(6)–C(5)	121.6(7)	C(32)–C(31)–C(30)	121.2(6)
O(2)–C(7)–C(12)	124.5(6)	C(31)–C(32)–C(27)	123.6(6)

O(2)–C(7)–C(8)	118.6(6)	C(31)–C(32)–N(2)	115.8(6)
C(12)–C(7)–C(8)	116.9(6)	C(27)–C(32)–N(2)	120.7(5)
C(9)–C(8)–C(7)	117.5(6)	C(36)–C(33)–C(35)	107.1(8)
C(9)–C(8)–C(13)	120.2(6)	C(36)–C(33)–C(34)	106.9(9)
C(7)–C(8)–C(13)	122.3(6)	C(35)–C(33)–C(34)	109.8(9)
C(8)–C(9)–C(10)	125.6(7)	C(36)–C(33)–C(28)	111.7(6)
C(11)–C(10)–C(9)	116.2(6)	C(35)–C(33)–C(28)	112.0(7)
C(11)–C(10)–C(17)	123.8(6)	C(34)–C(33)–C(28)	109.2(7)
C(9)–C(10)–C(17)	120.0(7)	C(38)–C(37)–C(40)	111(1)
C(10)–C(11)–C(12)	120.6(7)	C(38)–C(37)–C(39)	110(1)
C(11)–C(12)–C(7)	123.2(7)	C(40)–C(37)–C(39)	103(1)
C(11)–C(12)–N(5)	115.5(6)	C(38)–C(37)–C(30)	113.2(8)
C(7)–C(12)–N(5)	121.2(6)	C(40)–C(37)–C(30)	111.7(7)
C(16)–C(13)–C(15)	107.0(6)	C(39)–C(37)–C(30)	107.5(9)

Table A32: Anisotropic displacement parameters ( $\text{\AA}^2 \times 10^3$ ) for  $[\text{Cu}(\text{triaz})_2]$ . The anisotropic displacement factor exponent takes the form:  $-2p^2 [h^2 a^* U^{11} + \dots + 2 h k a^* b^* U^{12}]$

	U11	U22	U33	U23	U13	U12
Cu(1)	43(1)	68(1)	52(1)	-13(1)	-7(1)	-6(1)
Cl(1)	98(2)	112(3)	52(2)	0(2)	-15(1)	-17(2)
Cl(2)	90(2)	88(2)	83(2)	-46(2)	-7(2)	-2(2)
Cl(3)	101(8)	95(10)	87(8)	-15(7)	0(7)	-33(8)
Cl(4)	127(12)	127(14)	139(14)	-22(11)	-17(10)	16(11)
O(1)	44(3)	100(5)	49(3)	-11(3)	-8(2)	-10(3)
O(2)	42(2)	76(4)	64(3)	-28(3)	-14(2)	-2(3)
N(1)	50(3)	51(4)	43(3)	-2(3)	-16(3)	-2(3)
N(2)	51(3)	48(4)	44(3)	-6(3)	-9(3)	-1(3)
N(3)	52(3)	62(4)	56(4)	-1(3)	-4(3)	-17(3)
N(4)	48(3)	57(4)	46(3)	-6(3)	-3(3)	-11(3)
N(5)	41(3)	49(4)	47(3)	-5(3)	-7(2)	-3(3)
N(6)	40(3)	58(4)	61(4)	-5(3)	-10(3)	4(3)
C(1)	42(4)	59(5)	57(5)	-12(4)	-6(3)	-3(4)
C(2)	48(4)	66(6)	71(5)	-10(4)	-7(4)	1(4)
C(3)	68(5)	63(6)	72(6)	-14(4)	9(4)	-10(5)
C(4)	65(5)	59(6)	63(5)	-18(4)	10(4)	-13(5)
C(5)	50(4)	68(6)	56(5)	-17(4)	0(3)	-15(4)
C(6)	49(4)	49(5)	50(4)	-6(3)	-3(3)	-10(4)
C(7)	35(3)	49(5)	54(4)	-4(3)	-13(3)	-1(3)
C(8)	49(4)	44(5)	56(4)	-4(3)	-14(3)	-1(4)
C(9)	56(4)	48(5)	45(4)	-9(3)	-17(3)	4(4)
C(10)	44(4)	47(5)	58(4)	-6(3)	-16(3)	-2(4)
C(11)	42(4)	50(5)	56(4)	1(4)	-13(3)	-6(4)
C(12)	38(3)	46(5)	48(4)	-8(3)	-11(3)	0(3)
C(13)	54(4)	57(5)	57(5)	-20(4)	-10(3)	6(4)
C(14)	79(5)	79(7)	78(6)	-8(5)	-27(5)	17(5)
C(15)	64(5)	86(7)	90(7)	-34(5)	11(4)	-16(5)
C(16)	69(5)	74(6)	85(6)	-32(5)	-18(4)	10(5)
C(17)	59(4)	62(6)	72(5)	-10(4)	-26(4)	-11(4)
C(18)	100(7)	117(8)	63(6)	-18(5)	-37(5)	-25(6)

C(19)	102(7)	100(8)	117(8)	12(7)	-46(6)	-48(7)
C(20)	57(5)	102(8)	135(9)	-27(7)	-44(5)	-5(5)
C(21)	53(4)	51(5)	45(4)	-8(3)	-7(3)	-3(4)
C(22)	60(4)	75(6)	62(5)	1(4)	7(4)	-20(5)
C(23)	73(5)	67(6)	51(5)	0(4)	-4(4)	-11(5)
C(24)	71(5)	59(5)	45(4)	-5(4)	-10(4)	9(4)
C(25)	54(4)	56(5)	38(4)	-8(3)	-7(3)	4(4)
C(26)	47(4)	37(4)	52(4)	-6(3)	-4(3)	-1(3)
C(27)	45(4)	50(5)	57(5)	-12(3)	-7(3)	-7(4)
C(28)	52(4)	64(5)	50(4)	-11(4)	-5(3)	-12(4)
C(29)	57(4)	75(6)	52(4)	2(4)	-15(3)	-8(4)
C(30)	51(4)	65(5)	62(5)	3(4)	-22(4)	-13(4)
C(31)	48(4)	59(5)	56(5)	-2(4)	-17(3)	-10(4)
C(32)	46(4)	53(5)	41(4)	0(3)	-17(3)	-6(4)
C(33)	62(5)	102(7)	41(4)	-4(4)	-6(3)	-26(5)
C(34)	160(11)	192(14)	104(9)	-37(9)	25(8)	-125(11)
C(35)	71(6)	217(15)	79(7)	17(8)	18(5)	8(8)
C(36)	102(7)	198(13)	55(6)	31(7)	-14(5)	-63(8)
C(37)	80(6)	99(8)	68(6)	15(5)	-39(5)	-34(6)
C(38)	153(12)	390(30)	260(19)	240(20)	-162(13)	-138(16)
C(39)	119(10)	221(17)	219(16)	-90(13)	-81(10)	-39(11)
C(40)	60(6)	274(19)	124(10)	-22(11)	-35(6)	-3(9)

Table A33: Crystal data and structure refinement for OON2

empirical formula	C <sub>14</sub> H <sub>15</sub> NO <sub>2</sub>	
formula weight	229.27	
temperature	293(2) K	
wavelength	0.71073 Å	
crystal system	triclinic	
space group	P $\bar{1}$ (No. 2)	
unit cell dimensions	a = 7.671(2) Å	$\alpha$ = 108.17(2)°
	b = 8.050(1) Å	$\beta$ = 93.82(2)°
	c = 11.358(2) Å	$\gamma$ = 113.80(2)°
volume	594.6(2) Å <sup>3</sup>	
Z	2	
density (calculated)	1.281 gcm <sup>-3</sup>	
absorption coefficient	0.086 mm <sup>-1</sup>	
F(000)	244	
crystal size	0.5 x 0.7 x 1.1 mm <sup>3</sup>	
theta range for data collection	2.89 to 28.10°.	
index ranges	-10 < h < 10	
	-10 < k < 10	
	-15 < l < 14	
reflections collected	7187	
independent reflections	2652 [R(int) = 0.0331]	
data / restraints / parameters	2652 / 0 / 218	
Goodness-of-fit on F <sup>2</sup>	0.945	
final R indices [I > 2sigma(I)]	R1 = 0.0435, wR2 = 0.1012	

R indices (all data) R1 = 0.0811, wR2 = 0.1122  
 largest diff. peak and hole 0.171 and -0.147 e.Å<sup>-3</sup>

Table A34: Atomic coordinates ( $\times 10^4$ ) and equivalent isotropic displacement parameters ( $\text{Å}^2 \times 10^3$ ) for OON2. U(eq) is defined as one third of the trace of the orthogonalized  $U^{ij}$  tensor.

	x	y	z	U(eq)
O(1)	9628(2)	7355(2)	9479(1)	53(1)
O(2)	7474(2)	3188(2)	5763(1)	52(1)
N(1)	7495(2)	2675(2)	8646(1)	51(1)
C(1)	7228(2)	4057(2)	8367(1)	39(1)
C(2)	5411(3)	4053(3)	8246(2)	55(1)
C(3)	3840(3)	2585(3)	8407(2)	63(1)
C(4)	4113(3)	1155(3)	8682(2)	59(1)
C(5)	5933(3)	1247(3)	8786(2)	60(1)
C(6)	9029(2)	5741(2)	8282(1)	41(1)
C(7)	10711(3)	5243(3)	8077(2)	49(1)
C(8)	8531(2)	6388(2)	7228(2)	40(1)
C(9)	7822(2)	5070(2)	5961(2)	41(1)
C(10)	7493(3)	5676(3)	4988(2)	52(1)
C(11)	7847(3)	7605(3)	5277(2)	62(1)
C(12)	8488(3)	8901(3)	6508(2)	62(1)
C(13)	8825(3)	8292(2)	7484(2)	51(1)
C(14)	6933(3)	1836(3)	4491(2)	55(1)

Table A35: Bond lengths [ $\text{Å}$ ] and angles [ $^\circ$ ] for OON2

O(1)–C(6)	1.443(2)	C(4)–C(5)	1.363(3)
O(2)–C(9)	1.368(2)	C(6)–C(7)	1.510(2)
O(2)–C(14)	1.421(2)	C(6)–C(8)	1.530(2)
N(1)–C(1)	1.332(2)	C(8)–C(13)	1.385(2)
N(1)–C(5)	1.345(2)	C(8)–C(9)	1.404(2)
C(1)–C(2)	1.390(2)	C(9)–C(10)	1.385(2)
C(1)–C(6)	1.531(2)	C(10)–C(11)	1.386(3)
C(2)–C(3)	1.377(3)	C(11)–C(12)	1.368(3)
C(3)–C(4)	1.370(3)	C(12)–C(13)	1.392(3)
C(9)–O(2)–C(14)	118.3(2)	C(7)–C(6)–C(1)	112.8(1)
C(1)–N(1)–C(5)	117.7(2)	C(8)–C(6)–C(1)	111.1(1)
N(1)–C(1)–C(2)	121.5(2)	C(13)–C(8)–C(9)	118.1(1)
N(1)–C(1)–C(6)	117.5(1)	C(13)–C(8)–C(6)	121.4(1)
C(2)–C(1)–C(6)	120.8(1)	C(9)–C(8)–C(6)	120.4(1)
C(3)–C(2)–C(1)	119.7(2)	O(2)–C(9)–C(10)	123.2(2)
C(4)–C(3)–C(2)	118.8(2)	O(2)–C(9)–C(8)	116.0(1)
C(5)–C(4)–C(3)	118.5(2)	C(10)–C(9)–C(8)	120.9(1)
N(1)–C(5)–C(4)	123.9(2)	C(9)–C(10)–C(11)	119.4(2)
O(1)–C(6)–C(7)	108.6(1)	C(12)–C(11)–C(10)	120.7(2)
O(1)–C(6)–C(8)	108.1(1)	C(11)–C(12)–C(13)	119.8(2)
C(7)–C(6)–C(8)	109.5(1)	C(8)–C(13)–C(12)	121.0(2)
O(1)–C(6)–C(1)	106.6(1)		

Table A36: Anisotropic displacement parameters ( $\text{\AA}^2 \times 10^3$ ) for OON2. The anisotropic displacement factor exponent takes the form:  $-2p^2 [ h^2 a^2 U^{11} + \dots + 2 h k a^* b^* U^{12} ]$

	U11	U22	U33	U23	U13	U12
O(1)	54(1)	48(1)	44(1)	7(1)	3(1)	19(1)
O(2)	74(1)	40(1)	38(1)	13(1)	11(1)	24(1)
N(1)	46(1)	48(1)	58(1)	23(1)	7(1)	16(1)
C(1)	39(1)	42(1)	30(1)	9(1)	9(1)	14(1)
C(2)	49(1)	56(1)	71(1)	31(1)	21(1)	24(1)
C(3)	45(1)	67(1)	80(1)	33(1)	21(1)	22(1)
C(4)	45(1)	57(1)	58(1)	25(1)	8(1)	5(1)
C(5)	56(1)	52(1)	66(1)	30(1)	6(1)	14(1)
C(6)	41(1)	38(1)	35(1)	9(1)	8(1)	14(1)
C(7)	45(1)	54(1)	44(1)	20(1)	15(1)	17(1)
C(8)	33(1)	40(1)	46(1)	16(1)	14(1)	15(1)
C(9)	41(1)	40(1)	45(1)	19(1)	15(1)	18(1)
C(10)	55(1)	60(1)	49(1)	27(1)	14(1)	29(1)
C(11)	64(1)	70(1)	75(1)	47(1)	21(1)	36(1)
C(12)	57(1)	47(1)	91(2)	33(1)	22(1)	27(1)
C(13)	44(1)	40(1)	67(1)	19(1)	16(1)	18(1)
C(14)	64(1)	50(1)	42(1)	8(1)	10(1)	25(1)

Table A37: Crystal data and structure refinement for OON3

empirical formula	$C_{19}H_{17}NO_2$	
formula weight	291.34	
temperature	293(2) K	
wavelength	0.71073 $\text{\AA}$	
crystal system	triclinic	
space group	$P\bar{1}$ (No. 2)	
unit cell dimensions	a = 8.205(5) $\text{\AA}$ b = 8.721(5) $\text{\AA}$ c = 12.612(5) $\text{\AA}$	$\alpha = 71.752(5)^\circ$ $\beta = 73.840(5)^\circ$ $\gamma = 65.829(5)^\circ$
volume	770.1(7) $\text{\AA}^3$	
Z	2	
density (calculated)	1.256 $\text{gcm}^{-3}$	
F(000)	308	
crystal size	0.3 x 0.3 x 0.6 $\text{mm}^3$	
theta range for data collection	1.73 to 27.32 $^\circ$ .	
index ranges	-10 < h < 10 -11 < k < 11 -15 < l < 16	
reflections collected	7245	
independent reflections	3297 [R(int) = 0.0412]	
data / restraints / parameters	3297 / 0 / 257	
Goodness-of-fit on $F^2$	0.884	
final R indices [ $I > 2\sigma(I)$ ]	R1 = 0.0440, wR2 = 0.1027	
R indices (all data)	R1 = 0.0947, wR2 = 0.1254	

extinction coefficient	0.081(8)
largest diff. peak and hole	0.147 and $-0.152 \text{ e.}\text{\AA}^{-3}$

Table A38: Atomic coordinates ( $\times 10^4$ ) and equivalent isotropic displacement parameters ( $\text{\AA}^2 \times 10^3$ ) for OON3.  $U(\text{eq})$  is defined as one third of the trace of the orthogonalized  $U^{ij}$  tensor.

	x	y	z	$U(\text{eq})$
O(1)	436(2)	241(2)	3828(1)	64(1)
O(2)	3689(2)	-1072(2)	4395(1)	77(1)
N(1)	281(2)	2683(2)	1013(1)	72(1)
C(1)	-796(3)	3103(3)	237(2)	75(1)
C(2)	-1876(3)	2204(3)	327(2)	73(1)
C(3)	-1874(3)	826(3)	1223(2)	76(1)
C(4)	-794(3)	382(3)	2017(2)	65(1)
C(5)	262(2)	1330(2)	1904(1)	51(1)
C(6)	1467(2)	847(2)	2777(1)	50(1)
C(7)	1793(3)	2430(2)	2824(1)	53(1)
C(8)	3266(3)	2803(3)	2174(2)	60(1)
C(9)	3569(4)	4226(3)	2184(2)	76(1)
C(10)	2364(4)	5335(3)	2850(2)	78(1)
C(11)	864(4)	4996(3)	3506(2)	83(1)
C(12)	564(3)	3536(3)	3504(2)	69(1)
C(13)	3284(2)	-594(2)	2526(1)	51(1)
C(14)	4360(3)	-1554(2)	3372(2)	60(1)
C(15)	5981(3)	-2883(3)	3167(2)	75(1)
C(16)	6592(3)	-3261(3)	2110(2)	76(1)
C(17)	5595(3)	-2316(3)	1259(2)	69(1)
C(18)	3959(3)	-1000(2)	1474(2)	58(1)
C(19)	4600(4)	-2083(3)	5336(2)	103(1)

Table A39: Bond lengths [ $\text{\AA}$ ] and angles [ $^\circ$ ] for OON3

O(1)–C(6)	1.434(2)	C(9)–C(10)	1.371(4)
O(1)–H(20)	0.94(3)	C(9)–H(9)	1.08(3)
O(2)–C(14)	1.378(2)	C(10)–C(11)	1.366(4)
O(2)–C(19)	1.430(2)	C(10)–H(10)	0.99(3)
N(1)–C(5)	1.352(2)	C(11)–C(12)	1.393(3)
N(1)–C(1)	1.366(3)	C(11)–H(11)	0.99(3)
C(1)–C(2)	1.367(3)	C(12)–H(12)	0.94(2)
C(1)–H(1)	1.02(2)	C(13)–C(18)	1.386(3)
C(2)–C(3)	1.368(3)	C(13)–C(14)	1.406(2)
C(2)–H(2)	0.98(3)	C(14)–C(15)	1.383(3)
C(3)–C(4)	1.381(3)	C(15)–C(16)	1.380(3)
C(3)–H(3)	1.02(3)	C(15)–H(15)	0.95(2)
C(4)–C(5)	1.378(3)	C(16)–C(17)	1.372(3)
C(4)–H(4)	0.97(2)	C(16)–H(16)	0.98(3)
C(5)–C(6)	1.531(2)	C(17)–C(18)	1.386(3)
C(6)–C(7)	1.531(3)	C(17)–H(17)	0.98(2)
C(6)–C(13)	1.534(2)	C(18)–H(18)	0.97(2)
C(7)–C(8)	1.358(3)	C(19)–H(19A)	0.9600
C(7)–C(12)	1.386(3)	C(19)–H(19B)	0.9600
C(8)–C(9)	1.367(3)	C(19)–H(19C)	0.9600

C(8)–H(8)	0.67(2)		
C(6)–O(1)–H(20)	106(2)	C(11)–C(10)–C(9)	119.3(2)
C(14)–O(2)–C(19)	119.3(2)	C(11)–C(10)–H(10)	122(2)
C(5)–N(1)–C(1)	118.2(2)	C(9)–C(10)–H(10)	119(2)
N(1)–C(1)–C(2)	122.5(2)	C(10)–C(11)–C(12)	120.4(2)
N(1)–C(1)–H(1)	118(1)	C(10)–C(11)–H(11)	122(1)
C(2)–C(1)–H(1)	119(1)	C(12)–C(11)–H(11)	118(2)
C(1)–C(2)–C(3)	119.0(2)	C(7)–C(12)–C(11)	119.6(2)
C(1)–C(2)–H(2)	119(1)	C(7)–C(12)–H(12)	119(2)
C(3)–C(2)–H(2)	122(1)	C(11)–C(12)–H(12)	121(1)
C(2)–C(3)–C(4)	119.4(2)	C(18)–C(13)–C(14)	116.9(2)
C(2)–C(3)–H(3)	121(1)	C(18)–C(13)–C(6)	122.7(2)
C(4)–C(3)–H(3)	120(1)	C(14)–C(13)–C(6)	120.5(2)
C(5)–C(4)–C(3)	120.0(2)	O(2)–C(14)–C(15)	123.4(2)
C(5)–C(4)–H(4)	119(2)	O(2)–C(14)–C(13)	115.5(2)
C(3)–C(4)–H(4)	120(1)	C(15)–C(14)–C(13)	121.2(2)
N(1)–C(5)–C(4)	121(2)	C(16)–C(15)–C(14)	120.1(2)
N(1)–C(5)–C(6)	118.7(2)	C(16)–C(15)–H(15)	120(1)
C(4)–C(5)–C(6)	120.4(2)	C(14)–C(15)–H(15)	120(1)
O(1)–C(6)–C(7)	110.4(1)	C(17)–C(16)–C(15)	120.1(2)
O(1)–C(6)–C(5)	103.9(2)	C(17)–C(16)–H(16)	122(1)
C(7)–C(6)–C(5)	110.7(1)	C(15)–C(16)–H(16)	118(1)
O(1)–C(6)–C(13)	109.9(1)	C(16)–C(17)–C(18)	119.6(2)
C(7)–C(6)–C(13)	110.1(2)	C(16)–C(17)–H(17)	120(1)
C(5)–C(6)–C(13)	111.7(1)	C(18)–C(17)–H(17)	120(1)
C(8)–C(7)–C(12)	118.8(2)	C(13)–C(18)–C(17)	122.2(2)
C(8)–C(7)–C(6)	120.4(2)	C(13)–C(18)–H(18)	120(1)
C(12)–C(7)–C(6)	120.8(2)	C(17)–C(18)–H(18)	118(1)
C(7)–C(8)–C(9)	121.6(2)	O(2)–C(19)–H(19A)	109.5
C(7)–C(8)–H(8)	122(2)	O(2)–C(19)–H(19B)	109.5
C(9)–C(8)–H(8)	117(2)	H(19A)–C(19)–H(19B)	109.5
C(8)–C(9)–C(10)	120.3(3)	O(2)–C(19)–H(19C)	109.5
C(8)–C(9)–H(9)	123(2)	H(19A)–C(19)–H(19C)	109.5
C(10)–C(9)–H(9)	117(2)	H(19B)–C(19)–H(19C)	109.5

Table A40: Anisotropic displacement parameters ( $\text{\AA}^2 \times 10^3$ ) for OON3. The anisotropic displacement factor exponent takes the form:  $-2p^2 [ h^2 a^* 2U^{11} + \dots + 2 h k a^* b^* U^{12} ]$

	U <sup>11</sup>	U <sup>22</sup>	U <sup>33</sup>	U <sup>23</sup>	U <sup>13</sup>	U <sup>12</sup>
O(1)	63(1)	77(1)	46(1)	–2(1)	–8(1)	–29(1)
O(2)	79(1)	83(1)	58(1)	–13(1)	–32(1)	–8(1)
N(1)	80(1)	79(1)	61(1)	–1(1)	–26(1)	–34(1)
C(1)	85(2)	82(1)	61(1)	0(1)	–32(1)	–31(1)
C(2)	70(1)	83(1)	71(1)	–16(1)	–32(1)	–20(1)
C(3)	72(1)	82(1)	89(2)	–18(1)	–30(1)	–33(1)
C(4)	66(1)	64(1)	70(1)	–7(1)	–21(1)	–27(1)
C(5)	51(1)	54(1)	47(1)	–9(1)	–12(1)	–17(1)
C(6)	52(1)	55(1)	43(1)	–7(1)	–10(1)	–20(1)
C(7)	57(1)	52(1)	50(1)	–9(1)	–22(1)	–13(1)



C(8)	62(1)	58(1)	60(1)	-14(1)	-10(1)	-23(1)
C(9)	87(2)	69(1)	82(1)	-8(1)	-27(1)	-34(1)
C(10)	91(2)	60(1)	93(2)	-11(1)	-41(1)	-25(1)
C(11)	92(2)	63(1)	94(2)	-33(1)	-30(1)	-8(1)
C(12)	64(1)	68(1)	74(1)	-24(1)	-13(1)	-14(1)
C(13)	53(1)	49(1)	52(1)	-8(1)	-14(1)	-18(1)
C(14)	63(1)	58(1)	59(1)	-10(1)	-20(1)	-17(1)
C(15)	67(1)	66(1)	83(2)	-10(1)	-29(1)	-9(1)
C(16)	61(1)	65(1)	91(2)	-21(1)	-11(1)	-10(1)
C(17)	68(1)	66(1)	71(1)	-22(1)	-6(1)	-21(1)
C(18)	62(1)	56(1)	57(1)	-11(1)	-11(1)	-22(1)
C(19)	112(2)	111(2)	73(1)	-7(1)	-54(2)	-11(2)

Table A41: Crystal data and structure refinement for  $[\text{Co}(\text{OON3})_2(\mu\text{-Cl})_2\text{CoCl}_2]\cdot\text{C}_3\text{H}_6\text{O}$ 

empirical formula	$\text{C}_{41}\text{H}_{40}\text{Cl}_4\text{Co}_2\text{N}_2\text{O}_5$	
formula weight	900.41	
temperature	293(2) K	
wavelength	0.71073 Å	
crystal system	triclinic	
space group	$P\bar{1}$ (No. 2)	
unit cell dimensions	$a = 8.983(2)$ Å $b = 12.107(3)$ Å $c = 19.539(5)$ Å	$\alpha = 92.74(2)^\circ$ $\beta = 97.43(2)^\circ$ $\gamma = 94.01(2)^\circ$
volume	2098.7(8) Å <sup>3</sup>	
Z	2	
density (calculated)	1.425 gcm <sup>-3</sup>	
absorption coefficient	1.089 mm <sup>-1</sup>	
F(000)	924	
crystal size	0.3 x 0.4 x 0.4 mm <sup>3</sup>	
theta range for data collection	1.69 to 27.35°.	
index ranges	-11 < h < 10 -15 < k < 15 -24 < l < 25	
reflections collected	20125	
independent reflections	9100 [R(int) = 0.0982]	
data / restraints / parameters	9100 / 0 / 493	
Goodness-of-fit on F <sup>2</sup>	0.653	
final R indices [I > 2σ(I)]	R1 = 0.0477, wR2 = 0.0931	
R indices (all data)	R1 = 0.2007, wR2 = 0.1211	
largest diff. peak and hole	1.011 and -0.489 e.Å <sup>-3</sup>	

Table A42: Atomic coordinates (  $\times 10^4$ ) and equivalent isotropic displacement parameters (Å<sup>2</sup> $\times 10^3$ ) for  $[\text{Co}(\text{OON3})_2(\mu\text{-Cl})_2\text{CoCl}_2]\cdot\text{C}_3\text{H}_6\text{O}$ . U(eq) is defined as one third of the trace of the orthogonalized  $U^{ij}$  tensor.

	x	y	z	U(eq)
Co(1)	5950(1)	3457(1)	2214(1)	47(1)

Co(2)	8628(1)	5411(1)	2222(1)	56(1)
Cl(1)	8216(2)	4090(1)	3002(1)	62(1)
Cl(2)	6116(2)	5335(1)	1744(1)	61(1)
Cl(3)	9965(2)	4680(2)	1445(1)	76(1)
Cl(4)	9648(2)	7008(1)	2730(1)	92(1)
N(1)	4411(5)	2800(4)	1361(2)	46(1)
N(2)	4361(5)	3750(4)	2878(2)	48(1)
O(1)	7332(5)	2767(3)	1518(2)	51(1)
O(2)	6890(7)	3807(5)	267(3)	109(2)
O(3)	7788(6)	984(4)	3569(3)	88(2)
O(4)	5783(4)	1986(3)	2751(2)	49(1)
O(5)	7448(10)	-2095(7)	4663(4)	161(3)
C(1)	2916(8)	2988(5)	1242(4)	64(2)
C(2)	1979(8)	2673(6)	648(4)	73(2)
C(3)	2582(7)	2153(5)	118(4)	69(2)
C(4)	4087(7)	1947(5)	217(3)	58(2)
C(5)	4953(7)	2261(4)	824(3)	46(2)
C(6)	6592(6)	1965(4)	986(3)	43(1)
C(7)	6667(7)	837(4)	1298(3)	48(2)
C(8)	5452(8)	82(5)	1251(3)	56(2)
C(9)	5553(10)	-975(6)	1506(4)	80(2)
C(10)	6958(12)	-1247(6)	1818(4)	88(3)
C(11)	8182(10)	-497(7)	1878(4)	88(2)
C(12)	8136(9)	606(6)	1621(3)	87(3)
C(13)	7369(6)	2016(5)	336(3)	51(2)
C(14)	7499(8)	2966(6)	-11(4)	66(2)
C(15)	8195(8)	3068(7)	-599(4)	81(2)
C(16)	8729(9)	2122(9)	-862(4)	96(3)
C(17)	8600(8)	1153(8)	-557(4)	85(2)
C(18)	7926(7)	1097(6)	34(3)	63(2)
C(19)	7056(12)	4898(7)	-36(5)	140(4)
C(20)	3483(7)	4630(5)	2835(3)	60(2)
C(21)	2304(7)	4716(6)	3211(3)	66(2)
C(22)	1967(7)	3903(6)	3641(4)	67(2)
C(23)	2846(7)	3006(5)	3692(3)	61(2)
C(24)	4060(7)	2971(5)	3309(3)	49(2)
C(25)	5135(6)	2042(5)	3399(3)	48(2)
C(26)	4272(7)	938(5)	3484(3)	50(2)
C(27)	3550(8)	314(6)	2911(4)	70(2)
C(28)	2696(8)	-648(6)	2977(4)	74(2)
C(29)	2501(8)	-999(6)	3610(4)	80(2)
C(30)	3188(9)	-389(6)	4192(4)	78(2)
C(31)	4084(7)	575(5)	4121(3)	62(2)
C(32)	6380(7)	2361(5)	4003(3)	53(2)
C(33)	7736(8)	1805(6)	4062(4)	63(2)
C(34)	8880(9)	2090(7)	4593(5)	86(2)
C(35)	8720(10)	2917(8)	5079(5)	95(3)
C(36)	7409(11)	3450(7)	5045(4)	94(3)
C(37)	6273(8)	3168(6)	4505(4)	73(2)
C(38)	9050(12)	311(9)	3678(5)	180(6)
C(39)	6688(15)	-3830(10)	4225(7)	189(6)
C(40)	6799(12)	-2635(9)	4184(6)	98(3)

C(41)                      6041(17)                      -2291(13)                      3555(7)                      245(9)

---

Table A43: Bond lengths [Å] and angles [°] for [Co(OON3)<sub>2</sub>(μ-Cl)<sub>2</sub>CoCl<sub>2</sub>]:C<sub>3</sub>H<sub>6</sub>O

Co(1)–N(2)	2.086(5)	C(17)–C(18)	1.373(9)
Co(1)–N(1)	2.109(5)	C(17)–H(17)	0.9300
Co(1)–Cl(1)	2.441(2)	C(18)–H(18)	0.9300
Co(1)–Cl(2)	2.494(2)	C(19)–H(19A)	0.9600
Co(2)–Cl(4)	2.213(2)	C(19)–H(19B)	0.9600
Co(2)–Cl(3)	2.240(2)	C(19)–H(19C)	0.9600
Co(2)–Cl(1)	2.305(2)	C(20)–C(21)	1.372(8)
Co(2)–Cl(2)	2.321(2)	C(20)–H(20)	0.9300
N(1)–C(5)	1.368(7)	C(21)–C(22)	1.368(8)
N(1)–C(1)	1.370(7)	C(21)–H(21)	0.9300
N(2)–C(24)	1.331(7)	C(22)–C(23)	1.387(8)
N(2)–C(20)	1.368(7)	C(22)–H(22)	0.9300
O(1)–C(6)	1.449(6)	C(23)–C(24)	1.402(8)
O(1)–H(1)	0.8200	C(23)–H(23)	0.9300
O(2)–C(14)	1.316(8)	C(24)–C(25)	1.534(7)
O(2)–C(19)	1.480(8)	C(25)–C(26)	1.524(8)
O(3)–C(33)	1.358(8)	C(25)–C(32)	1.532(8)
O(3)–C(38)	1.442(8)	C(26)–C(31)	1.367(8)
O(4)–C(25)	1.461(6)	C(26)–C(27)	1.382(8)
O(4)–H(4)	0.8200	C(27)–C(28)	1.370(8)
O(5)–C(40)	1.18(1)	C(27)–H(27)	0.9300
C(1)–C(2)	1.365(8)	C(28)–C(29)	1.356(9)
C(1)–H(1)	0.9300	C(28)–H(28)	0.9300
C(2)–C(3)	1.375(9)	C(29)–C(30)	1.38(1)
C(2)–H(2)	0.9300	C(29)–H(29)	0.9300
C(3)–C(4)	1.383(8)	C(30)–C(31)	1.394(8)
C(3)–H(3)	0.9300	C(30)–H(30)	0.9300
C(4)–C(5)	1.355(8)	C(31)–H(31)	0.9300
C(4)–H(4)	0.9300	C(32)–C(37)	1.369(8)
C(5)–C(6)	1.536(8)	C(32)–C(33)	1.427(8)
C(6)–C(7)	1.525(7)	C(33)–C(34)	1.38(1)
C(6)–C(13)	1.529(8)	C(34)–C(35)	1.37(1)
C(7)–C(8)	1.364(8)	C(34)–H(34)	0.9300
C(7)–C(12)	1.438(9)	C(35)–C(36)	1.38(1)
C(8)–C(9)	1.399(8)	C(35)–H(35)	0.9300
C(8)–H(8)	0.9300	C(36)–C(37)	1.38(1)
C(9)–C(10)	1.40(1)	C(36)–H(36)	0.9300
C(9)–H(9)	0.9300	C(37)–H(37)	0.9300
C(10)–C(11)	1.37(1)	C(38)–H(38A)	0.9600
C(10)–H(10)	0.9300	C(38)–H(38B)	0.9600
C(11)–C(12)	1.451(9)	C(38)–H(38C)	0.9600
C(11)–H(11)	0.9300	C(39)–C(40)	1.45(1)
C(12)–H(12)	0.9300	C(39)–H(39A)	0.9600
C(13)–C(14)	1.368(8)	C(39)–H(39B)	0.9600
C(13)–C(18)	1.388(8)	C(39)–H(39C)	0.9600
C(14)–C(15)	1.383(9)	C(40)–C(41)	1.42(1)
C(15)–C(16)	1.38(1)	C(41)–H(41A)	0.9600
C(15)–H(15)	0.9300	C(41)–H(41B)	0.9600

C(16)–C(17)	1.35(1)	C(41)–H(41C)	0.9600
C(16)–H(16)	0.9300		
N(2)–Co(1)–N(1)	96.7(2)	H(19A)–C(19)–H(19B)	109.5
N(2)–Co(1)–Cl(1)	98.4(1)	O(2)–C(19)–H(19C)	109.5
N(1)–Co(1)–Cl(1)	164.8(1)	H(19A)–C(19)–H(19C)	109.5
N(2)–Co(1)–Cl(2)	97.7(1)	H(19B)–C(19)–H(19C)	109.5
N(1)–Co(1)–Cl(2)	92.6(1)	N(2)–C(20)–C(21)	122.0(6)
Cl(1)–Co(1)–Cl(2)	86.44(6)	N(2)–C(20)–H(20)	119.0
Cl(4)–Co(2)–Cl(3)	113.98(9)	C(21)–C(20)–H(20)	119.0
Cl(4)–Co(2)–Cl(1)	112.63(8)	C(22)–C(21)–C(20)	120.0(6)
Cl(3)–Co(2)–Cl(1)	107.93(7)	C(22)–C(21)–H(21)	120.0
Cl(4)–Co(2)–Cl(2)	117.49(7)	C(20)–C(21)–H(21)	120.0
Cl(3)–Co(2)–Cl(2)	108.94(8)	C(21)–C(22)–C(23)	118.7(6)
Cl(1)–Co(2)–Cl(2)	93.87(7)	C(21)–C(22)–H(22)	120.7
Co(2)–Cl(1)–Co(1)	86.45(6)	C(23)–C(22)–H(22)	120.7
Co(2)–Cl(2)–Co(1)	84.87(6)	C(22)–C(23)–C(24)	119.0(6)
C(5)–N(1)–C(1)	114.9(5)	C(22)–C(23)–H(23)	120.5
C(5)–N(1)–Co(1)	118.7(4)	C(24)–C(23)–H(23)	120.5
C(1)–N(1)–Co(1)	125.7(4)	N(2)–C(24)–C(23)	122.0(5)
C(24)–N(2)–C(20)	118.2(5)	N(2)–C(24)–C(25)	117.6(5)
C(24)–N(2)–Co(1)	117.9(4)	C(23)–C(24)–C(25)	120.3(5)
C(20)–N(2)–Co(1)	123.4(4)	O(4)–C(25)–C(26)	109.4(5)
C(6)–O(1)–H(1)	109.5	O(4)–C(25)–C(32)	109.8(5)
C(14)–O(2)–C(19)	118.3(7)	C(26)–C(25)–C(32)	112.5(5)
C(33)–O(3)–C(38)	115.8(7)	O(4)–C(25)–C(24)	104.0(4)
C(25)–O(4)–H(4)	109.5	C(26)–C(25)–C(24)	110.8(5)
C(2)–C(1)–N(1)	125.0(6)	C(32)–C(25)–C(24)	110.0(5)
C(2)–C(1)–H(1)	117.5	C(31)–C(26)–C(27)	117.8(6)
N(1)–C(1)–H(1)	117.5	C(31)–C(26)–C(25)	121.7(6)
C(1)–C(2)–C(3)	117.8(6)	C(27)–C(26)–C(25)	120.3(6)
C(1)–C(2)–H(2)	121.1	C(28)–C(27)–C(26)	121.3(7)
C(3)–C(2)–H(2)	121.1	C(28)–C(27)–H(27)	119.4
C(2)–C(3)–C(4)	119.0(7)	C(26)–C(27)–H(27)	119.4
C(2)–C(3)–H(3)	120.5	C(29)–C(28)–C(27)	120.7(7)
C(4)–C(3)–H(3)	120.5	C(29)–C(28)–H(28)	119.6
C(5)–C(4)–C(3)	120.3(6)	C(27)–C(28)–H(28)	119.6
C(5)–C(4)–H(4)	119.8	C(28)–C(29)–C(30)	119.5(7)
C(3)–C(4)–H(4)	119.8	C(28)–C(29)–H(29)	120.2
C(4)–C(5)–N(1)	122.9(5)	C(30)–C(29)–H(29)	120.2
C(4)–C(5)–C(6)	122.6(5)	C(29)–C(30)–C(31)	119.4(7)
N(1)–C(5)–C(6)	114.4(5)	C(29)–C(30)–H(30)	120.3
O(1)–C(6)–C(7)	106.1(4)	C(31)–C(30)–H(30)	120.3
O(1)–C(6)–C(13)	110.5(4)	C(26)–C(31)–C(30)	121.3(7)
C(7)–C(6)–C(13)	112.0(4)	C(26)–C(31)–H(31)	119.4
O(1)–C(6)–C(5)	107.1(4)	C(30)–C(31)–H(31)	119.4
C(7)–C(6)–C(5)	110.9(5)	C(37)–C(32)–C(33)	116.6(7)
C(13)–C(6)–C(5)	110.1(5)	C(37)–C(32)–C(25)	123.3(6)
C(8)–C(7)–C(12)	122.3(6)	C(33)–C(32)–C(25)	120.0(6)
C(8)–C(7)–C(6)	122.8(5)	O(3)–C(33)–C(34)	123.7(7)
C(12)–C(7)–C(6)	114.9(6)	O(3)–C(33)–C(32)	115.2(6)
C(7)–C(8)–C(9)	122.3(7)	C(34)–C(33)–C(32)	121.0(7)

C(7)–C(8)–H(8)	118.8	C(35)–C(34)–C(33)	119.9(8)
C(9)–C(8)–H(8)	118.8	C(35)–C(34)–H(34)	120.1
C(10)–C(9)–C(8)	117.7(7)	C(33)–C(34)–H(34)	120.1
C(10)–C(9)–H(9)	121.1	C(34)–C(35)–C(36)	120.4(9)
C(8)–C(9)–H(9)	121.1	C(34)–C(35)–H(35)	119.8
C(11)–C(10)–C(9)	120.7(7)	C(36)–C(35)–H(35)	119.8
C(11)–C(10)–H(10)	119.6	C(35)–C(36)–C(37)	119.3(8)
C(9)–C(10)–H(10)	119.6	C(35)–C(36)–H(36)	120.3
C(10)–C(11)–C(12)	123.5(8)	C(37)–C(36)–H(36)	120.3
C(10)–C(11)–H(11)	118.2	C(32)–C(37)–C(36)	122.7(7)
C(12)–C(11)–H(11)	118.2	C(32)–C(37)–H(37)	118.7
C(7)–C(12)–C(11)	113.3(8)	C(36)–C(37)–H(37)	118.7
C(7)–C(12)–H(12)	123.3	O(3)–C(38)–H(38A)	109.5
C(11)–C(12)–H(12)	123.3	O(3)–C(38)–H(38B)	109.5
C(14)–C(13)–C(18)	115.0(6)	H(38A)–C(38)–H(38B)	109.5
C(14)–C(13)–C(6)	122.0(6)	O(3)–C(38)–H(38C)	109.5
C(18)–C(13)–C(6)	122.9(5)	H(38A)–C(38)–H(38C)	109.5
O(2)–C(14)–C(13)	113.6(6)	H(38B)–C(38)–H(38C)	109.5
O(2)–C(14)–C(15)	121.6(7)	C(40)–C(39)–H(39A)	109.5
C(13)–C(14)–C(15)	124.8(7)	C(40)–C(39)–H(39B)	109.5
C(16)–C(15)–C(14)	116.5(7)	H(39A)–C(39)–H(39B)	109.5
C(16)–C(15)–H(15)	121.8	C(40)–C(39)–H(39C)	109.5
C(14)–C(15)–H(15)	121.8	H(39A)–C(39)–H(39C)	109.5
C(17)–C(16)–C(15)	121.6(8)	H(39B)–C(39)–H(39C)	109.5
C(17)–C(16)–H(16)	119.2	O(5)–C(40)–C(41)	129(1)
C(15)–C(16)–H(16)	119.2	O(5)–C(40)–C(39)	118(1)
C(16)–C(17)–C(18)	119.8(8)	C(41)–C(40)–C(39)	113(1)
C(16)–C(17)–H(17)	120.1	C(40)–C(41)–H(41A)	109.5
C(18)–C(17)–H(17)	120.1	C(40)–C(41)–H(41B)	109.5
C(17)–C(18)–C(13)	122.2(7)	H(41A)–C(41)–H(41B)	109.5
C(17)–C(18)–H(18)	118.9	C(40)–C(41)–H(41C)	109.5
C(13)–C(18)–H(18)	118.9	H(41A)–C(41)–H(41C)	109.5
O(2)–C(19)–H(19A)	109.5	H(41B)–C(41)–H(41C)	109.5
O(2)–C(19)–H(19B)	109.5		

Table A44: Anisotropic displacement parameters ( $\text{\AA}^2 \times 10^3$ ) for  $[\text{Co}(\text{OON}_3)_2(\mu\text{-Cl})_2\text{CoCl}_2] \cdot \text{C}_3\text{H}_6\text{O}$ . The anisotropic displacement factor exponent takes the form:  $-2p^2[h^2a^*2U^{11} + \dots + 2hk a^* b^* U^{12}]$

	U11	U22	U33	U23	U13	U12
Co(1)	48(1)	47(1)	45(1)	0(1)	8(1)	2(1)
Co(2)	54(1)	46(1)	66(1)	-3(1)	10(1)	0(1)
Cl(1)	57(1)	66(1)	61(1)	6(1)	4(1)	-8(1)
Cl(2)	57(1)	54(1)	72(1)	8(1)	6(1)	6(1)
Cl(3)	69(1)	82(1)	81(1)	1(1)	29(1)	7(1)
Cl(4)	85(1)	50(1)	129(2)	-12(1)	-16(1)	-3(1)
N(1)	46(3)	45(3)	49(3)	2(2)	12(3)	7(2)
N(2)	51(3)	51(3)	40(3)	1(2)	1(3)	1(3)
O(1)	56(3)	50(3)	49(3)	-4(2)	13(2)	1(2)
O(2)	147(5)	83(4)	100(4)	34(3)	25(4)	-3(4)
O(3)	79(4)	108(4)	81(4)	3(3)	2(3)	39(3)

O(4)	56(3)	51(3)	44(2)	5(2)	15(2)	12(2)
O(5)	147(7)	208(9)	124(6)	-51(6)	15(6)	30(6)
C(1)	61(5)	73(5)	57(5)	-8(4)	3(4)	11(4)
C(2)	52(4)	99(6)	64(5)	-12(4)	-7(4)	19(4)
C(3)	53(4)	85(5)	62(5)	-13(4)	-17(4)	15(4)
C(4)	56(4)	65(4)	50(4)	-16(3)	-2(4)	11(3)
C(5)	48(4)	43(3)	45(4)	-2(3)	5(3)	1(3)
C(6)	42(4)	42(3)	43(4)	-8(3)	4(3)	-4(3)
C(7)	63(4)	37(3)	44(4)	-4(3)	14(3)	0(3)
C(8)	73(5)	45(4)	51(4)	8(3)	14(4)	4(3)
C(9)	122(7)	58(5)	61(5)	0(4)	22(5)	-1(5)
C(10)	149(9)	57(5)	66(5)	12(4)	26(6)	24(6)
C(11)	96(7)	81(6)	90(6)	14(5)	9(5)	36(5)
C(12)	114(7)	98(6)	56(5)	1(4)	2(5)	67(5)
C(13)	49(4)	58(4)	48(4)	10(3)	10(3)	2(3)
C(14)	67(5)	65(5)	67(5)	-6(4)	11(4)	13(4)
C(15)	83(6)	103(6)	59(5)	38(5)	13(4)	-18(5)
C(16)	74(6)	140(8)	75(6)	-15(6)	25(5)	-6(6)
C(17)	67(5)	112(7)	76(6)	-15(5)	21(5)	2(5)
C(18)	60(4)	69(5)	61(5)	-4(4)	20(4)	-3(4)
C(19)	173(10)	100(7)	157(10)	45(7)	41(8)	17(7)
C(20)	55(4)	61(4)	63(5)	7(3)	2(4)	12(3)
C(21)	60(5)	72(5)	66(5)	-12(4)	10(4)	18(4)
C(22)	55(4)	84(5)	66(5)	-3(4)	21(4)	11(4)
C(23)	56(4)	68(4)	62(5)	9(4)	17(4)	3(4)
C(24)	51(4)	52(4)	45(4)	-2(3)	8(3)	5(3)
C(25)	49(4)	50(4)	47(4)	2(3)	7(3)	8(3)
C(26)	56(4)	42(3)	53(4)	6(3)	11(3)	4(3)
C(27)	85(5)	69(5)	53(5)	-2(4)	11(4)	-9(4)
C(28)	77(5)	65(5)	72(5)	-5(4)	1(4)	-19(4)
C(29)	75(5)	72(5)	90(6)	11(5)	13(5)	-16(4)
C(30)	93(6)	72(5)	66(5)	22(4)	9(5)	-22(4)
C(31)	67(4)	68(4)	49(4)	11(4)	4(4)	-14(4)
C(32)	54(4)	52(4)	50(4)	3(3)	7(3)	-8(3)
C(33)	56(5)	75(5)	58(5)	13(4)	4(4)	-2(4)
C(34)	56(5)	111(7)	85(6)	20(5)	-9(5)	-9(5)
C(35)	82(7)	116(7)	75(6)	15(6)	-20(5)	-28(6)
C(36)	114(7)	93(6)	65(6)	-14(5)	-9(6)	-10(6)
C(37)	71(5)	82(5)	61(5)	-11(4)	-3(4)	-1(4)
C(38)	154(10)	246(14)	147(10)	-24(9)	-15(8)	143(10)
C(39)	222(15)	147(11)	209(14)	-5(10)	73(12)	18(10)
C(40)	100(8)	109(8)	93(8)	-5(7)	33(7)	33(6)
C(41)	265(18)	380(20)	128(11)	73(13)	71(12)	187(17)

Table A45: Crystal data and structure refinement for  $[\text{Fe}(\text{OON1})\text{Cl}_2]_2$ 

empirical formula	$\text{C}_{26}\text{H}_{24}\text{Cl}_4\text{Fe}_2\text{N}_2\text{O}_4$
formula weight	681.97
temperature	293(2) K
wavelength	0.71073 Å
crystal system	triclinic

space group	$P\bar{1}$ (No. 2)	
unit cell dimensions	a = 9.882(5) Å b = 11.354(5) Å c = 14.259(5) Å	$\alpha = 79.901(5)^\circ$ $\beta = 87.670(5)^\circ$ $\gamma = 65.751(5)^\circ$
volume	1435(1) Å <sup>3</sup>	
Z	2	
density (calculated)	1.578 gcm <sup>-1</sup>	
absorption coefficient	1.418 mm <sup>-1</sup>	
F(000)	692	
crystal size	0.2 x 0.3 x 0.4 mm <sup>3</sup>	
theta range for data collection	2.26 to 28.10°	
index ranges	-13 < h < 13 -13 < k < 13 -18 < l < 18	
reflections collected	17384	
independent reflections	6418 [R(int) = 0.1593]	
data / restraints / parameters	6418 / 0 / 345	
Goodness-of-fit on F <sup>2</sup>	0.666	
final R indices [I > 2sigma(I)]	R1 = 0.0464, wR2 = 0.0692	
R indices (all data)	R1 = 0.1911, wR2 = 0.0944	
largest diff. peak and hole	0.391 and -0.484 e.Å <sup>-3</sup>	

Table A46: Atomic coordinates (  $\times 10^4$ ) and equivalent isotropic displacement parameters (Å<sup>2</sup> $\times 10^3$ ) for [Fe(OON1)Cl<sub>2</sub>]<sub>2</sub>. U(eq) is defined as one third of the trace of the orthogonalized U<sup>ij</sup> tensor.

	x	y	z	U(eq)
Fe(1)	7421(1)	4612(1)	3415(1)	32(1)
Fe(2)	7493(1)	3378(1)	1592(1)	30(1)
Cl(1)	5411(2)	6076(2)	3884(1)	54(1)
Cl(2)	9364(2)	5068(2)	3569(1)	53(1)
Cl(3)	9659(2)	1667(2)	1589(1)	55(1)
Cl(4)	5653(2)	3070(2)	1061(1)	55(1)
O(1)	7251(4)	3135(4)	2989(2)	36(1)
O(2)	7106(6)	-367(5)	3743(3)	68(2)
O(3)	7306(4)	5002(4)	2000(2)	33(1)
O(4)	7894(6)	8317(5)	1170(3)	66(1)
N(1)	7972(5)	3162(5)	4654(3)	39(1)
N(2)	7823(5)	4469(5)	335(3)	34(1)
C(1)	8410(8)	3274(8)	5511(4)	63(2)
C(2)	8742(8)	2301(9)	6295(5)	70(2)
C(3)	8615(8)	1188(8)	6215(5)	64(2)
C(4)	8176(7)	1054(6)	5359(4)	47(2)
C(5)	7854(6)	2052(6)	4584(4)	34(2)
C(6)	7354(7)	2003(6)	3637(4)	40(2)
C(7)	5866(7)	1865(6)	3666(4)	37(2)
C(8)	4552(7)	2983(7)	3647(4)	53(2)
C(9)	3214(9)	2903(9)	3638(5)	72(2)
C(10)	3155(10)	1739(10)	3639(5)	75(3)
C(11)	4412(10)	610(9)	3669(4)	69(2)

C(12)	5766(9)	701(7)	3688(4)	51(2)
C(13)	7104(10)	-1644(7)	3809(5)	89(3)
C(14)	8050(7)	4091(6)	-529(4)	47(2)
C(15)	8413(7)	5967(7)	-1231(4)	48(2)
C(16)	8364(7)	4788(7)	-1302(4)	51(2)
C(17)	8161(6)	6373(6)	-388(4)	43(2)
C(18)	7848(6)	5621(6)	393(3)	29(1)
C(19)	7525(6)	6022(6)	1369(3)	30(1)
C(20)	6219(7)	7341(6)	1335(3)	33(1)
C(21)	4794(7)	7436(6)	1405(4)	46(2)
C(22)	3588(8)	8608(8)	1404(4)	66(2)
C(23)	3870(10)	9711(8)	1346(5)	72(3)
C(24)	5255(10)	9682(7)	1259(4)	66(2)
C(25)	6460(9)	8448(6)	1248(4)	46(2)
C(26)	8241(9)	9424(8)	1167(5)	82(3)

Table A47: Bond lengths [ $\text{\AA}$ ] and angles [ $^\circ$ ] for  $[\text{Fe}(\text{OON1})\text{Cl}_2]_2$ 

Fe(1)–O(1)	1.951(4)	C(3)–C(4)	1.365(9)
Fe(1)–O(3)	1.986(3)	C(4)–C(5)	1.379(7)
Fe(1)–N(1)	2.109(5)	C(5)–C(6)	1.474(7)
Fe(1)–Cl(1)	2.173(2)	C(6)–C(7)	1.540(8)
Fe(1)–Cl(2)	2.212(2)	C(7)–C(12)	1.360(8)
Fe(2)–O(3)	1.965(4)	C(7)–C(8)	1.391(8)
Fe(2)–O(1)	1.981(3)	C(8)–C(9)	1.363(9)
Fe(2)–N(2)	2.088(4)	C(9)–C(10)	1.35(1)
Fe(2)–Cl(4)	2.176(2)	C(10)–C(11)	1.37(1)
Fe(2)–Cl(3)	2.223(2)	C(11)–C(12)	1.386(9)
O(1)–C(6)	1.414(6)	C(14)–C(16)	1.344(8)
O(2)–C(12)	1.373(8)	C(15)–C(17)	1.339(7)
O(2)–C(13)	1.437(8)	C(15)–C(16)	1.380(9)
O(3)–C(19)	1.422(6)	C(17)–C(18)	1.387(7)
O(4)–C(25)	1.364(8)	C(18)–C(19)	1.520(7)
O(4)–C(26)	1.431(8)	C(19)–C(20)	1.518(7)
N(1)–C(5)	1.333(7)	C(20)–C(25)	1.358(8)
N(1)–C(1)	1.356(7)	C(20)–C(21)	1.368(8)
N(2)–C(18)	1.335(7)	C(21)–C(22)	1.374(8)
N(2)–C(14)	1.355(7)	C(22)–C(23)	1.38(1)
C(1)–C(2)	1.370(9)	C(23)–C(24)	1.36(1)
C(2)–C(3)	1.34(1)	C(24)–C(25)	1.420(9)
O(1)–Fe(1)–O(3)	73.3(1)	C(3)–C(4)–C(5)	120.5(7)
O(1)–Fe(1)–N(1)	76.4(2)	N(1)–C(5)–C(4)	120.7(6)
O(3)–Fe(1)–N(1)	147.0(2)	N(1)–C(5)–C(6)	115.0(5)
O(1)–Fe(1)–Cl(1)	117.2(1)	C(4)–C(5)–C(6)	124.3(6)
O(3)–Fe(1)–Cl(1)	106.2(1)	O(1)–C(6)–C(5)	109.5(5)
N(1)–Fe(1)–Cl(1)	99.2(1)	O(1)–C(6)–C(7)	110.7(5)
O(1)–Fe(1)–Cl(2)	131.3(1)	C(5)–C(6)–C(7)	112.3(4)
O(3)–Fe(1)–Cl(2)	95.6(1)	C(12)–C(7)–C(8)	117.9(7)
N(1)–Fe(1)–Cl(2)	94.4(2)	C(12)–C(7)–C(6)	123.2(6)
Cl(1)–Fe(1)–Cl(2)	111.45(9)	C(8)–C(7)–C(6)	118.9(6)



O(3)–Fe(2)–O(1)	73.2(1)	C(9)–C(8)–C(7)	120.5(8)
O(3)–Fe(2)–N(2)	77.3(2)	C(10)–C(9)–C(8)	120.1(9)
O(1)–Fe(2)–N(2)	150.1(2)	C(9)–C(10)–C(11)	121.8(8)
O(3)–Fe(2)–Cl(4)	124.5(1)	C(10)–C(11)–C(12)	117.6(8)
O(1)–Fe(2)–Cl(4)	102.9(1)	C(7)–C(12)–O(2)	114.7(7)
N(2)–Fe(2)–Cl(4)	97.3(1)	C(7)–C(12)–C(11)	122.2(8)
O(3)–Fe(2)–Cl(3)	122.7(1)	O(2)–C(12)–C(11)	123.1(8)
O(1)–Fe(2)–Cl(3)	97.0(1)	C(16)–C(14)–N(2)	123.1(6)
N(2)–Fe(2)–Cl(3)	95.20(1)	C(17)–C(15)–C(16)	118.8(6)
Cl(4)–Fe(2)–Cl(3)	112.79(9)	C(14)–C(16)–C(15)	119.1(6)
C(6)–O(1)–Fe(1)	121.7(3)	C(15)–C(17)–C(18)	120.2(6)
C(6)–O(1)–Fe(2)	129.8(3)	N(2)–C(18)–C(17)	121.3(5)
Fe(1)–O(1)–Fe(2)	106.3(2)	N(2)–C(18)–C(19)	115.2(4)
C(12)–O(2)–C(13)	118.5(6)	C(17)–C(18)–C(19)	123.5(6)
C(19)–O(3)–Fe(2)	122.2(3)	O(3)–C(19)–C(20)	112.3(4)
C(19)–O(3)–Fe(1)	129.5(3)	O(3)–C(19)–C(18)	108.0(4)
Fe(2)–O(3)–Fe(1)	105.6(2)	C(20)–C(19)–C(18)	112.3(4)
C(25)–O(4)–C(26)	120.2(6)	C(25)–C(20)–C(21)	119.0(6)
C(5)–N(1)–C(1)	117.8(5)	C(25)–C(20)–C(19)	119.8(6)
C(5)–N(1)–Fe(1)	116.6(4)	C(21)–C(20)–C(19)	121.2(6)
C(1)–N(1)–Fe(1)	125.6(5)	C(20)–C(21)–C(22)	122.8(7)
C(18)–N(2)–C(14)	117.4(5)	C(21)–C(22)–C(23)	116.9(8)
C(18)–N(2)–Fe(2)	117.2(3)	C(24)–C(23)–C(22)	123.0(8)
C(14)–N(2)–Fe(2)	125.4(4)	C(23)–C(24)–C(25)	117.8(8)
N(1)–C(1)–C(2)	123.1(7)	C(20)–C(25)–O(4)	117.4(6)
C(3)–C(2)–C(1)	118.6(7)	C(20)–C(25)–C(24)	120.4(7)
C(2)–C(3)–C(4)	119.4(7)	O(4)–C(25)–C(24)	122.2(7)

Table A48: Anisotropic displacement parameters ( $\text{\AA}^2 \times 10^3$ ) for  $[\text{Fe}(\text{OON1})\text{Cl}_2]_2$ . The anisotropic displacement factor exponent takes the form:  $-2 \sum_{i,j} h^2 a_i^2 U^{11} + \dots + 2 h k a_i^* b^* U^{12}$

	U <sup>11</sup>	U <sup>22</sup>	U <sup>33</sup>	U <sup>23</sup>	U <sup>13</sup>	U <sup>12</sup>
Fe(1)	34(1)	27(1)	35(1)	–5(1)	4(1)	–13(1)
Fe(2)	32(1)	24(1)	36(1)	–5(1)	3(1)	–13(1)
Cl(1)	49(1)	45(1)	60(1)	–16(1)	19(1)	–11(1)
Cl(2)	44(1)	64(1)	60(1)	–12(1)	0(1)	–30(1)
Cl(3)	39(1)	35(1)	75(1)	0(1)	10(1)	–5(1)
Cl(4)	52(1)	64(1)	63(1)	–10(1)	–6(1)	–35(1)
O(1)	53(3)	22(2)	34(2)	2(2)	3(2)	–20(2)
O(2)	90(4)	36(3)	85(4)	–14(3)	19(3)	–32(3)
O(3)	48(3)	21(2)	36(2)	–1(2)	3(2)	–20(2)
O(4)	84(4)	42(4)	84(3)	–8(2)	13(3)	–41(3)
N(1)	47(3)	40(4)	34(3)	–4(2)	–1(2)	–21(3)
N(2)	39(3)	32(3)	31(3)	–7(2)	4(2)	–14(3)
C(1)	69(5)	70(6)	51(4)	–8(4)	–7(4)	–30(5)
C(2)	86(7)	79(7)	39(4)	15(4)	–20(4)	–33(5)
C(3)	61(6)	68(6)	43(4)	21(4)	–11(4)	–17(5)
C(4)	51(4)	33(4)	44(4)	3(3)	7(3)	–9(3)
C(5)	29(4)	33(4)	30(3)	4(3)	6(3)	–9(3)
C(6)	41(4)	21(4)	55(4)	1(3)	10(3)	–11(3)

C(7)	52(4)	30(4)	31(3)	-2(3)	6(3)	-21(3)
C(8)	48(5)	55(5)	55(4)	0(3)	7(3)	-25(4)
C(9)	52(6)	81(7)	85(6)	4(5)	10(4)	-36(5)
C(10)	63(7)	104(8)	73(5)	7(5)	-8(5)	-57(6)
C(11)	92(7)	87(7)	60(5)	-7(4)	10(5)	-71(6)
C(12)	72(6)	42(5)	46(4)	-5(3)	13(4)	-32(4)
C(13)	157(10)	40(6)	92(6)	-24(4)	17(6)	-58(6)
C(14)	61(5)	38(4)	52(4)	-15(3)	10(3)	-29(4)
C(15)	48(5)	55(5)	31(3)	2(3)	2(3)	-15(4)
C(16)	62(5)	59(5)	27(4)	-6(3)	8(3)	-21(4)
C(17)	47(4)	27(4)	50(4)	1(3)	7(3)	-14(3)
C(18)	23(3)	30(4)	30(3)	-2(3)	2(2)	-7(3)
C(19)	36(4)	29(4)	29(3)	-2(3)	-1(3)	-20(3)
C(20)	43(4)	22(4)	32(3)	-5(2)	0(3)	-11(3)
C(21)	41(4)	39(4)	51(4)	-5(3)	0(3)	-11(4)
C(22)	52(5)	60(6)	57(5)	-3(4)	9(4)	3(5)
C(23)	74(7)	45(6)	68(5)	-7(4)	8(4)	3(5)
C(24)	101(7)	28(5)	59(5)	-3(3)	18(5)	-19(5)
C(25)	65(5)	29(4)	42(4)	-5(3)	0(3)	-19(4)
C(26)	103(8)	53(6)	106(6)	-20(5)	8(5)	-48(5)

Table A49: Crystal data and structure refinement for  $[\text{Cu}(\text{OON1})\text{Cl}_2]_n$ 

empirical formula	$\text{C}_{13}\text{H}_{12}\text{Cl}_2\text{CuNO}_2$	
formula weight	348.68	
temperature	293(2) K	
wavelength	0.71073 Å	
crystal system	monoclinic	
space group	$P2_1/c$ (No. 14)	
unit cell dimensions	$a = 14.674(2)$ Å	$\alpha = 90^\circ$
	$b = 14.407(2)$ Å	$\beta = 103.84(2)^\circ$
	$c = 7.0563(9)$ Å	$\gamma = 90^\circ$
volume	$1448.5(3)$ Å <sup>3</sup>	
Z	4	
density (calculated)	$1.599$ gcm <sup>-3</sup>	
absorption coefficient	$1.872$ mm <sup>-1</sup>	
F(000)	704	
crystal size	$0.2 \times 0.2 \times 0.2$ mm <sup>3</sup>	
theta range for data collection	$2.83$ to $28.18^\circ$	
index ranges	$-19 < h < 19$	
	$-19 < k < 19$	
	$-8 < l < 8$	
reflections collected	13633	
independent reflections	3342 [R(int) = 0.1464]	
data / restraints / parameters	3342 / 36 / 193	
Goodness-of-fit on F <sup>2</sup>	0.845	
final R indices [I > 2sigma(I)]	R1 = 0.0467, wR2 = 0.0749	
R indices (all data)	R1 = 0.1452, wR2 = 0.0880	
largest diff. peak and hole	$0.407$ and $-0.512$ e.Å <sup>-3</sup>	

Table A50: Atomic coordinates ( $\times 10^4$ ) and equivalent isotropic displacement parameters ( $\text{\AA}^2 \times 10^3$ ) for  $[\text{Cu}(\text{OON1})\text{Cl}_2]_n$ .  $U(\text{eq})$  is defined as one third of the trace of the orthogonalized  $U^{ij}$  tensor

	x	y	z	U(eq)
Cu(1)	2981(1)	3003(1)	3619(1)	42(1)
Cl(1)	4041(1)	2148(1)	5738(2)	46(1)
Cl(2)	2007(1)	1825(1)	2386(2)	50(1)
O(01)	2174(3)	3822(2)	1644(6)	46(1)
O(2)	1251(7)	5261(7)	3140(20)	73(3)
O(3)	2376(9)	6118(7)	-1137(17)	80(4)
N(1)	3472(3)	4247(3)	4649(6)	40(1)
C(1)	2564(4)	4741(3)	1465(9)	48(2)
C(2)	1097(8)	5533(7)	1710(20)	129(6)
C(3)	3210(3)	4962(3)	3407(9)	44(2)
C(4)	4382(4)	5289(4)	6958(9)	61(2)
C(5)	3563(4)	5844(4)	3874(10)	68(2)
C(6)	2347(17)	6800(12)	-2500(30)	153(9)
C(7)	4030(4)	4416(4)	6388(8)	51(2)
C(8)	4149(4)	5999(4)	5652(11)	71(2)
C(9)	1788(5)	5433(4)	866(13)	75(3)
C(10)	577(14)	5360(13)	4110(30)	128(7)
C(11)	1749(8)	5987(6)	-750(20)	149(6)
C(12)	985(10)	6613(8)	-1390(30)	223(10)
C(13)	338(8)	6098(8)	1180(20)	192(8)
C(14)	323(11)	6607(7)	-270(30)	207(10)

Table A51: Bond lengths [ $\text{\AA}$ ] and angles [ $^\circ$ ] for  $[\text{Cu}(\text{OON1})\text{Cl}_2]_n$ 

Cu(1)–N(1)	2.001(4)	C(1)–C(9)	1.497(8)
Cu(1)–Cl(1)	2.249(1)	C(2)–C(9)	1.30(2)
Cu(1)–Cl(2)	2.255(1)	C(2)–C(13)	1.36(1)
O(01)–C(1)	1.461(6)	C(3)–C(5)	1.382(6)
O(2)–C(2)	1.05(2)	C(4)–C(8)	1.365(8)
O(2)–C(10)	1.34(2)	C(4)–C(7)	1.382(7)
O(3)–C(11)	1.04(1)	C(5)–C(8)	1.359(8)
O(3)–C(6)	1.37(2)	C(9)–C(11)	1.38(1)
N(1)–C(7)	1.325(6)	C(11)–C(12)	1.43(2)
N(1)–C(3)	1.348(6)	C(12)–C(14)	1.39(3)
C(1)–C(3)	1.502(7)	C(13)–C(14)	1.26(2)
N(1)–Cu(1)–Cl(1)	96.8(1)	N(1)–C(3)–C(1)	116.8(4)
N(1)–Cu(1)–Cl(2)	162.5(1)	C(5)–C(3)–C(1)	122.1(5)
Cl(1)–Cu(1)–Cl(2)	96.76(5)	C(8)–C(4)–C(7)	118.0(6)
C(2)–O(2)–C(10)	116(2)	C(8)–C(5)–C(3)	119.3(6)
C(11)–O(3)–C(6)	116(2)	N(1)–C(7)–C(4)	122.8(5)
C(7)–N(1)–C(3)	118.6(4)	C(5)–C(8)–C(4)	120.1(5)
C(7)–N(1)–Cu(1)	126.1(4)	C(2)–C(9)–C(11)	116(1)
C(3)–N(1)–Cu(1)	115.3(3)	C(2)–C(9)–C(1)	124.6(9)
O(01)–C(1)–C(3)	106.8(4)	C(11)–C(9)–C(1)	120(1)

O(01)–C(1)–C(9)	109.9(5)	O(3)–C(11)–C(9)	117(1)
C(3)–C(1)–C(9)	112.8(5)	O(3)–C(11)–C(12)	119(1)
O(2)–C(2)–C(9)	113(1)	C(9)–C(11)–C(12)	120(2)
O(2)–C(2)–C(13)	118(2)	C(14)–C(12)–C(11)	115(2)
C(9)–C(2)–C(13)	128(2)	C(14)–C(13)–C(2)	115(2)
N(1)–C(3)–C(5)	121.1(5)	C(13)–C(14)–C(12)	126(2)

Table A52: Anisotropic displacement parameters ( $\text{\AA}^2 \times 10^3$ ) for  $[\text{Cu}(\text{OON1})\text{Cl}_2]_n$ . The anisotropic displacement factor exponent takes the form:  $-2p^2 [h^2 a^* 2U^{11} + \dots + 2 h k a^* b^* U^{12}]$

	U <sup>11</sup>	U <sup>22</sup>	U <sup>33</sup>	U <sup>23</sup>	U <sup>13</sup>	U <sup>12</sup>
Cu(1)	46(1)	32(1)	42(1)	0(1)	-2(1)	-1(1)
Cl(1)	48(1)	46(1)	39(1)	5(1)	4(1)	5(1)
Cl(2)	56(1)	38(1)	49(1)	-1(1)	-2(1)	-9(1)
O(01)	51(2)	29(2)	51(3)	-11(2)	1(2)	-2(2)
O(2)	59(7)	80(7)	95(10)	-17(6)	48(7)	24(5)
O(3)	111(10)	56(6)	91(9)	42(6)	60(8)	20(6)
N(1)	39(3)	41(2)	38(3)	-4(2)	1(2)	-3(2)
C(1)	54(3)	33(3)	53(4)	6(2)	4(3)	0(2)
C(2)	87(8)	91(7)	165(13)	-72(8)	-57(9)	43(6)
C(3)	37(3)	30(3)	57(4)	-4(3)	-3(3)	-2(2)
C(4)	69(4)	59(4)	47(5)	-16(3)	-2(3)	-17(3)
C(5)	67(4)	36(3)	89(6)	5(3)	-4(4)	-11(3)
C(6)	230(30)	111(14)	150(20)	41(14)	113(17)	53(15)
C(7)	57(4)	50(3)	40(4)	-3(3)	3(3)	-10(3)
C(8)	68(5)	42(3)	92(6)	-12(4)	-5(4)	-13(3)
C(9)	62(5)	28(3)	106(7)	-9(3)	-36(4)	11(3)
C(10)	125(16)	141(16)	140(20)	-21(13)	73(15)	22(13)
C(11)	105(8)	75(6)	210(13)	83(7)	-75(8)	-33(6)
C(12)	177(14)	86(7)	322(19)	107(10)	-108(13)	-37(9)
C(13)	97(7)	97(8)	316(18)	-120(9)	-78(10)	49(7)
C(14)	154(12)	33(5)	350(20)	-46(9)	-108(13)	24(7)

Table A53: Crystal data and structure refinement for  $[\text{Cu}(\text{OON3})\text{Cl}_2]_2$

empirical formula	$\text{C}_{19}\text{H}_{17}\text{Cl}_2\text{CuNO}_2$	
formula weight	425.78	
temperature	293(2) K	
wavelength	0.71073 $\text{\AA}$	
crystal system	monoclinic	
space group	$P2_1/c$ (No. 14)	
unit cell dimensions	$a = 9.073(2) \text{\AA}$ $b = 11.196(2) \text{\AA}$ $c = 18.518(3) \text{\AA}$	$a = 90^\circ$ $b = 100.18(2)^\circ$ $g = 90^\circ$
volume	$1851.5(5) \text{\AA}^3$	
Z	4	
density (calculated)	$1.527 \text{ g cm}^{-3}$	
absorption coefficient	$1.480 \text{ mm}^{-1}$	

F(000)	868
crystal size	0.2 x 0.3 x 0.4 mm <sup>3</sup>
theta range for data collection	2.88 to 28.15°.
index ranges	-11 < h < 11 -14 < k < 14 -24 < l < 24
reflections collected	17270
independent reflections	4478 [R(int) = 0.2427]
data / restraints / parameters	4478 / 0 / 228
Goodness-of-fit on F <sup>2</sup>	0.655
final R indices [I>2sigma(I)]	R1 = 0.0452, wR2 = 0.0542
R indices (all data)	R1 = 0.2433, wR2 = 0.0824
largest diff. peak and hole	0.298 and -0.340 e.Å <sup>-3</sup>

Table A54: Atomic coordinates ( x 10<sup>4</sup>) and equivalent isotropic displacement parameters (Å<sup>2</sup>x 10<sup>3</sup>) for [Cu(OON3)Cl<sub>2</sub>]<sub>2</sub>. U(eq) is defined as one third of the trace of the orthogonalized U<sup>ij</sup> tensor

	x	y	z	U(eq)
Cu(1)	5985(1)	1089(1)	4740(1)	48(1)
Cl(1)	4577(2)	1165(2)	5638(1)	54(1)
Cl(2)	8181(2)	958(2)	5470(1)	90(1)
O(1)	4131(4)	1448(3)	4031(2)	44(1)
O(2)	1988(4)	2912(4)	4202(2)	57(1)
N(1)	6756(5)	1531(5)	3829(2)	50(2)
C(1)	8144(6)	1308(7)	3699(4)	72(2)
C(2)	8594(8)	1602(9)	3049(4)	100(4)
C(3)	7608(8)	2147(8)	2518(4)	85(3)
C(4)	6175(7)	2376(6)	2625(3)	61(2)
C(5)	5768(6)	2050(6)	3284(3)	46(2)
C(6)	4235(5)	2306(5)	3456(3)	33(1)
C(7)	3008(6)	2028(6)	2798(3)	41(2)
C(8)	2352(7)	2927(7)	2341(3)	62(2)
C(9)	1253(7)	2651(9)	1738(4)	83(3)
C(10)	802(8)	1517(10)	1616(4)	85(3)
C(11)	1443(8)	625(8)	2051(4)	78(3)
C(12)	2569(6)	871(7)	2656(3)	56(2)
C(13)	4102(6)	3539(5)	3755(3)	36(2)
C(14)	5068(7)	4461(7)	3657(3)	49(2)
C(15)	4912(9)	5592(8)	3908(4)	76(2)
C(16)	3779(11)	5806(7)	4263(4)	80(3)
C(17)	2773(8)	4963(8)	4384(4)	62(2)
C(18)	2956(6)	3846(7)	4116(3)	45(2)
C(19)	1053(8)	3031(7)	4735(4)	107(3)

Table A55: Bond lengths [Å] and angles [°] for [Cu(OON3)Cl<sub>2</sub>]<sub>2</sub>

Cu(1)–N(1)	1.999(4)	C(7)–C(8)	1.381(8)
Cu(1)–Cl(2)	2.207(2)	C(8)–C(9)	1.394(8)

Cu(1)–Cl(1)	2.271(2)	C(8)–H(8)	0.9300
Cu(1)–Cl(1)#1	2.644(2)	C(9)–C(10)	1.34(1)
Cl(1)–Cu(1)#1	2.644(2)	C(9)–H(9)	0.9300
O(1)–C(6)	1.448(6)	C(10)–C(11)	1.35(1)
O(1)–H(1)	0.8200	C(10)–H(10)	0.9300
O(2)–C(18)	1.393(7)	C(11)–C(12)	1.404(8)
O(2)–C(19)	1.417(6)	C(11)–H(11)	0.9300
N(1)–C(1)	1.347(6)	C(12)–H(12)	0.9300
N(1)–C(5)	1.357(6)	C(13)–C(18)	1.375(7)
C(1)–C(2)	1.377(8)	C(13)–C(14)	1.387(7)
C(1)–H(1)	0.9300	C(14)–C(15)	1.365(9)
C(2)–C(3)	1.35(1)	C(14)–H(14)	0.9300
C(2)–H(2)	0.9300	C(15)–C(16)	1.337(9)
C(3)–C(4)	1.374(8)	C(15)–H(15)	0.9300
C(3)–H(3)	0.9300	C(16)–C(17)	1.358(9)
C(4)–C(5)	1.384(7)	C(16)–H(16)	0.9300
C(4)–H(4)	0.9300	C(17)–C(18)	1.367(9)
C(5)–C(6)	1.509(7)	C(17)–H(17)	0.9300
C(6)–C(13)	1.499(7)	C(19)–H(19A)	0.9600
C(6)–C(7)	1.531(7)	C(19)–H(19B)	0.9600
C(7)–C(12)	1.367(9)	C(19)–H(19C)	0.9600
N(1)–Cu(1)–Cl(2)	96.9(1)	C(9)–C(8)–H(8)	120.1
N(1)–Cu(1)–Cl(1)	159.2(2)	C(10)–C(9)–C(8)	120.0(8)
Cl(2)–Cu(1)–Cl(1)	96.77(7)	C(10)–C(9)–H(9)	120.0
N(1)–Cu(1)–Cl(1)#1	95.3(1)	C(8)–C(9)–H(9)	120.0
Cl(2)–Cu(1)–Cl(1)#1	102.09(9)	C(9)–C(10)–C(11)	120.9(7)
Cl(1)–Cu(1)–Cl(1)#1	97.01(6)	C(9)–C(10)–H(10)	119.5
Cu(1)–Cl(1)–Cu(1)#1	82.99(6)	C(11)–C(10)–H(10)	119.5
C(6)–O(1)–H(1)	109.5	C(10)–C(11)–C(12)	120.5(8)
C(18)–O(2)–C(19)	118.5(5)	C(10)–C(11)–H(11)	119.7
C(1)–N(1)–C(5)	117.6(5)	C(12)–C(11)–H(11)	119.7
C(1)–N(1)–Cu(1)	125.6(5)	C(7)–C(12)–C(11)	119.0(7)
C(5)–N(1)–Cu(1)	116.7(4)	C(7)–C(12)–H(12)	120.5
N(1)–C(1)–C(2)	122.9(6)	C(11)–C(12)–H(12)	120.5
N(1)–C(1)–H(1)	118.6	C(18)–C(13)–C(14)	115.3(6)
C(2)–C(1)–H(1)	118.6	C(18)–C(13)–C(6)	121.7(5)
C(3)–C(2)–C(1)	118.9(6)	C(14)–C(13)–C(6)	122.9(5)
C(3)–C(2)–H(2)	120.6	C(15)–C(14)–C(13)	122.7(7)
C(1)–C(2)–H(2)	120.6	C(15)–C(14)–H(14)	118.7
C(2)–C(3)–C(4)	120.0(7)	C(13)–C(14)–H(14)	118.7
C(2)–C(3)–H(3)	120.0	C(16)–C(15)–C(14)	118.0(8)
C(4)–C(3)–H(3)	120.0	C(16)–C(15)–H(15)	121.0
C(3)–C(4)–C(5)	119.1(6)	C(14)–C(15)–H(15)	121.0
C(3)–C(4)–H(4)	120.5	C(15)–C(16)–C(17)	123.6(8)
C(5)–C(4)–H(4)	120.5	C(15)–C(16)–H(16)	118.2
N(1)–C(5)–C(4)	121.6(5)	C(17)–C(16)–H(16)	118.2
N(1)–C(5)–C(6)	115.9(5)	C(16)–C(17)–C(18)	116.6(7)
C(4)–C(5)–C(6)	122.4(6)	C(16)–C(17)–H(17)	121.7
O(1)–C(6)–C(13)	108.7(4)	C(18)–C(17)–H(17)	121.7
O(1)–C(6)–C(5)	102.2(4)	C(17)–C(18)–C(13)	123.8(7)
C(13)–C(6)–C(5)	113.0(4)	C(17)–C(18)–O(2)	121.7(6)

O(1)–C(6)–C(7)	108.5(4)	C(13)–C(18)–O(2)	114.5(6)
C(13)–C(6)–C(7)	112.7(5)	O(2)–C(19)–H(19A)	109.5
C(5)–C(6)–C(7)	111.1(5)	O(2)–C(19)–H(19B)	109.5
C(12)–C(7)–C(8)	119.7(6)	H(19A)–C(19)–H(19B)	109.5
C(12)–C(7)–C(6)	119.5(6)	O(2)–C(19)–H(19C)	109.5
C(8)–C(7)–C(6)	120.9(6)	H(19A)–C(19)–H(19C)	109.5
C(7)–C(8)–C(9)	119.9(7)	H(19B)–C(19)–H(19C)	109.5
C(7)–C(8)–H(8)	120.1		

Symmetry transformations used to generate equivalent atoms: #1  $-x+1, -y, -z+1$

Table A56: Anisotropic displacement parameters ( $\text{\AA}^2 \times 10^3$ ) for  $[\text{Cu}(\text{OON}_3)\text{Cl}_2]_2$ . The anisotropic displacement factor exponent takes the form:  $-2p^2 [h^2 a^* 2U^{11} + \dots + 2hk a^* b^* U^{12}]$

	U <sup>11</sup>	U <sup>22</sup>	U <sup>33</sup>	U <sup>23</sup>	U <sup>13</sup>	U <sup>12</sup>
Cu(1)	42(1)	49(1)	49(1)	-5(1)	1(1)	-6(1)
Cl(1)	71(1)	45(1)	47(1)	-10(1)	16(1)	-1(1)
Cl(2)	48(1)	146(2)	67(1)	0(2)	-13(1)	-13(1)
O(1)	33(2)	48(3)	50(3)	7(2)	9(2)	0(2)
O(2)	52(3)	73(4)	51(3)	-5(3)	21(2)	6(3)
N(1)	35(3)	65(5)	51(3)	-15(3)	9(3)	-9(3)
C(1)	33(3)	104(7)	74(5)	-23(5)	-1(3)	3(4)
C(2)	42(4)	198(12)	68(6)	-32(6)	29(4)	-8(5)
C(3)	52(5)	155(9)	53(5)	-23(5)	23(4)	-29(5)
C(4)	48(4)	99(6)	36(4)	-8(4)	9(3)	-16(4)
C(5)	38(4)	63(5)	38(4)	-8(4)	9(3)	-12(3)
C(6)	31(3)	38(4)	29(3)	5(3)	8(3)	-11(3)
C(7)	25(3)	59(5)	40(4)	-10(4)	7(3)	-5(3)
C(8)	55(4)	85(6)	41(4)	-5(4)	-6(3)	-10(4)
C(9)	55(5)	154(9)	36(4)	5(5)	-3(4)	-16(5)
C(10)	46(5)	162(11)	46(5)	-40(6)	8(4)	-44(6)
C(11)	64(5)	96(7)	78(6)	-48(5)	23(4)	-21(5)
C(12)	43(4)	74(7)	51(4)	-21(4)	5(3)	-11(4)
C(13)	36(3)	47(5)	23(3)	0(3)	2(3)	-9(3)
C(14)	63(4)	51(5)	32(4)	-2(4)	4(3)	-8(4)
C(15)	91(6)	56(7)	74(6)	13(5)	-8(5)	-18(5)
C(16)	113(7)	44(6)	67(6)	-4(5)	-29(5)	16(6)
C(17)	72(5)	62(6)	48(5)	-6(4)	-2(4)	15(5)
C(18)	46(3)	50(5)	36(3)	-2(4)	-3(3)	2(4)
C(19)	75(5)	175(9)	83(5)	-31(7)	47(4)	-18(6)

Table A57: Crystal data and structure refinement for  $[\text{Cu}(\text{py})_4(\text{OTf})_2] \cdot 2\text{C}_5\text{H}_5\text{N}$

empirical formula	$\text{C}_{32}\text{H}_{30}\text{CuF}_6\text{N}_6\text{O}_6\text{S}_2$
formula weight	836.28
temperature	293(2) K
wavelength	0.71073 $\text{\AA}$
crystal system	monoclinic
space group	$P2_1/c$ (No. 14)

unit cell dimensions	a = 19.545(5) Å b = 9.326(5) Å c = 20.958(5) Å	$\alpha = 90^\circ$ $\beta = 97.841(5)^\circ$ $\gamma = 90^\circ$
volume	3784(2) Å <sup>3</sup>	
Z	4	
density (calculated)	1.468 gcm <sup>-3</sup>	
absorption coefficient	0.767 mm <sup>-1</sup>	
F(000)	1708	
crystal size	0.4 x 0.4 x 0.6 mm <sup>3</sup>	
theta range for data collection	1.96 to 27.34°	
index ranges	-25 < h < 25 -10 < k < 11 -27 < l < 26	
reflections collected	47564	
independent reflections	8425 [R(int) = 0.1010]	
data / restraints / parameters	8425 / 0 / 558	
Goodness-of-fit on F <sup>2</sup>	0.702	
final R indices [I > 2sigma(I)]	R1 = 0.0388, wR2 = 0.0643	
R indices (all data)	R1 = 0.1332, wR2 = 0.0786	
largest diff. peak and hole	0.316 and -0.487 e.Å <sup>-3</sup>	

Table A58: Atomic coordinates (  $\times 10^4$ ) and equivalent isotropic displacement parameters (Å<sup>2</sup> $\times 10^3$ ) for [Cu(py)<sub>4</sub>(OTf)<sub>2</sub>] $\cdot$ 2C<sub>3</sub>H<sub>5</sub>N. U(eq) is defined as one third of the trace of the orthogonalized U<sup>ij</sup> tensor

	x	y	z	U(eq)
Cu(1)	7549(1)	-134(1)	3522(1)	49(1)
S(1)	8238(1)	2643(1)	4773(1)	54(1)
S(2)	6624(1)	-2922(1)	2443(1)	55(1)
O(1)	8048(1)	1832(3)	4190(1)	62(1)
O(2)	8705(1)	1913(3)	5249(1)	76(1)
O(3)	7675(1)	3357(3)	5006(1)	83(1)
O(4)	7151(1)	-2074(3)	2816(1)	67(1)
O(5)	6122(1)	-3510(3)	2810(1)	71(1)
O(6)	6350(1)	-2311(3)	1833(1)	82(1)
F(1)	9300(1)	3573(3)	4278(1)	112(1)
F(2)	8401(1)	4825(3)	4046(1)	118(1)
F(3)	8979(2)	4941(3)	4978(1)	147(1)
F(4)	7423(1)	-5109(3)	2751(1)	101(1)
F(5)	6699(2)	-5416(3)	1906(1)	124(1)
F(6)	7583(1)	-4102(3)	1875(1)	107(1)
N(1)	6630(1)	896(3)	3379(1)	49(1)
N(2)	7839(1)	892(3)	2753(1)	50(1)
N(3)	7231(1)	-1149(3)	4289(1)	49(1)
N(4)	8477(1)	-1157(3)	3688(1)	49(1)
N(5)	6020(3)	-8614(14)	531(6)	293(7)
N(6)	10817(3)	967(6)	3830(3)	138(2)
C(1)	6605(2)	2326(4)	3372(2)	60(1)
C(2)	5990(2)	3077(5)	3285(2)	78(1)
C(3)	5384(2)	2343(5)	3187(2)	83(1)



C(4)	5403(2)	886(5)	3191(2)	76(1)
C(5)	6027(2)	197(5)	3291(2)	62(1)
C(6)	8414(2)	1691(4)	2804(2)	58(1)
C(7)	8618(2)	2401(5)	2290(2)	73(1)
C(8)	8226(2)	2326(5)	1700(2)	73(1)
C(9)	7643(2)	1507(5)	1633(2)	69(1)
C(10)	7462(2)	815(4)	2167(2)	59(1)
C(11)	6989(2)	-416(5)	4756(2)	59(1)
C(12)	6752(2)	-1057(6)	5274(2)	73(1)
C(13)	6764(2)	-2537(6)	5310(2)	81(1)
C(14)	7020(2)	-3287(5)	4844(2)	72(1)
C(15)	7239(2)	-2571(5)	4334(2)	60(1)
C(16)	8710(2)	-1974(4)	3242(2)	62(1)
C(17)	9332(2)	-2697(5)	3352(2)	74(1)
C(18)	9729(2)	-2581(5)	3939(2)	76(1)
C(19)	9503(2)	-1750(4)	4400(2)	66(1)
C(20)	8881(2)	-1051(4)	4258(2)	59(1)
C(21)	8751(2)	4075(5)	4504(2)	75(1)
C(22)	7103(2)	-4470(5)	2229(2)	76(1)
C(23)	5426(6)	-7110(9)	215(5)	212(5)
C(24)	5575(12)	-8420(30)	152(7)	503(17)
C(25)	4993(4)	-7160(11)	699(5)	197(4)
C(26)	5625(4)	-9055(8)	1095(4)	180(3)
C(27)	5168(4)	-8159(11)	1169(3)	179(4)
C(28)	10281(3)	1441(8)	3395(3)	108(2)
C(29)	10221(3)	2666(9)	3160(2)	101(2)
C(30)	10689(5)	3604(7)	3348(3)	125(2)
C(31)	11259(4)	3282(8)	3784(3)	125(2)
C(32)	11316(3)	1957(9)	4023(3)	128(2)

Table A59: Bond lengths [ $\text{\AA}$ ] and angles [ $^\circ$ ] for  $[\text{Cu}(\text{py})_4(\text{OTf})_2] \cdot 2\text{C}_5\text{H}_5\text{N}$ 

Cu(1)–N(2)	2.022(3)	N(5)–C(26)	1.55(1)
Cu(1)–N(1)	2.023(3)	N(5)–C(23)	1.88(2)
Cu(1)–N(3)	2.035(3)	N(6)–C(32)	1.363(7)
Cu(1)–N(4)	2.036(3)	N(6)–C(28)	1.366(7)
Cu(1)–O(4)	2.399(2)	C(1)–C(2)	1.383(5)
Cu(1)–O(1)	2.429(2)	C(2)–C(3)	1.359(5)
S(1)–O(3)	1.427(2)	C(3)–C(4)	1.360(6)
S(1)–O(2)	1.430(2)	C(4)–C(5)	1.369(5)
S(1)–O(1)	1.442(2)	C(6)–C(7)	1.370(5)
S(1)–C(21)	1.807(4)	C(7)–C(8)	1.364(6)
S(2)–O(6)	1.435(2)	C(8)–C(9)	1.363(5)
S(2)–O(5)	1.436(2)	C(9)–C(10)	1.379(5)
S(2)–O(4)	1.442(2)	C(11)–C(12)	1.374(5)
S(2)–C(22)	1.811(4)	C(12)–C(13)	1.382(6)
F(1)–C(21)	1.317(4)	C(13)–C(14)	1.352(6)
F(2)–C(21)	1.303(4)	C(14)–C(15)	1.378(5)
F(3)–C(21)	1.310(4)	C(16)–C(17)	1.381(5)
F(4)–C(22)	1.324(4)	C(17)–C(18)	1.367(5)
F(5)–C(22)	1.310(4)	C(18)–C(19)	1.359(6)

F(6)–C(22)	1.318(4)	C(19)–C(20)	1.376(5)
N(1)–C(1)	1.335(4)	C(23)–C(24)	1.27(3)
N(1)–C(5)	1.337(4)	C(23)–C(25)	1.41(1)
N(2)–C(6)	1.341(4)	C(25)–C(27)	1.37(1)
N(2)–C(10)	1.345(4)	C(26)–C(27)	1.248(9)
N(3)–C(15)	1.329(5)	C(28)–C(29)	1.243(7)
N(3)–C(11)	1.332(4)	C(29)–C(30)	1.288(8)
N(4)–C(16)	1.335(4)	C(30)–C(31)	1.373(8)
N(4)–C(20)	1.343(4)	C(31)–C(32)	1.333(8)
N(5)–C(24)	1.11(2)		
N(2)–Cu(1)–N(1)	89.9(1)	N(1)–C(1)–C(2)	122.5(4)
N(2)–Cu(1)–N(3)	178.5(1)	C(3)–C(2)–C(1)	119.3(4)
N(1)–Cu(1)–N(3)	88.7(1)	C(2)–C(3)–C(4)	118.6(4)
N(2)–Cu(1)–N(4)	91.1(1)	C(3)–C(4)–C(5)	119.6(4)
N(1)–Cu(1)–N(4)	178.6(1)	N(1)–C(5)–C(4)	122.8(4)
N(3)–Cu(1)–N(4)	90.5(1)	N(2)–C(6)–C(7)	122.4(4)
N(2)–Cu(1)–O(4)	88.1(1)	C(8)–C(7)–C(6)	120.1(4)
N(1)–Cu(1)–O(4)	93.4(1)	C(9)–C(8)–C(7)	118.8(4)
N(3)–Cu(1)–O(4)	91.6(1)	C(8)–C(9)–C(10)	118.7(4)
N(4)–Cu(1)–O(4)	87.6(1)	N(2)–C(10)–C(9)	123.2(4)
N(2)–Cu(1)–O(1)	88.2(1)	N(3)–C(11)–C(12)	123.3(4)
N(1)–Cu(1)–O(1)	90.3(1)	C(11)–C(12)–C(13)	118.2(4)
N(3)–Cu(1)–O(1)	92.2(1)	C(14)–C(13)–C(12)	118.8(4)
N(4)–Cu(1)–O(1)	88.7(1)	C(13)–C(14)–C(15)	119.6(4)
O(4)–Cu(1)–O(1)	174.73(8)	N(3)–C(15)–C(14)	122.4(4)
O(3)–S(1)–O(2)	115.7(2)	N(4)–C(16)–C(17)	122.6(4)
O(3)–S(1)–O(1)	114.5(2)	C(18)–C(17)–C(16)	119.3(4)
O(2)–S(1)–O(1)	114.0(2)	C(19)–C(18)–C(17)	119.1(4)
O(3)–S(1)–C(21)	104.4(2)	C(18)–C(19)–C(20)	118.6(4)
O(2)–S(1)–C(21)	103.9(2)	N(4)–C(20)–C(19)	123.6(4)
O(1)–S(1)–C(21)	102.2(2)	F(2)–C(21)–F(3)	108.5(4)
O(6)–S(2)–O(5)	115.5(2)	F(2)–C(21)–F(1)	107.3(4)
O(6)–S(2)–O(4)	114.6(2)	F(3)–C(21)–F(1)	106.4(4)
O(5)–S(2)–O(4)	114.2(2)	F(2)–C(21)–S(1)	111.6(3)
O(6)–S(2)–C(22)	103.8(2)	F(3)–C(21)–S(1)	111.4(3)
O(5)–S(2)–C(22)	104.0(2)	F(1)–C(21)–S(1)	111.4(3)
O(4)–S(2)–C(22)	102.4(2)	F(5)–C(22)–F(6)	108.0(4)
S(1)–O(1)–Cu(1)	157.1(2)	F(5)–C(22)–F(4)	107.8(4)
S(2)–O(4)–Cu(1)	153.6(1)	F(6)–C(22)–F(4)	106.9(3)
C(1)–N(1)–C(5)	117.2(3)	F(5)–C(22)–S(2)	111.6(3)
C(1)–N(1)–Cu(1)	120.4(2)	F(6)–C(22)–S(2)	111.3(3)
C(5)–N(1)–Cu(1)	122.5(3)	F(4)–C(22)–S(2)	110.9(3)
C(6)–N(2)–C(10)	116.9(3)	C(24)–C(23)–C(25)	102(1)
C(6)–N(2)–Cu(1)	121.4(2)	C(24)–C(23)–N(5)	34.8(8)
C(10)–N(2)–Cu(1)	121.6(2)	C(25)–C(23)–N(5)	97.2(7)
C(15)–N(3)–C(11)	117.6(3)	N(5)–C(24)–C(23)	105(2)
C(15)–N(3)–Cu(1)	121.2(2)	C(27)–C(25)–C(23)	115.2(7)
C(11)–N(3)–Cu(1)	121.2(3)	C(27)–C(26)–N(5)	110.9(7)
C(16)–N(4)–C(20)	116.7(3)	C(26)–C(27)–C(25)	118.7(7)
C(16)–N(4)–Cu(1)	122.0(2)	C(29)–C(28)–N(6)	125.7(6)
C(20)–N(4)–Cu(1)	121.4(2)	C(28)–C(29)–C(30)	118.5(6)

C(24)–N(5)–C(26)	100(1)	C(29)–C(30)–C(31)	122.2(6)
C(24)–N(5)–C(23)	41(2)	C(32)–C(31)–C(30)	118.1(6)
C(26)–N(5)–C(23)	96.8(5)	C(31)–C(32)–N(6)	119.7(5)
C(32)–N(6)–C(28)	115.6(5)		

Table A60: Anisotropic displacement parameters ( $\text{\AA}^2 \times 10^3$ ) for  $[\text{Cu}(\text{py})_4(\text{OTf})_2] \cdot 2\text{C}_5\text{H}_5\text{N}$ . The anisotropic displacement factor exponent takes the form:  $-2p^2[h^2a^*2U^{11} + \dots + 2hk a^* b^* U^{12}]$

	U <sup>11</sup>	U <sup>22</sup>	U <sup>33</sup>	U <sup>23</sup>	U <sup>13</sup>	U <sup>12</sup>
Cu(1)	43(1)	56(1)	48(1)	9(1)	7(1)	4(1)
S(1)	59(1)	55(1)	50(1)	1(1)	7(1)	3(1)
S(2)	53(1)	57(1)	55(1)	-1(1)	5(1)	1(1)
O(1)	69(2)	66(2)	48(2)	-5(1)	-5(1)	-5(1)
O(2)	85(2)	85(2)	51(2)	9(1)	-11(1)	13(2)
O(3)	78(2)	87(2)	92(2)	2(2)	38(2)	23(2)
O(4)	59(1)	63(2)	77(2)	-14(1)	1(1)	-11(1)
O(5)	64(2)	73(2)	82(2)	2(1)	28(1)	-8(1)
O(6)	78(2)	100(2)	62(2)	19(2)	-8(1)	14(2)
F(1)	80(2)	122(2)	144(2)	-3(2)	48(2)	-20(2)
F(2)	135(2)	91(2)	130(2)	55(2)	23(2)	-2(2)
F(3)	204(3)	106(2)	133(2)	-48(2)	27(2)	-81(2)
F(4)	110(2)	83(2)	113(2)	27(2)	26(1)	36(2)
F(5)	148(2)	91(2)	137(2)	-55(2)	31(2)	-14(2)
F(6)	115(2)	107(2)	113(2)	9(2)	66(2)	26(2)
N(1)	47(2)	46(2)	53(2)	8(1)	6(1)	1(1)
N(2)	46(2)	56(2)	47(2)	5(1)	6(1)	3(1)
N(3)	46(2)	49(2)	53(2)	5(2)	9(1)	5(1)
N(4)	46(2)	54(2)	47(2)	7(2)	7(1)	2(1)
N(5)	119(5)	408(15)	377(13)	-242(12)	121(7)	-27(7)
N(6)	124(4)	148(5)	153(5)	19(4)	56(4)	17(4)
C(1)	45(2)	62(3)	71(3)	13(2)	2(2)	1(2)
C(2)	74(3)	51(3)	107(4)	17(3)	9(2)	13(2)
C(3)	55(2)	75(3)	116(4)	14(3)	4(2)	17(3)
C(4)	43(2)	76(3)	105(4)	-2(3)	-1(2)	1(2)
C(5)	53(2)	54(3)	77(3)	-2(2)	9(2)	2(2)
C(6)	53(2)	67(3)	53(2)	3(2)	11(2)	-1(2)
C(7)	69(3)	78(3)	77(3)	10(3)	27(2)	-7(3)
C(8)	96(3)	76(3)	53(3)	16(2)	33(2)	10(3)
C(9)	84(3)	77(3)	47(3)	9(2)	11(2)	5(2)
C(10)	59(2)	66(3)	52(2)	8(2)	4(2)	3(2)
C(11)	63(2)	60(3)	54(2)	2(2)	13(2)	6(2)
C(12)	79(3)	88(4)	57(3)	2(3)	23(2)	6(3)
C(13)	85(3)	94(4)	71(3)	27(3)	27(2)	3(3)
C(14)	84(3)	57(3)	80(3)	21(3)	22(2)	7(2)
C(15)	61(2)	61(3)	60(2)	8(2)	14(2)	9(2)
C(16)	52(2)	78(3)	54(3)	4(2)	7(2)	7(2)
C(17)	60(2)	85(3)	81(3)	5(3)	26(2)	22(2)
C(18)	44(2)	85(3)	98(4)	17(3)	9(2)	14(2)
C(19)	50(2)	74(3)	71(3)	8(2)	2(2)	7(2)
C(20)	53(2)	58(2)	65(3)	3(2)	6(2)	8(2)

C(21)	89(3)	63(3)	72(3)	-3(2)	13(2)	-16(2)
C(22)	79(3)	71(3)	80(3)	-4(3)	20(2)	5(2)
C(23)	265(11)	124(7)	274(12)	55(7)	140(9)	-15(7)
C(24)	650(40)	630(40)	174(12)	-180(17)	-144(16)	120(30)
C(25)	164(7)	229(10)	201(9)	-50(8)	31(7)	100(7)
C(26)	157(7)	133(6)	242(10)	88(6)	-2(6)	48(5)
C(27)	193(8)	245(10)	109(5)	68(6)	54(5)	78(7)
C(28)	78(3)	155(6)	89(4)	3(4)	1(3)	-22(4)
C(29)	78(3)	140(6)	79(3)	40(4)	-10(3)	19(4)
C(30)	180(7)	106(5)	100(5)	36(4)	62(5)	46(5)
C(31)	144(6)	133(6)	105(5)	-2(4)	49(4)	-65(5)
C(32)	61(3)	203(7)	118(5)	46(5)	6(3)	-18(4)

---

## **Erklärung :**

Ich versichere, daß ich die von mir vorgelegte Dissertation selbständig angefertigt, die benutzten Quellen und Hilfsmittel vollständig angegeben und die Stellen der Arbeit – einschließlich Tabellen, Karten und Abbildungen - , die anderen Werken im Wortlaut oder dem Sinn nach entnommen sind, in jedem Einzelfall als Entlehnung kenntlich gemacht habe; daß diese Dissertation noch keiner anderen Fakultät oder Universität zur Prüfung vorgelegen hat; daß sie – abgesehen von unten angegebenen Teilpublikationene – noch nicht veröffentlicht worden ist sowie, daß ich eine solche Veröffentlichung vor Abschluß des Promotionsverfahrens nicht vornehmen werde.

Die Bestimmungen dieser Promotionsordnung sind mir bekannt. Die von mir vorgelegte Dissertation ist von Prof. Dr. Axel Klein betreut worden.

Nachfolgend genannte Teilpublikation liegt vor:

A. Klein, K. Butsch, J. Neudörfl, *Inorg. Chim. Acta*, **2010**, :10.1016/j.ica.2010.06.011.

Ich versichere, daß ich alle Angaben wahrheitsgemäß nach bestem Wissen und Gewissen gemacht habe und verpflichte mich, jedmögliche, die obigen Angaben betreffenden Veränderungen, dem Dekanat unverzüglich mitzuteilen.

Datum

Unterschrift

## Katharina Butsch

Geboren am: 15.08.1983

Wohnhaft: Bonnstr. 151  
50321 Brühl

Familienstand: ledig

Schulbildung: 1990-1994 Martin Luther Grundschule, Brühl  
1994-2003 St. Ursula Gymnasium in Brühl

Studium : 10/2003-03/2008 Universität zu Köln, Diplom Studium  
07.07-03.08 Diplomarbeit im Arbeitskreis von Prof. Dr. A. Klein:  
„Organometallische Verbindungen des Palladiums mit biorelevanten Liganden“  
  
seit 04.08 Promotionsstudium bei Prof. Dr. A. Klein, Thema: „Copper Phenoxyl  
Complexes“

### Publikationen:

K. Butsch, S. Elmas, N. Sen Gupta, R. Gust, F. Heinrich, A. Klein, Y. von Mering, M. Neugebauer, I. Ott, M. Schäfer, H. Scherer, T. Schurr, *Organometallics*, **2009**, 28, 3906–3915.

A. Klein, S. Elmas, K. Butsch, *Eur. J. Inorg. Chem.* **2009**, 2271–2281.

K. Butsch, R. Gust, A. Klein, I. Ott, M. Romanski, *Dalton Trans.*, **2010**, 39, 18, 4331–4340.

A. Klein, Y. von Mering, A. Uthe, K. Butsch, D. Schaniel, N. Mockus, T. Woike, *Polyhedron*, **2010**, 29, 12, 2553–2559.

A. Klein, A. Lüning, I. Ott, L. Hamel, K. Butsch, M. Neugebauer, V. Lingen, F. Heinrich, S. Elmas, *J. Organomet. Chem.*, **2010**, 695, 1898–1905.

A. Klein, K. Butsch, J. Neudörfel, *Inorg. Chim. Acta*, **2010**, doi: 10.1016/j.ica.2010.06.011.

### Konferenzbeiträge:

International Conference on Coordination Chemistry (ICCC) in Jerusalem 2008  
Poster: “Synthesis & Analysis of DPPZ-derivatives and related Palladium Complexes”

European Conference on Chemistry for Life-sciences (ECCLS) in Frankfurt 2009  
Poster: “Exchange reactions of Nucleobase(analogue)-ligands on Pd(II)-complexes”

European Conference on Biological and Inorganic Chemistry (EuroBIC) in Thessaloniki 2010  
Poster: “Electron transfer studies on Cu(II) complexes bearing phenoxy-pincer ligands”